the horizontal natural frequency of a pendulum system from Eq. (13.3) if one replaces X_{st} in that equation by the pendulum length. Some commercial isolation systems combine pendulum action for horizontal isolation with spring action for vertical isolation.

Various exotic isolation systems have also been investigated or employed for special applications. These include systems in which the spring action is provided by magnetic or electrostatic levitation or by streams or thin films of gases or liquids.

Active isolation systems (see Chapter 18) have recently received increased attention. Such systems essentially are dynamic control systems in which the vibration of the item to be protected is sensed by an appropriate transducer whose suitably processed output is used to drive an actuator that acts on the item so as to reduce its vibration. Active systems are relatively complex, but they can provide better isolation than passive systems under some conditions, notably, in the presence of low-frequency disturbances, attenuation of which by passive means generally tends to be most difficult.

REFERENCES

1. W. T. Thomson, *Theory of Vibration with Applications*, 2nd ed., Prentice-Hall, Englewood Cliffs, NJ, 1981.
2. J. C. Snowdon, *Vibration and Shock in Damped Mechanical Systems*, Wiley, New York, 1968.
3. D. J. Mead, *Passive Vibration Control*, Wiley, New York, 1998.
4. E. I. Rivin, *Passive Vibration Isolation*, American Society of Mechanical Engineers, New York, 2003.
5. H. Himelblau, Jr. and S. Rubin, "Vibration of a Resiliently Supported Rigid Body," in C. M. Harris and C. E. Crede (Eds.), *Shock and Vibration Handbook*, 2nd ed. McGraw-Hill, New York, 1976.
6. J. N. Macduff and J. R. Curreri, *Vibration Control*, McGraw-Hill, New York, 1958.
7. C. E. Crede and J. E. Ruzicka, "Theory of Vibration Isolation," in C. M. Harris and C. E. Crede (Eds.), *Shock and Vibration Handbook*, 2nd ed., McGraw-Hill, New York, 1976.
8. E. E. Ungar and C. W. Dietrich, "High-Frequency Vibration Isolation," *J. Sound Vib.*, **4**, 224–241 (1966).
9. L. Cremer, M. A. Heckl, and E. E. Ungar, *Structure-Borne Sound*, 2nd ed., Springer-Verlag, Berlin, 1988.
10. E. E. Ungar, "Mechanical Vibrations," in H. A. Rothbart (Ed.), *Mechanical Design and Systems Handbook*, 2nd ed., McGraw-Hill, New York, 1985, Chapter 5.
11. D. Muster and R. Plunkett, "Isolation of Vibrations," in L. L. Beranek (Ed.), *Noise and Vibration Control*, McGraw-Hill, New York, 1971, Chapter 13.
12. E. E. Ungar, "Wave Effects in Viscoelastic Leaf and Compression Spring Mounts," *Trans. ASME Ser. B*, **85**(3), 243–246 (1963).
13. D. Muster, "Resilient Mountings for Reciprocating and Rotating Machinery," Eng. Rept. No. 3, ONR Contract N70NR-32904, July 1951.

CHAPTER 14

Structural Damping

ERIC E. UNGAR AND JEFFREY A. ZAPFE

Acentech, Inc.
Cambridge, Massachusetts

14.1 THE EFFECTS OF DAMPING

The dynamic responses and sound transmission characteristics of structures are determined by essentially three parameters: mass, stiffness, and damping. Mass and stiffness are associated with storage of kinetic and strain energy, respectively, whereas damping relates to the dissipation of energy, or, more precisely, to the conversion of the mechanical energy associated with a vibration to a form (usually heat) that is unavailable to the mechanical vibration.

Damping in essence affects only those vibrational motions that are controlled by a balance of energy in a vibrating structure; vibrational motions that depend on a balance of forces are virtually unaffected by damping. For example, consider the response of a classical mass–spring–dashpot system to a steady sinusoidal force. If this force acts at a frequency that is considerably lower than the system's natural frequency, the response is controlled by a quasi-static balance between the applied force and the spring force. If the applied force acts at a frequency that is considerably above the system's natural frequency, the response is controlled by a balance between the applied force and the mass's inertia. In both of these cases, damping has practically no effect on the responses. However, at resonance, where the excitation frequency matches the natural frequency, the spring and inertia effects cancel each other and the applied force supplies some energy to the system during each cycle; as a result, the system's energy (and amplitude) increases until steady state is reached, at which time the energy input per cycle is equal to the energy lost per cycle *due to damping*.

In light of energy considerations like the foregoing, one finds that increased damping results in (1) more rapid decay of unforced vibrations, (2) faster decay of freely propagating structure-borne waves, (3) reduced amplitudes at resonances of structures subject to steady periodic or random excitation with attendant reductions in stresses and increases in fatigue life, (4) reduced response to sound and increased sound transmission loss (reduced sound transmission) above the coincidence frequency (at which the spatial distribution of the disturbing pressure

Aroma360 - Exhibit 1027

the horizontal natural frequency of a pendulum system from Eq. (13.3) if one replaces X_{st} in that equation by the pendulum length. Some commercial isolation systems combine pendulum action for horizontal isolation with spring action for vertical isolation.

Various exotic isolation systems have also been investigated or employed for special applications. These include systems in which the spring action is provided by magnetic or electrostatic levitation or by streams or thin films of gases or liquids.

Active isolation systems (see Chapter 18) have recently received increased attention. Such systems essentially are dynamic control systems in which the vibration of the item to be protected is sensed by an appropriate transducer whose suitably processed output is used to drive an actuator that acts on the item so as to reduce its vibration. Active systems are relatively complex, but they can provide better isolation than passive systems under some conditions, notably, in the presence of low-frequency disturbances, attenuation of which by passive means generally tends to be most difficult.

REFERENCES

1. W. T. Thomson, *Theory of Vibration with Applications*, 2nd ed., Prentice-Hall, Englewood Cliffs, NJ, 1981.
2. J. C. Snowdon, *Vibration and Shock in Damped Mechanical Systems*, Wiley, New York, 1968.
3. D. J. Mead, *Passive Vibration Control*, Wiley, New York, 1998.
4. E. I. Rivin, *Passive Vibration Isolation*, American Society of Mechanical Engineers, New York, 2003.
5. H. Himelblau, Jr. and S. Rubin, "Vibration of a Resiliently Supported Rigid Body," in C. M. Harris and C. E. Crede (Eds.), *Shock and Vibration Handbook*, 2nd ed. McGraw-Hill, New York, 1976.
6. J. N. Macduff and J. R. Curreri, *Vibration Control*, McGraw-Hill, New York, 1958.
7. C. E. Crede and J. E. Ruzicka, "Theory of Vibration Isolation," in C. M. Harris and C. E. Crede (Eds.), *Shock and Vibration Handbook*, 2nd ed., McGraw-Hill, New York, 1976.
8. E. E. Ungar and C. W. Dietrich, "High-Frequency Vibration Isolation," *J. Sound Vib.*, **4**, 224–241 (1966).
9. L. Cremer, M. A. Heckl, and E. E. Ungar, *Structure-Borne Sound*, 2nd ed., Springer-Verlag, Berlin, 1988.
10. E. E. Ungar, "Mechanical Vibrations," in H. A. Rothbart (Ed.), *Mechanical Design and Systems Handbook*, 2nd ed., McGraw-Hill, New York, 1985, Chapter 5.
11. D. Muster and R. Plunkett, "Isolation of Vibrations," in L. L. Beranek (Ed.), *Noise and Vibration Control*, McGraw-Hill, New York, 1971, Chapter 13.
12. E. E. Ungar, "Wave Effects in Viscoelastic Leaf and Compression Spring Mounts," *Trans. ASME Ser. B*, **85**(3), 243–246 (1963).
13. D. Muster, "Resilient Mountings for Reciprocating and Rotating Machinery," Eng. Rept. No. 3, ONR Contract N70NR-32904, July 1951.

CHAPTER 14

Structural Damping

ERIC E. UNGAR AND JEFFREY A. ZAPFE

Acentech, Inc.
Cambridge, Massachusetts

14.1 THE EFFECTS OF DAMPING

The dynamic responses and sound transmission characteristics of structures are determined by essentially three parameters: mass, stiffness, and damping. Mass and stiffness are associated with storage of kinetic and strain energy, respectively, whereas damping relates to the dissipation of energy, or, more precisely, to the conversion of the mechanical energy associated with a vibration to a form (usually heat) that is unavailable to the mechanical vibration.

Damping in essence affects only those vibrational motions that are controlled by a balance of energy in a vibrating structure; vibrational motions that depend on a balance of forces are virtually unaffected by damping. For example, consider the response of a classical mass–spring–dashpot system to a steady sinusoidal force. If this force acts at a frequency that is considerably lower than the system's natural frequency, the response is controlled by a quasi-static balance between the applied force and the spring force. If the applied force acts at a frequency that is considerably above the system's natural frequency, the response is controlled by a balance between the applied force and the mass's inertia. In both of these cases, damping has practically no effect on the responses. However, at resonance, where the excitation frequency matches the natural frequency, the spring and inertia effects cancel each other and the applied force supplies some energy to the system during each cycle; as a result, the system's energy (and amplitude) increases until steady state is reached, at which time the energy input per cycle is equal to the energy lost per cycle *due to damping*.

In light of energy considerations like the foregoing, one finds that increased damping results in (1) more rapid decay of unforced vibrations, (2) faster decay of freely propagating structure-borne waves, (3) reduced amplitudes at resonances of structures subject to steady periodic or random excitation with attendant reductions in stresses and increases in fatigue life, (4) reduced response to sound and increased sound transmission loss (reduced sound transmission) above the coincidence frequency (at which the spatial distribution of the disturbing pressure

matches that of the structural displacement), (5) reduced rate of buildup of vibrations at resonances, and (6) reduced amplitudes of "self-excited" vibrations, in which the vibrating structure accepts energy from an external source (e.g., wind) as the result of its vibratory motion.

14.2 MEASURES AND MEASUREMENT OF DAMPING

Most measures of damping are based on the dynamic responses of simple systems with idealized damping behaviors. Damping measurements typically involve observation of some characteristics of these responses.

Decay of Unforced Vibrations with Viscous Damping

Many aspects of the behaviors of vibrating systems can be understood in terms of the simple ideal linear mass–spring–dashpot system shown in Fig. 14.1. If this system is displaced by an amount x from its equilibrium position, the massless spring produces a force of magnitude kx tending to restore the mass m toward its equilibrium position, and the massless dashpot produces a retarding force of magnitude $c\dot{x}$. Here k and c are constants of proportionality; k is known as the spring constant and c as the *viscous damping coefficient.*

If this system is displaced from its equilibrium position by an amount X_0 and then released, the resulting displacement varies with time t as[1]

$$x = X_0 e^{-\zeta\omega_n t} \cos(\omega_d t + \phi) \tag{14.1}$$

provided that $\zeta < 1$. Here ϕ represents a phase angle, which depends on the velocity with which the mass is released, and ω_n and ω_d represent the undamped and damped radian natural frequencies of the system. These obey

$$\omega_n = \sqrt{\frac{k}{m}} = 2\pi f_n \qquad \omega_d = \omega_n\sqrt{1-\zeta^2} \tag{14.2}$$

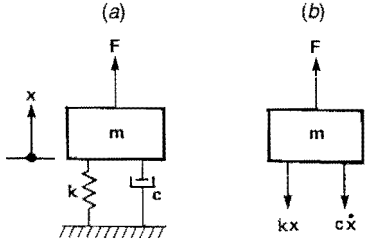


FIGURE 14.1 System with single degree of freedom: (*a*) schematic representation of mass–spring–dashpot system or of a vibrational mode of a structure; (*b*) free-body diagram of mass. Spring produces restoring force kx; dashpot produces retarding force $c\dot{x}$.

with f_n representing the cyclic (undamped) natural frequency. The constant ζ is called the *damping ratio* or *fraction of critical damping*; it is defined as

$$\zeta = \frac{c}{c_c} \qquad c_c = 2\sqrt{km} = 2m\omega_n \tag{14.3}$$

where c_c is known as the *critical damping coefficient.* For the small values of ζ one usually encounters in practice, ω_d is sufficiently close to ω_n so that one rarely needs to distinguish between the damped and the undamped natural frequencies. Furthermore, the foregoing expression for ω_d applies only for viscous damping; other relations hold for other damping models.

The right-hand side of Eq. (14.1) represents a cosine function with an amplitude $X_0 e^{-\zeta\omega_n t}$ that decreases as time t increases (see Fig. 14.2); its rate of decrease is $\zeta\omega_n$ and thus is proportional to ζ. However, Eq. (14.1) does not apply for values of ζ that equal or exceed unity (or for values of c that equal or exceed c_c). For such large values of ζ or c one obtains a nonoscillatory decay represented by pure exponential expressions instead of the decaying oscillation represented by Eq. (14.1). The critical damping coefficient c_c constitutes the boundary between oscillatory and nonoscillatory decays.

The *logarithmic decrement* δ is a convenient, time-honored representation of how rapidly a free oscillation decays. It is defined by[1]

$$\delta = \frac{1}{N}\ln\frac{X_i}{X_{i+N}} \tag{14.4}$$

where X_i represents the value of x at any selected peak and X_{i+N} represents the value at the peak at N cycles from the aforementioned one. It follows from Eq. (14.1) that $\delta = 2\pi\zeta$.

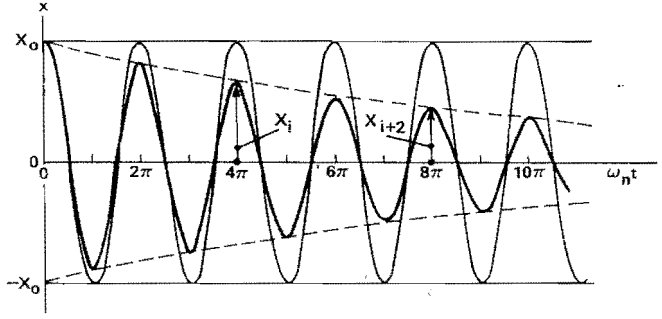


FIGURE 14.2 Time variation of displacement of mass–spring–dashpot system released with zero velocity from initial displacement X_0. *Light curve*: Undamped system ($c = \zeta = 0$); amplitude remains constant at X_0. *Heavy curve*: Damped system ($0 < c < c_c$; $0 < \zeta < 1$); amplitude decreases according to $x = X_0 e^{-\zeta\omega_n t}$, which is represented by upper dashed curve. Lower dashed curve corresponds to $x = -X_0 e^{-\zeta\omega_n t}$. Amplitudes X_i and X_{i+2} illustrate values that may be used to calculate logarithmic decrement from Eq. (14.4) for $N = 2$.

The utility of logarithmic measures of oscillatory quantities has long been recognized in acoustics, and definitions analogous to acoustical levels have come into use in the field of vibrations, particularly in regard to measurement. For example, one may define the displacement level L_x, in decibels, corresponding to an oscillatory displacement $x(t)$ in analogy to sound pressure level, as

$$L_x = 10 \log_{10} \frac{x^2(t)}{x_{\text{ref}}^2} \tag{14.5}$$

where x_{ref} denotes a (constant) reference value of displacement. One may then define a decay rate Δ, in decibels per second, and find that for a viscously damped system[2]

$$\Delta = -\frac{dL_x}{dt} = 8.69\zeta\omega_n = 54.6\zeta f_n \tag{14.6}$$

Also in analogy to acoustics, one may define the reverberation time T_{60} as the time it takes for the displacement level to decrease by 60 dB; thus,

$$T_{60} = \frac{60}{\Delta} = \frac{1.10}{\zeta f_n} \tag{14.7}$$

Because velocity and acceleration levels may be defined in full analogy to the definition of displacement level in Eq. (14.5), the decay rate and reverberation time expressions of Eqs. (14.6) and (14.7) also apply to these other vibration levels.

If any extended structure that is not too highly damped vibrates in the absence of external forces at one of its natural frequencies, all points on that structure move either in phase or in opposite phase with each other, and the structure is said to vibrate in one of its modes. In addition to the modal natural frequency, there corresponds to each mode a modal mass, a modal stiffness, and a modal damping value. With the aid of these parameters the behavior of a modal vibration may be described in terms of that of an equivalent simple mass–spring–dashpot system.[1,3,4] Thus, all of the foregoing discussion concerning this simple system also applies to structural modes.

Of course, extended structures also can exhibit wave motions at a given frequency in which all points are not in or out of phase with each other. Such motions, which can be described in terms of freely propagating waves, also decrease due to damping. For flexural waves on a beam or for nonspreading (straight-crested) flexural waves on a plate, the *spatial decay rate* Δ_λ, defined as the reduction in vibration level per wavelength, obeys[2] $\Delta_\lambda = 27.2\zeta$ in decibels per wavelength.

Steady Forced Vibrations

If the system of Fig. 14.1 is subject to a sinusoidal force $F(t) = F \cos \omega t$, then its equation of motion may be written as

$$m\ddot{x} + c\dot{x} + kx = F(t) = F \cos \omega t \tag{14.8}$$

One may find its steady-state solution by substituting $x(t) = X \cos(\omega t - \phi)$ and solving for X and ϕ. Alternatively, one may obtain this solution by taking $x(t) = \text{Re}[\overline{X}e^{j\omega t}]$, where $j = \sqrt{-1}$ and the complex amplitude or *phasor* $\overline{X} = Xe^{-j\phi}$ indicates both the amplitude and the phase of the vibration.* In terms of phasors (and omitting the writing of "Re"), the equation of motion may be written as

$$(-m\omega^2 + j\omega c + k)\overline{X} = (\overline{k} - m\omega^2)\overline{X} = F \tag{14.9}$$

In the foregoing there has been introduced the complex stiffness

$$\overline{k} = k + j\omega c = k + k_i = k\left(1 + \frac{jk_i}{k}\right) \tag{14.10}$$

which includes information about the system's damping as well as about it stiffness. By means of either solution approach one may determine that

$$\frac{X}{F/k} = \frac{X}{X_{\text{st}}} = \frac{1}{\sqrt{(1-r^2)^2 + (2r\zeta)^2}} \qquad \tan\phi = \frac{2r\zeta}{1-r^2} \tag{14.11}$$

where $r \equiv \omega/\omega_n$.

The deflection $X_{\text{st}} = F/k$, which was introduced in order to obtain a nondimensional expression, is the quasi-static or zero-frequency deflection that the system would experience due to a statically applied force of magnitude F. The ratio X/X_{st}, which indicates by what factor the amplitude under dynamic excitation exceeds the quasi-static deflection, is called the *amplification*.

The foregoing response expressions (and related ones that involve velocity V or acceleration A instead of displacement) depend on damping; thus, damping data may be extracted from corresponding measurements. Two widely used measures of damping may be derived readily from the amplification expressions of Eq. (14.11), a plot of which is shown in Fig. 14.3. One is the *amplification at resonance*, conventionally represented by the letter Q and often simply called "the Q" of the system.[2] This corresponds to the value of X/X_{st} that results if the excitation frequency ω is equal to the natural frequency ω_n and is related to the viscous damping ratio by $Q = 1/2\zeta$. The second commonly used measure is the *relative bandwidth* $b = \Delta\omega/\omega_n \approx 1/Q$, where $\Delta\omega$ represents the difference between the two frequencies† (one below and one above ω_n; see Fig. 14.3) at which the amplification is equal to $Q/\sqrt{2}$.

In view of Eq. (14.11), the phase lag ϕ also provides a measure of damping. It is particularly convenient to use phase information in "Nyquist plots," that is, in plots of the real and imaginary parts of responses at a number of frequencies, as illustrated in Fig. 14.4. These plots are circles or nearly circles, with a diameter that is equal to Q if the plots are appropriately nondimensionalized.[5,6]

*Note that $e^{jz} = \cos z + j \sin z$ for any real number z. The amplitude X is equal to the absolute value of the phasor; that is, $X = |\overline{X}|$.

†These frequencies often are called the *half-power points* because at these the energy stored in the system (and that dissipated by it), which is proportional to the square of the amplitude [see Eq. (14.6)], is half of the maximum value.

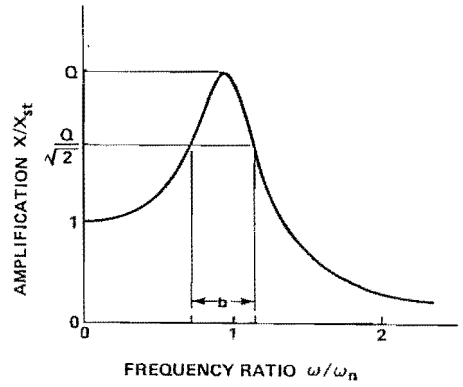


FIGURE 14.3 Steady-state response of mass–spring–dashpot system to sinusoidal force. See Eq. (14.11): Q = value of amplification X/X_{st} at resonance. Relative bandwidth $b = \Delta\omega/\omega_n$ is determined from "half-power points," that is from frequencies at which response amplitude is $1/\sqrt{2}$ times the maximum.

If the system of Fig. 14.1 (or a structural mode modeled by it) is subject to a broadband force (or broadband modal force) rather than a single-frequency sinusoidal force, then the mean-square displacement $\overline{x}^2$ of the mass is given by[7]

$$\frac{\overline{x}^2}{\pi S_F(\omega)\omega_n/k^2} = \frac{1}{2\zeta} \tag{14.12}$$

where $S_F(\omega)$ denotes the spectral density of the force in terms of radian frequency (i.e., the value of excitation force squared per unit radian frequency interval). Note that the spectral density in cyclic frequency obeys $S_F(f) = 2\pi S_F(\omega)$. The foregoing equation is exact for excitations with spectral densities that are constant for all frequencies. It is a good approximation for excitations with spectral densities that vary only slowly in the vicinity of the system's natural frequency ω_n; the spectral density value to be used in the equation then is that corresponding to ω_n.

Energy; Complex Stiffness

All of the measures of damping discussed so far are based on the motions of simple systems. However, since damping pertains to the dissipation of energy, damping measures that relate to energy are more basic and more general.

The *damping capacity* ψ is defined as the ratio of the energy that is dissipated per cycle to the total energy present in the vibrating system. The *loss factor* η is defined similarly as the ratio of the energy that is dissipated per radian to the total energy. If D denotes the energy dissipated per cycle and W the total energy in the system, then

$$\eta = \frac{\psi}{2\pi} = \frac{D}{2\pi W} \tag{14.13}$$

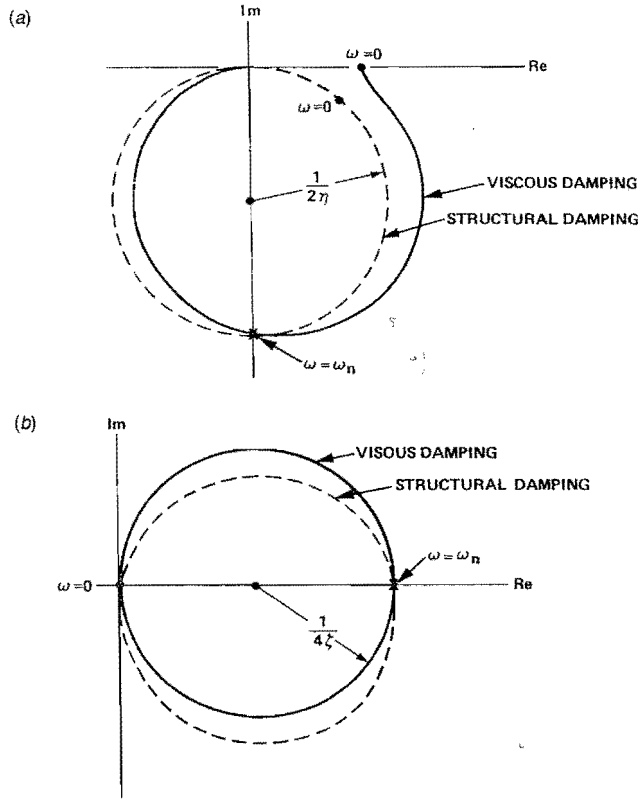


FIGURE 14.4 Nyquist plots of nondimensional responses of viscously and structurally damped mass–spring–damper systems. (*a*) Real and imaginary parts of amplification X/X_{st}. (*b*) Real and imaginary parts of mobility $Vk/F\omega_n = Vc_c/2F$. Amplification plot for structural damping and mobility plot for viscous damping are exact circles; others are approximate circles that become more nearly circular with decreased damping. Diameter is exactly or approximately equal to Q. Figure plots correspond to $\zeta = 0.2$, $\eta = 0.4$.

These expressions apply for any damping mechanism. However, it is interesting to relate them to the special case of a viscously damped mass–spring–dashpot system like that of Fig. 14.1. In this system the energy dissipated corresponds to the work that is done on the dashpot, and one may readily determine that the energy dissipated per cycle in a steady vibration at radian frequency ω and displacement amplitude X obeys $D = \pi\omega c X^2$. The total energy W stored by the system consists of the kinetic energy W_{kin} of the mass and the potential (or strain) energy W_{pot} in the spring. If the energy dissipated is small compared to the total energy stored, then W is approximately equal to the energy stored in the spring when the kinetic energy is zero—that is, when the spring is displaced to the full extent of its amplitude—and $W = W_{kin} + W_{pot} \approx kX^2/2$.

Thus, one finds by use of Eqs. (14.3) and (14.13) that for a viscously damped system

$$\eta \approx \frac{\omega c}{k} = \frac{2\zeta\omega}{\omega_n} = 2r\zeta \tag{14.14}$$

From Eq. (14.10) one finds that

$$\bar{k} = k(1 + j\eta) \qquad k_i/k = \eta \tag{14.15}$$

Equation (14.14) indicates that for the particular case of a viscously damped system the loss factor is proportional to the frequency. In cases where the loss factor exhibits some other frequency dependence, Eqs. (14.13) and (14.15) still apply—and Eq. (14.11) holds if $2r\zeta$ is replaced by η. These equations then permit one not only to consider the case of *structural damping*, which is characterized by a constant loss factor, but also to take into account experimentally determined frequency variations of the loss factor.

Interrelation of Measures of Damping

The following relations apply at all frequencies:

$$\eta = \frac{\psi}{2\pi} = \frac{k}{k_i} = |\tan\ \phi|_{r=0} \tag{14.16a}$$

but the relations of Eq. (14.16b) are exact only at resonance:

$$\eta = \frac{1}{Q} = 2\zeta \qquad \text{and} \qquad \eta \approx b \text{ for small damping} \tag{14.16b}$$

For systems with viscous damping,

$$2\zeta = \frac{\delta}{\pi} = \frac{2.20}{f_n T_{60}} = \frac{\Delta}{27.3 f_n} = \frac{\Delta_\lambda}{13.6} \tag{14.16c}$$

For systems with small damping, one may take $\eta \approx 2\zeta$, consider that the system behaves approximately like a viscously damped one, and use the relations of Eq. (14.16c).

Measurement of Damping

Most approaches to measurement of the damping of structures are based on the previously discussed responses of simple systems, which, as has been mentioned, also correspond to those of structural modes. However, unlike mass–spring–dashpot systems, structures have a multiplicity of modes and corresponding natural frequencies. Therefore, many of the approaches applicable to simple systems can be applied only to structural modes whose responses can be separated adequately from those of all others because of differences in their natural frequencies or mode shapes.

Measurement of logarithmic decrement δ typically is applicable only to the fundamental modes of structures for which a clear record of the amplitude-versus-time trace can be obtained. If more than one mode is present, their decaying responses are superposed and the record becomes difficult to interpret.

The counting of peaks that is required for determination of the logarithmic decrement from Eq. (14.4) is not needed if one focuses on the decaying signal's envelope. For purposes of evaluating this envelope it is particularly convenient to use a display of the logarithm of the rectified amplitude versus time. Rectification is needed because the logarithm of negative numbers is undefined. In such a logarithmic display the envelope becomes a straight line whose slope is proportional to $\zeta\omega_n$ and thus to the decay rate. Not only does measurement of the slope enable one to evaluate the damping, but also observation of deviations of the envelope from a straight line permit one to judge whether the structure's damping is indeed viscous and amplitude-independent and whether a superposition of responses with different decay rates is present.

Determination of decay rates is useful also in frequency bands in which a multitude of modes are excited. A typical measurement here involves excitation of a structure by a broadband force in a given frequency band, cutting off the excitation, then observing the envelope of the logarithm of the rectified signal obtained by passing the output of a transducer (usually an accelerometer) through a bandpass filter* tuned to the excitation band. The center frequency of this passband may be taken to represent ω_n for all modes in the band. Some judgment in interpreting the resulting envelopes and averaging of results from repeated measurements is generally required because different modes in the band may exhibit somewhat different decays.

A conceptually straightforward approach to measuring the damping of a structure involves the application of Eq. (14.13) to observed values of the energy dissipation and total vibrational energy W present in a structure in the steady state.[8] The structure is excited via an impedance head or a similar transducer arrangement that measures the force and motion at the excitation point. The instantaneous force and velocity values are multiplied and the product is time averaged to yield the average energy input per unit time, which is equal to the energy dissipated per unit time under steady-state conditions. For a given excitation frequency f, the energy D dissipated per cycle is equal to $1/f$ times the energy dissipated per unit time.

The energy W stored in the structure may be determined from its kinetic energy, which may be calculated from information on its mass distribution and from velocity values measured by a suitable array of accelerometers or other motion transducers. This measurement approach requires particular care in instrumentation selection and calibration, but it has a significant advantage: Because it involves direct measurement of the dissipated energy, it does not rely on any

*The filter's response must be fast enough so that it can follow the decaying signal; otherwise one observes the decay of the filter response instead of that of the structural vibration. Filters with wider passbands need to be used to observe the more rapid decays associated with greater damping.

particular model of dissipation. It also permits one, for example, to investigate how the loss factor varies with amplitude.

Force-and-motion transducer combinations may also be employed for the direct measurement of complex impedance or mobility (or of other force–motion ratios), from which damping information may be extracted, typically on the basis of Nyquist plots. Much corresponding specialized *modal testing* or *modal parameter extraction* instrumentation and software has recently become available.

Simple steady sinusoidal response measurements may also be made to measure Q and the half-power point bandwidth b directly on the basis of their definitions. These measurements require particular care to ensure that the near-resonance response of the mode of interest is not affected significantly by the responses of other modes with resonance frequencies near that of the mode of interest.

14.3 DAMPING MODELS

Analytical Models

Most of the foregoing discussion has dealt with "viscous" damping, where energy dissipation results from a force that is proportional to the velocity of a vibrating system and that acts opposite to the velocity. This viscous model of damping action has been used most widely because it results in relatively simple linear differential equations of system motion and because it yields a reasonable approximation to the action of some real systems, particularly at small amplitudes.

Among the many other models that have received considerable attention, most also involve a motion-opposing force that is a function of velocity. In *dry friction* or *Coulomb* damping, the force is constant in magnitude (but changes its algebraic sign when the velocity does). In *square law* and *power law* damping the force magnitude is proportional to the square or to some other power of velocity. Of course, modern numerical methods also permit one readily to analyze models involving other velocity dependences, such as one might obtain from corresponding experiments.

Whereas in viscous damping the retarding force is proportional to the velocity, in *structural damping* the retarding force is proportional to the displacement. As has been mentioned, structural damping is characterized by a constant loss factor η and the dimensionless response relation for a system with structural damping is given by Eq. (14.11) with $2r\zeta$ replaced by η. Because of the difference in the retarding forces, a structurally damped system behaves differently from a viscously damped one, except near the natural frequency. The structural damping model is often extended to loss factors that vary with frequency as determined from experimental data. With the appropriate frequency dependence of the loss factors, the structural damping model can be made to represent the sinusoidal response of viscously damped systems—and, indeed, of any system whose loss factor is independent of amplitude.*

*Caution is required if one wants to undertake transformations from the frequency to the time domain. Not all conceivable frequency variations of the loss factor lead to physically realizable results; e.g., some imply system motions that begin before application of a force.[9]

Applicability of Models

If one desires to determine the precise response of a system to a prescribed excitation, one generally needs to have a complete description of all forces, including the damping forces; that is, one needs a damping model that corresponds to the actual system. This is true, for example, if one wants to study the "wave shape" of the motion of a screeching brake or a chattering tool or if one needs to determine the response of a system to a transient, such as a shock.

In many practical instances, however, the details of the system's motion are of no interest and only the amplitudes are of concern. As has been mentioned, under steady resonant or free decay conditions (and in a few other situations), the amplitudes are established essentially by the energy in the system. For such conditions, the details of the damping model are unimportant as long as the model gives the correct energy dissipation per cycle. It is for this reason that measures of damping that involve only energy considerations have found wide acceptance.*

14.4 DAMPING MECHANISMS AND MAGNITUDES

Since damping involves the conversion of energy associated with a vibration to other forms that are unavailable to the vibration, there are as many damping mechanisms as there are ways to remove energy from a vibrating system. These include mechanisms that convert mechanical energy into heat, as well as others that transport energy away from the vibrating system of concern.

Energy Dissipation and Conversion

Material damping, mechanical hysteresis, and internal friction refer to the conversion of mechanical energy into heat that occurs within materials due to deformations that are imposed on them. This conversion may result from a variety of effects on the molecular, crystal lattice, or metal grain level, including magnetic, thermal, metallurgical, and atomic phenomena.[10] Figure 14.5 indicates the ranges of the loss factors reported for some common materials.

Damping of a vibrating structure may also result from friction associated with relative motion between the structure and solids or fluids that are in contact with it. Also, an electrically conductive structure moving in a magnetic field is subject to damping due to eddy currents that result from the motion and that are converted into heat.

A granular material, such as sand, placed in contact with a vibrating structure tends to produce damping by two different mechanisms. At small amplitudes, damping results predominantly from interaction of asperities on adjacent grains and the attendant energy loss due to mechanical hysteresis. At large amplitudes,

*Equivalent viscous damping, defined as viscous damping that results in the same energy dissipation as the damping actually present in the system, is often used in analyses. This damping model obviously should not be used where details of the system motion are of concern.

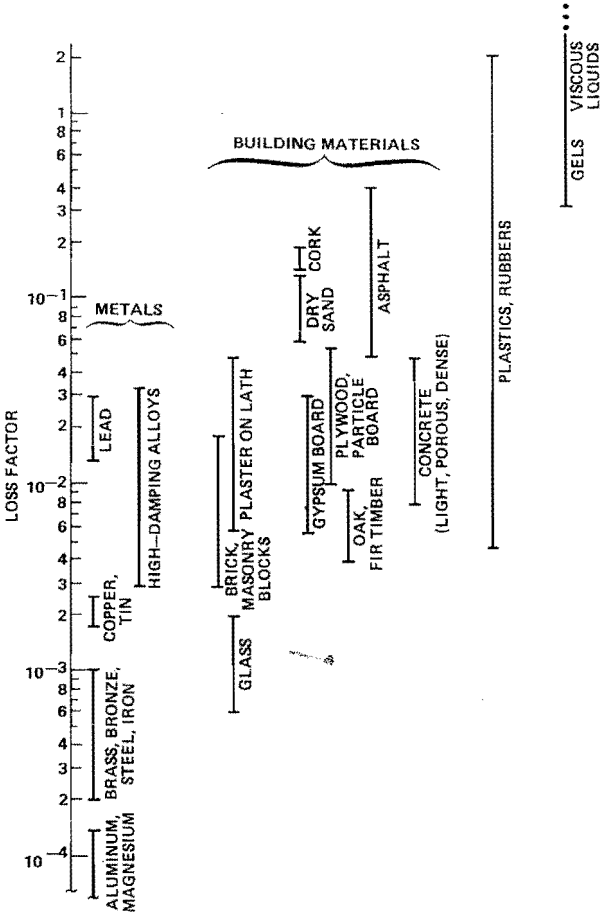


FIGURE 14.5 Typical ranges of material loss factors at small strains, near room temperature, at audio frequencies. The loss factors of metals tend to increase with strain amplitude, particularly near the yield point, but the loss factors of plastics and rubbers tend to be relatively independent of strain amplitude up to strains of the order of unity. The loss factors of some materials, particularly those that can flow or creep, tend to vary markedly with temperature and frequency.

damping results predominantly from impacts between the structure and the grains or between grains; these impacts produce high-frequency vibrations of the structure and of the granular material, and the energy that goes into these vibrations (which eventually is converted to heat) is no longer available to the structural vibrations of concern.[11] Impact dampers, in which a small element is made to rattle against a vibrating structure, similarly rely on conversion of the energy of the vibrating structure to higher frequency vibrations.

Damping due to Boundaries and Reinforcements

For panels or other structural components that may be considered as uniform plates, one may estimate the loss factor η_b associated with energy loss at the panel boundaries, due to both energy transport to adjacent panels and dissipation at its boundaries, from information on the boundary absorption coefficients.[12] For a panel of area A vibrating at a frequency at which the flexural wavelength λ on the panel is considerably shorter than a panel edge, this loss factor is given by

$$\eta_b = \frac{\lambda}{\pi^2 A} \sum \gamma_i L_i \tag{14.17}$$

where γ_i denotes the absorption coefficient of the ith boundary increment whose length is L_i and where the summation extends over all boundary increments.

At frequency f the flexural wavelength on a homogeneous plate of thickness h of a material with longitudinal wave speed c_L and Poisson's ratio ν is given by $\lambda = \sqrt{(\pi/\sqrt{3})hc_L/f(1-\nu^2)}$.

The absorption coefficient γ of a boundary element is defined as the fraction of the panel bending-wave energy impinging on the boundary element that is not returned to the panel. Although the absorption coefficient values associated with a given boundary element rarely can be predicted well analytically, they can often be determined experimentally. For example, one might add a boundary element of length L_0 to a panel, measure the resulting loss factor increase $\Delta\eta$ at various frequencies, and calculate the absorption coefficient values γ_0 of this boundary element from $\gamma_0 = (\Delta\eta)\pi^2 A/\lambda L_0$, which follows from Eq. (14.17). Both Eq. (14.17) and the expression for γ_0 are based on the assumption that the absorption coefficient of a boundary element is independent of its length, an assumption that generally holds true if the wavelength λ is considerably smaller than the element length.

Equation (14.17) also permits one to account for the damping effects of linear discontinuities, such as seams or attached reinforcing beams, on panels, provided one knows the corresponding absorption coefficients. Since plate waves can impinge on both sides of a discontinuity located within the panel area, for such a discontinuity location one needs to use in Eq. (14.17) twice the actual discontinuity length.

The energy that beams or reinforcements attached to a panel can dissipate, and thus the damping they can produce, depends markedly on the fastening method used. Metal beams attached to metal panels or seams in such panels generally produce little damping if they are continuously welded or joined by means of a rigid adhesive. However, they can contribute significant damping if they are fastened by a flexible, dissipative adhesive or if they are fastened at only a number of points, for example, by rivets, bolts, or spot welds. At high frequencies, at which the flexural wavelength on the panel is smaller than the distance between fastening points, damping results predominantly not from interface friction but from an "air-pumping" effect produced as adjacent surfaces (at locations between

the connection points) move away from and toward each other. Energy loss here is due to the viscosity of the air or other fluid present between the surfaces.[13–15]

The high-frequency absorption coefficient corresponding to a beam that is fastened to a panel at a multitude of points may be estimated from the experimental results summarized in Fig. 14.6, which shows how the beam's reduced absorption coefficient γ_r varies with reduced frequency f_r or with the ratio d/λ of fastener spacing to plate flexural wavelength. These reduced quantities, definitions of which are given in the figure, account for the absorption coefficients' dependence on beam width w, plate thickness h, fastener spacing d, and longitudinal wave speed c_L in the plate material by relating these to reference values of these parameters (indicated by the subscript 0). It should be noted that Fig. 14.6 pertains to panels immersed in air at atmospheric pressure; lesser absorption coefficient values apply for panels at reduced pressure and higher values for panels at greater pressures. A theory is available[13] to account for the effects of atmospheric pressure changes and for other gases or liquids present between the contacting surfaces.

Damping due to Energy Transport

Structural Transmission. Energy that is transported away from a vibrating structure constitutes energy lost from that structure and thus contributes damping. Energy transport may occur to neighboring structural elements or to fluids in contact with the vibrating structure.

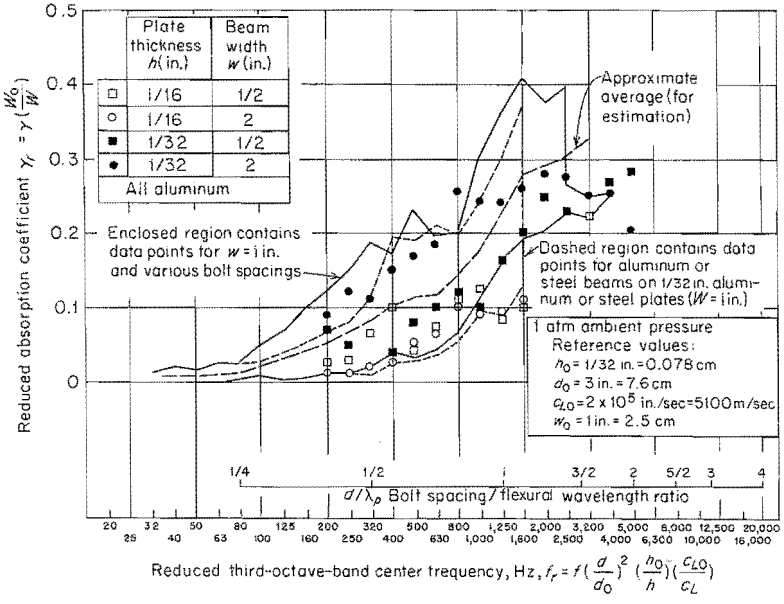


FIGURE 14.6 Summary of reduced absorption coefficient data for beams fastened to plates by rows of rivets, bolts, or spot welds.[15]

For example, a panel that is part of a multipanel array (such as an aircraft fuselage) is damped not only due to energy dissipation within the panel but also due to energy transport to adjacent panels. Energy transport makes it very difficult in practice to measure the dissipative damping of a structural component that is connected to others. Energy transported via the supports of test samples also tends to contaminate laboratory measurements of dissipative damping, potentially introducing large errors in measurements on samples with small inherent damping.

If a structural element is attached to a vibrating structure at a given point, then the energy D that is transported to the attached structure per cycle at frequency f is given by

$$D = \frac{V_S^2 \,\mathrm{Re}[Z_A]}{2f}\left|1 + \frac{Z_A}{Z_S}\right|^{-2} \tag{14.18}$$

Here V_S denotes the amplitude of the velocity of the vibrating structure at the attachment point before the added structure is attached; Z_A denotes the driving-point impedance of the attached structure, and Z_S denotes the impedance of the vibrating structure at the attachment point (with both impedances measured in the direction of V_S). The loss factor contribution due to an attached structure then may be found by use of Eq. (14.13).

A *waveguide absorber* is a damping device that is intended to conduct energy away from its attachment point and to dissipate that energy. Such an absorber consists essentially of a structural element along which waves can travel and which includes means for dissipating the energy transported by these waves. For example, a long slender beam (which may be straight or coiled in some fashion) that is made of a highly damped plastic or coated with a high-damping material may serve as a waveguide absorber at frequencies considerably above its fundamental resonance. To be effective, a waveguide absorber must support waves in the frequency range of interest, it must be attached at a point where the vibrating structure moves with considerable amplitude, and its impedance must be such that it does not excessively reduce the vibrating structure's motion at the attachment point.[16]

A *tuned damper*, often also called a *dynamic absorber* or *neutralizer*, may be visualized as a mass–spring–damper system whose spring base is attached to a point on a vibrating structure. In the region near its natural frequency a tuned damper tends to impede the motion of the attachment point and to dissipate considerable energy; outside this frequency region, the damping effect of such a damper typically is small. Any system, such as a beam or plate, which exhibits a resonance at the frequency of concern, can act as a tuned damper at that frequency. Considerable damping of a plate over a relatively wide frequency range can be obtained by distributing a number of small tuned dampers with slightly different natural frequencies over the plate surface.[17]

Sound Radiation. Sound radiated by a vibrating structure transports energy from the structure and thus contributes damping. For a homogeneous panel of

thickness h and material density ρ_p, one may calculate the panel's loss factor η_R at frequency f due to sound radiation from one side of the panel from its radiation efficiency σ by use of the relation[14]

$$\eta_R = \frac{\rho}{\rho_p}\frac{c}{2\pi f h}\sigma \tag{14.19}$$

where ρ and c denote the density of the ambient medium and the speed of sound in it, respectively. If the panel can radiate from both of its sides, η_R is twice as great as indicated by Eq. (14.19). The magnitude of the radiation efficiency σ depends on the vibratory velocity distribution on the panel, as well as on frequency, and thus generally is different for different excitation distributions.

For a plate that has little inherent damping and that is excited at a single point, the radiation efficiency σ obeys[18]

$$\sigma = \begin{cases} (Uc/\pi^2 A f_c)\sqrt{f/f_c} & \text{for } f \ll f_c \\ 0.45\sqrt{U f_c/c} & \text{for } f = f_c \\ 1.0 & \text{for } f \gg f_c \end{cases} \tag{14.20}$$

where A denotes the panel's surface area (one side), U its circumference, and f_c the coincidence frequency. This frequency, which is defined as that at which the plate flexural wavelength is equal to the acoustical wavelength in the ambient medium, is given by $f_c \approx c^2/1.8hc_L$, where c_L represents the longitudinal wave speed in the plate material. More detailed information on radiation efficiency is provided in Chapter 11. Equation (14.20) may be used for the general estimation of radiation efficiency values for plates that are not too highly damped. This equation also provides a reasonable estimate of the radiation efficiency of rib-stiffened plates if twice the total rib length is included in the circumference U.

14.5 VISCOELASTIC DAMPING TREATMENTS

Viscoelastic Materials and Material Combinations

Materials that have both damping (energy dissipation) and structural (strain energy storage) capability are called "viscoelastic." Although virtually all materials fall into this category, the term is generally applied only to materials, such as plastics and elastomers, that have relatively high ratios of energy dissipation to energy storage capability.

Structural materials with high strength-to-weight ratios typically have little inherent damping, as is evident from Fig. 14.5, whereas plastics and rubbers that are highly damped tend to have relatively low strength. This circumstance has led to the consideration of combinations of high-strength materials and high-damping viscoelastic materials for applications where both strength and damping are required. Additions of viscoelastic materials to structural elements have come to be known as viscoelastic damping treatments.

If a composite structure is deflected, it stores energy via a variety of deformations (such as shear, tension and compression, flexure) in each structural element. If η_i denotes the loss factor corresponding to the ith element deformation and W_i represents the energy stored in that deformation, then the loss factor η of the entire structure obeys[19]

$$\eta = \sum \eta_i \frac{W_i}{W_T} \tag{14.21}$$

where $W_T = \sum W_i$ denotes the total energy stored in the structure. The foregoing expression indicates that the loss factor η of the composite structure is equal to a weighted average of the loss factors corresponding to all of the element deformations, with the energy storages serving as the weighting factors. This expression also leads to an important conclusion: An element deformation can make a significant contribution to the total loss factor only if (1) the loss factor associated with it is significant *and* (2) the energy storage associated with it is a significant fraction of the total energy storage.*

Mechanical Properties of Viscoelastic Materials

Because viscoelastic materials have both energy storage and energy dissipation capability, it is convenient to describe their behavior in terms of elastic and shear moduli that are complex quantities, in analogy to the definition of the complex stiffness introduced in Eq. (14.10). The complex Young's modulus $\overline{E}$ of a material, defined as the ratio of the stress phasor to the strain phasor, may be written as[10] $\overline{E} = E_R + jE_I = E_R(1 + j\eta_E)$, where the real part E_R is called the storage modulus, the imaginary part E_I is called the loss modulus, and the loss factor η_E associated with Young's modulus is equal to E_I/E_R. A completely analogous definition applies to the complex shear modulus.†

For plastics and elastomers, the viscoelastic materials of greatest practical interest, the real and imaginary moduli as well as the loss factors vary considerably with frequency and temperature. However, these parameters usually vary relatively little with strain amplitude, preload, and aging.[10] The loss factor associated with the shear modulus typically is equal to that associated with the Young's modulus for all practical purposes, so that one generally need not distinguish between the two. Also, since most of the viscoelastic materials of practical interest are virtually incompressible, the shear modulus value is nearly equal to one-third of the corresponding Young's modulus value. One may also note that often $\eta_E^2 \ll 1$, so that $|\overline{E}| \approx E_R$.

*Equation (14.21) applies precisely only for cases where all energy storage elements are deflected in phase, so that they reach their maximum energy storages at the same instant.

†An advantage of the complex modulus representation is the ease with which it enables one to incorporate damping in an analysis. One merely needs to replace the real moduli in the undamped formulation of a problem by the corresponding complex moduli—or, equivalently, to replace the real stiffnesses by the corresponding complex stiffnesses—to obtain a formulation of the problem that includes damping. This approach applies for lumped-parameter dynamic systems as well as for continuous systems and can take account of different values of damping in different elements and materials.

Figure 14.7 shows how the (real) shear modulus and loss factor of a typical viscoelastic material vary with frequency and temperature. At low frequencies and/or high temperatures, the material is soft and mobile enough for the strain to follow an applied stress without appreciable phase shift so that the damping is small; the material is said to be in its "rubbery" state. At high frequencies and/or low temperatures, the material is stiff and immobile, may tend to be brittle, is relatively undamped, and behaves somewhat like glass; it is said to be in its "glassy" state. At intermediate frequencies and temperatures, the modulus takes on intermediate values and the loss factor is highest; the material is said to be in its "transition" state.

This material behavior may be explained on the basis of the interactions of the long-chain molecules that constitute polymeric materials. At low temperatures, the molecules are relatively inactive; they remain "locked together," resulting in high stiffness, and because they move little relative to each other, there is little intermolecular "friction" to produce damping. At high temperatures, the molecules become active; they move easily relative to each other, resulting in low stiffness, and because they interact little, there is again little energy dissipation due to intermolecular friction. At intermediate temperatures, where the molecules have intermediate relative motion and interaction, the stiffness also takes on an intermediate value and the loss factor is greatest. A similar discussion applies to the effect of frequency on the material properties, with the inertia of the molecules leading to their decreasing mobility and interaction with increasing frequency.

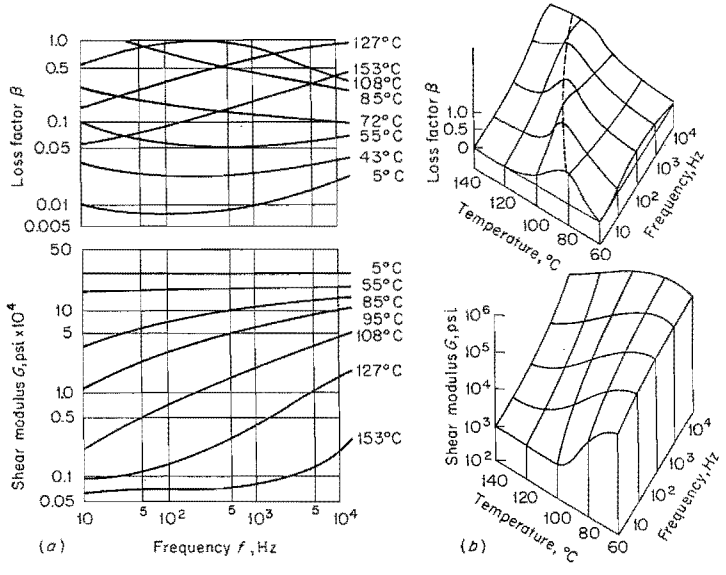


FIGURE 14.7 Dependence of shear modulus and loss factor of a polyester plastic on frequency and temperature[20]: (*a*) functions of frequency at constant temperature; (*b*) isometric plots on temperature–frequency plane. Note logarithmic frequency axes.

The observation that there exists a *temperature–frequency equivalence*, namely that an appropriate temperature decrease produces the same effect as a given frequency increase, has led to the development of convenient plots in which data for the frequency and temperature variations of each material modulus collapse onto single curves.[10,21] This collapse is achieved by plotting the data against a reduced frequency $f_R = f\alpha(T)$, where $\alpha(T)$ is an appropriately selected function of temperature T. In presentations of data in this form the function $\alpha(T)$ may be given analytically, in a separate plot or, as has recently been standardized[22,23], in the form of a nomogram that is superposed on the reduced data plot. Figure 14.8 is an illustration of such a plot and nomogram; its use is explained in the figure's legend.

Data on the properties of damping materials are available from knowledgeable suppliers of these materials. Compilations of data appear in references 10, 21, and 24. Key information on some of these materials appears in Table 14.1 in a form that is useful for preliminary material comparison and selection for specific applications in keeping with the concepts discussed in the later portions of this chapter. For each listed material the table shows the greatest loss factor value η_{max} exhibited by the material and the temperatures at which this value is obtained at three frequencies. The table also lists three values of the modulus of elasticity: E_{max}, the greatest value of Young's modulus, applies at low temperatures (i.e.,

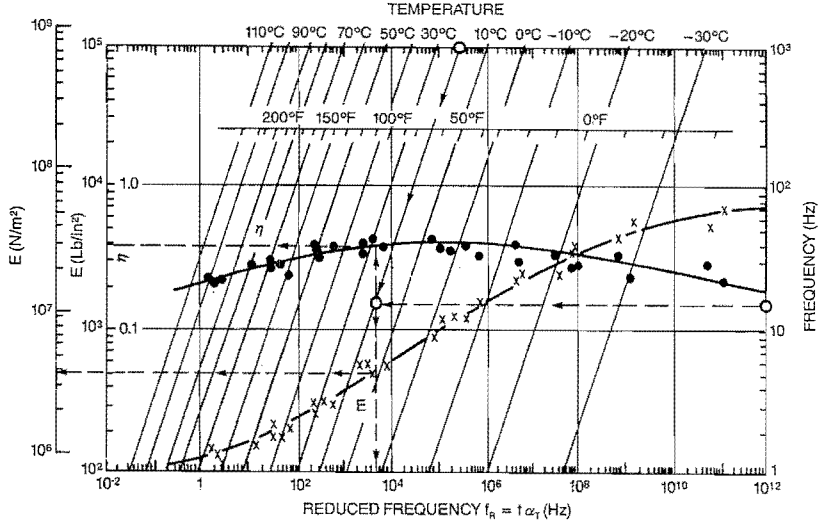


FIGURE 14.8 Reduced frequency plot of elastic modulus E and loss factor η of "Sylgard 188" silicone potting compound. (After Ref. 25) Points indicate measured data to which curves were fitted. Nomograph superposed on data plot facilitates determination of reduced frequency f_R corresponding to frequency f and temperature T. Use of nomogram is illustrated by dashed lines: For $f = 15$ Hz and $T = 20°C$, one finds $f_R = 5 \times 10^3$ Hz and $E = 3.8 \times 10^6$ N/m^2, $\eta = 0.36$.

TABLE 14.1 Properties of Some Commercial Damping Materials[a]

Material	Maximum Loss Factor	Temperature (°F)[b] for η_{max} at			Elastic Moduli (psi)[c]			
	η_{max}	10 Hz	100 Hz	1000 Hz	E_{max}	E_{min}	E_{trans}	$E_{I,max}$
Antiphon-13	1.8	25	75	120	3e5	1.2e3	1.9e4	3.e3e
blachford Aquaplas	0.5	50	80	125	1.6e6	3e4	2.2e5	1.1e5
Barry Controls H-326	0.8	−40	−25	−10	6e5	3e3	4.2e4	3.4e4
Dow Corning Sylgard 188	0.6	60	80	110	2.2e4	3e2	2.6e3	1.5e3
EAR C-1002	1.9	23	55	90	3e5	2e2	7.7e3	1.5e4
EAR C-2003	1.0	45	70	100	8e5	6e2	2.2e4	2.2e4
lord LD-400	0.7	50	80	125	3e6	3.3e3	1e5	7e4
Soundcoat DYAD 601	1.0	15	50	75	3e5	1.5e2	6.7e3	6.7e3
Soundcoat DYAD 606	1.0	70	100	130	3G5	1.2e2	6e3	6e3
Soundcoat DYAD 609	1.0	125	150	185	2e5	6e2	1.1e4	1.1e4
Soundcoat N	1.5	15	30	70	3e5	7e1	4.6e3	6.9e3
3M ISD-110	1.7	80	115	150	3e4	3e1	1e3	1.7e3
3M ISD-112	1.2	10	40	80	1.3e5	8e1	3.2e3	3.9e3
3M ISD-113	1.1	−45	−20	15	1.5e5	3e2	2.1e2	2.3e2
3m 468	0.8	15	50	85	1.4e5	3e1	2e3	1.6e3
3M ISD-830	1.0	−75	−50	−20	2e5	1.5e2	5.5e3	5.5e3
GE SMRD	0.9	50	80	125	e35	5e3	3.9e4	3.5e4

[a] Approximate values taken from curves in Ref. 11.

[b] To convert to °C, use the formula °C = $(\frac{5}{9})$(°F − 32) or the approximate table below:

°F	−80	−60	−40	−20	0	20	40	60	80	100	120	140	160	180	200
°C	−62	−51	−40	−29	−18	−7	4	16	27	38	49	60	71	82	93

[c] Numbers shown correspond to storage (real) values of Young's modulus, except that $E_{I,max}$ represents the maximum values of the loss (imaginary) modulus. E_{max} applies for low temperatures and/or high frequencies. E_{min} applies for high temperatures and/or low frequencies. E_{trans} and $E_{I,max}$ applies in the range of η_{max}. Divide by 3 to obtain the corresponding shear modulus values.
To convert to N/m^2, multiply tabulated values by 7×10^3. The number following e represents the power of 10 by which the number preceding e is to be multiplied; e.g., 1.2e3 represents 1.2×10^3

temperatures considerably below those corresponding to η_{max}); E_{min}, the smallest value of E, applies at high temperatures; the transition value E_{trans} applies in the η_{max} range; and $E_{I,max} \approx \eta_{max} E_{trans}$, the maximum value of the loss modulus, applies in the transition range.

It is important to keep in mind that the mechanical properties of polymeric materials, including plastics and elastomers, tend to be more variable than those of metals and other classical structural materials. Some of this variability results from a polymer's molecular structure and molecular weight distribution, which depend not only on the material's chemical composition but also on its processing. Additional variability results from the various types and amounts of plasticizers and fillers that are added to most commercial materials for a number of practical

purposes. Thus, it is quite common for nominally identical polymeric materials to exhibit considerably different mechanical behaviors. It may also occur that even material samples from the same production run have considerably different loss factors and moduli at frequencies and temperatures at which they are intended to be used, pointing toward the need for careful quality control and performance verification for critical applications.

Structures with Viscoelastic Layers

One may calculate the loss factor of a structure vibrating in a given mode by use of Eq. (14.21) if one knows the energies W_i stored in the various deformations of all of the component elements. Indeed, modern finite-element analysis methods[26–28] proceed by calculating the modal deflections, applying these to evaluate all the energy storage components, and then using Eq. (14.21) to find the loss factor.

Analytical results have been developed for flexure of uniform beam and plate structures under conditions that are often approximated in practice. These results, which are extremely useful for design guidance and for development of an understanding of the important parameters, apply to structures whose deflection distributions are sinusoidal.*

Two-Component Beams

In flexure of a uniform beam with an insert or added layer of viscoelastic material, as illustrated by Fig. 14.9, the energy storage (and dissipation) associated with shear and torsional deformations may generally be neglected. If contact between the components is maintained without slippage at all surfaces and if the loss factor of the basic structural (nonviscoelastic) component is negligible, then the

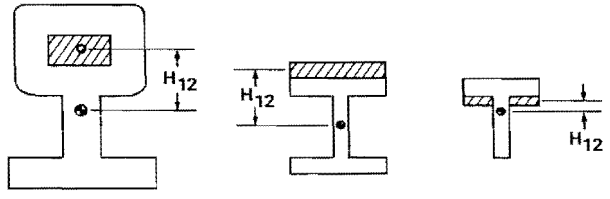


FIGURE 14.9 End views of beams with viscoelastic inserts or added layers. Structural material is unshaded, viscoelastic material is shown shaded; H_{12} represents distance between neutral axis of structural component and that of viscoelastic component. Beam deflection is vertical, with wave propagation along the beam length, perpendicular to the plane of the paper.

*The deflection distribution of any beam (or plate) vibrating in one of its natural modes is at least approximately sinusoidal (in one dimension for beams and in two dimensions for plates) at locations that are one wavelength or more from the boundaries, regardless of the boundary conditions. Therefore, the assumption of a sinusoidal deflection distribution is valid for a larger fraction of the structure as the frequency increases.

loss factor η of the composite beam is related to the loss factor β of the material of the viscoelastic component by[29,30]

$$\frac{\eta}{\beta} = \left[1 + \frac{k^2(1+\beta^2) + (r_1/H_{12})^2\alpha}{k[1+(r_2/H_{12})^2\alpha]}\right]^{-1} \tag{14.22}$$

where $\alpha = (1+k)^2 + (\beta k)^2$ and H_{12} denotes the distance between the neutral axes of the two components. With subscript 1 referring to the structural (undamped) component and subscript 2 referring to the viscoelastic component, $k = K_2/K_1$, where $K_i = E_i A_i$ denotes the extensional stiffness of component i, expressed in terms of its Young's modulus (real part) E_i and cross-sectional area A_i. Furthermore, $r_i = \sqrt{I_i/A_i}$ represents the radius of gyration of A_i, where I_i denotes the centroidal moment of inertia of A_i.

For the often-encountered case where the structural component's extensional stiffness is much greater than that of the viscoelastic component, $k \ll 1$ and Eq. (14.22) reduces to

$$\eta \approx \frac{\beta E_2 I_T}{E_1 I_1 + E_2 I_T} \approx \frac{\beta E_2}{E_1}\frac{I_T}{I_1} \tag{14.23a}$$

where $I_T = I_2 + H_{12}^2 A_2 = A_2(r_2^2 + H_{12}^2)$ denotes the moment of inertia of A_2 about the neutral axis of A_1.

The last expression in Eq. (14.23a) applies for $E_2 I_T \ll E_1 I_1$, which is generally true in practical structures where the area and elastic modulus of the viscoelastic component are small compared to those of the structural component. In this case the composite structure's neutral axis coincides very nearly with that of the structural component and the dominant energy storage is associated with flexure of the structural component (whose flexural stiffness is $E_1 I_1$). The dominant energy dissipation is associated with extension and compression of the viscoelastic component, with the average extension (equal to the extension at the viscoelastic component's neutral axis) resulting from the flexural curvature and the distance H_{12} between the neutral axes of the viscoelastic and the structural components.* The flexural curvature is greatest at the antinodes of the vibrating structure; most of the damping action thus occurs at these locations, with little damping resulting from the material near the nodes.

The second form of Eq. (14.23a) contains two ratios; the first involves only material properties and the second only geometric parameters. It indicates that the most important dynamic mechanical property of the viscoelastic material is its extensional loss modulus $E_I = \beta E_2$. In keeping with the conclusions based on the general energy expression [Eq. (14.21)], good damping of the composite structure can be obtained only from a viscoelastic material that has not only a high loss factor but also a considerable energy storage capability.

*A "spacer," a layer that is stiff in shear and soft in extension (e.g., like honeycomb), inserted between the structural and the viscoelastic component can increase H_{12} and thus the damping obtained with a given amount of viscoelastic material.[30]

Plates with Viscoelastic Coatings

A strip of a plate (see insert of Fig. 14.10) may be considered as a special case of a two-component beam, where the two components have rectangular cross sections. Thus Eqs. (14.22) and (14.23a) apply, with $r_i = H_i/\sqrt{12}$ and $H_{12} = \frac{1}{2}(H_1 + H_2)$, where H_i denotes the component thickness. The energy storage and dissipation considerations that were discussed in the foregoing section, as well as the foregoing remarks concerning the dominant damping material properties, apply here also.

Figure 14.10 is a plot based on Eq. (14.22) for $\beta^2 \ll 1$. It shows that for small relative thicknesses $h_2 = H_2/H_1$, the loss factor ratio η/β is proportional to the viscoelastic layer thickness, whereas for very large relative thicknesses the loss factor ratio approaches unity; that is, the loss factor of the coated plate approaches that of the viscoelastic coating, as one would expect.* As also is evident from

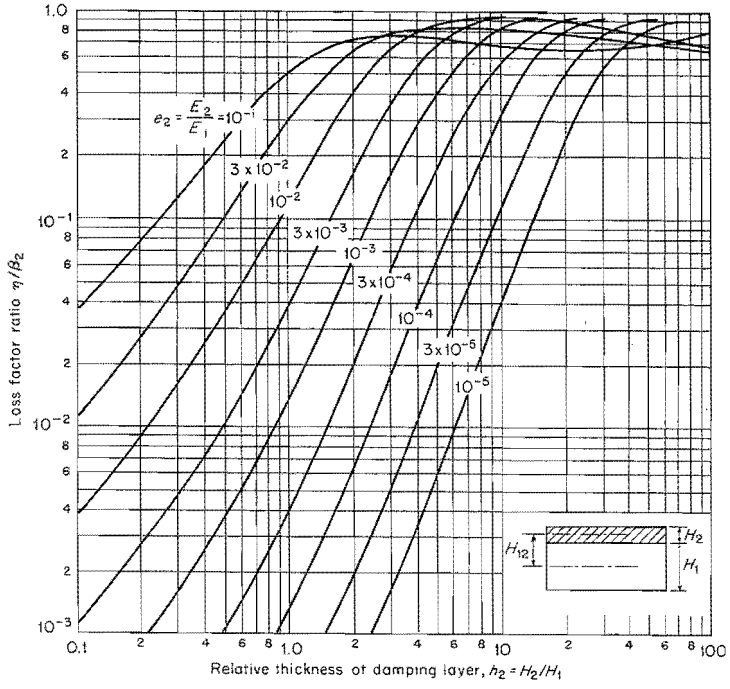


FIGURE 14.10 Dependence of loss factor η of plate strip with added viscoelastic layer on relative thickness and relative modulus of layer.[30] Curves apply for loss factors β of viscoelastic material that are small compared to unity.

*For very thick viscoelastic coatings, deformations in the thickness direction (which are not considered in this simplified analysis) also may play a significant role, particularly at frequencies at which standing-wave resonances may occur in the viscoelastic material.[31]

the figure, at small relative thicknesses the loss factor ratio is proportional to the modulus ratio $e_2 = E_2/E_1$. For small relative thicknesses, that is, in the regions where the curves of Fig. 14.10 are nearly straight, the loss factor of a coated plate may be estimated from[30]

$$\eta \approx \frac{\beta E_2}{E_1} h_2 \ (3 + 6h_2 + 4h_2^2) \tag{14.23b}$$

where $h_2 = H_2/H_1$.

If two viscoelastic layers are applied to a plate, one layer on each side, then the loss factor of the coated plate may be taken as the sum of the loss factors contributed by the individual layers, with each contribution calculated as if the other layer were absent, provided that each viscoelastic layer has low relative extensional rigidity, that is, that $E_2H_2 \ll E_1H_1$. If this inequality is not satisfied, a more complex analysis is required.

Three-Component Beams with Viscoelastic Interlayers

Figure 14.11 illustrates uniform beams consisting of two structural (nonviscoelastic) components interconnected via a relatively thin viscoelastic component. Such three-component beams may be preferable to two-component beams for practical reasons because the viscoelastic material is exposed only at its edges; however, such beams can also be designed to have higher damping than two-component beams of similar weight.*

In flexure of a three-component beam with a viscoelastic layer whose extensional and flexural stiffnesses are small compared to those of the structural components, the dominant energy dissipation is associated with shear in the viscoelastic component and the most significant energy storage occurs in connection with extension/compression and flexure of the two structural components. The shear in the viscoelastic component is greatest at the vibrating structure's nodes. Thus, most of the energy dissipation occurs in the viscoelastic material near

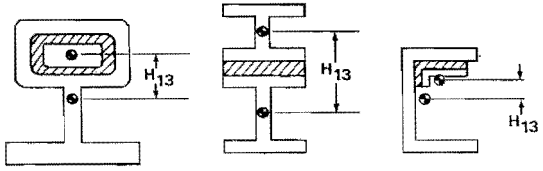


FIGURE 14.11 End views of composite beams made up of two structural components (unshaded) joined via a viscoelastic component (shaded); H_{13} is distance between neutral axes of structural components. Beam deflection is vertical, with wave propagation along the beam length, perpendicular to the plane of the paper.

*It should be noted that design changes to obtain increased damping generally also result in mass and stiffness changes, which tend to affect a structure's vibratory response and should be considered in the design process.[17,32,33]

the nodes, with relatively little resulting in that near the antinodes. For efficient damping, it is important that the shearing action in the viscoelastic material not be restrained (particularly at and near nodes) by structural interconnections, such as bolts.

The loss factor η corresponding to a spatially sinusoidal deflection shape of such a three-component beam is related to the loss factor β of the viscoelastic material by[29,30]

$$\eta = \frac{\beta Y X}{1 + (2 + Y)X + (1 + Y)(1 + \beta^2)X^2} \tag{14.24}$$

where

$$X = \frac{G_2 b}{p^2 H_2} S \qquad \frac{1}{Y} = \frac{E_1 I_1 + E_3 I_3}{H_{13}^2} S \qquad S = \frac{1}{E_1 A_1} + \frac{1}{E_3 A_3} \tag{14.25}$$

Here subscripts 1 and 3 refer to the structural components and 2 to the viscoelastic component; E_i, A_i, and I_i represent, respectively, the Young's modulus, cross-sectional area, and moment of inertia of component i; H_{13} denotes the distance between the neutral axes of the two structural components; and G_2 represents the shear modulus (real part) of the viscoelastic material, H_2 the average thickness of the viscoelastic layer, and b its length as measured on a cross section through the beam. The wavenumber p of the spatially sinusoidal beam deflection obeys

$$\frac{1}{p^2} = \left(\frac{\lambda}{2\pi}\right)^2 = \frac{1}{\omega}\sqrt{\frac{B}{\mu}} \tag{14.26}$$

where λ represents the bending wavelength and B denotes the flexural rigidity and μ the mass per unit length of the composite beam.

The *structural parameter* Y of three-component structures depends only on the geometry and Young's moduli of the two structural components, whereas the *shear parameter* X depends also on the properties of the viscoelastic layer and on the wavelength of the beam deflection. The shear parameter X is proportional to the square of the ratio of the beam flexural wavelength to the *decay distance*,[34] that is, the distance within which a local shear disturbance decays by a factor of e, where $e \approx 2.72$ denotes the base of natural logarithms; thus, X also is a measure of how well the viscoelastic layer couples the flexural motions of the two structural components.

The (complex) flexural rigidity of a three-component beam is given by

$$\overline{B} = (E_1 I_1 + E_3 I_3)\left(1 + \frac{X^* Y}{1 + X^*}\right) \qquad X^* = X(1 - j\beta) \tag{14.27}$$

Its magnitude is $B = |\overline{B}|$. Thus, for small X, the flexural rigidity B of the composite beam is equal to the sum of the flexural rigidities of the structural components, that is, to the total flexural rigidity that the two components exhibit if they are

not interconnected. For $X \gg 1$, however B approaches $1 + Y$ times the foregoing value, which is equal to the flexural rigidity of a beam with rigidly interconnected structural components 1 and 3.

For a given value of β and Y, the loss factor η of the composite beam takes on its greatest value,

$$\eta_{\max} = \frac{\beta Y}{2 + Y + 2/X_{\text{opt}}} \tag{14.28}$$

at the optimum value of X, which is given by

$$X_{\text{opt}} = [(1 + Y)(1 + \beta^2)]^{-1/2} \tag{14.29}$$

With the aid of these definitions, one may rewrite Eq. (14.24) in terms of the ratio $R = X/X_{\text{opt}}$ in the following form, which provides a convenient view of the damping behavior of three-component beams:

$$\frac{\eta}{\eta_{\max}} = \frac{2(1 + N)R}{1 + 2NR + R^2} \qquad N = (1 + \tfrac{1}{2}Y)X_{\text{opt}} \tag{14.30}$$

Figure 14.12, which is based on Eqs. (14.28) and (14.29), shows how $\eta_{\max}/\beta$ increases monotonically with Y, indicating the importance of selecting a configuration with a large value of Y in the design of highly damped composite structures.* Figure 14.13 gives approximate values of Y for some often encountered

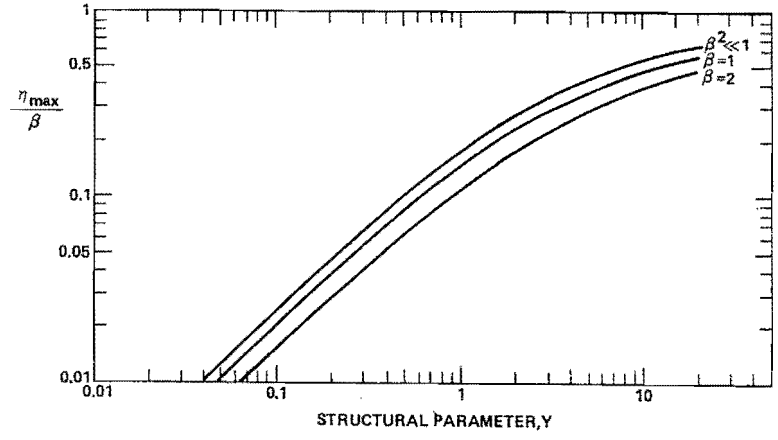


FIGURE 14.12 Dependence of maximum loss factor $\eta_{\max}$ of three-component beams or plates on structural parameter Y and loss factor β of viscoelastic material.

*A shear-stiff, extensionally soft "spacer" (e.g., honeycomb) inserted between the viscoelastic and one or both structural components can serve to increase H_{13} and, therefore, the value of Y. See Eq. (14.25). For a given deflection of the composite structure, a spacer increases the damping by increasing the shear strain—and thus the energy storage and dissipation—in the viscoelastic component.[30,34]

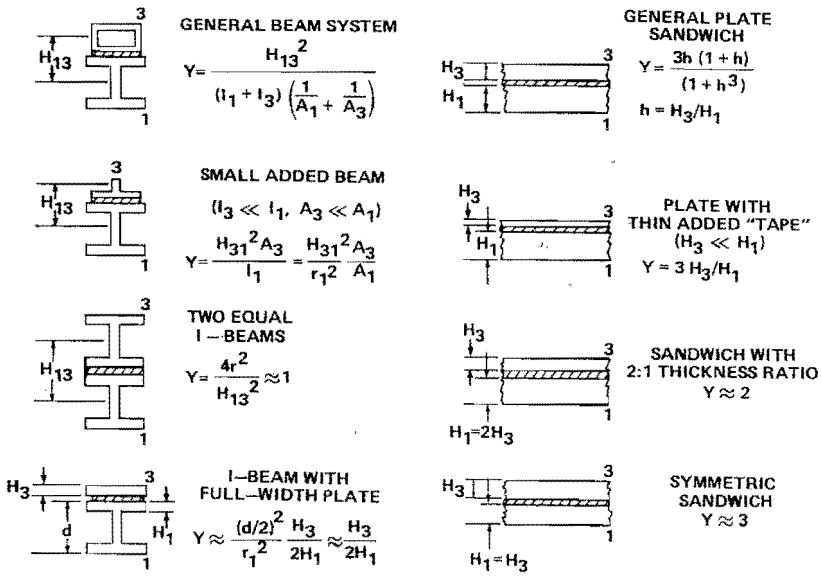


FIGURE 14.13 Values of structural parameter Y for three-component beam and plate configurations with thin viscoelastic components and with structural components of the same material; viscoelastic component is shown cross-hatched. I, moment of inertia; A, cross-sectional area; r, radius of gyration; H_{13}, distance between neutral axes.

configurations. Figure 14.14 shows how $\eta/\eta_{\max}$ varies with X/X_{opt}, indicating the importance of making the operating value of X of a given design match X_{opt} as closely as possible in order to obtain a loss factor that approaches $\eta_{\max}$.

If one knows the wavenumber $p = 2\pi/\lambda$ and the frequency associated with a given beam vibration, one may calculate the loss factor η of a composite beam simply by substituting the beam parameters and the material properties at any frequency (and temperature) of interest into Eqs. (14.24) and (14.25) or (14.28)–(14.30). The latter set of equations is particularly useful for judging how far from the optimum a given configuration may be operating.

If one knows only the frequency and not the wavenumber p corresponding to a beam vibration, one needs to use Eq. (14.26) to determine p. Substitution of B as calculated from Eq. (14.27) into Eq. (14.26), followed by substitution of the result into the first of Eqs. (14.25), leads to a cubic equation in X. Although one may solve this numerically, it is often more convenient to determine X by use of an iteration procedure like that indicated in Fig. 14.15.

In contrast to the previously discussed two-component beam, the loss factor η of a three-component beam does not depend primarily on the loss modulus (i.e., on the product of the loss factor β and storage modulus E_2 or G_2) of the viscoelastic material. The loss factor of a three-component beam depends on β and G_2 separately, and the separate dependences must be taken into account in

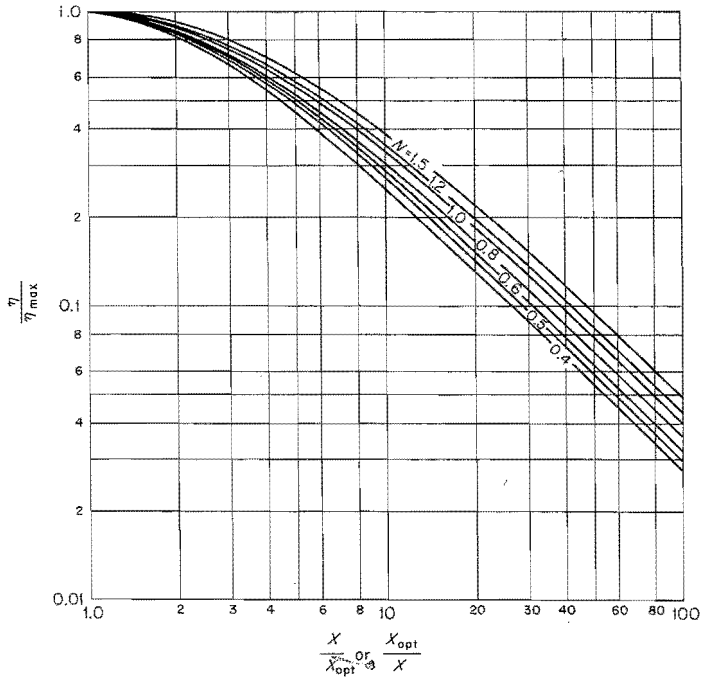


FIGURE 14.14 Dependence of loss factor η of three-component beam or plate on shear parameter X [from Eq. (14.30)].

the design of such a beam. Design of a highly damped three-component beam structure requires (1) choice of a configuration with a large structural parameter Y, (2) selection of a damping material with a large loss factor β in the frequency and temperature range of interest, and (3) adjustment of the damping material thickness H_2 and length b so as to make X [as calculated from Eq. (14.25) for the value of G_2 applicable to the frequency and temperature of concern] approximately equal to X_{opt} [given by Eq. (14.29)]. The resulting design then will have a loss factor approximately equal to $\eta_{\max}$ as given by Eq. (14.28).

The expected performance of any design should be checked for the frequency and temperature ranges of interest by means of the procedure described in the previous paragraph. Note that a given design may be expected to perform optimally—that is, to have X under operating conditions approximately equal to X_{opt}—only in a limited range of frequencies and temperatures, with reduced performance outside this range.

Plates with Viscoelastic Interlayers

A strip of a plate consisting of a viscoelastic layer between two structural layers may be considered as a special case of a three-component beam. In a plate strip,

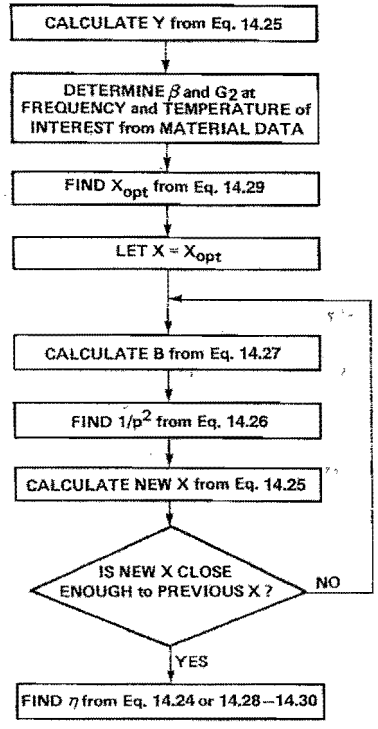


FIGURE 14.15 Iteration procedure for determination of loss factor of three-component beams or plates for which wavelength is not known initially.

all components have rectangular cross sections of the same width; Eqs. (14.25) accordingly become

$$X = \frac{G_2}{p^2 H_2} S \qquad \frac{1}{Y} = \frac{E_1 H_1^3 + E_3 H_3^3}{12 H_{31}^2} S \qquad S = \frac{1}{E_1 H_1} + \frac{1}{E_3 H_3} \tag{14.31}$$

If, furthermore, $E_1 I_1 + E_3 I_3$ in Eq. (14.27) is replaced by $\frac{1}{12}(E_1 H_1^3 + E_3 H_3^3)$ and if μ in Eq. (14.26) is interpreted as the mass per unit surface area of the plate, then all of the foregoing discussion pertaining to beams also applies to plates.

REFERENCES

1. W. T. Thomson, *Theory of Vibration with Applications*, 2nd ed., Prentice-Hall, Englewood Cliffs, NJ, 1981.
2. R. Plunkett, "Measurement of Damping," in J. F. Ruzicka (Ed.), *Structural Damping*, American Society of Mechanical Engineers, New York, 1959.

3. K. N. Tong, *Theory of Mechanical Vibration*, Wiley, New York, 1960.
4. E. E. Ungar, "Mechanical Vibrations," in H. A. Rothbart (Ed.), *Mechanical Design and Systems Handbook*, 2nd ed., McGraw-Hill, New York, 1985, Chapter 5.
5. D. J. Ewins, *Modal Testing: Theory and Practice*, Research Studies Press, Letchworth, Hertfordshire, England, 1986.
6. V. H. Neubert, *Mechanical Impedance: Modelling/Analysis of Structures*, Josens Printing and Publishing, State College, PA, distributed by Naval Sea Systems Command, Code NSEA-SSN, 1987.
7. B. L. Clarkson and J. K. Hammond, "Random Vibration," in R. G. White and J. G. Walker (Eds.), *Noise and Vibration*, Wiley, New York, 1982, Chapter 5.
8. B. L. Clarkson and R. J. Pope, "Experimental Determination of Modal Densities and Loss Factors of Flat Plates and Cylinders," *J. Sound Vib.*, **77**(4), 535–549 (1981).
9. S. H. Crandall, "The Role of Damping in Vibration Theory," *J. Sound Vib.*, **11**(1), 3–18 (1970).
10. A. D. Nashif, D. I. G. Jones, and J. P. Henderson, *Vibration Damping*, Wiley, New York, 1985.
11. G. Kurtze, "Körperschalldämpfung durch Körnige Medien" [Damping of Structure-Borne Sound by Granular Media], *Acustica*, **6**(Beiheft 1), 154–159 (1956).
12. M. A. Heckl, "Measurements of Absorption Coefficients on Plates," *J. Acoust. Soc. Am.*, **34**, 308–808 (1962).
13. G. Maidanik, "Energy Dissipation Associated with Gas-Pumping at Structural Joints," *J. Acoust. Soc. Am.*, **34**, 1064–1072 (1966).
14. E. E. Ungar, "Damping of Panels Due to Ambient Air," in P. J. Torvik (Ed.), *Damping Applications in Vibration Control*, AMD-Vol 38, American Society of Mechanical Engineers, New York, 1980, pp. 73–81.
15. E. E. Ungar and J. Carbonell, "On Panel Vibration Damping Due to Structural Joints," *AIAA J.*, **4**, 1385–1390 (1966).
16. E. E. Ungar and L. G. Kurzweil, "Structural Damping Potential of Waveguide Absorbers," *Trans. Internoise 84*, December 1985, pp. 571–574.
17. D. J. Mead, *Passive Vibration Control*, J Wiley, New York, 2002.
18. L. Cremer, M. Heckl, and E. E. Ungar, *Structureborne Sound*, 2nd ed., Springer-Verlag, New York, 1988.
19. E. E. Ungar and E. M. Kerwin, Jr., "Loss Factors of Viscoelastic Systems in Terms of Energy Concepts." *J. Acoust. Soc. Am.*, **34**(7), 954–957 (1962).
20. E. E. Ungar, "Damping of Panels," in L. L. Beranek (Ed.), *Noise and Vibration Control*, McGraw-Hill, New York, 1971, Chapter 14.
21. D. I. G. Jones, *Handbook of Viscoelastic Vibration Damping*, Wiley, New York, 2002.
22. ISO 10112, "Damping Materials—Graphic Presentation of the Complex Modulus," International Organization for Standardization, Geneva, Switzerland, 1991.
23. ANSI S2.24-2001, "Graphical Presentation of the Complex Modulus of Viscoelastic Materials," American National Standards Institute,Washington, DC, 2001.
24. J. Soovere and M. L. Drake, "Aerospace Structures Technology Damping Design Guide," AFWAL-TR-84-3089, Flight Dynamics Laboratory, Wright-Patterson Air Force Base, OH, December 1985.

25. D. I. G. Jones and J. P. Henderson, "Fundamentals of Damping Materials," Section 2 of Vibration Damping Short Course Notes, M. L. Drake (Ed.), University of Dayton, 1988.
26. M. L. Soni and F. K. Bogner, "Finite Element Vibration Analysis of Damped Structures." *AIAA J.*, **20**(5), 700–707 (1982).
27. C. D. Johnson, D. A. Kienholz, and L. C. Rogers, "Finite Element Prediction of Damping in Beams with Constrained Viscoelastic Layers," *Shock Vib. Bull.*, **51**(Pt. 1), 71–82 (1981).
28. M. F. Kluesner and M. L. Drake, "Damped Structure Design Using Finite Element Analysis," *Shock Vib. Bull.*, **52**(Pt. 5), 1–12 (1982).
29. E. E. Ungar, "Loss Factors of Viscoelastically Damped Beam Structures," *J. Acoust. Soc. Am.*, **34**(8), 1082–1089 (1962).
30. D. Ross, E. E. Ungar, and E. M. Kerwin, Jr., "Damping of Plate Flexural Vibrations by Means of Viscoelastic Laminae," in J. Ruzicka (Ed.), *Structural Damping*, American Society of Mechanical Engineers, New York, 1959, Section 3.
31. E. E. Ungar and E. M. Kerwin, Jr., "Plate Damping Due to Thickness Deformations in Attached Viscoelastic Layers," *J. Acoust. Soc. Am.*, **36**, 386–392 (1964).
32. D. J. Mead, "Criteria for Comparing the Effectiveness of Damping Materials," *Noise Control*, **1**, 27–38 (1961).
33. D. J. Mead, "Vibration Control (I)," in R. G. White and J. G. Walker (Eds.), *Noise and Vibration*, Ellis Horwood, Chichester, West Sussex, England, 1982.
34. E. M. Kerwin, Jr., "Damping of Flexural Waves in Plates by Spaced Damping Treatments Having Spacers of Finite Stiffness," in L. Cremer (Ed.), *Proc. 3rd Int. Congr. Acoust., 1959*, Elsevier, Amsterdam, Netherlands, 1961, pp. 412–415.

CHAPTER 15

Noise of Gas Flows

H. D. BAUMANN

Consultant
Rye, New Hampshire

W. B. CONEY

BBN Systems and Technologies Corporation
Cambridge, Massachusetts

15.1 INTRODUCTION

The sound produced by unsteady gas flows and by interactions of gas flows with solid objects is called *aerodynamic sound.* The same flows often excite structural modes of vibration in surfaces bounding the flow and are then said to generate *structure-borne sound.* Unwanted flow-generated sound, noise, is a common by-product of most industrial processes. It also accompanies the operation of ships, automobiles, aircraft, rockets, and so on, and can adversely affect structural stability and be an important source of fatigue.

A practical understanding of the sources of aerodynamic sound is necessary over the whole range of mean-flow Mach numbers, from the very lowest (0.01 or less) associated with flows in air conditioning systems and underwater applications to the high supersonic range occurring in jet engines and high-pressure valves. In subsonic flows, the sound may be attributed to three basic aerodynamic source types: monopole, dipole, and quadrupole.[1]

These fundamental source types are discussed in this chapter, together with a survey of noise mechanisms associated with turbulent jets, spoilers and airfoils, boundary layers and separated flow over wall cavities, combustion, and valves.

15.2 AEROACOUSTICAL SOURCE TYPES

Aerodynamic Monopole

Monopole radiation is produced by the unsteady introduction of mass or heat into a fluid. Typical examples are pulse jets (where high-speed air is periodically ejected through a nozzle), turbulent flow over a small aperture in a large wall

(where the flow induces pulsating motion in the aperture), unsteady combustion processes, and heat release from boundaries or from a pulsed laser beam.

The radiation from a monopole source in an otherwise stationary fluid is equivalent to that produced by a pulsating sphere (Fig. 15.1*a*). Both the amplitude and phase of the acoustical pressure are spherically symmetric. When the monopole sound is generated by unsteady flow velocities, the dimensional relation between the radiated sound power and the flow parameters is

$$W_{\text{monopole}} \propto \frac{\rho L^2 U^4}{c} = \rho L^2 U^3 M \tag{15.1}$$

where W_{monopole} = radiated sound power, W
ρ = mean speed of gas, kg/m^3
c = speed of sound in gas, m/s
U = flow velocity in source region, m/s
L = length scale of flow in source region, m
M = Mach number, $= U/c$, dimensionless

Aerodynamic Dipole

Dipole sources arise when unsteady flow interacts with surfaces or bodies, when the dipole strength is equal to the force on the body, or when there are significant variations of mean fluid density in the flow. This source type is found in compressors where turbulence impinges on stators, rotor blades, and other control surfaces. Similarly, the unsteady shedding of vorticity from solid objects,

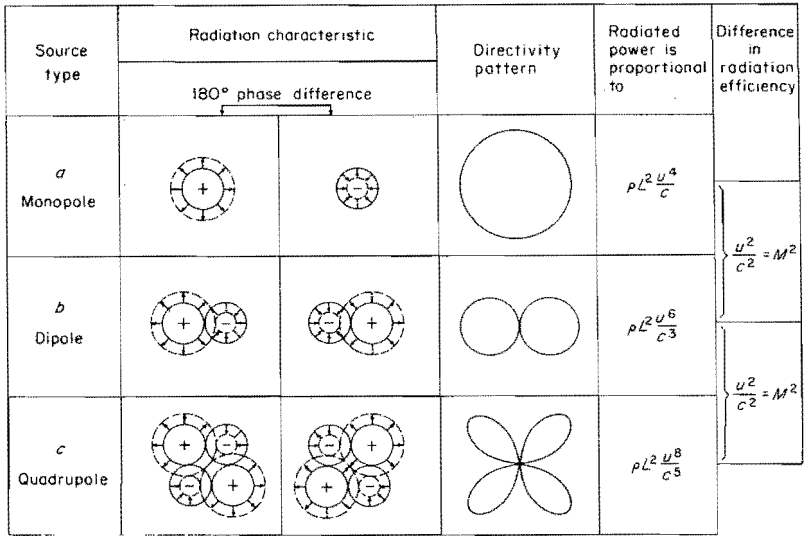


FIGURE 15.1 Aeroacoustical source types and their dimensional properties in fluid of uniform mean density. See also Fig. 1.2.

such as telegraph wires, struts, and airfoils, generates "singing" tones that are also attributable to dipole sources. Other examples include the noise generated by hot jets exhausting into a cooler ambient medium and by the acceleration of temperature (or "entropy") inhomogeneities in a mean pressure gradient, as in a duct contraction.

The dipole is equivalent to a pair of equal monopole sources of opposite phase separated by a distance that is much smaller than the wavelength of the sound. Destructive interference between the radiations from the monopoles reduces the efficiency with which sound is generated by the dipole relative to a monopole and produces a double-lobed, figure-eight radiation field shape proportional to the cosine of the angle measured from the dipole axis (Fig. 15.1*b*). In fluid of uniform mean density, the dimensional dependence of the aerodynamic dipole sound power is

$$W_{\text{dipole}} \propto \frac{\rho L^2 U^6}{c^3} = \rho L^2 U^3 M^3 \tag{15.2}$$

This differs by a factor M^2 from the power output of the monopole. In subsonic flow ($M < 1$) the dipole is a less efficient source of sound.

If the specific entropy or temperature of the flow in the source region is not uniform (e.g., in the shear layer of a hot jet exhausting into a cooler ambient atmosphere), the density must also be variable. The relatively strong pressure fluctuations in the turbulent flow are then scattered by the density variations and produce sound of the dipole type. The dipole strength is proportional to the difference between the actual acceleration of the density inhomogeneity in the turbulent pressure field and that which it would have experienced had the density been uniform.[2] The dimensional dependence of the corresponding sound power is

$$W_{\text{entropy}} \propto \frac{\rho L^2 (\delta T/T)^2 U^6}{c^3} = \rho L^2 \left(\frac{\delta T}{T}\right)^2 U^3 M^3 \tag{15.3}$$

where $(\delta T/T)^2$ is the mean-square fractional temperature fluctuation.

Aerodynamic Quadrupole

Quadrupole radiation is produced by the Reynolds stresses in a turbulent gas in the absence of obstacles. These arise from the convection of fluid momentum by the unsteady flow. The Reynolds stress forces must occur in opposing pairs, since the net momentum of the fluid is constant. Force pairs of this type are called quadrupoles and are equivalent to equal and opposite dipole sources (see Fig. 15.1*c*).

Aerodynamic quadrupoles and entropy dipoles are the dominant source types in high-speed, subsonic, turbulent air jets. The quadrupole strength is larger where both the turbulence and mean velocity gradients are high, for example, in the turbulent mixing layer of a jet.

The dimensional dependence of the radiated quadrupole sound power is

$$W_{\text{quadrupole}} \propto \frac{\rho L^2 U^8}{c^5} = \rho L^2 U^3 M^5 \tag{15.4}$$

This differs from the dipole power by a factor M^2. At subsonic speeds ($M < 1$), the quadrupole radiation efficiency is lower than that of the dipole because of the double cancellation illustrated in Fig. 15.1*c*.

The monopole, dipole, and quadrupole sources decrease in their respective radiation efficiencies for subsonic flows, but the dependencies of their radiated sound powers on flow velocity show the opposite trend, that is, the total radiated sound power varies as the fourth, sixth, and eighth powers of the flow speed U for monopole, dipole, and quadrupole sources, respectively. Thus, if the flow velocity is high enough, the radiation from the quadrupole sources may be the dominant source of sound even though the efficiency with which the sound is produced is small. This is usually the case for a jet engine at high subsonic exhaust velocities, although other internal sources caused by unsteady combustion or rough burning (predominantly monopole) or compressor noise (predominantly dipole) can also make a significant contribution to the total noise.

The value of the constant of proportionality for each type of source depends on both the sound-generating mechanism and the flow configuration. Thus, the constant for a singing wire differs from that of an edge tone, although both arise from unsteady surface forces (dipole sources). However, the proportionality relations (15.1)–(15.4) can be used to estimate the influence on radiated sound power of changes in one or more of the source parameters. A twofold increase in the exhaust velocity U of a jet (quadrupole-type source) causes the sound power level to increase by 24 dB (eighth power of flow velocity), whereas a doubling of the exhaust nozzle area A (proportional to L^2) increases the sound power level by only 3 dB. Because the thrust of a jet engine is proportional to AU^2, the increase in radiated sound will be smaller if a doubling of the thrust is achieved by increasing the nozzle area by a factor of 2 rather than the exhaust velocity by a factor of 1.4.

Aerodynamic Sources of Fractional Order

The efficiency with which sound is produced by aerodynamic dipole sources on surfaces whose dimensions greatly exceed the acoustical wavelength frequently differs from those implied by Eqs. (15.2) and (15.3). For example, the net dipole strength associated with turbulent flow over a smooth, plane wall is zero: The radiation is the same as that generated by the quadrupole sources in the flow when the wall is regarded as a plane reflector of sound. Similarly, the net strength of the dipoles induced by turbulence near the edge of a large wedge-shaped body varies with angle ν—being equivalent to that of a quadrupole when $\nu = 180°$ (i.e., for a plane wall) and to a *fractional* multipole order $\frac{3}{2}$ when $\nu = 0$ (knife edge). The latter case is important in estimating the leading and trailing edge noise of an airfoil, where at high enough frequency the sound power is proportional to $\rho L U^3 M^2$.

Influence of Source Motion

The directional characteristics of the radiation from acoustical sources are changed if the source moves relative to the fluid. Both the frequency and intensity of the sound are increased ahead of the source and decreased to its rear. It is usual to refer the observer to a coordinate system based on the source location at the time of emission of the received sound.

For a monopole source of strength $q(t)$ kilograms per second (equal to the product of the volume velocity and the fluid density) moving at constant speed U in the direction illustrated in Fig. 15.2, the acoustical pressure p in the far field is

$$p_{\text{monopole}} = \pm\left[\frac{dq/dt}{4\pi r(1 - M_{fr})^2}\right] \tag{15.5}$$

where the square brackets denote evaluation at the time of emission of the sound, (r, Φ) are coordinates defining the observer position relative to the source at the time of emission of the sound, and the plus and minus sign is taken according as $M_{fr} < 1$ or $M_{fr} > 1$, where

$$M_{fr} = \left(\frac{U}{c}\right)\cos\Phi \quad \text{(dimensionless)}$$

The frequency of the received sound is $f/(1 - M_{fr})$, where f, per second, is the frequency in a frame fixed relative to the source. The term $1/(1 - M_{fr})$ is called the *Doppler factor*. Its effect is to modify both the frequency and the amplitude of the acoustic field.

For a uniformly translating dipole of strength $f_i(t)$ (newtons), which is equivalent to an applied force in the i direction, and for a quadrupole $T_{ij}(t)$ (newtons-meters), specified by directions i, j (and equivalent to a force pair applied to the fluid), the respective acoustical pressure fields become

$$p_{\text{dipole}} = \pm\left[\frac{df_r/dt}{4\pi c r(1 - M_{fr})^2}\right] \qquad p_{\text{quadrupole}} = \left[\frac{d^2T_{rr}/dt^2}{4\pi c^2 r|1 - M_{fr}|^3}\right] \tag{15.6}$$

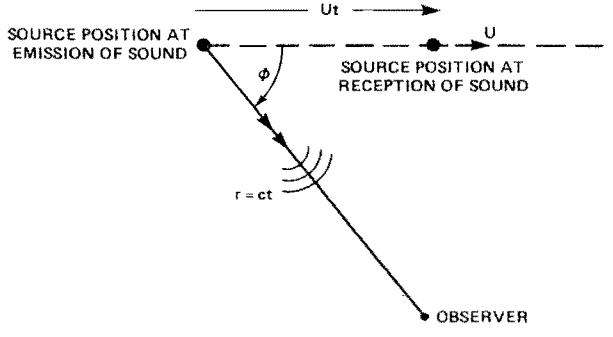


FIGURE 15.2 Coordinates defining the observer position at the time of emission of the received sound from a moving source.

where f_r, T_{rr} denote the components of the dipole and quadrupole source strengths in the observer direction at the time of emission of the sound and the plus and minus sign is taken according as $M_{fr} < 1$ or $M_{fr} > 1$.

These expressions are valid for ideal, point sources moving at constant velocity. The influence of source motion on real, aerodynamic sources is often much more complicated. For example, a pulsating sphere is a monopole source when at rest. In uniform translational motion, however, the radiation is amplified by a Doppler exponent of $\frac{7}{2}$ instead of the 2 of Eq. (15.5). This is because the monopole is augmented due to the motion by a dipole whose strength is proportional to the convection Mach number M_f. The interaction of the volume pulsations with the mean flow over the sphere produces a net fluctuating force on the fluid.

15.3 NOISE OF GAS JETS

The sound generated by high-speed jets is usually associated with several different sources acting simultaneously. *Jet mixing noise*, caused by the turbulent mixing of the jet with the ambient medium, and for imperfectly expanded supersonic jets *shock-associated noise*, produced by the convection of turbulence through shock cells in the jet, are the principal components of the radiation. The properties of sound sources in real jets differ considerably from those of the idealized models described in Section 15.2. Sources located within the "jet pipe" can also make a significant contribution to the noise. In the case of a gas turbine engine, the additional radiation includes combustion noise as well as tonal and broadband sound produced by interactions involving fans, compressors, and turbine systems. The following discussion is based on experimental data obtained and validated by several independent investigators and collated for prediction purposes by the Society of Automotive Engineers.[3] Formulas are given for predicting the *free-field* radiation from a jet in an ideal acoustical medium. In many applications it will be necessary to modify these predictions to account for atmospheric attenuation and interference caused by reflections from surfaces.

Jet Mixing Noise

Mixing noise is the most fundamental source of sound produced by a jet. The simplest free jet is an air stream issuing from a large reservoir through a circular convergent nozzle (Fig. 15.3). The gas accelerates from near-zero velocity in the reservoir to a peak velocity in the narrowest cross section of the nozzle. Sonic flow occurs at the nozzle exit when the pressure ratio p_0/p_s exceeds 1.89, where p_0 is the steady reservoir pressure and p_s is the ambient pressure downstream of the nozzle. An increase above this critical pressure ratio leads to the appearance of a shock cell structure downstream of the nozzle and "choking" of the flow unless the convergent part of the nozzle is followed by a divergent section in which the pressure decreases smoothly to p_s.

For the idealized, shock-free jet, no interaction is assumed between the gas flow and the solid boundaries. The noise is produced entirely by turbulent mixing

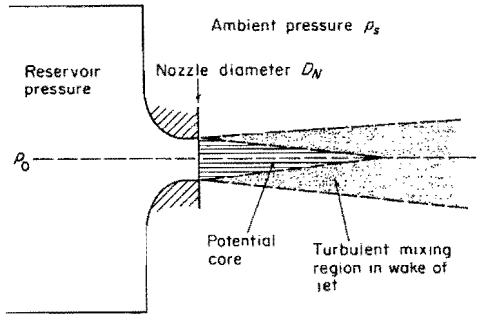


FIGURE 15.3 Subsonic turbulence-free jet.

in the shear layer. The sources extend over a considerable distance downstream of the nozzle. The high-frequency components of noise are generated predominantly close to the nozzle, where eddy sizes are small. Lower frequencies are radiated from sources further downstream where eddy sizes are much larger. The sources may be regarded as quadrupoles, whose strength and directivity are modified by the influences of nonuniform fluid density (temperature) and convection by the flow.

The total radiated sound power W in watts of the mixing noise may be expressed in terms of the mechanical stream power of the jet, equal to

$$W_{\text{mech stream}} = \tfrac{1}{2}mU^2 \tag{15.7}$$

where m = mass flow of gas, kg/s
U = fully expanded mean jet velocity, m/s

The dependence of $W/\frac{1}{2}mU^2$ on jet Mach number $M = U/c$ and density ratio ρ_j/ρ_s, where c is the ambient sound speed and ρ_j, ρ_s are respectively the densities (in kilograms per cubic meter) of the fully expanded jet and the ambient atmosphere, is illustrated in Fig. 15.4. For $M < 1.05$ the sound power increases as ρ_j/ρ_s decreases (i.e., as the jet temperature increases) and decreases at higher Mach numbers. When $M < 1$, W may be estimated from

$$\frac{W}{W_{\text{mech stream}}} = \frac{4 \times 10^{-5}(\rho_j/\rho_s)^{(w-1)}M^{4.5}}{(1 - M_c^2)^2} \qquad M < 1 \tag{15.8}$$

where $M_c = 0.62U/c$ and w is the jet density exponent given by[4]

$$w = \frac{3M^{3.5}}{0.6 + M^{3.5}} - 1 \tag{15.9}$$

Equation (15.9) is applicable for M greater than about 0.35, including the supersonic region and is also used in the formulas given below.

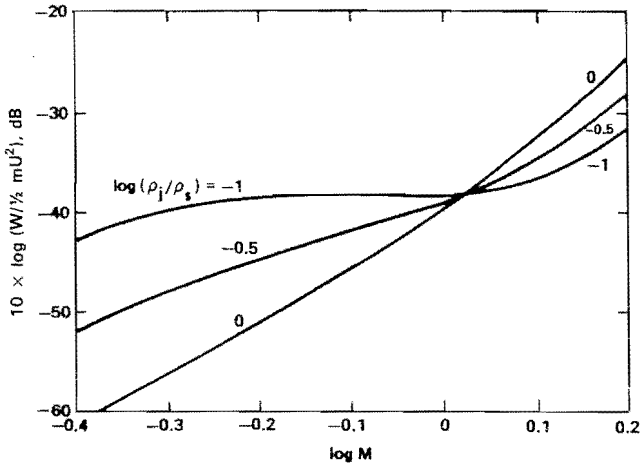


FIGURE 15.4 Ten times the logarithm of the ratio of acoustical power of jet mixing noise to mechanical stream power as a function of the fully expanded jet Mach number $M = U/c$ for different values of ρ_j/ρ_s.

The overall sound pressure level (OASPL) at any point in space is defined as

$$\text{OASPL} = 20 \times \log_{10} \frac{p_{\text{rms}}}{20\ \mu\text{Pa}} \qquad \text{dB} \tag{15.10}$$

where p_{rms} is the rms sound pressure in pascals (newtons per square meter) (see Chapter 2). Source convection and refraction in the shear layers causes the sound field to be directive, the maximum noise being radiated in directions inclined at angles θ to the jet axis between about 30° and 45°.

Typical field directivities at a fixed observer distance for an air jet at three different jet Mach numbers $M = U/c$ are shown in Fig. 15.5. The curves give the variation of OASPL(θ) − OASPL(90°), the sound pressure level relative to its value at $\theta = 90°$, and are approximated by the formula

$$\text{OASPL}(\theta) = \text{OASPL}(90°) - 30 \times \log\left[1 - \frac{M_c \cos\theta}{(1 + M_c^5)^{1/5}}\right] - 1.67 \times \log\left[1 + \frac{1}{10^{(40.56-\theta')} + 4 \times 10^{-6}}\right] \tag{15.11}$$

where $M_c = 0.62U/c$

$\theta' = 0.26(180 - \theta)M^{0.1}$, degrees

The final term on the right of (15.11) is negligible unless $\theta < 180° - 150°/M^{0.1}$, that is, except in directions close to the jet axis.

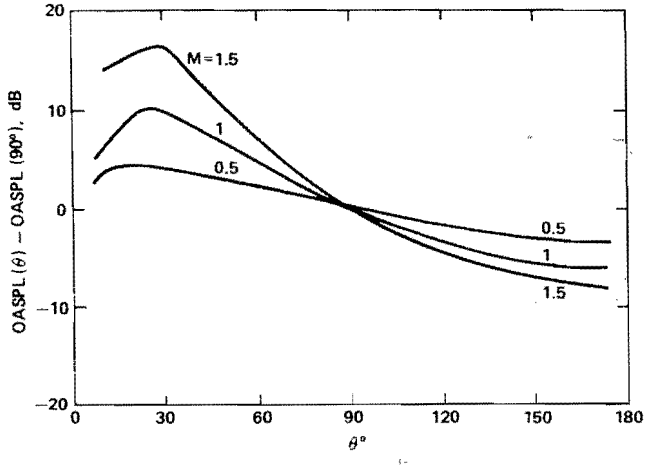


FIGURE 15.5 Directivity of jet mixing noise.

At $\theta = 90°$ the overall sound pressure level of jet mixing noise can be calculated from the formula

$$\text{OASPL} = 139.5 + 10 \times \log\frac{A}{R^2} + 10 \times \log\left[\left(\frac{p_s}{p_{\text{ISA}}}\right)^2 \left(\frac{\rho_j}{\rho_s}\right)^w\right] + 10 \times \log\left(\frac{M^{7.5}}{1 - 0.1M^{2.5} + 0.015M^{4.5}}\right) \tag{15.12}$$

where A = fully expanded jet area, $= \frac{1}{4}\pi D_N^2$ for a subsonic jet, m²

D_N = nozzle exit diameter, m

R = distance from center of nozzle exit, m

p_{ISA} = international standard atmospheric pressure at sea level, = 10.13 μPa

The dependence of OASPL(90°) − 10 × log(A/R^2) on jet Mach number M and density ratio ρ_j/ρ_s is illustrated in Fig. 15.6.

The sound-pressure-level (SPL) frequency spectrum of jet mixing noise is broadband and peaks at a frequency $f = f_p$ that is a function of the radiation direction θ, jet Mach number M, and temperature ratio T_j/T_s, where T_j (in kelvin) is the fully expanded jet temperature and T_s (kelvin) is the ambient gas temperature. The spectrum has a broad peak that occurs in the range $0.3 < S < 1$, where

$$S = \frac{f_p D_N}{U} \tag{15.13}$$

is the *Strouhal number* (dimensionless), tabulated in Table 15.1 for $\theta \geq 50°$ and for different values of T_j/T_s. For practical purposes the difference $\Delta =$

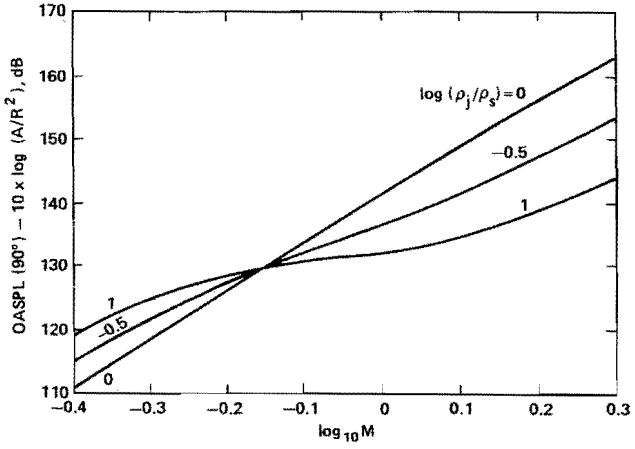


FIGURE 15.6 Overall sound pressure level at $\theta = 90°$.

TABLE 15.1 Values of Strouhal Number and $\Delta(\cdot)$ for Different Values of T_j/T_s[a]

T_j/T_s	$\theta = 50°$	$\theta = 60°$	$\theta = 70°$	$\theta = 80°$	$\theta \geq 90°$
1	0.7 (11 dB)	0.8 (11 dB)	0.8 (11 dB)	1.0	0.9
2	0.5 (10 dB)	0.4 (10 dB)	0.6 (11 dB)	0.5	0.6
3	0.3 (9 dB)	0.4 (10 dB)	0.4 (10 dB)	0.4	0.5

[a] Strouhal number $S = fD_N/U$ at the peak of the one-third-octave-band spectrum of jet mixing noise for $U/c \leq 2.5$ (left columns); $\Delta = \text{OASPL} - \text{SPL}_{\text{peak}} \cong 11$ dB for all $\theta \geq 80°$ except as indicated in parentheses (right columns).

OASPL $-$ SPL_{peak} between the peak of the one-third-octave-band spectrum and the overall SPL at the same value of θ may be taken to be 11 dB except as indicated in the table.

Figure 15.7 shows a typical relative one-third-octave-band SPL spectrum SPL(f) $-$ OASPL for $\rho_j = \rho_s$ and angles $\theta \geq 90°$. The characteristic shape is the same for all temperatures and angles, although there is significant dependence on temperature and Mach number when θ is smaller than about 50° and $f > f_p$ when refraction of sound by the jet shear layer becomes important. For subsonic jets, the spectrum varies roughly as f^3 at low frequencies and decays like $1/f$ for $f > f_p$.

Figures 15.4–15.7 and Table 15.1, supplemented when necessary by Eqs. (15.8) and (15.9), comprise a general procedure for estimating the SPL, directivity, and spectrum of jet mixing noise.

Example 15.1. Find the total jet mixing noise sound-power- and sound-pressure-level spectrum at 60° from the jet axis and 3 m from the nozzle of a 0.03-m-diameter air jet. The jet exhausts into ambient air (15°C, $p_s = 10.13$ μPa, $\rho_s = 1.225$ kg/m^3) at sonic ($U/c = 1$) exit velocity, that is, 340 m/s.

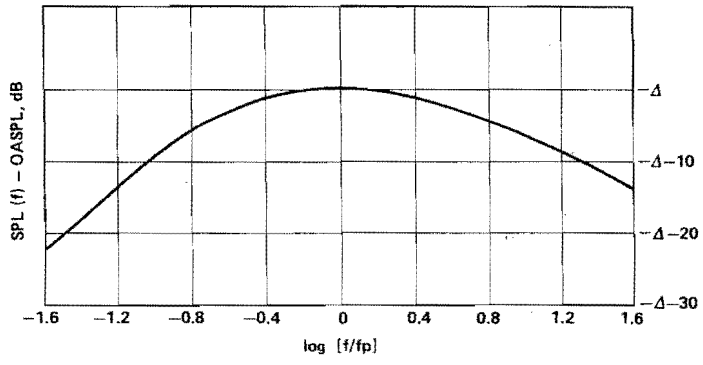


FIGURE 15.7 One-third-octave-band SPL $-$ OASPL (dB) for radiation directions $\theta \geq 90°$ and $\rho_j = \rho_s$.

Solution The mechanical stream power $\frac{1}{2}mU^2$ is 1.70×10^4 W. The ratios ρ_j/ρ_s and U/c are unity. Therefore, from Fig. 15.3 [or Eqs. (15.8) and (15.9)] the ratio of sound power to mechanical stream power is 1.0×10^{-4}. The resulting overall sound power is 1.7 W. From Fig. 15.6 [or Eq. (15.12)] the OASPL at 90° to the jet axis and $R = 3$ m is 98.8 dB re 20 μPa. From Eq. (15.11) the OASPL at 60° to the jet axis and $R = 3$ m is 103.5 dB, and the peak Strouhal number is 0.8. The one-third-octave-band SPL spectrum is found from Fig. 15.6 by adding 103.5 dB to the ordinate with $\Delta = 11$ dB (from Table 15.1).

Realistic jets exhausting from pipes and engine nozzles do not provide smooth, low-turbulence entrainment of flow but rather flow that has been disturbed or spoiled before leaving the nozzle. In this case, the above procedure is not valid unless the jet velocity U exceeds about 100 m/s. Below this speed major portions of the aerodynamically generated noise emanate from internal sources.

Noise of Imperfectly Expanded Jets

Supersonic, underexpanded, or "choked" jets contain shock cells through which the flow repeatedly expands and contracts (see inset to Fig. 15.8). Seven or more distinct cells are often visible extending up to 10 jet diameters downstream of the nozzle. They are responsible for two additional components of jet noise: *screech tones* and broadband *shock-associated noise*. Screech is produced by a feedback mechanism in which a disturbance convected in the shear layer generates sound as it traverses the standing system of shock waves. The sound propagates upstream through the ambient atmosphere and causes the release of a new flow disturbance at the nozzle exit. This is amplified as it convects downstream, and the feedback loop is completed when it encounters the shocks. A notable feature of the screech tones is that the frequencies are independent of the radiation direction, the fundamental occurring at approximately $f = U_c/L(1 + M_c)$, where $M_c = U_c/c$, U_c is the convection velocity of the disturbance in the shear layer, L is the axial length

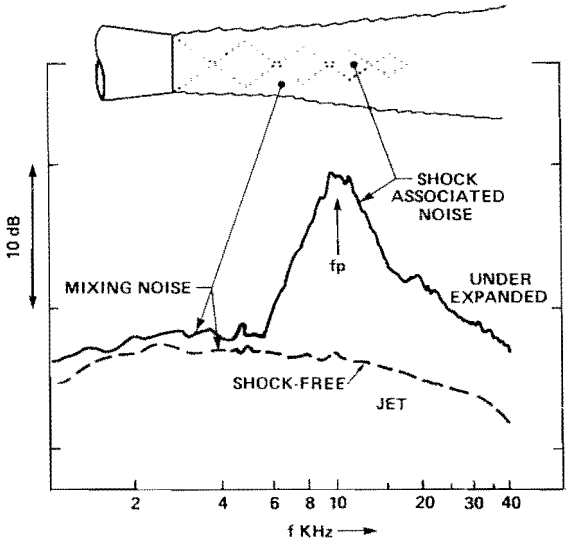


FIGURE 15.8 Jet noise spectra for shock-free and underexpanded jets at $\theta = 90°$, $\beta = 1$.

of the first shock cell, and c is the ambient speed of sound. Although screech is often present in model-scale experiments and can be important for choked jet engines, it is usually easy to eliminate by minor modifications to nozzle design, for example, by notching.

In practice, it is the broadband, shock-associated noise that is important for supersonic jet engines. It can be suppressed by proper nozzle design, but it is always present for a convergent nozzle. The dominant frequencies are usually higher than the screech tones and can range over several octave bands. For predictive purposes it is permissible to estimate separately the respective contributions of mixing noise and shock-associated noise to the overall sound power generated by the jet. The mixing noise predictions are the same as for a shock-free jet.

The overall SPL of shock-associated noise is approximately independent of the radiation direction and may be estimated from

$$\text{OASPL} = C_0 + 10 \times \log \frac{\beta^n A}{R^2}$$

$$C_0 = 156.5 \quad \text{(dB)} \quad n = \begin{cases} 4 & (\beta < 1) \\ 1 & (\beta > 1) \end{cases} \quad \frac{T_j}{T_s} < 1.1$$

$$C_0 = 158.5 \quad \text{(dB)} \quad n = \begin{cases} 4 & (\beta < 1) \\ 2 & (\beta > 1) \end{cases} \quad \frac{T_j}{T_s} > 1.1 \qquad (15.14)$$

where T_j = total (reservoir) jet temperature, K
T_s = total ambient temperature, K
$\beta = \sqrt{M_j^2 - 1}$
M_j = fully (ideally) expanded jet Mach number, based on sound speed in jet

The shock-associated noise spectrum exhibits a well-defined peak in the vicinity of

$$f_p = \frac{0.9U_c}{D_N \beta (1 - M_c \cos\theta)} \qquad (15.15)$$

where the convection velocity U_c meters per second is equal to $0.7U$ and θ is measured from the jet axis. When $T_j/T_s > 1.1$, the one-third-octave-band SPL (re 20 μPa) is given by

$$\text{SPL} = 143.5 + 10 \times \log \frac{\beta^n A}{R^2} - 16.13 \times \log \left(\frac{5.163}{\sigma^{2.55}} + 0.096\sigma^{0.74} \right)$$
$$+ 10 \times \log \left\{ 1 + \frac{17.27}{N_s} \cdot \sum_{i=0}^{N_s - 1} \left[C(\sigma)^{(i^2)} \right. \right.$$
$$\left. \left. \times \sum_{j=1}^{N_s - i - 1} \frac{\cos(\sigma q_{ij}) \sin(0.1158\sigma q_{ij})}{\sigma q_{ij}} \right] \right\} \qquad (15.16)$$

where $C(\sigma) = 0.8 - 0.2 \times \log_{10}(2.239/\sigma^{0.2146} + 0.0987\sigma^{2.75})$
$\sigma = 6.91\beta D_N f/c$, dimensionless
c = ambient speed of sound, m/s
$N_s = 8$ (number of shocks)
$q_{ij} = (1.7ic/U)\{1 + 0.06[j + \frac{1}{2}(i+1)]\}[1 - 0.7(U/c)\cos\theta]$

and n is defined as in (15.14). In the case of a "cold jet," for which $T_j/T_s < 1.1$, the prediction (15.16) should be reduced by 2 dB.

The prediction procedure for shock-associated noise is applicable over all angles θ where shock cell noise is important (say, $\theta > 50°$). When used in conjunction with the prediction procedure for jet mixing noise, the one-third-octave-band sound pressure spectrum for the overall jet noise may be estimated by adding the respective contributions to each frequency band of the mean-square acoustical pressures of the mixing noise and the shock-associated noise. The influence of shock-associated noise is illustrated in Fig. 15.8, which compares the spectrum of the jet mixing noise of a fully expanded, shock-free supersonic jet from a convergent–divergent nozzle at the same pressure ratio. In the latter case the spectral peak occurs at the frequency f_p given by Eq. (15.15).

Flight Effects

The noise generated by a jet engine in flight is modified because of the joint effects of Doppler amplifications (discussed in Section 15.2) and the reduction in mean shear between the jet flow and its environment. From an extensive series of experimental studies[3] empirical formulas have been developed to predict the SPL in flight in terms of the corresponding static levels.

In the Mach number range of $1.1 < M < 1.95$ jet mixing noise $\mathrm{OASPL}(\theta)_{\mathrm{flight}}$ is related to $\mathrm{OASPL}(\theta)_{\mathrm{static}}$ by

$$\mathrm{OASPL}(\theta)_{\mathrm{flight}} = \mathrm{OASPL}(\theta)_{\mathrm{static}} - 10 \times \log\left[\left(\frac{U}{U - V_f}\right)^{m(\theta)} (1 - M_f \cos \Phi)\right]$$

$$m(\theta) = \left[\left(\frac{6959}{|\theta - 125|^{2.5}}\right)^7 + \frac{1}{[31 + 18.5M - (0.41 - 0.37M)\theta]^7}\right]^{-1/7} \tag{15.17}$$

where θ = angle between jet axis and observer at retarded time of emission of sound, degrees
Φ = angle between flight direction and observer direction at retarded time of emission of sound, defined in Fig. 15.2
U = fully expanded jet velocity (relative to nozzle), m/s
V_f = aircraft flight speed, m/s
M_f = flight Mach number relative to sound speed in air, $= V_f/c$

The formula is applicable for $20° < \theta < 160°$. For $M < 1.1$ and $M > 1.95$, the relative velocity exponent $m(\theta)$ should be taken to be given by the above formula at $M = 1.1$, 1.95, respectively.

Estimates of the one-third-octave-band SPL spectrum in flight can be made by using Fig. 15.6 with the OASPL determined by (15.17) and the Strouhal number fD_N/U replaced by that based on the jet velocity: $fD_N/(U - V_f)$.

For shock-associated noise the influence of flight on both the spectrum and the OASPL is approximately given by

$$\mathrm{SPL}_{\mathrm{flight}} = \mathrm{SPL}_{\mathrm{static}} - 40 \log \times (1 - M_f \cos \Phi) \tag{15.18}$$

15.4 COMBUSTION NOISE OF GAS TURBINE ENGINES

Jet mixing noise and shock-associated noise of high-speed jet engines are the result of sources in the flow downstream of the nozzle. Their importance has progressively diminished in recent years with the introduction of large-diameter, high-bypass-ratio turbofan engines with much reduced mass efflux velocities. In consequence, greater attention has been given to noise generated within the engine (termed *core noise*), which tends to be predominant at frequencies less than 1 kHz. Combustion processes are a significant component of core noise,

both directly in the form of thermal monopole sources and indirectly through the creation of temperature and density inhomogeneities ("entropy spots"), which behave as dipole sources when accelerated in nonuniform flow.

The noise prediction scheme outlined below is based on an analysis of combustion noise of turbojet, turboshaft, and turbofan engines as well as model-scale data[3]. Annular, can-type, and "hybrid" combusters were all included in the valuation studies.

The overall sound power level (OAPWL, in decibels) is a function of the operating conditions of the combuster and the turbine temperature extraction and may be estimated from the equation

$$\mathrm{OAPWL} = -60.5 + 10 \times \log \frac{mc^2}{\Pi_{\mathrm{ref}}} + 20 \times \log \frac{(\Delta T/T_I)(P_I/p_{\mathrm{ISA}})}{[(\Delta T)_{\mathrm{ref}}/T_s]^2} \tag{15.19}$$

where m = combuster mass flow rate, kg/s
P_I = combuster inlet total pressure, Pa
ΔT = combuster total temperature rise, K
$(\Delta T)_{\mathrm{ref}}$ = reference total temperature extraction by engine turbines at maximum takeoff conditions, K
T_I = inlet total temperature, K
T_s = sea-level atmospheric temperature, 288.15 K
Π_{ref} = reference power, 10^{-12} W
p_{ISA} = sea-level atmospheric pressure, 10.13 kPa $= 1.013 \times 10^4$ N/m^2
c = sea-level speed of sound, 340.3 m/s

This formula is expected to yield predictions that are accurate to within ±5 dB.

The one-third-octave-band power level spectrum $\mathrm{PWL}(f)$ is given in terms of the OAPWL by

$$\mathrm{PWL}(f) = \mathrm{OAPWL} - 16 \times \log[(0.003037f)^{1.8509} + (0.002051f)^{-1.8168}]\ \mathrm{dB} \tag{15.20}$$

where f is frequency (in hertz) and the formula is applicable for 100 Hz $\leq f \leq$ 2000 Hz. The spectrum is essentially symmetric about a peak at $f = 400$ Hz (Fig. 15.9). In applications where the observed peak frequency f_p differs slightly from this value, the spectrum in the figure should be shifted, retaining its shape, so that the peak coincides with observation. In (15.20), f would be replaced by $400f/f_p$.

The one-third-octave-band sound power pressure spectrum may now be determined from the formula

$$\mathrm{SPL} = -10.8 + \mathrm{PWL}(f) - 20 \times \log R - 2.5 \times \log\left[\frac{1}{(10^{(1.633 - 0.0567\theta)} + 10^{(19.43 - 0.233\theta)})^{0.4}} + 10^{(4.333 - 0.115\theta)}\right] \tag{15.21}$$

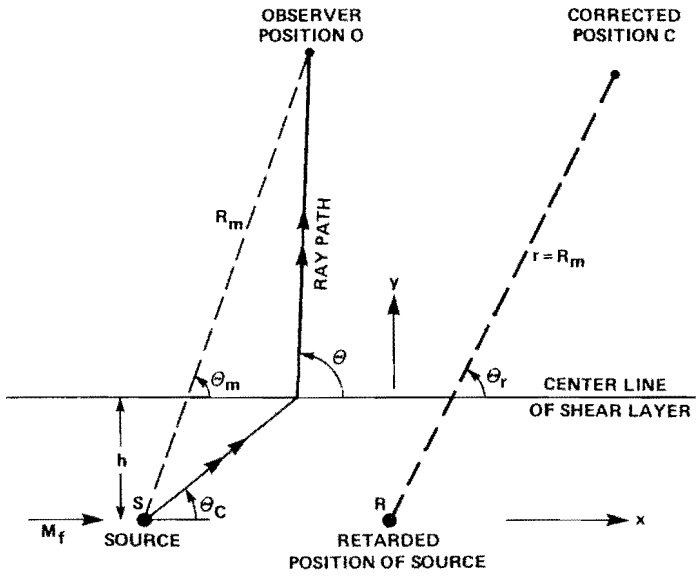


FIGURE 15.9 One-third-octave-band frequency power level spectrum of combuster noise.

where θ = angle from jet exhaust axis, degrees
R = observer distance, m

The peak radiation is predicted by (15.21) to occur at $\theta \approx 60°$, although at very low frequencies ($\leq$200 Hz) the peak may be shifted slightly toward the jet axis.

For an aircraft in flight at speed V_f, the modification of the predicted SPL may be estimated from Eq. (15.18).

15.5 TURBULENT BOUNDARY LAYER NOISE

The intense pressure fluctuations that can occur beneath a turbulent boundary layer are a source of sound and structural vibrations. The sound is produced directly by aerodynamic sources within the flow and indirectly by the *diffraction* at discontinuities in the wall (e.g., corners, ribs, support struts) of structural modes excited by the boundary layer pressures.

The pressure developed beneath a boundary layer on a *hard* wall is called the *blocked pressure* and is twice the pressure that a nominally identical flow would produce if the wall were absent. The rms wall pressure p_{rms} (in pascals) of the turbulent boundary layer can be estimated by[5]

$$\frac{p_{\text{rms}}}{q} \approx \sigma\varepsilon^* = \frac{\sigma}{\frac{1}{2}(1 + T_w/T) + 0.1(\gamma - 1)M^2} \tag{15.22}$$

where $\sigma = 0.006$, dimensionless
q = local dynamic pressure, $= \frac{1}{2}\rho U^2$, Pa
ρ = fluid density at outer edge of boundary layer, kg/m^3
U = free-stream velocity at outer edge of boundary layer, m/s
M = free-stream Mach number, $= U/c$, dimensionless
c = speed of sound at outer edge of boundary layer, m/s
T = temperature at outer edge of boundary layer, K
T_w = temperature of the wall, K
γ = ratio of specific heats of gas, dimensionless

The quantity $\sigma \equiv (p_{\text{rms}}/q)_{\text{incompressible}}$, and Eq. (15.22) represents a mapping from an incompressible flow to the compressible state by means of the compressibility factor, ε^*. Recent measurements[6] suggest that the currently accepted value $\sigma = 0.006$ may be too low and that a better approximation is $\sigma = 0.01$.

In many applications wall pressure fluctuations are substantially higher if the flow *separates*. For example, when separation occurs at the compression corner at a ramp or at an expansion corner, the rms wall pressure can typically exceed 2% of the local dynamic pressure q.

The structural response of a flexible wall to forcing by the boundary layer depends on both the temporal and spatial characteristics of the pressure fluctuations. When the wall is locally plane, these can be expressed in terms of the *wall pressure wavenumber–frequency spectrum* $P(\mathbf{k}, \omega)$. This is the two-sided Fourier transform $(1/2\pi)^3 \int_{-\infty}^{\infty} R_{pp}(x_1, x_3, t) \exp[-i(\mathbf{k} \cdot \mathbf{x} - \omega t)]\, dx_1\, dx_3\, dt$ of the space–time correlation function of the wall pressure R_{pp}. By convention, coordinate axes (x_1, x_2, x_3) are taken with x_1, x_3 parallel and transverse to the mean flow, respectively, x_2 measured outward of the wall, and the wavenumber $\mathbf{k} = (k_1, k_3)$ (in reciprocal meters) has components parallel to the x_1, x_3 axes only. The principal properties of the blocked-pressure spectrum $P_0(\mathbf{k}, \omega)$, say, are understood only for low-Mach-number flows ($M \ll 1$).

Wall Pressure Spectrum at Low Mach Number

Here, $P_0(\mathbf{k}, \omega)$ is an even function of ω, and its general features are shown in Fig. 15.10[7] for $\omega > 0$ The strongest pressure fluctuations are produced by eddies in the *convective ridge* of the wavenumber plane that convect along the wall at about 70% of the free-stream velocity. The region $k \equiv |\mathbf{k}| < \omega/c$ (c = speed of sound, in meters per second) is called the acoustical domain, and $k_0 = \omega/c$ is the acoustical wavenumber. The adjacent *subconvective* domain ($k_0 < k \ll \omega/U_c$) is important to determining the structural response of the wall to forcing by the turbulence pressures. In these regions $10 \times \log[P_0(\mathbf{k}, \omega)]$ is typically 30–60 dB below the levels in the convective domain.

Pressure fluctuations in the acoustical domain correspond to sound waves in the fluid. When the wall is smooth and flat, the generation of sound is dominated by quadrupole sources in the flow,[7] and the acoustical pressure frequency spectrum

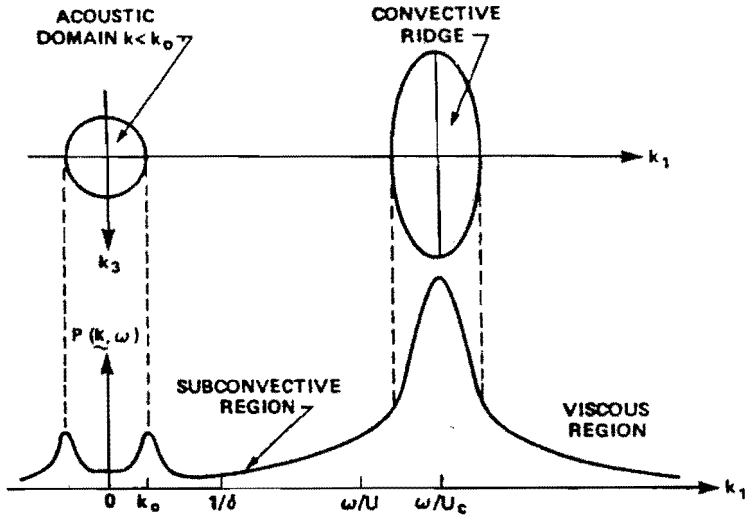


FIGURE 15.10 Turbulent boundary layer wall pressure spectrum at low Mach number for $\omega\delta/U \gg 1$, where δ is the boundary layer thickness (m).

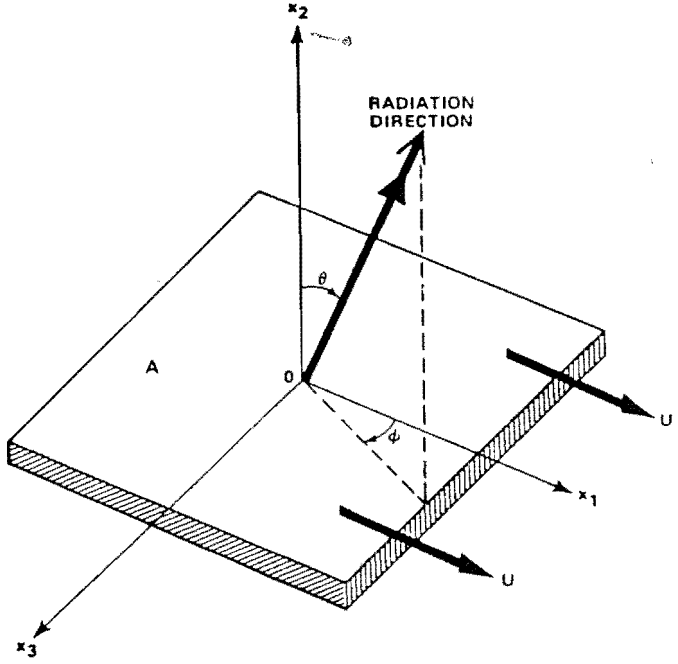


FIGURE 15.11 Coordinates defining the radiation of sound from a region of the wall of area A.

of sound produced by a fixed area of the wall (Fig. 15.11) is

$$\Phi(\omega) = 2\frac{A}{R^2}k_0^2 \cos^2\theta P_0(k_0 \sin\theta \cos\phi, k_0 \sin\theta \sin\phi, \omega) \tag{15.23}$$

where OASPL $= 10 \times \log\left[\int_0^\infty \Phi(\omega)\, d\omega/(20\ \mu\text{Pa})^2\right]$, dB
A = area of wall region, m^2
R = observer distance from center of A, m
(θ, ϕ) = polar angles of observer defined in Fig. 15.11

Chase[8] has proposed the following representation of the blocked-pressure spectrum that is applicable over the whole range of wavenumbers and is based on an empirical fit to experimental data in the convective and subconvective domains:

$$\frac{P_0(\mathbf{k},\omega)}{\rho^2 v_*^2 \delta^3} = \frac{1}{[(k_+\delta)^2 + 1.78]^{5/2}}\left\{\frac{0.1553(k_1\delta)^2 k^2}{|k_0^2 - k^2| + \beta^2 k_0^2} + 0.00078 \times \frac{(k\delta)^2[(k_+\delta)^2 + 1.78]}{(k\delta)^2 + 1.78}\left(4 + \frac{|k_0^2 - k^2|}{k^2} + \frac{k^2}{|k_0^2 - k^2| + \beta^2 k_0^2}\right)\right\}$$

$$\frac{\omega\delta}{U} > 1 \tag{15.24}$$

where δ = boundary layer thickness (distance from wall at which mean-flow velocity is equal to $0.99U$), m
ρ = mean fluid density, kg/m^3
v_* = friction velocity, $\approx 0.035U$, m/s
$U_c \approx 0.7U$, m/s
U = mainstream velocity at outer edge of boundary layer, m/s
ω = radian frequency, $= 2\pi f$, rad/s
$k_+ = \sqrt{(\omega - U_c k_1)^2/9v_*^2 + k^2}$, m^{-1}
$\beta \approx 0.1$, dimensionless

The first term in the curly brackets determines the behavior near the convective ridge and the second the low-wavenumber and acoustical domains. The numerical coefficient β controls the height of the spectral peak (Fig. 15.10) at the boundary $k = k_0$ of the acoustical domain and determines the intensity of the sound waves propagating parallel to the plane of the wall.

Example 15.2. Estimate the frequency spectrum $\Psi(\omega)$ of the power dissipated by flexural motion of a plane wall when the wall is excited by a low-Mach-number turbulent flow over a region of area A whose normal impedance $\mathbf{Z}(\mathbf{k}, \omega)$ (kg/m^2 · s) is independent of the orientation of $\mathbf{k}$.

Solution The impedance satisfies $Z(\mathbf{k}, \omega) = -p(\mathbf{k}, \omega)/v_2(\mathbf{k}, \omega)$, where p and v_2, respectively, denote the Fourier components of the pressure and normal velocity on the wall. Let $Z = R - iX$, where R and X are the resistive and reactive

components of the impedance, respectively. The total power delivered to the flexural motions is equal to $\int_0^\infty \Psi(\omega)\, d\omega$, where

$$\Psi(\omega) = 2A \int_{k>|k_0|}^{\infty} \frac{R(\mathbf{k}, \omega) P_0(\mathbf{k}, \omega)\ d^2\mathbf{k}}{R(\mathbf{k}, \omega)^2 + [X(\mathbf{k}, \omega) + \rho\omega/\sqrt{k^2 - k_0^2}]^2}$$

The flexural-mode wavenumbers are the roots $\mathbf{k} = \mathbf{k}_n, n = 1, 2, 3, \ldots,$ of $X(\mathbf{k}, \omega) + \rho\omega/\sqrt{k^2 - k_0^2} = 0$. In practice, these usually lie in the low-wavenumber region where $P_0(\mathbf{k}, \omega) \equiv P_0(k, \omega)$, so that, when $R \ll X$ and Z is a function of $k \equiv \mathbf{k}$ and ω only,

$$\Psi(\omega) \approx \sum_n \frac{4\pi^2 A k_n P_0(k_n, \omega)}{\left|(\partial/\partial k)\left[X(k, \omega) + \rho\omega\Big/\sqrt{k^2 - k_0^2}\right]\right|_{k_n}}$$

When the wall consists of a vacuum-backed, thin elastic plate of bending stiffness B (kg · m^2/s^2), mass density m (kg/m^2) per unit area, and negligible damping $R = 0$, we have $X = -(Bk^4 - m\omega^2)/\omega$, and there is only one flexural mode that occurs at $k = k_* > |k_0|$ such that

$$\Psi(\omega) = \frac{4\pi^2 A\omega(k_*^2 - k_0^2) P_0(k_*, \omega)}{5Bk_*^4 - 4B(k_0 k_*)^2 - m\omega^2}$$

where k_* is the positive root of $Bk^4 - m\omega^2 - \rho\omega^2/\sqrt{k^2 - k_0^2} = 0$. Numerical estimates may be made by substituting for $P_0(k_*, \omega)$ from (15.24).

15.6 NOISE FROM FLUID FLOW IN PIPES

Piping system noise typically comes mainly from control valves (see Section 15.11) and high-speeds machines (see Chapter 18). However, under some circumstances the noise induced by flow through milder discontinuities (bends, tees, swags, and other components) may be significant. Here we describe an approximate approach for estimating this type of flow-induced noise.

Pressure fluctuations in the turbulent boundary layer drive the wall of the pipe, causing it to radiate sound. As described in Section 15.5, the structural response of a flexible wall to forcing by the boundary layer depends in a complex manner on both the temporal and spatial characteristics of the pressure fluctuations. Seebold[9] suggested the following approximate method for estimating the noise produced by fluid flow in piping systems. The method estimates the noise that results from boundary layer pressure fluctuations in fully developed turbulent flow in uninterrupted straight pipes[10] and then applies a loss factor correction for local discontinuities. This loss factor correction is based on the notion that the sound power radiated at a discontinuity is approximately proportional to the square of the pressure drop Δp there and can therefore be related to the pressure head loss factor K, where $\Delta p = K(\frac{1}{2}\rho U^2)$.

The sound pressure level at a distance of 1 m from the pipe in the octave band centered on frequency f_c is approximated by

$$\text{SPL} = -3.5 + 40 \log U + 20 \log \rho + 20 \log K - 10 \log\left[\frac{t}{D}\left(1 + \frac{1.83}{D}\right)\right] - 5 \log\left[\frac{f_c}{f_r}\left(1 - \frac{f_c}{f_r}\right)\right] + \Delta L(f_c) \tag{15.25}$$

where U = gas flow velocity, m/s
ρ = fluid density, kg/m^3
t = pipe wall thickness, m
D = inside diameter of pipe, m
f_c = octave-band center frequency, Hz
f_r = ring frequency of pipe, Hz; = $1608/D$ for steel
K = total loss factor per 10-diameter pipe section, dimensionless

The spectral correction $\Delta L(f_c)$ depends on the ratio of the octave-band center frequency f_c to the Strouhal frequency of the pipe flow, $f_p = 0.2U/D$, as[11]

$$\Delta L = \begin{cases} 10.4 + 11.4 \log \dfrac{f_c}{f_p} & \text{for } \dfrac{f_c}{f_p} < 0.5 \\ 7 & \text{for } 0.5 \le \dfrac{f_c}{f_p} < 5 \\ 14 - 10 \log \dfrac{f_c}{f_p} & \text{for } 5 \le \dfrac{f_c}{f_p} < 12 \\ 41.9 - 36.1 \log \dfrac{f_c}{f_p} & \text{for } \dfrac{f_c}{f_p} \ge 0.5 \end{cases} \tag{15.26}$$

When employing (15.25), the piping system should be thought of as being composed of segments 10 diameters in length. The total loss factor K is determined by adding the individual loss factors K_i for the flow fittings and elements present within each 10-diameter segment of pipe. This total loss factor is then entered in Eq. (15.25) to estimate the flow noise emanating from that segment (at a distance of 1 m from the pipe wall). Loss factors for various piping components are provided in Table 15.2. For example, the loss factor for a straight pipe is taken to be 0.12 velocity heads per 10-diameter segment. On the other hand, a 10-diameter-long segment of piping containing an expander (1.5 : 1), an elbow (90°, $R/D = 1.5$), and a tee (flow-through run) would have a total loss factor of approximately 1, $K \approx 0.1 + 0.33 + 0.5 \approx 1$.

15.7 SPOILER NOISE

The term *spoiler noise* is used to characterize the noise produced by an obstacle or other obstruction that spans a duct carrying a mean flow. We shall discuss the case of air flowing in a duct or pipe that may be regarded as "semi-infinite" when

TABLE 15.2 Pressure Head Loss Factors[a] K

Straight pipes (10-diameter-long segment)		0.12				
45° Elbow	Screwed	0.42	Welded, $R/D = 1$	0.29	Welded, $R/D = 1.5$	0.21
90° Elbow	Screwed	0.92	Welded, $R/D = 1$	0.45	Welded, $R/D = 1.5$	0.33
180° Elbow	Screwed	2.00	Welded, $R/D = 1$	0.60	Welded, $R/D = 1.5$	0.43
Tees (screwed)	Thru branch	1.80	Thru run	0.50		
Tees (welded)	Thru branch	1.40	Thru run	0.40		
Reducer	$D_2/D_1 = 0.3$	0.25	$D_2/D_1 = 0.5$	0.17	$D_2/D_1 = 0.7$	0.07
Expander	$D_2/D_1 = 3$	0.80	$D_2/D_1 = 2$	0.56	$D_2/D_1 = 1.25$	0.10
Sudden Contraction	$D_2/D_1 = 0.1$	0.48	$D_2/D_1 = 0.33$	0.41	$D_2/D_1 = 0.8$	0.12
Sudden Expansion	$D_2/D_1 = 10$	0.98	$D_2/D_1 = 3$	0.79	$D_2/D_1 = 1.25$	0.12

[a] After Ref. 9.

it is desired to estimate the acoustical radiation from the open end. A spoiler-noise-generating system is shown schematically in Fig. 15.12. In practice, the spoiler may be a strut, stringer, guide vane, or other flow control device. The nominally steady mean flow exerts unsteady lift and drag forces on the spoiler, which accordingly behaves as an acoustical source of *dipole* type.

The following idealizations will be made:

1. The spoiler can be of arbitrary shape, but its cross-flow dimensions are small relative to the pipe cross section. This ensures that the flow speeds near the spoiler are not significantly greater than the pipe mean flow speed and therefore that turbulence mixing noise (quadrupole) can be neglected. Thus, the case of a valve, which produces a severe throttling of the flow, is excluded (see Section 15.11).
2. The peak frequency of the noise spectrum is below the "cutoff" frequency f_{co} of the pipe, which is given by

$$f_{co} = \begin{cases} 0.293c/r & \text{Hz (circular pipe)} \\ 0.5c/w & \text{Hz (rectangular pipe)} \end{cases} \qquad (15.27)$$

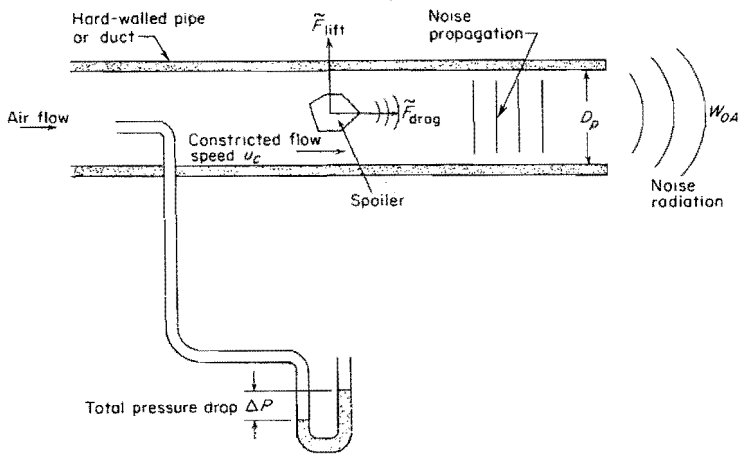


FIGURE 15.12 Flow spoiler system. The sound power is generated by the unsteady drag force on the spoiler and radiated from the open end of the pipe.

where c = sound speed, m/s
r = radius of circular pipe, m
w = largest transverse dimension of rectangular pipe, m

If this condition is not fulfilled, the propagated sound power near and above the peak frequency (which determines most of the overall sound power) will be influenced by transverse modes of the pipe.

3. The pipe wall is acoustically rigid. The fluctuating lift forces on the spoiler are then canceled by images in the wall, and sound is produced solely by the unsteady drag, which corresponds to an acoustical dipole whose axis is parallel to the mean flow. A low-noise spoiler system should therefore use bodies of low drag, such as airfoils, rather than grids or other oddly shaped bodies.

For several elementary flow spoiler configurations, such as the one shown in Fig. 15.12, the *fluctuating drag is directly proportional to the steady-state drag experienced by the body*. This depends on the pressure drop ΔP across the spoiler (as measured by an upstream and a downstream total-pressure probe), and the broadband noise radiated from the open end of the pipe is given by[12]

$$W_{OA} = \frac{k(\Delta P)^3 D_p^3}{\rho^2 c^3} \qquad (15.28)$$

where W_{OA} = overall radiated sound power, W
k = constant of proportionality, dimensionless

ΔP = total pressure drop across spoiler, Pa
D_p = pipe diameter, m
ρ = atmospheric density, kg/m^3
c = atmospheric sound speed, m/s

Specific information about spoiler geometry is absent from Eq. (15.28) but is implicit in the pressure drop ΔP. From a variety of experimental spoiler configurations the constant k is found to be about 2.5×10^{-4} for air.

Equation (15.28) determines the broadband sound power. It should strictly be regarded as a lower bound that is applicable only if there are no *discrete-frequency* components of the noise. These are present in certain conditions (e.g., excitation of edge tones) and may well stand out against the broadband levels.[13] When such a mechanism has been identified, the discrete tones can usually be eliminated or controlled by detuning or rounding off sharp corners or edges or cutting feedback paths by treating reflecting surfaces with sound-absorbent materials.

The frequency spectrum measured outside the pipe for the noise generated by the spoiler exhibits a haystack structure (Fig. 15.13) with a peak frequency given by

$$f_p \approx \frac{u_c}{db} \quad \text{Hz} \tag{15.29}$$

where u_c = constricted flow speed, m/s
d = projected width of spoiler, m
b = constant that equals 0.2 for pressure differences ΔP of the order 4000 Pa and 0.5 for ΔP of the order of 40,000 Pa

The constricted flow speed u_c for cold air is given in Table 15.3 as a function of ΔP. Values in between those in the table can be interpolated.

Example 15.3. Find the sound-power-level spectrum of noise produced by a spoiler consisting of a flat plate of width 2 cm stretching across a circular pipe of internal diameter $D_p = 5$ cm. The pressure drop across the spoiler is $\Delta P = 10,000$ Pa.

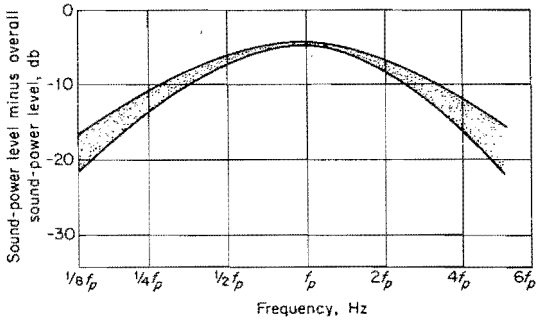


FIGURE 15.13 Generalized octave-band spectrum for in-pipe-generated spoiler noise referenced to the total power radiated from the open end and the peak frequency.

TABLE 15.3 Constricted Flow Speed u_c for Cold Air as Function of Pressure Drop

ΔP, Pa	2500	5000	10,000	20,000	30,000	40,000
u_c, m/s	63	90	124	173	209	238

Solution From Eq. (15.28) the total sound power $L_w \approx 101$ dB re 10^{-12} W. When $\Delta P = 10,000$ Pa, the peak frequency of the spectrum can be expected to be at $f_p \approx 0.35u_c/d$.

From Table 15.3, we find $u_c = 124$ m/s; hence $f_p \approx 2170$ Hz. The sound power spectrum in octave bands is obtained form Fig. 15.13 with 101 dB added to the ordinate.

15.8 GRID OR GRILLE NOISE

The characteristics of noise produced by flow through grids, grilles, diffusers, guide vanes, or porous plates, which often terminate air conditioning ducts, are similar to those of spoiler-generated sound. The principal differences are that (1) the grid is located at the open end of the duct, (2) the duct cross-sectional area is typically quite large (say, 0.04–1 m^2), and (3) the velocity of the air in the duct is usually small, rarely exceeding 30 m/s. The speed of the "air jets" exhausting from the individual air passages (or orifices) in a diffuser is generally low enough (<100 m/s) that jet mixing noise can be neglected. The dominant sound source is of dipole type and is associated with the interaction of the flow with the diffuser elements (e.g., guide vanes).

When a duct is terminated by a grid of circular rods (Fig. 15.14*a*), periodic shedding of vortices can occur, producing a fluctuating lift force on each rod and an associated *tonal* component of the radiated sound. This source is a dipole (whose axis is parallel to the lift direction) and is in addition to the drag dipole. The frequency of the tone is given approximately by

$$f = \frac{0.2u}{D_R} \tag{15.30}$$

where u = mean flow speed, m/s
D_R = diameter of rods, m

Tonal oscillations produced by a feedback mechanism can also arise when the duct termination consists of a plate perforated with sharp-edged circular cylindrical apertures (Fig. 15.14b).

In general, however, the noise produced by typical air conditioner grids is almost always broadband and of conventional dipole character, with the sound power varying as the sixth power of the velocity. As in the case of spoiler noise, the overall sound power can be related to the pressure drop ΔP across the grid,

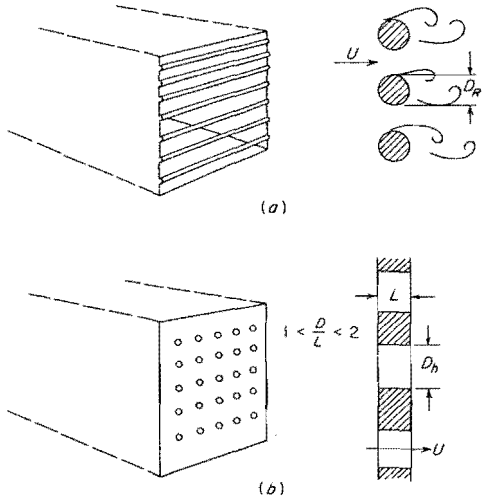


FIGURE 15.14 Special cases of duct terminations: (*a*) circular rods; (*b*) sharp-edge circular cylindrical holes.

independently of the specific grid geometry. To do this, we introduce the pressure drop coefficient

$$\xi = \frac{\Delta P}{\frac{1}{2}\rho u^2} \tag{15.31}$$

where ρ = density of air, kg/m^3
u = mean flow speed in duct prior to grid, m/s

Three typical diffuser configurations together with their pressure drop coefficients ξ are illustrated in Fig. 15.15.[14] The values of ξ for similar diffuser configurations are usually available from the manufacturer. If not, they may be estimated from this figure.

If not given by the manufacturer, the overall sound power level L_w from air conditioning diffusers can be estimated from the empirical formula[14]

$$L_w = 10 + 10 \times \log(S\xi^3 u^6) \quad \text{dB re } 10^{-12} \text{ W} \tag{15.32}$$

where S = area of duct cross section prior to diffuser, m^2
ΔP = pressure drop through diffuser, Pa

The noise spectra of different diffusers do not exhibit identical shapes even when normalized to similar flow speeds and exhaust areas. Construction differences tend to emphasize different frequency regimes, and poorly designed diffusers will radiate discrete-frequency sound. In practical noise control problems, however, a general spectrum shape $L_w - 10 \times \log_{10}(S\xi^3)$ (dB re 10^{-12} W) can be used for each duct velocity u (in meters per second) that fits most diffuser noise spectra to within about ±5 dB, as shown in Fig 15.16.

Configuration	Duct area, m^2	Comment	Pressure drop coefficient ξ
(a) 0.2 m, 0.1 m, 0.035 m	0.020	Parallel louvres	2.9
	0.020	Inclined louvres	2.7
(b) 0.29 m, 0.09 m, 0.07 m	0.028	Parallel louvres Open damper	4.8
	0.028	Parallel louvres Partially closed damper	7.3
(c) 0.24 m, 0.475 m, 0.475 m, 0.24 m, 0.025 m, 0.075 m, 0.145 m	0.046	Open stagnation disk Parallel damper vanes	5.6
	0.046	Closed stagnation disk Parallel damper vanes	6.2
	0.046	Open stagnation disk Deflected damper vanes	19.8
	0.046	Closed stagnation disk Deflected damper vanes	19.9

FIGURE 15.15 Various duct terminations and their pressure drop coefficients $\xi = \Delta P / \frac{1}{2}\rho u^2$. The duct area S is in square meters. (After Ref. 14.)

To estimate the sound power spectrum of the radiation from a given diffuser, first determine the relevant curve from Fig. 15.16 for the particular flow speed. The ordinate in the figure is then increased by $10 \times \log_{10}(S\xi^3)$ decibels to yield the desired one-third-octave-band spectrum with a margin of error of about ±5 dB.

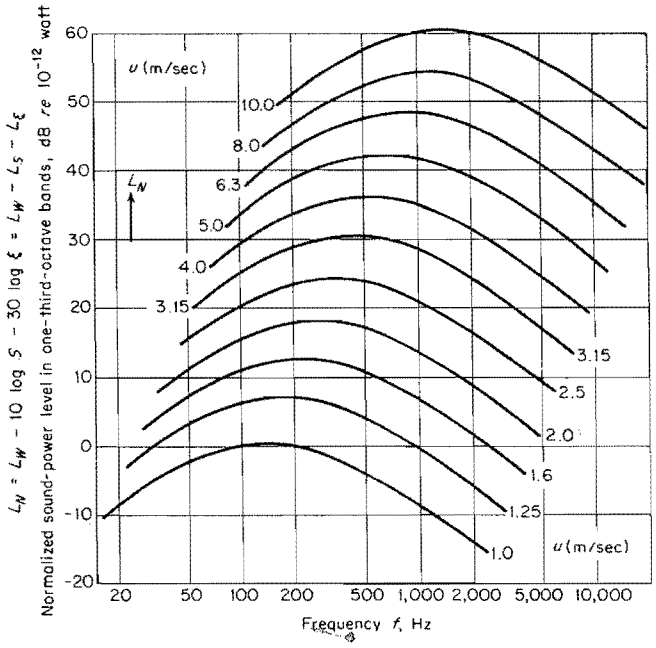


FIGURE 15.16 Normalized one-third-octave-band sound power level spectra for noise radiated from diffusers of various flow velocities. (After Ref. 14.)

15.9 SOUND GENERATION BY AIRFOILS AND STRUTS

Noise of a Strut in a Turbulent Stream

Long struts, airfoils, guide vanes, and so on, which offer negligible drag to a mean flow, frequently experience significant fluctuations in lift when exposed to a turbulent stream and behave as *dipole-type* sources of broadband sound. The strength of the radiation depends on the dimensions of the airfoil and on the turbulence intensity and correlation length of the velocity fluctuations.

A simple description of the radiation can be given when the mean flow is of low Mach number (say, <100 m/s in air) and when the distance to the nearest boundary (e.g., duct wall) is at least of the order of the acoustical wavelength. In these circumstances the *frequency spectral density* of the total radiated sound power $\Pi(\omega)$ is given approximately by

$$\Pi(\omega) = \frac{\pi l a^2 \rho u^2 M^3 (\omega\Lambda/U)^4}{4(1+\pi\omega a/U)[1+(\omega\Lambda/U)^2]^{5/2}[1+(\omega a/3c)^3]^{1/3}} \qquad (15.33)$$

where ω = radian frequency, $= 2\pi f$, f in Hz
a = chord of airfoil, m

l = span of airfoil, m
ρ = density of mean stream, kg/m^3
u = rms turbulence velocity in lift direction, m/s
U = velocity of mean stream, m/s
M = mean flow Mach number, $= U/c$, dimensionless
c = sound speed, m/s
Λ = integral scale of turbulence velocity, m

The total radiated sound power $W = \int_0^\infty \Pi(\omega)\, d\omega$, in watts, can be estimated from

$$W = \frac{1.78(la^2/\Lambda)\rho u^2 U M^3}{(1+10.71a/\Lambda)(1+1.79\ Ma/\Lambda)} \qquad 0 \le M \le 0.3 \qquad (15.34)$$

At low frequencies the acoustical intensity exhibits the characteristic dipole *field shape*, proportional to $\cos^2\theta$, where θ is measured from the direction of the mean lift. At higher frequencies (when the acoustical wavelength is much smaller than the chord of the airfoil but still exceeds the airfoil thickness), the field shape assumes a cardioid form, with a null in the forward direction and peaks close to the direction of the mean flow.

Airfoil Self-Noise

In addition to gust/inflow turbulence-induced noise, an airfoil can also generate *self-noise* when turbulence that arises from the natural instability of the boundary layers on the surface of the airfoil is swept past the trailing edge. This is usually important when the hydrodynamic wavelength of the turbulence eddies is larger than the airfoil thickness at the trailing edge. The mechanism of noise production tends to be weaker than at the leading edge, because the violence of the unsteady motion at the trailing edge is alleviated by vortex shedding into the wake, and to be more prominent at higher frequencies.[15]

The noise may be ascribed to a distribution of lift dipoles near the trailing edge. At low frequencies the acoustical intensity exhibits the characteristic dipole field shape, proportional to $\cos^2\theta$, with a null in the plane of mean motion of the airfoil. At higher frequencies (when the acoustical wavelength is smaller than the chord of the airfoil) the field shape assumes a cardioid form, with a null in the downstream direction and the peak in the forward direction. In either case, when the trailing edge is at right angles to the mean flow, the frequency spectral density of the overall sound power $\Pi(\omega)$ (in watt-seconds) is given approximately by

$$\Pi(\omega) = \frac{\pi l a \omega^2}{24\rho c^3[1+(\omega a/3c)^3]^{1/3}} \int_{-\infty}^{\infty} \frac{P_0(k_1, 0, \omega)}{|k_1|}\, dk_1 \qquad (15.35)$$

where $P_0(\mathbf{k}, \omega)$ = blocked-pressure wavenumber–frequency spectrum on airfoil just upstream of trailing edge (see Section 15.5)
k_1 = wavenumber component parallel to mean flow, m^{-1}

If the flow approaching the trailing edge is turbulent on both sides of the airfoil, $P_0(k_1, 0, \omega)$ in Eq. (15.35) should be replaced by the sum of the wall pressure spectra on the two sides.

When the Chase model [Eq. (15.24)] is used to estimate the integral in Eq. (15.35), the frequency spectral density of the sound power radiated by a section of the airfoil of spanwise length l (in meters) is

$$\Pi(\omega) = \frac{0.08al\delta\rho v_*^4 U_c(\omega\delta/U_c)^3}{c^3[1 + (\omega a/3c)^3]^{1/3}[(\omega\delta/U_c)^2 + 1.78]^2} \tag{15.36}$$

where δ = boundary layer thickness, m
v_* = friction velocity, m/s
$U_c \approx 0.7 \times$ velocity of mean stream, m/s

and other quantities are defined after Eq. (15.35).[16] However, measured levels of $\Pi(\omega)$ frequently exceed predictions of this formula. More detailed empirical formulas are given in the references.[16,17]

When the frequency is high enough [beyond the range of applicability of Eq. (15.36)] that the *Strouhal number* $\omega h/U \approx 1$, where h is the thickness of the trailing edge of the airfoil, the shedding of discrete vortices from the trailing edge can occur, provided the Reynolds number Ua/ν based on the chord a of the airfoil (dimensionless; ν is kinematic viscosity in square meters per second) does not exceed 10^6–10^7. This produces a distinct contribution to trailing-edge noise, often called "airfoil singing," whose amplitude is not easily predicted.[16]

15.10 FLOWS PAST CAVITIES

Sheared flow passing over a hole or opening in a wall can be the source of intense acoustical tones. Instability of the mean flow over such a wall cavity not only can excite hydrodynamic self-sustained oscillations but also can couple with resonant acoustical modes of the cavity, as in the Helmholtz resonator. Cavity tones are a frequent source of unwanted noise and vibration in branched duct and piping systems, turbomachinery, and exposed openings on automobiles, aircraft, and other high-speed vehicles. In this section we provide relationships for determining when flow over an opening that can be approximated as either a rectangular cavity (Fig. 15.17*a*) or a Helmholtz resonator (Fig. 15.17*b*) might be expected to exhibit strongly resonant behavior.

Flow over Cavities of Uniform Cross Section

For cavities of the type shown in Fig. 15.17*a*, resonant cavity oscillation occurs when the frequency associated with the shedding of vorticity from the upstream edge of the cavity is sufficiently high and the acoustical wavelengths within the cavity are sufficiently short as to allow standing waves inside the cavity. Longitudinal wave resonance is possible when the acoustical wavelength is less

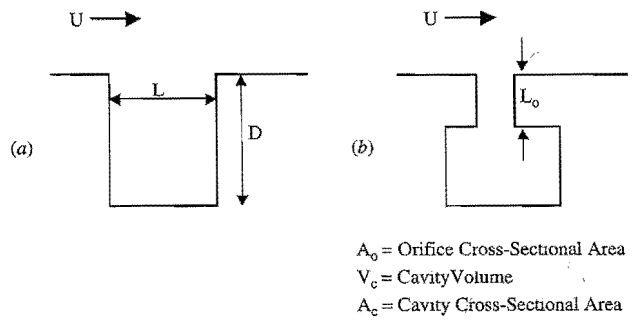


FIGURE 15.17 Examples of flows that sustain cavity resonances: (*a*) rectangular cavity of uniform cross section; (*b*) non-axisymmetric Helmholtz resonator.

than twice the cavity length, $c/f \leq 2L$, and depth resonance is observed when the acoustical wavelength is less than four times the cavity depth, $c/f \leq 4D$. For shallow cavities, where cavity length-to-depth ratio is large ($L/D > 1$), the longitudinal standing waves are dominant, while for deep cavities ($L/D < 1$) the depth resonance dominates.

Rossiter[18] derived the following equation for the Strouhal number associated with longitudinal cavity resonance modes:

$$\frac{fL}{U_\infty} = \frac{m - \xi}{M + 1/k_v} \tag{15.37}$$

where k_v = ratio of shear layer velocity to free-stream velocity, $= U_c/U_\infty \cong 0.57$
m = mode number, $= 1, 2, 3, \ldots$, dimensionless
ξ = empirical constant, $= 0.25$, dimensionless
L = cavity length, m
M = free-stream Mach number, $= U_\infty/c$, dimensionless

Block[19] developed the following relation for the longitudinal cavity modes that accounts for the dependence of the Strouhal number on the cavity L/D ratio as observed in experimental data for shallow ($L/D > 1$) cavities:

$$\frac{fL}{U_\infty} = \frac{m}{1.75 + M\,(1 + 0.514/(L/D))} \tag{15.38}$$

The following relation for depthwise modes of cavity oscillation was developed by East[20]:

$$\frac{fL}{U_\infty} = \left(\frac{1}{M}\right)\left(\frac{L}{D}\right)\left(\frac{0.25}{1 + 0.65(L/D)^{0.75}}\right) \tag{15.39}$$

Lucas,[21] after comparing the ranges of validity of various cavity oscillation models, recommends, for low to moderate Mach number, the use of Block's

formula (15.38) for shallow ($L/D > 1$) cavities. For deep cavities he suggests use of East's formula (15.39) to determine the resonance of the depth mode and Rossiter's formula (15.37) for the longitudinal resonance mode. For such deep cavities the depth resonance will be the dominant mode.

Block[19] combined Eqs. (15.38) and (15.39) so that the frequency for the shallow acoustical waves coincides with the depthwise acoustical modes, providing the following formula for estimating the Mach number at which a cavity begins to oscillate in a given mode m:

$$M = \frac{1.75L/D}{4m[1 + 0.65(L/D)^{0.75}] - [(L/D) + 0.514]} \tag{15.40}$$

Equation (15.40) was shown by Block[19] to give adequate agreement with experimental data for Mach numbers in the range of 0.1–0.5 and for $L/D < 2$.

Flow over a Helmholtz Resonator

The natural frequency f_n of the Helmholtz resonator shown in Fig. 15.17*b* is given by

$$f_n = \frac{c}{2\pi}\sqrt{\frac{A_o}{V_c L_{\text{eff}}}} \tag{15.41}$$

where c = sound speed, m/s
A_o = orifice cross-sectional area, m^2
V_c = cavity volume, m^3
L_{eff} = effective neck length of orifice, m

The following approximate expression[22] for the effective neck length L_{eff} in the presence of a mean flow over the Helmholtz resonator accounts for an end correction due to the entrained mass of the virtual piston forming the interface between the neck and the exterior space (length ΔL_o):

$$\begin{aligned} L_{\text{eff}} &= L_o + \Delta L_o \\ &= L_o + 0.48\sqrt{A_0} \end{aligned} \tag{15.42}$$

where L_o is the length of the neck length of the orifice in meters.

An experimental study by Panton and Miller[23] indicates a strong response of the Helmholtz resonator excited by a turbulent boundary layer when

$$\frac{2d_o f_n}{U_c} \cong 1 \tag{15.43}$$

where d_o = Helmholtz resonator neck diameter, m
U_c = boundary layer convection velocity, $\approx 0.7U$, m/s
U = mainstream velocity at outer edge of boundary layer, m/s

In Eq. (15.43) f_n is either the Helmholtz resonance frequency in Eq. (15.41) or the fundamental standing-wave (organ pipe) resonance. For the latter, the natural frequency is approximately given by

$$f_n \cong \frac{c}{2L_{\text{eff}}} \tag{15.44}$$

Example 15.4. Many automobiles have a sunroof opening in their roof. Under some conditions the interior volume of the automobile cabin can act in combination with such an opening to create a Helmholtz resonator. If no measures are taken to prevent such an occurrence, at what speed might we expect the automobile's passengers to experience intense pressure fluctuations given a cabin interior volume of approximately 3 m^2, a square opening in the roof 0.4 m on a side, and a combined thickness of the roof and edging surrounding the opening of approximately 10 cm.

Solution Assuming an air temperature of 20°C, the speed of sound $c = 331.5 + 0.58T$ (in °C) = 343.1 m/s. The orifice cross sectional area $A_o = 0.4 \times 0.4 = 0.16$ m^2. The effective length of the opening is given by Eq. (15.42) as $L_{\text{eff}} = 0.1 + 0.48\sqrt{0.16} = 0.29$ m. Applying the above values and the cavity volume of $V_c = 3$ m^2, from Eq. (15.41) we expect the Helmholtz resonance to occur at $f_n = 23.4$ Hz. We take the neck diameter to be given by the length of the opening, $d_o = 0.4$ m. Substituting this value and that of the resonance frequency into Eq. (15.43), we can solve for the convection velocity, $U_c \approx 2 \times 0.4 \times 23.4 = 18.7$ m/s. The corresponding velocity of the mainstream, and thus our estimate of the vehicle speed at which we expect to strongly excite the Helmholtz resonance, is $U = U_c/0.7 = 26.7$ m/s, or 96 kph.

15.11 AERODYNAMIC NOISE OF THROTTLING VALVES

The noise of gas control or throttling valves may generally be associated with two sources: (1) mechanical vibration of the trim and (2) aerodynamic throttling. Noise generation by these mechanisms rarely occurs simultaneously, but when it does, the cure of one is usually the cure of the other.

Aerodynamic Noise

The prediction of the noise radiated from the body of a valve and from the downstream piping connected to it involves the following conceptual steps: (1) prediction of the magnitude and the spatial and spectral distribution of the noise inside the pipe based on the aerodynamic characteristics of the valve and the cross sectional area of the pipe, (2) prediction of the vibration response of the pipe to the internal sound field, (3) prediction of the sound radiation of the vibrating pipe.

In Step 1, the sound power generated by the valve has two components. The first is owing to the dynamic drag and lift forces (dipole) generated by the interaction of the turbulent flow with the valve, which are roughly proportional to the sixth power of the flow velocity. The second is sound power generated by

the jet noise component (quadrupole), which is roughly proportional to the eighth power of the jet exit velocity. At very high pressure ratios, when the flow in the valve passage is supersonic, a shock pattern emerges downstream of the valve and generates intense screech noise. The dipole mechanism dominates the internal sound field at low Mach numbers and the quadrupole at high Mach numbers.

Based on the scaling of experimental data,[24] the lowest pipe wall attenuation occurs at $f_0 = (f_R/4)(c_{gas}(T)/c_0)$, where f_R is the ring frequency (Eq.15.58) and $c_{gas}(T)$ and $c_0 = 340$ m/s are the speed of sound of the gas in the pipe at local temperature and the that of air at room temperature respectively.

A fully analytical prediction procedure is too cumbersome. Consequently, the valve industry has adopted a prediction procedure based on both analytical and empirical methods that predicts the sound pressure level of the valve noise at 1 meter from the pipe wall directly from the aerodynamic properties of the valve and the geometric and material properties of the pipe. The rest of this chapter describes this semi-empirical prediction procedure.

Investigations of noise-induced pipe failures[25] have enabled maximum safe sound power levels to be established for given pipe sizes and wall thicknesses, as indicated in Fig. 15.18. The power levels shown in the figure correspond approximately to a sound level of 130 dBA at 1 m from the pipe wall downstream of the valve. Exceeding this level will most probably lead to piping failure, and a limit of 110 dBA at 1 m is recommended for safety and to maintain the structural integrity of valve-mounted accessories.

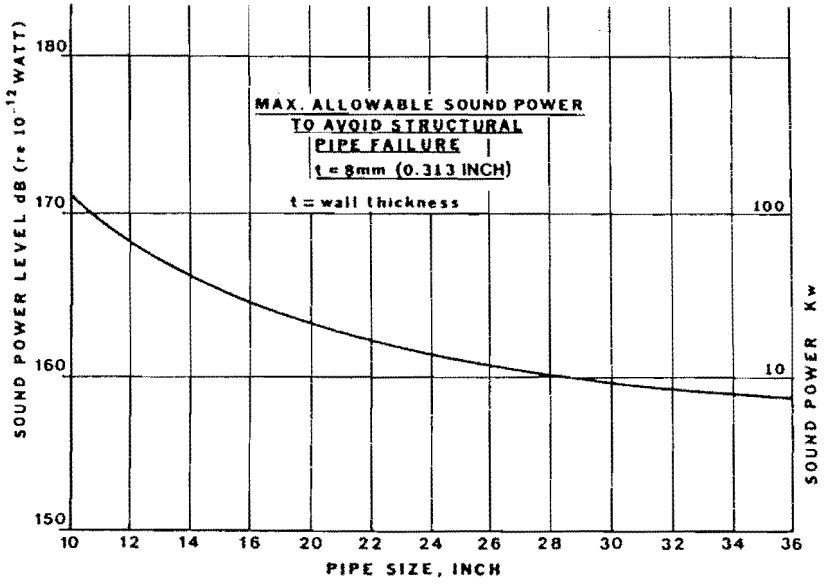


FIGURE 15.18 Suggested sound power level and sound power (Kw) limits inside pipe to avoid structural pipe failure based on actual occurrence.[24]

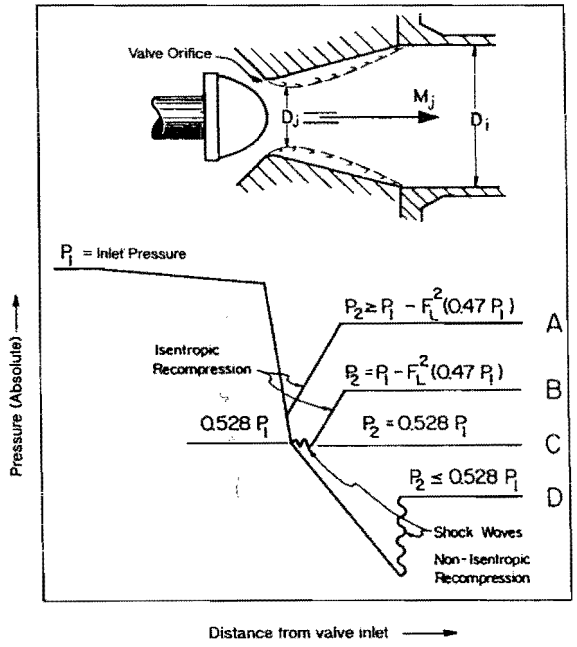


FIGURE 15.19 Schematic flow profile and static pressure diagram of throttling valve for various downstream pressures (P_2).

The aerodynamic noise is determined by the mechanical stream power $W_{\text{mech strm}} = \frac{1}{2}mU^2$ (m being the mass flow and U the velocity; see Section 15.3) that is converted from potential energy (inlet pressure) to kinetic energy (velocity head) within the valve and subsequently to thermal energy (corresponding to reduced downstream pressure and an increase in entropy).[26] The pressure reduction (i.e., the conversion of kinetic into thermal energy) occurs via the generation of turbulence or, when the flow is supersonic, through shock waves. The sound power is equal to $\eta W_{\text{mech strm}}$, where η is an acoustical efficiency factor. Unlike the case of a jet discharging into the atmosphere, the jet from a valve cannot expand freely, and only a fraction of the kinetic energy is converted by turbulence into thermal energy. This is illustrated in Fig. 15.19, which is a schematic view of a throttling valve and the associated pressure profile for various downstream pressures P_2.* On curve A the flow is subsonic, and turbulence-generated sound is predominantly of dipole type. At the critical pressure ratio ($P_1/P_2 = 1.89$ for air), curve B shows the presence of incipient shock waves followed by subsonic recompression, with both turbulence and shocks as noise sources. At higher pressure ratios recompression tends to be nonisentropic, and sound is produced predominantly by shock waves (curve D).

*In the rest of this chapter all pressures are absolute static pressures (in pascals).

Downstream of the vena contracta (D_j in Fig. 15.19) a portion of the velocity head is always recovered. The fraction lost is equal to F_L^2, where F_L is an experimentally determined pressure recovery coefficient that depends on valve type and size. The pressure drop $P_1 - P_2$ across the valve required to reach sonic velocity in the vena contracta is $F_L^2(P_1 - P_0)$, where P_0 is the static pressure in the vena contracta.[26] In subsonic flow the remaining portion of the jet power is recovered through isentropic recompression and is not converted to sound. If there were no pressure recovery at the valve orifice and assuming sonic flow at speed in c_0 meters per second (curve D in Fig. 15.19),

$$W_{\text{mech strm}} = \tfrac{1}{2}mc_0^2 \tag{15.45}$$

where m is the mass flow in kilograms per second, which also determines the valve flow coefficient C_v [see Eq. (15.50) or Table 15.4] together with the specific gravity G_f of the vapor or gas (relative to air = 1) and the valve inlet pressure P_1 (in pascals) such that

$$W_{\text{mech strm}} = 7.7 \times 10^{-11} C_v F_L c_0^3 P_1 G_f \quad \text{W} \tag{15.46}$$

The total sound power is then

$$W = \eta W_{\text{mech strm}} \quad \text{W} \tag{15.47}$$

$$L_W = 10 \times \log \frac{\eta W}{10^{-12}} \quad \text{dB} \tag{15.48}$$

When the pressure ratio is not sonic, η should be replaced by the acoustical power coefficient η_m determined below and (to simplify the calculations) should be used in conjunction with the sonic mechanical stream power given by Eq. (15.45). The acoustical power coefficient is further used in Eq. (15.53).

It may be remarked that the pressure recovery coefficient F_L can be used to predict the pressure P_0 in the vena contracta and also, to a satisfactory approximation, the area A_v of the vena contracta by

$$P_0 = P_1 - \frac{P_1 - P_2}{F_L^2} \tag{15.49a}$$

$$A_v = \frac{C_v F_L}{5.91 \times 10^4} \quad \text{m}^2 \tag{15.49b}$$

The valve's flow coefficient C_v can be calculated as follows:

$$C_v = \begin{cases} 2.14 \times 10^7 \dfrac{m}{\sqrt{\Delta P(P_1 + P_2)G_f}} & \Delta P \le \dfrac{1}{2}F_L^2 P_1 \\ 1.95 \times 10^7 \dfrac{m}{F_L P_1 \sqrt{G_f}} & \Delta P \ge \dfrac{1}{2}F_L^2 P_1 \end{cases} \tag{15.50}$$

TABLE 15.4 Factors for Valve Noise Prediction (Typical Values)

Valve Type	Flow To	Percentage of Capacity or Angle of Travel	$C_v/D^{2,a}$	F_L	F_d
Globe, single-port parabolic plug	Open	100%	0.020	0.90	0.46
Globe, single-port parabolic plug	Open	75%	0.015	0.90	0.36
Globe, single-port parabolic plug	Open	50%	0.010	0.90	0.28
Globe, single-port parabolic plug	Open	25%	0.005	0.90	0.16
Globe, single-port parabolic plug	Open	10%	0.002	0.90	0.10
Globe, single-port parabolic plug	Close	100%	0.025	0.80	1.00
Globe, V-port plug	Open	100%	0.016	0.92	0.50
Globe, V-port plug	Open	50%	0.008	0.95	0.42
Globe, V-port plug	Open	30%	0.005	0.95	0.41
Globe, four-port cage	Open	100%	0.025	0.90	0.43
Globe, four-port cage	Open	50%	0.013	0.90	0.36
Globe, six-port cage	Open	100%	0.025	0.90	0.32
Globe, six-port cage	Open	50%	0.013	0.90	0.25
Butterfly valve, swing-through vane	—	75° open	0.050	0.56	0.57
Butterfly valve, swing-through vane	—	60° open	0.030	0.67	0.50
Butterfly valve, swing-through vane	—	50° open	0.016	0.74	0.42
Butterfly valve, swing-through vane	—	40° open	0.010	0.78	0.34
Butterfly valve, swing-through vane	—	30° open	0.005	0.80	0.26
Butterfly valve, fluted vane	—	75° open	0.040	0.70	0.30
Butterfly valve, fluted vane	—	50° open	0.013	0.76	0.19
Butterfly valve, fluted vane	—	30° open	0.007	0.82	0.08
Eccentric rotary plug value	Open	50° open	0.020	0.85	0.42
Eccentric rotary plug value	Open	30° open	0.013	0.91	0.30
Eccentric rotary plug value	Close	50° open	0.021	0.68	0.45
Eccentric rotary plug value	Close	30° open	0.013	0.88	0.30
Ball valve, segmented	Open	60° open	0.018	0.66	0.75
Ball valve, segmented	Open	30° open	0.005	0.82	0.63

[a] D is the internal pipe diameter in mm.

Acoustical Efficiency

At Mach 1 a free jet has an acoustical efficiency $\eta \approx 10^{-4}$. If it is assumed that the sources of valve noise are dipoles and quadrupoles of equal magnitude (5×10^{-5}) at the Mach 1 reference point, then their respective efficiencies are represented by curves A and B in Fig. 15.20, and both curves can be combined to yield a subsonic slope C that originates at 1×10^{-4} and varies as $U^{3.6}$. This curve can be modified further to account for the decrease in $W_{\text{mech strm}}$ ($\propto U^3$) with subsonic velocities, leading to the final curve D for the effective efficiency (i.e., acoustical power coefficient) η_m that varies as $U^{6.6}$ or $(P_1/P_0 - 1)^{2.57}$ when $U \propto (P_1/P_0 - 1)^{0.39}$, P_0 being the static pressure in the vena contracta. This approximation gives satisfactory results for $0.38 \le M \le 1$ (i.e., down to $P_1/P_2 = 1.1$).

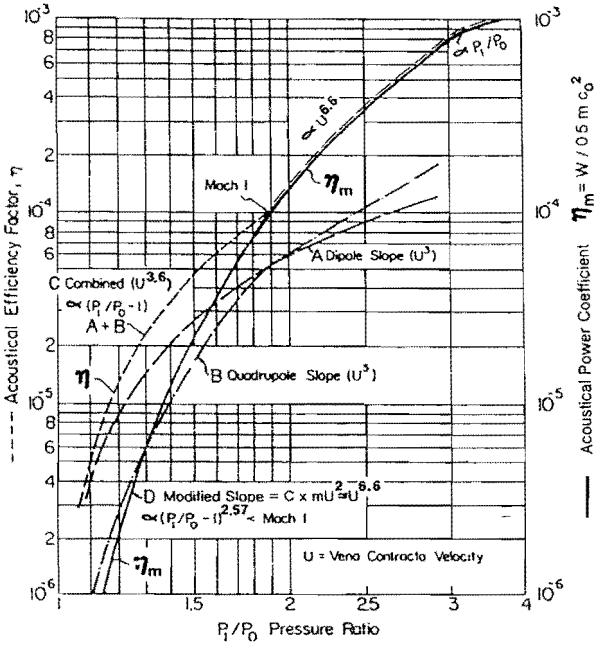


FIGURE 15.20 Slopes of dipole and quadrupole acoustical efficiency curves, assuming each has equal strength at Mach 1; their combined slope and the η_m curve after subtracting the effects of change in mass flow m and orificial velocity U for regions below Mach 1 from the combined curve.

For practical use it is convenient to express η_m in terms of P_1/P_2 = inlet pressure/outlet pressure. The following formulas[28,29] may be used for this purpose:

regime I: $P_1/P_2 < P_1/P_{2\text{critical}}$ (subsonic):

$$\eta_{m\text{I}} = 10^{-4} F_L^2 \left(\frac{P_1 - P_2}{P_1 F_L^2 - P_1 + P_2} \right)^{2.6} \tag{15.51a}$$

regimes II and III: $P_1/P_{2\text{critical}} < P_1/P_2 < 3.2\alpha$:

$$\eta_{m\text{II}} = 10^{-4} F_L^2 \left(\frac{P_1/P_2}{P_1/P_{2\text{critical}}} \right)^{3.7} \tag{15.51b}$$

regime IV: $3.2\alpha < P_1/P_2 < 22\alpha$ ($M_j > 1.4$):

$$\eta_{m\text{IV}} = 1.32 \times 10^{-3} F_L^2 \left(\frac{P_1/P_2}{P_1/P_{2\text{break}}} \right) \tag{15.51c}$$

regime V: $P_1/P_2 > 22\alpha$ (constant efficiency):

$$\eta_{m\text{V}} = \text{maximum value from regime IV} \tag{15.51d}$$

where
$$\alpha = (P_1/P_{2\text{critical}})/1.89$$
$$P_1/P_{2\text{break}} = \alpha\gamma^{\gamma/(\gamma-1)} \text{ at } M = \sqrt{2}$$
$$\gamma = \text{ratio of specific heat of gas}$$
$$P_1/P_{2\text{critical}} = P_1/(P_1 - 0.5 P_1 F_L^2)$$

The values of these parameters may be taken from Table 15.5.

When the downstream piping is straight and there are no sudden changes in cross-sectional area, the highest internal $\frac{1}{3}$-octave band sound pressure level L_{pi} (re 2×10^{-5} Pa) downstream of the valve is given by

$$L_{pi} = -61 + 10 \times \log \frac{\eta_m C_v F_L P_1 P_2 c_0^4 G_f^2}{D_i^2} \quad \text{dB} \tag{15.52}$$

where D_i = internal diameter of downstream pipe, m
G_f = specific gravity of gas relative to air at 20°C
$c_0 = \sqrt{\gamma P_0/\rho_0}$, m/s (speed of sound)
γ = ratio of specific heats
ρ_0 = gas density at vena contracta, kg/m^3

Pipe Transmission Loss Coefficient

Knowledge of the peak internal sound frequency f_p is crucial for a proper prediction of the pipe transmission loss coefficient T_L. The coefficient T_L does not vary significantly between the first cutoff frequency f_0 [see Eq. (15.58)] and the ring frequency f_R of the pipe (see lower curve in Fig. 15.21), but variations can be large at other frequencies. The slope of T_L is about −6 dB per octave below f_0 and +6 dB per octave above f_r.[28]

For Mach numbers in the pipe less than about 0.3 and for relatively heavy pipes (as found in typical process plants) it may be assumed that the *minimum*

TABLE 15.5 Important Pressure Ratios for Air[a]

F_L	0.5	0.6	0.7	0.8	0.9	1.0
P_1/P_2 critical	1.13	1.20	1.30	1.43	1.61	1.89
P_1/P_2 break	1.95	2.07	2.24	2.40	2.76	3.25
α Ratio	0.60	0.64	0.68	0.76	0.85	1.0
22α	13	14	15	16	19	22

Note: P_1/P_0 critical = 1.89.
[a]May be used for other gases with reasonable accuracy.

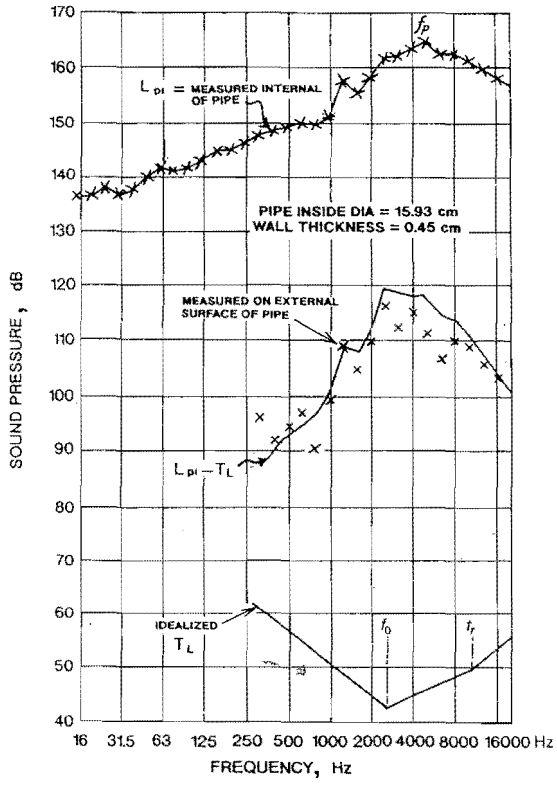


FIGURE 15.21 Test data taken on a 150-mm globe valve showing good agreement using the stated transmission loss equation. Notice the resultant shift in the peak sound frequency (f_p) from ~4.8 kHz inside the pipe to the first cutoff frequency of the pipe (f_0) at 2.5 kHz outside the pipe.

transmission loss occurs at f_0 and is given by[28]

$$T_{Lf_0} = 10 \times \log\left[9 \times 10^6 \frac{r t_p^2}{D_i^3}\left(\frac{P_2}{P_a} + 1\right)\right] \quad \text{dB} \tag{15.53}$$

where r = distance from pipe wall to observer, m
t_p = thickness of pipe wall, m
D_i = internal pipe diameter, m
P_2 = internal static pressure downstream of valve, Pa
P_a = external static pressure at same downstream distance, Pa

Typical values are given in Table 15.6. For fluids with higher sonic velocities and for thinner pipe walls, the minimum value of T_{Lf_0} shifts toward the ring frequency f_R [see Eq. (15.58)].

TABLE 15.6 Minimum Pipe Transmission Loss Coefficient T_{Lf_0}[a]

	Pipe Schedule	
Nominal Pipe Size, m	40	80
0.025	72	76
0.050	65	69
0.080	64	68
0.100	60	64
0.150	57	61
0.200	54	58
0.250	52	57
0.300	51	56
0.400	50	55
0.500	48	53

[a] At 1 m distance from steel pipe (dB) for 200 kPa internal and 100 kPa external air pressure. Pipe schedules per ANSI B36.10.

The total transmission loss coefficient for the valve is now expressed in the form

$$T_L = T_{Lf_0} + \Delta T_{Lf_p} \tag{15.54}$$

where the correction ΔT_{Lf_p} (in decibels) is determined by the peak noise frequency according to

$$\Delta T_{Lf_p} = \begin{cases} 20 \times \log \dfrac{f_0}{f_p} & f_p \le f_0 \\ 13 \times \log \dfrac{f_p}{f_0} & f_p \le 4f_0 \\ 20 \times \log \dfrac{f_p}{4f_0} + 7.8 & f_p > 4f_0 \end{cases} \tag{15.55}$$

The peak frequency is estimated from[29]

$$f_p = \begin{cases} \dfrac{0.2 M_j c_0}{D_j} & M_j < 4 \\ \dfrac{0.28 c_0}{D_j \sqrt{M_j^2 - 1}} & M_j > 4 \end{cases} \tag{15.56}$$

where c_0 = speed of sound at vena contracta, m/s
D_j = jet diameter at valve orifice

and

$$M_j = \left\{\frac{2}{\gamma - 1}\left[\left(\frac{P_1}{\alpha P_2}\right)^{(\gamma-1)/\gamma} - 1\right]\right\}^{1/2} \tag{15.57}$$

$$f_R = \frac{c_L}{\pi D_i} = 4f_0; \quad \text{for steel pipes and air} \quad f_R \approx \frac{5000}{\pi D_i} \tag{15.58}$$

For a gas other than air f_0 must be multiplied by $c_{0,\text{gas}}/c_{0,\text{air}}$.

The diameter D_j is difficult to determine because of the complex flow geometry in many valves. A reasonable approximation is to use the hydraulic diameter D_H as the jet diameter and make use of a valve-style modifier F_d (see Table 15.4) to obtain

$$D_j \approx 4.6 \times 10^{-3} F_d \sqrt{C_v F_L} \quad \text{m} \tag{15.59}$$

This formula is *not* applicable if jet portions combine downstream (usually at higher pressure ratios). This is common with multiple-hole valve cages,[30] short-stroke parabolic valve plugs in the "flow to close" direction, and butterfly valves at larger openings.

The external sound level (measured at 1 m from the wall) is now given by

$$L_a = 5 + L_{pt} - T_L - L_g \quad \text{dBA} \tag{15.60}$$

where L_g is a correction for fluid velocity in the pipe:

$$L_g = -16 \times \log\left(1 - \frac{1.3 \times 10^{-5} P_1 C_v F_L}{D_i^2 P_2}\right) \tag{15.61}$$

The laboratory test data shown in Fig. 15.21, taken with air on a DN150 globe valve, exhibits good agreement between predicted and measured external valve sound levels using T_L calculated from Eq. (15.54). In the absence of unusual phenomena such as jet "screech," Eq. (15.60) is found to be accurate to within ±3 dB assuming that all the valve coefficients are well established.

Accounting for Additional Noise due to High Velocities in Valve Outlet

Gas expanding in volume due to pressure reduction in a valve can cause high valve outlet velocities. These, in turn, can create secondary noise sources in the downstream pipe or pipe expander.[31,32]

The first step is to estimate the valve's outlet velocity (limited to sonic c_2):

$$U_R = 4\frac{m}{\pi \rho_2 (d_i^2)} \tag{15.62}$$

where d_i is the valve diameter in meters.

The internal sound pressure level produced by this velocity is

$$L_{piR} = 65 + 10 \log\left(M_R^3 \frac{W_{mR}}{D_i^2}\right) \tag{15.63}$$

Here

$$W_{mR} = \frac{m}{2} U_R^2 \left[\left(1 - \frac{d_i^2}{D_i^2}\right) + 0.2\right] \tag{15.64}$$

and

$$M_R = \frac{U_R}{c_2} \tag{15.65}$$

Use Eq. (15.60) to calculate the external sound level L_R, substituting L_{piR} for L_{pi}, and using Eq. (15.54) to calculate TL, here substituting f_{pR} for f_p, where

$$f_{pR} = 0.2\frac{U_R}{d_i} \tag{15.66}$$

The combined estimated external sound level at 1 m from the pipe from both the valve and the downstream piping now is

$$L_{ps} = 10 \log(10^{L_a/10} + 10^{L_R/10}) \tag{15.67}$$

The reader in encouraged to review reference 24, which illustrates the use of the prediction procedure in numerous examples.

Methods of Valve Noise Reduction

The two basic variables controlling the valve noise are the jet Mach number M_j and the internal peak frequency f_p. In subsonic flows lower jet velocities can be achieved by use of a valve trim that is less streamlined ($F_L \geq 0.9$, say).

At higher pressure ratios the only remedy is to use orifices or resistance paths in series, so that each operates subsonically. Such a "zig-zag" path valve is shown in Fig. 15.22. For example, for natural gas with an inlet pressure of 10,000 kPa that is to be throttled down to 5000 kPa and assuming a valve pressure recovery factor $F_L = 0.9$, the internal pressure ratio P_1/P_0 for a single-stage reduction would be $P_1/P_2\alpha = 2.35 : 1$. However, using the trim from Fig. 15.22 with 10 reduction steps, the orificial pressure ratio for each step is now only 1.603 : 1 with an acoustical power coefficient of only 1.1×10^{-7}. Ignoring the partial addition of 10 separate power sources, this represents a noise reduction of about 30 dB.

A less costly way to reduce "audible" valve noise is to increase the peak frequency by using multiorifice trim, as shown in Fig. 15.23. The throttling is still single stage, but the jets are divided into a number of parallel ports. This reduces the value of the valve style modifier $F_d \approx 1/\sqrt{n_o}$, where n_o is the number of equally sized parallel ports. Since F_d is proportional to jet diameter D_j, f_p can be shifted to higher levels. Thus if $n_o = 16$, as in Fig. 15.23, $F_d = 0.25$ and f_p is four times higher than for a single orifice ($F_d = 1$) with the same total flow area. If the peak frequency occurs in the mass-controlled region, an overall reduction in the external (audible) sound level of $\Delta T_{Lf_p} = 20 \times \log(f_{p_1}/f_{p_0}) = 20 \times \log(1/0.25) \approx 12$ dB is achieved.

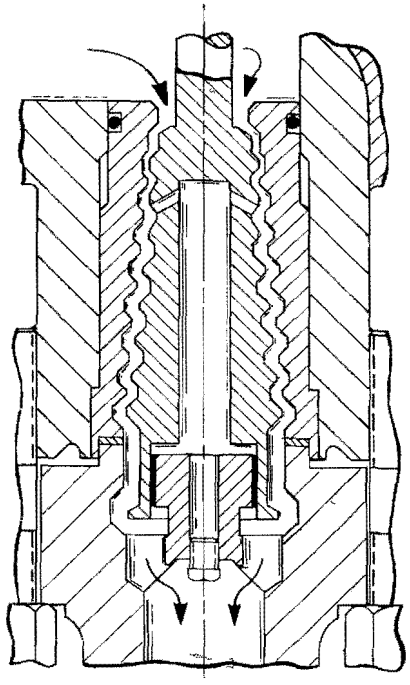


FIGURE 15.22 High-pressure reducing valve using multiple-step trim with a single flow path. Ideally each step will have subsonic orifice velocity.

The beneficial effects of a reduction in velocity combined with higher transmission loss caused by increased frequency are obtained with the elaborate arrangement shown in Fig. 15.24. This combines the multistep and multipath approach by use of a layer of disks having individually cast or etched channels.

A more economical solution is to couple a static downstream pressure-reducing device, such as a multihole restrictor, with a throttling valve with a fluted disk as indicated in Fig. 15.25. The fluted disk generates multiple jets with increased noise frequencies, although most of the energy is converted by the static pressure plate. At maximum design flow the valve is sized to have a low pressure ratio of 1.1 or 1.15 and the remainder of the pressure reduction occurs across the static plate having inherent low-noise throttling due to multistage, multihole design.

The most advanced and most compact form of a low noise valve trim is shown in Fig. 15.26. It consists of identical stamped or cut plates and constitutes a two-stage device, hence the narrow envelope. The device combines a supersonic first stage with a subsonic second stage for lowest overall acoustic efficiency, while retaining the final high frequency peak outlet sound level for high transmission losses.

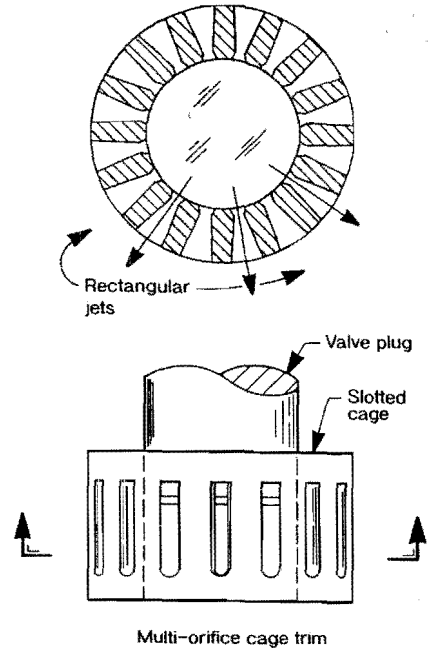


FIGURE 15.23 Slotted valve cage subdivides single-step flow path in 16 separate openings ($F_d = 0.25$) to increase peak frequency and thereby transmission loss.

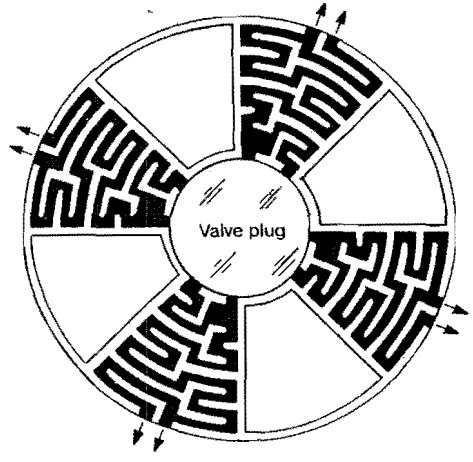


FIGURE 15.24 Labyrinth-type flow path cast or machined into each of a stack of metal plates surrounding a valve plug to provide a combination of multistep and multichannel flow paths in order to reduce throttling velocity and increase peak frequency.

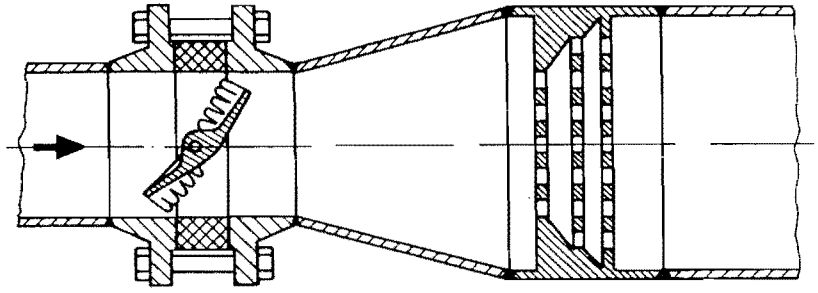


FIGURE 15.25 Modulating fluted butterfly valve cooperates with triple-stage static resistance plate for purposes of pressure reduction. Static plates see 90% of pressure drop at maximum design flow. Balance is handled by the valve.

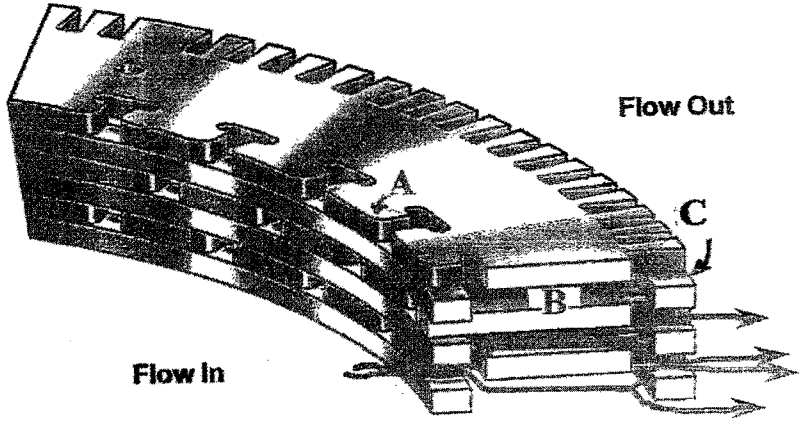


FIGURE 15.26 A stacked trim made from identical plates offers most advanced noise reduction. Here gas enters inlet orifices (A) configured as supersonic diffusers. These orifices convert about 95% of the stream power of the gas through a mechanism of shock waves; the gas then expands into sound-absorbing settling chambers (B) and finally exits the trim through a series of small subsonic passages (C).

Placing a silencer downstream of a valve is not cost effective because a good portion of the sound power travels upstream or radiates through the valve body and actuator, yielding noise reductions that typically do not exceed about 10 dB. Similar remarks apply to acoustical insulation of the pipe wall, where attenuations are limited to about 15 dB. The effectiveness of various abatement procedures is summarized below:

1. One-inch-thick pipe insulation: 5–10-dB reduction
2. Doubling thickness of pipe wall: 6-dB reduction

3. Silencer downstream: 10-dB reduction
4. Silencers upstream and downstream: 20-dB reduction
5. Multiport resistance plate downstream of valve: 15–20-dB reduction (use only 5–10% of valve inlet pressure as valve ΔP at maximum flow)
6. Special low-noise valve: 15–30-dB reduction

ACKNOWLEDGMENT

The authors wish to acknowledge the contribution of Dr. M. H. Howe for the portions of this chapter that have been retained from previous editions of this book.

REFERENCES

1. M. J. Lighthill, "On Sound Generated Aerodynamically. Part I: General Theory," *Proc. Roy. Soc. Lond.*, **A211**, 564–587 (1952).
2. M. S. Howe, "Contributions to the Theory of Aerodynamic Sound with Applications to Excess Jet Noise and the Theory of the Flute," *J. Fluid Mech.*, **71**, 625–673 (1975).
3. Society of Automotive Engineers, *"Gas Turbine Jet Exhaust Noise Prediction,"* Report No. SAE ARP 876C, Society of Automotive Engineers, Warrendale, PA, 1985.
4. J. R. Stone, "Prediction of In-Flight Exhaust Noise for Turbojet and Turbofan Engines," *Noise Control Eng.*, **10**, 40–46 (1977).
5. A. L. Laganelli and H. Wolfe, *"Prediction of Fluctuating Pressure in Attached and Separated Turbulent Boundary Layer Flow,"* Paper 89, American Institute of Aeronautics and Astronautics, Washington, DC, 1989, p. 1064.
6. M. S. Howe, "The Role of Surface Shear Stress Fluctuations in the Generation of Boundary Layer Noise," *J. Sound Vib.*, **65**, 159–164 (1979).
7. M. S. Howe, "Surface Pressures and Sound Produced by Low Mach Number Turbulent Flow over Smooth and Rough Walls," *J. Acoust. Soc. Am.*, **90**, 1041–1047 (1991).
8. D. M. Chase, "The Character of Turbulent Wall Pressure Spectrum at Subconvective Wavenumbers and a Suggested Comprehensive Model," *J. Sound Vib.*, **112**, 125–147 (1987).
9. J. G. Seebold, "Smooth Piping Reduces noise—Fact or Fiction?" *Hydrocarbon Process.*, September 1973, pp. 189–191.
10. D. A. Bies, *"A Review of Flight and Wind Tunnel Measurements of Boundary Layer Pressure Fluctuations and Induced Structural Response,"* NASA CR-626, NASA Langley Research Center, Hampton, VA, May 1966.
11. D. A. Nelson, *Reduced-Noise Gas Flow Design Guide*, NASA Glenn Research Center, Cleveland, OH, April 1999.
12. H. H. Heller and S. E. Widnall, "Sound Radiation from Rigid Flow Spoilers Correlated with Fluctuating Forces," *J. Acoust. Soc. Am.*, **47**, 924–936 (1970).
13. P. A. Nelson and C. L. Morfey, "Aerodynamic Sound Production in Low Speed Flow Ducts," *J. Sound Vib.*, **79**, 263–289 (1981).

14. M. Hubert, "Untersuchungen ueber Geraeusche durchstroemter Gitter," Ph.D. Thesis, Technical University of Berlin, 1970.
15. M. S. Howe, "The Influence of Vortex Shedding on the Generation of Sound by Convected Turbulence," *J. Fluid Mech.*, **76**, 711–740 (1976).
16. W. K. Blake, *Mechanics of Flow-Induced Sound and Vibration*, Vol. 2: *Complex Flow-Structure Interactions*, Academic, New York, 1986.
17. T. F. Brooks, D. S. Pope, and M. A. Marcolini, *"Airfoil Self-Noise and Prediction,"* NASA Reference Publication No. 1218, NASA Langley Research Center, Hampton, VA, 1989.
18. J. E. Rossiter, *"Wind Tunnel Experiments on the Flow over Rectangular Cavities at Subsonic and Transonic Speeds,"* RAE TR 64037, Royal Aircraft Establishment, Farnsborough, U.K., 1964.
19. P. J. W. Block, *"Noise Response of Cavities of Varying Dimensions at Subsonic Speeds,"* Technical Paper D-8351, NASA Langley Research Center, Hampton, VA, 1976.
20. L. F. East, "Aerodynamically Induced Resonance in Rectangular Cavities," *J. Sound Vib.*, **3**(3), 277–287 (1966).
21. M. J. Lucas, "Impinging Shear Layers," in M. J. Lucas et al., *Handbook of the Acoustic Characteristics of Turbomachinery Cavities*, American Society of Mechanical Engineers, New York, 1997, pp. 205–241.
22. M. C. Junger, "Cavity Resonators," in M. J. Lucas et al., *Handbook of the Acoustic Characteristics of Turbomachinery Cavities*, American Society of Mechanical Engineers, New York, 1997, pp. 13–38.
23. R. L. Panton and J. M. Miller, "Excitation of a Helmholtz Resonator by a Turbulent Boundary Layer," *J. Acoust. Soc. Am.*, **58**, 533–544 (1975).
24. IEC 60534-8-3, *"Control Valve Aerodynamic Noise Prediction Method,"* International Electrical Commission, Geneva, Switzerland, 2000.
25. V. A. Carucci and R. T. Mueller, *"Acoustically Induced Piping Vibration in High Capacity Pressure Reducing Systems,"* Paper No. 82-WA/PVP-8, American Society of Mechanical Engineers, New York, 1982.
26. H. D. Baumann, *"On the Prediction of Aerodynamically Created Sound Pressure Level of Control Valves,"* Paper No. WA/FE-28, American Society of Mechanical Engineers, New York, 1970.
27. ANSI/ISA S75.01-1985, *"Flow Equations for Sizing Control Valves,"* Instrument Society of America, Research Triangle Park, NC, 1985.
28. ANSI/ISA S75.17, *"Control Valve Aerodynamic Valve Noise Prediction,"* Instrument Society of America, Research Triangle Park, NC, 1989.
29. H. D. Baumann, *"A Method for Predicting Aerodynamic Valve Noise Based on Modified Free Jet Noise Theories,"* Paper No. 87-WA/NCA-7, American Society of Mechanical Engineers, New York, 1987.
30. C. Reed, "Optimizing Valve Jet Size and Spacing Reduces Valve Noise," *Control Eng.*, **9**, 63–64 (1976).
31. H. D. Baumann, "Predicting Control Valve Noise at High Exit Velocities," *INTECH*, February 1997, pp. 56–59.

CHAPTER 16

Prediction of Machinery Noise

ERIC W. WOOD AND JAMES D. BARNES

Acentech, Inc.
Cambridge, Massachusetts

Engineering information and prediction procedures are presented describing the sound power emission characteristics of various industrial machinery. The types of equipment addressed in this chapter include air compressors, boilers, coal-handling equipment, cooling towers, air-cooled condensers, diesel-engine-powered equipment, fans, feed pumps, gas turbines, steam turbines, steam vents, transformers, and wind turbines. The information has been extracted from consulting project files and the results of field measurement programs. The machinery noise prediction procedures are based on studies of empirical field data sponsored by numerous clients, including the Edison Electric Institute and the Empire State Electric Energy Research Corporation, for whom references 1–3 were prepared with the authors' colleagues: Robert M. Hoover, Laymon N. Miller, Susan L. Patterson, Anthony R. Thompson, and István L. Vér.

Characteristics identified and described for the noise produced by the machines discussed in this chapter include the estimated overall, A-weighted, and octave-band sound power levels (L_w) in dB re 1 pW, general directivity and tonal characteristics observed in the far field of the source, and temporal characteristics associated with the source operation. In addition, noise abatement concepts that have proven to be useful to the authors during previous consulting projects are described briefly. Successful noise control treatments often require a detailed understanding of site-specific operating and maintenance requirements as well as pertinent acoustical conditions at the site. We suggest that acoustical design handbooks or experienced acoustical engineering professionals be consulted when guidance is needed for specific design applications.

The information and procedures presented here can be used for numerous engineering applications requiring predictions of the approximate acoustical characteristics of new machinery installations and estimates of the noise attenuation that may be needed to meet local requirements. The prediction procedures are expected to provide A-weighted sound-power-level estimates that are generally accurate to within about ±3 dB. Individual octave-band sound-power-level estimates will necessarily be somewhat less accurate than A-weighted

14. M. Hubert, "Untersuchungen ueber Geraeusche durchstroemter Gitter," Ph.D. Thesis, Technical University of Berlin, 1970.
15. M. S. Howe, "The Influence of Vortex Shedding on the Generation of Sound by Convected Turbulence," *J. Fluid Mech.*, **76**, 711–740 (1976).
16. W. K. Blake, *Mechanics of Flow-Induced Sound and Vibration*, Vol. 2: *Complex Flow-Structure Interactions*, Academic, New York, 1986.
17. T. F. Brooks, D. S. Pope, and M. A. Marcolini, *"Airfoil Self-Noise and Prediction,"* NASA Reference Publication No. 1218, NASA Langley Research Center, Hampton, VA, 1989.
18. J. E. Rossiter, *"Wind Tunnel Experiments on the Flow over Rectangular Cavities at Subsonic and Transonic Speeds,"* RAE TR 64037, Royal Aircraft Establishment, Farnsborough, U.K., 1964.
19. P. J. W. Block, *"Noise Response of Cavities of Varying Dimensions at Subsonic Speeds,"* Technical Paper D-8351, NASA Langley Research Center, Hampton, VA, 1976.
20. L. F. East, "Aerodynamically Induced Resonance in Rectangular Cavities," *J. Sound Vib.*, **3**(3), 277–287 (1966).
21. M. J. Lucas, "Impinging Shear Layers," in M. J. Lucas et al., *Handbook of the Acoustic Characteristics of Turbomachinery Cavities*, American Society of Mechanical Engineers, New York, 1997, pp. 205–241.
22. M. C. Junger, "Cavity Resonators," in M. J. Lucas et al., *Handbook of the Acoustic Characteristics of Turbomachinery Cavities*, American Society of Mechanical Engineers, New York, 1997, pp. 13–38.
23. R. L. Panton and J. M. Miller, "Excitation of a Helmholtz Resonator by a Turbulent Boundary Layer," *J. Acoust. Soc. Am.*, **58**, 533–544 (1975).
24. IEC 60534-8-3, *"Control Valve Aerodynamic Noise Prediction Method,"* International Electrical Commission, Geneva, Switzerland, 2000.
25. V. A. Carucci and R. T. Mueller, *"Acoustically Induced Piping Vibration in High Capacity Pressure Reducing Systems,"* Paper No. 82-WA/PVP-8, American Society of Mechanical Engineers, New York, 1982.
26. H. D. Baumann, *"On the Prediction of Aerodynamically Created Sound Pressure Level of Control Valves,"* Paper No. WA/FE-28, American Society of Mechanical Engineers, New York, 1970.
27. ANSI/ISA S75.01-1985, *"Flow Equations for Sizing Control Valves,"* Instrument Society of America, Research Triangle Park, NC, 1985.
28. ANSI/ISA S75.17, *"Control Valve Aerodynamic Valve Noise Prediction,"* Instrument Society of America, Research Triangle Park, NC, 1989.
29. H. D. Baumann, *"A Method for Predicting Aerodynamic Valve Noise Based on Modified Free Jet Noise Theories,"* Paper No. 87-WA/NCA-7, American Society of Mechanical Engineers, New York, 1987.
30. C. Reed, "Optimizing Valve Jet Size and Spacing Reduces Valve Noise," *Control Eng.*, **9**, 63–64 (1976).
31. H. D. Baumann, "Predicting Control Valve Noise at High Exit Velocities," *INTECH*, February 1997, pp. 56–59.

CHAPTER 16

Prediction of Machinery Noise

ERIC W. WOOD AND JAMES D. BARNES

Acentech, Inc.
Cambridge, Massachusetts

Engineering information and prediction procedures are presented describing the sound power emission characteristics of various industrial machinery. The types of equipment addressed in this chapter include air compressors, boilers, coal-handling equipment, cooling towers, air-cooled condensers, diesel-engine-powered equipment, fans, feed pumps, gas turbines, steam turbines, steam vents, transformers, and wind turbines. The information has been extracted from consulting project files and the results of field measurement programs. The machinery noise prediction procedures are based on studies of empirical field data sponsored by numerous clients, including the Edison Electric Institute and the Empire State Electric Energy Research Corporation, for whom references 1–3 were prepared with the authors' colleagues: Robert M. Hoover, Laymon N. Miller, Susan L. Patterson, Anthony R. Thompson, and István L. Vér.

Characteristics identified and described for the noise produced by the machines discussed in this chapter include the estimated overall, A-weighted, and octave-band sound power levels (L_w) in dB re 1 pW, general directivity and tonal characteristics observed in the far field of the source, and temporal characteristics associated with the source operation. In addition, noise abatement concepts that have proven to be useful to the authors during previous consulting projects are described briefly. Successful noise control treatments often require a detailed understanding of site-specific operating and maintenance requirements as well as pertinent acoustical conditions at the site. We suggest that acoustical design handbooks or experienced acoustical engineering professionals be consulted when guidance is needed for specific design applications.

The information and procedures presented here can be used for numerous engineering applications requiring predictions of the approximate acoustical characteristics of new machinery installations and estimates of the noise attenuation that may be needed to meet local requirements. The prediction procedures are expected to provide A-weighted sound-power-level estimates that are generally accurate to within about ±3 dB. Individual octave-band sound-power-level estimates will necessarily be somewhat less accurate than A-weighted

sound-power-level estimates. The prediction procedures estimate the equivalent (energy average) L_{eq} sound power level during operation of one machine. For equipment with intermittent operating cycles, the estimated sound power levels may be reduced by 10 log (operating cycle) if long-term equivalent values are required. When several identical machines are operating simultaneously, the sound power levels can be increased by 10 log (number of machines). When equipment is located within a large plant, other nearby large equipment may provide some shielding that will reduce the noise radiated to distant neighbors in shielded directions (see Chapter 7). When equipment is located within an enclosed plant, a portion of the acoustical energy will be dissipated inside the plant, leading to further reductions in the far-field noise. One should note that doors, windows, and ventilation openings can substantially diminish the acoustical performance (composite sound transmission loss) of building exterior walls (see Chapter 12).

The reader should try to obtain actual field data and/or manufacturers' information whenever possible for machines being studied. Information about the noise produced by gas flows and fans in buildings is presented in Chapters 15 and 17. Noise abatement information is provided in several other chapters. Indoor sound field characteristics are described in Chapters 6 and 7, and outdoor sound propagation is discussed in Chapter 5. The noise emission information provided in this chapter is representative of equipment presently available in the United States. Equipment in use in other countries may produce noise levels that are somewhat different than presented here. Prediction formulas for the overall sound power level are provided in the text of this chapter. Adjustments to predict the A-weighted and octave-band sound power levels are provided in Table 16.1.

16.1 AIR COMPRESSORS

The noise produced by air compressors is radiated from the filtered air inlet, the compressor casing, the interconnected piping and interstage cooler, as well as the motor or engine used to drive the compressor. The noise produced by air compressors can exhibit a distinctive duty cycle based on the demand for compressed air and is generally considered omnidirectional and broadband and absent prominent discrete tones. The air inlet noise of certain vacuum pumps sometimes includes high levels of low-frequency pulsating noise.

Noise-estimating procedures presented in this section are applicable to conventional industrial-, utility-, and construction-type air compressors without special noise abatement packages. Air compressors are often available from their manufacturer with special noise abatement packages that include various types of inlet mufflers, laggings, insulations, and enclosures that provide varying degrees of noise reduction. Acoustical data for these low-noise compressors should be obtained directly from the manufacturer's literature.

TABLE 16.1 Adjustments Used to Estimate A-Weighted and Octave-Band L_w[a]

Line	Equipment[b]	A-Weighted	31.5	63	125	250	500	1000	2000	4000	8000
1	RR compressor	2	11	15	10	11	13	10	5	8	15
2	C Compressor case	2	10	10	11	13	13	11	7	8	12
3	C Compressor inlet	0	18	16	14	10	8	6	5	10	16
4	S boilers	9	6	6	7	9	12	15	18	21	24
5	L boilers	12	4	5	10	16	17	19	21	21	21
6	CC shakers	9	5	6	7	9	12	15	18	21	24
7	R car open	12	4	5	10	13	17	19	21	21	21
8	R car enclosed	10	3	5	11	14	14	14	18	19	19
9	BL unloaders	9	8	5	8	10	12	13	18	23	27
10	CS unloaders	11	3	8	12	14	14	16	19	21	25
11	Coal crushers	9	6	6	6	10	12	15	17	21	30
12	T towers	7	7	7	7	9	11	12	14	20	27
13	C mill (13–36)	5			4	6	8	11	13	15	
14	C mill (37–55)	5			6	7	4	11	14	17	
15	ND C towers	0			12	13	11	9	7	5	7
16	MD C towers	10	9	6	6	9	12	16	19	22	30
17	MD C towers 1/2S	5	9	6	6	10	10	11	11	14	20
18	A-C condenser	12	5	6	6	10	14	17	24	29	34
19	D engine	5		11	6	3	8	10	13	19	25
20	C fan I + O	5	11	9	7	8	9	9	13	17	24
21	C fan case	13	3	6	7	11	16	18	22	26	33
22	R fan case	12	10	7	4	7	18	20	25	27	31
23	Axial fan	3	11	10	9	8	8	8	10	14	15
24	S Fd pumps	4	11	5	7	8	9	10	11	12	16
25	L Fd pumps	1	19	13	15	11	5	5	7	19	23
26	C-C plant	11	7	3	7	13	15	17	19	23	21
27	S St turbines	5	11	7	6	9	10	10	12	13	17
28	L St turbines	12	9	3	5	10	14	18	21	29	35
29	SL blow-out	11		2	6	14	17	17	21	18	18
30	Transformers	0		−3	−5	0	0	6	11	16	23

[a] Subtract values shown from estimated overall L_w, except for transformers, subtract values from A-weighted sound level.

[b] RR: rotary and reciprocating; C: casing; S: small, L: large, CC: coal car; R: rotary car dumpers; BL: bucket ladder; CS: clamshell; T: transfer; C. coal; ND C: natural-draft cooling; MD C: mechanical-draft cooling; A-C: air cooled; D: diesel; C-C plant: inside combined-cycle power plant main building; SL: steam line.

The overall sound power level radiated by the casing and air inlet of rotary and reciprocating air compressors can be estimated using Eq. (16.1) (see also line 1 of Table 16.1). These relations for rotary and reciprocating compressors assume that the air inlet is equipped with a filter and small muffler as normally provided by the manufacturer:

$$\text{Rotary and reciprocating compressor, overall } L_w = 90 + 10 \log(\text{kW}) \quad \text{(dB)} \tag{16.1}$$

where kW is the shaft power in kilowatts. The casing and unmuffled air inlet overall sound power levels for centrifugal air compressors in the power range of 1100–3700 kW can be estimated using Eqs. (16.2) and (16.3) (see also lines 2

and 3 of Table 16.1). The insertion loss of any muffler installed at the air inlet should be deducted from the calculated inlet power levels:

$$\text{Centrifugal compressor casing, overall } L_w = 79 + 10 \log(\text{kW}) \quad \text{(dB)} \quad (16.2)$$

$$\text{Centrifugal compressor inlet, overall } L_w = 80 + 10 \log(\text{kW}) \quad \text{(dB)} \quad (16.3)$$

The term $\log(x)$ represents the common logarithm to base 10 of the value of x.

Equations (16.2) and (16.3) do not include the noise radiated by the motor or engine used to drive the compressor. Sound power levels calculated for the driving equipment should be added to the calculated sound power levels for the compressor.

Mufflers, laggings, barriers, and enclosures have all been used with varying degrees of success to control the noise radiated from compressors to nearby workspaces or neighborhoods. However, it is suggested that it is often most practical to specify and purchase a reduced-noise compressor from the manufacturer.

16.2 BOILERS

Two procedures are provided to predict the noise from boilers; one is for relatively small boilers in the range of about 50–2000 boiler horsepower (one boiler horsepower equals 15 kg of steam per hour). Another procedure is provided for large boilers of the type that serve electric-power-generating stations in the range of 100–1000 megawatts (MWe).

Small Boilers

The sound power output of small boilers is only weakly related to the thermal rating of the boiler. The combustion air fans and the burners probably radiate more noise than do the insulated sidewalls of small boilers. The overall sound power level of small boilers can be estimated using Eq. (16.4) (also see line 4 of Table 16.1):

$$\text{Small boiler, overall } L_w = 95 + 4 \log(\text{bhp}) \quad \text{(dB)} \quad (16.4)$$

Large Boilers

Noise levels measured in work spaces adjacent to large central-station boilers that are not enclosed in a building (open boilers) are often in the range of 80–85 dBA at the lower half and 70–80 dBA at the upper half of the boiler. Noise levels measured in the vicinity of enclosed boilers (generally found in areas with cold climates) are often about 5 dBA higher. The overall sound power output of large central-station boilers can be estimated by the relation given in Eq. (16.5) (also see line 5 of Table 16.1):

$$\text{Large boiler, overall } L_w = 84 + 15 \log(\text{MWe}) \quad \text{(dB)} \quad (16.5)$$

The noise from boilers is essentially omnidirectional and broadband in character. However, the combustion air or forced-draft fans, induced-draft fans, gas recirculation fans, overfire air fans, and drive motors sometimes produce tonal noise and may increase the noise levels on their side of the boiler. A small number of boilers have also been found to exhibit a strong discrete tone, usually at a frequency between about 20 and 100 Hz during operation at particular boiler loads. This can be caused by vortex shedding from heat exchanger tubes that excite an acoustical resonance within the boiler that in turn causes coherent (rather than random) vortex shedding to occur at a boiler resonance frequency. The low-frequency tonal noise that radiates from the boiler sidewalls has caused strong adverse reactions from residential neighbors. Boiler operators have also expressed concern about possible fatigue failure of vibrating tube sheets. Installation of one or more large metal plates to subdivide the interior of the boiler volume and thereby change its resonance frequency has successfully corrected this problem. Additional information about this resonant condition and its control is provided in references 4 and 5.

The typical broadband noise radiated by boiler sidewalls has been successfully reduced with the use of a well-insulated exterior enclosure, which also serves as weather protection for equipment and workers. The noise produced by fans serving the boiler can also be controlled as described in Section 16.6.

16.3 COAL-HANDLING EQUIPMENT

A wide variety of noise-producing equipment, such as railcar, ship and barge unloaders, transfer towers, conveyors, crushers, and mills, are used to unload, transport, and condition coal for use at large industrial and utility boilers. The results of numerous noise-level surveys have been studied and condensed to prepare the following general noise prediction procedures for this equipment.

Coal Car Shakers

Coal car shakers vibrate coal cars during bottom unloading. The unloading operation of each car often occurs for about 2–5 min when the coal is not frozen. When frozen coal is located in the car, the shake-out operation can last for up to 10 min or longer. Car shakers are often located inside a sheet metal or masonry building with little or no interior insulation for sound absorption. Shaker buildings include large openings at both ends and sometimes smaller openings and windows along the sidewalls. They also include dust collection and ventilation systems with fans that produce noise. The overall sound power produced during a coal car shake-out can be estimated using the following relation (also see line 6 of Table 16.1):

$$\text{Coal car shake-out, overall } L_w = 141 \text{ dB} \quad (16.6)$$

Noise produced by the dust collection and ventilation fans can be estimated using the relations provided in Section 16.6 and in Chapter 17.

The far-field noise produced by car shake-outs can be reduced by enclosing the operation inside a metal or masonry building or by reducing the openings in any existing building. In addition, modern car-shaking equipment is sometimes available that produces measured A-weighted sound levels about 10 dB lower than are estimated with Eq. (16.6). Careful train movements can reduce the impact noise associated with indexing the train through the shaker operation. Limiting the shake-out operation to daytime hours also reduces the community noise impacts.

Rotary Car Dumpers

Rotary car dumpers are often used to unload long unit trains equipped with special rotary couplings. It typically takes 2–3 min to unload unfrozen coal from each car. A 100-car unit train can be unloaded in about 3–5 h unless delays are encountered. The overall sound power produced during rotary car unloading cycles can be estimated using Eqs. (16.7) and (16.8) for open and enclosed facilities (also see lines 7 and 8 of Table 16.1). However, short-duration impact sounds can be as much as 10–25 dB greater than the equivalent values given by these relations:

$$\text{Rotary car open unloading, overall } L_w = 131 \text{ dB} \tag{16.7}$$

$$\text{Rotary car enclosed unloading, overall } L_w = 121 \text{ dB} \tag{16.8}$$

Noise abatement methods for rotary car dumpers are similar to those discussed previously for car shakers.

Bucket Ladder and Clamshell Bucket Unloaders

Bucket ladder and clamshell bucket unloaders are often used to unload coal delivered by ship or barge. This equipment is located outdoors along the dock line with the electric motors and speed reduction gears often inside metal enclosures for weather protection. Acoustical data studied to prepare the prediction relations provided here were obtained at bucket ladder unloaders with free-digging rates in the range of 1800–4500 metric tons per hour and clamshell unloaders with free-digging rates in the range of 1600–1800 metric tons per hour. The energy-averaged overall sound power level produced during operation of bucket ladder and clamshell bucket unloaders can be estimated using Eqs. (16.9) and (16.10) (see also lines 9 and 10 of Table 16.1):

$$\text{Bucket ladder unloader, overall } L_w = 123 \text{ dB} \tag{16.9}$$

$$\text{Clamshell bucket unloader, overall } L_w = 131 \text{ dB} \tag{16.10}$$

Noise control treatments for bucket ladder and clamshell bucket unloaders generally employ insulated enclosures for the drive equipment and limiting unloading operations to daytime hours.

Coal Crushers

Coal is sometimes conveyed to a crusher building where the chunks are reduced in size in preparation for firing in a power plant boiler. Noise produced during crushing operations is a composite of the crusher, metal chutes, conveyors, drive motors, and speed reducers. Coal crushing is usually an intermittent operation and the noise is often omnidirectional without major tonal components. The overall sound power level produced during operation of the crusher can be estimated in accordance with the following relation (also see line 11 of Table 16.1):

$$\text{Coal crusher, overall } L_w = 127 \text{ dB} \tag{16.11}$$

The far-field noise associated with coal-crushing operations can be reduced by using a well-insulated and ventilated building to enclose the operation.

Coal Transfer Towers

Transfer towers reload coal from one conveyor to another as the coal is relocated within the coal yard on its way to the plant. Transfer tower noise is comprised of coal impacts, local conveyors, drive motors, and dust collection and ventilation system fans. Coal transfer is usually an intermittent operation, and the noise is often omnidirectional without major tonal components. The overall sound power level produced during coal transfer in open buildings can be estimated in accordance with the following relation (also see line 12 of Table 16.1):

$$\text{Transfer tower, overall } L_w = 123 \text{ dB} \tag{16.12}$$

Coal transfer operations can be enclosed in a well-ventilated building to reduce the far-field community noise. In this case, the estimated far-field noise can be mitigated by the composite sound transmission loss of the exterior building walls. Fan noise associated with the ventilation system should be estimated with the relations given in Section 16.6 or Chapter 17.

Coal Mills and Pulverizers

Coal mills and pulverizers crush and size coal in preparation for burning in a boiler. The resulting noise is associated with internal impacts, drive motors, speed reducers, and fans. The noise is essentially broadband, omnidirectional, reasonably steady, and continuous while the plant is operating. The overall sound power level produced by a coal mill in a building with large openings can be estimated in accordance with the following relations for mills in the size ranges of 13–36 and 37–55 metric tons per hour (also see lines 13 and 14 of Table 16.1). When coal mills are located in a closed building, the estimated far-field noise can be reduced by the composite sound transmission loss of the exterior building walls:

$$\text{Coal mill, overall } L_w = \begin{cases} 110 \text{ dB} & 13\text{–}36 \text{ metric tons per hour} \quad (16.13) \\ 112 \text{ dB} & 37\text{–}55 \text{ metric tons per hour} \quad (16.14) \end{cases}$$

16.4 COOLING TOWERS

The sound power output of wet cooling towers is caused primarily by the water splash in the fill and in the basin as well as by the fans, motors, and gears used to provide draft in mechanical towers. The noise is usually continuous and somewhat directive for rectangular towers. The noise produced by a specific pair of large natural-draft hyperbolic cooling towers has been observed to include a modest low-frequency discrete tone associated with aerodynamic vortex shedding at the base of each tower.

Methods that can be used to estimate the sound power output of natural-draft and mechanical induced-draft cooling towers are provided below. Major tower manufacturers can provide additional useful information regarding noise estimates and noise abatement.

Natural-Draft Cooling Towers

The overall sound power radiated from the rim of large hyperbolic natural-draft wet cooling towers can be estimated with Eq. (16.15) (see line 15 in Table 16.1). Noise radiated by the top of the tower is usually not significant at ground elevations compared to the rim-radiated noise:

$$\text{Natural-draft cooling tower rim, overall } L_w = 86 + 10 \log Q \quad \text{(dB)} \tag{16.15}$$

where Q is the water flow rate in gallons per minute (one cubic meter per minute is equal to 264 U.S. gallons per minute).

Inlet mufflers and fan assistance have been installed to control rim-radiated noise for hyperbolic cooling towers in Europe when located near residential neighbors. However, noise abatement is expensive and not common for large hyperbolic towers.

Mechanical Induced-Draft Cooling Towers

The sound power produced by mechanical induced-draft wet cooling towers operating at full fan speed and at half fan speed can be estimated using the following relations (also see lines 16 and 17 of Table 16.1):

Mechanical-draft tower full speed, overall

$$L_w = 96 + 10 \log(\text{fan kW}) \quad \text{(dB)} \tag{16.16}$$

Mechanical-draft tower half speed, overall

$$L_w = 88 + 10 \log(\text{fan kW}) \quad \text{(dB)} \tag{16.17}$$

where kW is the full-speed fan power rating in kilowatts for both relations.

The above relations apply in all horizontal directions from round towers and most directions away from the inlet face of rectangular towers. For directions away from the enclosed ends of rectangular towers, the far-field noise is several decibels less than estimated above due to the effects of shielding by the solid closed ends. For a line of as many as 6–10 rectangular towers, the far-field noise from the enclosed ends could be as much as 5–6 dB less than estimated, based on omnidirectional radiation using Eqs. (16.16) and (16.17).

Reduced fan speed is a common method used to mitigate the noise from mechanical-draft cooling towers during evening and nighttime hours when excess cooling capacity may be available due to reduced ambient air temperatures. In multiple-cell tower installations, it is preferable to reduce the fan speed for all cells rather than to shut down unneeded cells; the fans' speeds should be properly selected to avoid introducing a strong acoustical beat. Another common noise control method is to install wide-chord high-efficiency fan blades that can provide the necessary fan performance at reduced speeds. In addition, mechanical-draft towers with centrifugal fans may be selected because they can sometimes be designed to produce less noise than towers with propeller fans, although at some energy cost. Mufflers have also been installed at the air inlet and discharge to reduce both the fan and water noise. However, the mufflers must be protected from the wet environment, can become coated with ice during freezing weather, and introduce an additional aerodynamic restriction that must be overcome by the fan. Barrier walls and partial enclosures have successfully shielded neighbors from cooling-tower noise; however, barrier walls that avoid excessive restrictions to the airflow often limit their acoustical benefit for protecting far-field locations.

16.5 AIR-COOLED CONDENSERS

The sound power output of air-cooled condensers (dry cooling systems) is caused primarily by the fans used to move air across the condenser with some additional noise contribution from the motors and gears. The noise is usually continuous and somewhat directive for rectangular installations. The sound power output of dry air-cooled condensers does not, of course, include the water splash noise associated with wet cooling towers.

The need to reduce water consumption is causing the increasing trend to install air-cooled condensers even at large industrial facilities. When installed at a moderate to large new combined-cycle power plant, the fans for the forced-draft air-cooled condenser can contribute approximately the same sound power output as the balance of equipment at the plant. Fortunately, low-noise fans are now readily available for air-cooled condensers that produce comparable airflow rates and 3–6 dBA less noise than do conventional fans. These low-noise fans include high-efficiency wide-chord blades operating at reduced tip speeds. For some installations, noise reductions greater than 6 dBA can be available.

To avoid water consumption, power consumption, and fan noise generation, air-cooled systems are installed in hyperbolic natural-draft towers.

The sound power produced by air-cooled condensers with low-noise fans operating at full speed can be estimated using the following relation (also see line 18 of Table 16.1):

$$\text{Air-cooled condenser full speed, overall } L_w = 84 + 10 \log(\text{fan kW}) \quad \text{(dB)} \quad (16.18)$$

where kW is the full-speed fan power rating in kilowatts.

The above relation applies in all horizontal directions from a low-noise unit; a standard unit will produce greater noise. It is suggested that fan- and air-cooled condenser manufacturers be contacted to obtain useful information regarding noise estimates and noise abatement for specific applications. See also references 6 and 7 for information about air-cooled condenser noise generation and propagation. Summary comparisons of the operating performance of wet, dry, and parallel condensing systems are provided in reference 8.

16.6 DIESEL-ENGINE-POWERED EQUIPMENT

When machinery such as compressors, generators, pumps, and construction equipment is powered by a diesel engine, it is usually the diesel engine that is the dominant noise source.

Mobile construction and coal yard equipment powered by diesel engines, such as dozers, loaders, and scrapers, often produces in-cab A-weighted noise levels as high as 95–105 dB. Methods to retrofit and reduce in-cab noise levels for several loaders and dozers have been developed, field tested, and documented in references 9 and 10. Well-designed cabs and noise control features are now often available from major manufacturers when purchasing new diesel-engine-powered mobile equipment.

A simple relation for estimating the maximum exterior overall sound power level for naturally aspirated and turbocharged diesel engines used to power equipment is provided in Eq. (16.19) (also see line 19 in Table 16.1):

$$\text{Diesel engine equipment, overall } L_w = 99 + 10 \log(\text{kW}) \quad \text{(dB)} \quad (16.19)$$

The above relation assumes that the engine has a conventional exhaust muffler in good working condition as typically provided by the engine manufacturer and further assumes that the engine is operating at rated speed and power. Noise associated with material impacts during equipment operation is not included.

Equipment used on construction sites often operates at part power. Measurements obtained at the operating equipment indicate that work-shift-long equivalent L_{eq} sound levels are therefore typically about 2–15 dB less than the maximum values provided by Eq. (16.19). It is assumed that the following values could be subtracted from the Eq. (16.19) maximum levels to obtain work-shift-long equivalent L_{eq} levels. When project-long equivalent L_{eq} levels are required, the estimated values can be further reduced to account for the percentage of time

that the equipment will actually operate on the construction site [10 log(operating time/project time)]:

3–4 dB	Backhoes, rollers
5–6 dB	Dozers, graders, haulers, loaders, scrapers
7–8 dB	Air compressors, concrete batch plants, mobile cranes, trucks
12–13 dB	Derrick cranes, paging systems

When stationary diesel-engine-driven equipment is located inside masonry or metal buildings, it is necessary to consider the sound power radiated by the engine inlet, the engine casing, the engine exhaust, and the engine cooling fan as well as the driven equipment. It is also necessary to account for the attenuation expected from the building walls and openings, the inlet filter/muffler, the exhaust muffler, and mufflers to be installed at building openings that serve ventilation and cooling systems. Additional information about the propagation of noise from equipment located inside buildings and about muffler systems is provided in Chapters 9 and 17.

16.7 INDUSTRIAL FANS

The noise produced by industrial fans is caused by the dynamic interaction of the gas flow with rotating and stationary surfaces of the fan. Noise produced by shear flow is usually not considered important. Broadband fan noise results from the random aerodynamic interactions between the fan and the gas flow. The prominent discrete tones produced by centrifugal fans result from the periodic interaction of the outlet flow and the cutoff located directly downstream of the blade trailing edges. Tonal noise produced by axial-flow fans results from periodic interactions between distorted inflow and the rotor blades as well as the rotor wakes and nearby downstream surfaces, including struts and guidevanes. This tonal noise is usually most prominent at the harmonics of the passing frequency of the fan blade (number of blades times the rotation rate in revolutions per second). Detailed information about the noise associated with gas flows and fans is provided in Chapters 15 and 17.

The noise produced by new forced-draft fans can be controlled most easily with the use of ducted and muffled inlets. Sometimes the ducted inlet is extended to a location in the plant where warm air is available and additional ventilation is needed. To provide further noise reduction, acoustical insulation lagging should be considered for the inlet and outlet ducts and the fan housing. Open-inlet forced-draft fans can be located within an acoustically treated fan room that contains the fan and its noise. However, workers inside the fan room during inspections and maintenance will be exposed to high levels of fan noise and should wear ear protection.

Discharge noise of large induced-draft fans radiated from the top of the stack to residential neighbors has caused serious community noise problems. The fan and duct system design should include provisions to control this noise if residential

areas are located within $\frac{1}{2}$–1 mile of the plant. Mufflers used for induced-draft fan service at boilers and furnaces should be of the dissipative, parallel-baffle, open-cavity type tuned to the harmonics of fan blade passing frequency. These mufflers are built to avoid fly-ash clogging and include erosion protection to ensure adequate long-term performance. They can usually be designed to introduce a pressure loss in the range of about 10–40 mm water gauge. Consideration should also be given to the noise attenuation that will be provided by any flue gas scrubbers, filters, or precipitators that are to be located between the induced-draft fan and its stack. Alternatively, variable-speed fan drives can be installed to reduce nighttime noise at cycling plants that shed load during nighttime hours. This has the added benefit of also reducing the power consumed by the fans and reducing the erosion rates and stresses of rotating components. When multiple fans are installed, they should be operated at the same speed to avoid acoustical beats between the fan tones. (see references 3 and 11).

When an induced-draft centrifugal fan discharges directly to a stack, it is not uncommon for the tonal fan noise to radiate relatively long distances from the top of the stack. This tonal noise is generated by the fluid dynamic interaction of the gas flow leaving rotating fan blades and the stationary cutoff of the fan. This noise propagates with little attenuation up the stack and radiates from the stack top. Some success in reducing the magnitude of this tonal noise at large industrial centrifugal fan installations has been achieved by modifying the geometry of the cutoff. The fabrication and installation of "slanted" and rounded cutoffs, as described in reference 12, have been shown to reduce the tonal noise level by about 3–10 dB with no observed loss in fan performance.

Well-designed and sized inlet and outlet ducts that properly manage the flow are essential to avoid excessive fan noise. Inlet swirl, distorted inflow, and excessive turbulence can result in high noise levels and reduced system efficiency. Useful design guidelines have been established by the Air Movement and Control Association (AMCA) for large industrial fan installations.

Procedures are provided in this section to estimate the overall sound power output of large industrial fans operating at peak efficiency conditions with undistorted inflow. Experience indicates that fans operating with highly distorted inflow or at off-peak efficiency conditions often produce sound power levels that may be 5–10 dB higher than indicated below. Centrifugal- and axial-flow fans produce less sound power when operating at low speeds and reduced working points than during full-load, high-speed operation. For part-speed operation, the sound power levels estimated below can be reduced by about 55 log(speed ratio). Additional information about fan noise generation and attenuation is provided in reference 13.

Centrifugal-Type Forced-Draft and Induced-Draft Fans with Single-Thickness, Backward-Curved or Backward-Inclined Blades or Airfoil Blades

The overall sound power level radiated from the inlet of forced-draft centrifugal fans and the outlet of induced-draft centrifugal fans (with single-thickness, backward-curved or backward-inclined blades or airfoil blades) can be estimated with the relationship provided in Eq. (16.20) (also see line 20 of Table 16.1):

$$\text{Centrifugal fan, overall } L_w = 10 + 10 \log Q + 20 \log(\text{TP}) \quad \text{(dB)} \quad (16.20)$$

where Q is fan flow rate in cubic meters of gas per minute and TP is fan total pressure rise in newtons per square meter at rated conditions.

To account for the tonal noise, 10 dB should be added to the octave bands containing the fan blade passing frequency and its second harmonic. For multiple-fan installations, the estimated sound power levels should be increased by 10 log N, where N is the number of identical fans.

The overall sound power level radiated from the uninsulated casing of centrifugal fans can be estimated with the relationship provided in Eq. (16.21) (also see line 21 of Table 16.1). To account for the tonal noise, 5 dB should be added to the octave band containing the fan blade passing frequency:

$$\text{Centrifugal fan casing, overall } L_w = 1 + 10 \log Q + 20 \log(\text{TP}) \quad \text{(dB)} \quad (16.21)$$

where Q and TP are as defined for Eq. (16.20).

The sound power radiated by the uninsulated discharge breaching is about 5 dB less than the sound power estimated using Eq. (16.21) for the fan casing.

The overall sound power level radiated from the casings of radial-blade centrifugal fans with ducted inlets and outlets, such as are sometimes used for gas recirculation and dust collection service, can be estimated with the relationship provided in Eq. (16.22) (also see line 22 of Table 16.1):

$$\text{Radial fan casing, overall } L_w = 13 + 10 \log Q + 20 \log(\text{TP}) \quad \text{(dB)} \quad (16.22)$$

where again Q and TP are as defined for Eq. (16.20).

To account for the tonal noise, 10 dB should be added to the octave bands containing the fan blade passing frequency and its second harmonic.

Axial-Flow Forced-Draft and Induced-Draft Fans

The overall sound power level radiated from the inlet of forced-draft axial-flow fans and the outlet of induced-draft axial-flow fans can be estimated with the following relation:

$$\text{Axial-flow fan, overall } L_w = 24 + 10 \log Q + 20 \log(\text{TP}) \quad \text{(dB)} \quad (16.23)$$

where Q and TP have been defined in Eq. (16.20).

To account for the tonal noise, 6 dB should be added to the octave band containing the fan blade passing frequency and 3 dB should be added to the octave band containing its second harmonic. For multiple-fan installations, the above estimated values should be increased by 10 log N, where N is the number of identical fans.

Ventilation Fans

The sound power output of industrial ventilation fans can be estimated using Eq. (16.20) for centrifugal ventilation fans or Eq. (16.23) for axial-flow ventilation fans; also see Chapter 17.

16.8 FEED PUMPS

It is common for the noise radiated by a pump motor set to be dominated by the motor noise. One exception is the relatively high-flow, high-head pumps used for boiler and reactor feedwater service in large modern power-generating stations that operate in the United States. These feed pumps are usually driven by an electric motor, an auxiliary steam turbine, or the main turbine-generator shaft. Midsize pumps generally produce broadband noise without strong tonal components. The larger pumps, however, commonly produce both broadband noise and strong midfrequency tonal noise. Feed pump noise is omnidirectional and continuous during plant operation.

A high-performance thermal-acoustical blanket insulation, described in reference 14, has been developed and evaluated at field installations specifically for use with equipment such as noisy feedwater pumps, valves, and turbines. This thermal-acoustical insulation provides far better noise attenuation than conventional blanket insulations. It is also easier to remove and reinstall during maintenance and inspections than most rigid insulations. It has been successfully used as a retrofit insulation at installed pumps, turbines, valves, and lines and has been used by equipment manufacturers at new installations requiring reduced noise levels. The use of flexible thermal-acoustical insulation to control noise avoids the mechanical, structural, and safety problems associated with the large rigid enclosures that have sometimes been used at boiler feedwater pump installations. Note that experience in Germany indicates that it is possible to design and operate boiler feedwater pumps that produce relatively low noise levels without external means for controlling the noise.

The overall sound power level radiated by boiler and reactor feedwater pumps can be estimated using the information provided below for pumps in the power range of 1–18 MWe:

Rated Power (MWe)	Overall Sound Power (dB)
1	108
2	110
4	112
6	113
9	115
12	115
15	119
18	123

Octave-band and A-weighted sound power levels for boiler and reactor feedwater pumps can be estimated by subtracting the values provided in line numbers 24 and 25 of Table 16.1 from the overall power level estimated above.

16.9 INDUSTRIAL GAS TURBINES

Industrial gas turbines are often used to provide reliable, economic power to drive large electric generators, gas compressors, pumps, or ships. A prediction scheme for the combustion noise of flightworthy gas turbine engines used in aircraft operations (turbojet, turboshaft, and turbofan engines) is provided in Chapter 15. The noise produced by industrial gas turbine installations is radiated primarily from four general source areas: the inlet of the compressor; the outlet of the power turbine; the casing and/or enclosure of the rotating components; and various auxiliary equipment, including cooling and ventilating fans, the exhaust-heat recovery steam generator, poorly gasketed or worn access openings, generators, and electric transformers. Each of the above areas should receive considerable attention if an industrial gas turbine is to be located successfully near a quiet residential area.

Operation of unmuffled industrial gas turbines of moderate size would produce sound power levels of 150–160 dB or greater. Because the resulting noise levels would be unacceptable, essentially all industrial gas turbine installations include at least some noise abatement provided by the manufacturer. Noise abatement performance requirements may call for reducing the sound power output to levels as low as 100 dB for installations located near sensitive residential areas.

Noise radiated from the compressor inlet includes high levels of both broadband and tonal noise, primarily at frequencies above 250–500 Hz. This mid- and high-frequency noise is controlled with the use of (a) a conventional parallel-baffle or tubular muffler comprised of closely spaced thin baffles and (b) inlet ducting, plenum walls, expansion joints, and access hatches that are designed to contain the noise and avoid flanking radiation.

Noise radiated by the casings of rotating components is typically contained with the use of thermal insulation laggings and close-fitting steel enclosures that include interior sound absorption and well-gasketed access doors. It is not uncommon for the enclosure to be mounted directly on the structural steel base that supports the rotating components. This encourages the transmission of structure-borne noise to the enclosure and can limit its effective acoustical performance at installations requiring high degrees of noise reduction. Off-base mounting of the enclosure can be considered for installations where noise abatement performance must be improved. In addition, many large industrial gas turbines are being installed within a turbine-generator building that provides weather protection and additional reduction of noise radiated through the enclosure from the rotating components.

Noise radiated from the power turbine outlet includes high levels of both broadband and tonal noise at low, mid, and high frequencies, with the low-frequency noise being the most difficult and expensive to control at simple-cycle

installations (without heat recovery boilers) located near residential areas. The wavelength of sound at about 30 Hz is on the order of 15–20 m in the gas stream at the back end of the power turbine, thereby increasing the required size of the discharge mufflers. Furthermore, low-frequency exhaust noise has caused significant community noise problems when the sound level in the 31-Hz octave band exceeded about 70 dB at sensitive residential areas. This low-frequency exhaust noise might be best controlled by the manufacturer with improved gas management designs behind the power turbine. The outlet noise is typically controlled with the use of (a) conventional parallel-baffle or tubular mufflers that include thick acoustical treatments; (b) additional dissipative or reactive muffler elements tuned to attenuate low-frequency noise; and (c) outlet ducts, plenum chamber, expansion joints, and access hatches that include adequate acoustical treatments to avoid flanking along these paths and their radiation of excessive noise.

At combined-cycle and cogeneration plants, heat recovery steam generators (HRSGs) are installed downstream of the power turbine to absorb waste heat from the exhaust stream. The HRSG also serves to attenuate the stack-radiated turbine exhaust noise, often by as much as 15–30 dBA, depending on the configurations and sizes of the gas turbine and HRSG. The HRSG can eliminate, or at least reduce, the performance requirements of the exhaust muffler. Also, the HRSG reduces the exhaust gas stream temperature, the wavelengths of the exhaust sounds, and the required size of an exhaust muffler. It is necessary to consider and account for the noise radiated from the surfaces and various steam vents of the HRSG. It is suggested that most HRSG manufacturers can provide technical information describing the noise radiated from their equipment. See also references 15–19 for additional information.

Noise produced by auxiliary cooling and ventilation fans can be controlled effectively with the use of high-performance low-speed fan blades, mufflers, or partial enclosures, depending on specific site and installation requirements. The control of transformer noise, if required for a specific installation, is discussed in Section 16.11. The control of noise radiated from the sidewalls of heat recovery steam generators can be accomplished with large barrier walls or an enclosing building.

Combined-cycle gas turbine power plants produce relatively steady noise as well as relatively brief intermittent loud noises often associated with steam venting and steam bypass operations. Noise levels of 75–80 dBA or greater at 300 m are not uncommon; however, these intermittent sources can usually be reduced 5–10 dBA or more. Further information about such intermittent loud noise from power plants is provided in reference 20.

Sound-power-level prediction procedures are not provided here specifically for industrial gas turbines because of the rather wide range of noise control treatments available within the industry. Many manufacturers offer their machines with a variety of optional noise abatement treatments, ranging from modest to highly effective. For example, 50–100-MWe installations, with or without heat recovery boilers, are readily available with noise abatement treatments resulting

in A-weighted noise levels in the range of 50–60 dB at 120 m. Installations with lower noise levels are available from certain manufacturers and can be designed by several independent professionals who have specialized in the control of noise from industrial gas turbines. Combined-cycle plants in the range of 500–600 MWe have been designed and constructed to meet 43 dBA at 300 m.

The overall sound power level of the combined-cycle equipment located within the main power building, including the combustion turbine, HRSG, steam turbine, generators, and support equipment can be estimated with the following relation (also see line 26 of Table 16.1):

$$\text{Inside main power building, overall } L_w = 96 + 10\log(A) \quad \text{(dB)} \quad (16.24)$$

where A is the wall and roof area of the building in square meters.

This relationship is based on field measurements obtained near the outer wall and roof areas at numerous combined-cycle and cogeneration power plants. Equation (16.24) assumes that the interior surfaces of the building have sound absorption, with a resulting average sound level of 85 dBA at the outer wall and roof areas. For buildings without significant sound absorption treatment, the estimates should be increased by 5 dB. The interior sound level and the building shell transmission loss will determine the amount of noise that radiates to the outdoors from the main plant equipment. For additional discussion on these plants, see reference 21.

One early but important step in the design of a new gas turbine installation is the preparation of a reasonable and well-founded technical specification by the buyer or buyer's acoustical consultant that fully describes the site-specific noise requirements. Methods and procedures for preparing gas turbine procurement specifications that describe expected noise-level limits are included in ANSI/ASME B133.8-1977 (R1996). If residential neighbors are near the site, the reader is cautioned to consider fully the site-specific needs when planning control of the low-frequency exhaust noise. Several independent consultants with many years of gas turbine experience have suggested that the noise-level threshold of complaints resulting from low-frequency noise in the 31-Hz octave band is about 65–70 dB, measured at residential wood-frame homes. Higher levels of low-frequency noise can sometimes vibrate the walls and rattle the windows and doors of wood-frame homes and result in varying degrees of annoyance. Gas turbine manufacturers, however, correctly indicate that low-frequency noise control treatments are expensive and that many industrial gas turbines are operating that produce higher levels of low-frequency noise in residential areas without causing complaints.

16.10 STEAM TURBINES

Two procedures are provided to predict the sound power radiation from steam turbines; one is for the relatively small turbines in the power range of 400–8000 kW that operate at about 3600–6000 rpm and are often used to drive auxiliary

equipment at a plant where steam is readily available. Another procedure is provided for large steam turbine generators in the range of about 200–1100 MWe used at central electricity-generating stations. Thermal-acoustical blanket insulation that has been developed to control noise radiated from equipment including steam turbines is discussed in Section 16.8 and reference 14.

Auxiliary Steam Turbines

The overall sound power output of auxiliary steam turbines, with common thermal insulation installed, can be estimated using Eq. (16.25) (see also line 27 of Table 16.1). This noise is considered to be omnidirectional, generally nontonal, and continuous when the driven equipment is operating:

$$\text{Auxiliary steam turbine, overall } L_w = 93 + 4 \log(\text{kW}) \quad (\text{dB}) \quad (16.25)$$

Large Steam Turbine-Generators

The overall sound power output of large steam turbine-generators can be estimated using Eq. (16.26). This includes the noise radiated by the low-pressure, intermediate-pressure, and high-pressure turbines as well as the generator and shaft-driven exciter. The turbine-generator produces both tonal and broadband noise. The tonal components produced by the generator are typically most noticeable at 60 and 120 Hz for 3600-rpm machines and 30, 60, 90, and 120 Hz for 1800-rpm machines:

$$\text{Large steam turbine-generator, overall } L_w = 113 + 4 \log(\text{MW}) \quad (\text{dB}) \quad (16.26)$$

Octave-band and A-weighted sound power levels for large steam turbine-generators can be calculated by subtracting the values provided in line 28 of Table 16.1 from the overall sound power level estimated using Eq. (16.26).

Most major manufacturers of large steam turbine-generators will provide their equipment with additional noise abatement features that reduce the noise by about 5–10 dBA, when required by a well-written purchase specification. The reverberant noise inside a turbine building can also be reduced through the proper selection of the building siding. The use of building siding with a fibrous insulation sandwiched between a perforated metal inner surface and a solid exterior surface will provide improved midfrequency sound absorption and thereby reduce the reverberant buildup of noise within the turbine building. It can also reduce the noise radiated to the outdoors.

16.11 STEAM VENTS

Atmospheric venting of large volumes of high-pressure steam is probably one of the loudest noise sources found at industrial sites. The overall sound power produced during steam line blow-outs at large central stations prior to starting a new boiler can be estimated using Eq. (16.27) (see also line 29 of Table 16.1).

This noise is broadband and only occurs for a few minutes during each blow-out for the first few weeks of boiler operation:

$$\text{Steam line blow-out, overall } L_w = 177 \text{ dB} \quad (16.27)$$

The actual sound power level produced during the venting of high-pressure gas is, of course, related to various factors, including the conditions of the flowing gas and the geometry of the valve and pipe exit. However, the above relationship will provide a reasonable estimate of the noise associated with the blow-out of steam lines at large boilers used for utility service.

Large heavy-duty mufflers are sometimes purchased or rented that reduce the noise by about 15–30 dB during steam line blow-outs. The noise produced by the more common atmospheric vents and commonly encountered valves can be estimated using prediction procedures available from many valve manufacturers and their representatives. Many manufacturers offer valves with special low-noise trims, orifice plates, and inline mufflers that effectively reduce noise generation and radiation. The low-noise trim can also reduce the vibration and maintenance that are sometimes associated with valves used in high-pressure-drop service.

16.12 TRANSFORMERS

The noise radiated by electrical transformers is composed primarily of discrete tones at even harmonics of line frequency, that is, 120, 240, 360, ... Hz when the line frequency is 60 Hz and 100, 200, 300, ... Hz when the line frequency is 50 Hz. This tonal noise is produced by magnetostrictive forces that cause the core to vibrate at twice the electrical line frequency. The cooling fans and oil pumps at large transformers produce broadband noise when they operate; however, this noise is usually less noticeable and therefore less annoying to nearby neighbors. The tonal core noise should be considered omnidirectional and continuous while the transformer is operating. The broadband fan and pump noise occurs only during times when additional cooling is required.

The technical literature includes numerous relations and guidelines for the prediction of noise produced by transformers. Reference 22 reports the results of measurements obtained at 60 transformer banks and indicates that the space-averaged A-weighted sound level produced by the core of the average transformer (without built-in noise abatement) at an unobstructed distance of about 150 m is well represented by the relationship given in Eq. (16.28). Ninety-five percent of the A-weighted noise data reported in reference 22 lies within about ±7 dB of this relation for transformers with maximum ratings in the range of 6–1100 MVA:

Average A-weighted core sound level at 150 m,

$$L_p = 26 + 8.5 \log(\text{MVA}) \quad (\text{dBA}) \quad (16.28)$$

where MVA is the maximum rating of the transformer in million volt-amperes.

The space-averaged sound pressure levels of the transformer core tones at 120, 240, 360, and 480 Hz at 150 m can be estimated by adding the following values to the A-weighted sound level of Eq. (16.28):

120	240	360	480
17	5	−4	−8

Another relation for transformer A-weighted sound levels versus distance, extracted from reference 23, is

$$\text{Space-averaged far-field sound level } L_p = L_n - 20(\log\ d/S^{1/2}) - 8 \quad \text{(dBA)} \tag{16.29}$$

where L_n = circumferential average sound pressure levels measured at National Electrical Manufacturers Association (NEMA) close-in measurement positions (A-weighted or tonal)
S = total surface area of four sidewalls of transformer tank
d = distance from transformer tank (in units that are compatible with tank sidewall area), must be greater than $S^{1/2}$

Equation (16.29) can be used if L_p and L_n represent the A-weighted sound levels or the sound pressure levels of the discrete tones produced by the transformer tank. The octave-band sound pressure levels of the transformer core noise can be obtained directly from the sound pressure levels of the discrete tones estimated above. The octave-band sound pressure levels of the total transformer noise with the cooling fans operating can be estimated by subtracting the values provided in line 30 of Table 16.1 from the A-weighted sound level estimated with Eq. (16.29). This applies to conventional cooling-fan systems with motors in the power range of about 0.15–0.75 kW operating at about 1000–1700 rpm with two- or four-bladed propeller fans. Further information about special low-noise cooling systems should be obtained from the manufacturer. Excess attenuation should be considered (see Chapter 5) when estimating sound levels at distances beyond about 150 m.

NEMA has published standard tables of close-in noise levels for transformers; see reference 24. Experience indicates that the noise near most operating transformers is often equal to or somewhat less than the NEMA standard values, and the noise near new high-efficiency transformers can be significantly less than the NEMA values. However, the noise produced by converter transformers operating at AC-to-DC converter terminals can include discrete tones at frequencies up to about 2000 Hz and can be about 5–10 dB greater than the NEMA standard values. This additional high-frequency noise has been found to be unusually noticeable and disturbing to residential neighbors when the converter transformer is located in quiet rural-suburban areas.

Two basic methods are available for reducing the far-field noise produced by transformers. First, manufacturers are able to respond to custom noise requirements and produce transformers with reduced flux density that generate noise levels as much as 10–20 dB lower than the NEMA standard values. New high-efficiency transformers with low electrical losses usually produce core noise levels that are less than the NEMA standard values. For the quieted-design transformers, reductions of the higher frequency tones (e.g., 480 and 600 Hz) are typically 1–3 dB more than the reductions of the lower frequency tones (e.g., 120, 240, and 360 Hz). High-efficiency low-speed cooling fans and cooling-fan mufflers are also available from some manufacturers when needed for special siting applications. In some cases, the cooling fans are eliminated from the transformer tank and replaced with oil-to-water heat exchangers.

Second, barrier walls, partial enclosures, and full enclosures can be provided to shield or contain the transformer noise. They are usually fabricated with masonry blocks or metal panels. The interior surfaces of the barrier or enclosure walls should usually include sound absorption that is effective at the prominent transformer tones. Care must be used to ensure adequate strike distances and space for cooling-air flows. If the fin-fan oil coolers are to be located outside of the enclosure, some attention should be given to the structure-borne and oil-borne noise from the core that can be radiated by the coolers. Space and provisions must be provided for inspections, maintenance, and transformer removal. It is also important to ensure that the enclosure walls are structurally isolated from the transformer foundation to avoid radiation of structure-borne noise resulting transformer-induced vibration. Further information about the control of transformer noise is available from most major transformer manufacturers as well as from reference 25. And a promising passive means of canceling tonal noise radiated from transformer sidewalls by means of an attached mechanical oscillator is discussed in reference 26.

As energy efficiency becomes increasingly important, new transformers are being purchased with low electrical losses reducing operating costs. Experience at numerous large electrical facilities indicates that new high-efficiency low-loss transformers also often produce core noise levels 5–10 dB less than the NEMA standard values.

Instead of, or in addition to, reducing the noise radiated from a transformer substation, it is sometimes possible to site a transformer far from residential neighbors or within an existing noisy area, such as close to a well-traveled highway, where the ambient sounds partially mask the transformer noise.

16.13 WIND TURBINES

The installation of modern wind energy systems is growing rapidly throughout many areas of the world. Installed capacity by 2001 exceeded 30,000 MWe as the reliability and efficiency of modern wind turbines increased and the costs declined. It has been estimated that wind turbines will generate more than 10% of the world's energy, more than 1200 GW, by year 2020. Wind turbine capacity is generally rated based on rotor diameter, rotor swept area, or generator capacity in watts. Small-capacity wind turbines are generally rated at less than about 5 kW, medium turbines at about 5–300 kW, and large wind turbines at about 500 kW and above. Large turbines are now available rated at up to 1–5 MW, and with

multiple turbines on a single tower, ratings can continue to increase. Wind turbine parks or farms are being developed onshore and offshore with rated capacities of 50–150 MWe and greater. The development of wind turbine rotors to operate with low wind speeds will increase the available resource area and will bring development closer to more people.

The main types of noise from wind turbines are aerodynamic, mechanical, and electrical. The principal sources of noise include the rotor blades, the gearbox, and the generator. Additional sources include the brakes, the electronics, and the tower. Earlier wind turbine installations produced both prominent tonal noise from the gear box and a strongly modulated "thumping" noise most often associated with the rotor blades passing through and interacting with the turbulent tower wake flow at downwind machines. Fortunately, the manufacturers of modern wind turbines have learned to avoid what were these most noticeable and annoying aspects of wind turbine noise.

Considerable progress in reducing noise generation and radiation continues to be made by the equipment manufacturers with ongoing technical support from research organizations (reference 27). Noise abatement for modern wind turbines includes increasingly efficient rotor blade profiles, variable-speed and variable-pitch rotors, advanced electronics, and low-noise gearboxes, as well as vibration isolation mounts and sound absorption within turbine nacelles. Noise from modern wind turbines is generally dominated by broadband rotor noise that is directly related to tip speed. Information about aeroacoustical noise generation is provided in Chapter 15.

Modern wind turbines are generally available that produce broadband noise without strong tonal components. The midfrequency aerodynamic rotor noise generally includes some noticeable time-varying amplitude modulation at the passing frequency of the rotor blade (number of blades times the rotation rate in revolutions per second). For a three-blade constant-speed turbine operating at 25 rpm, this is 1.25 Hz. For variable-rotor-speed turbines, the modulation frequency will often be in the range of 0.5–1 Hz.

The approximate A-weighted sound power level of modern medium to large wind turbines can be estimated with the relationships provided in Eq. (16.30) or (16.31), although the sound power level of some turbines will be as much as 10 dBA greater:

$$\text{Wind turbine, A-weighted sound power level} = \begin{cases} 86 + 10 \log D \quad \text{(dBA)} & (16.30) \\ 73 + 10 \log \text{kW} \quad \text{(dBA)} & (16.31) \end{cases}$$

where D is the rotor diameter in meters and kW is the rated turbine power.

Alternatively, the approximate footprint area surrounding a modern wind turbine within which the A-weighted sound level equals or exceeds 40 dBA can be estimated with the relationship provided in Eq. (16.32):

$$\text{Wind turbine 40 dBA footprint area in square meters} = 800 \times \text{kW} \quad (\text{m}^2) \qquad (16.32)$$

The operating characteristics, including noise generation under specific conditions, of most modern wind turbines have been certified in accordance with national and international standards. The special requirements associated with reliable measurements and specification of wind turbine noise are defined by International Standard IEC 61400-11, 1998, "Wind Turbine Generator Systems—Part 11: Acoustic Noise Measurement Techniques."

16.14 SUMMARY

The machinery noise prediction procedures and relations presented in this chapter are based primarily on extensive field measurement data collected by the authors and their colleagues during many years of consulting projects. The results obtained when using these relations should be useful for many engineering applications. The reader is cautioned, however, that site-specific installation conditions and individual equipment characteristics can cause noise levels to be somewhat higher or lower than predicted, and detailed knowledge of these exceptions can be important for critical applications. Also, many items of equipment can be purchased with reduced noise, can be installed so as to reduce noise, or can be fitted with effective noise control treatments.

The authors continue to add to and update their library of equipment noise emission data used in the preparation of this chapter. Readers with access to new or useful data or information on equipment noise characteristics or control and wanting to share their information are encouraged to send copies to the authors.

REFERENCES

1. L. N. Miller, E. W. Wood, R. M. Hoover, A. R. Thompson, and S. L. Patterson, *Electric Power Plant Environmental Noise Guide,* rev. ed., Edison Electric Institute, Washington, DC, 1984.
2. J. D. Barnes, L. N. Miller, and E. W. Wood, *Power Plant Construction Noise Guide*, BBN Report No. 3321, Empire State Electric Energy Research Corporation, New York, 1977.
3. I. L. Vér and E. W. Wood, *Induced Draft Fan Noise Control: Technical Report and Design Guide*, BBN Report Nos. 5291 and 5367, Empire State Electric Energy Research Corporation, New York, 1984.
4. I. L. Vér, "Perforated Baffles Prevent Flow-Induced Resonances in Heat Exchangers," in *Proceedings of DAGA*, Deutschen Arbeitsgemeinschaft fur Akustik, Göttingen, Germany, 1982, pp. 531–534.
5. R. D. Blevins, *Flow-Induced Vibrations*, Krieger Publishing Company, Melbourne, FL, 2001.
6. W. E. Bradley, "Sound Radiation from Large Air-Cooled Condensers," in *Proceedings of NoiseCon 2003*, June 2003, The Institute of Noise Control Engineering of the USA, Inc., Washington, DC, 2003.
7. J. Mann, A. Fagerlund, C. DePenning, F. Catron, R. Eberhart, and D. Karczub, "Predicting the External Noise from Multiple Spargers in an Air-Cooled Condenser Power

Plant," in *Proceedings of NoiseCon 2003*, June 2003, The Institute of Noise Control Engineering of the USA, Inc., Washington, DC, 2003.

8. L. De Backer and W. Wurtz, "Why Every Air-Cooled Steam Condenser Needs a Cooling Tower," *CTI J.*, **25** (1), 52–61 (Winter 2004).
9. *Bulldozer Noise Control*, manual prepared by Bolt Beranek and Newman for the U.S. Bureau of Mines Pittsburgh Research Center, Pittsburgh, PA, May 1980.
10. *Front-End Loader Noise Control*, manual prepared by Bolt Beranek and Newman for the U.S. Bureau of Mines Pittsburgh Research Center, Pittsburgh, PA, May 1980.
11. R. M. Hoover and E. W. Wood, "The Prediction, Measurement, and Control of Power Plant Draft Fan Noise," Electric Power Research Institute Symposium on Power Plant Fans—The State of the Art, Indianapolis, IN, October 1981.
12. J. D. Barnes, E. J. Brailey, Jr., M. Reddy, and E. W. Wood, "Induced Draft Fan Noise Evaluation and Control at the New England Power Company Salem Harbor Generating Station Unit No. 3," in *Proceedings of ASCE Environmental Engineering*, Orlando, FL, July 1987.
13. *Proceedings of Fan Noise Symposiums*, Senlis, France, 1992 and 2003.
14. C. C. Thornton, C. B. Lehman, and E. W. Wood, "Flexible-Blanket Noise Control Insulation-Field Test Results and Evaluation," in *Proc. INTER-NOISE* 84, June 1984, Noise Control Foundation, Poughkeepsie, NY, 1984, pp. 405–408.
15. G. F. Hessler, "Certifying Noise Emissions from Heat Recovery Steam Generators (HRSG) in Complex Power Plant Environments," in *Proceedings of NoiseCon 2000*, December 2000, The Institute of Noise Control Engineering of the USA, Inc., Washington, DC, 2000.
16. W. E. Bradley, "Integrating Noise Controls into the Power Plant Design," in *Proceedings of NoiseCon 2000*, December 2000, The Institute of Noise Control Engineering of the USA, Inc., Washington, DC, 2000.
17. J. R. Cummins and J. B. Causey, "Issues in Predicting Performance of Ducts and Silencers Used in Power Plants," in *Proceedings of NoiseCon 2003*, June 2003, The Institute of Noise Control Engineering of the USA, Inc., Washington, DC, 2003.
18. *Noise Prediction—Guidelines for Industrial Gas Turbines*, Solar Turbines, San Diego, CA, 2004.
19. R. S. Johnson, "Recommended Octave Band Insertion Losses of Heat Recovery Steam Generators Used on Gas Turbine Exhaust Systems," in *Proceedings of NoiseCon 1994*, May 1994, Noise Control Foundation, Poughkeepsie, NY, 1984, pp. 181–184.
20. D. Mahoney and E. W. Wood, "Intermittent Loud Sounds from Power Plants," in *Proceedings of NoiseCon 2003*, June 2003, The Institute of Noise Control Engineering of the USA, Inc., Washington, DC, 2003.
21. G. F. Hessler, "Issues In HRSG System Noise," in *Proceedings of NoiseCon 1997*, June 1997, The Institute of Noise Control Engineering of the USA, Inc., Washington, DC, 1997, pp. 297–304.
22. R. L. Sawley, C. G. Gordon, and M. A. Porter, "Bonneville Power Administration Substation Noise Study," BBN Report No. 3296, Bolt Beranek and Newman, Cambridge, MA, September 1976.
23. L. Vér, D. W. Anderson, and M. M. Miles, "Characterization of Transformer Noise Emissions," Vols. 1 and 2, BBN Report No. 3305, Empire State Electric Energy Research Corporation, New York, July 1977.

24. NEMA Standards Publication No. TR 1–1993 (R2000), "*Transformers, Regulators and Reactors*," National Electrical Manufacturers Association, Rosslyn, VA, 2000.
25. C. L. Moore, A. E. Hribar, T. R. Specht, D. W. Allen, I. L. Vér, and C. G. Gordon, "Power Transformer Noise Abatement," Report No. EP 9–14, Empire State Electric Energy Research Corporation, New York, October 1981.
26. J. A. Zapfe and E. E. Ungar, "A Passive Means for Cancellation of Structurally Radiated Tones," *J. Acoust. Soc. Am.*, **113** (1), 320–326 (January 2003).
27. P. Migliore, J. van Dam, and A. Huskey, "Acoustic Tests of Small Wind Turbines," AIAA-2004-1185, 23rd ASME Wind Energy Symposium, U.S. DOE National Renewable Energy Laboratory, Reno, NV, January 2004.

CHAPTER 17

Noise Control in Heating, Ventilating, and Air Conditioning Systems

ALAN T. FRY

Consultant
Colchester, Essex, United Kingdom

DOUGLAS H. STURZ

Acentech, Inc.
Cambridge, Massachusetts

This chapter provides guidelines, recommendations, and design tools useful in assessing and controlling noise and vibration stemming from mechanical systems serving buildings. Discussed are the transmission of noise along duct systems, airflow velocities at various points in duct systems that are consistent with particular noise goals, fan noise, terminal box noise, and special design features for especially quiet heating, ventilating, and air conditioning (HVAC) systems. Sound isolation for mechanical rooms and special consideration for the application of vibration isolation for mechanical equipment in buildings are also addressed. Further discussion and additional detailed design information can be found in references 1–5, and in Chapters 9–15 of this book.

17.1 DUCT-BORNE NOISE TRANSMISSION

It is of significant practical interest to predict the noise that transmits via a ducted system from a source to a receiver space to achieve a desired noise goal. This is typically done by starting with the noise of a known source (typically and primarily a fan) and subtracting from this the attenuation provided by each of the various duct elements that the noise encounters as it propagates along the duct path. Thus, from a known noise source level, one can predict the noise level that reaches the occupant of a space and can engineer any special attenuation treatments that may need to be incorporated in the duct system to help achieve a desired result. Alternatively, one can work backward from a desired noise goal in the receiving space to determine the permissible sound power level of a fan serving the system (or other source in the system). There are many acoustical complexities that are difficult to model precisely without exhaustive knowledge

of the duct construction and the nature of the sound field entering a duct element, and such details are generally not well known. The prediction procedure is really a guide to make decisions in order to achieve designs that are in the correct neighborhood of the goal, and generally the procedure is a good guide in the moderately lower frequency range that is of greatest interest for ventilation systems. There are many aspects of ducted systems which are strongly frequency dependent in the higher frequency range, and the precision of the calculations may be questionable for extensive systems in this frequency range. Fortunately, in designing noise control for ducted systems, when the lower frequencies are suitably controlled, the predicted noise levels at higher frequencies are dramatically lower than the goal and there is no need to make precise predictions in this higher frequency range. The following presents some of the data necessary to assess attenuation in the path of sound propagation from source to receiver. Considerations for some relevant noise sources are presented later.

Sound Attenuation in Straight Ducts

Even the attenuation of sound propagating in simple, straight ducts is quite complex. The sound attenuation in straight ducts of uniform cross section and wall construction is usually given in attenuation per unit length, decibels per meter or decibels per feet, assuming that every unit of duct length provides the same amount of attenuation. This is a considerable simplification because the attenuation is a function of the character of the sound field entering the duct section and the character of the sound field is constantly changing along the length of even a straight-duct run. At frequencies high enough for the duct to support higher order modes, these higher order modes are much more rapidly attenuated by duct attenuation treatments than the plane-wave fundamental mode. Attenuation of sound along a duct is a function of the sound dissipation when the sound wave interacts with the walls of the duct and this is determined by the impedance of the duct wall. Sound attenuation in lined ducts and silencers is treated in detail in Chapter 9. At high frequencies, energy loss due to sound transmission through the bare sheet metal duct walls yields only very little sound attenuation for the duct path. However, with sound-absorptive lining of the walls, high-frequency sound attenuation along the ducts can be quite high. At low frequencies, a substantial portion of the sound attenuation along the duct path is provided by energy transmission through the sheet metal walls of the duct—breakout. Form, stiffness, and surface weight control the low-frequency sound attenuation. Consequently, unlined form-stiff round ducts yield much less sound attenuation (and also much higher breakout sound transmission loss) than do ducts with rectangular or oval cross section and with large aspect ratio. The sound attenuation values represented herein are for typical duct construction within the range of constructions typically allowed by the Sheet Metal and Air Conditioning National Association (SMACNA) for low-pressure ductwork.

Estimation of the attenuation provided by unlined and lined ducts of round and rectangular duct constructions typically found in the field is presented in Tables 17.1–17.6.

TABLE 17.1 Sound Attenuation in Unlined Rectangular Sheet Metal Ducts

Duct Size, in. × in.	P/A, ft^{-1}	Attenuation by Octave-Band Center Frequency, dB/ft			
		63 Hz	125 Hz	250 Hz	>250 Hz
6 × 6	8.0	0.30	0.20	0.10	0.10
12 × 12	4.0	0.35	0.20	0.10	0.06
12 × 24	3.0	0.40	0.20	0.10	0.05
24 × 24	2.0	0.25	0.20	0.10	0.03
48 × 48	1.0	0.15	0.10	0.07	0.02
72 × 72	0.7	0.10	0.10	0.05	0.02

Source: 1999 ASHRAE *Applications Handbook*, © American Society of Heating, Refrigerating and Air Conditioning Engineers, Inc., www.ashrae.org.

Sound Attenuation by Duct Divisions

When sound propagating along a duct encounters a duct branch, the acoustical energy divides into the two branches according to the fraction of the area that each represents to the total area leaving the division. This is probably a reasonable approximation of what happens at lower frequencies, but at higher frequencies there are likely to be directional effects for which this simple model does not account. Fortunately, for most practical HVAC noise control concerns, the low-frequency range is of the greatest interest. The attenuation in decibels that occurs at a duct division is given by

$$\text{Attenuation} = 10 \log \left(\frac{A_1}{A_T} \right) \quad \text{dB} \tag{17.1}$$

where A_1 is the area of the duct leaving the division on the path being studied and A_T is the total area of all branches leaving the division.

Sound Attenuation by Duct Cross-Sectional Area Changes

Sound propagating along a duct is reflected back if it encounters a sudden cross-sectional area change. The strength of reflection at low frequencies, where only the fundamental plane wave can propagate in the duct, depends only on the ratio of the cross-sectional areas. Whether the sound is coming from the duct of the larger or smaller cross-sectional area, the resulting sound attenuation is given by

$$\text{Attenuation} = 10 \log \left\{ 0.25 \left[\left(\frac{A_1}{A_2} \right)^{0.5} + \left(\frac{A_2}{A_1} \right)^{0.5} \right]^2 \right\} \quad \text{dB} \tag{17.2}$$

TABLE 17.2 Insertion loss for Rectangular Sheet Metal Ducts with 1-in. Fiberglass Lining[a]

	Insertion Loss by Octave Band Center Frequency, dB/ft					
Dimensions, in. × in.	125 Hz	250 Hz	500 Hz	1000 Hz	2000 Hz	4000 Hz
6 × 6	0.6	1.5	2.7	5.8	7.4	4.3
6 × 10	0.5	1.2	2.4	5.1	6.1	3.7
6 × 12	0.5	1.2	2.3	5.0	5.8	3.6
6 × 18	0.5	1.0	2.2	4.7	5.2	3.3
8 × 8	0.5	1.2	2.3	5.0	5.8	3.6
8 × 12	0.4	1.0	2.1	4.5	4.9	3.2
8 × 16	0.4	0.9	2.0	4.3	4.5	3.0
8 × 24	0.4	0.8	1.9	4.0	4.1	2.8
10 × 10	0.4	1.0	2.1	4.4	4.7	3.1
10 × 16	0.4	0.8	1.9	4.0	4.0	2.7
10 × 20	0.3	0.8	1.8	3.8	3.7	2.6
10 × 30	0.3	0.7	1.7	3.6	3.3	2.4
12 × 12	0.4	0.8	1.9	4.0	4.1	2.8
12 × 18	0.3	0.7	1.7	3.7	3.5	2.5
12 × 24	0.3	0.6	1.7	3.5	3.2	2.3
12 × 36	0.3	0.6	1.6	3.3	2.9	2.2
15 × 15	0.3	0.7	1.7	3.6	3.3	2.4
15 × 22	0.3	0.6	1.6	3.3	2.9	2.2
15 × 30	0.3	0.5	1.5	3.1	2.6	2.0
15 × 45	0.2	0.5	1.4	2.9	2.4	1.9
18 × 18	0.3	0.6	1.6	3.3	2.9	2.2
18 × 28	0.2	0.5	1.4	3.0	2.4	1.9
18 × 36	0.2	0.5	1.4	2.8	2.2	1.8
18 × 54	0.2	0.4	1.3	2.7	2.0	1.7
24 × 24	0.2	0.5	1.4	2.8	2.2	1.8
24 × 36	0.2	0.4	1.2	2.6	1.9	1.6
24 × 48	0.2	0.4	1.2	2.4	1.7	1.5
24 × 72	0.2	0.3	1.1	2.3	1.6	1.4
30 × 30	0.2	0.4	1.2	2.5	1.8	1.6
30 × 45	0.2	0.3	1.1	2.3	1.6	1.4
30 × 60	0.2	0.3	1.1	2.2	1.4	1.3
30 × 90	0.1	0.3	1.0	2.1	1.3	1.2
36 × 36	0.2	0.3	1.1	2.3	1.6	1.4
36 × 54	0.1	0.3	1.0	2.1	1.3	1.2
36 × 72	0.1	0.3	1.0	2.0	1.2	1.2
36 × 108	0.1	0.2	0.9	1.9	1.1	1.1
42 × 42	0.2	0.3	1.0	2.1	1.4	1.3
42 × 64	0.1	0.3	0.9	1.9	1.2	1.1
42 × 84	0.1	0.2	0.9	1.8	1.1	1.1
42 × 126	0.1	0.2	0.9	1.7	1.0	1.0
48 × 48	0.1	0.3	1.0	2.0	1.2	1.2
48 × 72	0.1	0.2	0.9	1.8	1.0	1.0
48 × 96	0.1	0.2	0.8	1.7	1.0	1.0
48 × 144	0.1	0.2	0.8	1.6	0.9	0.9

[a] Add to attenuation of bare sheet metal ducts.

Source: 1999 ASHRAE *Applications Handbook*, © American Society of Heating, Refrigerating and Air Conditioning Engineers, Inc., www.ashrae.org.

TABLE 17.3 Insertion loss for Rectangular Sheet Metal Ducts with 2-in. Fiberglass Lining[a]

	Insertion Loss by Octave-Band Center Frequency, dB/ft					
Dimensions, in. × in.	125 Hz	250 Hz	500 Hz	1000 Hz	2000 Hz	4000 Hz
6 × 6	0.8	2.9	4.9	7.2	7.4	4.3
6 × 10	0.7	2.4	4.4	6.4	6.1	3.7
6 × 12	0.6	2.3	4.2	6.2	5.8	3.6
6 × 18	0.6	2.1	4.0	5.8	5.2	3.3
8 × 8	0.6	2.3	4.2	6.2	5.8	3.6
8 × 12	0.6	1.9	3.9	5.6	4.9	3.2
8 × 16	0.5	1.8	3.7	5.4	4.5	3.0
8 × 24	0.5	1.6	3.5	5.0	4.1	2.8
10 × 10	0.6	1.9	3.8	5.5	4.7	3.1
10 × 16	0.5	1.6	3.4	5.0	4.0	2.7
10 × 20	0.4	1.5	3.3	4.8	3.7	2.6
10 × 30	0.4	1.3	3.1	4.5	3.3	2.4
12 × 12	0.5	1.6	3.5	5.0	4.1	2.8
12 × 18	0.4	1.4	3.2	4.6	3.5	2.5
12 × 24	0.4	1.3	3.0	4.3	3.2	2.3
12 × 36	0.4	1.2	2.9	4.1	2.9	2.2
15 × 15	0.4	1.3	3.1	4.5	3.3	2.4
15 × 22	0.4	1.2	2.9	4.1	2.9	2.2
15 × 30	0.3	1.1	2.7	3.9	2.6	2.0
15 × 45	0.3	1.0	2.6	3.6	2.4	1.9
18 × 18	0.4	1.2	2.9	4.1	2.9	2.2
18 × 28	0.3	1.0	2.6	3.7	2.4	1.9
18 × 36	0.3	0.9	2.5	3.5	2.2	1.8
18 × 54	0.3	0.8	2.3	3.3	2.0	1.7
24 × 24	0.3	0.9	2.5	3.5	2.2	1.8
24 × 36	0.3	0.8	2.3	3.2	1.9	1.6
24 × 48	0.2	0.7	2.2	3.0	1.7	1.5
24 × 72	0.2	0.7	2.0	2.9	1.6	1.4
30 × 30	0.2	0.8	2.2	3.1	1.8	1.6
30 × 45	0.2	0.7	2.0	2.9	1.6	1.4
30 × 60	0.2	0.6	1.9	2.7	1.4	1.3
30 × 90	0.2	0.5	1.8	2.6	1.3	1.2
36 × 36	0.2	0.7	2.0	2.9	1.6	1.4
36 × 54	0.2	0.6	1.9	2.6	1.3	1.2
36 × 72	0.2	0.5	1.8	2.5	1.2	1.2
36 × 108	0.2	0.5	1.7	2.3	1.1	1.1
42 × 42	0.2	0.6	1.9	2.6	1.4	1.3
42 × 64	0.2	0.5	1.7	2.4	1.2	1.1
42 × 84	0.2	0.5	1.6	2.3	1.1	1.1
42 × 126	0.1	0.4	1.6	2.2	1.0	1.0
48 × 48	0.2	0.5	1.8	2.5	1.2	1.2
48 × 72	0.2	0.4	1.6	2.3	1.0	1.0
48 × 96	0.1	0.4	1.5	2.1	1.0	1.0
48 × 144	0.1	0.4	1.5	2.0	0.9	0.9

[a] Add to attenuation of bare sheet metal ducts.

Source: 1999 ASHRAE *Applications Handbook*, © American Society of Heating, Refrigerating and Air Conditioning Engineers, Inc., www.ashrae.org.

TABLE 17.4 Sound Attenuation in Straight Unlined Round Ducts

	Attenuation by Octave-Band Center Frequency, dB/ft						
Diameter, in.	63 Hz	125 Hz	250 Hz	500 Hz	1000 Hz	2000 Hz	4000 Hz
$D \leq 7$	0.03	0.03	0.05	0.05	0.10	0.10	0.10
$7 < D \leq 15$	0.03	0.03	0.03	0.05	0.07	0.07	0.07
$15 < D \leq 30$	0.02	0.02	0.02	0.03	0.05	0.05	0.05
$30 < D \leq 60$	0.01	0.01	0.01	0.02	0.02	0.02	0.02

Source: 1999 ASHRAE *Applications Handbook*, © American Society of Heating, Refrigerating and Air Conditioning Engineers, Inc., www.ashrae.org.

TABLE 17.5 Insertion Loss for Acoustically Lined Round Ducts with 1-in. Lining[a]

	Insertion Loss by Octave-Band Center Frequency, dB/ft							
Diameter, in.	63 Hz	125 Hz	250 Hz	500 Hz	1000 Hz	2000 Hz	4000 Hz	8000 Hz
6	0.38	0.59	0.93	1.53	2.17	2.31	2.04	1.26
8	0.32	0.54	0.89	1.50	2.19	2.17	1.83	1.18
10	0.27	0.50	0.85	1.48	2.20	2.04	1.64	1.12
12	0.23	0.46	0.81	1.45	2.18	1.91	1.48	1.05
14	0.19	0.42	0.77	1.43	2.14	1.79	1.34	1.00
16	0.16	0.38	0.73	1.40	2.08	1.67	1.21	0.95
18	0.13	0.35	0.69	1.37[a]	2.01	1.56	1.10	0.90
20	0.11	0.31	0.65	1.34	1.92	1.45	1.00	0.87
22	0.08	0.28	0.61	1.31	1.82	1.34	0.92	0.83
24	0.07	0.25	0.57	1.28	1.71	1.24	0.85	0.80
26	0.05	0.22	0.53	1.24	1.59	1.14	0.79	0.77
28	0.03	0.19	0.49	1.20	1.46	1.04	0.74	0.74
30	0.02	0.16	0.45	1.16	1.33	0.95	0.69	0.71
32	0.01	0.14	0.42	1.12	1.20	0.87	0.66	0.69
34	0	0.11	0.38	1.07	1.07	0.79	0.63	0.66
36	0	0.08	0.35	1.02	0.93	0.71	0.60	0.64
38	0	0.06	0.31	0.96	0.80	0.64	0.58	0.61
40	0	0.03	0.28	0.91	0.68	0.57	0.55	0.58
42	0	0.01	0.25	0.84	0.56	0.50	0.53	0.55
44	0	0	0.23	0.78	0.45	0.44	0.51	0.52
46	0	0	0.20	0.71	0.35	0.39	0.48	0.48
48	0	0	0.18	0.63	0.26	0.34	0.45	0.44
50	0	0	0.15	0.55	0.19	0.29	0.41	0.40
52	0	0	0.14	0.46	0.13	0.25	0.37	0.34
54	0	0	0.12	0.37	0.09	0.22	0.31	0.29
56	0	0	0.10	0.28	0.08	0.18	0.25	0.22
58	0	0	0.09	0.17	0.08	0.16	0.18	0.15
60	0	0	0.08	0.06	0.10	0.14	0.09	0.07

[a] Add to attenuation of bare sheet metal ducts.
Source: 1999 ASHRAE *Applications Handbook*, © American Society of Heating, Refrigerating and Air Conditioning Engineers, Inc., www.ashrae.org.

TABLE 17.6 Insertion Loss for Acoustically Lined Round Ducts with 2-in. Lining[a]

	Insertion Loss by Octave-Band Center Frequency, dB/ft							
Diameter, in.	63 Hz	125 Hz	250 Hz	500 Hz	1000 Hz	2000 Hz	4000 Hz	8000 Hz
6	0.56	0.80	1.37	2.25	2.17	2.31	2.04	1.26
8	0.51	0.75	1.33	2.23	2.19	2.17	1.83	1.18
10	0.46	0.71	1.29	2.20	2.20	2.04	1.64	1.12
12	0.42	0.67	1.25	2.18	2.18	1.91	1.48	1.05
14	0.38	0.63	1.21	2.15	2.14	1.79	1.34	1.00
16	0.35	0.59	1.17	2.12	2.08	1.67	1.21	0.95
18	0.32	0.56	1.13	2.10	2.01	1.56	1.10	0.90
20	0.29	0.52	1.09	2.07	1.92	1.45	1.00	0.87
22	0.27	0.49	1.05	2.03	1.82	1.34	0.92	0.83
24	0.25	0.46	1.01	2.00	1.71	1.24	0.85	0.80
26	0.24	0.43	0.97	1.96	1.59	1.14	0.79	0.77
28	0.22	0.40	0.93	1.93	1.46	1.04	0.74	0.74
30	0.21	0.37	0.90	1.88	1.33	0.95	0.69	0.71
32	0.20	0.34	0.86	1.84	1.20	0.87	0.66	0.69
34	0.19	0.32	0.82	1.79	1.07	0.79	0.63	0.66
36	0.18	0.29	0.79	1.74	0.93	0.71	0.60	0.64
38	0.17	0.27	0.76	1.69	0.80	0.64	0.58	0.61
40	0.16	0.24	0.73	1.63	0.68	0.57	0.55	0.58
42	0.15	0.22	0.70	1.57	0.56	0.50	0.53	0.55
44	0.13	0.20	0.67	1.50	0.45	0.44	0.51	0.52
46	0.12	0.17	0.64	1.43	0.35	0.39	0.48	0.48
48	0.11	0.15	0.62	1.36	0.26	0.34	0.45	0.44
50	0.09	0.12	0.60	1.28	0.19	0.29	0.41	0.40
52	0.07	0.10	0.58	1.19	0.13	0.25	0.37	0.34
54	0.05	0.08	0.56	1.10	0.09	0.22	0.31	0.29
56	0.02	0.05	0.55	1.00	0.08	0.18	0.25	0.22
58	0	0.03	0.53	0.90	0.08	0.16	0.18	0.15
60	0	0	0.53	0.79	0.10	0.14	0.09	0.07

[a] Add to attenuation of bare sheet metal ducts.
Source: 1999 ASHRAE *Applications Handbook*, © American Society of Heating, Refrigerating and Air Conditioning Engineers, Inc., www.ashrae.org.

Equation (17.2) yields an attenuation of only 0.5 dB for a cross-sectional area change of $A_1/A_2 = 2$ or $A_2/A_1 = 0.5$ and that of 2 dB for a 1 : 4 or 4 : 1 change. Since large abrupt changes in duct cross-sectional area do not occur very often for aerodynamic reasons, the attenuation attributable to duct cross-sectional area changes usually encountered in HVAC duct design is very small.

Sound Attenuation by Elbows

When sound propagating along a duct encounters an elbow, some of the sound is reflected back in the direction from which it was coming, some is dissipated, and

some continues to propagate along the duct path. The fraction of sound energy that is reflected or dissipated determines the attenuation. The attenuation is a function of frequency and size of the elbow. The attenuation is also impacted by the type of elbow (mitered, mitered with vanes, and radiused) and the presence (or absence) of sound-absorbing lining in the duct (or on the turning vanes). Mitered elbows with vanes and radiused elbows tend to transmit more higher frequency energy around the bend than mitered elbows without vanes and so they provide less attenuation for the duct path. However, they yield lower pressure drop and therefore are commonly used. Tables 17.7–17.9 present the estimated sound attenuation for various elbow types.

TABLE 17.7 Insertion Loss of Unlined and Lined Rectangular Elbows without Turning Vanes

	Insertion Loss, dB	
	Unlined Elbows	Lined Elbows
$fw < 1.9$	0	0
$1.9 \leq fw < 3.8$	1	1
$3.8 \leq fw < 7.5$	5	6
$7.5 \leq fw < 15$	8	11
$15 \leq fw < 30$	4	10
$fw > 30$	3	10

Note: $fw = f \times w$, where f = center frequency, kHz, and w = width, in.
Source: 1999 ASHRAE *Applications Handbook*, © American Society of Heating, Refrigerating and Air Conditioning Engineers, Inc., www.ashrae.org.

TABLE 17.8 Insertion Loss of Unlined and Lined Rectangular Elbows with Turning Vanes

	Insertion Loss, dB	
	Unlined Elbows	Lined Elbows
$fw < 1.9$	0	0
$1.9 \leq fw < 3.8$	1	1
$3.8 \leq fw < 7.5$	4	4
$7.5 \leq fw < 15$	6	7
$fw > 15$	4	7

Note: $fw = f \times w$, where f = center frequency, kHz, and w = width, in.
Source: 1999 ASHRAE *Applications Handbook*, © American Society of Heating, Refrigerating and Air Conditioning Engineers, Inc., www.ashrae.org.

TABLE 17.9 Insertion Loss of Unlined Round Elbows

	Insertion Loss, dB
$fw < 1.9$	0
$1.9 \leq fw < 3.8$	1
$3.8 \leq fw < 7.5$	2
$fw > 7.5$	3

Note: $fw = f \times w$, where f = center frequency, kHz, and w = width, in.
Source: 1999 ASHRAE *Applications Handbook*, © American Society of Heating, Refrigerating and Air Conditioning Engineers, Inc., www.ashrae.org.

Prefabricated Sound Attenuators

Prefabricated sound-attenuating devices (duct silencers) are available from a variety of manufacturers in a variety of styles, configurations, and constructions to fit virtually every HVAC system application and to meet every sound attenuation requirement. The sound-absorptive media may be conventional dissipative materials such as glass fiber, mineral wool, or nylon wool covered by a perforated metal facing sheet to provide physical protection for the fibrous sound-absorbing material from erosion by the turbulent flow. For low-velocity flows the sound-dissipating material may be protected only by a thin surface layer of flow-resistive facing such as applied on the surface of duct liners. For special applications, to prevent any fibrous material from getting into the air stream, the fill material can be sealed in thin plastic bagging. This typically will slightly increase the acoustical attenuation at specific low and midfrequencies and diminish it substantially at high frequencies compared to unfaced fill. Special construction details are typically required to prevent the film from sealing the holes in the perforated metal protective facing and to avoid chafing of the film on sharp edges formed on the back of the perforated metal in the punching process. Detailed information on the design and prediction of dissipative silencers is given in Chapter 9. There are also silencers without traditional dissipative fill but with special acoustically reactive surfaces lining the air channels which remove acoustical energy from the air stream.

Basic silencers have a straight-through air path with aerodynamic inlet and discharge geometry to help minimize pressure losses which are greatest at the flow transition points. Silencers are also available with special flow configurations for special applications. For HVAC system applications, elbow configuration silencers are particularly notable since these can help to avoid difficult flow conditions that could otherwise exist or even be caused by aerodynamically poor application of a straight silencer.

Manufacturers' information should be used for the prediction of the sound attenuation, pressure drop, and flow-generated noise. For a given application

there are typically several silencers that might be able to provide the desired acoustical performance. The noise control and HVAC design engineers must select one that also yields a suitably low pressure drop and trade-offs will need to be considered between the length and the resistance class of the silencer. For most typical HVAC system applications the pressure drop across the silencer should be limited to about 0.30 in. water gauge (wg). The pressure loss can be higher, but the designer needs to be sure the extra pressure loss will not have undesirable impacts on the system. The energy consumed to overcome the pressure drop of the silencer should be considered in deciding what pressure loss is acceptable. Over the lifetime of the system, significant energy cost savings will result from having a silencer that has a particularly low pressure drop. The savings may be much more than the extra initial cost of the lower pressure drop model. Silencers should not be placed in the duct just upstream of a fan to avoid having the turbulent flow from the tail end of the baffles interact with the fan blade, which will increase the fan's broadband and blade passage tone noise.

Ideally, the airflow entering and leaving the silencer should be straight and smooth to approach the conditions under which the sound attenuation, pressure drop, and flow noise of the silencer are tested in accordance with ASTM E-477 or ISO 7235. In the field, such ideal conditions seldom occur, and there is some degree of excess pressure drop beyond the catalogued value for the application due to system effects. The system designer needs to consider these when making pressure drop predictions. To the extent that the silencers are placed in positions where the inflow is distorted and turbulent, there will be extra pressure drop. Figure 17.1 presents some common flow configurations and the associated extra pressure drop multiplier to be applied to the catalogued silencer pressure loss.

Because of the high velocity flows through the narrow silencer channels and the imperfect conversion of velocity pressure to static pressure at the discharge, turbulence is generated in the flow through silencers and this creates flow noise. The manufacturers typically tabulate the flow-generated noise of their silencers at various face velocities. The total flow-generated sound power is a function of the face velocity and the area of the silencers, and the noise generated by the silencer will typically be published for various face velocities and for a specific cross-sectional area. This data must be adjusted for the cross-sectional size of the silencer actually used when one predicts the flow-generated noise by adding 10 log A_1/A_0 to the published data (where A_1 is the actual silencer area and A_0 is the area that is the basis for the presented data, in consistent units). The noise generated by the silencer becomes another source of noise that propagates along the duct and needs to be addressed. The closer the silencer is placed to the receiving space and the quieter the receiving space, the more care needs to be taken in controlling flow-generated noise because there is less opportunity to attenuate it before it reaches the receiving space. For duct systems serving spaces where the noise goal is moderate (perhaps NC-35 to NC-40; NC = noise criterion) silencers located near the occupied space (such as on the room-side of a terminal box) typically need to be sized for less about 0.10 in. wg pressure drop. Where the noise goal is more stringent, the pressure loss through the silencer

DUCT ELEMENT	SILENCER SYSTEM EFFECT FACTOR: DUCT ELEMENT ON... SILENCER INLET	SILENCER DISCHARGE
TRANSITIONS		
$7\frac{1}{2}$ degrees per side		
Distance of transition from silencer		
$D = 1$	1.0	1.0
$D = 2$	1.1	1.1
$D = 3$	1.2	1.1
25 degrees per side		
Distance of transition from silencer		
$D = 1$	1.3	1.1
$D = 2$	1.5	1.1
$D = 3$	1.8	1.1
45 degrees per side		
Distance of transition from silencer		
$D = 1$	1.7	1.1
$D = 2$	1.9	1.1
$D = 3$	2.0	1.1
ELBOW-RADIUS TYPE		
Distance of radius elbow from silencer		
$D = 0$	1.2	1.4
$D = 1$	1.1	1.2
ELBOW-MITERED TYPE WITH SHORT TURNING VANES		
Distance of mitered elbow from silencer		
$D = 0$	1.2	1.1
$D = 1$	1.2	1.1
$D = 2$	1.2	1.2
ELBOW-MITERED TYPE WITH NO TURNING VANES		
Distance of mitered elbow from silencer		
$D = 0$	1.2	2.9
$D = 1$	1.0	1.8
$D = 2$	1.1	1.4
ABRUPT ENTRY OR EXIT		
Smooth inlet or discharge		
Distance of entry or exit from silencer		
$D = 0$	1.1	1.8
$D = 1$	1.0	1.4
$D = 2$	1.0	1.1
$D = 3$	1.0	1.0
ABRUPT ENTRY OR EXIT		
Sharp inlet or discharge		
Distance of entry or exit from silencer		
$D = 0$	1.2	2.0
$D = 1$	1.1	1.5
$D = 2$	1.0	1.2
$D = 3$	1.0	1.0
CENTRIFUGAL FAN		
Distance of centrifugal fan from silencer		
$D = 0$	1.5	2.0
$D = 1$	1.2	1.7
$D = 2$	1.1	1.5
$D = 3$	1.0	1.2
AXIAL FAN		
Distance of axial fan from silencer		
$D = 0$	1.5	2.0
$D = 1$	1.2	1.7
$D = 2$	1.1	1.5
$D = 3$	1.0	1.2

D is the diameter of round duct or equivalent diameter of rectangular duct.

FIGURE 17.1 Factor by which catalogue silencer pressure loss is multiplied for various applications. (Reproduced with permission from Vibro-Acoustics.)

needs to be commensurately lower. When silencers are located near the fans, at the beginning of systems, the noise of the fan on the building side of the silencer will often still be substantially higher than the flow-generated noise of the silencer (if selected for reasonable pressure loss), so that flow noise is not of concern. The lower the noise goal, the more carefully this needs to be checked.

Poorly selected and positioned silencers, which produce excessive pressure drop, can cause more noise problems than they solve.

Sound Attenuation by Plenums

Plenums in duct systems can often provide significant sound attenuation for the ducted path. The extent of the attenuation depends upon the size of the plenum compared to the connecting ducts, the orientation of the inlets and outlets, and the absorptivity of the inner walls. Equations (17.3)–(17.5) as applied to Fig. 17.2 provide a method for estimating the attenuation provided by plenums:

$$\mathrm{TL} = -10 \log_{10}\left[S_{\text{out}}\left(\frac{Q\cos\theta}{4\pi r^2} + \frac{1-\alpha_A}{S\alpha_A}\right)\right] \tag{17.3}$$

where (refer to Fig. 17.2)

where TL = transmission loss, dB
S_{out} = area of outlet section of plenum, ft^2
S = total inside surface area of plenum minus inlet and outlet area, ft^2
r = distance between centers of inlet and outlet sections of plenum, ft
Q = directivity factor, which may be taken as 4
α_A = average absorption coefficient of the plenum lining
θ = angle of vector representing r to long axis l of plenum

The average absorption coefficient α_A of the plenum lining is

$$\alpha_A = \frac{S_1\alpha_1 + S_2\alpha_2}{S} \tag{17.4}$$

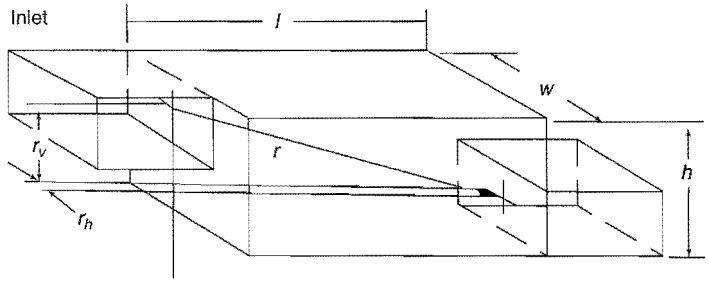


FIGURE 17.2 Schematic of plenum chamber. *Source*: 1999 ASHRAE *Applications Handbook*, © American Society of Heating, Refrigerating and Air Conditioning Engineers, Inc., www.ashrae.org.

where α_1 = sound absorption coefficient of any bare or unlined inside surfaces of plenum
S_1 = surface area of bare or unlined inside surface of plenum, ft^2
α_2 = sound absorption coefficient of any acoustically lined inside surfaces of plenum
S_2 = surface area of acoustically lined inside surface of plenum, ft^2

The value of cos θ is obtained from

$$\cos\theta = \frac{l}{r} = \frac{l}{(l^2 + r_v^2 + r_h^2)^{0.5}} \tag{17.5}$$

where l = length of plenum, ft
r_v = vertical offset between axes of plenum inlet and outlet, ft
r_h = horizontal offset between axes of plenum inlet and outlet, ft

The precision of plenum insertion loss predictions is generally not considered to be very good, and research is being conducted currently to improve the accuracy of the predicted attenuation of these duct elements. The results of the above equations are only valid where the wavelength of sound is small compared to the characteristic dimensions of the plenum. Equation (17.3) is not valid below the cutoff frequency of the entering and exiting ducts, given as

$$f_{\text{co}} = \frac{c_0}{2a} \quad \text{for rectangular ducts}$$

and

$$f_{\text{co}} = \frac{0.586c_0}{d} \quad \text{for circular ducts}$$

where f_{co} = cutoff frequency, Hz
c_0 = speed of sound in air, m/s
a = larger cross-sectional dimension of duct, m
d = diameter of duct, m

End-Reflection Loss

When sound propagating along ducts reaches an abrupt change in cross-sectional area (such as the termination of a duct system at a diffuser or grille) and there is no disturbance of the sound field as it makes the transition, some low-frequency sound reflects back from the point of the abrupt change and does not propagate on toward the receivers of concern. The end-reflection loss is a function of the size of the termination compared with the acoustical wavelength and the specific location of the duct termination within the room. Typical values of end reflections are given in Table 17.10. Note that these are for idealized conditions. If there is a grille or diffuser at the termination of the duct system or if the grille or diffuser is not in the middle of a large plane (like the ceiling) but is in a two- or three-dimensional corner of the room, the end reflection will be lower. For each factor that deviates

TABLE 17.10 Duct End-Reflection Loss

Duct Diameter, in.	End Reflection Loss by Octave-Band Center Frequency, dB					
	63 Hz	125 Hz	250 Hz	500 Hz	1000 Hz	2000 Hz
	Duct Terminated in Free Space					
6	20	14	9	5	2	1
8	18	12	7	3	1	0
10	16	11	6	2	1	0
12	14	9	5	2	1	0
16	12	7	3	1	0	0
20	10	6	2	1	0	0
24	9	5	2	1	0	0
28	8	4	1	0	0	0
32	7	3	1	0	0	0
36	6	3	1	0	0	0
48	5	2	1	0	0	0
72	3	1	0	0	0	0
	Duct Terminated Flush with Surface					
6	18	13	8	4	1	
8	16	11	6	2	1	
10	14	9	5	2	1	
12	13	8	4	1	0	
16	10	6	2	1	0	
20	9	5	2	1	0	
24	8	4	1	0	0	
28	7	3	1	0	0	
32	6	2	1	0	0	
36	5	2	1	0	0	
48	4	1	0	0	0	
72	2	1	0	0	0	

Source: 1999 ASHRAE *Applications Handbook*, © American Society of Heating, Refrigerating and Air Conditioning Engineers, Inc., www.ashrae.org.

from the ideal case, one might consider the effective duct emitting area to be 4 times the actual duct size when entering the chart.

Note that end-reflection losses are not limited to the duct terminations but can be a useful technique within a ducted system to get low-frequency attenuation, for instance where a duct abruptly enters a large highly sound absorptive plenum volume.

Room Effect

Room effect is the translation of the sound power emitted into the room from the duct system to the sound pressure level that results in the space at a given location. The process of predicting the sound pressure level from the sound power level is treated in detail in Chapter 7.

The classical method to relate the sound pressure that results in a room to the sound power emitted from a source is modeled by a point sound source for small-size sources, such as round or rectangular diffusers, and by a line sound source in the case of strip diffusers or duct breakout. Note that the amplitude of the reverberant sound field, which dominates at large distances from the source, is independent of the nature of the source. However, the amplitude of the direct sound, which dominates in the vicinity of the sound source, strongly depends on how the sound energy spreads from the source.

For a point sound source radiating into the room the sound pressure level at a distance r (resulting from the power-based addition of the direct and reverberant fields) is given in the equation

$$L_p(r) = L_w + 10 \log_{10}\left(\frac{Q}{4\pi r^2} + \frac{4}{R}\right) \tag{17.6}$$

where L_w = source sound power level, dB re 10^{-12}W
L_p = sound pressure level, dB re 2×10^{-5}N/m^2
R = room constant, $= S\alpha_A/(1-\alpha_A)$, m^2
S = total room absorption, m^2
α_A = average absorption coefficient of room surfaces
r = source–receiver distance, m
Q = inverse of fraction of sphere to which sound energy radiates

For a case where there is only one source of concern for design, using this equation is simple and sufficient. However, where there are multiple noise sources such as various diffusers or grills with close to the same noise emission level and producing close to the same noise level at the receiver position, some way to adjust the room effect for the multiple diffusers is needed. This might be done by adjusting the room effect by 10 log N decibels, where N is the effective number of outlets contributing to the sound at the critical receiver location. Other, more sophisticated, methods based of sound propagation modeling in rooms presented in Chapter 7 may be used when dealing with special situations.

17.2 FLOW NOISE IN DUCTED SYSTEMS

The noise generated by flow in duct systems is a concern for noise transmission inside the duct along the duct path and that radiated from the outside surface of the duct. Noise generated at particular fittings or duct elements can be estimated in accordance with the methods presented in Chapter 15. Flow-generated noise propagates down the ducts just like noise from any other sources in the duct system. It is typically in the mid- and higher frequency range and thus is relatively easily attenuated by dissipative treatments such as silencers or lining. When attenuating elements do not exist in the ductwork between the source and the occupied space, this noise can become a concern.

TABLE 17.11 Recommended Airflow Velocities in Lined Duct Systems[a,b]

	Airflow Velocities (fpm) Consistent with Indicated Noise Criterion (NC) through Net Free Area of Duct Section or Device							
	NC 15		NC 20		NC 25		NC 30	
Duct Element or Device	Supply	Return	Supply	Return	Supply	Return	Supply	Return
Terminal device[c] ($\frac{1}{2}$in. minimum slot width)	250	300	300	360	350	420	425	510
First 8–10 ft of duct	300	350	360	420	420	490	510	600
Next 15–20 ft of duct	400	450	480	540	560	630	680	765
Next 15–20 ft of duct	500	570	600	685	700	800	850	970
Next 15–20 ft of duct	640	700	765	840	900	980	1080	1180
Next 15–20 ft of duct	800	900	960	1080	1120	1260	1360	1540
Maximum within space[b]	1000	1100	1200	1320	1400	1540	1700	1870

Note: Fan noise must be considered separately. Reduce duct velocities (not diffuser/grille velocities) by 20% if ductwork is unlined.

[a] All ducts with 1-in.-thick internal sound absorptive lining.

[b] Above mineral fiber panel ceiling. Lower velocities 20% if open or acoustically transparent ceiling.

[c] No dampers, straighteners, deflectors, equalizing grids, etc. behind terminal devices.

The following guidelines are offered for duct sizing based on the location, type, and class of ductwork:

- <3000 feet per minute (fpm) velocity in round ducts in mechanical rooms and shafts,
- <2500 fpm velocity in rectangular ducts in mechanical rooms and shafts,
- <2000–2500 fpm velocity in the ceiling of occupied spaces with mineral fiber ceiling for NC-35 to NC-40 goal,
- <1500–2000 fpm velocity in the ceiling of occupied spaces with open or acoustically transparent ceiling for NC-35 to NC-40 goal,
- <1500 fpm velocity in larger final distribution ducts serving NC-35 to NC-40 spaces,
- <a friction rate (pressure loss rate) of 0.10 in. wg/100 ft of duct run in smaller final duct distribution for NC-40, and
- <a friction rate (pressure loss rate) of 0.08 in. wg/100 ft of duct run in smaller final duct distribution for NC-35.

Airflow velocity guidelines for the design of special low noise spaces (typically NC-30 and lower) are presented in Table 17.11 for lined duct systems.

17.3 SYSTEM DESIGN FOR ESPECIALLY QUIET SPACES

The lower the noise goal for a particular space, the more carefully the duct arrangement needs to be considered from the air balance and aerodynamic

standpoints. In particular, the duct system needs to be designed to be as naturally balanced as possible. That is, if the system is turned on, the airflow naturally delivered from each outlet would match the desired airflow with little or no damper throttling to control the flow. Creating systematically branching duct arrangements to an array of diffusers or grilles is typically a good approach. There should be suitably long straight ducts between the branches for the flow to straighten out and divide, as desired at the next branch. However, not all buildings and conditions can accommodate this design concept. Often there is a need to have a series of diffusers or branches to diffusers off the side of a large main duct. Having at least a modest length (a duct diameter) of straight duct run out to the diffuser is always preferred to improve the airflow presentation to the back of the diffuser and to create a more desirable position for a damper that can be used to control the flow at a point that is away from the diffuser. For these cases, it is often best to have the main duct that feeds the diffusers remain a constant size so that the pressure drop along the main "header" duct becomes small and the flow distribution is controlled by the pressure drop of the runouts. To achieve a naturally balanced design, it is generally best to have the diffusers and grilles be in a reasonably cohesive grouping rather than be widely spaced out.

It is recommended to avoid having a tight cluster of diffusers serving a critical space and then a long "tail" duct extending downstream, because to balance the system, it will be necessary to throttle dampers near the diffusers serving the critical space, and this will cause noise to be generated.

Dampers should be provided in duct systems as needed to control the flow, but they must be located sufficiently far from the terminal devices so that the turbulence and noise they generate can be sufficiently attenuated before it reaches the occupied space. For especially quiet systems, dampers should not be placed at or near the face of the diffusers and grilles. It is essential to use dampers well back in the duct system to adjust for major deviations from a natural air balance design.

The airflow velocity near diffusers and grilles needs to be appropriately slow to avoid excessive noise generation. As one moves back in the duct system away from the critical space, flow velocities can progressively increase. Ideally, the velocities would step down in moving toward the critical space in a manner that is consistent with the desired systematic branching pattern. The best correlation between airflow velocities and the noise resulting in the space of interest is for noise from grilles and diffusers in the room and for the ducts closest to the room. The correlation between noise reaching the space of interest and the flow velocity becomes less direct as one moves further into the duct system, away from the receiving space. Thus, there is not much room for compromise in velocities close to the occupied space, but there may be room for compromise from an ideal design at greater distances from the occupied space.

Table 17.11 presents suggested velocities in duct systems serving quiet spaces to help ensure achieving particular noise goals with acoustically lined ductwork. These suggested flow velocities generally assume that the duct configuration will be only average in terms of its aerodynamics. If very desirable airflow geometry

is achieved, somewhat higher velocities can be allowed. The suggested velocities through the net free area of the diffusers and grilles, given in Table 17.11, assumes a nominal slot width of about 1/2 in. To the extent that wider slot widths are used, higher velocities can be allowed for a given noise goal. Typically, there might be an allowable increase in slot velocity of 15–20% for each doubling of the nominal slot width up to about 2-in.-wide slots. Special nozzle-type diffusers are available to operate more quietly so that they can throw the air further for a given noise level. The manufacturer's noise data should be reviewed for special diffuser applications, being sure that the noise generation is adjusted from the conditions under which the devices are tested to the actual conditions of use. Because, at the indicated velocities, it is difficult to blow the air very far, for quiet systems, supply air is often delivered using a distributed array of diffusers at the ceiling rather than from the sidewalls of a space. This is not to say that sidewall blow applications need to be avoided; they just need to be limited to covering a small zone at the sides of the space rather than trying to condition the entire space from this position. Using a combination of ceiling diffusers and sidewall blow diffusers can be a useful technique to divide the main ducts into smaller pieces that will fit through the building more easily than handling all the airflow in fewer large ducts. Note that to help fit ducts into buildings it is often better to avoid having diffusers or grilles directly off the sides of a main duct because the entire airflow in the main duct will have to run at a very low velocity and this duct will be very large. However, in applications where there is ample space for large ducts or where ducts are exposed, this may be a simple, neat, and clean approach to the design. Developing the duct distribution in a systematic branching pattern naturally allows the ducts that have the large airflow quantity to be sized at a higher velocity, which helps them fit in the building more easily. For quiet systems, the space required to handle the airflow at the desired velocities can be considerable and this can translate into requiring more building volume in which to maneuver the ducts. Considering the system design concept and velocities early in the design can allow the building to be more economical from the standpoint of the sheet metal that is used and the building volume that is constructed. Not considering the duct system requirements early in the design may result in an undesirable compromise in the design and/or the noise levels that can be achieved.

Note that about a 20% change in velocity is generally associated with a 5-NC point change in noise level in the occupied spaces. Thus, a compromise of increasing the airflow velocities in a project design by 20% will generally increase the noise by about 5 NC points. Also, lowering the noise level by about 5 NC points requires about 20% lower velocities; this translates into only about 10–15% increase in the dimensions and surface area of round and (reasonably square) rectangular ducts. Increasing the noise goal by 5 NC points will only save about 10–15% of the sheet metal cost.

The airflow velocity guidelines in Table 17.11 assume that there will be lining in the duct system, and this is generally recommended to control the noise generated by flow in the ducts at fittings and unexpected flow obstacles in systems that are to be especially quiet. For lower noise goals, more things need to be done properly in the implementation of the design and there is less margin for error. If the ductwork does not have lining, it is suggested that the velocities in the ductwork (not at the diffusers and grilles) be about 20% lower than indicated to allow about a 5-dB margin for the lack of attenuation in the duct path.

17.4 DIFFUSER AND GRILLE SELECTION

The airflow velocities for low-noise spaces presented in Table 17.11 are only guidelines which include a number of assumptions, including that the nominal slot width is about 1/2 in. and the ductwork leading to the diffuser is only nominally configured. This also includes assumptions regarding the room effect and the number of diffusers that are contributing to the sound field at the receiving position. Note that the larger the room, the more likely it is that diffusers will be more numerous (and hence there will be more sources of noise), but in this case, it is also more likely that the diffusers will be further from the receiver and hence the room effect will be larger. These two factors tend to counter each other so that a single velocity guideline chart can cover a wide range of applications.

Manufacturers often provide data for the noise generated by their diffusers and typically these are boiled down to a single NC rating for the diffuser at a particular flow. Be careful in applying manufacturers' data because they are generated under ideal flow conditions and often include very favorable room effects so that the reported noise levels are as favorable as possible. Also, they typically are reported for one diffuser or for a short section of a linear diffuser where the application may have many more such elements contributing to the noise level at a receiver location. It is necessary to account for the sum of the noise that is generated by multiple diffusers/grilles which reach the receiver as well as to make other adjustments to correct the assumptions in the presented data to match the actual conditions of a project. It is also essential to make adjustments to the ideal flow condition used as the basis for the data to get to the actual applied flow condition. For especially quiet spaces, use of the velocity guidelines may be a preferable approach for establishing the selection parameters for the diffusers and grilles.

The noise produced by dampers needs to be assessed separately from diffuser and grille noise, but having two flow turbulence-producing devices closely spaced in series may add to the noise each device produces by itself.

Displacement ventilation systems which deliver air to the occupied zone through diffusers at the floor can often be very quiet. This is largely because air is introduced to the space in small quantities at any one location and the flow velocity at the diffuser needs to be particularly low for comfort reasons. The result can be a system with little diffuser-generated noise and this can be a favorable design approach for spaces that need to be very quiet.

17.5 NOISE BREAKOUT/BREAK-IN

When ducts containing high levels of noise pass though spaces with low or moderate noise goals, it is necessary to consider whether the noise that transmits

out through the surface of the sheet metal duct (called the breakout noise) is suitably controlled. Similarly, when a duct in which the sound field inside has been quieted passes near a noisy piece of mechanical equipment prior to penetrating the mechanical room wall, noise may break into the duct and travel down the duct to a receiving space of concern. To minimize concern for noise breakout/break-in, it is usually best to position the high-insertion-loss elements in the duct system (the silencer) at or very near the penetration of the mechanical room boundary. However, it is not always possible to achieve this goal along with the goal of achieving good aerodynamics for the application of the silencer. Special elbow (or other configuration) silencers can help achieve the goal of the desired position of the silencer for breakout/break-in considerations while avoiding poor flow. This is a very good use of special silencers.

The noise that breaks out of and into ducts can be predicted using Eqs. (17.7) and (17.8), respectively:

$$L_{w(\text{out})} = L_{w(\text{in})} - \text{TL}_{\text{out}} + 10 \log\left(\frac{S}{A}\right) - C \tag{17.7}$$

$$L_{w(\text{in})} = L_{w(\text{out})} - \text{TL}_{\text{in}} - 3 \tag{17.8}$$

where $L_{w(\text{out})}$ = sound power level of sound radiated from outside surface of duct walls, dB
$L_{w(\text{in})}$ = sound power level of sound inside duct, dB
S = surface area of outside sound-radiating surface of duct, in.^{2}
A = cross-sectional area of inside of duct, in.^{2}
TL_{out} = duct breakout transmission loss, dB
C = correction factor as follows for values of $\Delta = \text{TL}_{\text{out}} - 10 \log(S/A)$

Δ	C
$> +10$	0
$+8$ to $+5$	1
$+4$ to $+2$	2
$+1$ to -1	3
-2 to -3	4
-4	5
-5	6
-6	7
-7	8
-8	9
<-9	$-\Delta$

Note: These breakout and break-in equations should not be used where $\Delta < -10$. Also, where Δ is a negative number, the precision of the result is questionable. The value of Δ tends to go negative with relatively long duct sections. This approach does not take into account any dissipative attenuation along the duct path, but at the low frequencies principally of concern for breakout and break-in issues, dissipative attenuation is usually small along the duct path in the length of duct sections for which the approach should be used.

The noise breakout formula can further lead to prediction of the sound pressure level in a receiving space by applying an appropriate room effect and including the sound isolation of any intervening construction. The noise break-in equation will determine the sound power that can then be used as a source level and the propagation of this noise can be traced along the duct system. Treatments for noise breakout/break-in typically include increasing the surface weight of the duct construction, stiffening the duct, applying a flexible mass barrier material on resilient backing (such as a glass fiber mat or foam), or enclosing the duct in gypsum board using a variety of possible details. Prediction of the insertion loss achieved by various types of wrappings is given in Chapter 13. The further the enclosing mass layer is from the duct surface and the heavier the enclosure material, the better this will control low-frequency sound, which is most typically the concern. Circular ducts are inherently stiffer than rectangular ducts made of flat metal sheets, and for this reason, distribution systems using circular ducts are often less prone to breakout/break-in noise problems. Note that there is a particular concern for breakout/break-in noise when glass fiber panel or other acoustically transparent ceilings are used in occupied spaces in buildings. Where there is a solid gypsum board ceiling, breakout noise is naturally less of a concern than where there is a conventional mineral fiber acoustical ceiling.

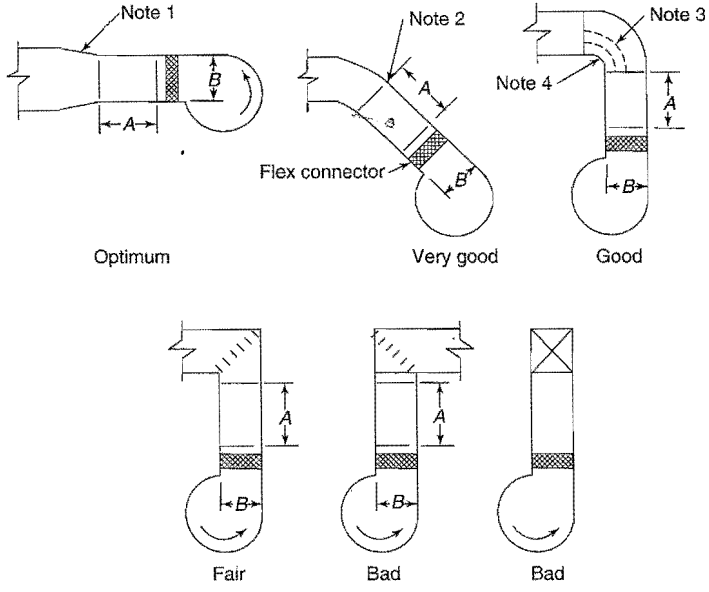
Ducts that drop out of the bottom of rooftop air-handling units into the ceiling plenums above occupied spaces are a classic case where duct breakout noise is a problem, and this typically is worst when the supply duct discharges directly down into the ducts rather than into a plenum within the unit. Elbow silencers with high-transmission-loss casings can be a convenient method of addressing this problem. If a straight silencer is used and is located well away from the elbow that turns in the ceiling space, there can be a significant amount of duct wall which can radiate noise to the occupied space and may need to be treated. This is discussed further under the rooftop unit section (Section 17.10). Most of the duct enclosure treatments to address this concern are very difficult to install, especially when there is limited space and the building is finished. Whenever possible, designs should be developed which avoid the need for this sort of treatment.

17.6 FANS

Fans are typically the major source of noise emission into duct systems. The various fan types have differing noise spectrum and magnitude characteristics and this is also a function of the duty. Certain fans are aerodynamically better suited for particular flow and pressure applications. This needs to be considered for the full operating range of the application. Many older references, such as

older editions of the ASHRAE handbooks, include generic methods to predict the noise generated by fans, and such sources can provide useful guidance in the absence of more specific data from the manufacturer for the fans that are planned. If such data are used, remember that, due to changes in manufacturing methods, modern fans may not be made the same way as the fans used as the basis for the generic prediction methodology. Often new fans are made more economically and produce more noise that older fans. It is best to obtain the noise data for the fan from the prospective manufacturer, tested in accordance with the most current applicable standards. These data should be used as a guide in the selection of the fan and as a point of comparison between candidate fans for an application. In addition, the quietest of the reasonable fans should be selected for a given application. Such a process should help avoid selecting a particularly noisy fan, which could lead to unexpected noise problems or noise control treatment which could unduly burden the system.

The manufacturer's noise emission data for fans are based on a standard test which may or may not closely match the conditions of a particular field



Notes:
1. Slopes of 1 in 7 preferred. Slopes of 1 in 4 permitted below 200 fpm.
2. Dimension *A* should be at least 1.5 times *B*, where *B* is the largest discharge duct dimension.
3. Rugged turning vanes should extend the full radius of the elbow.
4. Minimum 6-in. radius required.

FIGURE 17.3 Various outlet configurations for centrifugal fans and their possible rumble conditions. *Source*: 1999 ASHRAE *Applications Handbook*, © American Society of Heating, Refrigerating and Air Conditioning Engineers, Inc., www.ashrae.org.

application. The noise radiated by the fan into the duct will vary with the particular acoustical impedance of the connected ductwork. Consequently, the actual sound power of the fan that is emitted into a duct system may differ from the manufacturer's data.

Particular care should be given to the inlet and outlet flow conditions for fans. Poor inlet flow can unbalance the flow over a fan wheel, causing performance problems and excess noise generation at the anticipated speed for the application. The fan speed may need to be increased to compensate for unexpected pressure losses and thus generate more noise than expected. Inlet vanes or substantial flow distortion due to flexible connections protruding into the flow can easily cause an increase of noise on the order of 6 dB across the full frequency spectrum. The local airflow velocities on the discharge of fans can be quite high in some regions and probably will not be uniform over the outlet area. This needs to be taken into account in the system design and arrangement. It is often not possible to create ideal flow conditions, but it is important to create at least reasonable flow conditions and to avoid poor flow conditions which can create severe noise problems. Figure 17.3 illustrates some favorable fan discharge conditions as well as conditions that need to be avoided. It is always necessary to consider the flow arrangement on the discharge of a fan or air-handling unit to be sure that the duct and fan geometry work together as well as possible for the condition and, most essentially, to avoid poor conditions. Poor flow conditions at the fans can lead to low-frequency noise generation, either by the fan or due to large-scale turbulence in the ductwork which will drum the duct walls, causing a low-frequency noise problem that can be very difficult to solve.

17.7 TERMINAL BOXES/VALVES

Many HVAC systems serving buildings include a variety of terminal boxes or valves to control the amount of air delivered to the occupied zone. Some boxes are used to vary the airflow to the room in accordance with thermal load. Others provide a constant amount of flow to assure ventilation rates and control zone pressurization. Some boxes incorporate fans to mix plenum air with a variable amount of main system air to maintain a minimum amount of air movement while delivering variable heating/cooling. All of these boxes and valves have in common that they produce a pressure drop from the higher pressure in the main duct system to a low pressure in the final distribution ductwork on the room side of the box. In throttling the pressure from the main to the final distribution ductwork, noise is generated and this noise needs to be considered in the design to meet desirable noise levels in the occupied spaces. The greater the airflow quantity through the box, the greater the noise that is generated. However, the most significant factor is that the noise boxes generate is a strong function of the pressure drop across the valve. Boxes on a system that are near the fans naturally see a higher pressure in the main duct than boxes near the ends of the system, and boxes close to the beginning of the system will generate more noise than

comparable boxes located toward the end of the system. Excess static pressure in the main ducts can be a significant factor in noisy systems as the terminal boxes in the system are throttling hard (have large pressure differential across them) to control the excess pressure.

The manufacturers of terminal boxes generally provide noise data for their boxes rated at various flow rates and pressure losses, and these data can be used for noise analysis of the ducted system just as fan noise propagation down the ducts is done. In such an analysis, the pressure loss that is of interest in determining the noise of the box is the actual pressure drop that the box is expected to produce in the field, not the minimum pressure at which the box will satisfactorily control flow or some arbitrary pressure loss that is assigned. Because of airflow control considerations, the boxes in many applications have inlet flow conditions that are reasonably close to the ideal flow condition under which the terminal box is tested for flow and noise. However, if there are adverse flow conditions, the noise generated by the boxes may be higher than the manufacturer's rating.

Noise radiation from the casings of the boxes can also impact the occupied spaces near them, and to enable assessment of this, manufacturers also publish casing radiated noise data. For fan-power boxes, these data include the noise that radiates from the fan out of the plenum air inlet and this can be a significant issue. In some cases it is necessary to provide attenuation for the plenum air inlet to the box. Most moderate-size terminal boxes operating at nominal pressures can be located in the ceilings of occupied spaces where the noise goal is NC-35 or higher when there is a conventional mineral fiber ceiling. Where boxes are in the ceilings of spaces with noise goals more stringent than NC-35, where system pressures are anticipated to be high, and/or where ceilings with lower transmission loss are used, special consideration should be given to the issue of casing radiated noise. In particular, be cautious of exposed box applications or where glass fiber, perforated, or open-slat ceilings are used.

The manufacturer's noise data should be reviewed for verification, but typically the frequency band of concern for flat-plate damper boxes is the 250-Hz octave band; for pneumatic-style boxes, the 500-Hz octave band; and for plunger-style valves, the 1000-Hz octave band. The type of noise control treatments that are applied in the duct systems should ideally be selected to treat the particular noise spectrum that is expected based on the box/valve type that is used.

For systems that utilize terminal boxes/valves it is usually a good idea to try to conceive the main duct system to be able to deliver the design airflow with the minimum overall pressure loss and the minimum differential in pressure arriving at the various boxes in the system. Consider gradually reducing the flow resistance in the main duct as the duct proceeds toward the end of the run and the magnitude of air being handled is reduced. The overall velocity in the duct system is often a significant factor determining the pressure drop from beginning to end, and the design velocities should be as low as reasonably possible. Use aerodynamically favorable fittings. Try to avoid particularly long duct runs by using more vertical shafts in the building to minimize the length of duct runs on the floors served. Where it is possible and acceptable to create ring ducts fed from both ends to serve the floor plate of a building, this can favorably reduce the pressure that is needed in the system. Consideration of these design features can help avoid noise problems and/or minimize the magnitude of attenuation treatments that are needed.

Always be sure that the final setup and balancing have the system operating at the lowest pressure that is consistent with delivering design airflow. This includes making sure that the system pressure cannot be further lowered without jeopardizing the required flow at the extremes of the duct system and making sure that the fan is operating at the lowest speed that will deliver design flow. If there are inlet vanes on the fan to control capacity, they should be nearly fully open when the system is demanding full design flow. The inlet vanes should not be constricting the airflow when the demand is full; if they are, the fan can probably be slowed, which should reduce noise emission.

17.8 MECHANICAL PLANT ROOM SOUND ISOLATION AND NOISE CONTROL

Good space planning is the best way to avoid sound isolation and noise problems at mechanical rooms. Avoid a common wall with a noise-sensitive space that would require a substantial and expensive wall construction. Very high sound isolation walls typically require discontinues in or special protection of the flanking structural paths; such treatments can be cumbersome and expensive. Having a common wall also invites penetration of that wall with ducts and pipes. Since creating a sufficiently tight seal around a single wall that is penetrated can often be difficult and risky, these should be avoided. Creating a buffer zone of less critical space between a mechanical room and noise-sensitive space allows simpler and less costly constructions to provide the desired isolation, and this minimizes the risk of noise leaks at penetrations. It is good practice to position particularly noisy equipment in mechanical rooms away from critical sound-isolating walls to avoid exposure of critical constructions to unnecessarily high levels of noise. Especially avoid locating equipment extremely close to walls where the sound has no opportunity to lose intensity owing to spreading losses.

Building constructions that provide a good deal of sound isolation can be constructed well, but there is always a door into the space, which is a weak sound isolation condition, and the location of doors needs special planning. Certainly it is necessary to avoid doors to mechanical rooms directly from noise-sensitive rooms. To the extent that it is possible to naturally create a double-door entrance vestibule ("noise-lock") to the mechanical room, such as by accessing the room off of a back-of-the-house corridor that is separated with another door from more public space, this is a good idea since good isolation can be reliably achieved with ordinary door construction.

Mechanical plant rooms often contain equipment which radiate relatively high levels of low-frequency noise, and it is necessary to have heavy constructions,

such as masonry walls, surrounding the room. Lighter constructions such as gypsum board on stud can be used, but double-wall constructions with a substantial air space between the two sides of the wall will likely be required. Hence, light weight wall construction alternatives may take up more floor space. To the extent that there is auxiliary equipment associated with the main plant equipment that is wall mounted, it is often wise to have a double-wall construction so that minor vibration and structure-borne noise that might get coupled to the inner wall of the mechanical room will not get strongly transmitted to the side of the wall construction in the occupied space that is to be protected.

Creating an air-tight seal, as is always necessary for sound isolation, at the heads of walls can be particularly problematic. Necessary firestopping can be achieved for walls with fibrous packing and coating with intumescent material, but this is not a suitable seal for sound control purposes where the basic construction needs to close within a typical caulk joint of the abutting construction. Closing concrete block construction to the underside of fluted metal deck and beams can be very difficult. It is also difficult to create a seal when concrete block comes up under roof constructions that are sloped for drainage or need to accommodate structural deflection. The seals that are needed under these conditions need to be considered early in the design, and practical methods to accomplish the necessary seal in the field need to be detailed.

Floating concrete floors are sometimes required to separate mechanical spaces from noise-sensitive spaces that are above or below the mechanical room. Prediction of the insertion loss of floating floors is provided in Chapter 11. These constructions consist of a concrete slab (typically 4 in. thick) which is supported above the structural floor on resilient mounts. Systems to accomplish this are available from the various isolation product vendors. These constructions can and do provide effective control of sound transmission through floors, but they take up space that needs to be allocated from the start. They also require careful coordination and implementation in the field in order to function as planned. Floating floors are not generally designed as part of a vibration isolation scheme for plant equipment; their primary use is for airborne sound isolation. Concentrated loads such as from equipment can be accommodated on floated floors with appropriate planning and design of the floated floor, but it can also be acceptable to have such loads supported on small structural piers (housekeeping pedestals) that penetrate through the floated floor. To avoid a sound isolation concern at support points that penetrate the floors, these need to be kept as small as practical and typically complete housekeeping pads are not used. The sizes and positions of support piers need to be carefully coordinated in the field. Rather than use floating floors to provide high-level sound isolation to spaces above or below mechanical rooms, it is sometimes necessary to have special sound-isolating ceilings above or below the mechanical spaces. These can be complex to implement and require special coordination of the building services to avoid or minimize penetrations for supports through the ceiling. The timing of construction of the ceiling relative to installation of the building services needs forethought since it typically cannot follow the usual sequence.

17.9 VIBRATION ISOLATION CONSIDERATIONS FOR BUILDING MECHANICAL SYSTEMS

Technical aspects of isolation of vibration sources are treated in detail in Chapter 13. This section will provide some practical guidance regarding the application of vibration isolation systems and devices to building mechanical systems.

Numerous references, such as the sound and vibration control chapters of the ASHRAE *Applications Handbook*,[1] and vibration isolation equipment vendors provide guidance regarding the application of isolation devices for building equipment, and the reader is referred to such sources for specific isolation selections based on the type of equipment, the speed of the equipment, the location in the building, and the sensitivity of the application. For application to building equipment, the selection of vibration isolators is reduced to identifying the deflection of the isolation element under the static load. The deflection of the isolator under load is related to the natural frequency (the frequency at which resonance occurs) of the isolation system by the equation

$$f_n = 3.13\left(\frac{1}{d}\right)^{0.5} \tag{17.9}$$

where f_n = isolator natural (resonance) frequency, Hz
d = isolator deflection, in.

Generally, to provide effective isolation, the natural frequency of the isolation system needs to be no more than 0.30–0.10 times the drive frequency (RPM/60) of the equipment. At ratios greater than 0.30 isolation efficiency will be minimal, and at a ratio of 0.70 there is theoretically no isolation at all. Clearly, it is necessary to avoid having the equipment operate at or near the natural frequency of the equipment. There is generally little point in an isolation system that has a ratio of isolation system natural frequency to equipment drive speed smaller than 0.10 since little additional effectiveness is gained for practical installations and the stability of the equipment on the isolation system can be marginal.

Many pieces or equipment are equipped with variable-speed drives and, in this case, it is generally appropriate to select the isolation system for the normal full speed of the equipment. As the equipment slows down and operates closer to the natural frequency of the isolation system, the isolation system will provide less isolation efficiency, but fortunately, the magnitude of the machine vibration force will be reduced at approximately the same rate. So, there are generally no problems with this. The natural frequency of the isolator should typically be no more than about half of the lowest operating frequency of the equipment to prevent operation too close to resonance, but for more difficult applications, this might be as high as 0.7. If it is not feasible to select large deflection springs, sometimes it is necessary to limit the operating range of the equipment to avoid operating too close to the isolation system natural frequency. This possibility should be considered early in the design. In some cases it might be worthwhile to

judiciously increase the deflection of the springs to lower the natural frequency to avoid impacting equipment operation and efficiency. However, an isolation system should not be so flexible that it creates instability or operational problems such as with alignment or stress transfer.

Inertia bases are used with many pieces of equipment to lower the center of gravity and to reduce the vibratory movement of the equipment when it is resiliently supported. Movement due to starting torque, resistance to forces created by the static pressure a fan develops, and turbulent flow in large fan systems are also reasons such bases are recommended for equipment. The inertia bases only reduce the motion of the equipment on the isolation system. They do not change the inherent unbalanced forces of the equipment, even though the magnitude of vibratory movement of the equipment on the base will be lower. The vibratory displacement of the base and that of the equipment rigidly mounted on it will be lower because the mass that the forces are now acting on is the combined mass of the equipment and the inertia base compared with the mass of the equipment alone. Note that the inertia base does not change the vibration forces that are transmitted to the building assuming that the deflection of the isolation system remains the same. This is because, for the same static deflection, the springs need to be stiffer to support the additional weight of the equipment plus its inertia base.

In theory, the weight of the inertia base would be determined by the desired reduction of the magnitude of the vibratory movement, but the magnitude of the motion of the equipment is not well known, so it is difficult to tell what mass ratio to use. In practice, the weight of the inertia base for building mechanical equipment is often determined by the weight of concrete fill in a steel frame that approximates the rectangular outline of the equipment footprint (with allowance for fastening), and the depth is determined by the need to make the base suitably stiff. The depth of the base is often related to the length of the base and is typically about $\frac{1}{10}$ to $\frac{1}{12}$ the longest dimension. Experience indicates that for many pieces of mechanical equipment, the base weight that results from this methodology is sufficient to control excessive movement and prevent undue forces from being transmitted to connected pipes and appurtenances.

Spring isolators most typically are manufactured to achieve rated deflections of approximately 1, 2, 3, and 4 in. This means that when the full design load for the spring is applied, the spring will approximately deflect this rated distance, and at this condition, the spring will also achieve other desirable design features such as for lateral stability, horizontal stiffness, and deflection reserve to bottoming out. The rated deflection has nothing to do with the deflection actually achieved in the field under the actual equipment load applied. For example, a spring that has a rated deflection of 1 in. for a 1000-lb load will only deflect 0.10 in. if it is supporting 100 lb. The only thing that is important in terms of the isolation efficiency of the mounting is the actual static deflection that results under the applied load and, in the case of this example, the natural frequency would be determined by 0.1 in. deflection. Isolation devices need to be properly selected to achieve the desired minimum static deflection and hence the desired isolation

efficiency. Underloading an isolator can result in achieving less than the desired isolation efficiency and overloading can cause the spring to collapse (bottom out) so that it provides no isolation at all. If a spring is specified to achieve 1 in. minimum deflection under load, there is only one load that will exactly satisfy the requirement if a spring is selected from a 1-in. rated series of springs, and that is the maximum load that the mount can support; lower loads will achieve less than 1 in. deflection and will not meet the required minimum deflection, and greater loads will overload the spring. To achieve the required minimum deflection in this case, a 2-in. rated deflection spring would need to be used so that as long as it is loaded between half and full load, it will achieve the required minimum deflection. This can cause unnecessary expense for isolators that have substantially more capacity than needed. To clarify the performance desired and to avoid unnecessarily costly springs, it is often better to specify spring deflections of 0.75, 1.5, 2.5, and 3.5 in., as expected from 1,2, 3, and 4-in. rated static deflection springs, respectively, so that there is a reasonable selection range available.

For applications where the weight of the isolated equipment may vary substantially from time to time, such as for a cooling tower or chiller if the water is drained for maintenance, the isolation devices that are used need to incorporate some method to restrain the upward movement of the equipment as the weight is removed because this can put excessive stress on connecting pipes. Equipment that is located outdoors may be exposed to wind and exhibit lateral movement which needs to be restrained. Special travel-limited isolators have been developed for this application which will snub the movement of the equipment under such conditions, typically at about 1/4 in.

Many pieces of equipment need to be specially restrained to avoid damage to the equipment or the building if a seismic event occurs. This applies to many pieces of equipment, whether resiliently mounted or not, but clearly, equipment that is resiliently supported could easily fall off its mounts if there is a seismic event. Seismic restraint of equipment is an entirely separate issue from vibration isolation; it is essentially a structural issue. Isolation and seismic restraint become related because so many pieces of equipment that are resiliently supported need restraint. There are seismic restraints available from vendors which are completely separate devices from vibration isolators. In some cases it is convenient to incorporate seismic restraint into the isolators, and products that do this are available from vibration isolation vendors, but it may not be necessary to use combination devices. Where the equipment has no other point of attachment but the mounting points at which suitable support and restraint can be achieved, a combination device is necessary. It is essential that the seismic restraint not compromise the performance of the vibration isolation system, and this is not an easy task considering the relatively tight installation tolerances that are required for both seismic restraints and vibration isolators. Often isolators with combined seismic restraint can help achieve the desired level of installation more reliably, and this is another benefit that such devices provide.

Electrical connections to vibration isolated equipment need to be made flexible to avoid creating a problematic vibration transmission path to the building structure. These are typically made with either a section of flexible conduit or a special flexible electrical coupling. For small-size equipment and conduits, practical lengths of flexible conduit are effective and sufficient. As the size of the equipment and the connecting conduit increase, the flexibility of these systems may diminish and it may be necessary to use special flexible electrical couplings. The flexible connections should be installed in whatever manner creates a slack condition.

Piping that connects to isolated equipment also needs to avoid creating a vibration transmission path to the building. There are flexible pipe connections available for many applications, but because vibration can travel through the fluid in the pipes (which is often highly incompressible), vibratory energy is often not stopped sufficiently by them. Such connections are best used (or not) based on considerations other than vibration control (e.g., thermal expansion/contraction or alignment). To control vibration transmission to the building via pipes, it is usually necessary to resiliently support the pipes for some prescribed extent, but that extent is not easy to describe and could vary substantially from project to project. Many schemes have been devised to describe the scope of pipe isolation in buildings, such as a prescribed length of pipe or a certain multiple of the pipe diameter, and this is somewhat dependent on the designer's philosophical approach. The fixed length of pipe isolation from a vibration source approach does not account for variations of pipe stiffness based on size. Clearly, a 1-in. pipe for a particular duty is much more flexible over a given distance than a 12-in. pipe for a similar duty. Prescribing the length of isolation in pipe diameters partly addresses this issue, but this approach can be difficult to work with in the field. In practice, there needs to be some compromise between a practical scheme that can be implemented in the field, a system that makes sense economically, and a scheme which will provide the isolation that is needed for the size of pipes and the vibration sources involved. There are many possible approaches to this specification depending upon what is workable and cost effective. There may be a generic scheme that is appropriate for many applications, but this should be carefully considered for each project before finalizing the scheme. The designer should keep in mind that a resilient connection between a pipe and the building structure provides a reduction of the vibratory force only if the local impedance of the supporting structure is high compared to the impedance of the isolation device. Little isolation will be gained if a moderately stiff isolator like a neoprene pad is used to resiliently support a pipe from a lightweight and flexible gypsum board on stud wall.

Classic vibration isolation theory assumes that isolators sit on supports that are infinitely stiff and massive. This is reasonably the case for support conditions at slab-on-grade floors, but this may not be the case for support conditions at all structures above grade. Most isolation application guides take this into account and provide recommendations for a variety of less than perfect support conditions such as on above-grade structures. The implications of structural flexibility on

vibration isolation for most above-grade support conditions are rather modest where the structure is reasonably massive (such as a concrete floor) and is suitably strong to support mechanical service equipment. This accommodation involves only slightly softer isolators than would be used on grade, but the isolators are still within the range of conventional products that are economically available. When the supporting structure is particularly lightweight, such as wood frame construction or a simple metal deck roof, special attention needs to be given to the support condition, and it may be necessary to create special load transfer schemes to transfer the load to more substantial points of structure such as columns.

17.10 ROOFTOP AIR CONDITIONING UNITS

Many HVAC systems employ a variety of types of packaged rooftop air conditioning units with circulating fan systems and sometimes with integral compressor/condenser sections. Because such equipment is often noisy and typically supported on a lightweight structure directly above occupied space, this equipment is one of the most common sources of noise problems in buildings. Because of space limitations and the magnitude and frequency of excess noise that results, problems with this equipment are often very difficult and expensive to address, especially once the equipment is installed. Sometimes it is not practical and economically feasible to fully resolve the problems presented by this equipment at the initially chosen location and major system changes are needed. The best way to address noise from this equipment is to have it installed at the outset according to a well-conceived noise and vibration control scheme. The necessary installation features to control noise and vibration may be new and unusual to some installers, and it is wise to take the extra steps to clearly document all the necessary details so they can be properly implemented.

The roof construction needs to extend fully under the equipment and needs to close tightly around any penetrating elements such as pipes and ducts. The roof construction needs to be appropriate to control airborne sound transmission to the occupied space, including sound that might transmit both through the roof deck directly under the unit and off to the side of the unit (for some distance from the unit). If concrete is used in the roof deck, this is very good and can help to address, in a simple manner, both airborne noise and vibration isolation issues. Concrete is not always necessary and lighter weight sound isolation alternatives can be conceived, but they may be unfamiliar to some installers.

Having the supply fan discharging directly down into the supply duct entering the ceiling of an occupied space is often a problem and does not allow easy opportunities to incorporate silencing devices. If possible, it is usually much better to have the fan discharge horizontally within the unit, into a discharge plenum (also in the unit), before the air is delivered to the duct system. The discharge plenum presents an opportunity to incorporate sound attenuation treatment before the air stream enters the duct in the ceiling of the occupied space. In some cases it is acceptable to run the ductwork across the roof before penetrating the roof,

and this is always a favorable noise control approach since it allows space for turbulent airflow to smooth out, allows room for substantial silencing treatments before the ductwork gets into the ceiling of the occupied space, avoids what are often poor duct flow geometries at the fan discharge which occur when the duct drops directly out of the bottom of the unit, and allows low-frequency fan and duct rumble noise in the initial duct sections to dissipate outdoors rather than radiate in the ceiling of occupied space. However, such ducts may present practical and aesthetic design issues. The return/relief air path associated with rooftop units can present similar issues as discussed for the supply air path, but typically conditions at the return are not as severe because the flow conditions are not as bad and there is less fan noise. Similar noise control treatments might be considered for the return as for the supply.

Be sure that the duct geometry on the discharge of the supply fan is as reasonably advantageous as possible and avoid poor geometries as discussed above.

Silencers are often needed in the supply and return ducts and this attenuation should ideally happen before the ducts enter the occupied space, but if the ductwork from the unit drops directly into the ceiling and then has to turn into the horizontal ceiling plane, there is no aerodynamically appropriate location to put the silencer close to the unit discharge. Often, an elbow silencer can work well for these applications. When the silencer is moved away from the roof penetration, it is often necessary to encase the ductwork between the roof penetration and the silencer in a special noise barrier construction. The silencers for these applications also often need to have special high-transmission-loss casings or be encased along with the adjacent ductwork. All of these details are awkward, expensive, and difficult to construct within the limited ceiling space that typically exists. Sometimes, special curbs are created under the units to allow the return air to flow back to the units within the curb space, such as shown in Figure 17.4. With appropriate design and detailing, this can facilitate very good and practical ways to incorporate noise control treatments for both the supply and return paths.

Vibration isolation of packaged rooftop HVAC equipment can present problems, but this most often results when the units have integral compressor/condenser sections. When the unit just has basic supply and return/relief fans in the cabinet, vibration isolation can usually be satisfactorily accomplished with conventional, suitably soft, spring isolation for the fans within the unit. In this case, such units can externally be rigidly supported to the building in whatever manner is desired based on other considerations. When a unit has a compressor/condenser section, there is a concern for vibration isolation even though the compressor may be "internally" isolated. This is because the refrigerant piping within the unit is typically not adequately internally isolated, allowing vibration transmission to the equipment casing and hence to the building. In this case it is necessary to externally vibration isolate the entire unit with a spring isolation system. This is done in either of two ways, depending upon how the unit is intended to be supported and how the building designer plans to transfer the load to the building structure. There are special curb isolation devices available for equipment that requires curb support and closure of the space below the unit,

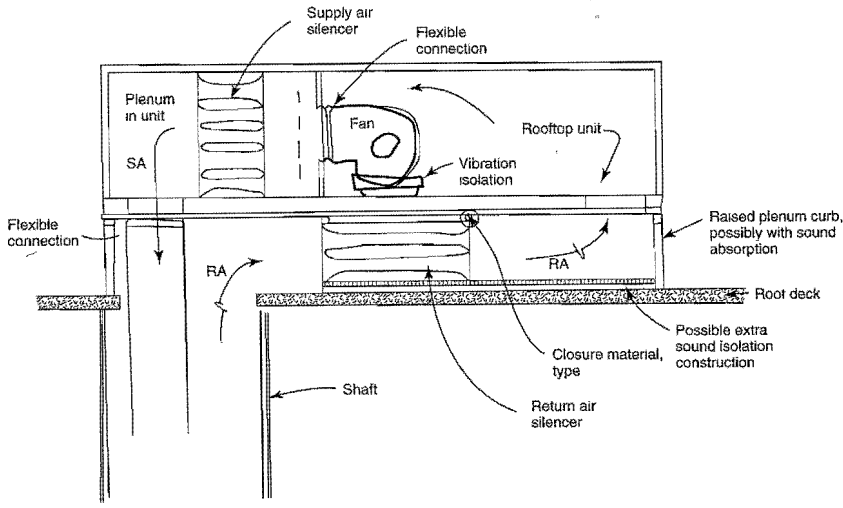


FIGURE 17.4 Rooftop unit with curb plenum return air. RA = return air, SA = supply air.

and some of these products can accommodate the aforementioned in-curb return airflow path scheme. If the load is to be transferred to the roof via a structural system raised above the roof, then point isolators are used. If the unit is intended for curb support but is raised above the roof in this manner, it may be necessary to mockup a structural curb for the unit to transfer its load to the point isolators.

17.11 OUTDOOR NOISE EMISSIONS

Many local authorities have noise regulations to control noise impact on neighboring properties and generally throughout the community. These need to be uncovered as part of the code searches at the outset of a building project so that they can be addressed in the mechanical system concept for the building. Typically, either fixed noise limits for specific receivers are established or the allowable noise level is based on the existing ambient noise level in the impacted area. If the noise requirement is based on the existing ambient noise condition, the existing noise has to be measured. Where neighbors are close by, requirements are stringent, and/or the receivers look down on the noise sources, meeting the noise requirements can be quite challenging.

Many pieces of equipment that are particularly economical (such as many air-cooled devices) are quite noisy and may not easily conform to noise regulations. Fortunately, equipment and mechanical schemes that produce less noise are often available, and, although they may be more expensive at the outset, they often provide some energy payback in the long run. Quieting the noise at the

source is almost always the best approach to controlling outdoor noise emissions. Evaporative cooling equipment is usually quieter than air-cooled equipment. Equipment incorporating centrifugal fans is usually much quieter for a given duty than comparable equipment with propeller fans. Propeller fans can be quieted by using larger and/or slower moving fan blades, even if more fans are required for the duty. There are several degrees of propeller blade technology available (particularly for moderate to larger blade size applications) which can provide worthwhile noise reduction at an affordable cost. Typically, propeller blade noise reduction is achieved by having more aerodynamically efficient blades with wider chords so that they move more air with each rotation and can move a given quantity of air with lower fan speeds. Some equipment can be equipped with variable-speed drives so that when the demand on the equipment is low, the equipment (typically fans) can operate more slowly and therefore with lower noise emission levels. This is of course statistical noise reduction and will not produce noise reduction when full speed is required. However, this is particularly useful for equipment such as cooling towers where the heat rejection requirements at night are lower than the design condition and it is easier to reject heat to the cooler nighttime environment. The noise reduction that results with variable-speed drives often works naturally with the typical diurnal noise cycle which has lower noise conditions at night. It is best to avoid equipment which has a noise emission spectrum that is particularly tonal since many regulations prohibit or more strictly limit tonal sounds. Tonal sounds are typically judged to be more annoying than an equivalent level of broadband sound, so the likelihood of avoiding a noise complaint is better with broadband sources than with tonal sources. For a given level of satisfaction with the noise level achieved, a greater degree of noise control will need to be applied to tonal sources.

Sometimes equipment cannot be purchased suitably quiet within practical or economical limits, and it is necessary to apply noise control treatments. For many pieces of equipment and systems this can be reasonably and economically accomplished, such as with silencers or by building a noise barrier to block sound emissions in a particular direction. However, some pieces of equipment are not well suited to having noise control applied and treatments (such as barriers) can inhibit airflow. For instance, propeller fans produce dramatically lower airflow when working against even small degrees of extra pressure loss, and it is difficult to apply silencing devices to such equipment without degrading mechanical performance. Heat rejection equipment such as cooling towers and condensers need to avoid having the hot discharge air be recirculated back into the inlet because this can reduce efficiency and limit the mechanical capacity of the unit. Providing high levels of noise control to such equipment is often not possible and alternate equipment selection may become essential. The ability to adapt noise control treatments to equipment, if required, is a factor that should be considered in selecting the basic equipment and mechanical scheme. For small amounts of excess noise (typically less than about 10 dBA) it may be possible to create a noise barrier with sound-attenuating louvers which can allow some airflow to help mitigate the adverse airflow due to the barrier.

REFERENCES

1. *Applications Handbook*, American Society of Heating, Refrigerating and Air Conditioning Engineers, Inc., Atlanta, GA, 1999, Chapter 46.
2. C. Harris, *Handbook of Acoustical Measurements and Noise control*, 3rd ed., McGraw-Hill, New York, 1991.
3. A. T. Fry (Ed.), *Noise Control in Building Services*, Pergamon, Oxford, 1988.
4. M. E. Schaffer, *A Practical Guide to Noise and Vibration Control for HVAC Systems*, American Society of Heating, Refrigerating and Air Conditioning Engineers, Inc., Atlanta, GA, 1991.
5. R. S. Johnson, *Noise and Vibration Control in Buildings*, McGraw-Hill, New York, 1984.

CHAPTER 18

Active Control of Noise and Vibration

RONALD COLEMAN AND PAUL J. REMINGTON

BBN Technologies
Cambridge, Massachusetts

18.1 INTRODUCTION

The term active noise and vibration control (ANVC) refers to systems that use externally powered actuators to generate sound and/or vibration to reduce responses caused by unwanted disturbances. These systems consist of a set of reference sensors that monitor the source and a set of control, or residual, sensors that monitor system response. In some cases (e.g., feedback control) the reference and control sensors are the same. The signals from these sensors are inputs to an electronic controller, which filters the sensor signals to generate drive signals for the actuators. In a well-designed system the actuators excite a structure and/or sound field in such a way as to interfere with the disturbance and reduce the unwanted noise and/or vibration. The advent of modern digital signal processing hardware and software has allowed the controller in the system to be extremely flexible and even to adapt to changing conditions.

While ANVC has become a powerful tool for the noise control engineer, it is not a "silver bullet," and careful consideration must be given to passive mitigation approaches in any noise and vibration control problem. At low frequencies where the offending source consists of a small number of discrete frequencies and where the system to be controlled has only a small number of degrees of freedom, ANVC can be very cost effective. Passive treatments can also be utilized successfully on tonal sources at low frequency, but because the acoustic and structural wavelengths can be very long, the weight and size of the treatments must often be quite large to be effective.

Broadband sources of noise and vibration at high frequency, the other extreme, are often best controlled using passive techniques because many passive approaches are broadband in nature. In addition, because the acoustic and structural wavelengths in the system to be controlled are short, the treatments need not be large and heavy to be effective. On the other hand, active systems are usually less effective against broadband sources, and higher frequencies can place considerably higher demands on the controller hardware.

As the above discussion indicates, ANVC can be effectively employed against narrow-band disturbances at low frequencies where the system to be controlled has a small number of degrees of freedom. The term *degrees of freedom* refers to the number of ways that the system to be controlled can respond. The number of modes contributing significantly to the response of a system is an example of the number of degrees of freedom. It is important in ANVC because, as will be discussed later, the number of degrees of freedom corresponds to the number of actuators needed to provide effective control. As the number of input and output channels to the controller, the frequency range for control, and the performance goals increase, so do the risks associated with the stability, robustness, and costs of the resulting control system. In general, one wants to employ the system of minimum complexity to achieve the design goals. In many cases the use of a hybrid system employing both passive and active components is the best approach and the most likely to succeed.

This chapter is designed to provide the practicing noise control engineer with an overview of the technology currently employed in the application of ANVC. Enough detail is included in the hope of allowing readers to assess the applicability of the technology to their problem and to allow them to lay out an approach to the solution of that problem appropriate for ANVC. We begin with a brief discussion of some basic issues underlying ANVC technology, including conceptual overviews of several types of ANVC systems. Modern-day ANVC systems rely on digital signal processing technology, and the heart of digital signal processing technology is, of course, the digital filter. These are discussed in Section 18.3. The design of digital filters is a rich topic that has seen many years of development. Here we can only scratch the surface and hope to give the reader some appreciation of the power of the technology. Sections 18.4 and 18.5 deal with feedforward and feedback control architectures, respectively. The chapters compare the two architectures, provide guidelines for design of optimal controllers, including adaptation, and discuss system identification issues. For feedback a suboptimal heuristic design approach is also presented. The next section deals with practical design considerations. The topics include the determination of the number and location of actuators and sensors, selection of control architecture and hardware, performance simulations, and controller implementation and testing. The final section provides a detailed discussion of three ANVC systems that have been successfully implemented.

18.2 BASIC PRINCIPLES

Placement and Selection of Control Sources/Actuators

The basic concept behind active noise control is illustrated in Fig. 18.1. There a loudspeaker has been placed a distance L from an unwanted source of sound. The intent is to create sound from the *control* loudspeaker that will be out of phase with and will cancel the sound from the *disturbance* source. Ideally it would be desirable to control the sound radiation in all directions (global cancellation),

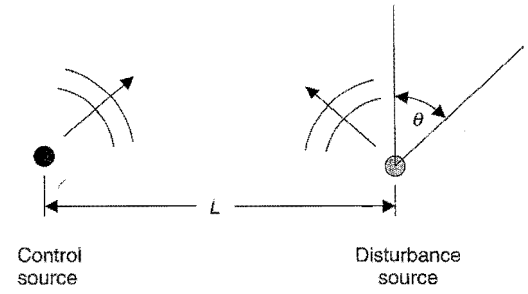


FIGURE 18.1 Disturbance source and control source.

and if the distance between the control source and disturbance source is small compared to a wavelength of sound, excellent global cancellation is possible. This comes about because the phases of the sound fields surrounding the two sources are very nearly the same at every location. Consequently, if one source is out of phase with the other two, the sound fields will cancel everywhere. On the other hand, if the separation distance is large compared to a wavelength, the two sound fields will have very different phases with the differences depending on location. As a result, the two sound fields will in some locations cancel and in others reinforce one another. This is illustrated in Fig. 18.2, where the change in the sound radiation from the disturbance source is shown as a function of angle θ. For $k_0L = 0.1$ in the figure, where k_0 is the acoustical wavenumber and L the distance between the disturbance source and the control source, the change is a reduction of 20 dB or more for all angles. However, as the frequency increases and k_0L increases, the global reductions decrease. For example, in the figure, for $k_0L = 1$ the reductions are limited to a small range of angles around $\pm 90^\circ$ and for $k_0L = 10$ there is a 6-dB increase for most angles. The figure clearly shows that it is desirable to locate the control source as close as possible to the disturbance source. In some cases, however, when the physical dimensions of the source are comparable to or larger than a wavelength at the frequencies of interest, the control source cannot be located close enough to the disturbing source. Figure 18.3 shows the effect of source separation on the overall radiated acoustic power (the integral over all angles in Fig. 18.2). The figure shows that for separation distances greater than one-quarter of an acoustic wavelength the total radiated power will actually increase. This is a fundamental limitation on ANVC that can only be overcome through the use of additional control sources. The use of multiple sources in a prototype system for controlling locomotive exhaust noise is discussed in Section 18.7 under MIMO Feedforward Active Locomotive Exhaust Noise Control System with Passive Component.

One of the earliest demonstrations of active noise control was carried out by Conover[1] and Conover and Ringlee[2] of General Electric in the early 1950s to control the noise from a high-voltage transmission line transformer. Using a single loudspeaker, he utilized the electrical line signal to drive the speaker and

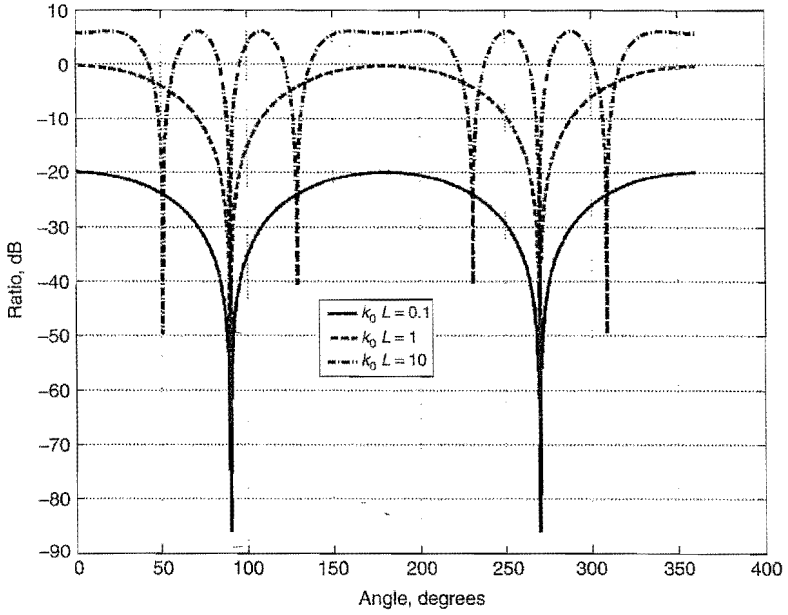


FIGURE 18.2 Change in the ratio of the controlled to the uncontrolled sound pressure level as a function of frequency and angle.

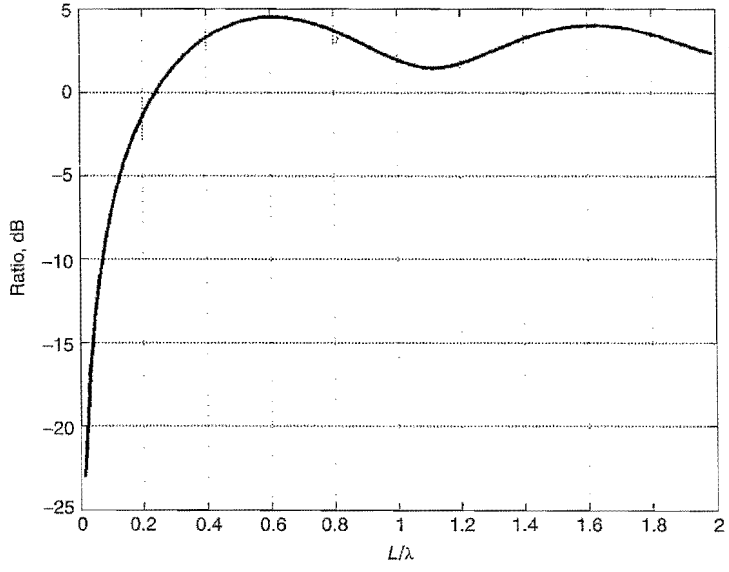


FIGURE 18.3 Change in the overall radiated output power as a function of the separation between sources.

appropriately amplified and phase shifted the harmonics of the line frequency to achieve the desired control. Because the system was not adaptive, occasional manual adjustment was required to correct for changes in sound propagation at the test site. In addition, because of the large size of the transformer, even at the low frequencies he was concerned with (120 Hz), he could not achieve global cancellation but had to be satisfied with ~10 dB of cancellation over a beam width of about 23°, corresponding to a point somewhere between the curves for $k_0L = 1$ and $k_0L = 10$ in Fig. 18.2. Remarkably, Conover was able to achieve this level of performance using purely analog hardware. Digital hardware did not come into use until the 1970s. Among the first to employ digital electronics were Kido[3] and Chaplin and Smith.[4] Kido used digital hardware to implement an active system to control transformer noise similar to Conover's and Chaplin and Smith developed a digital system for controlling tonal exhaust noise.

While the above discussion has focused on acoustical sources, similar principles apply to structural systems. Consider, for example, a plate with a point force disturbance applied as illustrated in Fig. 18.4 with a control actuator located as shown. In this example the plate is 10×5 ft and $\frac{1}{2}$-in-thick steel with a loss factor of 10% and the disturbance force and control actuator are about 1.4 ft apart. Because the plate in this example is finite in size, there will be resonant modes, which will add further complications to the selection of the number and location of the actuators. In this example, the control actuator is applying a force to the plate, the amplitude and phase of which is designed to control the first mode. Figure 18.5 shows the contribution of each mode to the plate response with and without activating the control actuator. Comparing the two plots in the figure, one can see that activating the control actuator has suppressed the first mode, and, in addition, the second and third modes have also been reduced. Higher

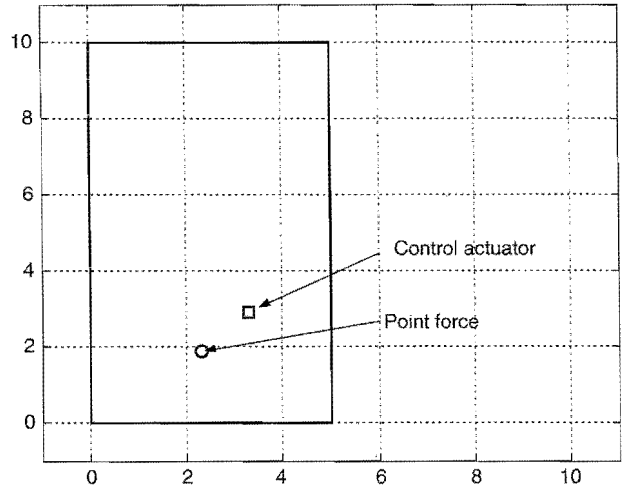


FIGURE 18.4 Plate with disturbance force and control actuator.

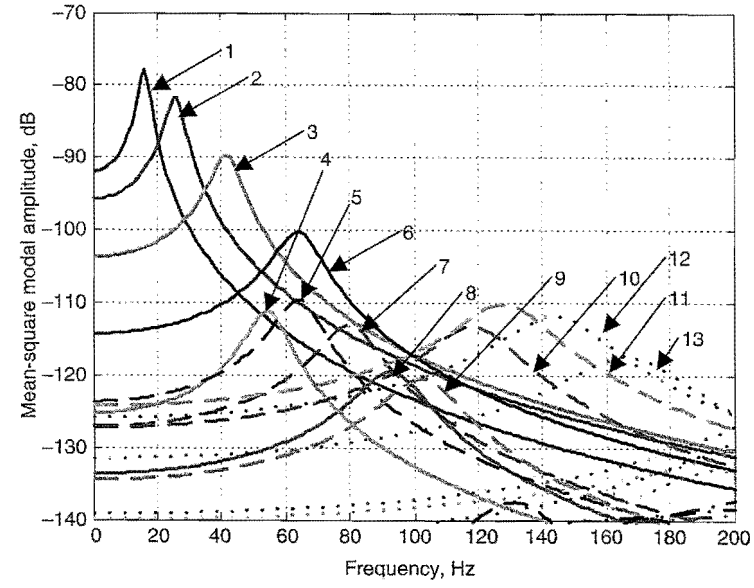


FIGURE 18.5 Modal amplitudes: (*a*) uncontrolled; (*b*) controlled.

order modes, however, have generally increased in amplitude. This increase in the amplitude of uncontrolled modes is referred to as *modal spillover*. Modes that are not targeted to be controlled can increase in amplitude. We can overcome this problem by moving the control actuator closer to the point of application of the disturbance force or we can add additional actuators, one for each mode that we wish to control. In general, placing the actuator as close as possible to the disturbance source will result in the best reduction in vibration. For example, in Fig. 18.6 the mean-square plate displacement averaged over the area of the plate is shown uncontrolled and controlled with a single actuator 1.4 ft away from the disturbance force and 0.28 ft away. When the actuator and disturbance are 1.4 ft apart, the vibration below 40 Hz is well controlled, but above about 50 Hz the control actuator increases the plate vibration due to modal spillover. When the control actuator is moved closer, spillover is virtually eliminated in the frequency range shown.

We can also increase the number of actuators, which will enable us to control additional modes and increase the frequency range over which the control will be effective. As an example consider the four control actuators located as shown in Fig. 18.7. These will be used to control the first four modes.* The result is shown in Fig. 18.8. While spillover has not been eliminated at all frequencies,

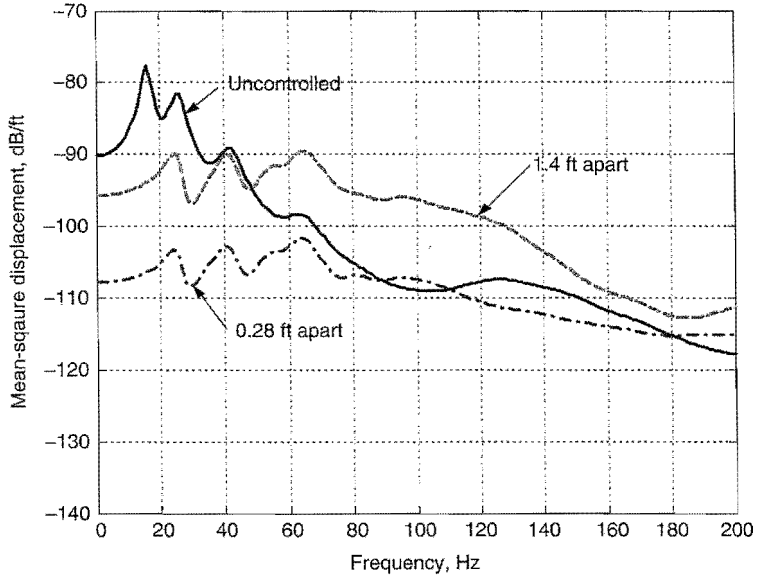


FIGURE 18.6 Controlled and uncontrolled plate response.

*Note that the actuator positions have been selected to ensure that at least one actuator is capable of exciting each of the four modes. If the actuators are placed near the node of a mode to be controlled, the actuator will be ineffective in controlling that mode.

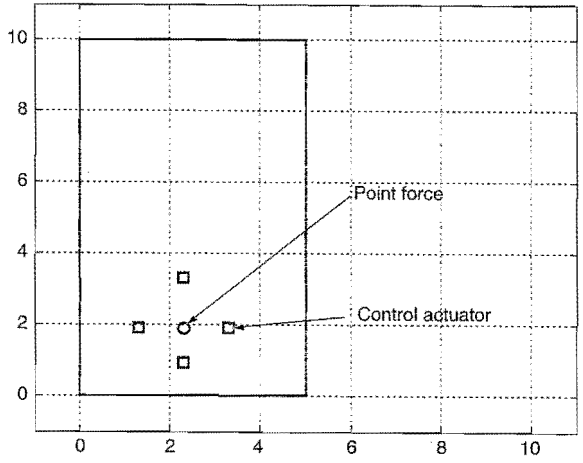


FIGURE 18.7 Location of four control actuators.

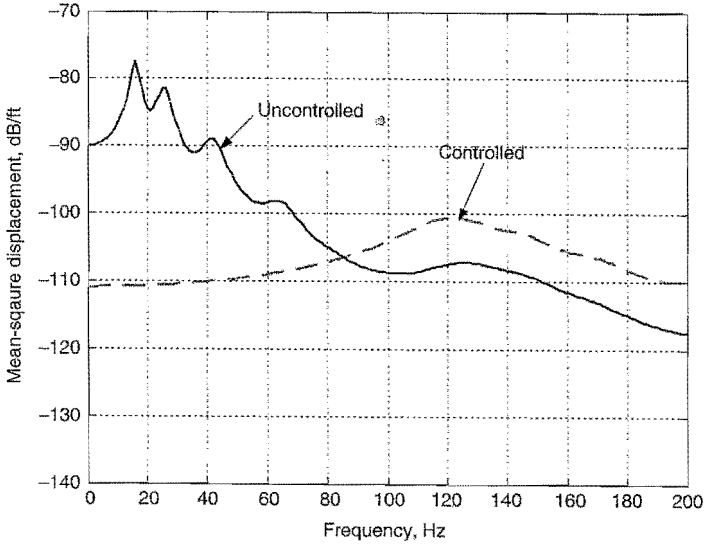


FIGURE 18.8 Change in mean-square plate vibration using four control actuators.

below 80 Hz the reduction in vibration is comparable to that achieved by bringing the control actuator very close to the disturbance point force. Good performance above 80 Hz can be achieved by continuing to increase the number of actuators and targeting more and more modes for control. Note that similar modal issues come into play in active noise control when the noise control is to be carried out in a confined space rather than in the free field in the first example.

The lesson to be learned from all of this is that, when possible, placing the control sources as close as feasible to the offending sources will provide the best noise and vibration reduction performance. When this is not possible due to the size of the source, lack of access, and so on, the loss in performance can be made up, in principle, by employing a larger number of control sources. However, increasing the number of control sources will increase the complexity of the controller needed to drive them and will certainly increase the cost of the entire system.

Control sources come in a wide variety of forms. For acoustic applications, loudspeakers are typically employed. The active elements in the speakers may be electrodynamic (voice coil), piezoelectric, or electromagnetic, to mention a few. The active element might be used to move a speaker cone, modulate airflow, or deform a structure. The most common configuration is a speaker cone driven by a voice coil. Whatever the configuration, the speaker usually needs to be enclosed for protection against physical damage, weather protection, and performance enhancement.[5] Figure 18.9 shows an enclosure arrangement developed for the active control system discussed in Section 18.7 under MIMO Feedforward Active Locomotive Exhaust Noise Control System with Passive Component. These enclosures are bandpass enclosures designed to enhance the speaker output between 40 and 250 Hz. Each contains 2–12-in. loudspeakers and 10 were employed to control the locomotive exhaust noise. Despite these efforts the

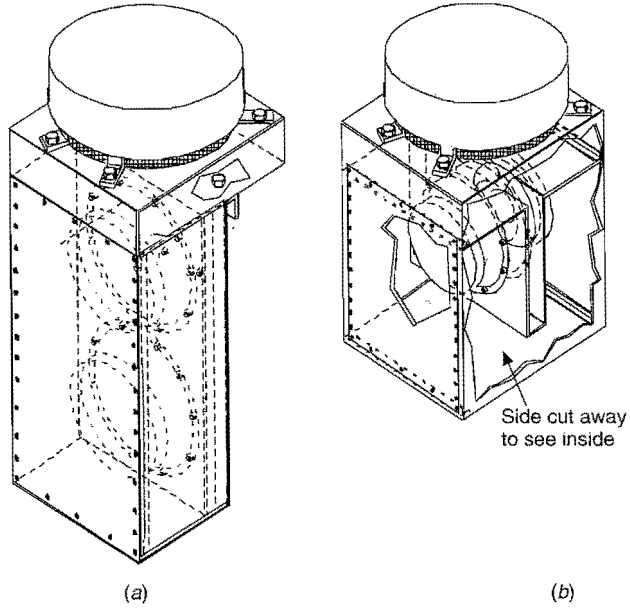


FIGURE 18.9 Typical loudspeaker enclosure arrangement.

performance of the active noise control system was limited by the output of these control sources. This is typically described as having insufficient *control authority*. Insufficient control authority is a problem often encountered in active noise control systems, and an assessment of the control source requirements is one of the first things that should be done before proceeding with any active noise and vibration control system design. If there is not sufficient space and power available to ensure adequate control authority, the active system is doomed to have inferior performance.

A wide variety of devices are available to be employed as structural control actuators. Typically these are devices that generate a force that is reacted against an inertial mass (inertial shaker) or against another part of the structure (interstructural shaker). The active element may be pneumatic,[6] hydraulic,[7] electrodynamic,[8] electromagnetic,[9] piezoelectric,[10] electrostatic,[11] or magnetostrictive,[12] to mention a few. A large-capacity electromagnetic inertially referenced shaker designed for use in an active control system is shown in Fig. 18.10.

In place of shakers piezoelectric[13] patches are sometimes applied directly to panels to control vibration or to radiate sound for noise control. Any of these devices can be very effective,* but the critical issue still remains. The device must provide sufficient control authority.

Control Sensors and Control Architectures

Sensors provide the input signals that the controller filters to drive the control sources and actuators. Sensors provide two functions, and to discuss those

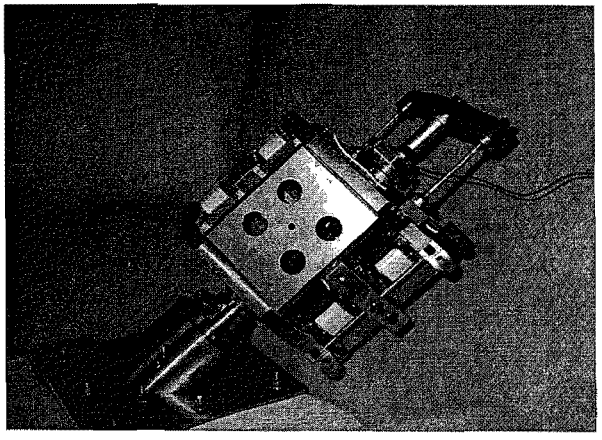


FIGURE 18.10 A 2000-lb-capacity electromagnetic inertial shaker.

*The inertial shaker usually provides better performance than the interstructural shaker, especially if the interstructural shaker creates a flanking path outside of the frequency range where the control system is functioning, but the interstructural device may be preferred when high control authority is needed with minimum weight.

functions, we need to describe the two commonly used control architectures: feedforward and feedback. The two architectures are illustrated in Fig. 18.11. In the feedforward system (Fig. 18.11*a*) one or more reference sensors measure a signal that is correlated with the disturbance to be controlled. The reference sensor output is sent to a control filter, which acts on the signal to generate an output signal that is used to drive the control actuators. The control actuators drive the system to be controlled (the plant function P in the figure) and the response of the plant is monitored by one or more residual sensors. The residual sensors are sometimes called the control sensors or error sensors. The purpose of the residual sensors is to monitor the performance of the control system. In later sections we will see how the reference and residual sensors are use to define and/or adapt the control filter.

In a feedback system (Fig. 18.11*b*) there are only residual sensors, or, to put it in other terms, the sensors in a feedback system provide both reference and residual functions. As in a feedforward system, the residual sensors monitor the performance of the control system. In addition, their signals are fed to the control filter, which acts on the signals to generate an output signal that is used to

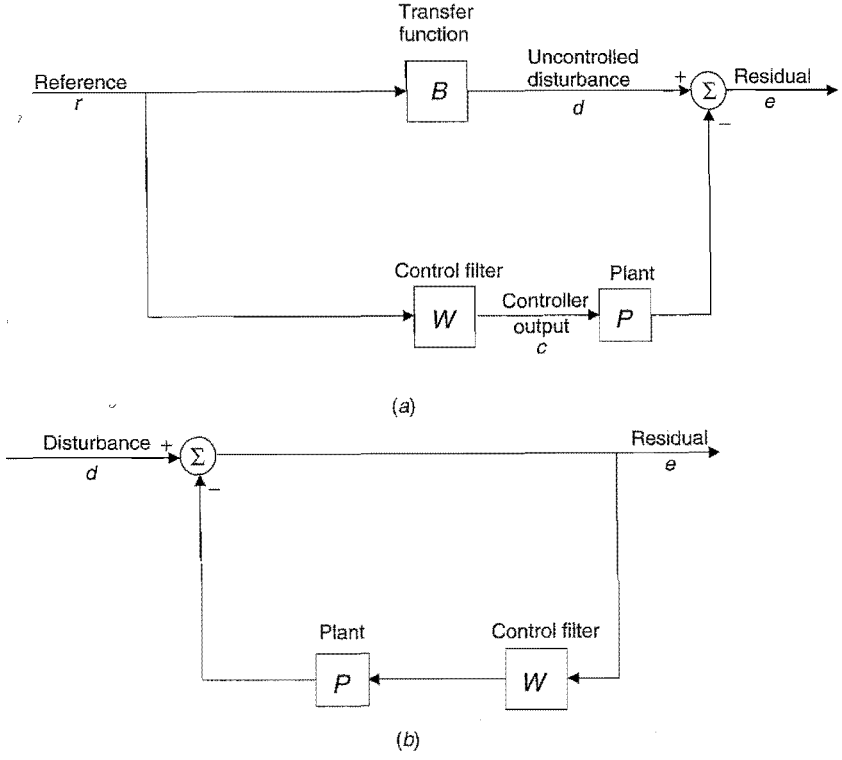


FIGURE 18.11 (*a*) Feedforward and (*b*) feedback architectures.

drive the control actuators. The control actuators drive the system and generate responses in the residual sensors through the plant transfer function, P.

The choice of whether to use feedback or feedforward architectures depends on a number of factors. In general, if reference sensors can be placed to measure a system response that is well correlated with the disturbance and residual sensors can be placed on the system such that there is sufficient delay between the reference and residual sensors (i.e., the reference sensors receive their signals before the residual sensors), then feedforward is the architecture of choice. This is especially true if the reference sensors are unaffected by the operation of the control actuators, such as would occur with a tachometer reference, for example. Feedforward is preferred (as we shall see in later sections of this chapter) because the algorithms are simple and easy to implement and the bandwidth requirements on a feedforward system are much less stringent than for feedback.

If a suitable set of reference and residual sensors satisfying the above requirements does not exist, then feedback must be used. As will be shown in later sections of this chapter, feedback control systems can present special problems. In particular, stability and out-of-band amplification requirements* can force the bandwidth of the system to be up to 100 times the control bandwidth.

As with actuators there is a wide variety of sensors used in active noise and vibration control systems. For systems designed to control only tones, a tachometer is often the reference sensor of choice, because in most cases the operation of the control system does not affect the tachometer, making the implementation of a feedforward system much easier. Other sensors that are commonly used include, accelerometers, force gauges, strain gauges and piezoelectric patches, proximity sensors, linear variable differential transformers (LVDTs), microphones, hydrophones, and pressure sensors. The requirements on the sensors are the same as for any high-quality instrumentation system: sufficient sensitivity to measure the phenomena of interest, low noise, stable operation, durability, and so on.

Performance Expectations

Active noise and vibration control systems can be powerful tools in the hands of a knowledgeable noise control engineer. In many cases, significant reductions in noise and vibration can be achieved with active systems that cannot be achieved using passive treatments with the same space and weight constraints. This is especially true at low frequencies. Despite the power of the technology, there are realistic limits on what reductions can be achieved. Figure 18.12 shows the performance achieved by the prototype active system described in Section 18.7 under Active Machinery Isolation. We present it here because it reflects the performance that is normally achievable in a properly designed active system. The figure shows the reduction in force transmitted by an active vibration isolation

*Outside of the frequency band where control is desired, the active system can amplify the disturbance unless great care is exercised in implementing the system filters to frequencies well beyond the frequency band for control.

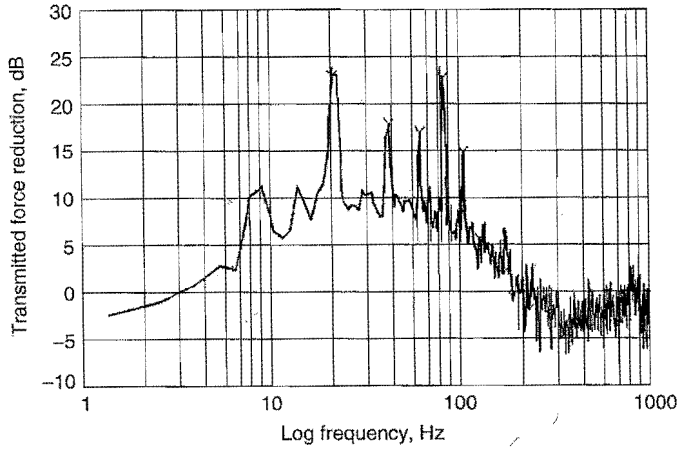


FIGURE 18.12 Typical performance of an active vibration control system.

mount. The system was a single-input, single-output (SISO) feedback control system designed for suppression of both broadband and narrow-band vibration. The narrow peaks in the figure with amplitudes of 15 to nearly 25 dB reflect the reduction in tonal components of the force transmitted by the mount. These values are what one would typically expect in tonal suppression from an active system. In addition to the peaks there is broad hill beneath them that in the frequency range of 10–100 Hz has an amplitude of from 6 to 10 dB. This too is typical of what one might expect from a system designed to provide control of broadband noise and vibration. Of course, there are many factors that go into determining the performance of an ANVC system, and there is no substitute for careful analytical/empirical modeling helping to direct the design process, but these values represent reasonable expectations for system performance when the technology is properly implemented.

Examples of Prototype ANVC Systems

There have been a vast number of ANVC prototype systems implemented over the past 50 years or so. Here we present a few examples of those systems to give the reader a sense of how the technology has been applied, where it has been most successful, and where additional technology and research is required. For a more detailed look at the early development of the technology the reader is referred to a number of review articles.[14–17]

The first patents proposing the use of a sound to cancel unwanted sound in the early 1930s proposed the type of system[18,19] illustrated in Fig. 18.13. These early proposals focused on the control of sound in a duct and involved the use of a reference microphone to sense the unwanted sound. In Fig. 18.13 the signal from that microphone was then acted on by appropriate electronics to synthesize

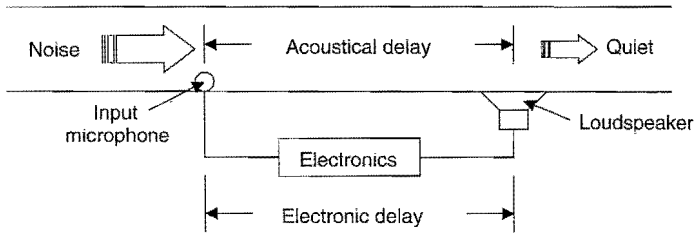


FIGURE 18.13 Schematic diagram of the active noise control concept for controlling sound in ducts.

a signal to drive a loudspeaker downstream from the microphone. The sound wave from the loudspeaker then cancels the unwanted sound. The use of active systems to control sound in ducts has received a great deal of attention over the years. Swinbanks[20] provided an extensive theoretical foundation in the early 1970s focusing on various arrangements of control sources at two different axial positions in a duct to minimize propagation of canceling sound back to the reference microphone. Other researchers[21,22] examined more complex control source configurations to deal with the control-source-to-reference coupling. Eventually laboratory experiments were carried out using analog electronics to confirm the predictions of the analysts[23] and to demonstrate both narrow-band and broadband control.[24] Eriksson's work in this area is particularly noteworthy.[25–28] His theoretical and experimental work eventually resulted in a commercially available active duct silencer utilizing digital electronics that was sold through Digisonix,* a subsidiary of Nelson Industries. The system configuration was very similar to that shown in Fig. 18.13.

Another early concept (1950s) for active noise control is illustrated in Fig. 18.14. This idea was developed by Olsen and May[29] while at the Radio

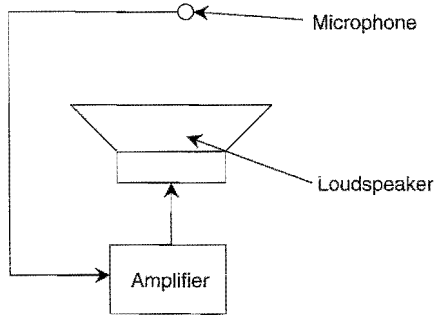


FIGURE 18.14 Olsen and May's "electronic sound absorber".

*Nelson Industries is currently owned by the Cummins Engine Company and Digisonix is no longer in business.

Corporation of America. The concept utilizes a microphone placed close to a loudspeaker in which the microphone detects the unwanted sound and the speaker generates a canceling signal that creates a zone of silence around the microphone. They assembled and successfully demonstrated their concept using only analog components. This basic concept has been extended and utilized in a number of applications, including control of automobile[30–34] and aircraft[35–38] interior noise and noise-reducing headsets.[39–41] The example in Section 18.7 under Active Control of Airborne Noise in a High-Speed Patrol Craft describes a system that uses this concept to reduce the noise in the berthing spaces of a high-speed patrol craft.

Figure 18.15 shows a schematic diagram of a notional active automotive interior noise control system. As shown, the system is designed to control noise generated by the propagation of vibration from the vehicle's suspension to the passenger compartment where it is radiated as sound to the vehicle interior (road noise) and engine noise. Feedforward active control architectures have usually been used to attack this problem. A number of reference accelerometers are placed on vehicle suspension components and in the engine compartment. Reference microphones might also be used. The reference signals are fed to a controller, which generates signals to drive the control loudspeakers in the passenger compartment. Residual microphones are located in the passenger compartment near the ears of the occupants so as to generate a zone of silence around the head of each occupant. Because of the nature of the interior noise, the control system must reduce both narrow-band and broadband noise. While the system concept is fairly simple, its successful implementation has proven difficult. First the number of residual sensors needed to sample all of the suspension sources can be quite large[42] (10–20). This can lead to significant costs due to the high channel count. In addition, the reductions achievable seem to be limited to about 6 dBA and the zone of silence around the control microphones is usefully large only at low

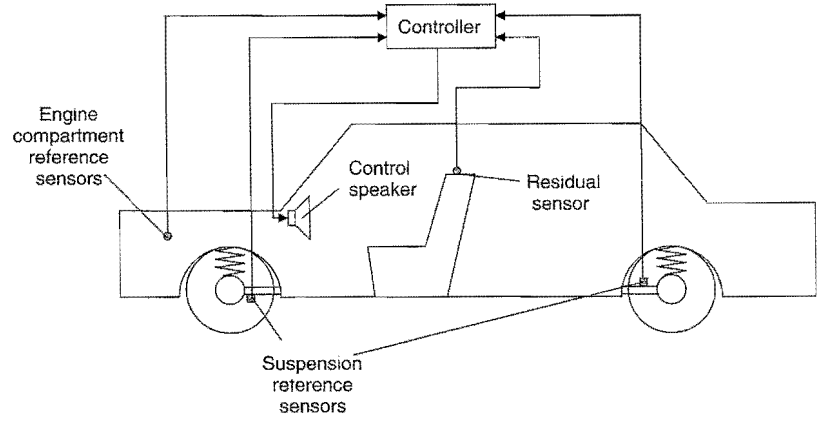


FIGURE 18.15 Schematic of an active automobile interior noise suppression system.

frequency (up to a few hundred hertz), limiting the useful frequency range of the system. Consequently, active systems providing broadband automobile interior noise control are not presently commercially available.

Systems for the control of aircraft interior noise have generally focused on tonal noise, that is, the propeller blade passage frequency and its harmonics. A schematic of a typical system is shown in Fig. 18.16. Experimental systems like that shown have generally provided about 10 dB of tonal interior noise control at the blade passage frequency and somewhat less at the higher harmonics. The system in the figure is similar to the automotive interior noise control system except that the reference is now a tachometer from the aircraft engine. The schematic shows control speakers as the actuators, but piezoelectric patches on the fuselage panels and inertial shakers on the ribs and stringers have also been tried, effectively turning the fuselage into a loudspeaker. Systems suitable for small propeller-driven business aircraft are presently commercially available from Ultra Electronics.

A number of manufacturers now provide reasonably priced active noise cancellation headsets. Figure 18.17 shows one arrangement. The figure shows the shell of one side of the headset in which there is a small speaker and colocated microphone. The signal that the wearer wishes to hear drives the speaker, the output of which is picked up by the microphone. The microphone also picks up any noise that passes through the shell. The microphone signal is then fed back, as shown in the block diagram in the figure. By increasing the gain of the filter,

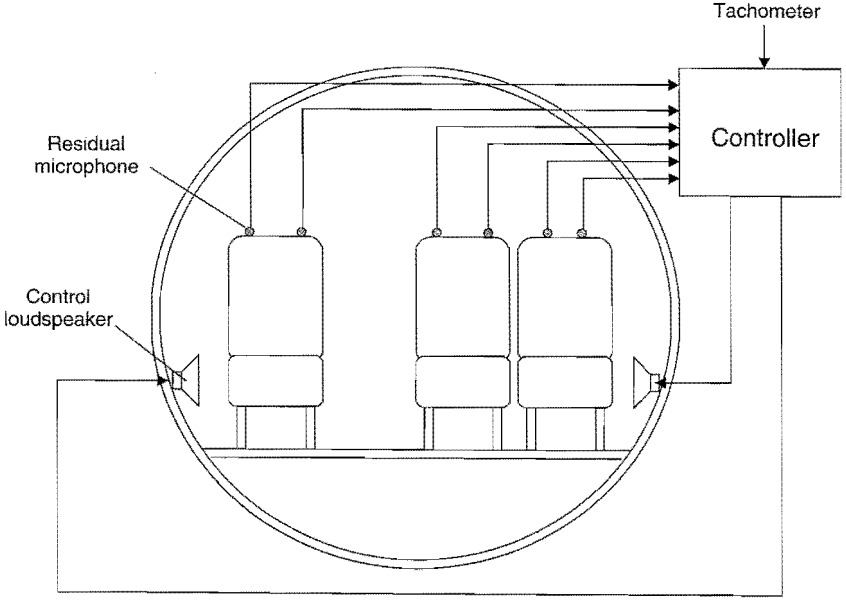


FIGURE 18.16 Schematic of an active aircraft interior noise control system.

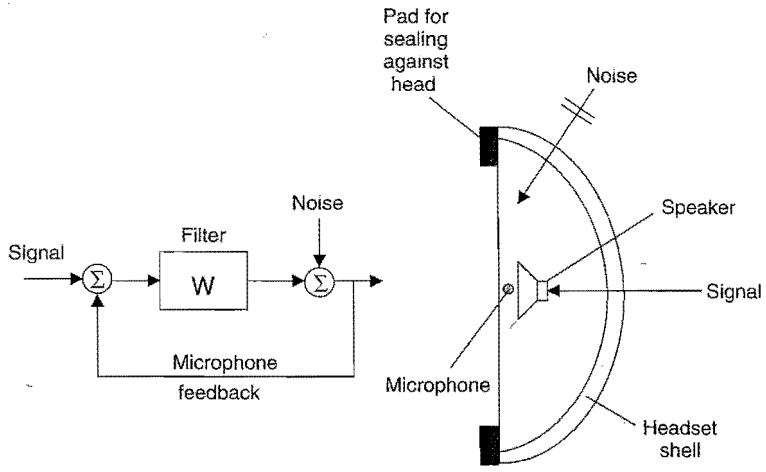


FIGURE 18.17 Typical noise cancellation headset.

W, in the block diagram* (typically an analog filter in commercial products rather than a digital one), the signal will pass through unchanged and the noise will be attenuated. Of course, this gain cannot be increased without limit, since too high a gain can result in instability and ringing. These devices produce noticeable improvement (10–15 dB) in the passive performance of hearing protection headsets above 100 Hz. The improvement gradually decreases with increasing frequency until at ~1 kHz most of the improvement has gone away. In very loud environments headsets can be limited in performance by the sound level the small speaker can generate within the shell.

Another area that has received considerable attention in recent years is the active control of tonal noise from turbofan engines.[43–50] Tonal noise from these engines is caused primarily by the interaction between the fan blade wakes and the stator vanes. The control systems for the most part have been feedforward systems utilizing a tachometer for a reference sensor. Since the fan and stator vanes are located in the bypass duct, the systems need to take into account the complex physics of the propagation of sound in ducts. The physics dictates that the fan–stator interaction noise will propagate down the duct as, so-called, spinning modes. These modes have a sinusoidal pressure variation in the circumferential directions that rotates as the mode propagates, hence the term *spinning mode*. Only a selected number of these modes are excited by the fan–stator interaction and a still smaller number propagate. Consequently, the control actuators must also generate spinning modes in order to cancel the fan–stator interaction noise without generating additional propagating modes in the duct. Figure 18.18 shows a schematic drawing of one such active noise control system. This particular

*In the block diagram W also contains the frequency response between the speaker input and the microphone output.

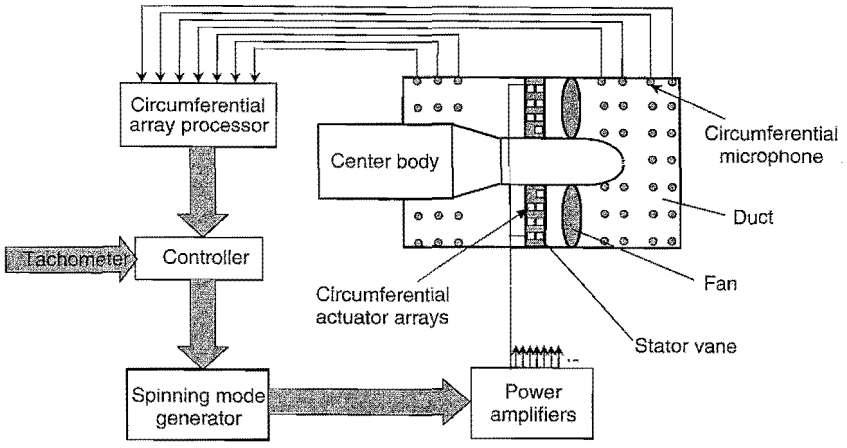


FIGURE 18.18 Schematic of the active noise control system for controlling fan-stator interaction noise.

system utilizes actuators in the stator vanes. Actuators have also been installed in the walls of the duct. The system must be designed with a sufficient number of actuators to ensure that the propagating modes to be controlled can be generated by the array without aliasing into other modes that will propagate.

Each array is driven by a single signal passed through analog or digital electronics (spinning-mode generator) that properly phase shifts the actuators in each array to produce a spinning mode of the desired circumferential order. Each actuator in the array must be the same. If there are large variations in amplitude and phase between actuators when driven by the same signal, then modes other than the desired mode will be generated, resulting in noise generation rather than suppression if the spurious modes propagate. The control sensors are typically wall-mounted microphones arranged in circumferential arrays and each array is steered (circumferential array processor) to accept a spinning mode of the circumferential mode order that is to be controlled. In a laboratory setting, systems of this type are capable of reducing the tonal noise from fan–stator interaction by 10–20 dB. In real high bypass turbofan engines, however, especially in modern-day large engines, none of the actuators tested to date have sufficient control authority to be able to overcome the disturbance. In addition, at the present time, while the controller channel count can be fairly low, typically equal to the number of modes to be controlled, the number of actuators and sensors needed to field a system can be quite large. It is very likely, however, that if active noise control is included early in the design process of an engine along with passive noise control treatments, the number of actuators and sensors needed could be substantially reduced. If more powerful actuation systems become available, commercially available active systems for the control of fan–stator interaction noise in turbofan engines may become a reality.

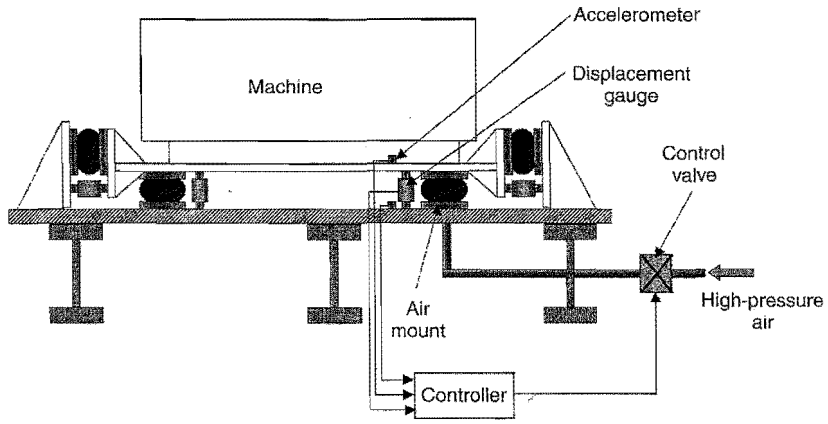


FIGURE 18.19 Notional activated vibration isolation mount.

In the 1950s Olsen[51] was the first to suggest extending active control to the control of machinery vibration. Since that time numerous studies have been carried out into the activation of vibration isolation mounts.[52–55] Figure 18.19 shows a schematic drawing of a notional active vibration isolation system. In this case, we envision a set of mounts supporting a vibrating machine on the deck of a ship. In the figure only one mount is shown activated. In actuality all (possibly 10 or 12 mounts) would be. It is desired to reduce the vibration excitation of the deck while maintaining the position of the machine, which is in a confined space, so that it does not strike any of the ship structure surrounding it during ship maneuvers. These two requirements are conflicting. Good vibration isolation performance requires a mount that is as compliant as possible while good position keeping requires a stiff mount. Two approaches can be taken to the activation of the mount. We can employ a mount that is stiff enough to ensure good position keeping and use an active system to increase the compliance of the mount at higher frequency where good vibration isolation performance is desired. We will refer to this type of system as the active isolation system. Another approach is to use a very compliant mount that provides the desired vibration isolation performance at high frequency and use the active system to provide position keeping at low frequency. We will refer to this system as the position-keeping system. For either concept to work the frequencies associated with ship maneuvers should be much lower than the frequencies where vibration isolation performance is desired. The notional system that we have shown in Fig. 18.19 incorporates air mounts. Since air mounts tend to be very compliant, they would be most appropriate for the position-keeping approach. The system would require 10–12 mounts to conveniently control all six rigid-body degrees of freedom. Each mount incorporates sensors for measuring relative displacement between the machine and the deck and for measuring the acceleration on the deck and the machine. These sensors would be used in the controller to generate a frequency-dependent linear

combination of relative displacement, velocity, and acceleration at each mount. Those inputs would then be used by the controller in a feedback architecture to drive the control valves, which can inject high-pressure air into or vent it from the air mounts. Since the frequencies associated with ship maneuvers tend to be lie below 1 Hz, the machine would most likely act as a rigid body, significantly simplifying the system transfer functions and making the controller simpler as well. This approach does have some disadvantages. For example, it would require about 10–12 air mounts to conveniently implement it. In addition, all mounts must be coupled in the controller, making it a multiple-input, multiple-output (MIMO) system. On the other hand, there would only need to be six independent channels in the controller to control the six rigid-body degrees of freedom of the machine. Multi-degree-of-freedom systems of this type and of even greater complexity have been implemented in research programs, but none are commercially available. However, there remains considerable interest in active isolation systems and position-keeping systems for both military and civilian applications.

The above examples of types of ANVC systems represent only a taste of the many noise cancellation problems that have been addressed using the technology. In Section 18.7 we present three detailed examples of ANVC systems to provide the reader with a more in-depth look at the development, implementation, and performance of real prototype systems.

18.3 DIGITAL FILTERS

Advantages of Digital Filters

Active noise and vibration controllers are basically filters. The inputs are sensor signals and the outputs are the drive signals to the actuator electronics, which impart desired control forces to the physical system being controlled. For some ANVC applications, implementing these filters using analog electronics is an efficient and cost-effective approach. In particular, analog controllers should be considered for applications where the required magnitude and phase responses of the filters are a relatively simple function of frequency and when these filters are not required to change over time. An example of an application where analog controllers have been used effectively is active headsets. However, when the required magnitude and phase responses vary significantly as a function of frequency and the characteristics of these filters are required to change over time to maintain a desired level of performance, digital controllers are often the best choice. The filters implemented within these digital controllers are referred to as digital filters.

Digital controllers offer many advantages over analog controllers. As discussed by Nelson and Elliott,[56] these advantages include the following:

Flexibility. Digital controllers implement digital filters by running programs written to operate on digital signal processor (DSP) chips. The codes to implement these filters can be written to allow for these filters to change their characteristics over time (i.e., adapt). Further, these codes can be written to accommodate increases in the number of input and output channels. Additionally, the complexity of the digital filters can be increased or decreased by modifying the codes running on the DSPs.

Accuracy. Many DSPs support floating-point computations running in either single- or double-precision arithmetic. Although greater accuracy in the calculations can be achieved using double precision, this increased precision is seldom required and comes at the cost of increased memory requirements. The accuracy of single-precision controllers has been demonstrated for a wide variety of ANVC applications, including those with large numbers of input and output signals and digital filters requiring very complex magnitude and phase responses as a function of frequency.

Adaptability. Applications of ANVC often require the controller to alter filtering characteristics over time to maintain a desired level of performance. Controllers that satisfy this requirement are said to be "adaptive." An example of an adaptive controller is ANVC applied to systems whose dynamics (as a function of frequency) change over time. Digital controllers implemented using DSPs can be designed to adapt to these changes.

Cost. The cost of DSPs has continued to drop over the past 15 years. At the same time, the computational and memory capabilities of these chips have continued to increase. Currently available DSPs deliver up to 1×10^9 floating-point operations per second (1 gigaflop, abbreviated Gflop) and are equipped with up to 256 Mbytes of local, fast-access memory. In addition, the architecture of these chips has expanded to allow communications between DSPs to support efficient implementation of digital controllers employing multiple DSPs for large-scale applications. Both fixed- and floating-point DSPs are available. Fixed-point processors are cheaper than floating-point processors but are generally more difficult to program, resulting in increased software development costs.

In the following section the concepts of digital sampling and filtering are discussed. Subsequent sections use these concepts to summarize optimal digital and adaptive digital filter designs.

Description of Digital Filters

There are many good texts covering the concepts of digital sequences, sampling, and filtering.[56–59] For purposes here, we summarize these concepts following the developments of Nelson and Elliott[56] and Oppenheim and Schafer.[57] The interested reader should look to these references for more detailed discussions.

The input to a digital controller is typically an analog signal from a sensor that passes through an analog-to-digital (A/D) converter. The purpose of the A/D converter is to sample the input signal at regular time intervals (Δt) to produce a sequence of numbers corresponding to the amplitude of the input signal at each sample time. A schematic of the operation of an A/D converter is shown in

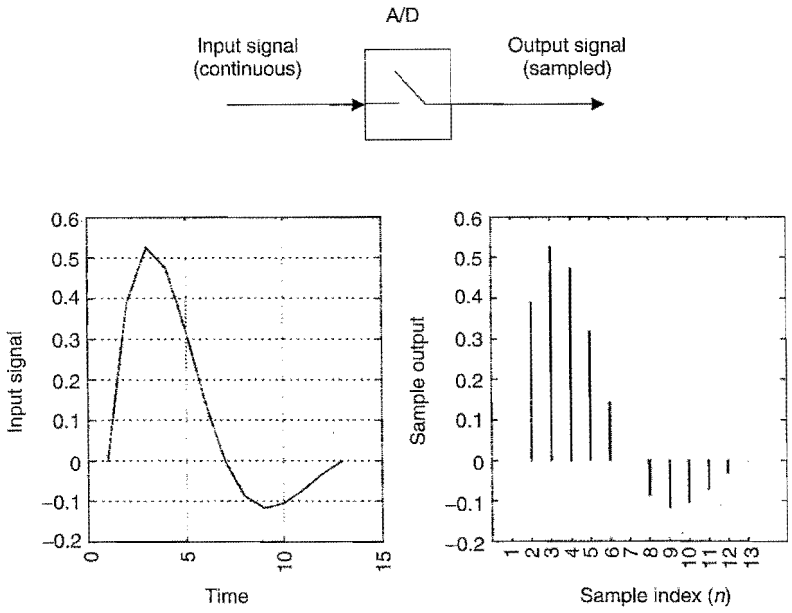


FIGURE 18.20 Digital sampling of an analog signal.

Fig. 18.20. The output of the A/D converter can be related to the continuous-time input signal through the following relationship:

$$f(n) = \sum_{i=-\infty}^{\infty} f(i)\delta(n-i) \tag{18.1}$$

where $\delta(n-i)$ is called the Kronecker delta function, or unit-sample sequence, and is defined as

$$\delta(n-i) = \begin{cases} 1 & n = i \\ 0 & n \neq i \end{cases} \tag{18.2}$$

The sampled signal in Eq. (18.1) is only defined for integer values of n. That is, $f(n)$ is only defined for $n = 0, \pm 1, \pm 2, \ldots$. An example of a continuous-time signal and the corresponding sampled signal $f(n)$ is shown in the lower portion of Fig. 18.20. The sample index n can be related to a discrete time by $t_n = n\ \Delta t$, where Δt is the fixed time interval between samples.

A digital system (e.g., digital filter) operates on a sequence of numbers to produce an output sequence. This is shown schematically in Fig. 18.21. The *impulse response* $w(n)$ of the digital system W is defined as the output corresponding to a unit-sample input [i.e., $\delta(n-i)$, $i = 0$]:

$$w(n) = W\{\delta(n)\} \tag{18.3}$$

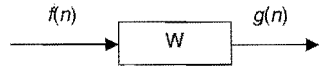


FIGURE 18.21 Digital filter operating on input $f(n)$ to produce an output $g(n)$.

where $w(i) = 0$ for $i < 0$ ensures that the output of the filter does not occur before the input sequence is applied. Filters that obey this constraint are referred to as *causal* filters.

The filter operation implied by the block diagram of Fig. 18.21 can be expressed mathematically as

$$g(n) = \sum_{i=0}^{I-1} w(i) f(n-i) \tag{18.4}$$

where the impulse response of the digital filter $w(i)$ in Eq. (18.4) is assumed to be a sequence of numbers of length I. It is common to refer to these numbers as the coefficients, taps, or weights of the digital filter. For example, $w(i)$ is called the ith coefficient of the digital filter w. Using this nomenclature, Eq. (18.4) states that the output of the digital filter w at time step n is equal to the summation over i of the ith coefficient of w times the input at time step $n-i$. In vector notation, this operation is equivalent to the inner product of a row vector and a column vector such that

$$g(n) = \mathbf{f}^{\mathrm{T}}(n)\mathbf{w} \tag{18.5}$$

where $(\cdot)^{\mathrm{T}}$ represents the vector transpose operator and $\mathbf{w}$ and $\mathbf{f}(n)$ are defined as

$$\begin{aligned} \mathbf{w}^{\mathrm{T}} &= [w(0), w(1), w(2), \ldots, w(I-1)] \\ \mathbf{f}^{\mathrm{T}}(n) &= [f(n), f(n-1), \ldots, f(n-I+1)] \end{aligned} \tag{18.6}$$

An example of this filtering process is shown schematically in Figs. 18.22 and 18.23. Figure 18.22 shows the input time sequence $f(n)$ and the impulse response of the digital filter $w(i)$. Figure 18.23 depicts the filtering of Eq. (18.4) at three increments in time during the filtering operation. The upper three charts plot the input sequence $f(n-i)$ for $n = 0, 4, 9$. The middle three charts plot the impulse response of the digital filter w. The lower three charts plot the output $g(n)$ at time step $n = 0, 4, 9$. As shown in these figures, the output of the filter is obtained by computing the summation of the time-reversed input signal as it slides past the impulse response of the filter.

The digital filter of Eq. (18.4) depends only on current and past values of the input sequence and is limited in length to I coefficients. These types of digital filters are referred to as finite impulse response (FIR) filters because their impulse response is zero after a finite number of taps or coefficients. These filters are also known as "tapped delay line," "moving-average" (MA), "nonrecursive," "all zero," or "transversal" filters.

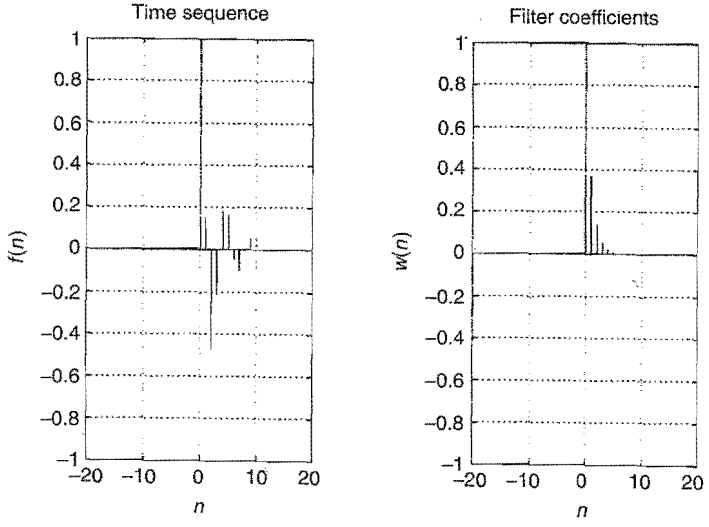


FIGURE 18.22 Example input sequence and impulse response.

A more general class of filters is defined as

$$g(n) = \sum_{i=0}^{I-1} a_i f(n-i) + \sum_{k=1}^{K} b_k g(n-k) \tag{18.7}$$

In addition to depending on current and past values of the inputs, the current output of the digital filter represented by Eq. (18.7) depends on past values of the output. Digital filters of this type are referred to as infinite impulse response (IIR) filters because, in general, the impulse response of these filters never decays to zero. These filters are also known as "recursive," "pole-zero," or "autoregressive moving average" (ARMA) filters. The general form of Eq. (18.7) reduces to a FIR filter when $b_k = 0$ for all k.

Implementations of FIR and IIR filters can be represented schematically if we define a delay operator z^{-k} such that

$$f(n-k) = z^{-k}\{f(n)\} \tag{18.8}$$

Using the property of the delay operator in Eq. (18.8) and the general filter representation in Eq. (18.7), a FIR filter can be implemented as shown in Fig. 18.24. A corresponding implementation for an IIR filter is shown in Fig. 18.25. A desired filter response can be approximated digitally using either the FIR or IIR filter structures discussed above. The choice between these two involves certain trade-offs, including the following:

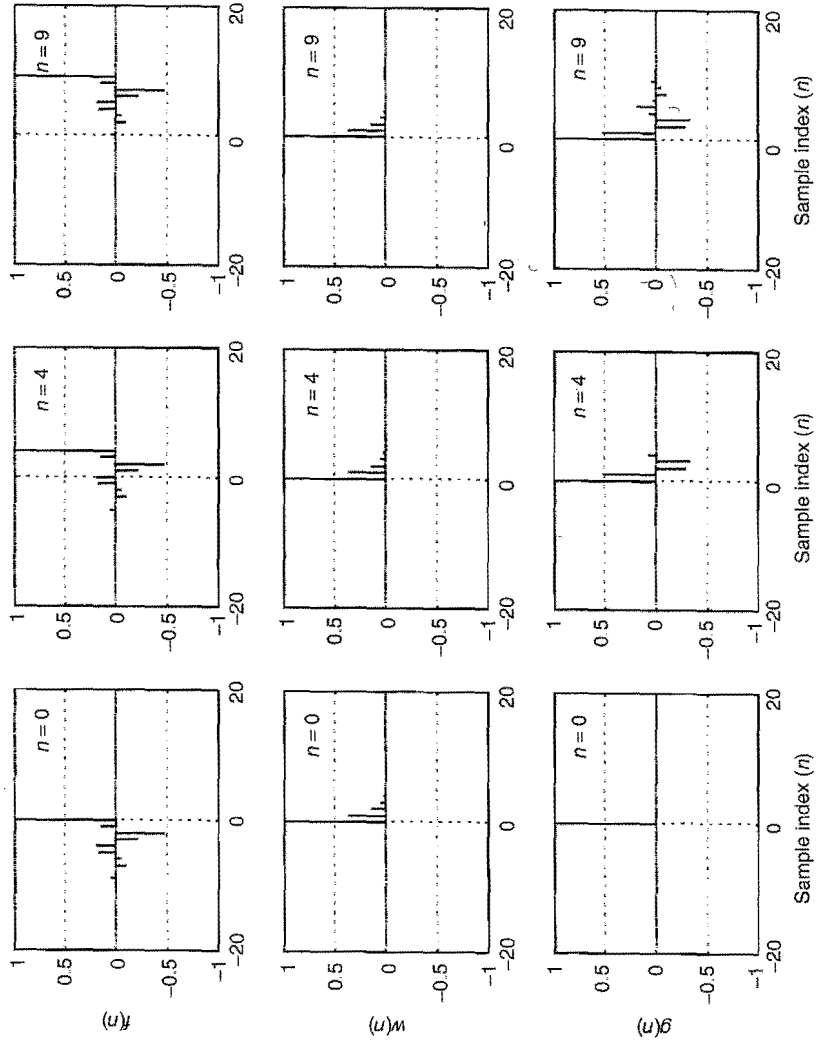


FIGURE 18.23 Representation of digital filtering as a discrete convolution.

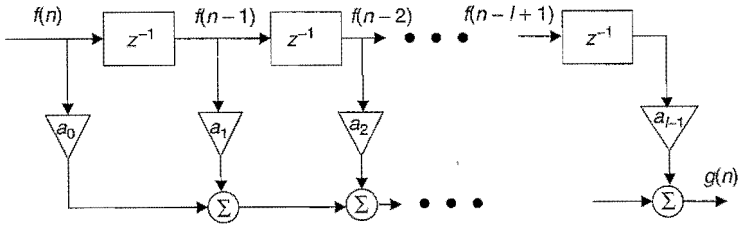


FIGURE 18.24 Implementation of a FIR filter using current and delayed values of the input.

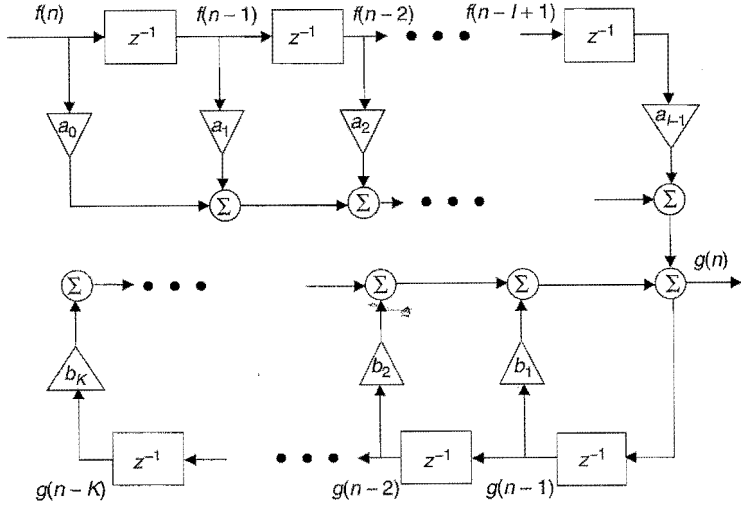


FIGURE 18.25 Implementation of an IIR filter using current input and delayed values of the inputs and outputs.

- FIR filters are guaranteed to be stable provided the coefficients are finite: Bounded inputs produce bounded outputs.
- IIR filters can be unstable even when all coefficients are finite: Bounded inputs can produce unbounded outputs.
- IIR filters may require fewer coefficients than FIR filters to approximate the frequency response necessary to provide active noise and vibration control: Typical transfer functions associated with structural acoustics include both poles and zeros, as do IIR filters, whereas FIR filters have only zeros.
- Design procedures to solve for FIR filter coefficients are generally numerically better behaved than those to solve for IIR filter coefficients.

Although there are advantages and disadvantages to both approaches, the vast majority of ANVC applications rely on the numerically stable design procedures and guaranteed stability associated with FIR filters and consequently implement the digital filters within ANVC controllers as FIR filters or composites of FIR filters.

Optimal Digital Filter Design

Having described the concept of digital filtering in the previous section, we focus in this section on design procedures to solve for the optimal coefficients of a digital filter for a particular class of problems. The class of problems considered is illustrated in Fig. 18.26. This problem is referred to as the electrical noise cancellation problem and is discussed in detail in references[56,58, and 59]. This is an important class of problems because it introduces the concept of minimizing a mean-square error metric and because it has strong parallels to problems encountered in ANVC applications; the main difference is that ANVC applications will have a nonunity transfer function relating the output of the control filter to the error signal response.

As shown in Fig. 18.26, the input signal $f(n)$, which is also referred to as the reference signal, is filtered by the FIR filter $\mathbf{w}$ to produce an output sequence $y(n)$. The desired signal, $\hat{d}(n)$, is contaminated by noise correlated with the input signal but presumably uncorrelated with the desired signal. The resulting signal plus noise is shown in the figure as $d(n)$. The correlation of the noise and the input signal is indicated by the unknown physical impulse response function h_i. The objective for this problem is to solve for the coefficients of the FIR filter that will take the input sequence $f(n)$ and generate the output sequence $y(n)$ that will remove the unwanted noise from the signal $d(n)$. In other words, we seek to design the optimal FIR filter to remove the part of $d(n)$ that is correlated with the input signal $f(n)$. If successful, the error signal $e(n)$ will be uncorrelated with the input signal when the filter is in place.

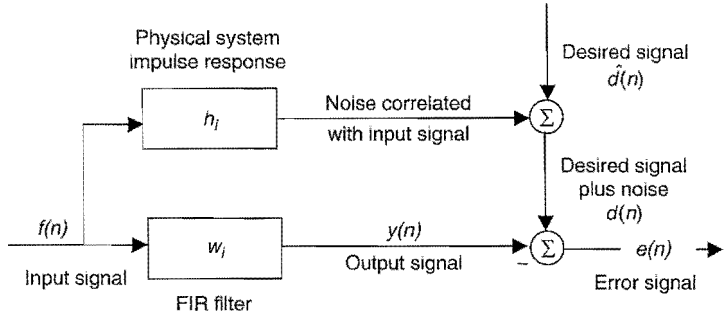


FIGURE 18.26 Electrical noise cancellation problem.

Following the developments in references 56 and 58 the error signal can be expressed in terms of the desired signal plus noise, the input signal, and the FIR filter coefficients:

$$e(n) = d(n) - \sum_{i=0}^{I} w(i) f(n-i)$$
$$= d(n) - \mathbf{w}^{\mathrm{T}}\mathbf{f}(n) = d(n) - \mathbf{f}^{\mathrm{T}}(n)\mathbf{w} \tag{18.9}$$

where the lower equation has been used to express this relationship using vector inner products and $f(n)$ is defined in Eq. (18.6).

An expression for the mean-square error can be obtained by expanding terms in Eq. (18.9) and taking the expected value:

$$E\{e^2(n)\} = E\{d^2(n)\} - 2\mathbf{w}^{\mathrm{T}}E\{\mathbf{f}(n)d(n)\} + \mathbf{w}^{\mathrm{T}}E\{\mathbf{f}(n)\mathbf{f}^{\mathrm{T}}(n)\}\mathbf{w} \tag{18.10}$$

Equation (18.10) is a key result because it reveals that the mean-square error is a quadratic function of the weights of the FIR filter. The quadratic function will have a *global minimum* provided that the matrix $E\{\mathbf{f}(n)\mathbf{f}^{\mathrm{T}}(n)\}$ in the third term is *positive definite*,[56,58–60] which means that all of its eigenvalues are greater than zero. Assuming this requirement is met, if one were to plot the mean-square error as a function of any two of the coefficients of the FIR filters, the "error surface" would be a bowl, as shown in Fig. 18.27. As a consequence, the FIR filter coefficients that correspond to the minimum mean-square error can be determined by differentiating Eq. (18.10) with respect to each coefficient of the FIR filter and setting the resulting set of equations equal to zero.

This process of differentiating and equating the results to zero will produce a set of linear equations in terms of the unknown coefficients of the FIR filter. This matrix equation can be expressed as

$$[\mathbf{A}]\mathbf{w} = \mathbf{b} \tag{18.11}$$

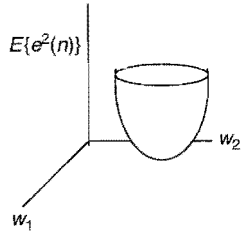


FIGURE 18.27 Error surface for a quadratic function in terms of coefficients w_1 and w_2.

where [**A**] is the *input correlation matrix* defined as

$$[\mathbf{A}] = \begin{bmatrix} R_{ff}(0) & R_{ff}(1) & \cdots & R_{ff}(I-1) \\ R_{ff}(1) & R_{ff}(0) & & \\ \vdots & & \ddots & \vdots \\ R_{ff}(I-1) & & & R_{ff}(0) \end{bmatrix} \tag{18.12}$$

where

$$R_{ff}(m) = E\{f(n)f(n-m)\} = E\{f(n)f(n+m)\} \tag{18.13}$$

The vector **b** in Eq. (18.11) corresponds to the lag values of the cross correlation between the reference sequence and the desired sequence given by

$$\mathbf{b} = [\, R_{fd}(0) \quad R_{fd}(1) \quad \cdots \quad R_{fd}(I-1)\,]^{\mathrm{T}} \tag{18.14}$$

where

$$R_{fd}(m) = E\{f(n)d(n+m)\} = E\{f(n-m)d(n)\} \tag{18.15}$$

With the above definitions for [**A**] and **b**, the coefficients of the optimal FIR filter can be expressed in terms of auto- and cross-correlation functions of the input and the desired signals. Provided that the input correlation matrix [**A**] is invertible, the optimal coefficients are given by

$$\mathbf{w}_{\mathrm{opt}} = [\mathbf{A}]^{-1}\mathbf{b} \tag{18.16}$$

where $[\mathbf{A}]^{-1}$ is the inverse of the matrix [**A**]. As discussed by Widrow and Stearns[59] and Elliott,[58] the solution of Eq. (18.16) is called the *Wiener filter*. It can be shown that using this filter will cause the cross correlation between the error signal and input signal to be zero over the length of the filter $(I-1)$. For the problem posed in Fig. 18.26, this implies that the Wiener filter will remove any portion of the signal, $d(n)$, that is correlated with the input signal $f(n)$.

The residual mean-square error can be determined by substituting Eq. (18.16) into Eq. (18.10):

$$E\{e^2(n)\}_{\min} = E\{d^2(n)\} - \mathbf{b}^{\mathrm{T}}[\mathbf{A}]^{-1}\mathbf{b} \tag{18.17}$$

Solving for $\mathbf{w}_{\mathrm{opt}}$ in Eq. (18.16), however, requires computing the inverse of the input correlation matrix [**A**], which can be computationally expensive and may be numerically ill-conditioned (i.e., singular). As a consequence, procedures have been developed to search for the minimum of Eq. (18.10) using iterative techniques. One of the most computationally efficient iterative techniques, the least mean-square (LMS) algorithm, is introduced in the next section.

Adaptive Digital Filter Design

Gradient Descent Algorithms. As discussed in the previous section, the mean-square error is a quadratic function in terms of the optimal weights of

the FIR filter. As such, gradient descent algorithms are guaranteed to converge to the global minimum, provided [**A**] is positive definite and the algorithm is itself stable.

The basic concept of a gradient descent algorithm is to estimate the gradient (i.e., derivative) of the mean-square error with respect to the FIR filter coefficients and update the filter coefficients by moving in the direction of the negative of the local gradient. There are many different algorithms that can be used to adaptively determine the filter coefficients corresponding to the global minimum. These algorithms include Newton-based algorithms, steepest-descent algorithms, and the LMS algorithm, which was introduced by Widrow and Stearns.[59] These algorithms typically trade off convergence speed versus numerical stability (for IIR filters) and computational complexity. Details of these algorithms can be found in texts written by Widrow and Stearns[59] and Elliott.[58] While sometimes having performance advantages over FIR filters, IIR filters can encounter numerical stability problems during design and can converge to nonglobal minima, resulting in less than optimal performance. On the other hand, the LMS algorithm discussed in the next section (for FIR filter design) approximates the gradient term, thus significantly reducing the required number of computations while ensuring convergence to the optimal coefficient vector.

LMS Algorithm. Widrow and Stearns[59] developed an elegant algorithm that greatly simplifies the computational complexity yet still converges to the optimal coefficient vector (i.e., Wiener filter). This algorithm estimates the gradient term using the instantaneous value of the error, as opposed to performing a matrix inversion or estimating expected values as required by Newton's algorithm and steepest-descent algorithm, respectively. As a consequence, the gradient term is approximated as [see Eq. (18.10)]

$$\frac{\partial E\{e^2(n)\}}{\partial \mathbf{w}} \approx 2e(n)\frac{\partial e(n)}{\partial \mathbf{w}} \approx -2\mathbf{f}(n)e(n) \tag{18.18}$$

Using this expression for the gradient, the update equation of the filter coefficients using the LMS algorithm is given by

$$\mathbf{w}(n+1) = \mathbf{w}(n) + 2\mu\mathbf{f}(n)e(n) \tag{18.19}$$

where μ is a constant known as the adaptation coefficient, which characterizes the speed of convergence of the algorithm. This equation states that the vector of filter coefficients at time step $n+1$ can be determined from the vector of coefficients at time step n plus a correction term in the direction of the negative of the gradient of the error surface as estimated by Eq. (18.18).

Widrow and others have shown that this algorithm will converge to the optimal solution and is guaranteed to be stable provided that the value of the convergence parameter satisfies the relationship

$$0 < \mu < \frac{2}{m\overline{f^2}} \tag{18.20}$$

The denominator of the right-hand term is an approximation to the trace of the input correlation matrix, where m is the number of FIR filter coefficients and $\overline{f^2}$ is equal to the mean-square value of $f(n)$.

Another important parameter associated with the LMS algorithm is termed the *misadjustment*, which is the ratio of the excess mean-square error to the minimum mean-square error. Essentially, this is a measure of how close the algorithm will converge toward the bottom of the quadratic performance surface (see, e.g., Fig. 18.27) for a particular value of μ. It can be shown that the *misadjustment* is equal to the convergence parameter times the trace of the input correlation matrix for the LMS algorithm.[59] If we invoke the same approximation to this trace as in Eq. (18.20), we obtain an expression for the convergence parameter in terms of the misadjustment and mean-square value of the input sequence:

$$\mu_{\max} = \frac{\rho}{m\overline{f^2}} \tag{18.21}$$

where ρ is the misadjustment factor. This final expression provides a useful procedure for selecting the convergence parameter. In fact, it is often useful to specify the desired misadjustment (e.g., $\rho = 0.01$) and let the adaptation coefficient be calculated from Eq. (18.21). In this way, the resulting adaptation coefficient will be normalized by the power of the reference signal. When the adaptation coefficient is adjusted to be inversely proportional to the power of the input signal, the algorithm is referred to as the *normalized* LMS algorithm. In practice, the value of the convergence coefficient obtained in this way serves as a starting point and manual adjustment is often necessary to obtain the desired performance.

To preserve clarity, we have presented the LMS algorithm assuming a SISO error signal. However, the algorithm is easily extendable to the MIMO case. Details for the MIMO implementation can be found in Widrow and Stearns,[59] Nelson and Elliott,[16] and Elliott.[58]

Because of its computational simplicity and good convergence properties, the LMS algorithm has been used extensively in a variety of applications (e.g., in-wire cancellation, system identification) and is the basis for the filtered-x LMS algorithm that is most often used in ANVC applications. In fact, the LMS algorithm is typically used to estimate the impulse response between the filter output and the error signal (i.e., plant), which is needed for the implementation of the filtered-x LMS algorithm. Details and examples of the filtered-x LMS algorithm are covered in the next section.

18.4 FEEDFORWARD CONTROL SYSTEMS

Basic Architecture

The basic architecture of a feedforward active control system is shown in Fig. 18.28. The figure shows a disturbance d exciting a system which is to be controlled. A transfer function T relates the disturbance to the system output o.

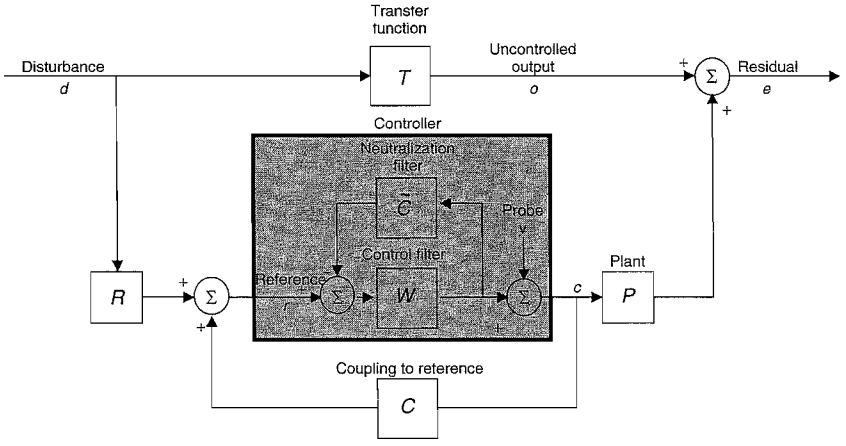


FIGURE 18.28 Basic feedforward architecture without adaptation.

A reference signal r correlated with the disturbance is used by the controller to generate a signal that drives a control actuator to excite the system and reduce the system response to the disturbance. The transfer function R is shown simply to indicate that the disturbance and the reference are correlated. The transfer function P, referred to as the plant, relates the controller output to the system output. The block diagram shows that the actuator, when driven by the controller output, is coupled not only to the system output but also to the reference through the transfer function C. The feedback to the reference signal is not desirable and the controller contains a filter $\tilde{C}$ the transfer function of which is a copy of the coupling transfer function between the control actuator and the reference sensor. The purpose of this neutralization filter is to cancel or neutralize the coupling between actuator and reference signal. In addition to $\tilde{C}$, the controller contains a second filter, W, the purpose of which is to take the reference signal and generate a signal to drive the actuator to reduce the system output o. If the neutralization filter performs properly, the coupling to the reference is removed and the block diagram simplifies to that shown in Fig. 18.29. Note that an alternate approach has been pioneered by Eriksson and his colleagues in which the designs of W and $\tilde{C}$ are combined in a slightly different architecture from that shown here. The interested reader is referred to references 25 and 61–63.

To see what the block diagram in Fig. 18.28 means physically, consider the duct problem described in Section 18.2. Figure 18.30 show a schematic of the duct with a reference microphone, controller, and control speaker. The disturbance, a sound wave of amplitude d, can be seen to the left propagating down the duct toward the control speaker. The transfer function T relates the disturbance pressure to the uncontrolled pressure, o, downstream of the speaker location in the duct. The reference microphone senses the disturbance pressure and sends a reference signal r to the controller. The control filter W operates

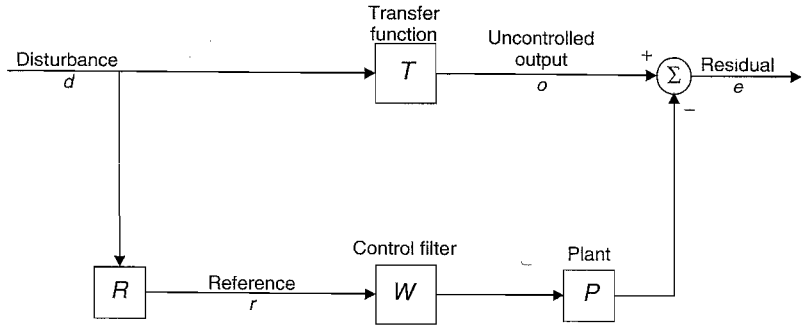


FIGURE 18.29 Simplified feedforward architecture with coupling to reference removed.

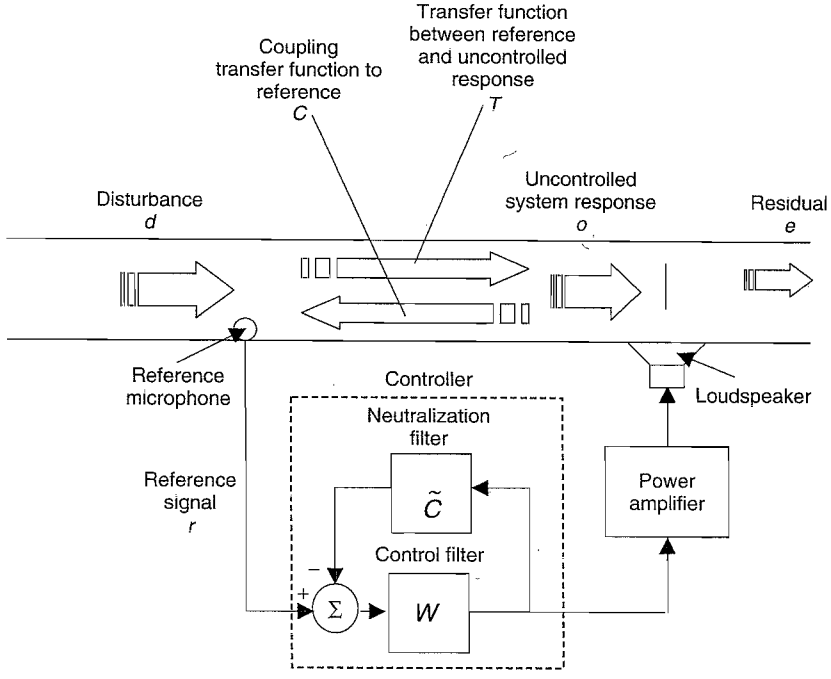


FIGURE 18.30 Feedforward architecture applied to the control of noise in a duct.

on the reference and sends the resulting signal to the power amplifier, which in turn drives the speaker. The transfer function relating the controller output signal to the pressure in the duct at the speaker is the plant transfer function P. The pressure generated by the speaker interacts with the disturbance propagating down the duct, reducing the amplitude and producing the residual sound wave

of amplitude e. In an adaptive system there would be a microphone in the duct downstream of the control speaker to sense this residual. As we shall see later, this residual, or error, signal and the reference signal can then be used in the controller electronics to update, or adapt, the coefficients of the control filter. In addition to generating a sound wave that interferes with the sound propagating down the duct, the speaker also generates a sound wave which travels upstream to the reference microphone, contaminating the reference signal. The filter $\tilde{C}$ is a copy of the transfer function relating the controller output to the pressure at the reference microphone. It electronically removes the contamination from the control speaker in the reference microphone before it reaches the control filter W.

The architecture in Figs. 18.28 and 18.29 has been discussed as if there were only one reference signal and one residual. In fact, the controller need not be restricted to the SISO case. There commonly are cases with multiple references and multiple residuals. In fact, for feedforward systems the procedures for estimating the optimum control filter W for the MIMO case as well as the SISO case are well in hand. In addition the block diagrams in Figs. 18.28 and 18.29 are completely general and apply equally to SISO or MIMO systems. The only difference is that the blocks, which for SISO systems are transfer functions, for MIMO systems become transfer function matrices.

Optimal Control Filter Estimation

Tonal Disturbances. We will first consider the case of narrow-band, or tonal, disturbances. To do so, we will first modify the block diagram of Fig. 18.29 by showing a functional connection between the reference and the disturbance indicated by the transfer function B, as shown in Fig. 18.31. Mathematically this is equivalent to setting $T = 1$ and $B = R^{-1}$. A simple equation can be written for the residual e in terms of the controller transfer function in Fig. 18.31:

$$e(\omega) = d(\omega) - P(\omega)W(\omega)r(\omega) \tag{18.22}$$

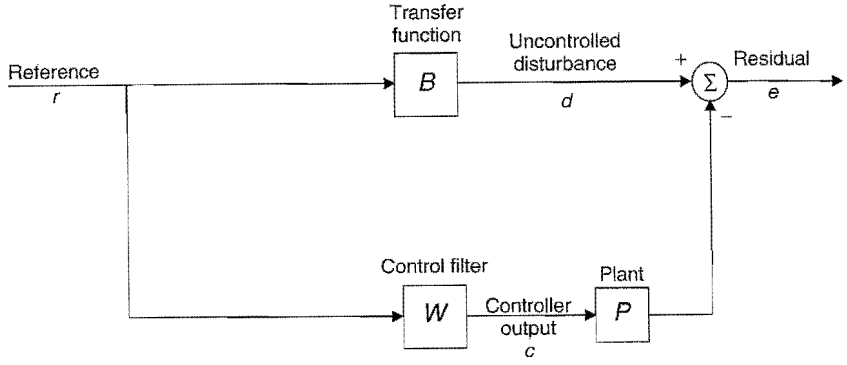


FIGURE 18.31 Simplified feedforward block diagram.

where ω is the frequency of the disturbance, the other variables are defined in Fig. 18.31, and all of the variables are scalars. We can use this equation to express the autospectrum of the residual as $S_{ee}(\omega) = E\{e(\omega)e^*(\omega)\}$, where $E\{\cdot\}$ means the expected value. Substituting Eq. (18.22) into this equation, we obtain

$$\begin{aligned} S_{ee}(\omega) = {} & S_{dd}(\omega) - P(\omega)W(\omega)S_{rd}(\omega) \\ & - P^*(\omega)W(\omega)^*S_{dr}(\omega) + |P^2(\omega)|S_{rr}(\omega)|W(\omega)^2| \end{aligned} \tag{18.23}$$

where $(\cdot)^*$ means complex conjugate, S_{dd} is the autospectrum of the disturbance, S_{rr} is the autospectrum of the reference, $S_{dr} = E\{dr^*\}$ is the cross-spectra of the disturbance and the reference, and $S_{rd} = E\{rd^*\}$ is the complex conjugate of that cross-spectrum. If we take the derivative of Eq. (18.23) with respect to W and equate it to zero and solve for $W(\omega)$, we obtain

$$W(\omega) = \{|P^2(\omega)|S_{rr}(\omega)\}^{-1}P^*(\omega)S_{rd}(\omega) = P^{-1}(\omega)\left\{\frac{S_{rd}(\omega)}{S_{rr}(\omega)}\right\} = P^{-1}(\omega)B(\omega) \tag{18.24}$$

where we have taken advantage of the fact that $\{S_{rd}(\omega)/S_{rr}(\omega)\}$ is an estimate of the transfer function between the disturbance and the reference. In Eq. (18.24) W is the optimum control filter. It consists of the inverse of the plant times an estimate of the transfer function between the reference and the disturbance. Such a form for the control filter makes a lot of sense, because W is attempting to take the reference signal r and turn it into the disturbance d. To do so, the filter must first remove the influence of the plant transfer function, which is the purpose of the plant inverse. It then must include an estimate of the transfer function between the reference and the disturbance, which is the purpose of the term in brackets.

If we substitute Eq. (18.24) into Eq. (18.23), we can obtain an estimate of the spectrum of the residual when this control filter is used:

$$S_{ee}(\omega) = S_{dd}(\omega) - \frac{|S_{rd}(\omega)|^2}{S_{rr}(\omega)} \tag{18.25}$$

This equation shows that for perfect correlation between the reference and disturbance ($d = \gamma r$), where γ is constant, the spectrum of the residual goes to zero.

Note that this approach does not guarantee that the control filter will be causal. As discussed in Section 18.3, a causal filter is one whose impulse response is zero for $t < 0$. Causal filters can be formulated as FIR or stable IIR digital filters. Noncausal filters cannot. Consequently, a digital representation of a noncausal filter cannot be found for use in a control system. The filter is simply not realizable.

In some cases using the above control filter can result in excessive demands on the actuators, in which case it is useful to be able to limit the output of the control filter. Control effort weighting is one means of reducing the actuator

effort. It can be included in the design equations for the filter by adding a term to Eq. (18.23), the equation for the residual. The term that is added is the weighted output of the controller given by

$$\alpha^2(\omega)|W(\omega)^2|S_{rr}(\omega) \tag{18.26}$$

where α^2 is a real positive scalar that might be a function of frequency. By selecting increasing values of α^2, the minimization of the residual can be adjusted. If α^2 is very small, the control filter will be designed as if there were no control effort weighting. If α^2 is large, the control effort will be reduced, and the performance of the control system will also be reduced. Including Eq. (18.26) in Eq. (18.23) results in a control filter given by

$$W(\omega) = \{[|P^2(\omega)| + \alpha^2(\omega)]S_{rr}(\omega)\}^{-1} P^*(\omega)S_{rd}(\omega) \tag{18.27}$$

and the residual is given by

$$S_{ee}(\omega) = S_{dd}(\omega) - \left\{\frac{|P^2(\omega)|}{|P^2(\omega)| + \alpha^2(\omega)}\right\}\left\{2 - \frac{|P^2(\omega)|}{|P^2(\omega)| + \alpha^2(\omega)}\right\}\frac{|S_{rd}(\omega)|^2}{S_{rr}(\omega)} \tag{18.28}$$

It is clear from this equation that as α^2 approaches zero the residual becomes the same as Eq. (18.25) with no control effort weighting. However, as α^2 becomes large, $S_{ee} \to S_{dd}$ and the control performance is reduced. Similarly the spectrum of the controller output c (see Fig. 18.31) is given by

$$S_{cc}(\omega) = |W^2(\omega)|S_{rr}(\omega) = \frac{|P^2(\omega)|}{\{|P^2(\omega)| + \alpha^2(\omega)\}^2}\frac{|S_{rd}(\omega)|^2}{S_{rr}(\omega)}$$

This equation shows that as α^2 increases the spectrum of the controller output will decrease, reducing the drive to the actuators. As a result increasing the control effort weighting will decrease the actuator drive at the cost of increasing the residual.

Broadband Disturbances. For a pure-tone disturbance, Eqs. (18.24) and (18.27) provide the proper control filter representation (amplitude and phase) at the frequency of the disturbance. For a broadband disturbance, if the broadband filter defined by these equations is noncausal, as it often is, then, a different approach that includes a constraint on causality needs to be employed to determine the optimum causal filter. We can ensure that the control filter is causal by inserting the form of a causal filter into Eq. (18.23) and carrying out the same optimization procedure. Because it results in a set of linear equations, we will use the form of an FIR digital filter given by

$$W(\omega) = \sum_{n=0}^{N-1} W_n e^{-j\omega n\Delta t} \tag{18.29}$$

where N is the number of taps in the filter, W_n is the real amplitude associated with each tap, and Δt is the sampling period (1/sampling rate). Before substituting Eq. (18.29) into (18.23) we need to modify Eq. (18.23) slightly. Since we are now concerned with a broadband disturbance, we need to integrate the residual spectrum over the frequency range where control is desired. Following the same procedure as for Eq. (18.23), we obtain for the optimum control filter the matrix equation

$$\begin{Bmatrix} W_0 \\ W_1 \\ \vdots \\ W_{N-1} \end{Bmatrix} = \begin{bmatrix} C_0 & C_{-1} & \cdots & C_{1-N} \\ C_1 & C_0 & \cdots & C_{2-N} \\ \vdots & & & \vdots \\ C_{N-1} & C_{N-2} & \cdots & C_0 \end{bmatrix}^{-1} \begin{Bmatrix} A_0 \\ A_1 \\ \vdots \\ A_{N-1} \end{Bmatrix} \tag{18.30}$$

where

$$A_p = \mathrm{Re}\left\{\sum_{k=0}^{K-1} P(k)S_{rd}(k)e^{-jpk(2\pi/K)}\right\}$$

$$C_{(p-m)} = \mathrm{Re}\left\{\sum_{k=0}^{K-1}\left\{|P^2(k)| + \alpha^2(k)\right\}S_{rr}(k)e^{-j(p-m)k(2\pi/K)}\right\} \tag{18.31}$$

and $p = 0, 1, \ldots, N-1$ and $m = 0, 1, \ldots, N-1$. In writing this equation, we have substituted a discrete sum for the integrals. The knowledgeable reader will recognize that Eq. (18.31) is in the form of the discrete Fourier transform (DFT), allowing for the efficient use of the fast Fourier transform algorithm in the evaluation of the vector and matrix elements in Eq. (18.30). In the equations K is the number of elements in the DFT.

Example. To illustrate these ideas, we will compute the noncausal and causal control filters for a simple example. We will use the following parameters:

$$S_{dd} = 1 \qquad S_{rr} = 1$$

$$S_{rd} = e^{-j\omega T}\left\{\frac{\omega_{\mathrm{BW}}^4}{\omega^4 + \omega_{\mathrm{BW}}^4}\right\} \tag{18.32}$$

$$P = \frac{\omega_0^2}{-\omega^2 + j\eta\omega_0\omega + \omega_0^2} \tag{18.33}$$

$$T = 0.02 \text{ s} \qquad f_0 = \frac{\omega_0}{2\pi} = 25 \text{ Hz}$$

$$\eta = 0.1 \qquad f_{\mathrm{BW}} = \frac{\omega_{\mathrm{BW}}}{2\pi} = 40 \text{ Hz}$$

Sampling rate = 200 Hz Filter length = 100 taps

In this case the autocorrelations of the disturbance and reference are taken as unity. The cross-spectral density S_{rd} shows a delay of $T = 0.02$ s and includes a transfer function (in brackets) that decreases with increasing frequency. The plant P is a simple second-order system with a natural frequency of 25 Hz and a loss factor of 0.1. For the causal control filter estimation procedure we will use the indicated sampling rate and filter length.

Figure 18.32 compares the frequency responses of the control filters estimated using the noncausal and causal estimation procedures. The two estimation procedures give different filters but not markedly so. The difference is slightly more evident in Figs. 18.33*a* and 18.33*b*, where the impulse response of the control filter estimated using the noncausal approach and the filter tap coefficients of the filter from the causal procedure are compared. Bear in mind that if we plot the filter tap coefficients separated by the sampling period (0.005 s at 200 Hz sampling rate), we will obtain a graph corresponding to the impulse response of the filter. The two figures are similar except that in the noncausal impulse response there is a small increase near the end of the time interval. Because of the periodicity of the impulse response of the filter obtained using the DFT, the increase at the end of the time interval actually indicates that the filter is responding before $t = 0$ and consequently that the filter is noncausal. The effect in this

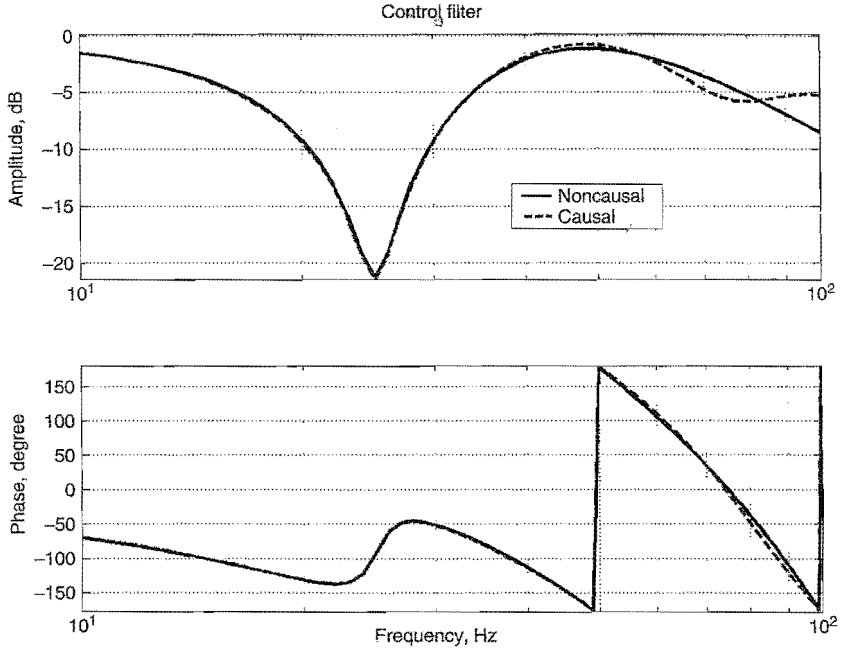


FIGURE 18.32 Control filter frequency response using the noncausal and causal estimation procedures.

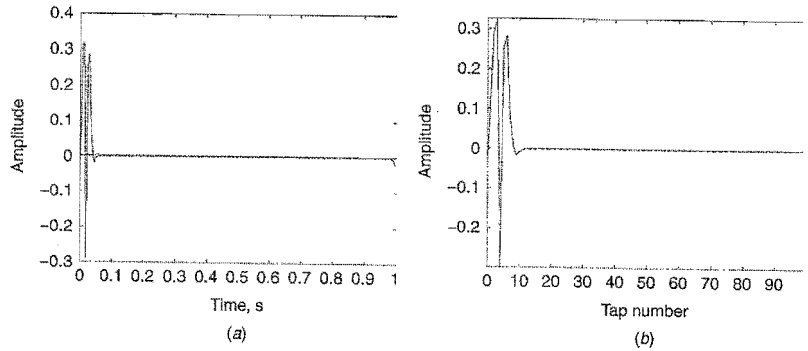


FIGURE 18.33 Comparison of the impulse response of (*a*) the noncausal control filter and (*b*) the tap coefficients of the causal filter.

instance is small; however, in later examples where we bring more realism into the calculation by including anti-aliasing filters and other practical considerations we will see much larger noncausal effects. Note that the tap coefficients of the filter estimated using the causal procedure show no such increase and the higher tap coefficients decrease to zero.

The performance of this system using the causal control filter is shown in Fig. 18.34. The figure shows the ratio of the spectrum of the controlled residual to the spectrum of the uncontrolled residual $\{S_{ee}(\omega)/S_{dd}(\omega)\}$ as a function of

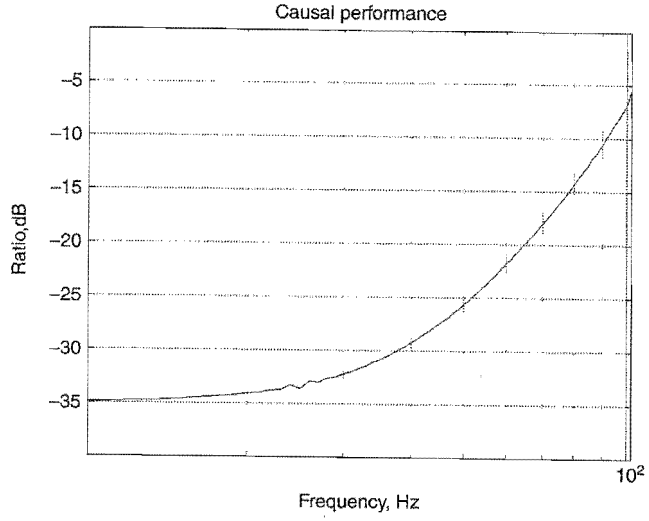


FIGURE 18.34 Ratio of the residual to the disturbance using the control filter in Fig. 18.32.

frequency out to the Nyquist frequency. Note that the performance of the non-causal filter (not shown in the graph) would be predicted to be perfect, that is, the residual would be zero for all frequencies.

The performance shown in the Fig. 18.34 is unrealistically large for a broadband active control system. This is a consequence of the fact that, at this stage, we have neglected to include other elements in the analysis that would add more realism to the estimate, such as system delays, anti-aliasing filters, sensor noise, and so on. In addition the figure only shows system performance up to the Nyquist frequency (one-half the sampling frequency). As we shall see in a later section, the digital control filter is periodic in frequency with a period equal to the sampling frequency. Consequently, the performance above the Nyquist frequency may also need to be controlled, especially if there is significant energy in the disturbance at those frequencies. We will see how this is done in a later section.

Adaptive Control

In the previous section we discussed the design of a control filter to reduce optimally a chosen residual in a least-squares sense. In that derivation the system to be controlled was assumed to be fixed. In reality the transfer functions defining dynamic systems often change with time. This means that those transfer functions must be measured periodically and the new results used to update the control filter coefficients. We will discuss this process of system identification in the next section. Here we examine an adaptive control algorithm based on the LMS algorithm that continuously updates the control filter coefficients in order to minimize the chosen residual sensor signals. The filtered-x algorithm, as it has come to be called, updates the control filter coefficients at each time step.

The filtered-x LMS algorithm, a modification of the LMS algorithm[59] commonly used for cancellation of electronic noise, was first proposed by Morgan.[64] If used unmodified in an active cancellation system, the LMS algorithm can lead to instabilities because the signal from the controller must pass through the plant dynamics where it will experience amplitude changes and phase shifts. The solution to this problem proposed by Morgan was also proposed independently by Widrow et al.[65] and Burgess.[66] Morgan's solution, which has come to be called the filtered-x LMS algorithm, is used extensively today and has been generalized to MIMO systems by Elliott and Nelson.[67]

Figure 18.35*a* shows a block diagram of a simplified feedforward control system. If we change the order of the plant and control filter in the block diagram, the response will be unchanged as long as the system is linear. The resulting block diagram is shown Fig. 18.35*b*. The result is a new reference signal u that is the original reference signal filtered by the plant transfer function P. The residual of this new system can be written as

$$e(n) = d(n) - \sum_{n=0}^{N_w-1} w(k)u(n-k) = d(n) - \mathbf{w}^{\mathrm{T}}\mathbf{u} \qquad (18.34)$$

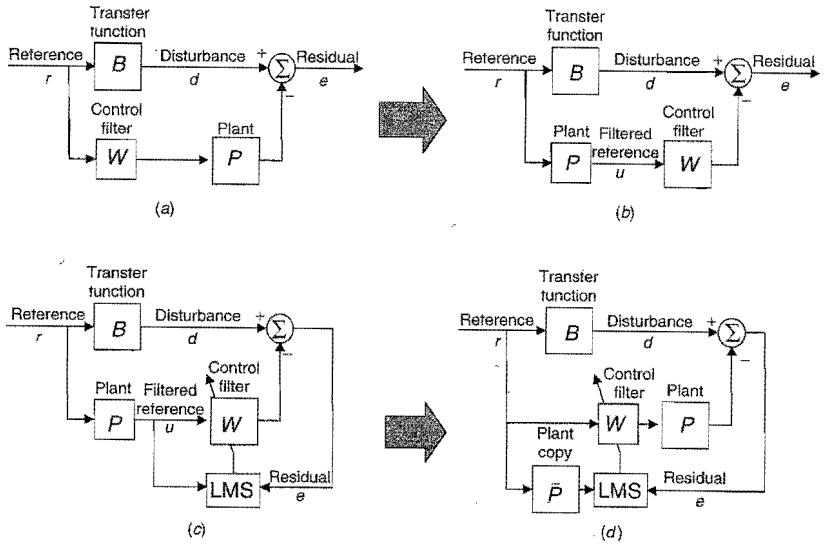


FIGURE 18.35 Feedforward block diagram with and without adaptation showing the progression to the LMS filtered-x algorithm: (*a*) original diagram; (*b*) changing the order of plant and control filter; (*c*) LMS algorithm; (*d*) filtered-x algorithm.

where $e(n)$ is the nth element of a time sequence e, $d(n)$ is similarly defined, $\mathbf{w}^{\mathrm{T}}$ is the transpose of a vector, the N_w elements of which are the control filter tap coefficients, and $\mathbf{u}$ is a column vector of the last N_w samples in the filtered reference, which is given by

$$u(n) = \sum_{m=0}^{N_w-1} p(m)r(n-m) \qquad (18.35)$$

where p is the impulse response of the system estimate of the plant filter P and r is the reference signal time sequence. The block diagram showing the adaptation process is shown in Fig. 18.35*c*, and a slight rearrangement of the blocks in the block diagram in Fig. 18.35*d* results in the specialized LMS algorithm called the filtered-x LMS algorithm.

Unlike the direct-estimation approach in the previous section in which the filter coefficients are estimated in a single calculation, the filtered-x algorithm uses an iterative approach which updates the estimate at each time step. The update equation for the control filter is derived similarly to that for the LMS algorithm (see Adaptive Digital Filter Design in Section 18.3). The resulting equation to estimate the coefficients of w is typically written as

$$\mathbf{w}(n+1) = \mathbf{w}(n) + 2\mu e(n)\mathbf{u}(n) \qquad (18.36)$$

where

$$\mathbf{w}(n) = \begin{Bmatrix} w(0) \\ w(1) \\ \vdots \\ w(N_w - 1) \end{Bmatrix}$$

is a column vector of the nth estimate of the N_w control filter coefficients, $w(0)$ is the first filter coefficient, $w(1)$ is the second, and so on,

$$\mathbf{u}(n) = \begin{Bmatrix} u(n) \\ u(n-1) \\ \vdots \\ u(n - N_w + 1) \end{Bmatrix}$$

is a column vector of the last N_w samples in the filtered reference, and μ is a scalar convergence coefficient set by the user to ensure stable convergence to the optimum filter coefficients. This equation is very similar to that derived for the LMS algorithm, the only difference being that the filtered reference $\mathbf{u}(n)$ is used in the update equation rather than the reference itself.

In Eq. (18.36) the larger is μ, the faster the algorithm will converge to the optimum filter coefficients. However, if μ is too large, the algorithm will go unstable and will not converge. The convergence coefficient can be selected using the following rule of thumb[58]:

$$0 < \mu \leq \frac{1}{N_w E\{u^2\}} \tag{18.37}$$

where N_w is the number of control filter coefficients and $E\{u^2\}$ is the mean-square value of the filtered reference. This is very similar to the rule of thumb for the LMS algorithm presented in Section 18.3 except that the mean-square value of the filtered reference, $E\{u^2\}$, is substituted for mean-square value of the reference itself, $E\{r^2\}$.

Equation (18.36) along with Eq. (18.35) states the SISO filtered-x algorithm. This algorithm has enjoyed a great deal of popularity because it is very easy to implement and functions well in the presence of errors in the plant estimate used to filter the reference. If the convergence rate is kept slow enough, the algorithm will still find the optimum filter coefficients even in the presence of plant phase errors of up to 90°.[64] In addition, the algorithm can be very effective in maintaining control even if the reference is nonstationary. Finally, it is possible to introduce something comparable to control effort weighting as discussed in the previous section. In the filtered-x algorithm this is referred to as *leakage*. By reducing the control filter coefficients by a small percentage at each time step,[59] the effect is similar to broadband control effort weighting.

Example. To illustrate the application of this algorithm, we will utilize it to design an optimum filter for the system of the previous section. To do so, we will require the impulse response function (IRF) associated with the cross-spectrum between disturbance and reference, S_{rd}, and the IRF of the plant, P. We obtain these by simply inverse Fourier transforming the FRF functions in Eqs. (18.32) and (18.33), respectively, and retaining a sufficient number of terms to ensure that we capture all of the impulse response. Figure 18.36 illustrates the two IRFs. The plant IRF is a decaying sinusoid with a frequency of 25 Hz, the natural frequency of the plant. The cross-spectrum IRF shows the delay of 0.02 s introduced into the model. We will retain the full 1 s duration (200 taps at a sampling rate of 200 Hz) of the IRFs in the figure, although it would probably be sufficient to retain substantially less. The filter coefficients obtained using the direct [Eq. (18.30)] and filtered-x [Eqs. (18.35) and (18.36)] estimation procedures are compared in Fig. 18.37, and the frequency response functions are compared in Fig. 18.38. There are clear differences between the two control filters that may be a consequence of the fact that the filtered-x procedure is still converging. That the procedure is still converging can be seen in Fig. 18.39, which shows a time history of the residual, or controlled disturbance. Even after over 80 s the residual still shows a tendency to decrease. Figure 18.40 shows the ratio of the spectrum of the controlled disturbance to the spectrum of the uncontrolled disturbance as a function of frequency at the end of the time interval in Fig. 18.39. Also shown in the figure is the same ratio for the direct-estimation procedure. In this case the two procedures give comparable results despite the differences in the control filters.

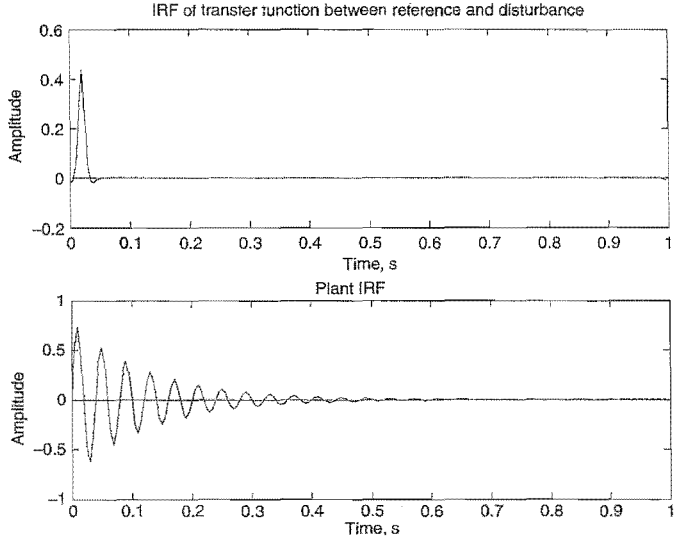


FIGURE 18.36 Impulse response functions for S_{rd} (top) and the plant, P (bottom).

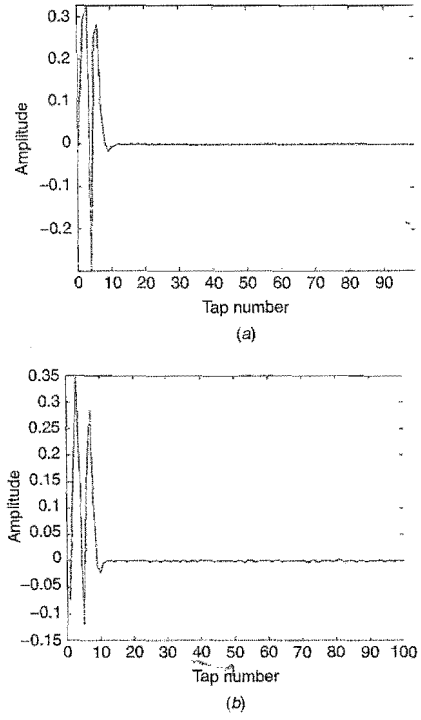


FIGURE 18.37 (*a*) Direct-estimation control filter coefficient compared to (*b*) filtered-x control filter coefficients.

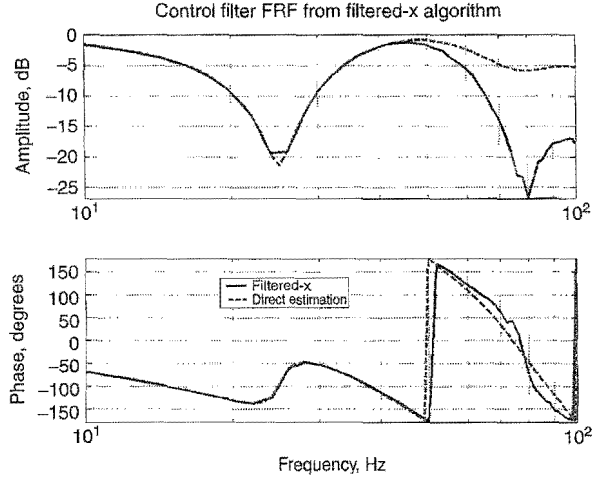


FIGURE 18.38 Filtered-x control filter frequency response compared to the direct estimation control filter frequency response.

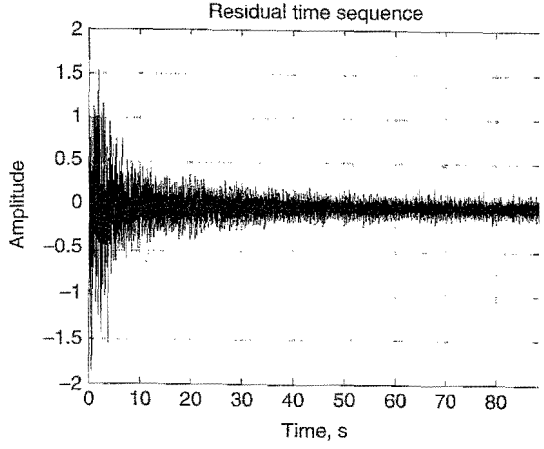


FIGURE 18.39 Time history of the residual.

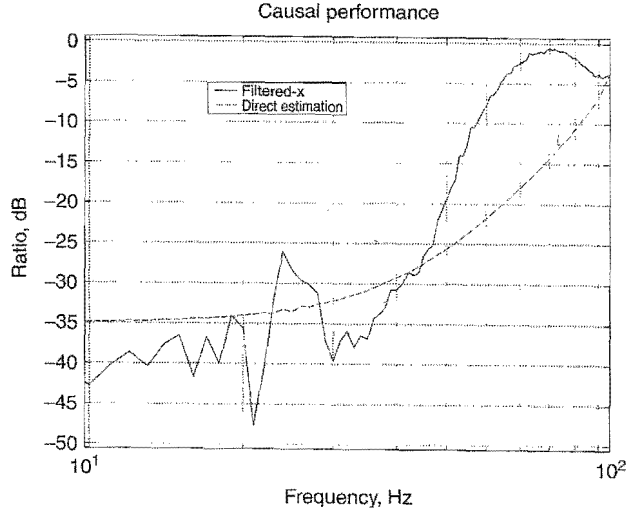


FIGURE 18.40 Ratio of controlled to uncontrolled disturbance.

Control of Aliasing Effects

In the previous sections we have focused on control of the disturbance below the Nyquist frequency. In fact, because digital filters are periodic in the frequency domain with a period equal to the sampling frequency, we must also concern ourselves with the performance above the Nyquist frequency, especially if the disturbance has significant amplitude there. Figure 18.41 shows the ratio

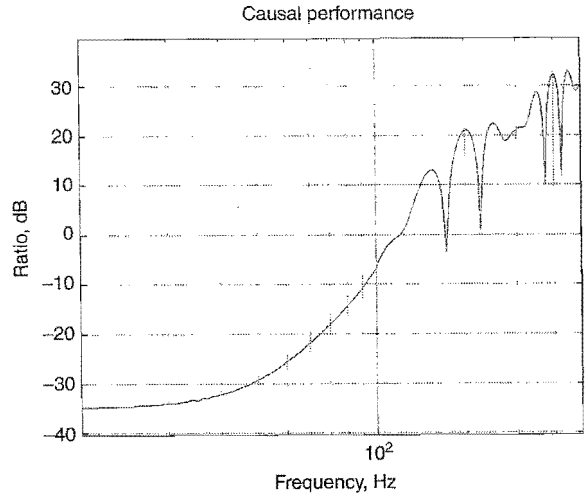


FIGURE 18.41 Change in the ratio of controlled to uncontrolled disturbance beyond the Nyquist frequency.

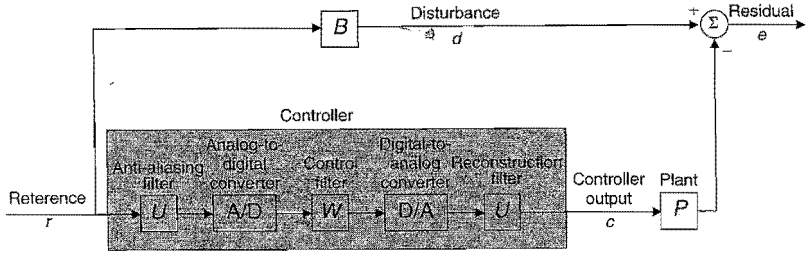


FIGURE 18.42 Feedforward block diagram further simplified (adaptation blocks not shown).

of the controlled-to-uncontrolled disturbance beyond the Nyquist frequency for the direct-estimation case in the previous section on optimal control filter estimation. Above ~125 Hz the figure shows that the control system will amplify the disturbance. To control this out-of-band amplification, one usually employs anti-aliasing filters, low-pass filters that minimize energy above the Nyquist frequency entering the controller. In addition, there are other low-pass filters and delays that should be included in a more realistic model of the active control system. To that end Fig. 18.42 shows the controller expanded into five blocks. First the analog reference signal needs to be digitized before the controller can utilize it. That is the function of the A/D converter shown as the second block in the controller. The first block is a low-pass filter called the anti-aliasing filter. Its cutoff frequency is usually set slightly below the Nyquist frequency in order

to reduce aliasing in the digital controller, as described above. The third block is the digital control filter, the output of which is fed to a D/A converter to convert the digital signals to analog signals. The D/A converter is usually a sample-and-hold device that produces a signal with discrete steps or jumps at the sampling rate. Consequently, there is usually a low-pass filter at the output of the D/A converter, typically called a reconstruction filter, to smooth or reconstruct the signal. This filter is typically the same as the anti-aliasing filter, although there is no requirement that the two filters be the same. The output of the reconstruction filter is an analog signal, c, that is applied to power electronics that will in turn drive a speaker or other actuator. The plant, P, accounts for all of the dynamics relating the controller output to the control signal, which cancels the disturbance d. In designing the control filter there may be significant delays associated with the anti-aliasing filter, the reconstruction filter, and the D/A converter, which need to be included in designing and evaluating the control filter. The delays associated with the A/D converter are usually small and can, in most cases, be neglected. The delays associated with the D/A converter, on the other hand, are on the order of half a sample period and usually need to be included in the design and evaluation process. To carry out the analysis, the anti-aliasing filter, reconstruction filter, and sample-and-hold delay (D/A converter) are usually lumped in with the plant transfer function. The D/A converter is typically modeled by a simple delay of one-half of the sample period. The total plant then becomes

$$U^2(\omega)P(\omega)e^{-j\omega\Delta T/2} \tag{18.38}$$

where ΔT is the sample period and $U^2(\omega)$ is the product of the frequency response functions of the anti-aliasing and reconstruction filters. To illustrate the impact on the design process and on the resulting performance, we will select an anti-aliasing filter and go through the design process once again using the same plant and disturbance-to-residual transfer function as used in Section 18.4 and given by Eqs. (18.32) and (18.33). As will be discussed in Section 18.6 under Hardware Selection, there is a wide variety of low-pass filter types that are commonly used for anti-aliasing and reconstruction, such as Butterworth, Bessel, and elliptical (Cauer), to name just a few. In this example we will use the third-order elliptical filter whose frequency response function is shown in Fig. 18.43. The filter has a cutoff frequency of 70 Hz, slightly below the Nyquist frequency, and the ratio of passband to stop-band amplitude is nominally 50 dB.

Using the direct-estimation procedure outlined in Section 18.4 under Optimal Control Filter Estimation, we obtain the causal control filter whose frequency response is shown in Fig. 18.44. Also shown in the figure is the noncausal control filter given by $B(\omega)\{U^2(\omega)P(\omega)\}^{-1}e^{j\omega\Delta T/2}$. The frequency response functions of the two filters are clearly quite different, but the difference is more clearly seen in Figs. 18.45*a* and *b*, where the impulse response function of the noncausal control filter and the filter coefficients of the causal control filter, respectively, are compared. The noncausal filter IRF shows a strong increase at the end of the time interval, which, as explained earlier, indicates that the filter responds before

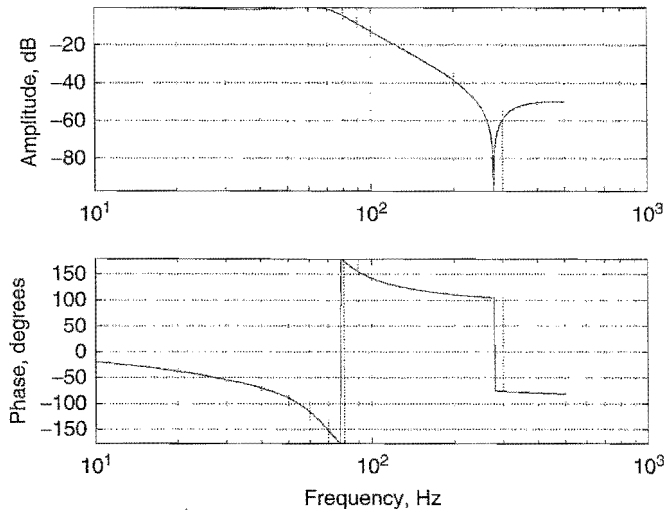


FIGURE 18.43 Frequency response function for a third-order elliptical filter with a cutoff frequency of 70 Hz and a passband–stop band ratio of 50 dB.

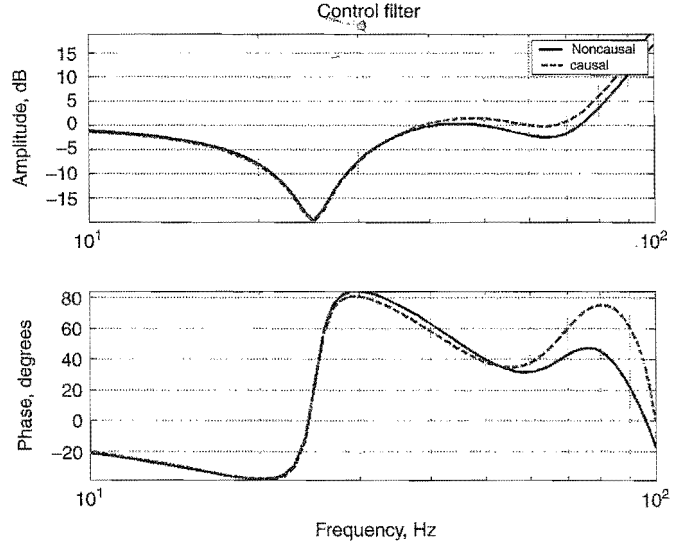


FIGURE 18.44 Comparison of the causal and noncausal control filter frequency response functions.

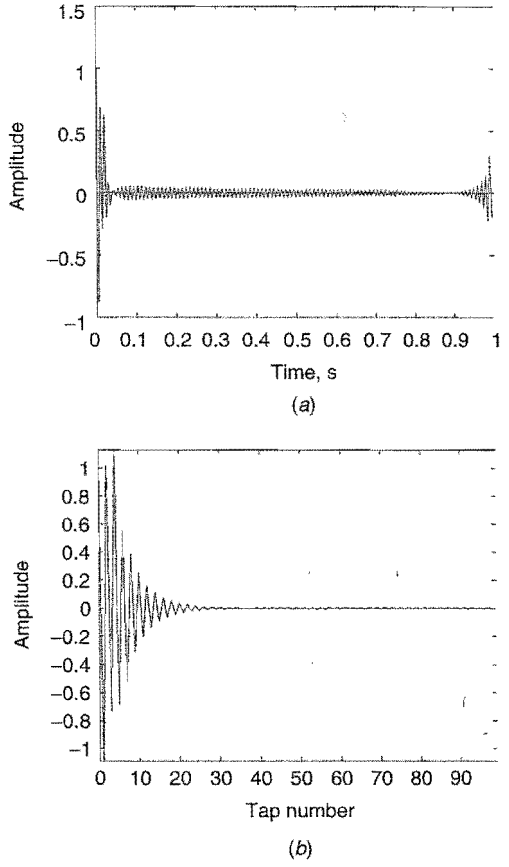


FIGURE 18.45 Comparison of (*a*) the noncausal control filter impulse response function and (*b*) the filter coefficients of the causal control filter.

it receives an input signal and is clearly noncausal. The filter coefficients of the causal filter, on the other hand, decay away to zero. The performance of the active control system is shown in Fig. 18.46. The figure shows the ratio of the controlled disturbance spectrum to the uncontrolled spectrum. The performance has clearly been degraded, especially in the vicinity of the Nyquist frequency. Nevertheless, the out-of-band amplification clearly visible in Fig. 18.41 has been completely removed through the use of the anti-aliasing and reconstruction filters.

System Identification

The control algorithms discussed in the previous sections require internal models of the transfer functions between the outputs of the controller (i.e., the signals sent

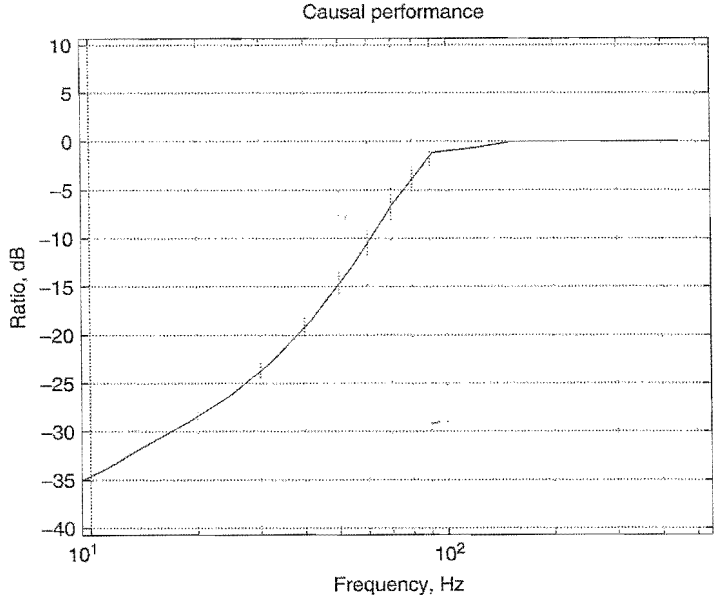


FIGURE 18.46 Ratio of controlled to uncontrolled disturbance with anti-aliasing filters, reconstruction filters, and D/A converter delays.

to the D/A converters) and the inputs to the controller from the residual sensors (i.e., outputs from the A/D converters). These transfer functions are commonly referred to as *plant* transfer functions. The procedure used to measure these transfer functions (or equivalently impulse response functions) is referred to as *system identification*. In this section, we discussed system identification approaches that apply to feedforward controllers.

Since most control algorithms require plant models for the control algorithms to converge to (or solve directly for) the optimal control filters,[58] system identification must be performed prior to any adjustments to the control filters. As such, when system identification is performed with control filters set to zero (i.e., all coefficients are equal to zero), it is referred to as "*open-loop*" system identification. It derives this name because the system identification algorithms are run when the control loop is open (i.e., no signals are allowed to pass through the control filters). The plant estimates obtained during open-loop system identification are used to initialize the plant models within the controller to support the control algorithms that subsequently adjust the control filter coefficients.

For systems where the plant transfer functions are expected to be time invariant (i.e., they do not change characteristics as a function of time), the plant estimates obtained during open-loop system identification can be held constant as the control filter coefficients are adjusted. It is more common, however, to expect that these transfer functions will change over time. These changes may

occur because of changes in environmental conditions (e.g., temperature, pressure), changes in the operating conditions of the system to be controlled (e.g., speed, load), or the presence of external factors (e.g., number and movement of passengers in an automobile).

There are two basic approaches to account for time-varying transfer functions that may be encountered in ANVC systems: the use of robust control algorithms and periodic system identification. Control algorithms are often formulated to allow for certain levels of uncertainty associated with the internal plant models. For example, the magnitude and phase response of the plant at a given frequency may only be known to within, say, ±2 dB in magnitude and ±10° in phase. In effect, these algorithms recognize that the internal plant model is "close" to the actual plant transfer function but not exact. Control algorithms that are stable and provide performance in the presence of this plant uncertainty are called "robust." For example, the filtered-x LMS algorithm is robust to errors in the plant model of up to 90°.[68] The second approach to account for time-varying transfer functions is to perform system identification at the same time that control filter coefficients are being adjusted. This approach provides *periodically updated* plant models to the control algorithms that track changes in the plant over time. System identification performed in this manner is referred to as *closed-loop* or *concurrent* since it occurs while the control loop is closed.

In practice, a combination of both approaches is often required to account for time-varying plants while at the same time maximizing achievable system performance. Control algorithms that rely on exact models of the plants to be controlled can offer maximum performance but are also very sensitive to slight changes in the plant transfer function. As such, small changes in the plant can lead to instability, and for this reason such systems are rarely used in practice. On the other hand, algorithms that make do with very inaccurate plant models will often provide very little performance. As such, there is a trade-off between control system robustness and performance. These trade-offs ultimately influence the approach chosen for system identification.

We now discuss procedures for open- and closed-loop system identification that are applicable to feedforward control systems. Consider first the feedforward system of Fig. 18.47. For this system, the plant, P, is the transfer function between the output of the control filter, y, and the response of the residual sensor, e. Though not shown explicitly, the plant transfer function P is assumed to include the following: D/A sample and hold, smoothing filters, transfer function through the structure to be controlled, anti-alias filters, and A/D converters. An open-loop estimate of P can be performed by setting the coefficients of the control filter, W, to zero and injecting a band-limited probe signal v into the output of the control filter. The probe signal is therefore a digital signal that adds to the output of the control filter y to produce a net signal c at the output of the controller.

The bandwidth of the probe signal is chosen to span the frequency range over which control performance is desired. For a tonal control problem, where the tone is nominally fixed in frequency, the probe signal may span only a few hertz.

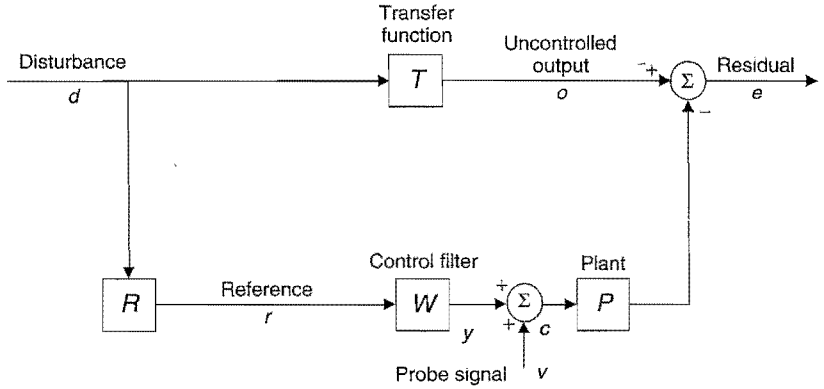


FIGURE 18.47 Probe signal injection for system identification in a feedforward system with no coupling between actuators and reference.

For broadband control, the probe signal bandwidth is often chosen to extend marginally beyond the control bandwidth to ensure an accurate plant estimate throughout the bandwidth for control.

The transfer function between the probe, v, and the residual, e, can be estimated in the frequency domain using the expression

$$\hat{P} = -S_{ve}S_{vv}^{-1} \tag{18.39}$$

where $\hat{P}$ = estimate of plant transfer function P
S_{ve} = cross-spectrum between probe and residual
S_{vv} = autospectrum of probe

This expression will provide an unbiased estimate of the plant transfer function for $W = 0$ (i.e., open-loop system identification) as well as for $W \neq 0$ (i.e., closed-loop system identification) provided the probe signal is uncorrelated with the disturbance and sufficient averaging time is allowed to obtain good estimates of S_{ve}.

An estimate of the plant transfer function in Fig. 18.47 can be made in the frequency domain using Fourier transforms of the probe and residual signals as outlined above. Alternatively, an estimate of the plant *impulse response* can be obtained using the optimal or adaptive FIR filter design procedures discussed in Section 18.3.

An example of system identification using the LMS algorithm integrated into a filtered-x control algorithm is depicted in Fig. 18.48. The filtered-x algorithm adapts the coefficients of the control filter W using the filtered reference signal and a modified residual signal (see later) as inputs. A separate LMS algorithm is used to identify the plant impulse response as shown in the lower portion of the figure. A probe signal v is injected into the control loop and sums with

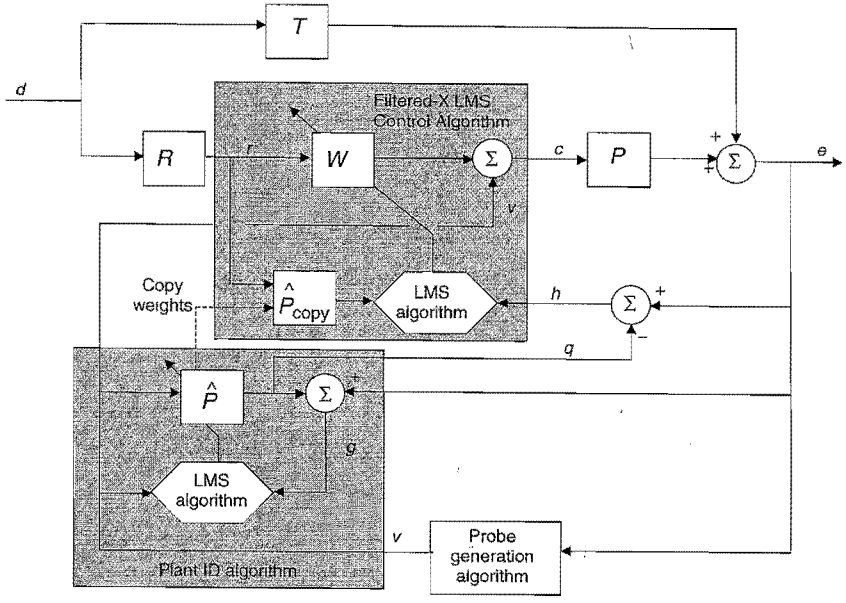


FIGURE 18.48 System identification using the LMS algorithm, embedded within filtered-x LMS controller.

the output of the control filter. The probe signal is also filtered by the adaptive FIR filter that is labeled $\hat{P}$. Finally, the probe signal is an input signal to the LMS algorithm that adapts the coefficients of $\hat{P}$. The output of $\hat{P}$ is summed with the residual signal e to form the error signal g, which is the second input to the LMS algorithm adapting the coefficients of $\hat{P}$. The coefficients of $\hat{P}$ are adapted to minimize the contribution in g that is correlated with the probe, v, in a least-squares sense. An optimal estimate of $\hat{P}$ is achieved when the LMS error signal g becomes uncorrelated with the probe, v. The coefficients of $\hat{P}$ are copied periodically into the filter, $\hat{P}_{\text{copy}}$, which filters the reference signal r, as required by the filtered-x LMS control algorithm.

Following the development of Section 18.3 under Adaptive Digital Filter Design, the update equation for the plant estimate is

$$\hat{\mathbf{p}}(n+1) = \hat{\mathbf{p}}(n) + 2\mu\mathbf{v}(n)g(n) \tag{18.40}$$

where

$$\hat{\mathbf{p}}^{\mathrm{T}} = [\hat{p}(0), \hat{p}(1), \hat{p}(2), \ldots, \hat{p}(I-1)] \tag{18.41}$$
$$\mathbf{v}^{\mathrm{T}}(n) = [v(n), v(n-1), \ldots, v(n-I+1)]$$

We note here that the convergence behavior of the LMS algorithm of Eq. (18.40) is improved if the portion of the residual signal correlated with the reference is removed before being used as input for the plant estimate. This can be achieved by including a third LMS algorithm with the reference and residual signals as inputs, and the modified residual signal as output. The update equation is similar to that in Eq. (18.40). Though not shown explicitly in Fig. 18.84 to preserve clarity, this approach was used for the adaptive feedforward control example presented near the end of this chapter (MIMO Feedforward Active Locomotive Exhaust Noise Control System with Passive Component) and is illustrated there in Fig. 18.93.

A consequence of being able to periodically update the model of the plant using the system identification procedure outlined in Fig. 18.48 is that the injected probe signal will increase the residual signal e. For purposes of system identification, it is desirable to used high-level probe signals because the probe signal will dominate the response at the residual sensor, and consequently accurate plant estimates can be obtained in a shorter length of time. During open-loop identification of ANVC systems, it is often acceptable to use high levels of probe signals. During closed-loop operation, however, the use of high-level probe signals is not acceptable since performance gains achieved as a result of the control filter will be overwhelmed by the presence of the probe signals reaching the residual. As a consequence, low-level (i.e., *covert*) probe signals are required during closed-loop operation.* The drawback to using low-level probes is that the plant estimate will adapt slowly and will not be able to track changes in the plant that occur over relatively short time frames. When this is the case, the control algorithms must be adjusted to deal with larger levels of uncertainty in the plant models or alternative strategies involving gain scheduling[69] must be considered.

For systems where the time constants of plant changes are *large* relative to the adaptation time of the LMS algorithm when using low-level probes, the system identification approach of Fig. 18.48 has been used effectively. For these cases, the probe signals can be generated using low-level band-limited "white" noise. However, fixed-level, white-noise probe signals are not necessarily the best choice. In particular, drawbacks of using white-noise probes include the following:

- The magnitude of the probe signal is held constant. Therefore, as the magnitude of the disturbance increases, the effective convergence rate for the plant filter will decrease. Alternatively, as the disturbance decreases relative to the probe, the convergence rate will increase at the expense of increasing the level of the closed-loop residual signals.
- The spectral shape of the probe signal is independent of the spectral shape of the residual signal and plant transfer function. Consequently, the quality (e.g., estimation errors) of the plant estimate will vary as a function of frequency. This can lead to temporary losses in system performance for control of slewing tonals and nonuniform control of broadband noise.

*Typically the probe signal is sized such that the resulting signal at the residual sensors is nominally 6 dB below the closed-loop signal (absent the probe) in those sensors.

For ANVC applications where white-noise probes may not be appropriate, probe-shaping algorithms can be employed to generate probe signals that provide plant estimates with nominally uniform estimation errors as a function of frequency. Further, these algorithms can account for changes in the disturbance spectrum and plant transfer functions over time.[70–72] Probe generation approaches are depicted collectively by the *probe generation* block in Fig. 18.48.

The final aspect to discuss concerning Fig. 18.48 is possible interaction between the filtered-x LMS algorithm adapting the control filter and the LMS algorithm adapting the plant estimate. In particular, we consider the effects of probe signal injection on convergence of the control filters. Note that the injected probe signal used for system identification contributes to the net residual signal e, which is typically used to adapt the control filter coefficients using the filtered-x LMS algorithm. The contribution from the probe signal is, by design, uncorrelated with the reference signal r. However, its presence in the residual signal will impact the instantaneous residual signal used in the gradient estimate and reduce the convergence speed of the filtered-x algorithm. As a consequence, it is beneficial to remove an estimate of the probe's contribution to the residual signal by subtracting the output of the filter, $\hat{P}$ (labeled q in Fig. 18.48), from the residual, e. This modified residual signal (labeled h in Fig. 18.48) is then used to adapt the control filter coefficients using the filtered-x LMS algorithm.

Up to this point, we have assumed that any coupling from the actuators back to the reference sensors is negligible (i.e., sufficiently small that it can be ignored with respect to system performance and stability). This is not always the case. In general, there exists physical coupling which must be accounted for by both the control algorithm and the system identification algorithms. Control algorithms that account for this path include *feedback neutralization* and Eriksson's *filtered-U* algorithm, both of which were discussed in the previous section. A fully adaptive filtered-U algorithm that includes concurrent system identification is discussed by Eriksson and Allie.[61] In those instances where the physical coupling to the references becomes so strong that electronic cancellation of the coupling may be ineffective, other approaches must be employed to minimize the physical coupling, such as the use of directional reference sensors and selection of alternate sensors.

Figure 18.49 shows the injection of a probe signal in a feedforward system that contains coupling C from the controller output to the reference input and neutralization filter $\tilde{C}$ in the controller to minimize the effects of this feedback path. The procedures for open-loop identification of the coupling transfer function C follows from the discussion above for identifying P, provided the reference signals are used in place of the residual signals. As such, unbiased estimates of the coupling transfer function can be obtained during open-loop operation, provided that the probe signal is uncorrelated with the disturbance. During closed-loop operation, however, transfer functions from the probe signal to the residual and

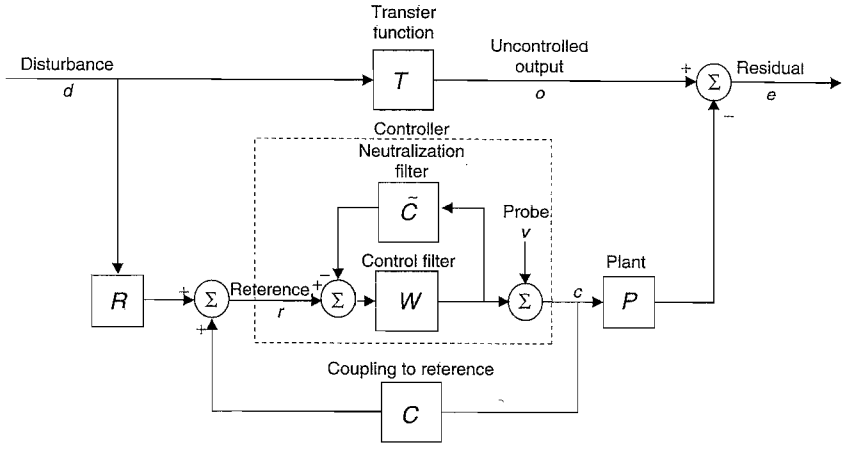


FIGURE 18.49 Probe signal injection in feedforward system with coupling to reference sensor and feedback neutralization filter.

reference sensors no longer provide unbiased estimates of P and C. Instead, these transfer functions include the loop gain associated with the feedback loop comprised of the coupling transfer function, neutralization filter, and control filter.

Following the nomenclature of Fig. 18.49, these transfer functions are given by

$$G_e = \frac{S_{ve}}{S_{vv}} = \frac{-P}{1-(C-\tilde{C})W} \qquad G_r = \frac{S_{vr}}{S_{vv}} = \frac{C}{1-(C-\tilde{C})W} \tag{18.42}$$

These expressions for G_e and G_c contain the desired transfer functions for P and C in the numerator, but both contain the impact of the feedback loop in the denominator. The denominator term can be isolated by estimating the transfer function from the probe signal to the controller output signal c. This transfer function is given by

$$G_c = \frac{S_{vc}}{S_{vv}} = \frac{1}{1-(C-\tilde{C})W} \tag{18.43}$$

Asymptotically unbiased estimates for the plant and coupling transfer functions can then be obtained by combining Eqs. (18.42) and (18.43) such that

$$\hat{P} = \frac{-G_e}{G_c} = P \qquad \tilde{C} = \frac{G_r}{G_c} = C \tag{18.44}$$

This approach for closed-loop identification is known as the joint input–output method.[73] Estimates of P and C can be made in the frequency domain by estimating the cross-spectra in Eqs. (18.42) and (18.43) and taking the ratios as

indicated in Eq. (18.44). Alternatively, multiple-embedded LMS algorithms could be employed to adapt estimates of P and C on a sample-by-sample basis.

Although we have discussed the joint input–output method applied to a feedforward system with feedback to the reference sensors, it is a general approach that is applicable to traditional feedback systems. As such, this method of concurrent system identification can be used to implement fully adaptive feedforward and feedback control systems. Further, the method is valid for use during open- and closed-loop operation. An example of a fully adaptive feedback control system using this approach to system identification when applied to an active machinery mount can be found in Berkman et al.,[74] Curtis et al.,[75] and Berkman and Bender[76] and is included here as an example in Section 18.7 under Active Machinery Isolation.

Extension to MIMO Systems

The equations and examples so far have considered only SISO controllers. In many instances there will be the need to design controllers that can handle multiple inputs and/or multiple outputs. While a complete consideration of the issues involved in the design of MIMO systems is beyond the scope of this chapter, we provide here a brief look at the algorithms for the design of optimum MIMO control filters.

Let us begin by defining a notional MIMO system like that shown in Fig. 18.50, where K reference signals, $\mathbf{r}$, are applied to a control filter which in turn generates M output signals, $\mathbf{u}$, to drive actuators on the system to be controlled. The system has L control sensors to monitor the system performance. Since there are multiple inputs and multiple outputs to each of the blocks in Fig. 18.50, the variables in the blocks $B(\omega)$, $W(\omega)$, and $P(\omega)$ no longer represent scalar transfer functions but must be transfer function matrices. For example, if there are M actuators driving the plant and L control sensors monitoring the system response, the plant transfer function $P(\omega)$ between the sensors and the

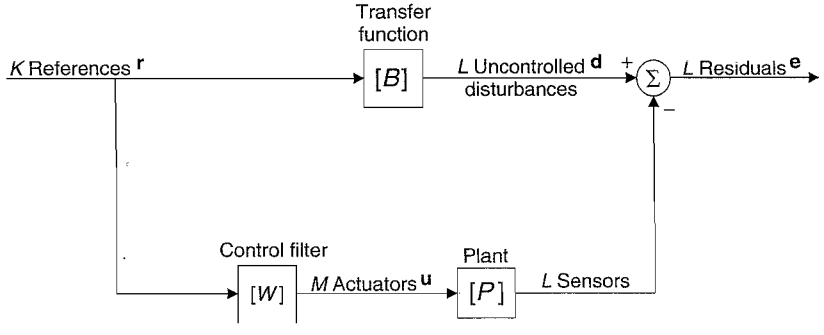


FIGURE 18.50 Notional MIMO control system.

actuators becomes the matrix of transfer functions $[P(\omega)]$:

$$[P(\omega)] = \begin{bmatrix} P_{11}(\omega) & P_{12}(\omega) & \cdots & P_{1M}(\omega) \\ P_{21}(\omega) & & & \vdots \\ \vdots & & \ddots & \\ P_{L1}(\omega) & \cdots & \cdots & P_{LM}(\omega) \end{bmatrix} \tag{18.45}$$

where the $P_{nm}(\omega)$ are each frequency response functions relating sensor output n to actuator input m.

In Eq. (18.24) we defined an optimum SISO control filter for tonal disturbances given by $W(\omega) = P(\omega)^{-1}B(\omega)$. It turns out that the optimal MIMO control filter is given by a very similar expression if the plant is a square transfer function matrix, that is, $L = M$:

$$[W(\omega)] = [P(\omega)]^{-1}[B(\omega)] \tag{18.46}$$

In the equation the square brackets indicate that the variables are transfer function matrices and not scalar transfer functions. For the more general case of a nonsquare plant matrix of K rows and L columns the same expression applies except that the pseudoinverse of the plant matrix is substituted for the normal inverse:

$$[W(\omega)] = [P(\omega)]^{\#}[B(\omega)] \tag{18.47}$$

where the pseudoinverse of the plant, $[P(\omega)]^{\#}$, is given by

$$[P]^{\#} = \begin{cases} \{[P]^H[P]\}^{-1}[P]^H & \text{for } K \leq L \\ [P]^H\{[P][P]^H\}^{-1} & \text{for } K > L \end{cases}$$

where $[\cdot]^H$ means the complex conjugate of the transpose of the matrix. Since for broadband disturbances Eq. (18.47) can result in noncausal control filters, there is a need to apply causality constraints to the MIMO filter design process similar to those applied to the SISO case in Section 18.4 under Optimal Control Filter Estimation. Unfortunately the derivation of the direct-estimation equations for the optimal MIMO control filter is very involved and beyond the scope of this chapter. The interested reader is referred to reference 77.

Fortunately the MIMO filtered-x algorithm is much simpler than the MIMO direct-estimation algorithm, and the equations have been developed by Nelson and Elliott.[16,67] The residual that we are seeking to minimize is given by

$$e_l(n) = d_l(n) - \sum_{m=1}^{M}\sum_{j=0}^{J-1} P_{lmj}u_m(n-j) \tag{18.48}$$

where P_{lmj} is the jth filter coefficient of the plant transfer function relating the ith sensor output to the mth actuator input, M is the number of actuators, J is

the length of the digital representation of the plant transfer functions, and u_m is the mth output of the control filter driven by the K references as indicated in the equation

$$u_m(n) = \sum_{k=1}^{K}\sum_{i=0}^{I-1} w_{mki}r_k(n-i) \tag{18.49}$$

In this equation w_{mki} is the ith coefficient of the control filter relating the mth actuator drive signal to the kth reference, I is the length of each control filter, and r_k is the kth reference signal input to the control filters. The MIMO filtered-x update equation for each control filter coefficient is given by

$$w_{mki}(n+1) = w_{mki}(n) + 2\mu\sum_{l=1}^{L} e_l(n)q_{lmk}(n-i) \tag{18.50}$$

where $w_{mki}(n)$ is the existing estimate of the ith filter coefficient for the control filter connecting reference k to actuator m, $w_{mki}(n+1)$ is the new estimate, and

$$q_{lmk}(n) = \sum_{j=0}^{J-1} P_{lmj}r_k(n-j) \tag{18.51}$$

Equation (18.50) is the MIMO filtered-x control filter update equation for multiple references, multiple sensors, and multiple actuators. It is similar in form (except for the sum over control sensors) to the SISO case, since the coefficients are updated by the product of the residual and the reference filtered by the plant transfer function. Its simple form allows for easy, computationally efficient implementation and, as a consequence, has become a very popular MIMO algorithm for feedforward applications. Furthermore, as we shall see in the next section, it can also be applied to feedback systems.

18.5 FEEDBACK CONTROL SYSTEMS

Basic Architecture

The block diagram of Fig. 18.51 shows the basic architecture of a SISO feedback control system. Such a block diagram might arise from the notional physical system shown in Fig. 18.52. The physical system consists of a second-order oscillator with a control sensor, an accelerometer for example, to monitor the motion of the mass. In addition there is a control actuator which can apply forces to the mass to control its motion. In the block diagram the residual, e, is the output signal from the residual sensor. That output is fed to a control filter,

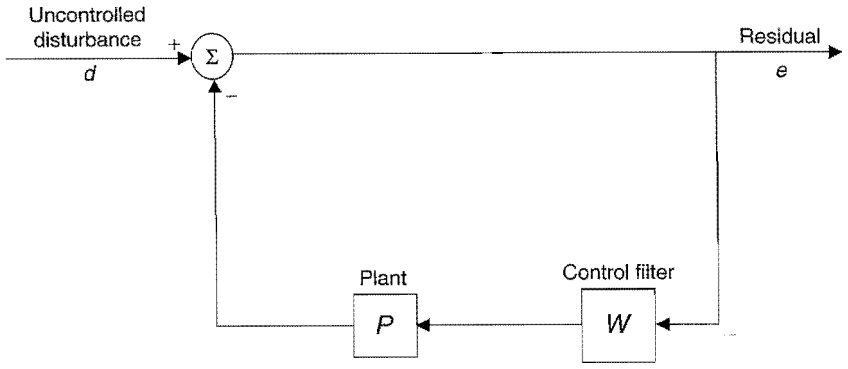


FIGURE 18.51 Basic feedback architecture.

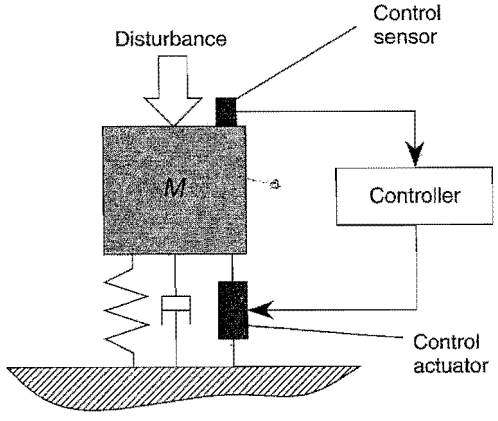


FIGURE 18.52 Notional system with a feedback controller.

which is shown as W in the block diagram. The control filter output drives an actuator that is used to control the motion of the mass.

The plant transfer function P in the block diagram relates the control filter output signal, which drives the actuator to the residual sensor output. In Fig. 18.51 the control filter drives the actuator in such a way as to reduce the input to the control filter. This is in contrast to feedforward systems in which the input to the control filter is a reference signal correlated with the disturbance. In one sense, feedback control systems can be thought of as feedforward systems in which the reference and control (residual) sensors are the same.

The solution for the closed-loop response is given by

$$e(\omega) = \{1 + P(\omega)W(\omega)\}^{-1} d(\omega) \tag{18.52}$$

Clearly the residual will be small if $PW \gg 1$, and in the limit the residual amplitude will become

$$e(\omega) = \{P(\omega)W(\omega)\}^{-1} d(\omega) \tag{18.53}$$

The quantity PW is referred to as the loop gain and the residual amplitude will be inversely proportional to the loop gain. Consequently, good performance from a feedback controller will be achieved if the loop gain is made sufficiently large. In addition, when the loop gain is large, the phase of PW is immaterial to the performance such that if the control filter deviates somewhat from its design goals the performance will suffer only minimally.

The above discussion makes the design of a feedback control filter seem easy. Unfortunately, stability considerations limit our ability to increase the loop gain without limit. Stability issues will be discussed more fully below under Alternate Suboptimum Control Filter Estimation, where the compensator-regulator approach to feedback control filter design is discussed.

Optimal Control Filter Estimation

The literature dealing with the design of optimal feedback controllers is vast and beyond the scope of what can be reasonably included in this chapter. Instead we will focus on two approaches—one optimal and one suboptimal—that each provide tools for the design of SISO or MIMO controllers. The collection of methods often referred to as *modern optimal control theory* will not be dealt with here. Those methods, while providing powerful tools for control filter design when an analytical model of the plant dynamics is available, are not especially well suited to the types of problems where only measured data on the plant dynamics are available. While curve-fitting techniques can be utilized to obtain an analytical model that approximates the measured data, many of those techniques begin to founder if the order of the system model (number of states) becomes too large. For a sampling of the technology in this field the interested reader is referred to references[78–81].

In this section, we focus on what has come to be called the Youla transform or inner model formulation. Through selection of a particular feedback architecture, the Youla transform allows the feedback problem to be transformed into a feedforward problem, making it possible for the feedforward control filter design techniques in Section 18.4 to be used for feedback. In addition, because the system is effectively transformed to a feedforward system, the resulting system is guaranteed to be stable, provided an accurate digital model of the plant has been utilized.

Figure 18.53 shows a simplified block diagram of the Youla transform. In the figure a second feedback loop has been inserted around the control filter. In that second loop a digital filter approximating the plant transfer function has been inserted. The term *inner model* is often used when referring to this approach, precisely because a digital model of the plant is inserted into the control filter.

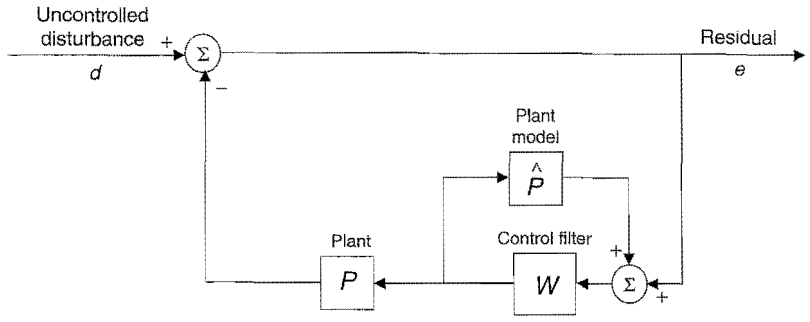


FIGURE 18.53 Youla transform architecture.

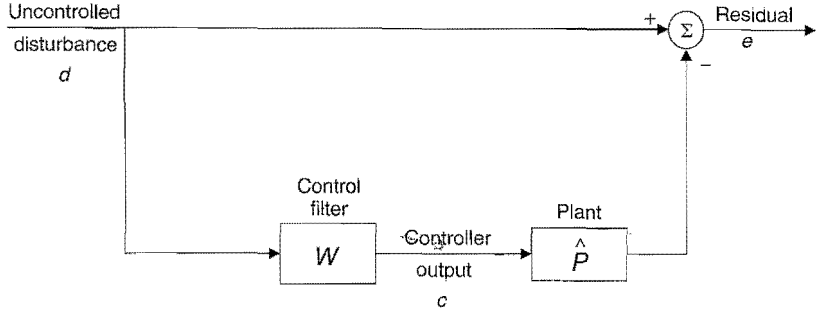


FIGURE 18.54 Feedforward system resulting from the Youla transform.

By making this change in the architecture of the feedback system, we have modified the transfer function from that shown in Eq. (18.52) to the following:

$$e(\omega) = \{1 - \hat{P}(\omega)W(\omega)\}\{1 + (P(\omega) - \hat{P}(\omega))W(\omega)\}^{-1}d(\omega) \tag{18.54}$$

Note that if $\hat{P}$ is a good match to P, then Eq. (18.54) simplifies to

$$e(\omega) = \{1 - \hat{P}(\omega)W(\omega)\}d(\omega) \tag{18.55}$$

Equation (18.55) is the equation for the residual of a feedforward system, the block diagram for which is shown in Fig. 18.54. The resulting block diagram is identical to the feedforward block diagram in Fig. 18.31 if the transfer function $B(\omega)$ is set to unity. Consequently, virtually all of the control filter design equations in Section 18.4 can be applied to a feedback system to which the Youla transform has been applied provided $B(\omega) = 1$. From Eq. (18.24) the noncausal control filter becomes

$$W(\omega) = \hat{P}^{-1}(\omega) \tag{18.56}$$

For the filtered-x algorithm Eqs. (18.35) and (18.36) can be applied to the Youla transform feedback system by simply changing the reference time sequence $r(n)$ in the equations to the disturbance time sequence $d(n)$ in Fig. 18.54:

$$\mathbf{w}(n+1) = \mathbf{w}(n) + \mu e(n)\mathbf{u}(n) \tag{18.57}$$

where $\mathbf{w}(n+1)$ is the new vector of filter coefficients, $\mathbf{w}(n)$ is the old vector,

$$\mathbf{u}(n) = \begin{Bmatrix} u(n) \\ u(n-1) \\ \vdots \\ u(n-N_w+1) \end{Bmatrix} \qquad u(n) = \sum_{m=0}^{N_w-1} \hat{p}(m)d(n-m)$$

and $\hat{p}(m)$ is the mth filter coefficient of the FIR filter representation of the plant frequency response function $\hat{P}(\omega)$.

The equations for determining the optimum feedforward control filter with causality constraints using the direct-estimation approach can be similarly employed by simply interchanging the disturbance d for the reference r. In this case what are affected are the autospectra and cross-spectra in the equations. Modifying Eqs. (18.30) and (18.31), we obtain for a control filter with N taps

$$\begin{Bmatrix} W_0 \\ W_1 \\ \vdots \\ W_{N-1} \end{Bmatrix} = \begin{bmatrix} C_0 & C_{-1} & \dots & C_{1-N} \\ C_1 & C_0 & \dots & C_{2-N} \\ \vdots & \vdots & \ddots & \vdots \\ C_{N-1} & C_{N-2} & \dots & C_0 \end{bmatrix}^{-1} \begin{Bmatrix} A_0 \\ A_1 \\ \vdots \\ A_{N-1} \end{Bmatrix} \tag{18.58}$$

where the coefficients in the matrix equation become

$$A_p = \mathrm{Re}\left\{\int_{\omega_1}^{\omega_2} P S_{dd} e^{-jp\omega\Delta t} d\omega\right\}$$

$$C_{(p-m)} = \mathrm{Re}\left\{\int_{\omega_1}^{\omega_2} \{|P^2| + \alpha^2\} S_{dd} e^{-j(p-m)\omega\Delta t} d\omega\right\} \tag{18.59}$$

where $p, m = 0, 1, \dots N-1$, S_{dd} is the autospectrum of the disturbance, and α^2 is the control effort weighting factor.

For MIMO systems the equations of Section 18.4 under Extension to MIMO Systems can be similarly adjusted for the design of a MIMO controller in the Youla feedback architecture.

The transformation of Eq. (18.54), a feedback system, into Eq. (18.55), a feedforward system, only occurs if $\hat{P} = P$. Consequently, one would expect that the digital representation of the plant transfer function would have to be fairly accurate. If it is not, the term

$$\{1 + (P(\omega) - \hat{P}(\omega))W(\omega)\}^{-1} \tag{18.60}$$

may indeed lead to instability if the error in the plant model is large enough. If we substitute $E(\omega)$ for the difference between the true plant and the digital representation, Eq. (18.60) becomes

$$\{1 + E(\omega)W(\omega)\}^{-1} \tag{18.61}$$

A simple criterion to ensure that the feedback system remains stable is to require for all frequencies where the controller is functioning that

$$|E(\omega)W(\omega)| < 1 \tag{18.62}$$

where $|\cdot|$ means the absolute value. Furthermore, it can be easily shown that $|E(\omega)W(\omega)| = |E(\omega)||W(\omega)|$. Consequently, we can write a simple criterion for the maximum allowable error in the plant model:

$$|E(\omega)| = |\hat{P}(\omega) - P(\omega)| \leq \frac{\beta}{|W(\omega)|} \qquad 0 < \beta < 1 \tag{18.63}$$

where the criterion applies to all frequencies where the control system is functioning and β provides some stability margin. For example, if $\beta = 0.1$, Eq. (18.63) will provide, at least, 20 dB of stability margin. This is a very simple criterion requiring that we know only the amplitude of the control filter as a function of frequency. No phase information is required. However, it is also very conservative, and systems that violate it may not necessarily be unstable. A more precise method for determining stability is to employ the Nyquist criterion, which we will discuss in the next section. Note that a similar criterion can be fashioned for MIMO systems based on the maximum singular values of the matrices $[E(\omega)]$ and $[\hat{P}(\omega)]$. The interested reader is referred to references 80 and 81.

Alternate Suboptimum Control Filter Estimation

Compensator-Regulator Architecture. The compensator-regulator approach to feedback controller design results in a suboptimal system but provides useful insights into functions performed by the controller by breaking the control filter up into a cascade of two filters, as illustrated in Fig. 18.55. The compensation filter is designed to approximate the plant inverse and *compensate* for its amplitude and phase over a range of frequency, which we will refer to as the compensation band. Consequently, if the compensation filter is given by

$$G(\omega) \approx P(\omega)^{-1} \tag{18.64}$$

then we conclude from Eq. (18.52) that the closed-loop residual response $e(\omega)$ is related to the disturbance $d(\omega)$ by

$$\frac{e(\omega)}{d(\omega)} = \frac{1}{1 + H(\omega)} \tag{18.65}$$

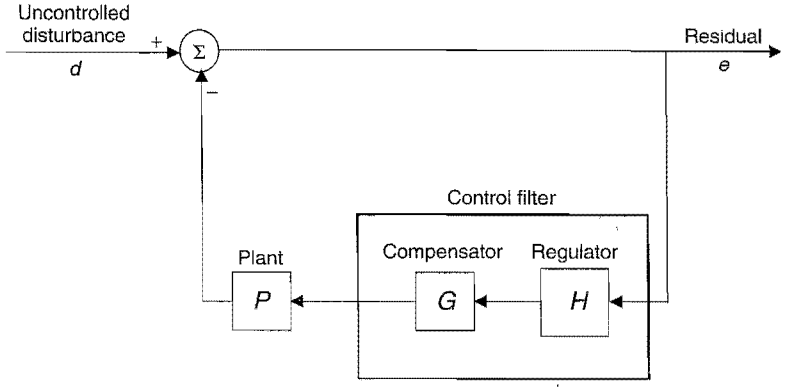


FIGURE 18.55 Compensator-regulator controller architecture.

where $H(\omega)$ is the regulation filter. As this equation shows, to provide reduction in the residual, $|H(\omega)| \gg 1$. When $|H(\omega)| \gg 1$,

$$\frac{e}{d} = \frac{1}{H(\omega)} \ll 1$$

and when $|H(\omega)| \ll 1$,

$$\frac{e}{d} = 1$$

As a result, the design of the regulation filter involves making its magnitude or loop gain large at those frequencies where control is desired (the regulation band) and small where control is not desired. As we shall see in the next section, the trick is to reduce the magnitude and phase of $H(\omega)$ in such a way as to maintain stability and avoid excessive noise amplification outside of the regulation band.

Regulation Filter Design. The range of frequency over which $|H(\omega)| \gg 1$ is referred to as the regulation band. To ensure stability as the magnitude of $H(\omega)$ is reduced outside of the regulation band, the phase of $H(\omega)$ should not exceed 180° until the magnitude is less than 1. This requirement is a consequence of the Nyquist stability criterion.

To employ the Nyquist criterion, one must plot in the phase plane the loop gain, or the change in amplitude and phase as a signal propagates around the feedback loop. In Eq. (18.65) $H(\omega)$ is the loop gain. In the phase plane, the real part of the loop gain is plotted on the horizontal axis and the imaginary part is plotted on the vertical axis such that as the frequency changes, a curve is traced out in two dimensions, as illustrated in Fig. 18.56. In the phase plane, the radius from the origin to a point on the curve represents the magnitude of the loop gain at a particular frequency, and the angle the radius makes with the positive horizontal axis is the phase angle. This is shown in Fig. 18.56 for

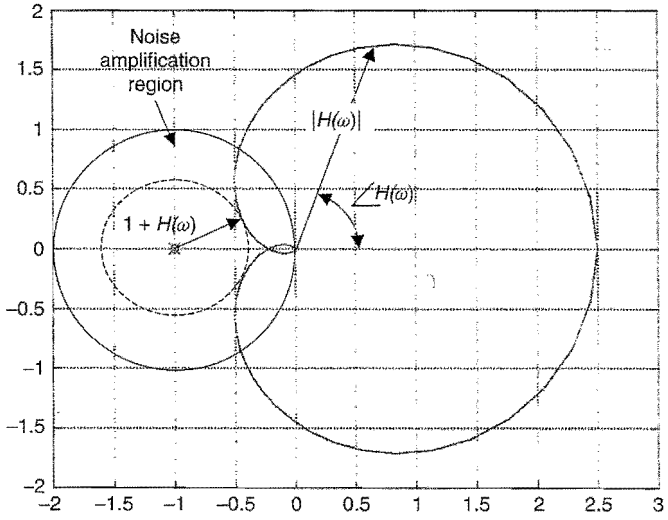


FIGURE 18.56 Stability and noise amplification requirement in the phase plane.

the case where the loop gain is $H(\omega)$. We will not present any proof here of the Nyquist criterion but will simply illustrate its application. For the interested reader, detailed discussions of the Nyquist criterion can be found in a number of texts on control theory.[56,82]

To apply the Nyquist criterion, one simply plots $H(\omega)$ on the phase plane as the frequency ω varies from $-\infty$ *to* ∞ and counts the number of times that -1 is encircled. That number is equal for most cases of interest to the number of unstable poles of $\{1 + H(\omega)\}^{-1}$. Figure 18.56 shows a Nyquist plot of a notional $H(\omega)$ in the phase plane. The amplitude and phase of $H(\omega)$ at a particular frequency are shown in the figure when the phase is less than 180° but the amplitude is greater than 1. As the frequency increases and the phase of $H(\omega)$ approaches 180° in the figure, the amplitude decreases to less than 1, satisfying the criterion. As the figure shows, this ensures that that the curve of $H(\omega)$ will not encircle -1 and that the system is stable.

In the figure, when the phase of $H(\omega)$ is 180°, the amplitude is ~0.2, which gives a modest gain margin of ~14 dB. This means that the amplitude of $H(\omega)$ would have to be 14 dB higher before the feedback control system would go unstable. Similarly, when the amplitude of $H(\omega)$ is unity, the phase is approximately 120°, giving a phase margin of 60°, meaning that the phase would have to increase by approximately 60° before the system would go unstable.

To ensure that there will be no noise amplification as the magnitude of $H(\omega)$ is reduced outside of the regulation band, the curve traced out by $H(\omega)$ in the phase plane should not enter a circle of unit radius centered on -1. This last requirement is also illustrated in Fig. 18.56. There, the trajectory of $H(\omega)$ is seen

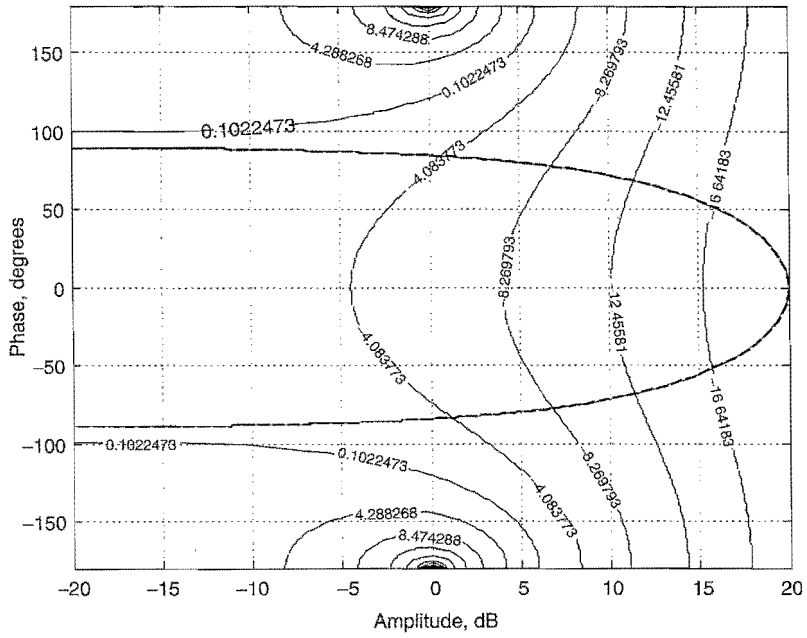


FIGURE 18.57 Nichols plot showing noise amplification in a feedback system as a function of the amplitude and phase of the loop gain.

entering the unit circle, indicating that some degree of noise amplification will occur.

While the loop gain plot in the phase plane can be used to estimate the noise amplification, the so-called Nichols plot provides that information more directly. Figure 18.57 shows a Nichols plot. In the figure, the phase of the loop gain is plotted on the vertical axis and the amplitude is plotted on the horizontal axis. The dashed curve in the figure is the loop gain of a second-order filter.* The contour lines in the plot show the noise amplification. Whenever the dashed curve crosses one of the contour lines, the feedback system with that loop gain will have the noise amplification in decibels indicated by the number on the contour line. For example, Fig. 18.57 shows that the second-order filter with the loop gain given by the dashed curve will never have a noise amplification greater than 0 dB. In fact, a simple examination of the Nyquist and Nichols plots will show that *any*

*The form of the filter is given by

$$H(\omega) = K\left\{\frac{j(\omega/\omega_0)}{(1-(\omega/\omega_0)^2 + j\eta\omega/\omega_0)}\right\}$$

where ω is the frequency and the other terms are constants.

filter whose phase is bounded by ±90°, as the second-order filter is, will always be stable with 0 dB noise amplification when placed in a feedback loop.

All of the above discussion assumes that $P(\omega)$ has been measured accurately and that a good causal representation of $P(\omega)^{-1}$ exists. If, however, the causal representation of $P(\omega)^{-1}$ is imperfect, then the loop gain in the controller will not be just $H(\omega)$ but will be $P(\omega)G(\omega)H(\omega)$. The same criteria for stability and noise amplification apply to this modified loop gain. The consequence is that $H(\omega)$ may need to be designed with larger gain and/or phase margins to maintain stability, and this may result in decreased performance. In addition, the imperfectly compensated system may also have increased noise amplification.

Another consideration is the frequency band over which the compensation filter, $G(\omega)$, must be a good representation of $P(\omega)^{-1}$. In general, the compensation bandwidth must be much greater than the regulation bandwidth to ensure stability and to control noise amplification. To determine the required compensation bandwidth, we first consider noise amplification. The basic approach is to compensate the plant until $H(\omega)$ is small enough so that uncompensated variations in the plant, $P(\omega)$, times the aliased compensation filter, $G(\omega)$, will not lead to noise amplification greater than that specified. If there are measurements of $P(\omega)$ up to frequencies well beyond even the compensation bandwidth, then it is possible to construct the Nyquist plot similar to that shown in Fig. 18.56 for $P(\omega)G(\omega)H(\omega)$ and determine the noise amplification for candidate compensation bandwidths in the same way as illustrated in the figure. Unfortunately, information on the plant is rarely available over such a broad bandwidth, and one must design in robustness by utilizing margins of safety. For example, let us assume that 2 dB of noise amplification is all that is allowed. For this to be true for any phase angle, the amplitude of the regulation filter must satisfy $|H(\omega)| < 0.206$ (−14 dB). If we have a margin of safety of, say, 6 dB to allow for uncompensated plant variations, we must compensate the plant until the regulation filter has declined to −20 dB. If we design the regulation filter to provide 10 dB of performance reduction in the residual, then $H(\omega)$ must have an amplitude of at least 10 dB in the regulation band. Consequently, we will need to compensate the plant out to frequencies beyond the regulation frequency until the amplitude of $H(\omega)$ has decreased by 30 dB from its maximum. Since we must not allow $H(\omega)$ to decrease too rapidly with increasing frequency or instability will result, the resulting compensation bandwidth can easily exceed the regulation bandwidth by a factor of 10–100.

To illustrate these concepts, we will carry out an example for narrow-band control and broadband control, in both cases assuming perfect compensation. For the narrow-band case we choose

$$H(\omega) = K\frac{j\omega/\omega_0}{1-(\omega/\omega_0)^2 + j\eta(\omega/\omega_0)} \tag{18.66}$$

where K and η are constant, $\omega = 2\pi f$, and f is the frequency in hertz. Equation (18.66) is a narrow-band regulation filter with high gain near $\omega = \omega_0$. The frequency response is shown in Fig. 18.58 for $\eta = 0.1$ and $K = 1$. This filter will provide approximately 20 dB of loop gain at the center frequency and

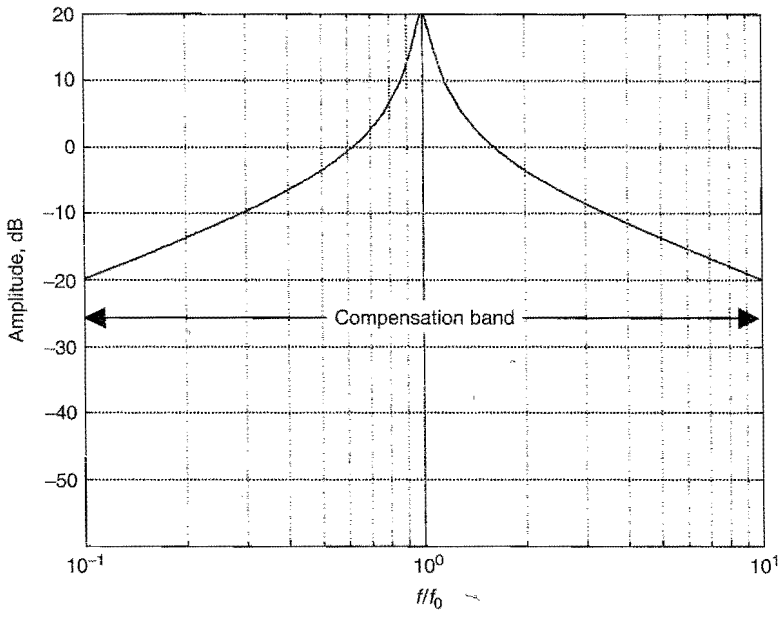


FIGURE 18.58 Narrow-band regulation filter.

consequently we would expect about 20 dB reduction in the residual. In addition, as mentioned above, the phase of the filter is bounded by ±90° and consequently, when placed in the feedback loop, will be stable with 0 dB noise amplification.

Figure 18.59 shows the reduction in the residual with this regulation filter in the feedback loop. The system frequency response looks like a notch filter with approximately 20 dB of noise reduction over a bandwidth of about 5% of the center frequency f_0. It shows no out-of-band noise amplification, as expected.

These estimates have assumed that the compensation for the plant is perfect and that $G(\omega) = P(\omega)^{-1}$ for all frequencies. In reality we need to define a realistic range over which the plant will be measured and the compensation filter will be designed to work. The compensation band should be extended out far enough in frequency such that the regulation filter gain is small enough to ensure that no matter what uncompensated plant phase is introduced, the noise amplification will not exceed a design value (e.g., 2 dB). Earlier we determined that that criterion would be satisfied if $|H(\omega)| < 0.206$ (−14 dB). To allow for possible increases in loop gain as the compensation is gradually turned off, we introduce some margin by reducing this value by an additional factor of 2 (6 dB). Consequently, the plant will be compensated until the regulation filter reduces its amplitude to −20 dB. From Fig. 18.58 we can see that the compensation bandwidth must extend from $\sim 0.1 f_0$ to $\sim 10 f_0$, or 2 decades. This is substantially broader than the control bandwidth.

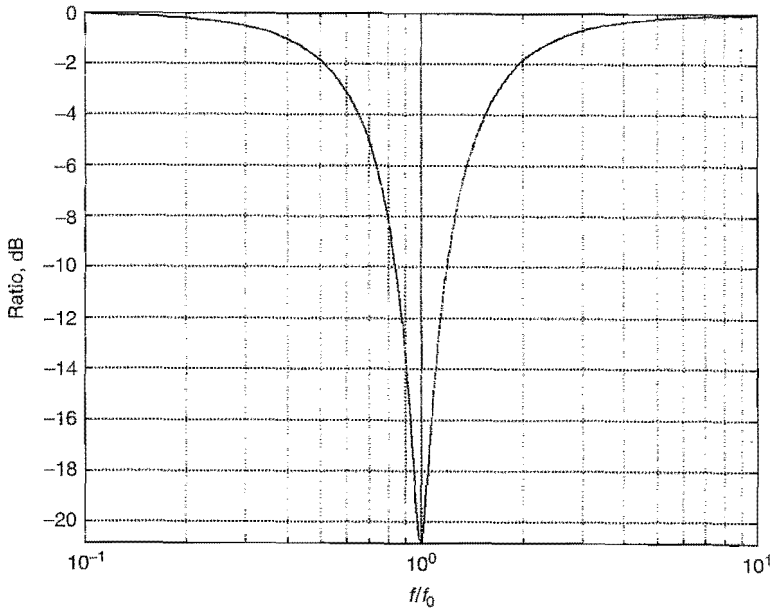


FIGURE 18.59 Ratio of controlled to uncontrolled residual for the narrow-band regulation filter.

Note that the bandwidth and noise reduction in Fig. 18.59 can be adjusted by varying the parameters of the regulation filter. For example, increasing η will increase the bandwidth but decrease the noise reduction performance of the feedback system, essentially broadening the notch and decreasing its depth in Fig. 18.59. Increasing K will increase the noise reduction performance, essentially deepening the notch in the figure but requiring that we compensate the plant out to still higher frequency to control noise amplification.

For broadband control we will use a second-order bandpass filter for the regulation filter given by

$$H(\omega) = Kb\left\{\frac{j(\omega/\omega_0)}{(j\omega/\omega_0 + a)(j\omega/\omega_0 + b)}\right\} \tag{18.67}$$

where ω_0 is the center frequency of the filter.

The frequency response of the filter with $K = 3$, $a = 0.1$, and $b = 10$ is shown in Fig. 18.60. The phase of this filter (not shown) is also bounded by $\pm 90°$ and hence the system would be expected to be stable with no noise amplification, provided the plant is properly compensated. The noise reduction performance of the feedback system employing this regulation filter is shown in Fig. 18.61. The figure shows about 10 dB or more of noise reduction for $0.12f_0 < f < 8f_0$. It

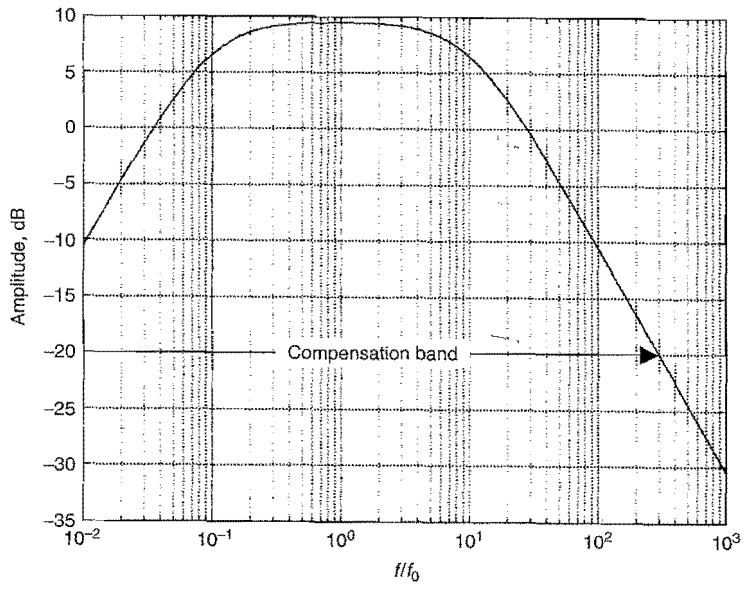


FIGURE 18.60 Frequency response of the broadband second-order regulation filter.

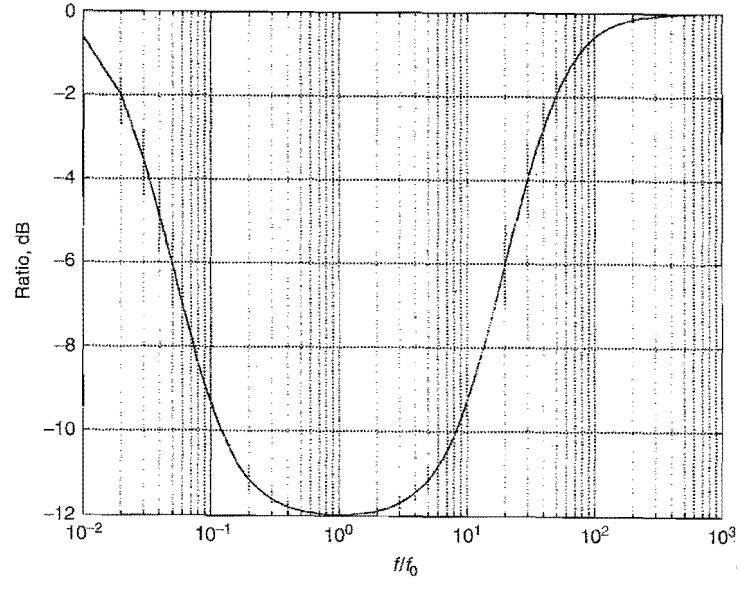


FIGURE 18.61 Ratio of controlled to uncontrolled residual for the broadband regulation filter.

also shows that there is no out-of-band noise amplification above and below the regulation frequency band, as expected.

The above calculations assume that the plant has been perfectly compensated. As for the narrow-band case, the compensation band should be extended out at least far enough in frequency such that the regulation filter gain is small enough to ensure that no matter what the phase, the noise amplification will not exceed 2 dB. Earlier we determined that that criterion would be satisfied if $|H(\omega)| < 0.206$ (−14 dB). Again, to allow for possible increases in loop gain as the compensation is gradually turned off, we introduce some margin by reducing this value by a factor of 2 (6 dB). Consequently, the plant will be compensated until the regulation filter reduces its amplitude to −20 dB. From Fig. 18.60 we can determine that the compensation band must extend out to $300 f_0$, or almost 40 times the highest frequency in the regulation frequency band. Since this is a fairly broad band over which to provide good compensation, it would be interesting to examine what would happen if we used a higher order filter. Since the loop gain associated with a higher order regulation filter would decrease more rapidly with frequency, the compensation band should be narrower. For example, if we simply square the frequency response function of the second-order filter in Eq. (18.67), we would have a fourth-order filter given by

$$H(\omega) = Kb\left\{\frac{j(\omega/\omega_0)}{(j\omega/\omega_0 + a)(j\omega/\omega_0 + b)}\right\}^2 \tag{18.68}$$

The frequency response function of this filter is shown in Fig. 18.62, which indicates that this filter rolls off much more quickly than the second-order filter. The compensation band now extends out to $\sim 50 f_0$ rather than $300 f_0$. There is, however, a penalty for this higher rolloff. That penalty is illustrated in the Nyquist and Nichols plots of Fig. 18.63 and the noise reduction performance plot of Fig. 18.64. The Nyquist plot shows that the system is stable but that the curve formed by $H(\omega)$ enters the noise amplification region. The Nichols plot shows that the expected noise amplification should be about 2.5 dB, which is confirmed in Fig. 18.64. Finally the regulation frequency band over which the noise reduction is 10 dB or more has been reduced slightly due to the more rapid rolloff of this higher order filter. The noise reduction performance and regulation bandwidth issues can be dealt with by changing the parameter values in the filter frequency response function (with concomitant increases in the compensation bandwidth and noise amplification). However, *the noise amplification generated by this higher order filter occurs even with perfect compensation and is the real reason the low-order filter is preferred.*

Compensation Filter. There are a number of approaches that can be applied to designing the compensation filter. Here we will examine the use of feedforward control filter design techniques, as discussed in Section 18.4, to design a control filter that will converge to the inverse of the plant. The notion for this approach is illustrated in the feedforward control architecture of Fig. 18.65. There the plant,

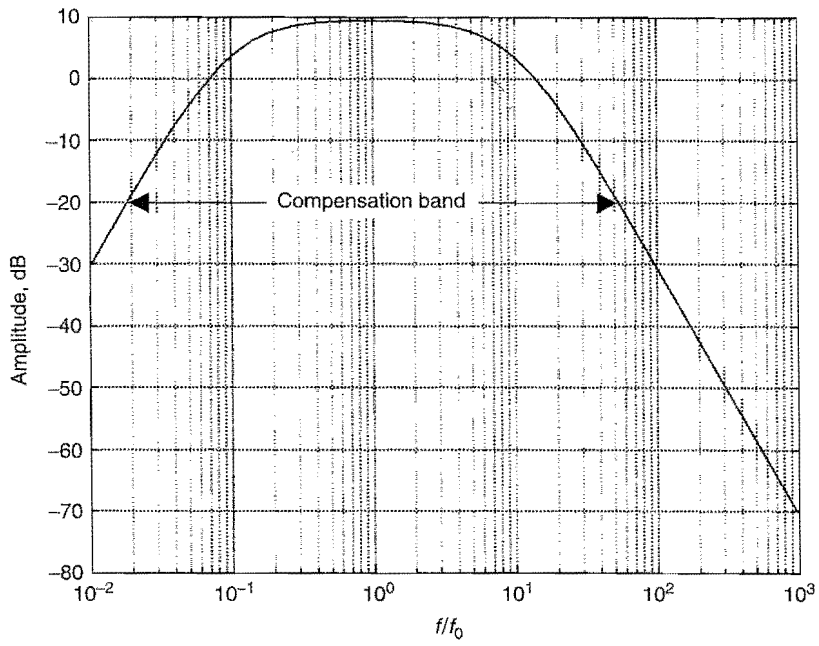


FIGURE 18.62 Frequency response of the broadband fourth-order regulation filter.

$P(\omega)$, and the compensation filter, $G(\omega)$, are connected in series and the disturbance and the residual are the same function, that is, the transfer function $B(\omega)$ in the simplified feedforward architecture of Fig. 18.31 is unity. With this arrangement, the control filter design algorithms will attempt to make $G(\omega)P(\omega) = 1$ or $G(\omega) \approx P(\omega)^{-1}$. Both the direct-estimation and filtered-x design tools can be applied to this problem and the inverses of both MIMO and SISO plants can be determined.

Example. To illustrate this approach, we define the notional position-keeping system for the suspended mass shown in Fig. 18.66. The mass might be machinery that is vibration isolated from the deck of a ship. For frequencies well above ω_0 the suspension system under the mass will reduce the excitation of the deck due to machine vibration from imbalance, for example. Our position-keeping system prevents the machinery from striking the deck when the ship encounters rough seas. In this system the relative displacement between the machine and the deck is measured and used as the input to a controller. The controller in turn generates a control force to minimize that relative deflection so that the machine and the deck do not come into contact. The control force could be generated by an inertial shaker or an interstructural shaker between the deck and the machine.

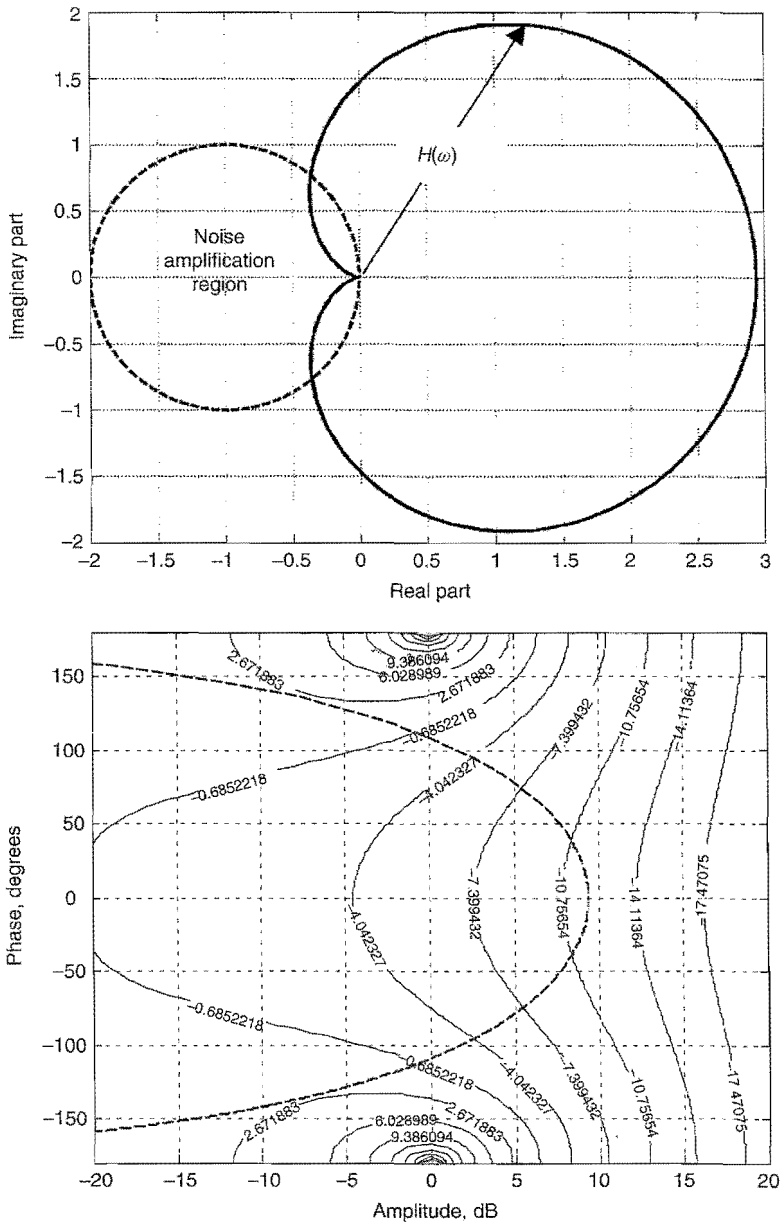


FIGURE 18.63 Nyquist and Nichols plot for the broadband fourth-order regulation filter.

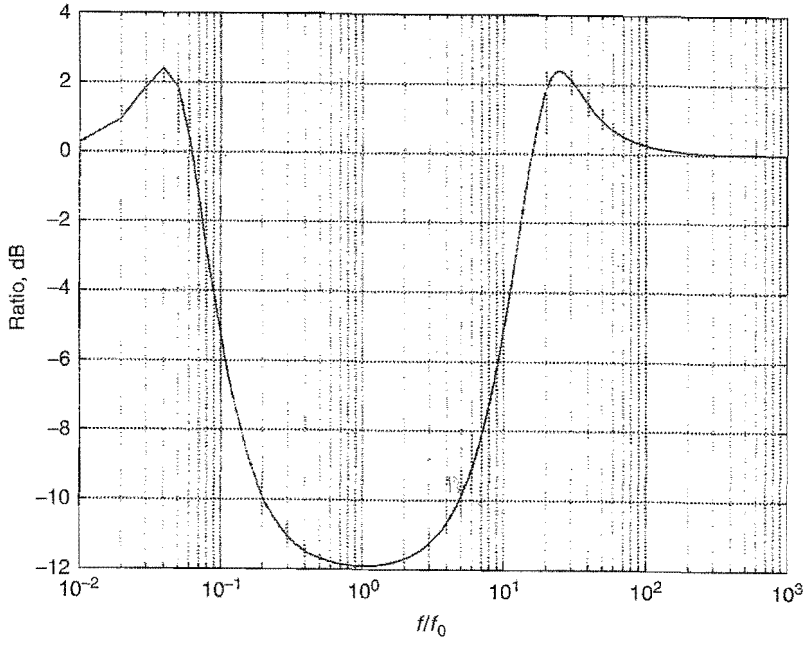


FIGURE 18.64 Ratio of controlled to uncontrolled residual for the broadband fourth-order regulation filter.

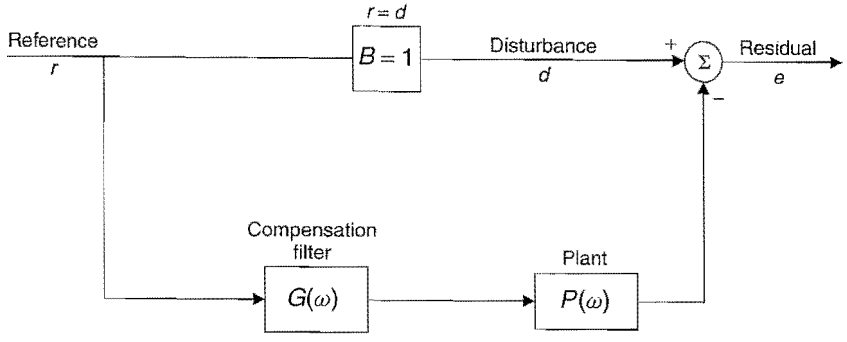


FIGURE 18.65 Feedforward architecture for estimating the plant inverse.

The plant for this system, which is the ratio of the relative deflection between deck and machine to actuator force is given by

$$P(\omega) = \frac{1}{M\omega_0^2\{1 - (\omega/\omega_0)^2 + j(\omega/\omega_0)\eta\}} \tag{18.69}$$

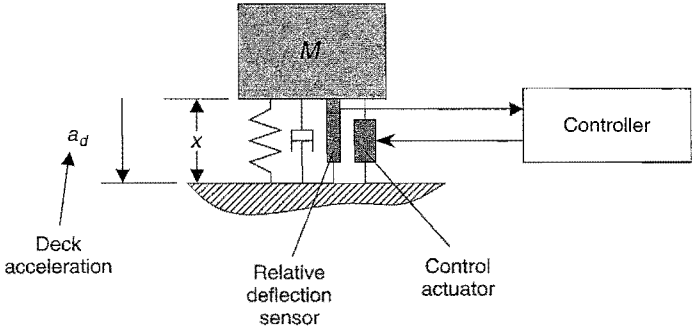


FIGURE 18.66 Notional feedback position-keeping system.

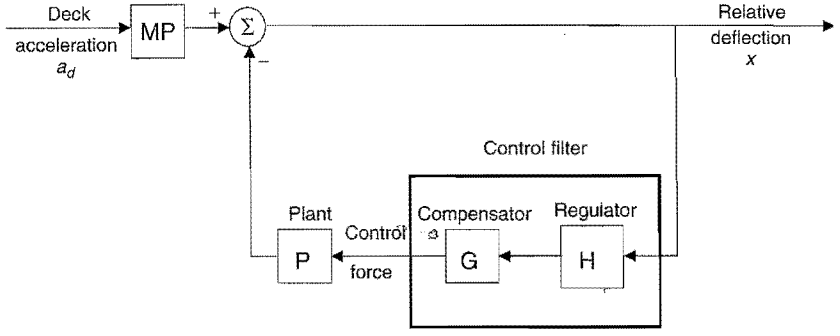


FIGURE 18.67 Block diagram of the notional feedback position-keeping system.

where ω_0 is the natural frequency of the mass on its suspension and η is the loss factor for the system. The feedback control system block diagram for our notional position-keeping system is shown in Fig. 18.67.

The parameter values that we will use are

$$f_o = \frac{\omega_0}{2\pi} = 25 \text{ Hz} \qquad \eta = 0.1$$

For this calculation we will not use any anti-aliasing or reconstruction filters but will rely on the plant itself to provide low-pass filtering. If we were to use any additional low-pass filtering, the frequency response of those filters would simply be included with the plant, since the compensation filter will have to compensate for the amplitude and phase variations of those components as well. In a real system with more complex high-frequency response than our simple notional system we would probably not be able to eliminate anti-aliasing and reconstruction filters, but eliminating them here simplifies the example. Finally, we must account

for the half-sample delay introduced by the sample-and-hold D/A converters. We simply include that delay in the plant frequency response function.

For a regulation filter we will use the second-order broadband filter of Eq. (18.67) with the following parameters:

$$K = 3 \qquad a = 0 \qquad b = 10$$
$$f_o = \frac{\omega_0}{2\pi} = 1$$

These parameters make the regulation filter have the low-pass characteristics illustrated in Fig. 18.68. The filter has a nominal loop gain of ~10 dB out to ~10 Hz.

Based on the results in Fig. 18.60, we know that the compensation band will need to extend out to about 40 times the highest frequency in the regulation band or out to 400 Hz. Since we cannot expect to design a compensation filter that will be effective right out to the Nyquist frequency (one-half the sampling rate), we will put in a margin of safety and use a sampling rate of 1000 Hz, which gives a Nyquist frequency of 500 Hz. Using the direct-estimation filter design technique

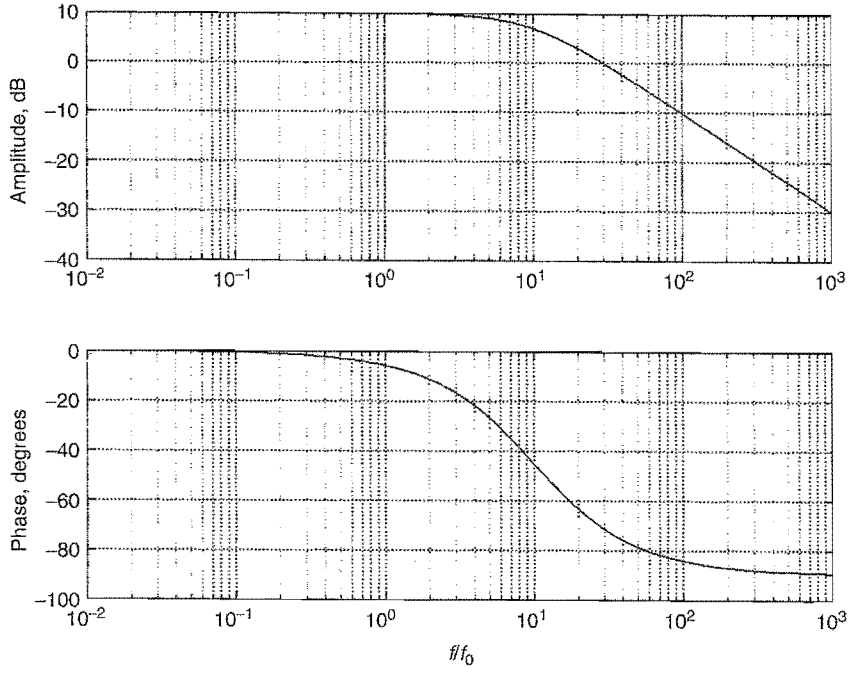


FIGURE 18.68 Amplitude and phase of the regulation filter.

of Section 18.4 for the system in Fig. 18.65, we obtain a 50-tap compensation filter $G(\omega)$ that when multiplied by the plant transfer function gives the result shown in Fig. 18.69. If the filter were a perfect compensator, the amplitude of $G(\omega)P(\omega)$ would be unity and the phase would be zero.

The figure shows that the amplitude is very close to unity almost all the way to the Nyquist frequency.* The phase, however, reaches almost 180° at 300 Hz, which indicates that we should expect some noise amplification due to imperfect compensation. That expectation is confirmed in the Nichols plot of Fig. 18.70 and the noise reduction performance plot of Fig. 18.71, which each slow a little over 2 dB of noise amplification. The Nyquist plot also in Fig. 18.70 shows that the system is stable. The noise reduction performance in Fig. 18.71 shows that 10 dB of noise reduction has been achieved up to more than 10 Hz.

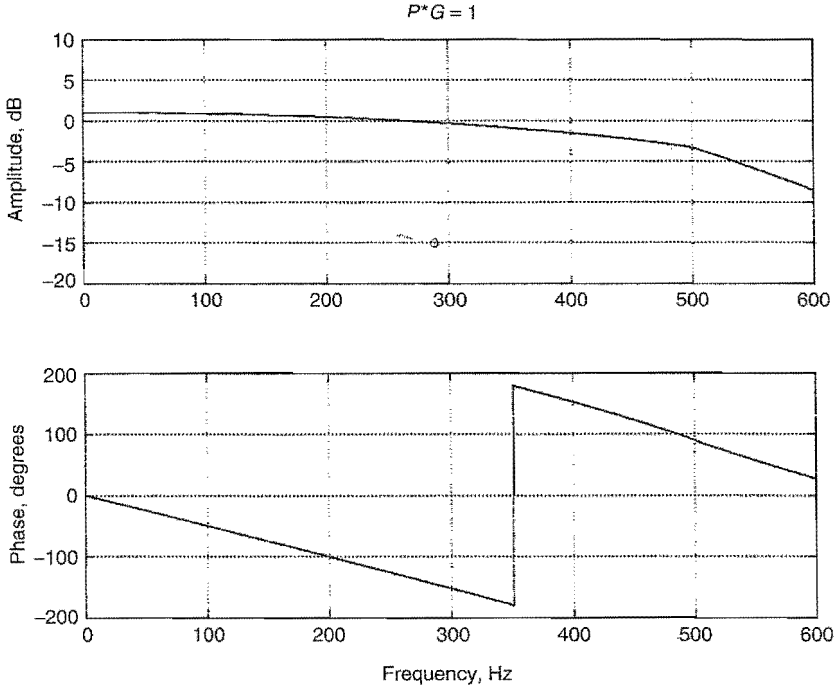


FIGURE 18.69 Amplitude and phase of the product of the compensation filter and the plant transfer function $\{G(\omega)P(\omega)\}$ as a function of frequency.

*Note that in computing the compensation filter using the direct-estimation approach it is sometimes necessary to introduce a small delay in the block diagram of Fig. 18.65 to deal with uncompensatable delays in the plant. Instead of setting $B(\omega) = 1$, we set it to $B(\omega) = e^{-j\omega\lambda T}$, where T is the sample period and λ a constant representing the length of the delay in sample periods. While introducing some phase error in the compensator, this approach often results in a better plant compensator than if no delay were introduced. For the case examined here best results were obtained with $\lambda \sim 1.5$.

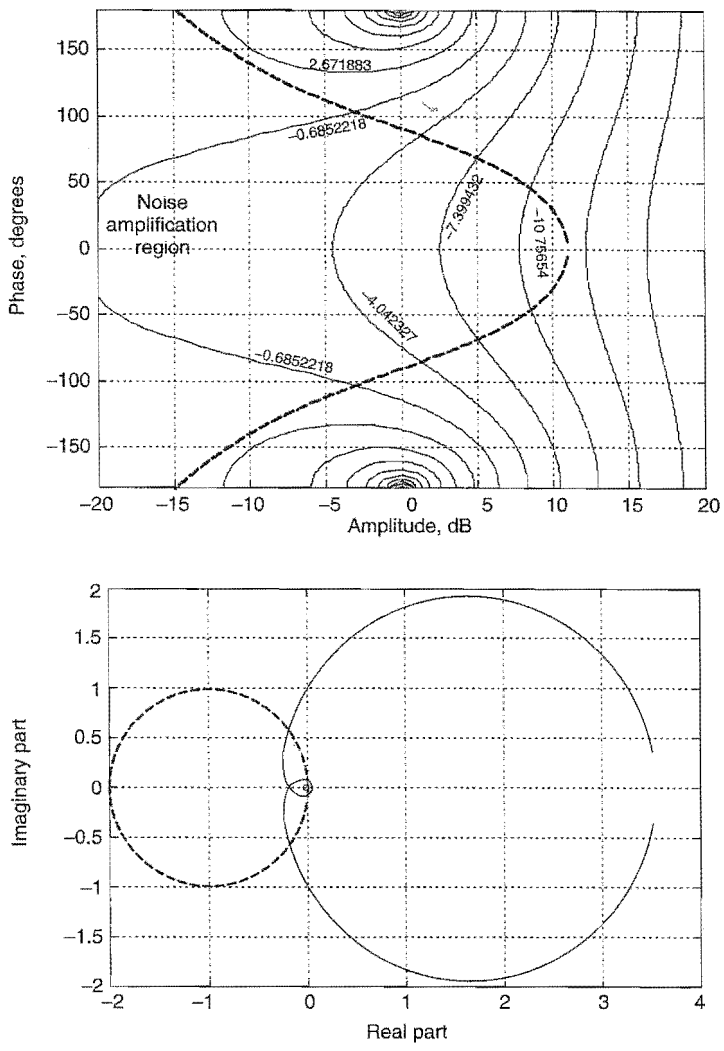


FIGURE 18.70 Nichols and Nyquist plots for the feedback control system of Fig. 18.67.

This example points out how feedback control systems can make severe demands on hardware, typically much more severe than feedforward systems. To achieve 10 dB of noise reduction out to 10 Hz required in this case a sampling rate of 1 kHz, 100 times higher than the regulation bandwidth. *Such a huge factor between regulation bandwidth and compensation bandwidth is not uncommon and is one of the reasons why feedforward systems are often favored over feedback.*

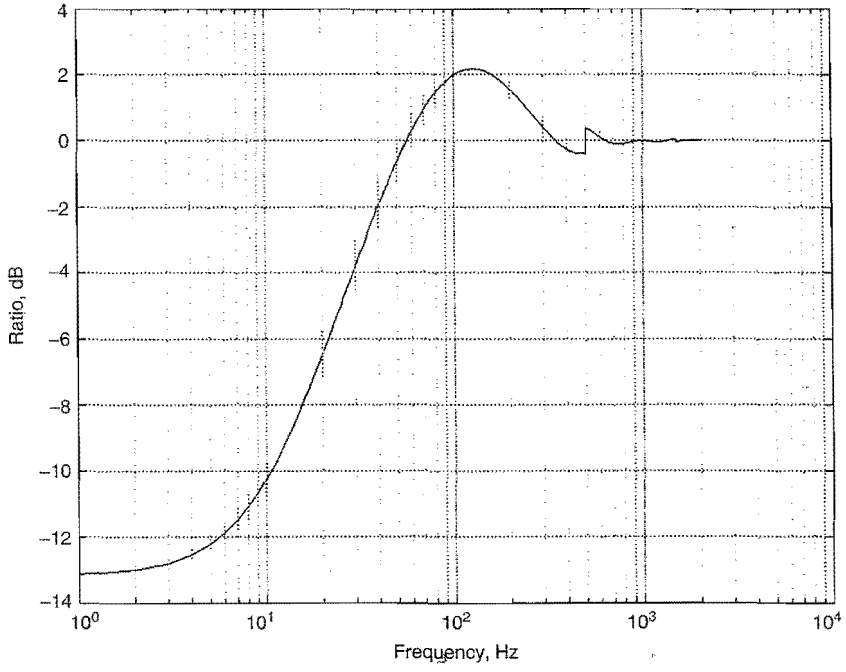


FIGURE 18.71 Ratio of controlled to uncontrolled residual for the feedback control system of Fig. 18.67.

18.6 CONTROL SYSTEM DESIGN CONSIDERATIONS

In this section, we discuss the process and steps involved in designing and implementing a successful ANVC system. This process is illustrated in the flow chart of Fig. 18.72 As shown, the first step is to establish design goals and requirements, which include performance goals and objectives. These goals, together with experimental data or structural–acoustic models, are used to conduct simulations to predict achievable system performance. These performance simulations typically involve trade-off studies of system performance as a function of actuator output levels, sensor dynamic ranges and noise floors, control algorithms, architecture, and controller parameters (e.g., sample rate, analog filter characteristics, digital filter sizes, computational load, and memory requirements). These simulations ultimately guide decisions concerning hardware selection, such as analog filtering, A/D and D/A converters, and digital-controller hardware. The output of this simulation step is a set of design specifications for the sensor and actuator subsystems as well as for the controller (i.e., control algorithm and architecture). Preliminary and detailed designs are then performed to produce sets of component specifications for each subsystem as well as interface control documentation between each subsystem and with the system to be controlled. At this

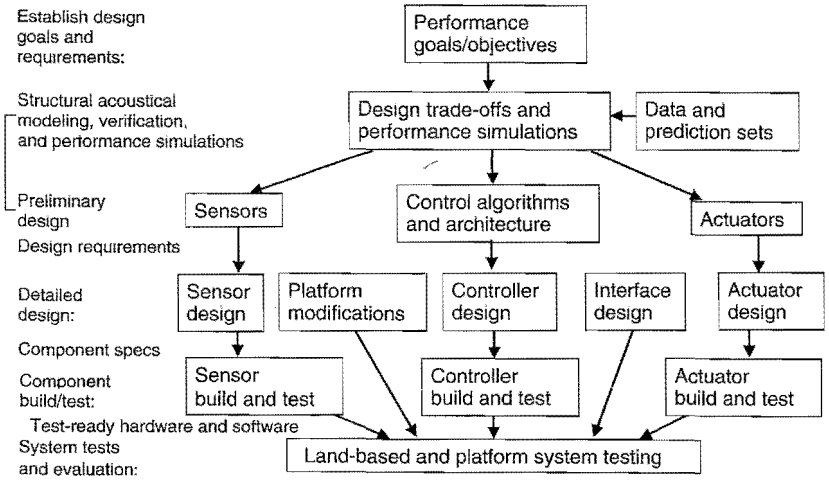


FIGURE 18.72 Flow chart for ANVC system development and implementation.

point, the subsystems are acquired if they are commercially available and fabricated if not. Each is then tested to ensure that both hardware and software meet specifications. The components are then integrated with the system to be controlled. Typically, a series of tests is conducted to validate system performance. If successful, more extensive in-service testing is usually performed to determine long-term performance and reliability before the prototype system is transformed into a commercial product or deployable system. That transformation, which can be an extensive and costly process, is not discussed here.

In the sections that follow, we discuss the major steps in this development process, including identification of performance goals, specification of actuator and sensor requirements, and selection of control architecture. Also discussed in what follows are the benefits of conducting both non causal and causal performance simulations; practical considerations concerning hardware selection of analog filters, D/A and A/D converters, and digital signal processors; and an overview of issues related to control system user interface, operating modes of the system, and system testing guidelines.

Identifying Performance Goals

Identifying performance goals is an important, yet often overlooked, first step in developing an ANVC system. Performance goals state what effect the control system should have on a particular physical quantity as a function of frequency. A schematic that is useful for discussing performance goals is shown in Fig. 18.73. This figure shows two conceptual curves as a function of frequency. The solid curve is representative of the uncontrolled response (e.g., mean-square vibration level on a particular component). The dashed curve is the desired mean-square

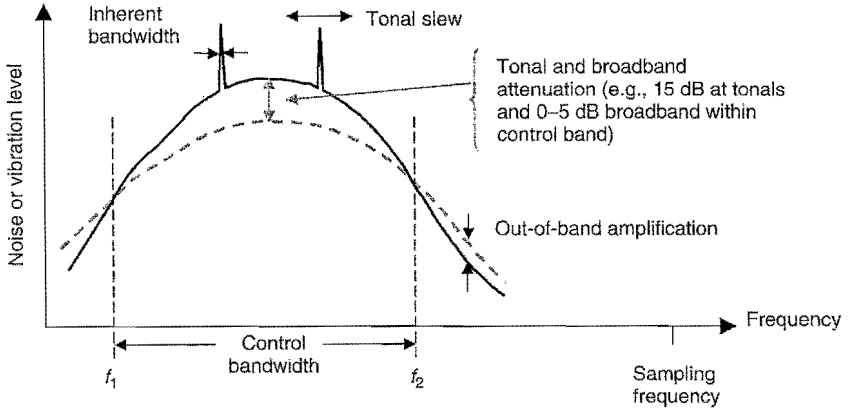


FIGURE 18.73 Schematic of performance goal specification, uncontrolled response (solid line), controlled response (dashed line).

response as a result of implementing an ANVC system. This desired response may be required to meet product specifications or may be related to meeting certain radiated noise specifications. In either case, the difference between these two curves identifies the reductions, as a function of frequency, that are required. As an example, the performance goals for the case illustrated in Fig. 18.73 might include the following:

- Reduce tonal components in mean-square vibration response by at least 15 dB.
- Maintain tonal performance in the presence of slewing tonals (e.g., where the tonal frequency changes over time at a rate of less than 3 Hz/s).
- Reduce broadband mean-square response in the control band (i.e., between frequencies f_1 and f_2) by 0–5 dB.
- Maintain performance in the presence of changes in the dynamics of the system (i.e., plant) that will occur over time.
- Limit out-of-band noise amplification to less than 2 dB at any frequencies outside the control band.

Identifying performance goals is important for several reasons. First, the expectations for the ANVC system are clearly stated and can be evaluated versus practically achievable ANVC performance. For example, typical ANVC systems can provide 15–20 dB of tonal reductions, depending on the slew rate of the tonals. Further, broadband performance in excess of 10 dB is typically associated with some level of out-of-band amplification. Second, these specifications will directly impact implementation aspects of the ANVC system. With regard to the above example, we can make the following initial observations. The broadband performance requirement will require a feedback implementation

or a feedforward implementation with reference sensors that are well correlated with the mean-square response to be controlled. The need to provide additional reductions at slewing tonal frequencies will require control filters that adapt relatively quickly in response to changing tonal frequency. In addition, since the plant transfer functions are expected to change over time, the control system will need to support concurrent system identification and adaptation to track relatively slower changes in the system dynamics. Finally, the constraint on noise amplification will impact the bandwidth of a feedback implementation (as discussed in Section 18.5) and probe signal design (as discussed in Section 18.4 under System Identification).

In general, the performance goals will have a direct impact on *all* aspects of the ANVC system design (e.g., sensors, actuators, and controller). In the next sections, we discuss how the performance goals impact each of these subsystems. In particular, we discuss procedures to answer the following questions:

- What number of actuator channels is required?
- Where should the actuators typically be located?
- What are the output drive requirements (force, volume velocity, etc.) for the actuators?
- What is the number of sensor channels required?
- Where should sensors typically be located?
- What control algorithm/architecture can be used to design control filters that will maximize achievable system performance?
- Is it likely that the program goals can be met (at least throughout the frequency range of the available models) with a reasonable number of actuator and sensor channels and with a causal controller?

These questions will be addressed within the context of the technical approach illustrated in the flow diagram of Fig. 18.74. As shown along the left side, the approach involves three sequential studies:

- Controllability: where to place the actuators.
- Observability: where to place the sensors.
- Realizability: how to design causal control filters.

Number, Location, and Sizing of Actuators

Actuator and sensor placement studies require either a model of the system to be controlled [e.g., finite-element model (FEM), lumped-parameter model] or access to experimental data from the system itself. The first questions to be addressed are where actuators should be located, how many are necessary as a function of achievable performance, and what size of actuator is needed (shaker maximum force output, speaker maximum volume velocity, etc.) to effectively drive the system and provide control.

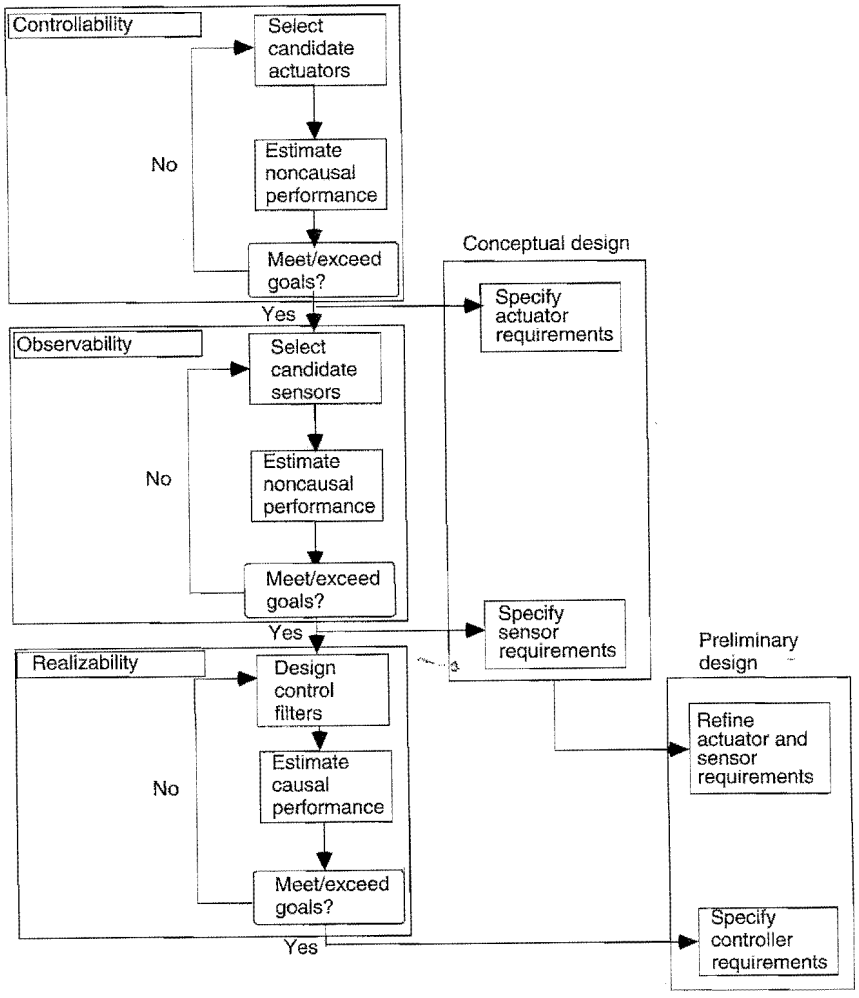


FIGURE 18.74 Flow diagram for ANVC strategy selection.

Number of Actuators. The question of how many actuator channels are required can be roughly estimated from experimental data or model results of the response to be controlled. For example, suppose that the response to be controlled is the mean-square vibration response on a component that is characterized by L point response measurements. The minimum number of actuator channels is equal to the number of independent ways the system is responding at the L measurement locations (referred to as *response dimensionality*) on a frequency-by-frequency basis. The response dimensionality can be estimated by computing the singular-valued decomposition (SVD) of the cross-spectral density (CSD) matrix of the L responses. We can express this CSD matrix as

$$[\mathbf{S_{ee}}] = [\mathbf{T}][\mathbf{S_{dd}}][\mathbf{T}]^H \tag{18.70}$$

where $[\mathbf{S_{dd}}]$ = cross-spectral density matrix of disturbance
$[\mathbf{T}]$ = transfer function matrix from source(s) to L response locations
$[\cdot]^H$ = conjugate transpose of matrix

Note that $[\mathbf{S_{ee}}]$ can be evaluated directly by measuring the CSD matrix of a number of sensors at candidate locations. As an alternate approach analytical/numerical models of the system to be controlled can be used to estimate $[\mathbf{T}]$ along with approximations to $[\mathbf{S_{dd}}]^*$ in Eq. (18.70) to estimate $[\mathbf{S_{ee}}]$.

The SVD of a matrix $[\mathbf{A}]$ is defined as

$$\text{svd}\{[\mathbf{A}]\} = [\mathbf{U_A}][\boldsymbol{\lambda}_\mathbf{A}][\mathbf{V_A}]^\mathrm{T} \tag{18.71}$$

where $[\mathbf{U_A}]$ and $[\mathbf{V_A}]$ are unitary matrices containing the left and right singular vectors of $[\mathbf{A}]$ and $[\boldsymbol{\lambda}_\mathbf{A}]$ is a diagonal matrix containing the singular values for $[\mathbf{A}]$ ranked from largest to smallest.[60] A typical plot of the singular values of $[\mathbf{S_{ee}}]$ (i.e., diagonal elements of $[\boldsymbol{\lambda}_\mathbf{e}]$) at a particular frequency will reveal several large (i.e., significant) singular values followed by a transition to a region containing smaller (i.e., less significant) singular values. An example of this type of plot, where the singular values are normalized by the largest, is shown in Fig. 18.75. These types of plots can be conveniently generated using the svd function in MATLAB.

The number of large singular values of $[\mathbf{S_{ee}}]$ at a given frequency indicates the number of significant and independent ways in which the disturbances on the system express themselves at the L measurement locations. At any frequency, the number of significant singular values is equal to the minimum of

- the number of independent disturbances acting on the structure (termed *source dimensionality*),
- the number of structural degrees of freedom (i.e., modes),
- the number of measurement responses (ie, sensors), and
- degrees of freedom of spectral estimates (i.e., number of ensemble averages in estimating the CSD matrix from experimental data).

As such, care must be taken to ensure that the estimated response dimensionality is not limited by using too few sensors, by insufficient averaging if $[\mathbf{S_{ee}}]$ is measured, or by too few sources and sensors if analytical models are used to estimate $[\mathbf{S_{ee}}]$. We note that controlling the response characterized by the L measurement

*For analytical/numerical simulations, where the CSD of the disturbances may be unknown, it is often sufficient to assume a large number of candidate disturbance locations and use a disturbance CSD matrix in Eq. (18.70) equal to the identity matrix at all frequencies of interest. This corresponds to the case where the sources are statistically independent with unit variance at each frequency.

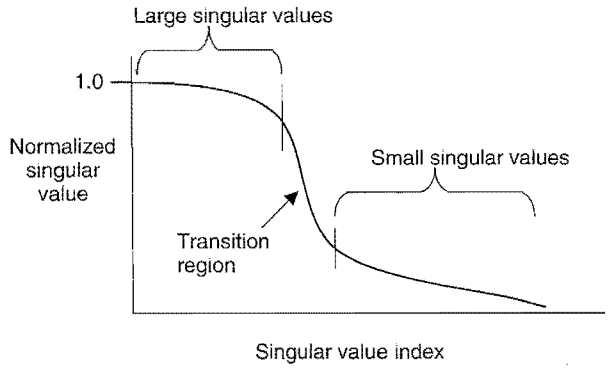


FIGURE 18.75 Typical decay of singular values of a sensor CSD matrix, normalized by the largest singular value.

locations will require at least as many actuator *channels** as significant singular values of $[\mathbf{S}_{ee}]$. Thus, this approach establishes a lower bound on the number of required actuator channels.

Finally, we make two remarks concerning the use of SVD spectra to determine lower bounds on the number of actuator channels. First, since the number of significant singular values will typically increase as a function of frequency (because the number of modes supported by the system increases with frequency), the number of required actuator channels is often dictated by the singular-value spectra at high frequency. Second, the transition region in Fig. 18.75 may be gradual rather than showing a distinct "knee." For those cases, a useful "rule of thumb" is that the number of significant singular values at a given frequency is equal to the number of singular values whose magnitude is within, say, 30 dB of the largest singular value.

Actuator Locations. The selection of specific actuator locations is typically the result of an optimization procedure to select the best K locations from a set of M possible locations ($M > K$). This procedure requires the response CSD discussed above as well as the $L \times M$ transfer function matrix $[\mathbf{P}]$ between the M possible actuator locations and the L sensor responses. An exhaustive search over all combinations to determine the optimal set of K actuator locations would require a search of $\dfrac{M!}{[K!(M-K)!]}$ possibilities. This can be a daunting task for even modest values of K and M. When this is the case, it is often useful to invoke suboptimal techniques to choose a "good" set of actuators.

One suboptimal approach that has been used successfully is based on Gram–Schmidt orthogonalization.[60] Given M candidate actuator locations,

*The term *actuator channels* is not necessarily the same as the number of actuators. For instance, a group of 10 actuators driven coherently requires only a single output channel from a controller.

choose the one that maximizes reductions in the trace of $[\mathbf{S}_{ee}]$. In this context, the best candidate is the column of $[\mathbf{P}]$ that is "most parallel" to the L sensor responses caused by the disturbances, integrated across frequency. Once an actuator (i.e., column of $[\mathbf{P}]$) is chosen, components of $[\mathbf{S}_{ee}]$ and remaining columns of $[\mathbf{P}]$ in the direction of the chosen column of $[\mathbf{P}]$ are removed. The process is repeated K times, where the value of K is estimated from SVD spectra of $[\mathbf{S}_{ee}]$. Variants of this procedure are discussed by LePage et al.[42] and Heck et al.[83] An interesting comparison of alternative procedures for selecting source locations based on using genetic algorithms and simulated annealing is discussed by Elliott.[58]

Regardless of the selection procedure, the mean-square response of the L sensors can be estimated assuming all actuators chosen so far can be used in an optimal, unconstrained sense. That is, we assume a controller can be developed to produce the required magnitude and phase spectra to drive each output channel. At each frequency, the L *vector* of residual responses $\boldsymbol{\varepsilon}$ can be expressed in terms of the L *vector* of uncontrolled responses $\mathbf{e}$ and the k *vector* of actuator drive signals $\mathbf{a}$ (for $k \leq K$) acting though the $L \times k$ plant transfer function matrix $[\mathbf{P}]$:

$$\boldsymbol{\varepsilon} = [\mathbf{T}]\mathbf{d} + [\mathbf{P}]\mathbf{a} = \mathbf{e} + [\mathbf{P}]\mathbf{a} \tag{18.72}$$

The optimal solution for $\mathbf{a}$ to reduce the residual mean-square response $\mathrm{tr}\{[\mathbf{S}_{ee}]\}$ at each frequency is

$$\mathbf{a} = -[\mathbf{P}]^{\#}\mathbf{e} \tag{18.73}$$

where # signifies the pseudoinverse, which can be conveniently computed using the pinv function in MATLAB or by the expression defined in Section 18.4 under Extension to MIMO Systems.

As a consequence, the optimal noise reduction (NR, in decibels) of the mean-square response using the selected actuators is

$$\mathrm{NR} = -10 \log_{10}\left(\frac{\mathrm{tr}\{[\mathbf{S}_{\varepsilon\varepsilon}]\}}{\mathrm{tr}\{[\mathbf{S}_{ee}]\}}\right) \tag{18.74}$$

where

$$[\mathbf{S}_{ee}] = E\{\mathbf{e}\mathbf{e}^{\mathbf{H}}\} = [\mathbf{T}][\mathbf{S}_{dd}][\mathbf{T}]^{\mathbf{H}}$$
$$[\mathbf{S}_{\varepsilon\varepsilon}] = [\mathbf{I} - \mathbf{P}\mathbf{P}^{\#}][\mathbf{S}_{ee}][\mathbf{I} - \mathbf{P}\mathbf{P}^{\#}]^{\mathbf{H}} \tag{18.75}$$

In Eq. (18.75), $[\mathbf{S}_{ee}]$ is the CSD matrix of the *uncontrolled* responses at the L residual sensor locations. This can be estimated from experimental data (i.e., $E\{\mathbf{e}\mathbf{e}^{\mathbf{H}}\}$) or can be computed using transfer functions from source-to-residual locations, $[\mathbf{T}]$, based on analytical models (i.e., lumped-parameter or FEM), and an assumed CSD matrix of the sources, $[\mathbf{S}_{dd}]$, for example, the unit matrix as described above.

Equation (18.74) can be plotted frequency by frequency (or integrated across the frequency bandwidth of concern) to determine an upper bound on system performance, parameterized by the number of assumed actuators, as shown in Fig. 18.76. These performance predictions represent upper bounds because at this point we have not placed any causality constraints on the control filter, and we have not identified what sensor signals will be used as inputs to the controller. As such, these predictions are referred to as noncausal predictions, corresponding to those identified in Fig. (18.74) pertaining to controllability. Since Eq. (18.74) represents an upper bound on achievable performance as a function of frequency for the selected actuator set, it provides a first-order assessment as to whether the identified performance goals are achievable.

Actuator Sizing. A critical issue in the design of an active control system is the sizing of the actuators. Actuators with too little drive capacity will result in an underperforming control system, while actuators with too much capacity may impose excessive weight or cost penalties. A rough guide is that the actuators must be able to create response levels at the residual sensors that are comparable to the levels observed there due to the disturbance. A more precise estimate of the required drive levels from the actuators can be determined from the diagonal elements of $[\mathbf{S_{aa}}]=[\mathbf{P}]^{\#}[\mathbf{S_{ee}}][\mathbf{P}^{\#}]^{\mathbf{H}}$, which correspond to the power spectra of the required drive signals to each actuator. For this calculation $[\mathbf{S_{ee}}]$ should be based on measurements unless good analytical models of the disturbances and their CSD matrix, $[\mathbf{S_{dd}}]$, are available. The square root of the integrated mean-square levels of each diagonal term across frequency provides an estimate of the rms levels for each drive signal. Peak drive requirements can be estimated from these

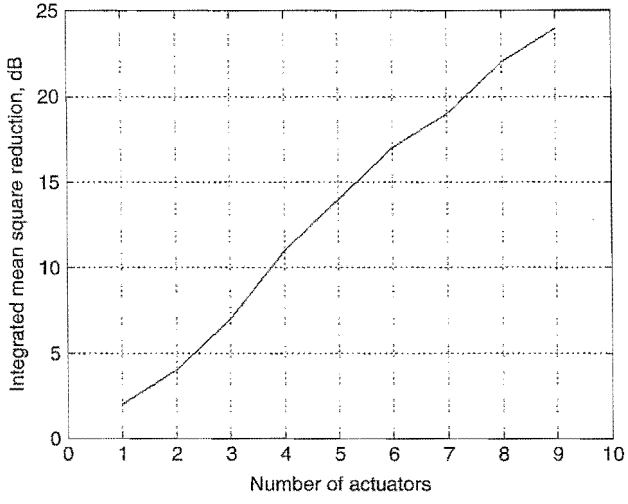


FIGURE 18.76 Example of noncausal performance versus number of actuator channels.

rms levels by applying an appropriate crest factor (i.e., ratio of the peak value of a waveform to its rms value). For pure-tone cases, the crest factor is 1.41; for broadband noise, the crest factor will depend on the statistics of the disturbance. A useful approximation to the crest factor for random noise is 4.

Note that if the plant [**P**] used in the equations above relates actuator output (force, volume velocity, etc.) to the residual channel responses, then the diagonal elements of $[\mathbf{S_{aa}}]$ (and the associated rms and peak levels) correspond to the actual actuator drive level (e.g., pounds, cubic feet per minute) that must be delivered to the structure by the actuators to produce the predicted performance. As such, these predictions provide initial actuator sizing information.

Number and Location of Sensors

The goals and requirements for selecting residual and reference channels are summarized below.

Residual Sensor Channel Selections for Feedforward and Feedback Strategies. The goal is to determine a minimal set of measurable responses that are

- well correlated with the radiated noise or vibration response to be controlled,
- nominally colocated with actuators for feedback control, and
- consistent with satisfying "obvious" causal constraints*: at or "downstream" of actuators for feedforward control strategy.

Reference Sensor Channel Selection (for Only Feedforward Strategy). The goal is to determine a minimal set of measurable responses that are

- well correlated with the disturbance sources,
- well correlated with candidate residual channels,
- consistent with satisfying obvious causal constraints: with sufficient "lead time" to implement an effective causal controller (i.e., located sufficiently "upstream" of the actuators).

Approaches for determining sensor channels that meet these goals and requirements are presented below.

Number of Sensors. If the number of residual sensors is equal to the number of control actuators, it is theoretically possible to achieve infinite noise reduction in a feedforward system. Of course, very large noise reduction at residual

*By obvious causal constraints, we rule out consideration of residual sensors that are closer to the sources than the selected actuator locations (i.e., upstream of the actuator locations). Similarly, we rule out consideration of reference sensor locations that are downstream of (farther away from the sources than) the actuator locations.

sensors does not necessarily mean that the system will also provide good noise reduction globally. Alternatively, if the number of control actuators exceeds the number of residual sensors, the system is overdetermined and the control effort may be excessive with some actuators competing against others unless control effort weighting is carefully included in the control filter design algorithm. Most practical systems have more residual sensors than control actuators so that the noise reduction is less concentrated at the residual sensor locations, resulting in more uniform global control.

The selection of residual and reference sensors (when required or available) can be determined following similar procedures to those outlined for actuator selection. As before, it is advisable to perform SVD analyses of candidate residual and reference CSD matrices to determine the minimum number of channels necessary to characterize the response caused by the disturbances at those locations. Since response dimensionality will never increase as measurement locations move away from the sources, it is common that the response dimensionality at the reference sensor locations will exceed that at the residual sensor locations. We note, however, that the number of sensors necessary to characterize the response dimensionality may exceed the number of sensor channels determined by the dimensionality studies, as, for example, when arrays of sensors are processed to characterize modal responses of a system.

If the response to be controlled is already known, the choice of residual sensing may be relatively straightforward. For example, if the mean-square response of a plate structure on a machine is to be reduced, it may be sufficient to instrument that plate with L point sensors, where L exceeds the response dimensionality of the plate (e.g., number of significant modes). Subsets of these L sensors can also be considered to determine the sets that when minimized in an optimal sense will produce the largest mean-square reductions of the full set of L sensors. Again, either exhaustive or suboptimal search techniques can be used.

For cases where reducing radiated noise is the main objective, it may not be possible to use residual sensor inputs to the controller that directly measure the noise field. Instead, for these cases, residual sensors must be located on the machine or device to be controlled. Selection of these on-board sensors is typically the result of using detailed radiation models to determine which on-board sensor responses are highly correlated with the radiated noise. If models or experimental data that include radiated noise information are available for this purpose, then candidate residual sensors can be selected using the exhaustive or suboptimal search techniques discussed above.

Residual Sensor Evaluation. As was done when considering actuator selection, the resulting sets of residual sensors obtained at each step can be evaluated to assess the maximum achievable performance as a function of the number of residual channels. In particular, reductions in the mean-square response of the selected residual channels can be determined using Eq. (18.74), where the optimal drive vector $\mathbf{a}$ in Eq. (18.73) is chosen to minimize only the candidate set of residual channels. These drives are then used in Eq. (18.72) to estimate the

reductions in mean-square performance across a larger and more complete set of residual channels, or the radiated noise response. Again, these predictions represent upper bounds on achievable noncausal performance assuming fixed sets of actuators and residual sensors. That is, we again assume that a controller can be developed to produce the spectral magnitudes and phases that are necessary to drive each output channel to reduce the mean-square residual response in an optimal sense.

Alternatively, residual sensors can be selected simultaneously with implementing the procedure for estimating performance. A similar approach can be used to select reference sensors for a feedforward system. Details of this approach are discussed below with respect to evaluating reference and residual sensors for the case where residual sensors cannot directly measure radiated noise.

Assuming statistical quantities, we define the following frequency domain relationships between the vectors of radiated pressures (or some other desired residual which cannot be measured directly by the control system) $\mathbf{p}$, residual channels $\mathbf{e}$, and reference channels $\mathbf{r}$ and the vector of disturbances $\mathbf{d}$,

$$\mathbf{p} = [\mathbf{Q}]\mathbf{d} \qquad \mathbf{e} = [\mathbf{T}]\mathbf{d} \qquad \mathbf{r} = [\mathbf{R}]\mathbf{d} \tag{18.76}$$

where $[\mathbf{Q}]$, $[\mathbf{T}]$, and $[\mathbf{R}]$ are the transfer function matrices relating the disturbances to the radiated pressure, residual channels, and reference channels, respectively. For purposes of the discussion below, we assume that either the transfer functions $[\mathbf{Q}]$, $[\mathbf{T}]$, and $[\mathbf{R}]$ are available from analytical models (e.g., lumped-parameter or FEM) or the response vectors $\mathbf{p}$, $\mathbf{e}$, and $\mathbf{r}$ are available from experimental data.

The radiated pressure can be related to the residual channels as

$$\mathbf{p} = [\mathbf{H}_e]\mathbf{e} + \mathbf{n} \tag{18.77}$$

where $\mathbf{n}$ represents the radiated pressure response that is uncorrelated with (or unobserved by) the residual channels. Assuming that $\mathbf{e}$ and $\mathbf{n}$ are independent statistical responses, we can obtain an expression for $[\mathbf{H}_e]$ in terms of the CSD matrix of the uncontrolled residual $[\mathbf{S}_{ee}]$ and the CSD matrix between the pressure and residual channels $[\mathbf{S}_{ep}]$:

$$[\mathbf{H}_e] = [\mathbf{S}_{ep}][\mathbf{S}_{ee}]^{-1} \tag{18.78}$$

As discussed earlier with regards to Eq. (18.75), $[\mathbf{S}_{ee}]$ is the CSD matrix of the *uncontrolled* responses at the L residual sensor locations and can be estimated from experimental data (i.e., $E\{\mathbf{e}\mathbf{e}^{\mathbf{H}}\}$) or can be computed by using transfer functions from source-to-residual locations, $[\mathbf{T}]$, based on analytical models (i.e., lumped-parameter or FEM), and an assumed CSD matrix of the sources, $[\mathbf{S}_{dd}]$. Similarly, $[\mathbf{S}_{ep}]$ is the CSD matrix of the uncontrolled responses of the pressure and residual sensors. It can be estimated from experimental data (i.e., $E\{\mathbf{p}\mathbf{e}^{\mathbf{H}}\}$) or

be computed from analytical models for [T] and [Q] together with an assumed CSD matrix of the sources, $[\mathbf{S}_{dd}]$:

$$[\mathbf{S}_{ep}] = [\mathbf{Q}][\mathbf{S}_{dd}][\mathbf{T}^H] \tag{18.79}$$

We can now write an expression for the maximum noise reduction, at each frequency, that can be achieved by eliminating the response in the radiated pressure that is correlated with the chosen set of residual channels:

$$\mathrm{NR}_p = 10 \log_{10} \left(\frac{\mathrm{tr}\{[\mathbf{S}_{pp}] - [\mathbf{H}_e][\mathbf{S}_{ee}][\mathbf{H}_e^H]\}}{\mathrm{tr}\{[\mathbf{S}_{pp}]\}} \right) \tag{18.80}$$

where

$$[\mathbf{S}_{pp}] = [\mathbf{Q}][\mathbf{S}_{dd}][\mathbf{Q}^H] \qquad [\mathbf{S}_{ee}] = [\mathbf{T}][\mathbf{S}_{dd}][\mathbf{T}^H] \tag{18.81}$$

Note that if there is no correlation between the residual sensors and radiated pressure, then NR_p will equal 0 dB. If the output is entirely due to the input (i.e., the residual sensors are perfectly correlated with the radiated pressure, then NR_p will be infinite (i.e., $-\infty$ decibels).

The evaluation of Eq. (18.80) requires either measured data or analytical/numerical models of the system to be controlled. If *simultaneous* measurements of the residual sensors, **e**, and the desired residual, **p**, are available, then the data can be processed to generate the cross-spectra density matrices $[\mathbf{S}_{ep}]$, $[\mathbf{S}_{ee}]$, and $[\mathbf{S}_{pp}]$. Equation (18.78) can then be used to determine $[\mathbf{H}_e]$, which can then be substituted along with $[\mathbf{S}_{ee}]$ and $[\mathbf{S}_{pp}]$ into Eq. (18.80). If, on the other hand, analytical/numerical models are available, they can be used to estimate the transfer function matrices [Q] and [T]. If the CSD of the disturbance $[\mathbf{S}_{dd}]$ is then taken to be the unit matrix as described earlier, then $[\mathbf{S}_{ep}]$, $[\mathbf{S}_{ee}]$, and $[\mathbf{S}_{pp}]$ can be easily estimated from the equations given above, allowing the evaluation of Eq. (18.80) as if measured data were available.

Reference Sensor Evaluation. In a similar fashion, the procedure outlined above can be used to select reference sensors that are highly correlated with the residual and/or radiated pressure. The residual channels can be related to the reference channels as

$$\mathbf{e} = [\mathbf{H}_r]\mathbf{r} + \mathbf{m} \tag{18.82}$$

where **m** represents the response in the residual channels that is uncorrelated with (or unobserved by) the reference channels. Following the procedure outlined above, the maximum reduction in the mean-square response of the residual channels, **e**, assuming a set of reference sensors **r** is given by

$$\mathrm{NR}_e = 10 \log_{10} \left(\frac{\mathrm{tr}([\mathbf{S}_{ee}] - [\mathbf{H}_r][\mathbf{S}_{rr}][\mathbf{H}_r^H])}{\mathrm{tr}([\mathbf{S}_{ee}])} \right) \tag{18.83}$$

where

$$[\mathbf{S}_{ee}] = [\mathbf{T}][\mathbf{S}_{dd}][\mathbf{T}^H] \qquad [\mathbf{S}_{rr}] = [\mathbf{R}][\mathbf{S}_{dd}][\mathbf{R}^H] \tag{18.84}$$

and

$$[\mathbf{H}_r] = \mathbf{S}_{re}[\mathbf{S}_{rr}]^{-1} \tag{18.85}$$

The expression given in Eq. (18.83) represents the maximum reduction, at each frequency, that can be achieved by eliminating the response in the residual channels that is correlated with the chosen reference channels. If there is no correlation between the residual sensors and radiated pressure, then NR_e will equal 0 dB. If the output is entirely due to the input (i.e., the residual sensors are perfectly correlated with the radiated pressure, then NR_e will be infinite.

As with the residual sensors the evaluation of Eq. (18.83) requires either measured data or analytical/numerical models of the system to be controlled. If simultaneous measurements of the residual sensors, **e**, and the reference sensors, **r**, are available, then the data can be processed to generate the cross-spectra density matrices $[\mathbf{S}_{er}]$, $[\mathbf{S}_{ee}]$, and $[\mathbf{S}_{rr}]$. Equation (18.85) can then be used to determine $[\mathbf{H}_r]$, which can then be substituted along with $[\mathbf{S}_{ee}]$ and $[\mathbf{S}_{rr}]$ into Eq. (18.83). If, on the other hand, analytical/numerical models are available, they can be used to estimate the transfer function matrices [R] and [T]. If the CSD of the disturbance $[\mathbf{S}_{dd}]$ is then taken to be the unit matrix as described earlier, then $[\mathbf{S}_{er}]$, $[\mathbf{S}_{ee}]$, and $[\mathbf{S}_{rr}]$ can be easily estimated from the equations given above, allowing the evaluation of Eq. (18.83) as if measured data were available.

Sensor Selection and Noncausal Performance. Choices for candidate residual and reference sensors are typically guided by an understanding of the physics of energy propagation for the system to be controlled as well as guidance on the required number of channels required based on SVD analyses. Assuming candidate actuator, reference, and residual locations have been identified using the procedures discussed above, an upper bound on achievable performance for this set of transducers can be obtained by estimating the noncausal performance. These predictions correspond to those identified in Fig. 18.74 under the observability phase. For a feedforward system, this means that we assume the controller can implement whatever filter is necessary to relate the reference sensor responses to the required actuator drive signals to minimize the mean-square residual response. For this case, the uncontrolled and controlled mean-square residual responses are given by

$$\mathrm{tr}([\mathbf{S}_{ee}]) = \mathrm{tr}([\mathbf{T}][\mathbf{S}_{dd}][\mathbf{T}^H]) \tag{18.86}$$

and

$$\mathrm{tr}([\mathbf{S}_{\varepsilon\varepsilon}]) = \mathrm{tr}(\{\mathbf{I}-[\mathbf{P}][\mathbf{P}^\#]\}[\mathbf{H}_r][\mathbf{S}_{rr}][\mathbf{H}_r]^H\{\mathbf{I}-[\mathbf{P}][\mathbf{P}^\#]\}^H) \tag{18.87}$$

where $[\mathbf{S_{ee}}]$ and $[\mathbf{S_{rr}}]$ are defined in Eq. (18.84), $[\mathbf{H_r}]$ is defined in Eq. (18.85), and the noise reduction is given by

$$\mathrm{NR} = 10 \log_{10} \left(\frac{\mathrm{tr}([\mathbf{S}_{ss}])}{\mathrm{tr}([\mathbf{S_{ee}}])} \right) \tag{18.88}$$

As described in the above discussion for the residual and reference sensors, Eq. (18.88) can be evaluated using either measured data or analytical/numerical models. The one difference here is that measurements or analytical/numerical predictions of the plant transfer function matrix $[\mathbf{P}]$ are also required.

On a final note, we remark that while the required numbers of reference and residual channels are typically determined by the system response at the highest frequency of interest, they may be more than is necessary at lower frequencies. As a consequence, the CSD matrices of the reference and residual sensors (and the plant matrix) may be ill-conditioned (i.e., noninvertible) at low frequencies, which may impact the matrix inverses in Eqs. (18.78), (18.85), and (18.87). For these situations, it may be necessary to add small values to the diagonal elements of these matrices before computing the inverse. This procedure is referred to as "regularization." The values added are ideally a function of frequency and will have a larger influence at low frequencies (where the matrices are ill-conditioned) than at high (where the matrices are not ill-conditioned). One procedure that satisfies this requirement (and has been used successfully in many ANVC applications) is to add a scalar times the maximum singular value of the matrix to each diagonal element of the matrix on a frequency-by-frequency basis.

Controller Architecture and Performance Simulations

The upper bound predictions given in the sections above on the number, location, and sizing of sensors and actuators provide a series of tools for bounding system performance as more of the control system is defined. As more realism is included (e.g., identifying both actuator and sensor numbers and locations), the bounds on achievable performance typically get smaller but also more realistic. Comparisons of these bounds with performance goals can be made at each step to determine if the control system under consideration is likely to meet its objectives. Should the system still appear feasible after selecting both actuator and sensor locations [i.e., from Eqs. (18.86) and (18.87)], the next step is to add more realism related to the implementation of the controller.

In this section, we consider the impact of controller architecture on achievable performance. In particular, we discuss procedures to include effects of analog filtering, sample rate, and length of control filter.

As an introduction to these issues, consider the signal path from sensor inputs to actuator drive signals for a conventional digital controller as shown in Fig. 18.77. With reference to this figure, a digital controller requires that the analog signals from the sensors be sampled and digitized at the sample rate of the controller. The sample rate of the controller is usually expressed in terms of a sampling rate or frequency (f_s), which implies that the signals are sampled

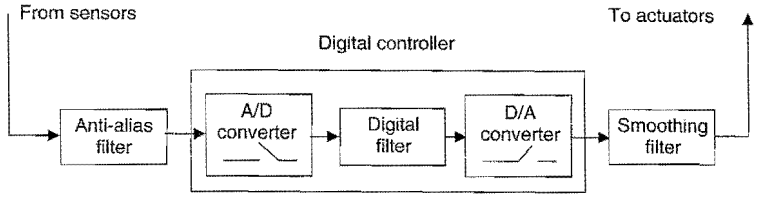


FIGURE 18.77 Signal path from sensor input to actuator drive signal for a digital controller.

at a time interval (T_s) equal to the inverse of the sample rate. For example, a sample rate $f_s = 1000$ Hz corresponds to a sample interval $T_s = 0.001$ s. To satisfy Nyquist's sampling theorem,[57] the sample rate of the controller must be at least twice the highest frequency of interest for the controller. For feedforward systems, the sample rate may be a factor of 4 above the highest frequency to be controlled. For broadband feedback systems, as discussed in Section 18.5 under Alternate Suboptimum Control Filter Estimation, it is not uncommon for the controller sample rate to be a factor of 100 above the highest frequency to be controlled (to minimize the effects of time delay through the controller and quantization noise on system performance).

Once the sample rate has been chosen, analog filters must be used to limit the frequency content of the analog sensor signals to below the Nyquist frequency of the controller, where

$$f_{\mathrm{nyq}} = \tfrac{1}{2} f_s \tag{18.89}$$

These filters are called "anti-alias" filters, and their output is passed to an A/D converter, which in turn samples and quantizes the signal. Similarly, the output of the digital controller is converted to an analog signal by a D/A converter. Before these output signals are sent to the actuators, however, they must be filtered to band limit the signals below the Nyquist frequency; otherwise signals above the Nyquist frequency will be sent to the actuators. These filters are referred to as "reconstruction" or "smoothing" filters

Although issues regarding the selection of anti-alias and smoothing filters are discussed in the next section, we note here that a major consequence of filtering is that it introduces a delay in the signal path, which is referred to as the "group delay" of the filter. This delay is related to the derivative of the phase response of the filter:

$$\tau_g(\omega) = \frac{d\varphi(\omega)}{d\omega} \tag{18.90}$$

In addition to the filters, delays in the signal path of Fig. 18.77 are also associated with the A/D converter, sample-and-hold functionality of the D/A, and the processing time associated with implementing the digital filter. With regards to the A/D converter, delays can be kept sufficiently small by choosing successive-approximation A/D converters. Issues related to A/D selection for applications where time delay is not a limiting factor in controller performance (e.g., tonal

control systems or for residual sensing in some feedforward applications) are discussed in the next section. The delay associated with the sample and hold of the D/A converter $\tau_{D/A}$ is directly related to the sample rate of the controller:

$$\tau_{D/A} = \frac{1}{2f_s} \tag{18.91}$$

For efficient implementations, the delay (τ_{DSP}) associated with implementing the digital filter within a DSP chip can be limited typically to a few tens of microseconds. These implementations require that the sample clock controlling the D/A converters be offset relative to the sample clock for the A/D converters. As such, output samples can be sent to the D/A converters as soon as they are computed so that the processing delay can be held to a fraction of a sample interval. This sampling strategy is in contrast to one that waits until the next time step to output a sample. The latter approach imposes a minimum one-sample delay in the processing, which can be unacceptable for certain applications.

The total delay from analog signal input to analog signal output is termed the *latency* of the controller. Where appropriate, any delay associated with the amplifiers and actuators will also contribute to the latency. Latency is an important parameter since it can directly limit achievable performance of broadband feedforward and feedback systems. As such, it is important to limit overall latency in ANVC control systems consistent with achieving performance goals.

At this point, specific characteristics of the analog filtering, sampling, and control filter parameters can be merged with model or experimental results to make causal performance predictions. The steps involved are as follows:

- Specify a system sample rate based on control bandwidth and architecture (feedforward or feedback).
- Modify the transfer function matrices involving sensor inputs and actuator outputs to include
  - — transfer functions of anti-alias (AA) and smoothing filters (SF),
  - — delay associated with D/A converter sample and hold ($\tau_{D/A}$),
  - — controller processing delay (τ_{DSP}), and
  - — transfer functions of amplifiers and actuator (SH).
- Specify cost function (including control effort and robustness constraints) to be minimized.
- Specify number of control filter coefficients.
- Solve for control filter coefficients using the procedures outlined in Sections 18.4 and 18.5.
- Estimate causal mean-square residual performance and actuator output drive requirements: Compare estimated performance to performance goals.

If transfer functions of the filters, amplifiers, and actuators are not available, initial causal performance estimates can be made by assuming flat magnitude

spectra with linear phase spectra, which correspond to pure time delays that bound expected delays for those components. When this is the case, Elliott[58] suggests approximating the group delay of the anti-alias or smoothing filters as

$$\tau_g \approx \frac{n}{8f_c} \tag{18.92}$$

where n is the order of the filter and f_c is the cutoff frequency.

Hardware Selection

In this section, we discuss some of the practical issues related to selecting analog filters, A/D converters, and DSPs. Although a complete discussion of these issues is beyond the scope of this book, we present general guidelines and considerations. Detailed discussions of each of these issues can also be found in reference 58.

Anti-Alias and Reconstruction Filters. As discussed earlier, the main purpose of anti-alias and reconstruction filters is to attenuate signals above the Nyquist frequency. The anti-alias filters minimize contamination of frequencies below the Nyquist frequency by attenuating the spectral content of the signals above the Nyquist frequency. These higher frequencies are interpreted as lower frequencies because of the nonlinear sampling process of the A/D converter. This phenomenon is referred to as *aliasing*. Similarly, reconstruction filters attenuate components of the drive above the Nyquist frequency, which occur as a consequence of sampled signals at the output of the D/A converter. The benefits of using anti-alias and reconstruction filters in combination with A/D and D/A converters are discussed below

The amount of attenuation required from an anti-alias filter depends on the spectral shape of the sensor response and the desired bandwidth over which the controller needs an accurate representation of the signal. A sensor response that is inherently band limited below the Nyquist frequency may require only a low-order anti-alias filter or possibly none. Alternatively, a sensor response that is flat or increasing with frequency will require a higher order anti-alias filter. For purposes here, we assume that the sensor response is flat versus frequency. In addition, we impose a requirement of at least 40 dB attenuation of contributions from aliasing frequencies at the highest frequency that is important to the controller (f_a). From the context of controller implementation, however, we wish to achieve this attenuation while minimizing the group delay of the filter to acceptable levels.

There are two basic approaches to selecting the filter. The first is to use a low-order filter with a relatively low cutoff frequency. The second is to use a high-order filter with a higher cutoff frequency. Figure 18.78 compares the magnitude spectra and group delays for a fourth-order Butterworth filter and a sixth-order Cauer filter, both of which were designed to provide at least 40 dB of attenuation above $f_{40\ dB} = 600$ Hz. Both filters will meet the attenuation requirements for

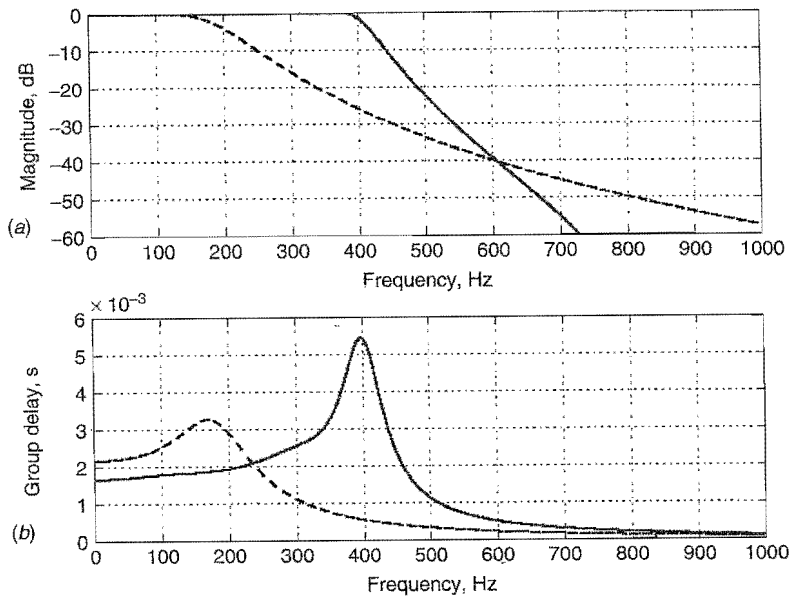


FIGURE 18.78 Comparison of (*a*) magnitude spectra and (*b*) group delay for fourth-order Butterworth (dashed curve) and sixth-order Cauer (solid curve) filters.

frequencies below their respective cutoff frequencies (i.e., $f_a < f_c$) provided that the system sample rate is chosen such that

$$f_s \geq f_a + f_{40\text{dB}} \tag{18.93}$$

Consider first the case with f_a less than the cutoff frequency of the Butterworth filter (nominally 200 Hz) and a sample rate of 800 Hz. For this case, attenuation of aliasing components is assessed by "folding" the magnitude response of the filters about the Nyquist frequency of $800/2 = 400$ Hz. As such, both filters provide the required attenuation of aliasing components in the frequency band below f_a. However, the group delay associated with the Cauer filter is less than that for the Butterworth for all frequencies below f_a, particularly near 200 Hz.

Now consider the case with $f_a = 350$ Hz and a sample rate of 950 Hz. For this case, attenuation of aliasing components is assessed by folding the magnitude response of the filters about the Nyquist frequency of $950/2 = 475$ Hz. The Cauer filter again satisfies the attenuation requirement because the sample rate satisfies Eq. (18.93). However, the attenuation requirement is not met by the Butterworth filter. In fact, less than 20 dB attenuation of aliasing components is achieved at 350 Hz (i.e., the difference in the magnitude responses at 350 Hz and $950 - 350 = 600$ Hz. Further, note that the maximum group delay of both filters in the frequency band below f_a is approximately the same.

The above comparisons suggest that using higher order filters with high cutoff frequencies is preferable to using low-order filters with low cutoff frequencies. Although the preceding discussion centered on selecting anti-alias filters, similar conclusions apply to reconstruction filters provided that the control filters are designed to reduce output levels above f_a. Unfortunately, the cost of implementing high-order filters will exceed the cost of using low-order filters. As a consequence, the performance benefits must be balanced against considerations of additional cost, as will be discussed further in the example ANVC system in Section 18.7 under MIMO Feedforward Active Locomotive Exhaust Noise Control System with Passive Component.

Analog-to-Digital and Digital-to-Analog Converters. A typical data path from sensor input to actuator drive signal was shown in Fig. 18.77. That figure illustrates the use of both types of data converters required for implementing digital controllers, namely A/D and D/A converters. The purpose of A/D converters is to sample the continuous-time signals from the sensors at uniform time intervals ($T_s = 1/f_s$) and quantize the amplitude to a discrete set of amplitude levels. Because the sampling process is a nonlinear operation, anti-alias filters are typically used to band limit the sensor signals below the Nyquist frequency ($f_s/2$) before sending the signals to the A/D converter. This minimizes the possibility that frequencies above Nyquist will contaminate the sensor response below Nyquist, which is referred to as aliasing.

Figure 18.79 shows a frequency domain schematic of how anti-aliasing filters are used in combination with A/D converters to minimize aliasing effects. The upper curve in Fig. 18.79*a* represents the spectrum of an unfiltered continuous-time signal presented at the input of an A/D converter. For an A/D converter operating at a sample rate of f_s, signals above the Nyquist frequency ($F_{\text{nyq}} = f_s/2$) will be interpreted as frequency below Nyquist. Fig. 18.79*a* illustrates schematically how frequencies above the Nyquist frequency will fold down into the frequency region below Nyquist. The estimated spectrum below Nyquist will be the sum of the true spectrum below Nyquist plus any aliasing components resulting from the frequency content of the signal that is above the Nyquist frequency. As a consequence, aliasing components can cause the estimated spectrum to differ from the true spectrum of the signal in the frequency region below Nyquist. Anti-alias filters are typically used to band limit the signals prior to the conversion process to reduce the magnitude of any aliasing components. Figure 18.79*b* is a plot of the magnitude response of an anti-alias filter designed to reject frequencies above the Nyquist frequency. When this filter is applied to the unfiltered signal of Fig. 18.79*a*, the resulting spectrum of the signal presented at the input to the A/D converter is that shown in Fig. 18.79*c*. As shown in this figure, much of the effects of aliasing components on the estimated spectrum are removed, thus ensuring that the estimated spectrum is a more accurate representation of the true spectrum of the signal below the Nyquist frequency.

Digital-to-analog converters are used to convert the digital sequences from the controller into analog signals that can ultimately be used as drive signals to actuator electronics. In the frequency domain, the sample output sequence

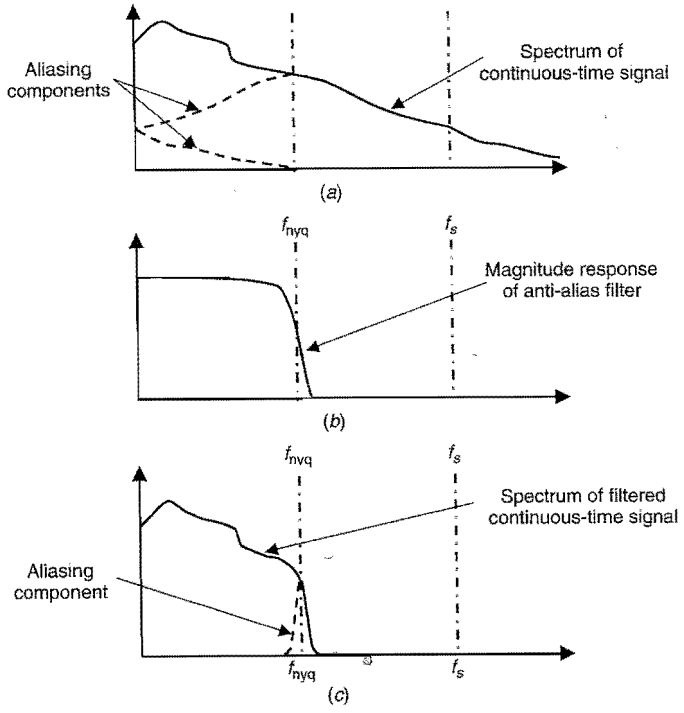


FIGURE 18.79 Use of anti-alias filters to minimize aliasing effects during A/D conversion: (*a*) aliasing components of an unfiltered continuous-time signal digitized at sample rate f_s; (*b*) magnitude spectrum of anti-alias filter; (*c*) aliasing components of filtered continuous-time signal digitized at sample rate f_s.

produces a spectrum that contains "images" of the signal spectrum below the Nyquist frequency, which occur at frequencies above the Nyquist frequency. These image spectra are shown schematically in Fig. 18.80. The effects of the images must be minimized. Otherwise, the controller will drive the actuators at frequencies above the Nyquist frequency, resulting in increased out-of-band noise amplification. These out-of-band effects are reduced to some extent by the sample-and-hold (S&H) functionality that is integral to most D/A converters. As discussed earlier, the S&H introduces a delay equal to one-half the sample interval ($T_s/2$). In addition, it provides some filtering of the output spectrum, as illustrated in Figs. 18.80*b* and 18.80*c*. To suppress the remaining signals above the Nyquist frequency, D/A converters are typically followed by smoothing or reconstruction filters. The effect of applying reconstruction filters on the D/A output signal is shown in Fig. 18.80*e*.

Two basic types of A/D converters are applicable for use in ANVC systems. The first type is referred to as "successive-approximation" (SA) A/D converters. The second type is referred to as "sigma–delta" ($\Sigma\Delta$) A/D converters. Table 18.1

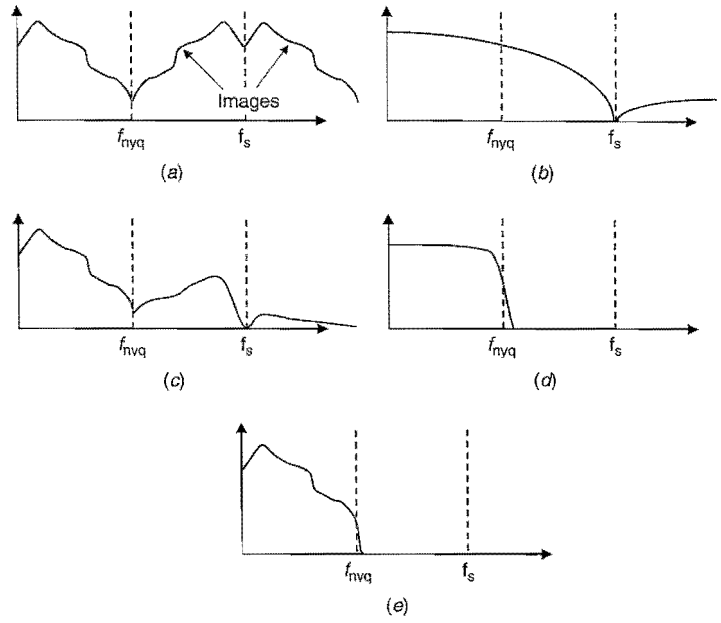


FIGURE 18.80 Use of reconstruction filters to reduce image spectra at the output of D/A converters: (*a*) spectrum of digitized output signal at sample rate f_s, (*b*) magnitude response of zero-order sample-and-hold integral to D/A converter; (*c*) spectrum of analog output of D/A converter prior to reconstruction filter; (*d*) magnitude response of reconstruction filter; (*e*) spectrum of analog signal at output of reconstruction filter.

compares some of the important features and differences between these two types of converters.

The choice of A/D converter for an ANVC application will depend on the control architecture (i.e., feedforward or feedback), the type of sensor signals (i.e., reference or residual sensors), and the performance goals. For broadband ANVC applications that require minimal latency through the controller (e.g., reference sensors in a feedforward system or residual sensors in a feedback system), the delay associated with $\Sigma\Delta$ A/D converters is unacceptable. As a consequence, SA A/D converters should be used for those applications, and the extra cost of the converters and anti-alias filtering should be included in the total cost of the ANVC system. We note, however, that low latency is not a necessary requirement for the residual sensors of a feedforward implementation. These sensor signals are used in the design of the control filters but are not themselves filtered by the control filter to produce output signals to the actuators. However, the latency associated with $\Sigma\Delta$ A/D converters used on the residual signals will be seen as a delay in the plant transfer functions. This added delay will in turn reduce allowable convergence coefficients for LMS-based algorithms[58] but does not preclude their use.

TABLE 18.1 Comparison of Successive-Approximation and Sigma-Delta A/D Converters

Successive-Approximation Converters	Sigma-Delta Converters
Sample input signal at rate f_s	Over sample input signal nominally at 64 times desired sample rate (i.e., $f_{\Sigma\Delta} = 64 f_s$)
Require use of relatively high-order anti alias filters to bandlimit signals below Nyquist frequency	Only low-order (if any) anti-alias filters required to bandlimit signals below $f_{\Sigma\Delta}/2$. Integral high-order (linear-phase) digital filters bandlimit signal below Nyquist frequency ($f_s/2$). Output is decimated (i.e., keep only every 64th sample) to produce sampled sequence at f_s sample rate.
Low latency (on the order of a few μs)	High throughput latency (typically $32T_s$, where $T_s = 1/f_s$)
Quantize signal at multiple bit levels (e.g., 12 or 16 bits)	One-bit quantization at oversampled rate to provide comparable multi-bit quantization (e.g., 12 or 16 bits) at f_s sample rate
Relatively expensive compared to $\Sigma\Delta$ converters	Relatively inexpensive compared to SA converters

When low latency is not required, the use of $\Sigma\Delta$ converters can significantly reduce the costs associated with digitizing the sensor signals. For example, a tonal feedforward ANVC system can use a $\Sigma\Delta$ A/D converter to digitize the reference signal. As before, digitization of the residual signals for this example can be done using $\Sigma\Delta$ A/D converters, provided that the extra delay is acceptable in terms of convergence rate (if adaptive algorithms are used). The choice of D/A converter is governed by similar arguments concerning allowable latency. For instance, when low latency is not required, $\Sigma\Delta$ D/A converters can be used. Alternatively, when latency must be minimized, conventional D/A converters should be used.

For most ANVC applications, it is desirable to initiate the sampling across all A/D converters using a common clock signal. In this way, all A/D inputs will be synchronously sampled. Similarly, it is advantageous to sample all the D/A converters using a common clock signal as well. The D/A converters could be clocked using the same clock pulse as for the A/D converters; however, to minimize latency through the controller, it is useful to offset the D/A clock relative to the A/D clock. In this way, subsample latency can be achieved by sending signals to the D/A when they are ready, as opposed to waiting for a full sample period.

The final aspect of converter selection is quantization noise. When analog signals are quantized to a finite number of amplitude values (e.g., 16-bit A/D converter), the errors in the conversion process can be thought of as noise. For the signals of interest for ANVC, this noise is modeled as uniformly distributed

from—LSB/2 to LSB/2. Here, LSB stands for the *least-significant bit* and is given by

$$\text{LSB} = \frac{V}{2^{M-1}} \tag{18.94}$$

where V corresponds to the voltage range of the converter (i.e., $\pm V$) and M is the number of resolution bits (e.g., 16 for a 16-bit converter). For the assumed uniform probability distribution of the noise, the rms of the quantization noise (QN_{rms}) is equal to

$$QN_{\text{rms}} = \frac{LSB}{\sqrt{12}} \tag{18.95}$$

For a sample rate f_s, the spectrum of the quantization noise ($QN_{\text{psd}}(f)$) is white (i.e., flat) with a power spectral density (PSD) amplitude given by

$$QN_{\text{psd}}(f) = \frac{LSB^2/12}{fs/2} \tag{18.96}$$

As an example, for a 16-bit converter with a voltage range of ± 10 V and a sample rate of 1 kHz, the rms quantization noise [from Eq. (18.95)] is 88 μV, and the PSD level is -108 dB re 1 V^2/Hz.

At this point, it is useful to compare plots of

- the expected signal levels (in volts from the sensor),
- electrical noise floors (associated with the sensors, analog filters, and gain), and
- quantization noise.

To support a common comparison, all of these voltage levels should be referenced to a common point in the signal path (e.g., the amplifier input). These plots should be generated corresponding to both open- and closed-loop sensor responses. Sensor sensitivities, signal gain, and quantization noise can then be assessed within a common framework. The goal is to choose each of these to ensure that sensor signals will have sufficient signal-to-noise ratio (SNR) throughout the bandwidth of interest.

To illustrate some of the issues related to A/D converter selection, consider the example shown in Fig. 18.81. The various curves grouped in the center of this plot correspond to the expected signal levels from multiple residual sensors, expressed in dB re V^2/Hz, referenced to the input of a bank of sixth-order Cauer filters. The filters are used to provide anti-alias filtering as well as programmable gain for these channels. The cutoff frequency is approximately 800 Hz. The power spectral density of the noise from the anti-aliasing filters at their input (labeled PFI *noise* in the figure) falls between -155 dB and -150 dB re 1 V^2/Hz. The spectral density of the sensor noise floor reference to the filter input is

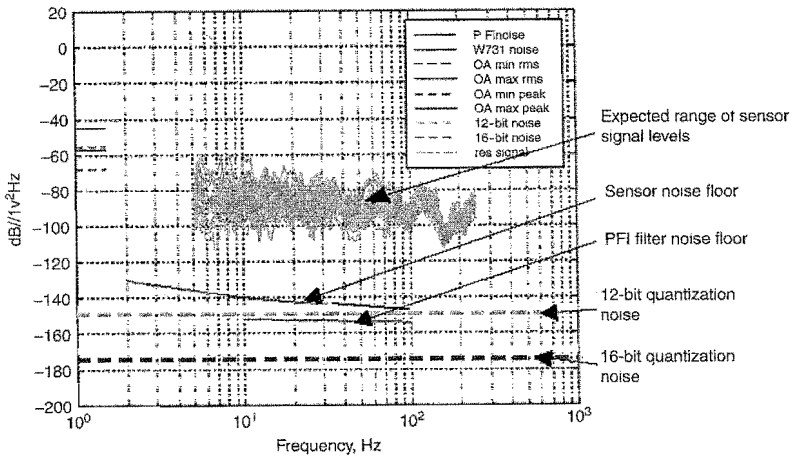


FIGURE 18.81 Comparison of signal level versus electrical and quantization noise.

approximately −130 dB re 1 V^2/Hz at 2 Hz and drops to −145 dB re 1 V^2/Hz at 100 Hz.

The rms levels for the sensor signals (needed for quantization noise estimates as indicated below) are determined by integrating the mean-square voltage responses across frequency and taking the square root. For these spectra, the largest rms level is approximately −57 dB re 1 V. Assuming the statistics of these responses is random (i.e., with a crest factor of 4 or 12 dB), a peak voltage response for this group of sensors is estimated to be approximately −45 dB re 1 V. The spectrum level of the digitization noise (at the filter input) can be estimated from Eq. (18.96), where the voltage V in Eq. (18.94) is taken (at the moment) to be the peak voltage of the sensor signals (i.e., −45 dB re 1 V = 5.5 mV). As such, the spectral levels of digitization noise for 12- and 16-bit converters, assuming a sample rate of 2 kHz, are −152 dB and −176 dB re 1 V^2/Hz, respectively. The SNR for these sensor measurements is a function of frequency and corresponds to the spread in decibels between the estimated signal responses and the maximum of the electrical noise (from filters and sensors) or the digitization noise. The SNR is nearly 30 dB throughout the frequency band of concern.

For the example shown in Fig. 18.81, it is sufficient to use a 12-bit converter since the SNR is limited by sensor noise as opposed to digitization noise up to about 100 Hz. Above that frequency, the SNR will be limited by digitization noise if a 12-bit converter is used or by PFI noise if a 16-bit converter is used. Further, if the converter (12- or 16-bit) has a voltage range of ±1 V, the programmable gain should be set at approximately 33 dB to allow 1–2 bits of headroom to avoid clipping.

The example case in Fig. 18.81 illustrates the relatively complex interdependencies that must be considered when selecting ANVC hardware to ensure adequate SNR, which in general will be a function of sensor noise and sensitivity, anti-alias filter noise, A/D converter quantization noise and voltage range, system gain, and sample rate.

Digital Signal Processors. As discussed earlier, the rapid growth in ANVC systems and applications over the past 25 years can be traced in large part to the advent of DSP chips. These chips are optimized to perform operations on a sample-by-sample basis. That is, these chips read in data one sample at a time, perform large numbers of computations, and then output a sample. This is in contrast to other central-processing units (CPUs) that read in groups (i.e., buffers or blocks) of data, operate on the entire buffer, and then output buffers of data. These later processors can often perform larger numbers of computations than DSP chips, but their latency is on the order of the block size.

Digital signal processors are ideally suited to perform the low-latency digital filtering required by ANVC algorithms. As such, they are widely used in the design of adaptive control systems based on the algorithms presented in this chapter. In addition, current DSP technology supports high-speed communication between DSPs to support applications with large numbers of inputs and outputs (e.g., many tens of inputs and outputs) as well as large digital filter sizes (e.g., IIR filters with over 5000 taps per filter). For these large-scale problems, efficient low-latency implementation of the digital filters can be achieved by combining DSPs with high-powered CPU compute engines such as PowerPC (PPC) chips. Further, the relatively large latency associated with the PPC chips may be acceptable to perform much of the "off-line" algorithms associated with system identification and control filter design when using direct estimation as opposed to adaptive filter algorithms.

Once the control algorithms have been selected, the computation and memory requirements can be determined for all "in-line" filtering and "off-line" processes. These requirements should then be mapped to DSPs and PPC chips, as necessary. Floating-point DSPs such as the TMS320C6701 are rated at 1 Gflop and include up to 128 MB of fast-access memory. Compute engines like the PPC7410 are rated at 2 Gflops with up to 512 MB of local memory. In addition, PC or VME (workstation) boards are currently available with up to four of each type of processor per board and support high-speed communications between processors on a given board as well as processors located on other boards. These processor-to-processor communications are supported by high-speed interconnect architectures such as Mercury RACE^{++}, Spectrum DSPLink, and SKYchannel.

As an example, Fig. 18.82 shows the hardware architecture for a large-scale ANVC system incorporating both DSPs and PPC chips, including high-speed communication over a Mercury RACEWAY interconnect. The signal path from the reference sensors to the actuator drive signals includes high-order anti-alias and reconstruction filters with cutoff frequencies near the Nyquist frequency. Successive-approximation converters are used to minimize latency associated with the conversion. A combination of DSPs and PPC chips are used to efficiently implement the digital control filters to minimize latency.[84] The residual sensor

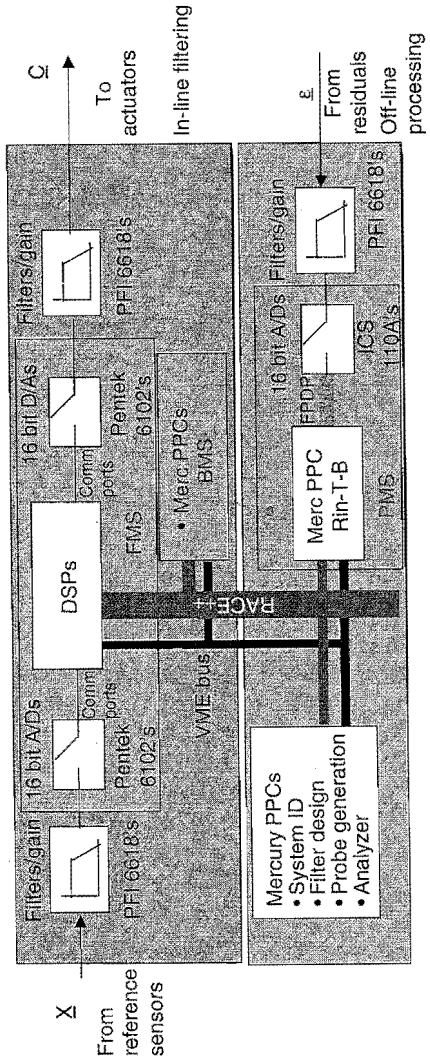


FIGURE 18.82 Control architecture using combination of DSPs and PPCs.

signals pass through anti-alias filters and are digitized using sigma–delta converters. These data support off-line functionality associated with system identification, control filter design, and probe-signal injection, which are performed on multiple PPC chips. Communications between the DSPs and PPC chips are primarily carried over Mercury's RACE^{++} interconnect bus, with additional communications occurring over the VME bus. In this way, the compute power associated with PPC chips can be used to efficiently perform off-line functions (e.g., direct estimation of plant and control filters), which can be passed to the in-line processors (DSPs and PPC chips) to support adaptation of the control filters.

Finally, we note that fixed-point DSPs as well as floating-point DSP devices are available. The floating-point devices are much easier to program and are often chosen for proof-of-principle systems or for final systems that are not highly cost sensitive. When cost is a driving issue, fixed-point devices should be considered. The final choice must balance the higher nonrecurring cost associated with programming fixed-point devices and the potential increased CPU overhead due to implementing floating-point arithmetic on a fixed-point device against the lower recurring per-unit cost

Control System Implementation and Testing

Once the simulations and hardware selections have been made, the control system is implemented and performance tests are conducted. In this section, we discuss the basic operating modes and features of a controller that should be considered during implementation to support the subsequent testing phase.

For each of the modes discussed below, parameters that can be changed during system operation (referred to as "soft" parameters) and those that cannot be changed during operation (referred to as "hard" parameters) must be identified. Soft parameters provide the flexibility to modify and tune certain parameters during system operation, which is often an invaluable feature in prototype systems. Allowing parameters to be changed "on-the-fly," however, adds complexity to the implementation. As such, lists of desired soft and hard parameters should be identified early on in the implementation phase so that the appropriate communications between a user interface and the embedded controller codes can be included. The typical operating modes and features of a controller are summarized in Table 18.2, including references to soft parameters that are useful in supporting each mode.

As indicated, an ANVC controller will typically have two primary operating modes, namely system identification and control. The purpose of system identification is to estimate the transfer functions (or equivalently impulse response functions) from the actuator control signals to sensor responses (both references and residuals). This identification is initially performed with the control filter set to zeros but can subsequently be performed during closed-loop operation, as discussed in Section 18.4 under System Identification. Once an initial plant estimate has been obtained, operational measurements of the system responses are obtained to characterize the "uncontrolled" (i.e., open-loop) response. These

TABLE 18.2 Controller Operating Modes and Features

Operating Mode	Description and Features
Open-loop characterization of system response	Collect measurement of residual sensors during normal "uncontrolled" (i.e., open-loop operation)
Open-loop system identification	Estimate plant models between actuator drive signals and sensors. Soft parameters include probe strength, adaptation coefficients, leakage coefficients, regularization parameters, and actuator channel selection.
Closed-loop operation with filter design based on open-loop response and system identification	Collect measurements of residual sensors during "controlled" (i.e., closed-loop) operation. Soft parameters include adaptation and leakage parameters, control effort and robustness weighting parameters, and regularization parameters.
Concurrent closed-loop system identification and control-filter adaptation	Collect measurements of residual sensors during "controlled" (i.e., closed-loop) operation, while probe signals are injected for the purpose of closed-loop system identification. Soft parameters include those cited above for system identification and closed-loop operation. In addition, software flags should be included to initiate use of updated plant models in the control filter design algorithm.
Save operational "state"	All controller information necessary to restart the controller should be saved. This includes, plant and control filter coefficients, all hard and soft parameters, operating mode, and probe signal path parameters.
Load saved "state" and restart controller	Load in a saved "state" and start operation using saved parameters and filters.

responses are also used to design control filters to support operation in the control mode. Once in the control mode, probe signals can be injected to support closed-loop system identification and to support adaptation of control filter coefficients. Soft parameters can be adjusted to optimize performance. Closed-loop system responses should then be collected and compared with open-loop responses to evaluate system performance versus performance objectives and goals.

The final two rows of Table 18.2 indicate the desire to be able to save the "state" of the controller at any point in time. By state, we mean all controller parameter values and filter coefficients are saved for the purpose of restarting the system at that state in the future. As such, the controller can be started from a closed-loop operating state or from some initial operating state (e.g., open loop). It is convenient for prototype systems to include a graphical user interface (GUI) through which operation mode, soft parameter values, performance assessments, and save/load state functionality can be monitored and controlled. Once an ANVC system has been successfully tested, values of soft parameters and logic for progressing from open-loop to closed-loop operation can be automated within the software, thus resulting in a stand-alone ANVC system.

18.7 EXAMPLES OF ANVC SYSTEMS

In this section we present three prototype active systems that illustrate the application of the principles outlined in the previous sections of this chapter. All of these systems were developed to demonstrate the technology and one is currently operational on a complete class of U.S. Navy ships. All three demonstrate the effectiveness of active noise and vibration control technology when appropriate design procedures are followed. The first example involves the synergistic application of a combination of active and passive noise reduction treatments. The example demonstrates the successful control of a source of noise that would have been difficult using only passive or only active approaches. The second example demonstrates the application of feedback technology to the control of both broadband and narrow-band vibration transmission through a vibration isolation mount. The final example illustrates the use of active noise control technology to generate a zone of silence in a noisy environment.

MIMO Feedforward Active Locomotive Exhaust Noise Control System with Passive Component

Problem Description. When operated at full power diesel-electric locomotives generate significant noise and can have a significant adverse impact on the quality of life near major railroad lines. The sources of noise are shown in Fig. 18.83.[85] As indicated in the figure, the primary sources of diesel-electric locomotive noise are the engine exhaust and the cooling fans, both of which must be reduced before significant noise reductions can be realized. The active noise control system developed for this application focused on just the exhaust noise, fully recognizing that later efforts would have to attack cooling-fan noise if significant overall locomotive noise reductions were to be achieved. Active technology was considered for this application because locomotive exhaust noise is significant at very low frequencies (below 40 Hz), and passive noise control treatments (e.g., dissipative or reactive mufflers) that could achieve the desired noise reduction would simply be too large to fit in the space available.

The basic concept for the system[86,87] is illustrated in Fig. 18.84, where a plan view of the top of the locomotive hood is shown near the exhaust stack. The figure shows a number of loudspeakers, the control actuators, surrounding the exhaust

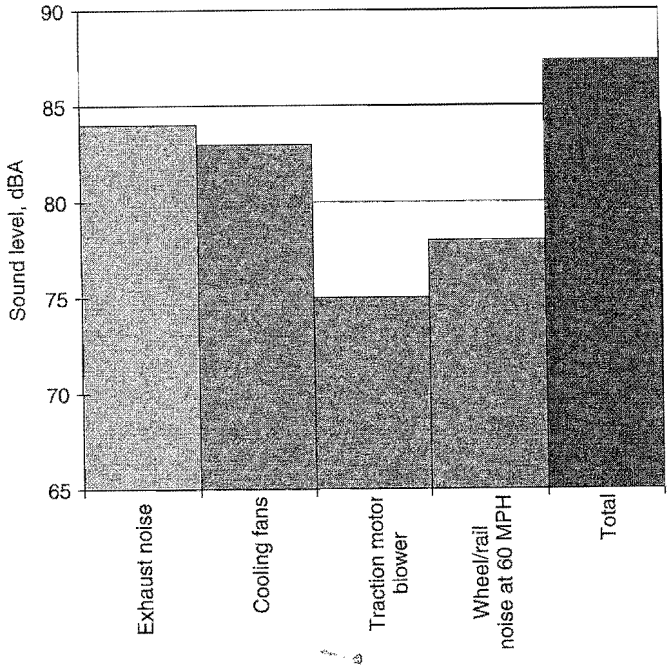


FIGURE 18.83 Noise sources on an SD40-2 diesel electric locomotive measured at 100 ft with the locomotive running at throttle 8 at full load.

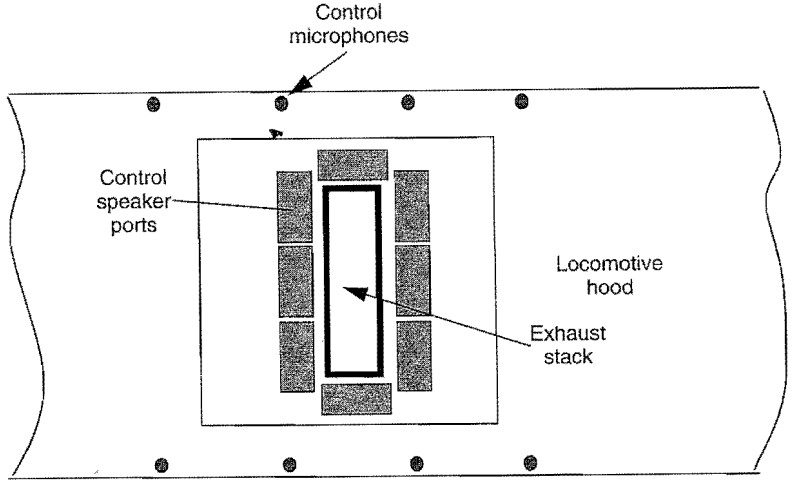


FIGURE 18.84 Plan view of the locomotive hood with the basic system concept.

stack and a number of control microphones located near the edge of the hood that will act as the residual sensors. It was determined based on exhaust noise measurements that at low frequencies where the active system would be designed to operate, the noise was primarily tonal and so a feedforward architecture was selected that used a tachometer on the locomotive diesel engine as the reference signal.

Performance Goals. Based on the source information in Fig. 18.83, it was decided that 10 dBA of overall reduction in exhaust noise would be desirable to have a significant impact on community noise (assuming of course that cooling-fan noise would eventually be similarly reduced). After examining the locomotive exhaust noise spectra we determined that to achieve 10 dBA of overall noise reduction would require that the exhaust noise be controlled out to at least 5 kHz. Since extending the bandwidth of the active system out to so high a frequency and requiring broadband control would place excessive demands on the technology, we decided on a hybrid approach. At low frequency where the noise is primarily tonal we decided to employ an active system. At high frequency where the noise is primarily broadband in character we determined that a passive silencer would be most advantageous. Such an approach is desirable because active technology is well developed for the control of low-frequency tonal noise and at high frequency passive silencers can be effective without having to be large in size. Both technologies were required because we found that

- active control of tones in the exhaust below 250 Hz with no broadband control at the higher frequencies would result in less than 1 dBA of noise reduction and
- no control of tones in the 0–250-Hz band would limit the maximum reduction of exhaust noise to ~5 dBA.

We ultimately decided that 10 dBA of exhaust noise reduction could be achieved with

- an active system providing 10 dB reduction of exhaust tones below 250 Hz along with
- a passive silencer providing 5 dB of broadband noise reduction from 250 to 500 Hz and 15 dB reduction from 500 to 5500 Hz.

Figure 18.85 shows the silencer designed to provide the above noise reduction performance. It is a very compact design with the center body and side chambers designed to provide the necessary insertion loss while maintaining the back pressure low enough to meet locomotive diesel engine specifications. The silencer was designed to allow the speaker enclosures to surround it, with the whole assembly fitting within a protective enclosure in the engine compartment. While the passive silencer was a critical component in the entire system design,

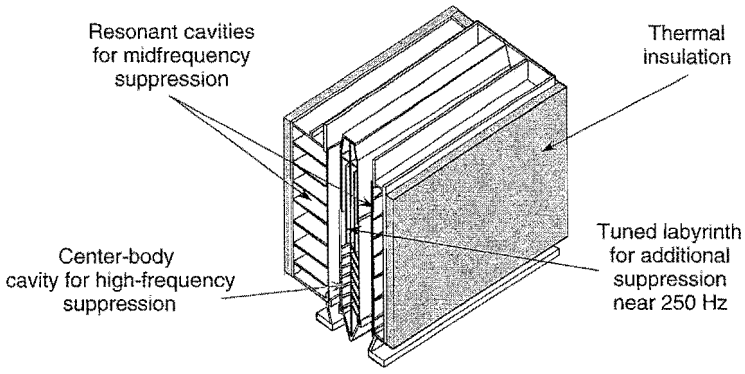


FIGURE 18.85 Compact passive silencer design.

we focus here only on the active system. Details on the passive silencer can be found in references 86 and 87.

Number and Location of Actuators. We began the design process by determining the number and location of control actuators (loudspeakers). Figure 18.86 shows a typical arrangement of actuators that we examined in simulations in which the exhaust stack and control actuators were treated as point sources. In the simulations we formed a matrix of transfer functions relating the sound pressure at 90 locations in the horizontal plane 30 m from the exhaust stack to the control speaker volume velocities at 32 speaker locations around the exhaust stack, as illustrated in Fig. 18.86. Figure 18.87 shows the ratio of the significant singular values to the largest singular value as a function of frequency for that transfer function matrix. In principle the number of significant singular values tells us the minimum number of actuators needed to provide significant control of the source. We found (not surprisingly), while carrying out calculations of this type, that the minimum number of singular values (control sources) was achieved when the control sources were placed as close as possible to the exhaust stack. Consequently, we carried out a preliminary design of the control speaker enclosures to determine a realistic minimum spacing between the exhaust stack and the enclosure outlets. The calculations in Fig. 18.87 were carried out for that minimum spacing. The figure shows that at 250 Hz eight singular values (including the largest) lie within 20 dB of the maximum. Since we are looking for only 10 dB reduction in noise, the use of eight actuators arranged as shown in Fig. 18.85 seemed to be a conservative choice. The performance predicted by this arrangement is shown in Fig. 18.88. While the noncausal noise reduction predicted by this calculation is much larger than we would expect to achieve, it was comforting to see that eight control actuators seemed to be more than adequate.

Number and Location of Control Sensors. The evaluations in the previous section placed the control sensors in the far field. In reality the microphones

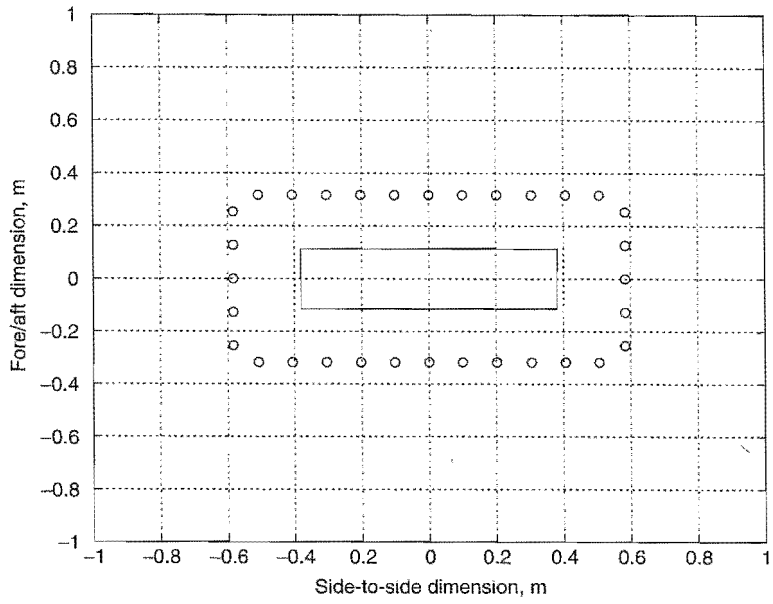


FIGURE 18.86 Candidate control source locations.

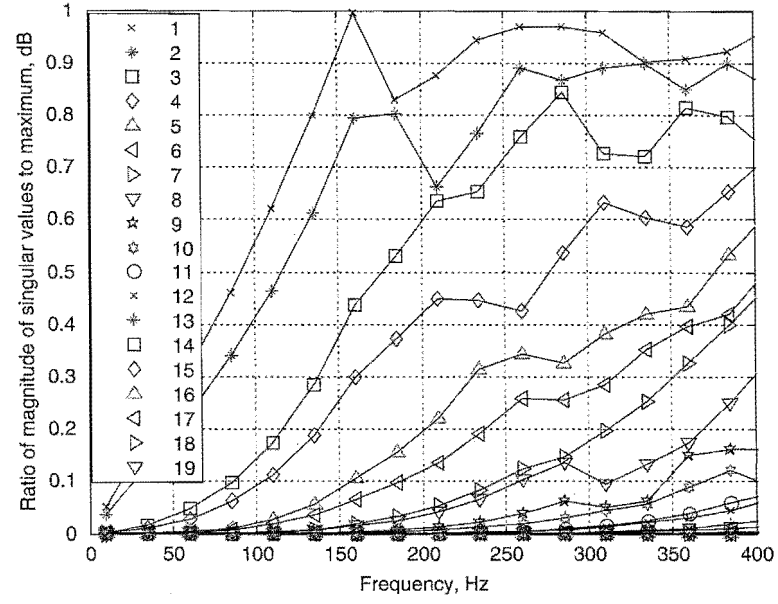


FIGURE 18.87 Ratio of each singular value to the largest singular value as a function of frequency.

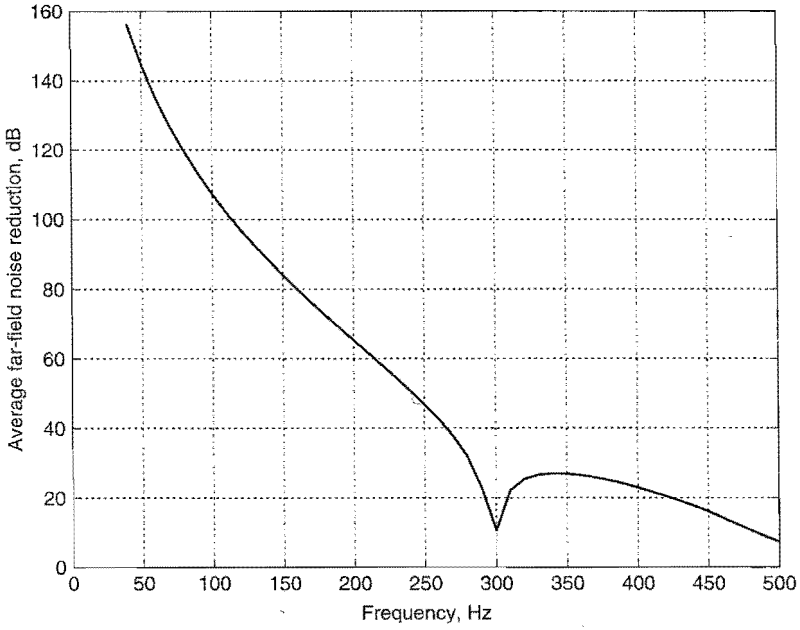


FIGURE 18.88 Predicted far-field performance of eight control actuators.

will have to be placed somewhere on the locomotive hood. Consequently, we developed an additional set of transfer function matrices relating the sound pressure at candidate control microphone locations on the locomotive hood to control speaker volume velocity at the previous 32 locations around the exhaust stack. We then determined the volume velocity required to minimize the pressure at the control microphones and then used those values with the previous transfer function matrix to predict the reduction in far-field pressure. Figure 18.89 shows the results of that calculation for a number of different control sensor locations. The solid curve in the figure is for the final control sensor placement, a line of four sensors along the two edges of the locomotive hood, similar to that shown in Fig. 18.84. A number of calculations of this type were used to help in the selection of control sensor locations. Other issues that came into play in the selection included the degree of dominance of exhaust noise over other sources at the candidate sensor locations, interference with other locomotive components, heat, and routing of cabling.

Control Actuator Design. The simulations for control sensor placement can provide, as part of the calculation, the estimated volume velocities required from the control speakers, provided realistic values of the uncontrolled sound pressure at the control sensors are used in the calculations. Measurements of the sound pressure at various locations on the hood of a test locomotive were acquired to

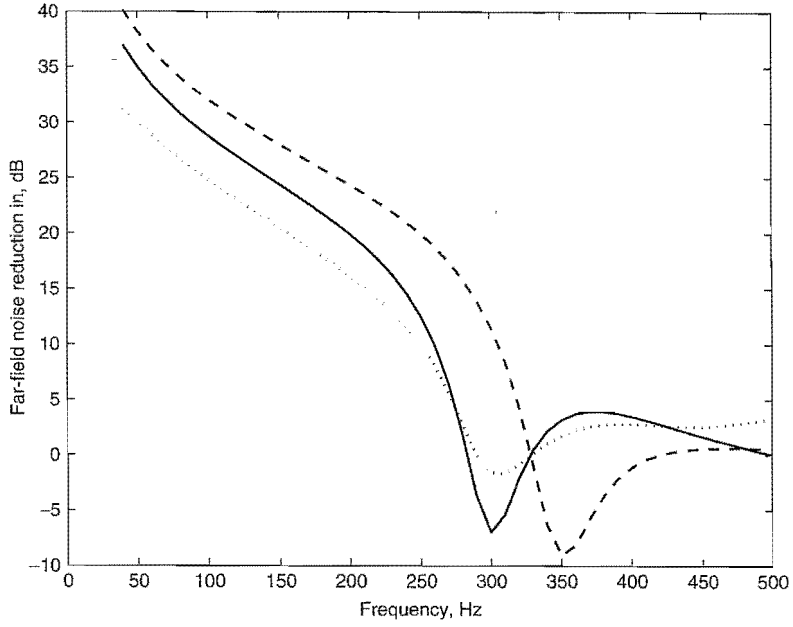


FIGURE 18.89 Predicted far-field noise reduction of eight control actuators with various configurations of eight control sensors.

provide those data. Simulations were then performed to determine the optimum control speaker volume velocities. That information was used in the selection of the control speakers and the design of the speaker enclosures. The enclosure design is shown in Fig. 18.90. Two different enclosure geometries were required to allow the necessary number of enclosures to fit in the space available around the exhaust duct. Each enclosure contains two 12-in.-diameter high-fidelity speakers and is designed to provide bandpass frequency response, enhancing the volume velocity in the 40–250-Hz frequency range. The enclosure–speaker system was designed using a commercially available computer program.

Figure 18.91 shows the arrangement of the control speaker enclosures around the exhaust stack. By careful design we were able to fit 10 enclosures in the space available. However, we retained only eight independent channels to drive the speakers. Because the simulations indicated that very high volume velocity would be required of the speakers on the centerline of the locomotive, we placed two speaker enclosures on each side of the centerline, as indicated in Fig. 18.91, rather than a single one on the centerline. We then drove each of the two pairs of enclosures with a single controller output channel.

Control Architecture. As indicated above, we decided early in the design process to use a feedforward control architecture since the technology is well

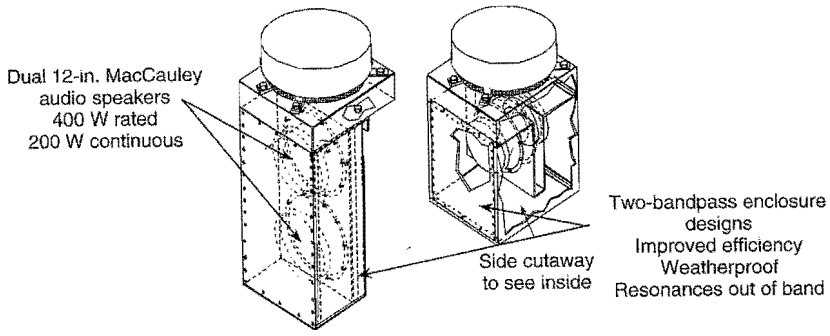


FIGURE 18.90 Control speaker enclosure design.

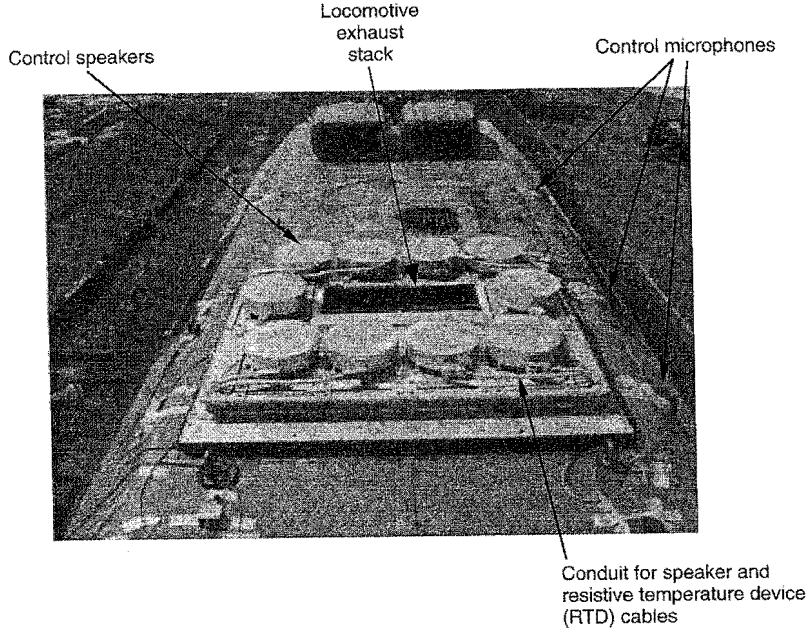


FIGURE 18.91 Control speaker arrangement in the locomotive.

developed for tonal control problems. A simplified control block diagram is shown in Fig. 18.92. The figure shows the typical adaptive MIMO LMS filtered-x architecture with eight control filters and an 8×8 plant transfer function matrix. A more detailed block diagram is shown in Fig. 18.93, where probe injection is shown for plant identification along with the additional LMS blocks for estimating the plant while minimizing the noise in the estimate.

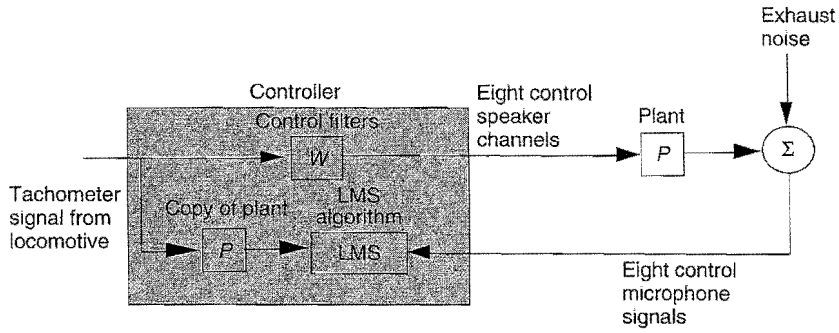


FIGURE 18.92 Simplified basic block diagram of the control architecture.

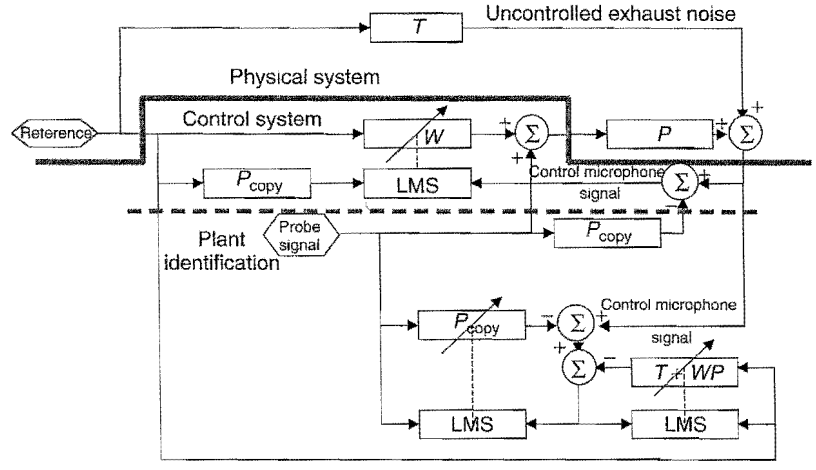


FIGURE 18.93 Detailed controller block diagram.

Hardware Selection. We decided early in the design process to use 12-bit successive-approximation A/D converters, since the lower discretization noise associated with 16-bit converters was not needed in this application. A commercially available input–output (I/O) board from Loughborough Sound Images was found that provided 16 input channels (A/D converters) and 8 output channels (sample-and-hold D/A converters) and in addition provided third-order low-pass Butterworth filters for anti-aliasing and reconstruction. We decided to use the on-board filters because providing a separate set of filters would have been too costly. Since these filters roll off very slowly with increasing frequency, we needed to use a sampling frequency much higher than would be needed to achieve the desired control bandwidth. Consequently, we sampled at 2000 Hz and set the cutoff frequency of the filters to 720 Hz; however, in the control computations

we downsampled the digital signals by a factor of 4. This gave us an effective sampling rate of 500 Hz and a control bandwidth on the order of 250 Hz.

Estimates of computational load and memory requirements for the application are shown in Table 18.3. These estimates were based on up to 200 taps for each of the plant filters and 180 taps for each control filter. The table is divided into two functions: in-line control and system identification. In-line control is the function associated with implementing the control algorithm and system identification is the measurement of the plant transfer function, which must be updated periodically to maintain good control performance. It was decided to use two Texas Instruments TMS320C44 DSP chips available on a commercially available carrier board from Loughborough Sound Images. The board provided more than sufficient memory for the two operations. Each DSP chip is clocked at 60 MHz and is capable of up to 30 million floating-point operations per second (Mflops). It was decided to separate the two functions mentioned above with the primary DSP providing all of the control processing and the secondary DSP carrying out all of the system identifications tasks.

System Performance. The control system described above was implemented on an F40PH passenger locomotive operated by Chicago Metra, a commuter rail line in the Chicago metropolitan area. Testing was carried out at the 51st St. Rail Yard in Chicago. The microphone locations for the evaluation are shown in Fig. 18.94. The number of available microphone locations was limited because of the presence of other equipment and structures in the yard that would have interfered with the acoustical evaluation. Uncontrolled measurements were made before installation of the passive silencer. The performance of the system was then measured with the passive silencer in place and with the active system turned on and turned off.

Figure 18.95 shows the reduction of the tonal noise at microphone 5 on the roof of the locomotive due to the use of the active system for the locomotive operating loaded at throttle 4.* The figure shows significant reduction of all of the important tones with some amplification of the low-amplitude tones.

TABLE 18.3 DSP Computation Requirements for the Active System

Operation	MFLOPS	Memory (Kbytes)
Control	22.4	107
System identification	9.6	10
Total	32.0	117.0

*The locomotive diesel engine was loaded by passing the power from the alternator driven by the engine through the locomotive dynamic brake grids (large resistors cooled by the dynamic brake fan). The locomotive can be operated unloaded at idle and can be operated loaded or unloaded in any one of eight throttle setting. Throttle 1 corresponds to the lowest speed and lowest power and throttle 8 is the highest speed at full power.

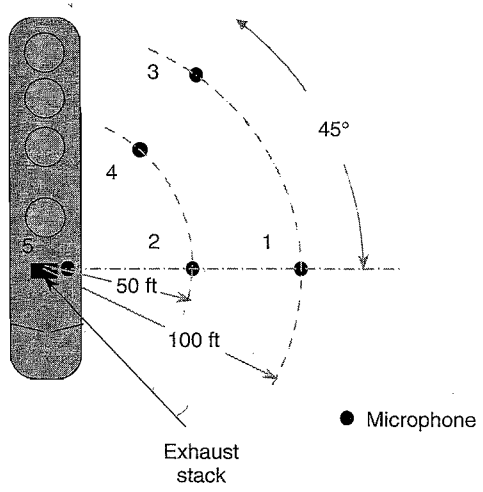


FIGURE 18.94 Microphone locations for the evaluation measurements.

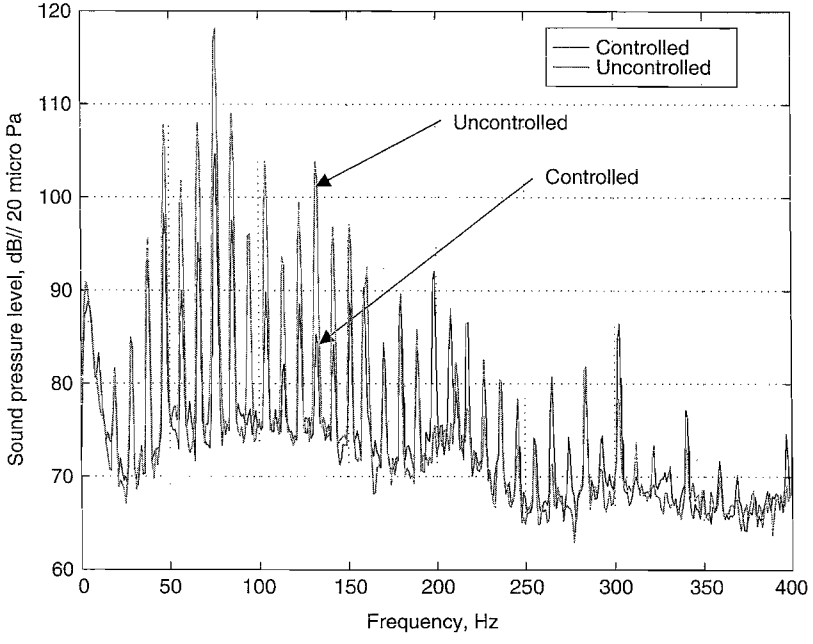


FIGURE 18.95 Noise reduction performance of the active system at throttle 4 loaded as measured at a microphone on the roof of the locomotive.

TABLE 18.4 Estimated Noise Reduction at the Far-Field Microphones

Throttle	Load	mic 5	mic 1	mic 2	mic 3	mic 4
idle	unloaded	5.1	5.2	6.5	6.1	6.4
hi idle	unloaded	8.7	6.5	8.9	5.8	7.4
t4	unloaded	6.9	5.2	4.1	5.6	5.4
t6	unloaded	7.7	6.6	5.6	6.4	6.0
t8	unloaded	5.8	−0.1	3.7	6.2	4.7
t4	loaded	6.4	5.2	4.1	4.7	4.6
t6	loaded	4.3	−1.9	1.2	2.8	1.7
t8	loaded	6.9	2.9	6.5	6.6	6.6

The reduction of the overall sound level below 250 Hz is in excess of 12 dB. Table 18.4 shows the overall A-weighted noise reduction due to the passive silencer and active system operating together. The reductions are somewhat less that the 10-dBA goal but are still significant for most operating conditions and for most microphone locations, showing that the hybrid active–passive system has provided significant broadband global noise reduction.

Active Machinery Isolation

Problem Description. It is difficult to achieve desired vibration isolation at low frequency using passive machinery mounts. Often, to achieve low-frequency isolation, two-stage isolators are employed, which incurs a very large weight penalty for the intermediate mass between the two isolators. In some applications, such as marine vessels or aircraft, the weight of the intermediate mass has an adverse economic and vehicle performance impact.

The forces transmitted into machinery foundations generally contain narrow-band and broadband components. Reduction of the continuous or broadband spectral components as well as the discrete or narrow-band spectral components is often necessary to meet noise or vibration goals. In addition, the tonal frequencies of the narrow-band excitation can change quite rapidly with time due to changes in operating speed. Further, the plant transfer function (i.e., the transfer function between the drive signal to the actuator and the sensor response) is expected to vary with time.

Finally, the machinery foundations of interest are often complex, large, distributed mechanical structures that are lightly damped and have a large number of resonant modes in the frequency range of interest. Thus, typically, plant transfer functions are of high order with high-Q response components. Moreover, the order (e.g., complexity) of the plant increases as the bandwidth of the controller is increased.

Based on the above observations, the control problem is defined as follows:

- Provide both narrow-band and broadband reduction of forces transmitted into the machinery foundation structures.

- Adapt rapidly to variations in the tonal frequencies of narrow-band excitations. Adapt at a relatively slower rate to variations in the plant.
- Minimize controller bandwidth to minimize complexity of the plant transfer function and consequently the controller.
- Provide the desired performance while avoiding out-of-band vibration amplification.

The final item is based on our experience with applications which require increased isolation performance within a certain frequency range but which will not tolerate significant degradation in isolation system performance outside the regulation bandwidth of the active system. Acceptable levels of out-of-band enhancement (i.e., noise amplification) are typically 2–3 dB.

In the following section, we describe an active isolation system designed to meet these requirements. We consider a feedback algorithm, because in general there is not a suitable reference sensor available to achieve broadband control using feedforward control. Although this discussion pertains to SISO control, the algorithms and control architecture are extensible to MIMO control.

Description of Control Strategy.

Real-Time Control Processing The basic real-time controller structure is shown in Fig. 18.96. This is the compensator-regulator architecture that was introduced in Section 18.5, where the plant, designated as $P(\omega)$ in Fig. 18.96, is the transfer function between the output of the controller and the net force transmitted to the foundation.

The controller is implemented as a cascade of two filters because we wish to adapt the low-order regulation filter coefficients quickly to track changes in the center frequency of narrow-band components of the disturbance. At the same time, we choose to adapt the relatively high-order compensation filter at a slower rate to track changes in the plant transfer function.

Adaptation Processing The full functionality of the adaptive controller is shown in Fig. 18.97. The "concurrent adaptation processing" block provides two types of adaptation:

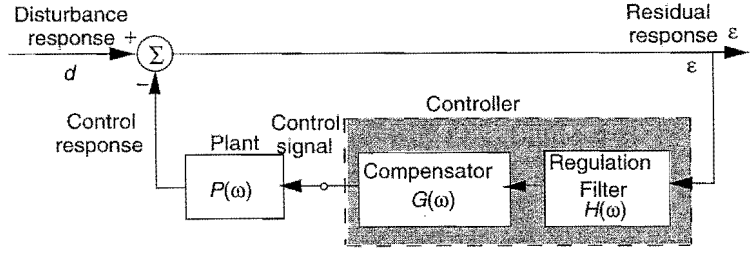


FIGURE 18.96 Feedback compensator regulator.

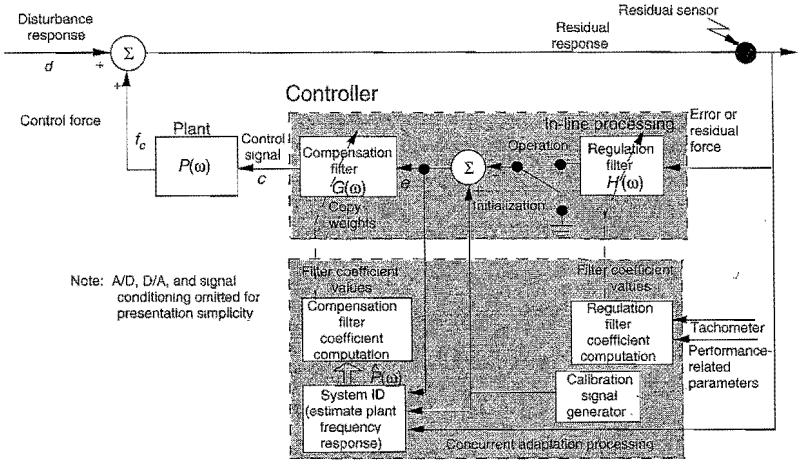


FIGURE 18.97 Controller functionality.

1. Variable narrow-band center frequency adaptation:
   - measurement via a tachometer (or other distinct speed or repetition rate measurement sensor) and a tracking filter of the center frequency of narrow-band response due to periodic excitation and
   - computation and updating of filter coefficients of the digital narrow-band regulation filters based on the currently measured center frequency and rate of change of the center frequency.
2. Variable plant adaptation:
   - system identification in the sense of plant frequency response estimation and
   - computation and updating of filter coefficients of the digital broadband compensation filter.

System identification is performed during closed-loop operation using the procedure outlined in Section 18.4. The major aspects of this procedure include (a) inserting a low-level calibration signal, which is uncorrelated with the external disturbance, into the compensation filter; (b) estimating the cross-spectra of the calibration signal with both the plant input and output; and (c) estimating the plant transfer function as the ratio of these two cross-spectra. Details of the processing of cross-spectra to estimate the plant as well as the design and injection of a covert probe signal are also discussed in Section 18.4 under System Identification.

The probe signal is sufficiently low in level that it does not add appreciably to the residual, and its bandwidth is matched to the full compensation band. Although it is low level, a good-quality estimate of the plant transfer function can be obtained with sufficient averaging time. In the performance plots that follow, estimates of the plant were updated approximately every 2 min.

Since we are concerned with a lightly damped mechanical structure and relatively large compensation bandwidths (e.g., 800 Hz), a FIR filter implementation of the compensation filters would have required a large number of coefficients. To reduce both the off-line and on-line computation load, we opted to use IIR filters designed by a multistep Yule–Walker method.

Hardware Description. Figure 18.98 presents a block diagram of the controller hardware. The algorithmic functionality of the controller is performed by four TMS320C30 DSP chips operating in parallel. The allocation of controller functionality to the individual DSP processors can be summarized as follows:

In-Line Processor. Performs the digital filtering of the regulation and compensation filters for the in-line data path.

Desamp Processor. Responsible for all off-line tasks associated with generating the desampled data buffers presented to the system identification algorithm. Replication filters and reference signal processing are also performed in this processor.

Sys_ID Processor. Performs the system identification and compensation filter weight algorithms. The compensation filter weights are then copied to the in-line processor.

Monitor Processor. Collects data from the other processors and uploads data to the host for monitoring and evaluating system performance.

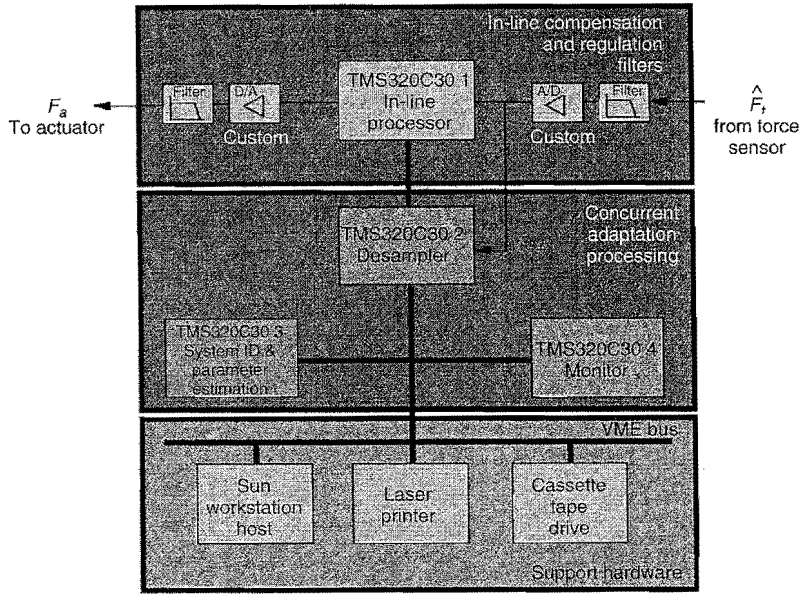


FIGURE 18.98 Controller hardware block diagram.

The controller implementation included custom-built A/D and D/A converter boards plus a logic controller board. The controller board provided a high-speed two-way interface between the DSP processors and the A/D and D/A boards. Two Sky Challenger boards, each of which contain two TMS320C30 chips per board, communicated with each other and the host computer over the VME bus and provide up to 132 Mflop computation rate. A SPARC workstation was chosen as the host computer.

Performance Example. The controller was connected to a prototype active/passive machinery mount located between one leg of a 1300-lb, 140 brake horsepower (BHP) at 2800 rpm, Detroit Diesel model 4–53 engine and a representative complex foundation structure. A picture of the active/passive mount and a schematic of the system are shown in Fig. 18.99. A detailed discussion of the engine, active/passive mount design, and test rig can be found in reference 88.

The test objectives were to provide at least 15 dB of narrow-band regulation at the fundamental and next four harmonics of the piston-firing frequency. In

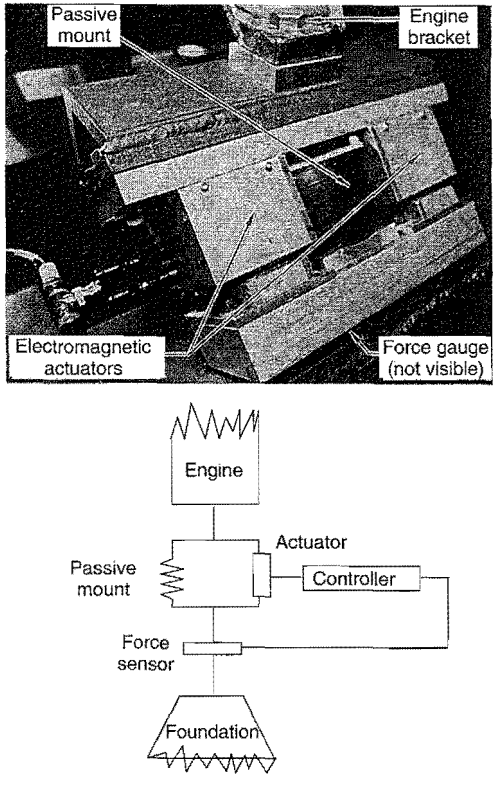


FIGURE 18.99 Active/passive mount and schematic of system.

addition, 10 dB of broadband regulation was desired over the frequency interval from 10 to 80 Hz while maintaining noise amplification below 5 dB outside the regulation bandwidth. To meet these objectives, a compensation bandwidth of 833 Hz and the system sample rate of 10 kHz were chosen. Latency of the digital system (including delay associated with the sample-and-hold on the D/A converter) was 60 μs.

The closed-loop performance of the active isolation system is shown in Fig. 18.100. This plot presents the ratio of the open- to closed-loop residual force transmitted into the foundation structure. As shown in this figure, narrow-band reductions in excess of 15 dB are achieved at the first five piston-firing tonals. In addition, approximately 10 dB of broadband regulation is achieved from about 15 to 80 Hz, which spans most of the frequency interval containing the tonals. Finally, this performance is achieved while limiting noise amplification to approximately 5 dB outside the regulation bandwidth. The very fine structure at higher frequencies of the measured ratio of open- to closed-loop forces, which sometimes goes below −5 dB, is due to harmonic distortion of the actuators (which were being driven very hard), rather than any shortcoming of the control processor.

Active Control of Airborne Noise in a High-Speed Patrol Craft

The Navy's new high-speed patrol crafts are powered by four main propulsion diesel engines that deliver a total of 13,000 shaft horsepower to a set of four propulsion shafts. The operation of these engines produces propeller blade rate tonal noise and broadband cavitation noise that propagate through the hull, producing high noise levels in the aft-crew berthing compartment, which is located

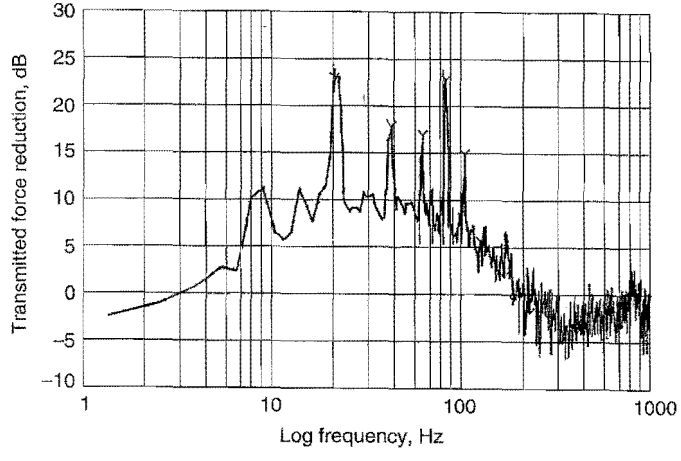


FIGURE 18.100 Reduction of transmitted force into foundation for active/passive mount relative to passive mount.

just forward of the propellers. Although extensive passive noise control treatments have been applied to reduce the noise in this compartment (including floating floors, double bulkheads, and constrained-layer damping), the 63- and 125-Hz octave-band and overall (dBA) airborne noise levels exceeded the Navy's acoustical habitability specifications. Table 18.5 compares measured third-octave-band and overall sound levels in the aft-crew berthing compartment for the first three ships of the class to the noise specification limits.[89] These measurements indicated that reductions in the 63- and 125-Hz octave bands were necessary to reduce overall A-weighted noise to acceptable levels.

To address this problem, several options were explored for reducing the low-frequency noise in the aft-crew compartment. Because passive treatments are least effective in this frequency region, several active noise and vibration control concepts were evaluated. These concepts included methods for both global and local control, using feedforward and feedback control strategies, and with digital and analog control hardware. To assess the benefits of each approach, a set of acoustical trials were conducted initially to measure the operational noise characteristics, path transfer functions, and compartment acoustical characteristics. These data were used to simulate performance of the various control options.

The approach chosen for implementation was local control of the sound field near the head of each bunk using a SISO feedback control strategy. This approach creates an effective "zone of silence" in the immediate vicinity of the occupant's head. This approach is shown schematically in Fig. 18.101. Laboratory simulations using measured data and a mock-up of one rack of bunks suggested that the necessary reductions at the occupant's head location could be achieved using this approach.

The active noise control system for a single bunk is contained within a single prismatic-shaped enclosure that is located in the upper corner of the bunk above and behind the occupant's head. Each unit contains a loudspeaker to create the cancellation noise, a pair of microphones to sense the noise field to be controlled, and a microprocessor to compute the cancellation signal in real time. The control algorithm implemented on the microprocessor was an adaptive feedback algorithm (based on the adaptive Youla transform discussed in Section 18.5) to reduce both narrow-band and broadband noise. The reading light originally placed in this location was incorporated into the active noise control (ANC) enclosure design.

TABLE 18.5 Average Aft Crew Berthing Octave-Band and A-Weighted Noise Levels at Full-Speed[89]

	31.5 Hz	63 Hz	125 Hz	250 Hz	A-Weighted
Noise Specification	105	100	95	90	82
Ship 1	98	113	100	88	87
Ship 2	97	104	94	85	85
Ship 3	95	111	96	86	86

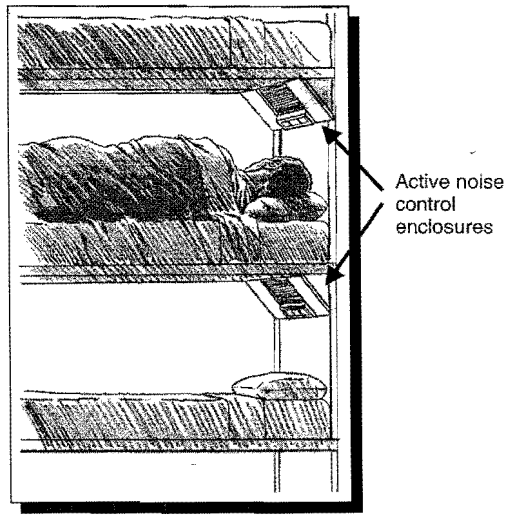


FIGURE 18.101 Schematic of active zone-of-silence approach.

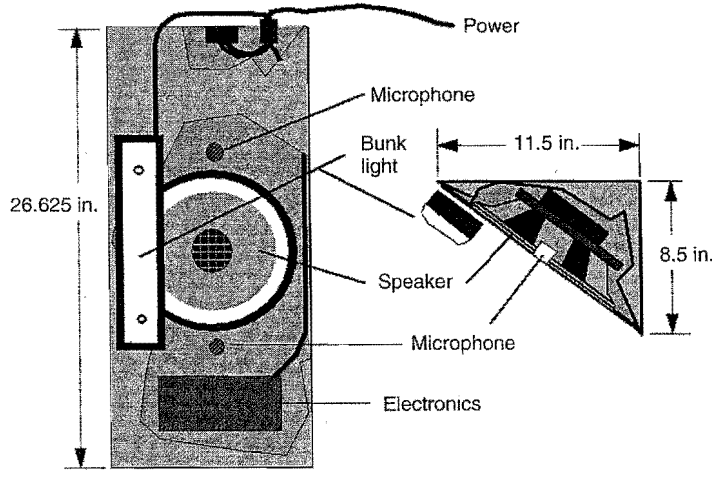


FIGURE 18.102 Components of the ANC enclosure.

The components of the ANC enclosure are illustrated in Fig. 18.102. Pictures of the actual implementation are contained in Figs. 18.103 and 18.104.

The prototype control system described above was evaluated during underway testing. A narrow-band plot of the measured noise reduction at the occupant's head location (not at the control microphones, where greater reductions were achieved) is shown in Fig. 18.105. This plot compares the noise spectra obtained

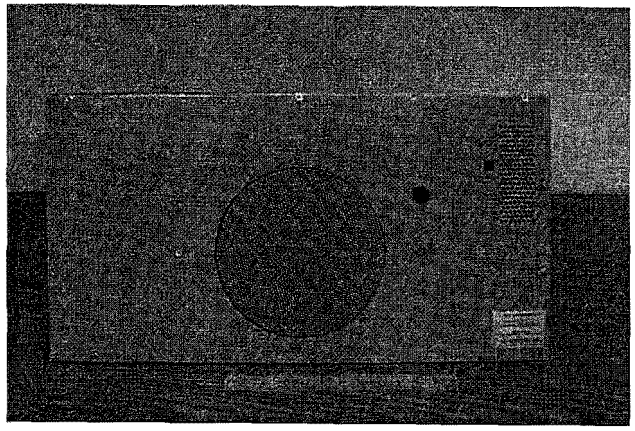


FIGURE 18.103 Faceplate of the ANC enclosure (integrated reading light not shown).

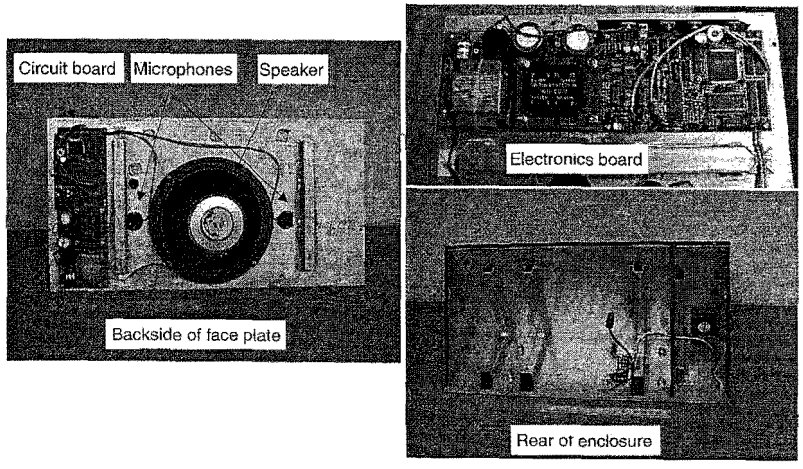


FIGURE 18.104 Pictures of the internal components of the ANC enclosure.

during full-speed operation when the control system was turned *off* to that when the control system was turned *on*. As shown in this plot, reductions at the dominant blade-rate tonals (at approximately 60 Hz) were greater than 15 dB, while 7–10 dB of broadband noise reduction was achieved between 30 and 85 Hz. Third-octave-band performance is summarized in Fig. 18.106. This summary shows that the system reduced the third-octave-band levels to below the limits of the Navy's acoustical habitability specifications, the goal of the program. Based on extensive testing of the prototype system on one patrol craft, the Navy contracted for production units for the entire class of PC1 patrol craft.

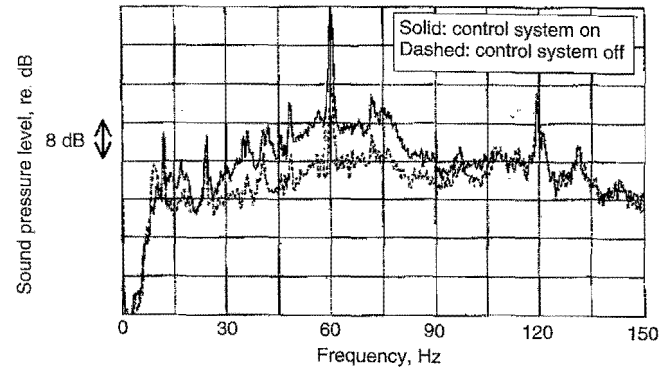
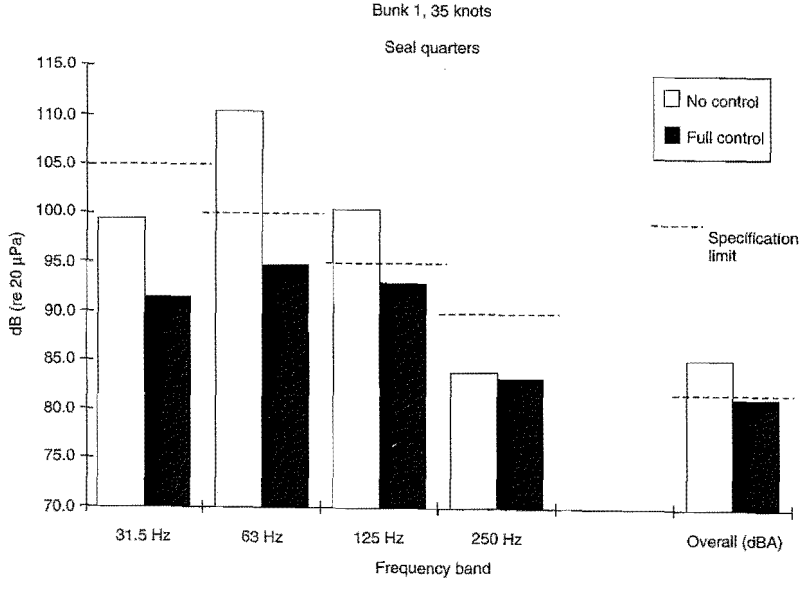


FIGURE 18.105 Narrow-band plot of noise reduction at occupant's head location during full-speed operation.



Acoustical data, dB re 20 μPa

Octave band	No control	Control	Attenuation
31.5	99.5	91.5	8
63	110.5	95	15.5
125	100.5	93	7.5
250	84	83.5	0.5
Overall dBA	85.5	81.5	4

FIGURE 18.106 Summary of third-octave-band performance at occupant's head location.

REFERENCES

1. W. B. Conover, "Fighting Noise with Noise," *Noise Control*, **2**, 78–82 (1956).
2. W. B. Conover and R. J. Ringlee, "Recent Contributions to Transformer Audible Noise Control," *Trans. AIEE Pt. III Power Apparatus and Systems*, **74**, 77–90 (1955).
3. K. Kido, "Reduction of Noise by Use of Additional Noise Sources," *Proc. Internoise 75*, 1975, pp. 647–650.
4. G. B. B. Chaplin and R. A. Smith, "The Sound of Silence," *Engineering*, **218**, 672–673 (1978).
5. L. A. Blondel and S. J. Elliott, "Tuned Loudspeaker Enclosures for Active Noise Control," paper presented at Internoise 96, International Congress on Noise Control Engineering, Liverpool, United Kingdom, July 30–August 2, 1996. Proceedings, pp. 1105–1108; Abstract, p. 67.
6. G. J. Stein, "A Driver's Seat with Active Suspension of Electro-pneumatic Type," *ASME J. Vib. Acoust.*, **119**, 230–235 (1997).
7. J. der Hagopian, L. Gaudiller, and B. Maillard, "Hierarchical Control of Hydraulic Active Suspensions of a Fast All-Terrain Military Vehicle," *J. Sound Vib.*, **222**, 723–752 (1999).
8. A. K. Abu-Akeel, "The Electrodynamic Vibration Absorber as a Passive or Active Device," ASME Paper 67-Vibr-18, *ASME J. Eng. Ind.*, **89**, 741–753 (1967).
9. S. Ikai; K. Ohsawa, K. Nagaya, and H. Kashimoto, "Electromagnetic Actuator and Stacked Piezoelectric Sensors for Controlling Vibrations of a Motor on a Flexible Structure," *J. Sound Vib.*, **231**, 393–409 (2000).
10. S. W. Sirlin and R. A. Laskin, "Sizing of Active Piezoelectric Struts for Vibration Suppression on a Space-Based Interferometer," paper presented at the First Joint U.S./Japan Conference on Adaptive Structures, Maui, HI, November 13–15, 1990. Proceedings, pp. 47–63.
11. P. K. C. Wang, "Feedback Control of Vibrations in a Micromachined Cantilever Beam with Electrostatic Actuators," *J. Sound Vib.*, **213**, 537–550 (1998).
12. D. L. Hall and A. B. Flatau, "Broadband Performance of a Magnetostrictive Shaker," in C. J. Radcliffe, K.-W. Wang, H. S. Tzou, and E. W. Hendricks (Eds.), *Active Control of Noise and Vibration*. Papers presented at the ASME Winter Annual Meeting, Anaheim, CA, November 8–13, 1992.*ASME Book DSC-Vol. 38*, pp. 95–104, American Society of Mechanical Engineers, New York.
13. B-T. Wang, R. A. Burdisso, and C. R. Fuller, "Optimal Placement of Piezoelectric Actuators for Active Structural Acoustic Control," *J. Intelligent Material Syst. Struct.*, **5**, 67–77 (1994).
14. G. E. Warnaka, "Active Attenuation of Noise—The State-of-the-Art," *Noise Control Eng.*, May/June 1982, pp. 100–110.
15. D. Guicking, *Active Noise and Vibration Control Reference Bibliography*, 3rd ed., Dritte Physicalisches Institut, University of Göttingen, Göttingerm 1988 and 1991 supplement.
16. S. J. Elliott and P. A. Nelson, "Active Noise Control," *IEEE Signal Process. Mag.*, October 1993, pp. 12–35.
17. C. Fuller, "Active Control of Sound and Vibration," tutorial lecture presented at the 120th Acoustical Society of America Meeting, San Diego, November 26, 1990.

18. H. Coanda, "Procédé de Protection Contre les Bruits," French Patent No. 722274, filed October 21, 1930, patented December 29, 1931, published March 15, 1932.
19. P. Lueg, "Process of Silencing Sound Oscillations," U. S. Patent 2,043,416, June 19, 1936.
20. M. A. Swinbanks, "The Active Control of Sound Propagation in Long Ducts," *J. Sound Vib.*, **27**(3), 411–436 (1973).
21. M. J. M. Jessel, "Sur les absorbeur actif," in *Proceedings of the sixth International Congress on Acoustics*, Paper F 5–6 82, Tokyo, 1968.
22. M. J. M. Jessel and G. Magiante, "Active Sound Absorbers in an Air Duct," *J. Sound Vib.*, **23**, 383–390 (1972).
23. H. G. Leventhall, "Developments in Active Attenuators," in *Proceedings of the 76 Noise Control Conference*, Warsaw, Poland, 1976, pp. 175–180.
24. G. Canevet, "Active Sound Absorption in an Air Conditioning Duct," *J. Sound Vib.*, **58**, 333–345 (1978).
25. L. J. Eriksson, M. C. Allie, and R. A. Greiner, "The Selection and Application of IIR Adaptive Filter for Use in Active Sound Attenuation," *IEEE Trans. Acoust. Speech Signal Process.*, **ASSP-35**, 433–437 (1987).
26. L. J. Eriksson and M. C. Allie, "A Digital Sound Control System for Use in Turbulent Flows," Paper presented at NOISE-CON 87, National Conference on Noise Control Engineering, State College, PA, June 8–10, 1987. Proceedings, pp. 365–370.
27. L. J. Eriksson and M. C. Allie, "A Practical System for Active Attenuation in Ducts," *Sound Vib.*, **22**(2), 30–34 (February 1988).
28. L. J. Eriksson, "The Continuing Evolution of Active Noise Control with Special Emphasis on Ductborne Noise," in C. A. Rogers and C. R. Fuller (Eds.), *Proceedings of the First Conference on Recent Advances in Active Control of Sound and Vibration*, Blacksburg, VA, April 15–17, 1991, pp. 237–245.
29. H. F. Olsen and E. G. May, "Electronic Sound Absorber," *J. Acoust. Soc. Am.*, **25**, 1130–1136 (1953).
30. D. C. Perry, S, J, Elliott, I. M. Stothers, and S. J. Oxley, "Adaptive Noise Cancellation for Road Vehicles," in *Proceedings of the Institution of Mechanical Engineers Conference on Automotive Electronics*, 1989, pp. 150–163.
31. S. Hasegawa, T. Tabata, A. Kinsohita, and H. Hyodo, "The Development of an Active Noise Control System for Automobiles," SAE Technical Paper Series, Paper No. 922087, Society of Automotive Engineers, Warrendale, PA. 1992.
32. R. J. Bernhard, "Active Control of Road Noise Inside Automobiles," in *Proceedings of ACTIVE 95, The 1995 International Symposium on Active Control of Sound and Vibration*, Newport Beach, CA, July 6–8, 1995, pp. 21–32
33. S. J. Elliott, P. A. Nelson, T. J. Sutton, A. M. McDonald, D. C. Quinn, I. M. Stothers, and I. Moore, "The Active Control of Low Frequency Engine and Road Noise Inside Automotive Interiors," Paper presented at ASME Winter Annual Meeting, Session NCA-8, Dallas, TX, Nov. 25–30, 1990. Proceedings, pp. 125–129.
34. W. Dehandschutter, R. Van Cauter, and P. Sas, "Active Structural Acoustic Control of Structure Borne Road Noise: Theory, Simulations, and Experiments," in S. D. Sommerfeldt and H. Hamada (Eds.), *Proceedings of ACTIVE 95, The 1995 International Symposium on Active Control of Sound and Vibration*, Newport Beach, CA, July 6–8, 1995, pp. 735–746.

35. S. J. Elliott, P. A. Nelson, and I. M. Stothers, "In Flight Experiments on the Active Control of Propeller Induced Cabin Noise," *J. Sound Vib.*, **140**, 219–238 (1990).

36. C. F. Ross and M. R. J. Purver, "Active Cabin Noise Control," in S. J. Elliott and G. Horváth (Eds.), *Proceedings of ACTIVE 97, The 1997 International Symposium on Active Control of Sound and Vibration*, Budapest, Hungary, August 21–23, 1997, pp. 39–46.

37. G. P. Mathur, B. N. Tran, and M. A. Simpson, "Active Structural Acoustic Control of Aircraft Cabin Noise Using Optimized Actuator Arrays—Laboratory Tests," AIAA Paper 95-082, presented at the First Joint CEAS/AIAA Aeroacoustics Conference (AIAA 16th Aeroacoustics Conference), München, DE, June 12–15, 1995.

38. M. A. Simpson, T. M. Luong, M. A. Swinbanks, M. A. Russell, and H. G. Leventhall, "Full Scale Demonstration Tests of Cabin Noise Reduction Using Active Noise Control," Paper presented at Internoise 89, International Congress on Noise Control Engineering, Newport Beach, CA, December 4–6, 1989. Proceedings, pp. 459–462.

39. P. D. Wheeler, "The Role of Noise Cancellation Techniques in Aircrew Voice Communications Systems," in *Proceedings of the Royal Aeronautical Society Symposium on Helmets and Helmet Mounted Devices*, 1987.

40. I. Veit, "Noise Gard—An Active Noise Compensation System for Headphones and Headsets," NATO Research Study Group (RSG) 11, Panel 3: Proceedings of the Workshop on Active Cancellation of Sound and Vibration, 22nd Meeting, Vicksburg, MS, October 31, 1990, and 23rd Meeting, Bremen, DE, June 5, 1991, pp. 164–167.

41. B. Rafaely and M. Jones, "Combined Feedback-Feedforward Active Noise-Reducing Headset—The Effect of the Acoustics on Broadband Performance," *J. Acous. Soc. Am.*, **112**, 981–989 (2002).

42. K. D. LePage, P. J. Remington, and A. R. D. Curtis, "Reference Sensor Selection for Automotive Active Noise Control Applications," Paper presented at 130th Meeting of the Acoustical Society of America, Adam's Mark Hotel, St. Louis, MO, November 27–December 1, 1995.

43. P. Remington, D. Sutliff, and S. Sommerfeldt, "Active Control of Low Speed Fan Tonal Noise Using Actuators Mounted in Stator Vanes Part 1: Control System Design and Implementation," Paper No. AIAA-2003-3191, presented at the AIAA/CEAS Aeroacoustics Conference, Hilton Head, SC, 2003.

44. D. Sutliff, P. Remington, and B. Walker, "Active Control of Low Speed Fan Tonal Noise Using Actuators Mounted in Stator Vanes Part 3: Results," Paper No. AIAA-2003-3193, presented at the AIAA/CEAS Aeroacoustics Conference, Hilton Head, SC, 2003.

45. A. R. D. Curtis, "Active Control of Fan Noise by Vane Actuators," BBN Report 1193, BBN Technologies, Cambridge, MA, 1998.

46. P. Joseph, P. A. Nelson, and M. J. Fisher, "Active Control of Turbofan Radiation Using an In-Duct Error Sensor Array," in S. J. Elliott and G. Horvath (Eds.), *Proceedings of ACTIVE 97, the 1997 International Symposium on Active Control of Sound and Vibration*, Active 97, Budapest, Hungary, August 21–23, 1997, pp. 273–286.

47. R. H. Thomas, R. A., Burdisso, C. R. Fuller, and W. F. O'Brien, "Active Control of Fan Noise from a Turbofan Engine," *AIAA J.*, **32**(1), 23–30 (1994).

48. R. A. Burdisso, R. H. Thomas, C. R. Fuller, and W. F. O'Brien, "Active Control of Radiated Inlet Noise from Turbofan Engines," in *Proceedings of the 2nd Conference on Recent Advances in Active Control of Sound and Vibration*, Blacksburg, VA, April 28–30, 1993, pp. 848–860.

49. R. G. Gibson, J. P. Smith, R. A. Burdisso, and C. R. Fuller, "Active Reduction of Jet Engine Exhaust Noise," Paper presented at Internoise 95, International Congress on Noise Control Engineering, Newport Beach, CA, July 10–12, 1995. Proceedings, pp. 518–520.

50. J. P. Smith, R. A. Burdisso, and C. R. Fuller, "Experiments on the Active Control of Inlet Noise from a Turbofan Jet Engine Using Multiple Circumferential Control Arrays," AIAA Paper 96–1792, presented at the 2nd AIAA/CEAS Aeroacoustics Conference, State College, PA, May 6–8, 1996.

51. H. F. Olsen, "Electronic Control of Noise, Vibration and Reverberation," *J. Acoust. Soc. Am.*, **28**, 966–972 (1956).

52. E. F. Berkman, "An Example of a Fully Adaptive Integrated Narrowband/Broadband SISO Feedback Controller for Active Vibration Isolation of Complex Structures," Paper presented at the ASME Annual Meeting, November 1992.

53. J. Scheuren, "Principles, Implementation and Application of Active Vibration Isolation," Paper C3, presented at the International Workshop on Active Control of Noise and Vibration in Industrial Applications, CETIM, Senlis, France, April 9–12, 1996.

54. P. Gardonio and S. J. Elliott, "Active Control of Structural Vibration Transmission between Two Plates Connected by a Set of Active Mounts," Proceedings of ACTIVE 99, Paper presented at the 1999 International Symposium on Active Control of Sound and Vibration, Ft. Lauderdale, FL, December 2–4, 1999, pp. 118–128

55. A. H. von Flotow, "An Expository Overview of Active Control of Machinery Mounts," Paper presented at the 27th IEEE Conference on Decision and Control (CDC), Austin, TX, December 7–9, 1988. Proceedings, Vol. 3, pp. 2029–2032.

56. P. A. Nelson and S. J. Elliott, *Active Control of Sound*, Academic, San Diego, CA, 1992.

57. A. V. Oppenheim and R. W. Schafer, *Digital Signal Processing*, Prentice-Hall, Englewood Cliffs, NJ, 1975.

58. S. J. Elliott, *Signal Processing for Active Control*, Academic, San Diego, CA, 2001.

59. B. Widrow and S. D. Stearns, *Adaptive Signal Processing*, Prentice-Hall, Englewood Cliffs, NJ, 1985.

60. G. H. Golob and C. F. Van Loan, *Matrix Computations*, Johns Hopkins University Press, Baltimore, MD, 1983.

61. L. J. Eriksson and M. J. Allie, "Use of Random Noise for On-Line Transducer Modeling in an Adaptive Active Attenuation System," *J. Acoust. Soc. Am.*, **85**, 797–802 (1989).

62. L. J. Eriksson, "Active Sound Attenuation System with On-Line Adaptive Feedback Cancellation," U. S. Patent 4,677,677, June 30, 1987.

63. L. J. Eriksson, "Active Attenuation System with On-Line Modeling of Speaker, Error Path and Feedback Path," U. S. Patent 4,677,676, June 30, 1987.

64. D. R. Morgan, "An Analysis of Multiple Correlation Cancellation Loops with a Filter in the Auxiliary Path," *IEE Trans. Acoust. Speech Signal Process.*, **ASSP-28**, 454–467 (1980).

65. B. Widrow, D. Shur, and S. Shaffer, "On Adaptive Inverse Control," in *Proceeding of the 15th ASILOMAR Conference on Circuits, Systems and Computers*, Pacific Grove, CA, November 9–11, 1981, pp. 185–195.

66. J. C. Burgess, "Active Adaptive Sound Control in a Duct: A Computer Simulation," *J. Acoust. Soc. Am.*, **70**, 715–726 (1981).

67. S. J. Elliott and P. A. Nelson, "Algorithm for Multi-Channel LMS Adaptive Filtering," *Electron. Lett.*, **21**, 978–981 (1985).

68. C. C. Boucher, S. J. Elliott, and P. A. Nelson, "The Effects of Errors in the Plant Model on the Performance of Algorithms for Adaptive Feedforward Control," *Proc. IEE-F*, **138**, 313–319 (1991).

69. K. J. Astrom and B. Wittenmark, *Adaptive Control*, Addison-Wesley, Reading, MA, 1989.

70. R. B. Coleman, E. F. Berkman, and B. G. Watters, "Optimal Probe Signal Generation for On-Line Plant Identification within Filtered-X LMS Controllers," paper presented at the ASME Winter Annual Meeting 1994, Chicago, IL, November 1994.

71. R. B. Coleman and E. F. Berkman, "Probe Shaping for On-line Plant Identification," in *Proceedings of ACTIVE 95, the 1995 International Symposium on Active Control of Sound and Vibration*, Newport Beach, CA, July 6–8, 1995.

72. R. B. Coleman, B. G. Watters, and R. A. Westerberg, "Active Noise and Vibration Control System Accounting for Time Varying Plant, Using Residual Signal to Create Probe Signal," U.S. Patent 5,796,849, August 18, 1998.

73. I. Gustavsson, L. Lyung, and T. Soderstrom, "Survey Paper: Identification of Processes in Closed Loop—Identifiability and Accuracy Aspects," *Automatica*, **13**, 59–75 (1977).

74. E. F. Berkman, R. B. Coleman, B. Watters, R. Preuss, and N. Lapidot, "An Example of a Fully Adaptive Integrated Narrowband/Broadband SISO Feedback Controller for Active Vibration Isolation of Complex Structures," paper presented at the ASME Annual Meeting, New York November 1992.

75. A. R. D. Curtis, E. F. Berkman, R. B. Coleman, and R. Preuss, "Controller Strategies for Fully Adaptive Integrated Narrowband and Broadband Feedback Control for Active Vibration Isolation of Complex Structures," in *Active Control of Noise and Vibrations in Industrial Applications*, CETIM, Senlis, France, April 1996.

76. E. F. Berkman and E. K. Bender, "Perspectives on Active Noise and Vibration Control," *Sound Vib.*, 30th anniversary issue, January 1997.

77. R. D. Preuss, "Methods for Apparatus Designing a System Using the Tensor Convolution Block Toeplitz Preconditioned Conjugate Gradient Method," U. S. Patent 6,487,524 B1, November 26, 2002.

78. M. Athans and P. L. Falb, *Optimal Control: An Introduction to the Theory and Its Application*, McGraw-Hill, New York, 1966.

79. H. Kwakernaak and R. Sivan, *Linear Optimal Control Systems*, Wiley-Interscience, New York, 1972.

80. M. A. Dahleh and I. J. Diaz-Bobillo, *Control of Uncertain Systems*, Prentice-Hall, Englewood Cliffs, NJ, 1995.

81. K. Zhou and J. C. Doyle, *Essentials of Robust Control*, Prentice-Hall, Upper Saddle River, NJ, 1998.

82. J. E. Gibson, *Nonlinear Automatic Control*, McGraw-Hill, New York, 1963.

83. L. P. Heck, J. A. Olkin, and H. Naghshineh, "Transducer Placement for Broadband Active Vibration Control Using a Novel Multidimensional QR Factorization," *ASME J. Vib. Acoust.*, **120**, 663–670 (1997).

84. R. D. Preuss and B. Musicus, "Digital Filter and Control System Employing Same," U.S. Patent 5,983,255, awarded November 9, 1999.

85. P. J. Remington and M. J. Rudd. "An Assessment of Railroad Locomotive Noise," Report No. DOT-TSC-OST-76-4/FRA-OR&D-76-142, U.S. Department of Transportation, Washington, DC, August 1976.

86. P. J. Remington, S. Knight, D. Hanna, and C. Rowley, "A Hybrid Active-Passive System for Controlling Locomotive Exhaust Noise," Paper No. IN2000/0035, presented at Internoise 2000, Nice, France, 2000.

87. P. J. Remington, S. Knight, D. Hanna, and C. Rowley, "A Hybrid Active/Passive Exhaust Noise Control System (APECS) for Locomotives," BBN Report No. 8302, BBN Technologies, Cambridge, MA, March 29, 2001.

88. B. G. Watters et al., "A Perspective on Active Machinery Isolation," in *Proceedings of 27th Conference on Decision and Control*, Austin, TX, December 1988.

89. M. Dignan et al., "The Active Control of Airborne Noise in a High Speed Patrol Craft," paper presented at Noise-Con 94, Ft. Lauderdale, FL, May 1994.

CHAPTER 19

Damage Risk Criteria for Hearing and Human Body Vibration

SUZANNE D. SMITH

Air Force Research Laboratory
Wright-Patterson Air Force Base, Ohio

CHARLES W. NIXON

Consultant
Kettering, Ohio

HENNING E. VON GIERKE

Consultant
Yellow Springs, Ohio

19.1 INTRODUCTION

Noise and vibration are closely related biodynamic environments in terms of their origins, manifestations, and effects on people. Those effects on people that are undesirable are often threatening, induce fatigue, compromise working performance, modify physiological responses, and harm human systems. At the present time, avoidance of excessive noise and vibration exposure is the only assured way to prevent these major hazardous effects.

The practical alternative to complete avoidance is to limit exposures in these environments to those defined as acceptable by appropriate standards, guidelines, and damage risk criteria. Scientific exposure guidelines and criteria established to curtail these effects are vital parts of comprehensive protection programs of concern to governments, industry, and affected personnel. Most adverse effects of these commonly encountered mechanical forces on human systems can be minimized and controlled through engineering and design efforts. Central to these programs and actions are guidelines and criteria that describe potential damage risk and/or establish acceptable exposure limits.

Criteria and limits define conditions above which the risk of damage due to an exposure is considered substantial or unacceptable. Noise and vibration criteria describe exposure characteristics and corresponding undesirable effects such as noise-induced hearing loss, vibration-induced hand–arm vibration syndrome

(HAVS), and vibration-related spinal injury. Damage risk criteria have been developed and implemented worldwide. The basic exposure–effects relationships that underlie these criteria are reasonably well understood and are derived from observations and experience as well as good laboratory and field studies. The various criteria contain different limiting values because of variations in interpretations of the basic data and in the rationale used to establish them. The rationale may include practical, legal, and economic considerations as well as humanitarian concerns. It is very important that the rationale underlying damage risk criteria is fully understood by the user to ensure that the application is justified and accurate.

Estimates of noise and vibration exposures and of their probable effects on populations are usually expressed in terms of population distribution statistics. These group population effects are not precise descriptors, and they are not appropriate for evaluating an individual. Nevertheless, they are adopted by nations and incorporated into national regulations and laws. Many become mandatory requirements included in governmental and industrial activities involving exposure of people to noise and vibration environments.

This chapter presents contemporary regulatory and voluntary noise and vibration exposure standards and criteria along with background information that will facilitate their understanding and application in engineering control and design.

19.2 DAMAGE RISK CRITERIA FOR THE AUDITORY RANGE

Noise Factor

Permanent hearing loss and its associated problems are clearly the most critical and widespread of the various consequences of excessive noise exposure. The extent of damage to the hearing mechanism caused by noise is related to the amount of acoustical energy reaching the hearing mechanism. Such damage cannot be estimated accurately for an individual because of the variability of the noise and the susceptibility of the exposed ears. The primary factors in noise-induced hearing loss are the level of the noise, the frequency content or spectrum of the noise, the duration or time course of the noise exposure, and the susceptibility of the ear.

Exposure limits are defined in terms of level, spectrum, and duration of the noise. A-weighted sound energy of an exposure is directly related to noise-induced hearing loss. No other measure of noise exposure provides a better *cause–effect* relationship with hearing loss.[1] Impulse noise is also included in this measure for many criteria, as was concluded by a special workshop on impulse noise.[2] It was agreed that there is no convincing evidence against acceptance of A-weighting measurement of all noises from 20 to 20,000 Hz in determining their permanent threshold shift (noise-induced hearing loss that does not recover to preexposure levels after cessation of exposures) hazard except when their unweighted, instantaneous, peak-sound-pressure levels exceed approximately 145 dB. Consequently, exposures are typically described in terms of the average A-weighted levels, or the equivalent continuous A-weighted sound pressure level (L_{eq}), over an average workday.

Practical measures for the prevention of noise-induced hearing loss are centered in hearing conservation programs. These programs involve definitions of acceptable noise exposure, personal hearing protection, monitoring the hearing of the affected personnel, and appropriate administrative actions to minimize and eliminate identified temporary hearing problems before they become permanent. The basis of a hearing conservation program is the definition of acceptable noise exposure or exposure criteria that specify the acceptable exposure limits and the proportion of the population to be protected. The criteria of various hearing conservation programs and applications differ in their limiting values.

The parameters of particular exposure criteria are selected to satisfy the needs of the user. Factors that may influence these selections are various interpretations of available data, policies or requirements of organizations, and the remaining uncertainty in the noise exposure–hearing loss databases. Consequently, criteria may differ in such features as estimates of beginning hearing loss, corrections for nonnoise effects such as aging, percentage of the population to be protected, and the extent of protection to be provided.

The most obvious differences among noise exposure criteria are the sound level at which the implementation occurs and how the duration of the exposure and the sound level of the noise are combined.[3] The duration–sound level relationships are referred to as time–intensity trading rules, which assume that damage to hearing is related to total A-weighted sound level and the duration of exposure time. The equal energy relationship between these parameters results in the 3-dB rule. This and other relationships are shown in Table 19.1 which displays permissible noise exposures in A-weighted sound pressure levels for the cited criteria. The permissible A-weighted level for an 8-h exposure ranges from 75 dBA for the Environmental Protection Agency (EPA) to 90 dBA for the Occupational Safety and Health Administration (OSHA).

Most criteria utilize the 3-, 4-, or 5-dB rule. The 3-dB rule is based on the equal-energy concept and is the most conservative or protective of the three rules. The 4- and 5-dB rules assume that intermittency and interruptions of exposures reduce the risk to less than that expected from the total energy. Consequently, a 50% increase in exposure duration corresponds to sound-level decreases of 3 and 5 dB for the respective 3- and 5-dB rules (Table 19.1). Intermittency of exposure is discussed later in the chapter.

Hearing Sensitivity

The human ear is sensitive to a much wider range of sounds than the generally cited 20 Hz–20 kHz audio frequency range. A compilation of independent measurement studies by several investigators using a wide variety of instrumentation and methodologies shows very good agreement and provides confidence in the data summarized in Fig. 19.1 Infrasound (<20 Hz) and ultrasound (traditionally >20,000 Hz but practically above about 12,000 Hz) are normally detected by the ear only at very high sound pressure levels. The traditional audio frequency

TABLE 19.1 Equal Energy and Other Trading Rules Used to Define Permissible Noise Exposures in A-Weighted Sound Pressure Level (dBA) and Exposure Time (h)

Duration of Exposure (h)	Equal Energy[a]	OSHA	EPA	NIOSH[b]	Army	Navy	Air Force	Music
24								
16								
8	90	90	75[c]	85	85	84	85	
4	93	95		88	88	88	88	
2	96	100		91	91	92	91	94[d]
1	99	105		94	94	96	94	
0.5	102	110		97	97	100	97	
0.25	105	115[e]		100	100	104	100	

[a]Equal energy rule of 3-dB decrease for doubling of exposure applied to a basic 8-h criterion of 90 dBA.
[b]National Institute of Occupational Safety and Health.
[c]Threshold for detectable noise-induced permanent threshold shift (NIPTS) at 4000 Hz: exposures exceeding 75 dBA may cause NIPTS exceeding 5 dB in 100% of the population after cumulative noise exposure of 10 years.
[d]Time-averaged A-weighted sound level, in dB, over a 2-h period once a week.
[e]Ceiling on exposure level and duration.

region (20 Hz–20 kHz) is well defined for stimuli including discrete tones, bands of noise, speech materials, loudness, comfort, and acceptibility. These databases provide the information necessary to support the development of noise exposure criteria.

The sensitivity of human hearing for high-frequency sounds (3000–4000 Hz and above) gradually decreases with advancing age. This process is called *presbyacusis*. Auditory system components are affected in both the peripheral and the central nervous systems. Although individual patterns of presbyacusis vary widely, normative data describing hearing sensitivity as a function of age have been compiled for various segments of society (some are reported in ref. 5). Loss of sensitivity due to accident, disease, or substances toxic to the auditory system is called *nosoacusis* while that attributed to the noises of everyday living is *sociacusis*. The major high-level noises to which people are exposed are the occupational environments.

Environmental noise occurs over the full spectrum to which the human auditory system is sensitive. Exposure to various segments of this sensory continuum produces differential effects on humans. Limiting levels and durations of acoustical exposure are defined for a number of specific portions of this spectrum, which include infrasound (0.5–20 Hz), audio frequencies (20 to about 12,000 Hz), ultrasound (12,000 to about 40,000 Hz), and impulsive sounds (characterized by rapid onset and durations of less than 1 s) described in terms of peak sound pressure level and duration. Some of these limits are well substantiated by experience and experimental evidence while others remain tentative until more evidence is available.

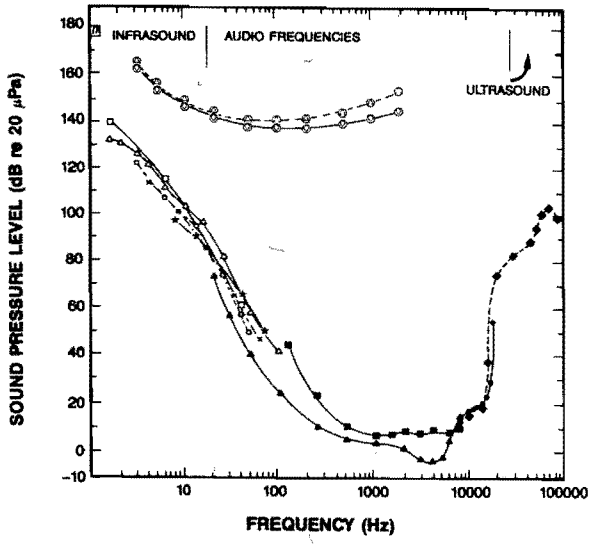


FIGURE 19.1 Human auditory sensitivity and pain thresholds for pure tones, octave bands of noise, and static pressure: (◬) BENOX (1953), pain MAP tones; (◬) pain static pressure; (◎) tickle, pain tones; (□) Bekesy (1960), MAP tones; (▲) ISO R226 (1961), MAF tones; (♦) Corso (1963) bone conduction minus 40-dB tones; (○) Yeowart, Bryan, and Tempest (1960), MAP tones; (×) MAP octave bands of noise; (■) standard reference threshold values (American National Standard on Specifications for Audiometers) (1969), MAP tones; (●) Northern et al. (1972), MAP tones; (△) Whittle, Collins, and Robinson (1972), MAP tones; (★) Yamada et al. (1986), MAF tones. (Data adapted from Ref. 4.) Minimum audible pressure (MAP) indicates that the sound was presented to the ears through earphones and the sound pressure levels were measured in an earphone–microphone coupler that approximated the cavity created by the earphone/pinna. Minimum audible field (MAF) indicates that the sound was presented to the listeners facing a loudspeaker and located in anechoic space. The sound pressure levels for MAF were measured at the location of the center of the head without the listener present. For the same listeners, MAP thresholds are generally several decibels higher than MAF thresholds.

19.3 AUDIO FREQUENCY REGION

CHABA

Noise exposure criteria for the audio frequency region (20–12,000 Hz) were developed by the National Academy of Sciences—National Research Council, Committee on Hearing, Bioacoustics and Biomechanics (CHABA) in 1965.[6] This method described noise exposure in terms of pure tones, third-octave, and octave bands of noise, and it includes the audio frequencies of 100–7000 Hz. Acceptable exposures to noise can be determined from 11 sets of curves. An environmental noise is considered acceptable if it produces, on average, a NIPTS after 10 years

or more of near daily exposure of no more than 10 dB at 1000 Hz and below, 15 dB at 2000 Hz, and no more than 20 dB at 3000 Hz and above. These criteria are based on the assumption that noise exposures producing temporary threshold shifts (TTSs) would eventually produce permanent threshold shifts (PTSs). The possible relationship that TTS is a precursor to PTS is still an open question. The CHABA criteria have been widely used and are an excellent tool. However, they are not simple to use or to relate to current standards, regulations, and guidelines and are less preferred than criteria employing A-weighted sound level.

OSHA

The Occupational Safety and Health Administration has adopted a noise exposure limit of 90 dBA with a 5-dB trading relationship to control excessive noise exposure in industry (Table 19.1). When employees are exposed to noise at different levels during the day, ratios of the actual to the allowed duration for that level are computed and the fractions summed for the day. Total daily exposure calculated from these fractions or ratios must not exceed unity. No other corrections or adjustments are applied to these criteria.

The OSHA noise exposure criteria were verified in 1983 with the publication of "Occupational Noise Exposure; Hearing Conservation Amendment; Final Rule."[7] The basic conditions of the original OSHA noise exposure regulation remain the same with a few exceptions. Continuous A-weighted sound levels are not permitted above 115 dBA regardless of duration. A permissible exposure level (PEL) is defined as that noise dose that would result from a continuous 8-h exposure to a sound level of 90 dBA. The limit of 90 dBA is a dose of 100%, which is the basic criterion level. A *time-weighted average* (TWA) is the sound level that would produce a given noise dose when the employee is exposed to that level continuously over an 8-h workday regardless of the length of the work shift. Workday exposures of 4 h at 90 dB, 8 h at 85 dB, or 12 h at 82 dB all correspond to a TWA of 85 dBA and a noise dose of 50%. The Hearing Conservation Amendment includes computational formulas and tables showing the time–intensity relationships for the 5-dB rule and conversions of dose to time-weighted averages. Guidance is given on calculations of age corrections to audiograms. However, the use of age correction procedures is not required for compliance.

A noise dose of 50% or a TWA of 85 dB is the "action level" at which hearing conservation measures must be implemented. All workers receiving noise doses at or above the action level must be included in a hearing conservation program that requires noise monitoring, audiometric testing, hearing protection, employee training, and record keeping. A baseline audiogram is one taken within six months of the employee's first exposure above the action level, against which subsequent audiograms can be compared. An annual audiogram must be taken for each employee exposed at or above the action level. A *standard threshold shift* (STS) is a change in hearing sensitivity from the baseline audiogram that exceeds an average of 10 dB or more at 2000, 3000, and 4000 Hz in either ear. Appropriate action by the employer must be taken in response to the STS to ensure the continued protection of the hearing of the employee.

Environmental Protection Agency

The EPA published "Information on Levels of Environmental Noise Requisite to Protect Public Health and Welfare with an Adequate Margin of Safety"[1] in 1974 in response to the Noise Control Act of 1972. The objective was to identify levels of environmental noise required to protect the public from adverse health and welfare effects. The levels for noise-induced hearing loss described in this document were based upon reviews and analyses of scientific materials as well as consultations and interpretations of experts. It was concluded that an L_{eq} of 70 dB over a 24-h day (over a 40-year working life) would protect virtually the entire population (96th percentile) for hearing conservation purposes. An $L_{eq(8)}$ limit of 75 dB was considered appropriate protection for the typical 8-h daily work period. This criterion is considered to be very restrictive for most applications, and it has not been incorporated into any DRC for occupational noise exposures.

Air Force

The U.S. Air Force (USAF) hearing conservation criterion is 85 dBA for a maximum allowable 8-h daily exposure. The trading relationship of 3 dB allows such exposures as 16 h at 82 dBA and 4 h at 88 dBA. Higher level continuous exposures for shorter durations, such as 94 dBA for 1 h, are limited to a maximum level of 115 dBA. The ratios of the actual to the allowable daily exposure times are not to exceed unity. Air Force criteria also include limiting conditions for infrasound, ultrasound, and impulse noises.

Army

The U.S. Army (USA) hearing conservation program criterion is 85 dBA as the maximum allowable exposure regardless of duration. Personnel experiencing these exposures must be enrolled in the hearing conservation program. In training and noncombat scenarios single hearing protection will be worn in steady noises of 85–107 dBA and double hearing protection for 108–118 dBA. Protection requirements for unique military noise sources are determined individually. The Army criteria also include limiting exposures for impulsive noises.

Navy

All noise-exposed Navy personnel are required to wear hearing protection when exposed to environmental noise exceeding the criterion of 84 dBA or 140 dB peak, regardless of duration. Personnel are entered into the hearing conservation program based on the 84-dBA damage risk criterion for an 8-h work day, with a 4-dB exchange rate. Double hearing protection is required when sound levels exceed 104 dBA, which administratively assumes 20 dB of single protection from an approved earplug or earmuff.

ISO-1999

The International Organization for Standardization (ISO) standard ISO-1999 (1990), "Acoustics—Determination of Occupational Noise Exposure and Estimation of Noise-Induced Hearing Impairment,"[5] is a landmark document that establishes practical procedures for estimating noise-induced hearing loss in populations. Standard ISO-1999 does not provide a specific formula for assessing risk of hearing handicap, but it specifies uniform methods for the prediction of hearing impairment that can be used for assessment of handicap according to the formula stipulated in a specific nation. The procedures are based on the equal-energy, 3-dB rule (adopted by the ISO and member nations as a conservative criterion) and deal with the measurement and description of noise exposure, the prediction of effects of noise on hearing threshold, and the assessment of risk of noise-induced hearing impairment and handicap. Annexes, which are not part of the standard, provide calculation procedures, examples, tabular data used in the calculations, and a method for relating this information to that of the preceding standard, ISO-1999 (1975). These procedures allow agencies, industries, and governments to select parameters and establish criterion values according to their respective needs. This document will form the basis for legislation in many countries.

The ISO method describes all exposures during an average work day in terms of the A-weighted sound exposure or energy average. The integration period is taken as a working day or a working week. All noises are included in the exposure, ranging from steady state to impulses. Exposures that contain steady tonal noise or impulsive/impact noise are considered about as harmful as the same exposure without these components but about 5 dB higher in level. Exposure can be measured with personal noise dosimeters or an integrating-averaging sound-level meter. Direct and indirect methods for the determination of exposure level are discussed as well as sampling methods.

The only measure of environmental noise needed to calculate hearing impairment or risk of hearing handicap under the following conditions is the energy-averaged daily noise exposure. The maximum instantaneous sound pressure level must be less than 140 dB, the average 8-h daily exposure must not exceed 100 dBA, and the maximum individual daily exposure must not be more than 10 dB above the average of all daily exposures to permit this determination of energy-averaged daily exposure.

Implementation of this standard follows a well-defined series of operations. The first involves determination of the age-related hearing levels of the target population for all test frequencies (e.g., population of 50-year-old males, 90th percentile at 500–6000 Hz). The long-standing difficulties of defining a "normal" population for this purpose were overcome with the utilization of two databases. Database A contains standardized distributions of hearing threshold of an ideal "highly screened" population free from all signs of ear disease, obstructions of wax, and without undue history of noise exposure. Database B can be any carefully collected database covering an *occupationally non-noise-exposed population* considered to be a valid control for the noise-exposed population under consideration. Each user of the standard can select the subpopulation most appropriate for its analysis. As an example, for database B the standard provides the data from the U.S. Public Health Service Surveys reported in 1965.[8]

Next, the predicted NIPTS of the population is calculated for all test frequencies by considering both the number of years of exposure and the average daily noise exposure levels. Data in the standard for calculating NIPTS are valid for frequencies from 500 to 6000 Hz, exposure times of 0–40 years, and average daily noise exposure levels between 75 and 100 dB.

The hearing handicap or risk of hearing handicap may be calculated using the appropriate NIPTS values and a formula selected by the user or a member nation. The document contains nine formulas that are proposed or commonly used among nations for assessing hearing handicap by averaging hearing threshold levels at selected audiometric test frequencies. In the United States, hearing handicap for conversational speech is assessed using the average of the hearing levels at 500, 1000, 2000, and 4000 Hz. Other procedures are available for determining overall percentage of hearing loss for purposes of compensation.

Long-Duration Noise Exposure

Noise exposure durations that exceed 8 h may occur in some work assignments and when substantial nonoccupational noise is added to that received at work. These longer duration exposures are extended by noises from daily living activities, recreation, transportation, proximity to industry, and even other vocational activities. Although the baseline of most criteria is the allowable exposure for an 8-h day, many do extend their time–intensity trading relationship to 16 or 24 h as additional guidance.

Although the 8-h day, 5-day work week is considered standard, numerous variations are employed for many occupations. Some of these are four 10-h days with three days off, three 12-h days with three and four days off, and 12 h on and 12 h off. The noise exposure criteria do not cover these exposures with the same degree of accuracy as with the standard work week. However, it is reasonable to consider the exposure per work week as a basis for calculating noise exposure (i.e., the 3-dB rule).

An important discovery in studies of effects of long-duration exposure to continuous (nonimpulsive) noise of 24 h and longer on human hearing was the phenomenon represented in Fig. 19.2 and called asymptotic threshold shift (ATS).[9] Hearing threshold levels progressively increased with time until the exposure durations reached 8–16 h. Hearing threshold levels reached a plateau or asymptote between 8 and 16 h and did not increase further with continuation of the same exposure levels for 24 and 48 h. Recovery from these asymptotic levels to the preexposure threshold levels was related to exposure time. Even though the asymptotic levels were the same for 24- and 48-h exposures to a particular stimulus, the time needed to recover was significantly longer for the 48- than for the 24-h exposures. The longer period of time to recover is interpreted by

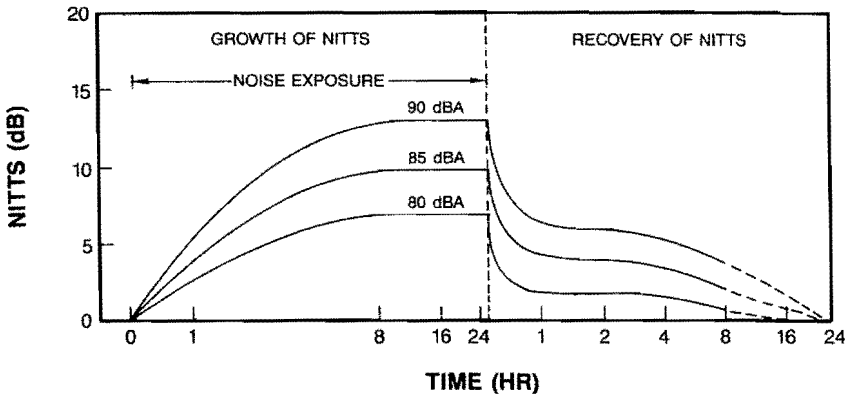


FIGURE 19.2 Growth recovery of noise-induced temporary threshold shift (NITTS) measured during and following the noise exposure at the times marked on the abscissa. The stimulus was a third-octave band of random noise centered on 1000 Hz presented at 80, 85, and 90 dBA. The curves represent the averages of the hearing levels (HLs) for the 1000-, 1500-, and 2000-Hz test frequencies $\frac{1}{3}(HL_{1000} + HL_{1500} + HL_{2000})$.

some as an indication of greater risk to hearing from the same stimulus (same asymptotic threshold level) for 48 than for 24 h. On the basis of analyses of the actual recovery times the guideline was established that the period of time in effective quiet required for recovery should be at least as long as the duration of the exposure.

Audiometric data on the crew members and information on the internal noise levels of the *Voyager* lightweight aircraft (two 110-hp piston engines) during a practice (five days) and a round-the-world flight (nine days) have provided additional important data points. The overall noise environments at the crew locations ranged between 99 and 103 dBA. Crew members wore communications headset and earplug equipments that allowed estimations of the exposures at the ears to be between 84 and 95 dB for the octave band at 500 Hz. Comparisons of preflight and postflight audiograms for both flights revealed substantial shifts of hearing levels. The threshold shifts from the nine-day flight were no greater than those for the five-day flight. One week following the nine-day flight the hearing thresholds of both crew members had returned to their preflight levels.

The hearing level data on the five- and nine-day exposures is consistent with laboratory data derived from both human studies of shorter duration and animal studies of similar duration. It is considered acceptable by some criteria to extend the 8-h limits to as much as 24 h using appropriate trading relationships. Noise exposures of atypical work schedules such as four 10-h days with three days off and 12 h on, 12 h off might be calculated on the bases of work week. Although recovery of the hearing thresholds occurred prior to nine days for these crew members, it remains reasonable to have personnel remain in effective quiet for a period at least as long as the exposure prior to reentering the noise.

Music Exposure Criteria

The USAF has adopted music exposure criteria that consider customers or clients of military "clubs" to be "recreationally exposed" and employees to be "occupationally exposed." The occupationally exposed persons are governed by the same provisions as those of workers exposed in any other occupational noise. A separate set of criteria are used to control or limit the recreational exposures.

An average A-weighted sound level of 94 dB is considered acceptable when it does not exceed 2 h duration once a week. It is important to recognize that the 94-dBA guideline is not a peak of a maximum level value but is the average sound level. The average sound-level concept does not specify a fixed maximum level or eliminate crescendos and special effects or even some selections. It does permit these intermittent high levels of entertainment music to be averages in such a way that the overall performance is acceptable.

19.4 IMPULSE NOISE

Impulse or impact noise is a very brief sound or short burst of acoustical energy with a sound pressure rise of 40 dB in 0.5 s or faster that may occur singly or as a series of events. The noise may be treated as steady state when the repetition rate of a series of impulses exceeds 10 per second and the decay from the individual peaks to minima does not exceed 6 dB.

The effects on the auditory system have been examined for such characteristics of the impulsive stimulus as frequency spectrum, duration, peak pressure level, total energy, type of impulse, and rise time. Although work continues with some of these characteristics, present exposure criteria use only peak pressure level and duration and type of impulse to describe safe impulse exposures.

In 1968, CHABA developed exposure criteria for impulse noise[10] based on extensive work in the United Kingdom on firing small arms.[11] The limiting noise exposure values for the impulsive stimuli are summarized in Fig. 19.3. These criteria define exposures that should produce, on average, no more NITTS than 10 dB at 1000 Hz, 15 dB at 2000 Hz, and 20 dB at 3000 Hz and above in 95% of the exposed ears. The criteria provide for adjustments or corrections for exposure situations that vary from the basic condition. The criteria provide for a daily exposure of 100 impulses during any time period ranging from about 4 min to several hours. The values are increased for fewer and decreased for more than 100 impulses per day by a factor of 1.5 dB for each doubling or halving of the number of impulses. The allowable level must be decreased by 5 dB for impulses that strike the ear at perpendicular incidence.

Simple, nonreverberating impulses that occur in open spaces are evaluated using the A-duration or pressure wave duration, which is the time required for the initial or principal wave to reach peak pressure level and return momentarily to zero (Fig. 19.3). The B-duration or pressure envelope duration is used for impulses that occur under various reverberant conditions and is the total time that the envelope of the pressure fluctuations (positive and negative) is within 20 dB

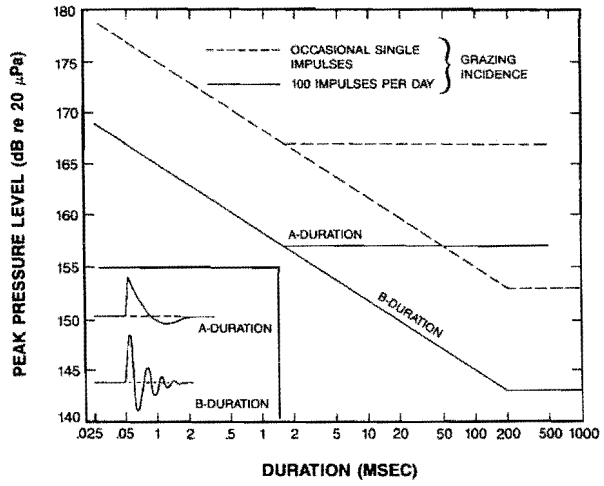


FIGURE 19.3 Proposed damage risk criteria for impulse noise arriving from the front or from behind (grazing incidence) exposed persons. The *A*-duration curve reflects the simple, nonfluctuating impulse that occurs in open areas. The *B*-duration curve reflects the pressure fluctuations of impulses that occur under various reverberant conditions.

of the peak pressure level, including reflected waves. The 143-dB floor of the B-duration curve represents the reduction of the energy entering the ear after 200 ms by action of the acoustic reflex (reflex contraction of the middle-ear muscles that reduces the transmission of energy to the inner ear). This comprehensive dose–response curve (DRC) for impulses continues to represent the present data and scientific understanding of impulse noise effects on hearing.

The OSHA amendment, the Air Force, and the Army, all limit exposure to impulse or impact noises to 140 dB peak sound pressure level. The Army has unique equipment that generates high-level impulse noises that are measured and treated individually.

Sonic booms do not constitute a threat of noise-induced hearing loss for human beings. Most of the energy in sonic booms generated by aircraft in supersonic flight is in the low and infrasonic frequency ranges and contributes little to the A-weighted sound level. Field and laboratory investigations with human exposures have revealed no significant effects on hearing from sonic booms at levels typically experienced in the community. One field study involving human exposures to extremely intense sonic booms ranging in level from about 50 to 144 lb/ft^2 observed no changes in the hearing levels of the participants.[12] Naturally, such intense sonic booms may generate higher A-weighted levels indoors than outdoors due to rattling of windows and doors.

Air bag systems are designed to provide crash protection of occupants during side and forward impacts of motor vehicles. These systems generate a loud, impulse noise inside the vehicle upon inflation of the air cushion. In an early

study[13] of a prototype system, 91 volunteers experienced this air bag deployment inside a small automobile at a median peak pressure level of 168 dB. Some TTS was experienced by about 50% of the subjects. About 95% of those with TTS recovered preexposure hearing levels on the same day. About 5% required longer times for recovery with one subject showing a gradually returning shift at one frequency that persisted for several months.

19.5 INFRASOUND

Relationships among human exposures to infrasound (0.5–20 Hz) and resulting hearing loss are presently not sufficiently understood for the establishment of national (U.S.) or international standards on exposure limits. Few investigations have been conducted because of difficulties in measuring hearing thresholds for infrasound and in producing infrasound stimuli free from audible overtones that are required for exposure studies. Tentative criteria have been established on the basis of laboratory investigations and field experiences with noises containing intense infrasound components. These criteria have been incorporated in some Department of Defense regulations on hazardous noise exposure.[14]

Human whole-body vibration exposures in intense levels of infrasound that exceeded 150 dB sound pressure level were reported in a classic study.[15] The sample size was small. However, the subjects were highly experienced professionals. Relationships were observed between exposure levels and human tolerance as a function of subjective "symptoms." These symptoms are described in Section 19.8 for airborne vibration. Certain exposures were judged to be very close to tolerance limits. Hearing levels of the subjects were measured 3 min following termination of these very intense exposures and no changes were found in hearing sensitivity.

The absence of hearing sensitivity effects immediately following the intense infrasound exposures verifies laboratory findings that infrasound is not a major threat to hearing. The exposure criteria in Fig. 19.4 have been developed on the basis of data such as that in the cited report and that presented in Fig. 19.5.[16] Numerous experimental subjects experienced exposures to 10 Hz at 144 dB for 8 min with no adverse effects. This set of safe exposure conditions was accepted as a baseline exposure from which 8-h limits (136 dB at 1 Hz and 123 dB at 20 Hz) and 24-h limits (130 dB at 1 Hz and 118 dB at 20 Hz) were extrapolated. (Development of this sound pressure level formulation is described in ref. 16.)

19.6 ULTRASOUND

Ultrasound (~16–40 kHz) is widespread in our society due to sources such as ultrasonic cleaners, measuring devices, drilling and welding processes, animal repellants, alarm systems, and communications control applications as well as a wide range of medical applications. Although the number of people exposed to

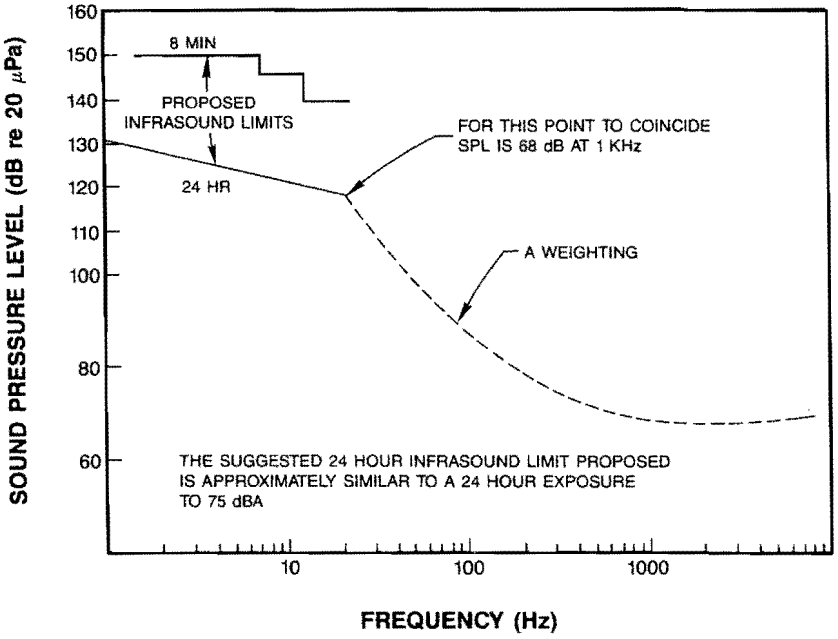


FIGURE 19.4 Infrasound 8-min and 24-h exposure limits.

ultrasound is large, it poses no threat to human hearing because neither temporary nor permanent hearing loss caused by ultrasound has been reported, with one exception. Temporary threshold shift was reported following experimental exposures to discrete tones in the region of 17–37 kHz at levels of 148–154 dB. The TTS occurred at subharmonics of the stimulus frequency and was likely caused by nonlinear distortion of the eardrum.

Nevertheless, ultrasound continues to be viewed as a threat to hearing as well as a cause of other subjective symptoms. Ultrasound is readily absorbed by air and its intensity diminishes rapidly with increasing distance from the source. The impedance match with human flesh is poor, and much energy is reflected away from the surface of the body. Consequently, the ear is the primary channel for transmitting airborne ultrasound to the internal systems.

Ultrasonic energy at frequencies above about 17 kHz and at levels in excess of about 70 dB may produce adverse subjective effects experienced as fullness in the ear, tinnitus, fatigue, headache, and malaise. These subjective effects are mediated through the hearing mechanism and are related to hearing ability. Persons who do not hear in this frequency region do not experience these subjective symptoms. Women experience the symptoms more often than men, and younger individuals report them more often than older ones. This reporting is consistent with the relative hearing abilities of the three groups. Neither disorientation nor loss of balance has been attributed to ordinary exposures to ultrasound.

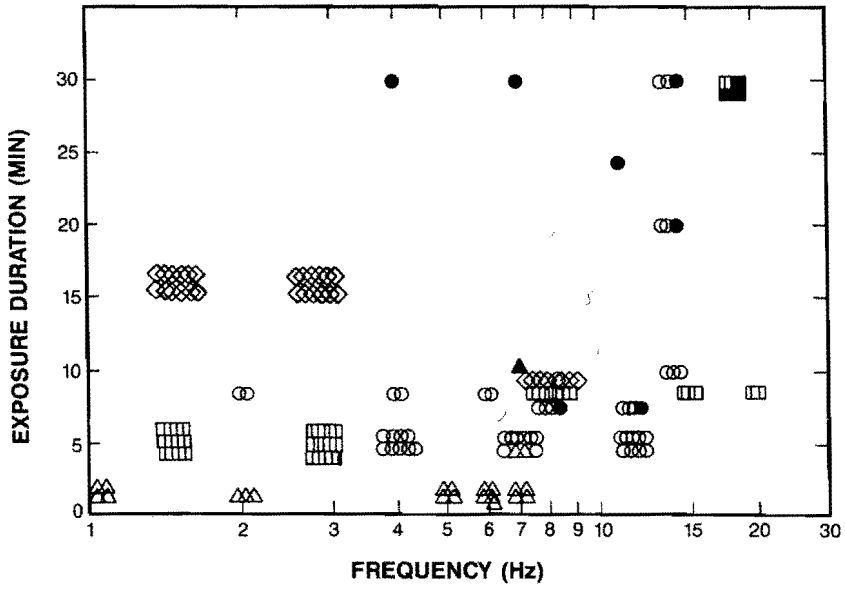


FIGURE 19.5 Infrasound exposure effects on hearing. Exposure levels (filled symbols indicate that some TTS has occurred): (△) > 150 dB; (○) 140–149 dB; (□) 130–139 dB; (◇) 120–129 dB.

Ultrasound exposures usually contain various amounts of high audio frequency energy (5–20 kHz). Subjective effects attributed to the ultrasound are usually caused by the audio frequency energy. Reducing the level of the audio frequency energy in the exposure usually results in the disappearance of the auditory and subjective symptoms.

Criteria for limiting the levels of ultrasound to control auditory and subjective effects are very similar. The data refer to the ultrasound levels at the head of the exposed person. The limiting levels at 20 kHz and above apply to protection from the subjective symptoms described earlier. Representative international and national criteria adopted by the World Health Organization (WHO), Norway, Sweden, and the American Conference of Governmental Industrial Hygienists (ACGIH) are displayed in Fig. 19.6. Norway accepts a level of 120 dB for frequencies higher that 22 kHz.

19.7 HEARING PROTECTION

The damage risk or noise exposure criteria presented above define allowable exposures for unprotected ears. These criteria are also used to identify exposure conditions above which personnel should be included in hearing conservation programs and where hearing protection should be worn. Hearing protection extends

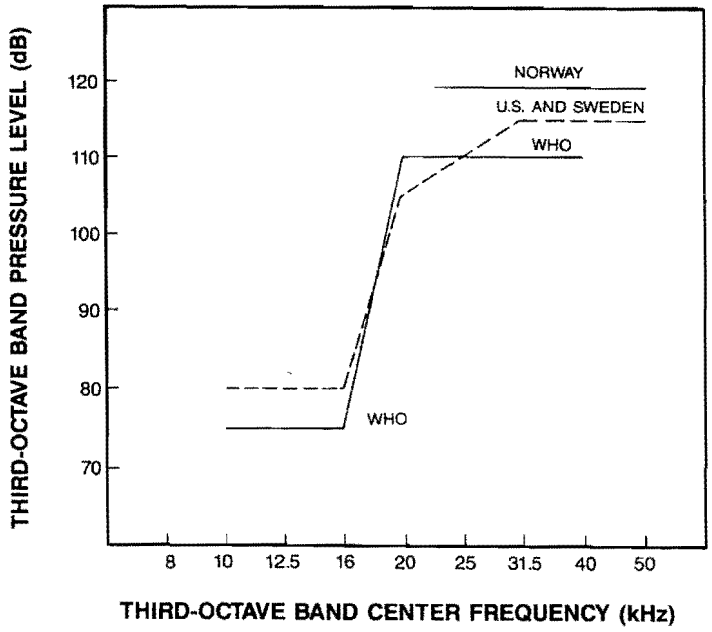


FIGURE 19.6 International and national criteria for exposure to airborne ultrasound.

the limits of allowable exposures by reducing the levels at the ear, allowing personnel to experience more intense and longer duration exposures than with unprotected ears and still remain within established whole-body exposure criteria.

Hearing protector performance is influenced by characteristics of the wearer, the protective device, and the noise exposure. Protection is best with devices that provide good attenuation, are comfortable, fit properly, are easy to use, are in a good state of repair, and are worn. Hearing protector effectiveness is reduced by air leaks, transmission properties of the materials, and noise-induced motion of the device that produces sound under the protector. A limit on performance of ideal devices is imposed by the sound conduction properties of the tissue and bone of the head. In high-level acoustical fields, sound travels "around" the protector to the inner ear through the tissue and bone of the head. The level of the sound reaching the ear by such means is about 50 dB below that of air conduction reaching the ear through an open ear canal. Bone-conducted sound is not a major concern for most noise environments. Total-head enclosures extend the tissue and bone limits by about 10 dB.

Infrasound

Good insert-type hearing protection devices should provide attenuation of infrasound approaching that observed at the 125-Hz third-octave band. Earmuff

hearing protectors provide very little protection and may even amplify the sound at some of these infrasonic frequencies. Exposures to levels of infrasound above 150 dB should be avoided even with maximal hearing protection because of possible adverse nonauditory effects.

Audio Frequency Region

Hearing protection performance varies as a function of the frequency spectrum of the noise. In general, conventional earplugs and earmuffs provide good sound protection at higher frequencies (above 1000 Hz). Earplugs provide effective protection at both high and low frequencies. Ample protection is observed across all frequencies with certain foam insert earplugs. Earmuffs provide poor attenuation at the low frequencies.

A combination of earplug and earmuff is required when an individual protector is unable to reduce a noise to an acceptable level. The resulting attenuation is not the sum of the two protectors but an amount determined by the particular combination of devices. The attenuation of the combined units often reaches the bone conduction limits at the high frequencies. At the mid- and lower frequencies the amount of attenuation is determined primarily by the earplug. Selection of a good earplug for use with a muff will provide good double hearing protection at all frequencies.

Special earmuff hearing protectors called nonlinear devices allow face-to-face speech communication at low levels of noise and provide typical amounts of earmuff protection at high levels. Active noise reduction (ANR) earmuffs employ electronic (noise cancellation) and acoustical means of reducing low-frequency noise at the ears. This active earmuff can increase intelligibility and comfort and reportedly reduce fatigue when used with speech communication systems in noise. The ANR earmuffs are widely used in such areas as communications, private aircraft, entertainment, and sport activities and by passengers in commercial aircraft.

Hearing protection devices have the potential capability to reduce and eliminate most noise-induced hearing loss. However, issues such as comfort, selection, fit, training, use, motivation, and others limit the full-performance capability of the devices to be realized in the workplace.

Long-Duration Exposures

Long-duration noise exposures are typically steady state, continuous, and generally within the audio frequency range. The information on hearing protection for audio frequencies is also appropriate for long-duration noises.

Ultrasound

Conventional hearing protection devices, earplugs and earmuffs, provide good protection against airborne ultrasound at frequencies above about 20,000 Hz.

Attenuation exceeding 30 dB is generally provided for frequencies from about 10,000 to 20,000 Hz. Hearing protection is most effective in eliminating subjective symptoms that occur when protectors are not worn. Reduction and elimination of subjective symptoms is also a good indication of the effectiveness of the hearing protector.

Impulses

Earmuff and earplug protectors should provide adequate attenuation for impulses comprised primarily of high-frequency energy, such as small-arms fire. Earmuff attenuation decreases as the concentration of energy in the impulses moves to the lower frequencies, as with large-caliber weapons (the attenuation vs. frequency of the protectors is not changing, only the spectral distribution of the impulse is different). The reduction of the peak sound pressure level of a particular earmuff is about 30 dB for pistol fire, about 18 dB for rifle fire, and as little as 5 dB for cannon fire. The peak level of the impulses of most pistol and standard rifle shots is reduced to less than 140 dB by good earmuffs. A combination of earplugs and earmuffs should be used for impulses requiring good low-frequency attenuation.

The USAF and the USA require single hearing protection when impulses reach 140 dB peak positive pressure and double hearing protection when the levels reach 160 dB (USAF) and 165 dB (USA).

19.8 HUMAN VIBRATION RESPONSE

The human body is a dynamic system, possessing mass and the ability to achieve relative motion between parts of the body (elasticity). It can therefore be affected by exposure to oscillatory motion or vibration. Although the ear is the most sensitive body organ for the reception of vibratory energy in the auditory frequency range, structure-borne and airborne vibration occurring at lower frequencies can be transmitted to a variety of anatomical structures, including skin, bone, muscles, joints, and internal organs. Most of our population is exposed to occasionally moderate levels of vibration with relatively harmless effects. Occupational exposures to vibration are more severe than nonoccupational exposures and have been associated with biological, psychological, and human performance effects.

Vibration is transmitted to the human body via the oscillatory motion from vibrating structures in contact with the body surface (structure borne) or via the transmission of sound pressure waves in high-noise environments (airborne). In structure-borne whole-body vibration, oscillatory motions enter the body usually at the feet (standing) or buttocks (sitting) at the supporting surface and can be transmitted throughout the body to other anatomical structures (such as the head).[17] The major sources of nonoccupational whole-body exposures include transportation vehicles such as automobiles, buses, trains, airplanes, and boats. Whole-body occupational vibration is experienced by operators of agricultural and forestry tractors, earth-moving and construction equipment, all types

of trucks, sea-going ships, airplanes and helicopters, as well as mining and factory workers on vibrating platforms. Structure-borne hand-transmitted vibration is isolated to a very specific anatomical region, primarily through the operation of vibrating hand tools such as jackhammers, chipping hammers, chain saws, grinders, and other types of pneumatic or electric hand-held devices. In airborne whole-body vibration, oscillatory motions enter the body via high levels of low-frequency sound pressure waves. Substantial airborne vibration occurs during aircraft engine run-ups and ground-based maneuvering, particularly in military environments where ground crews are required to work close to powerful aircraft in restrictive areas.

The absorption of vibratory energy by the body is determined by the body's characteristics as a mechanical system.[18] Engineering techniques (transfer function, power absorption) have been used and continue to be improved for defining these characteristics and for developing various models of the whole body and its subsystems (such as the hand–arm). These methods and models give insight into the energy transmission through the body and are useful tools for identifying the overall sensitivity of the body as well as for explaining the various effects on specific target organs and structures.

Whole-Body Vibration Effects

For whole-body vibration, the mechanical stresses imposed on the body can potentially lead to interference with bodily functions and tissue damage in practically all parts of the body. Historically, the major concern has focused on whole-body vertical vibration. More recent research includes multiaxis vibration effects. Figure 19.7 illustrates the short-time, 1-min, and 3-min tolerance limits reported by healthy adult male subjects exposed to vertical sinusoidal vibration.[19] Human tolerance to vibration tends to decrease with longer exposure periods. While acute exposures in the vicinity of human tolerance have not resulted in demonstrable harm or injury, prolonged and repeated exposures to these levels are considered to have a high potential for producing bodily damage. For vertical vibration, minimal tolerance occurs between 4 and 8 Hz.[19] This frequency range coincides with the major whole-body resonance observed in biodynamic data. Most physiologic effects in the region of 2–12 Hz are associated with excessive movement of the thoraco-abdominal viscera that can interfere with respiration and cause changes in cardiovascular functions that typically resemble the response to exercise.[20] Prolonged and repeated (chronic) occupational exposures, as they occur in drivers of tractors and earth-moving equipment, are implicated by many investigations in the development of spinal column and other joint disorders and pathologies and of stomach and duodenal diseases.[21,22] However, their causal relationship with vibration stress has not been clearly proven. For example, back pain and back disorders have been reported for other occupations with no vibration. These symptoms have also been associated with poor body posture. Studies, including the early study by Coermann,[23] have shown that body posture can affect whole-body vibration response.

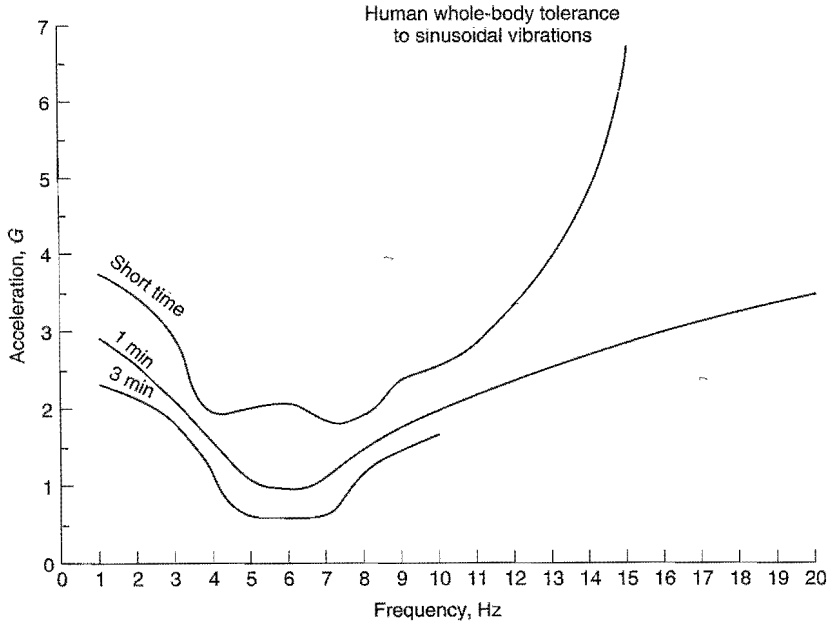


FIGURE 19.7 The short-time, 1-min, and 3-min tolerance limits reported during vertical sinusoidal vibration.[19]

Whole-body vibration can also influence working performance. It can cause involuntary body motions that interfere with the active motor control of the operator with undesirable effects. Relative motion of the eye with respect to an object or target can cause difficulty in reading instruments and performing visual searches.[24] This is particularly a concern at low frequencies where there is a high propensity for head movement in the region of whole-body resonance (below 10 Hz). Below about 20 Hz, compensatory eye movement aids in stabilizing the line of sight to a stationary object during head vibration.[25] When the image moves with the head, as occurs with a helmet-mounted display, compensatory eye movement becomes ineffective, increasing the potential for visual blurring.[26] Eye resonance has been reported to occur in a broad frequency range between 20 and 70 Hz.[25] Relatively high levels of whole-body vibration or direct contact of the head with the vibrating structure are necessary to induce visual blurring due to the body's damping effect at these higher frequencies.

With regard to airborne vibration, the mismatch between the acoustical impedance of air and the human body surfaces prevents significant amounts of acoustical energy from entering the body, particularly at higher frequencies.[27] With decreasing frequencies below 1000 Hz, more acoustical energy is absorbed in the form of transverse shear waves. With exposure to high-intensity noise levels [120 dB sound pressure level (SPL)] between 100 and 1000 Hz, tissue vibration

occurs and the noise is felt via the stimulation of somatic mechanoreceptors.[28] Below 100 Hz, intense noise can cause whole-body vibration that not only affects motion in the chest, abdominal wall, viscera, limbs, and head but also can generate motions in the body cavities and air-filled or gas-filled spaces.[28] Von Gierke and Nixon[27] reported that resonance of the chest wall and air-filled lungs occurs around 60 Hz. For noise exposures below 150 dB, the most common symptom reported by subjects was mild to moderate chest vibration.[15] Above 150 dB, symptoms included mild nausea, giddiness, subcostal discomfort, cutaneous flushing and tingling (around 100 Hz, 153 dB); coughing, severe substernal pressure, choking respiration, salivation, pain on swallowing, hypopharyngeal discomfort, and giddiness (60 Hz, 154 dB and 73 Hz, 150 dB); and headache (50 Hz, 153 dB).[15] More recent efforts have been made to measure the biodynamic response of the body to airborne vibration and compare the body acceleration spectra to the noise spectra.[29] The preliminary results for exposures to jet aircraft noise during engine run-ups confirm the upper torso resonance reported by von Gierke and Nixon.[27]

Hand-Transmitted Vibration Effects

Hand–arm vibration syndrome (HAVS) refers to the "complex of peripheral vascular, neurological, and musculoskeletal disorders associated with exposure to hand-transmitted vibration" (ref. 30, p. 11). HAVS is recognized worldwide as a health concern. Prolonged and repeated exposure to hand-transmitted vibration can lead to a very specific disease called vibration-induced white finger (VWF), or Raynaud's phenomenon. This impairment of the blood circulation of the hand progresses with exposure time from intermittent numbness and tingling in selected fingers to extensive blanching of most fingers, first only in combination with cold and finally at all environmental temperatures. In the final stages the disease interferes severely with social activities and continuation of the occupation. According to Taylor and Pelmear,[31] the clinical manifestations of the finger-blanching attacks progress in four stages, with stage 1 signaling the onset of the disease, mainly outdoors in winter. While symptoms of the first stages might still be reversible if vibration exposure is discontinued, the later stages are considered irreversible by most researchers. In later stages, the vascular manifestations are reported to be accompanied by nerve, bone, joint, and muscle involvement.[32] Studies have shown that HAVS, specifically VWF, is influenced by several factors, including the frequency, magnitude, and duration of the exposure, in addition to the type of tool. As with whole-body vibration, the symptoms of VWF appear to increase with exposure duration.

19.9 HUMAN VIBRATION EXPOSURE GUIDELINES

Extensive research over the last four decades has led to a reasonable understanding of the potential pathological and physiological effects of structure-borne

whole-body as well as hand-transmitted vibration, although the mechanisms of these effects continue to be topics of research. Frequency-dependent sensitivity curves have been derived for the whole-body and for the hand–arm from both subjective and objective frequency response characteristics. These sensitivity curves form the basis for current whole-body and hand-transmitted vibration standards. There are major national and international standards that provide guidelines and recommended criteria for safe vibration exposure based on these curves and that are generally relied upon in designing vehicles, equipment, tools, and mitigation strategies for use in vibration environments. These standards are periodically revised as vibration research continues and new data become available.

Structure-Borne Whole-Body Vibration Criteria

The International Organization for Standardization (ISO) is the most widely recognized body for providing the basic guidelines for assessing the damage risk of structure-borne whole-body vibration (ISO 2631). As of 2004, the standard entitled "Mechanical Vibration and Shock—Evaluation of Human Exposure to Whole-Body Vibration" included three parts: ISO 2631-1:1997,[33] ISO 2631-2:2003,[34] ISO 2631-4:2001,[35] and ISO 2631-5:2004.[36] Part 1, entitled "General Requirements," describes the general methods for measuring whole-body vibration. Informative annexes are included that give guidance on possible effects of vibration on comfort, perception, health, and motion sickness based on current knowledge in these areas. In 2002, the American National Standards Institute (ANSI) accepted the ISO 2631-1:1997 as a nationally adopted international standard (ANSI S3.18–2002),[37] replacing the long-standing 1979 version. For whole-body vibration, the frequency range considered is 0.5–80 Hz although the range from 1 to 80 Hz can be used if appropriate. When the vibration is transmitted by a resilient structure, such as a seat cushion, a suitably shaped transducer support is interposed between the person and that structure. The standard recommends the collection of acceleration data between the body and three supporting surfaces for the seated occupant, including the seat pan or surface, seat back, and feet. For the recumbent occupant, the supporting surfaces include the pelvis, back, and head. Translational vibrations are typically measured in the three axes defined by an orthogonal coordinate system. For standing, seated, and recumbent whole-body vibration, the x axis is defined in the back-to-chest (fore-and-aft) direction, the y axis for the side-to-side (lateral) direction, and the z axis for the foot- (or buttocks-) to-head (vertical) directions.[33] Rotational vibration may also be measured or estimated. There are three primary frequency-weighting curves (including motion sickness) and three additional frequency-weighting curves that are applied to the acceleration–time histories or frequency response spectra depending on the measurement site and the particular effect being assessed. Figure 19.8 illustrates the two primary frequency weightings that reflect the sensitivity of the body in the respective directions.

The overall weighted root-mean-square (rms) acceleration is determined in the time or frequency domain in each axis. The assessment is made based on

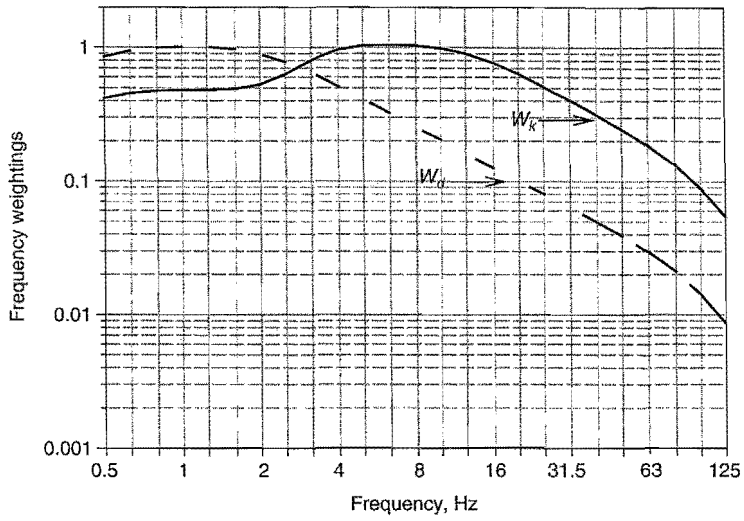


FIGURE 19.8 ISO 2631-1:1997[33] frequency-weighting curves for whole-body vibration in the horizontal (W_d) and vertical (W_k) directions. (Redrawn with permission. Copyright by the International Organization for Standardization. Standard can be obtained from any member body or directly from the ISO Central Secretariat, ISO, Casepostal 56, 1211 Geneva 20, Switzerland.)

the highest weighted acceleration level. If vibration in two or more directions is comparable, then additional direction-dependent multiplying factors are applied and the vibration total value (VTV) or vector sum is calculated.

Other methods are also described, including the running rms method and fourth-power vibration dose method (using the vibration dose value, or VDV). The VDV is more sensitive to peaks in the exposure. Figure 19.9 depicts the Health Guidance Caution Zones provided in the ISO 2631-1:1997 and ANSI S3.18–2002. These guidance zones apply to the overall weighted accelerations determined at the seat pan in the three translational directions. In the figure, the zones defined by the solid lines are applicable to the rms acceleration level. The zones defined by the dotted lines are applicable to the fourth-power vibration dose method. Below the zones, health effects have not been clearly documented or observed. Within the zones, caution is indicated for potential health risks. Above the zones, health risks are likely.[33]

For estimating the effects of structure-borne whole-body vibration on comfort and perception, rotational frequency weightings and multiplying factors are included for the seated occupant.[33] The VTV is recommended for assessing comfort. The standard ISO 2631-1:1997 provides six comfort reactions to vibration and the associated overall weighted acceleration levels ranging from "not uncomfortable" to "extremely uncomfortable." These reactions have no time dependency.

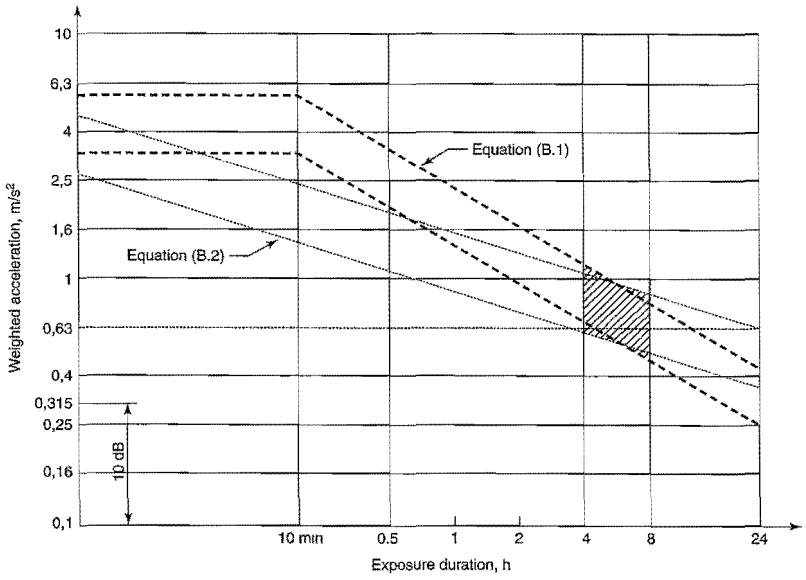


FIGURE 19.9 ISO 2631-1:1997 Health Guidance Caution Zones.[33] Equations (B.1) and (B.2) are defined in the standard. (Reprinted with permission. Copyright by the International Organization for Standardization. Standard can be obtained from any member body or directly from ISO Central Secretariat, ISO, Casepostal 56, 1211 Geneva 20, Switzerland.)

Guidelines on motion sickness are primarily applicable to ships and other sea vessels. The weighted rms acceleration is determined between 0.1 and 0.5 Hz in the vertical direction at the supporting surface. Two methods are given for calculating the motion sickness dose value ($MSDV_z$). An approximation of the percentage of individuals who may vomit is given by $K_m(MSDV_z)$, where $K_m = \frac{1}{3}$ for a population of unadapted male and female adults.[33]

The standard ISO 2631-2:2003, entitled "Part 2: Vibration in Buildings (1 Hz to 80 Hz)," is directed toward human exposure in buildings with respect to comfort and annoyance. A single frequency weighting, W_m, is defined that is related to the combined-response rating curve used in the older 1989 edition. The general guidelines for measuring the vibration are similar to those given in ISO 2631-1:1997. The vibration is measured in the three orthogonal axes with the directions relating to the structure and defined for the standing individual (Part 1). The measurements are made at a location where the highest frequency-weighted vibration occurs. Categories of sources are provided and include (a) continuous or semicontinuous processes (e.g., industry), (b) permanent intermittent activities (e.g., traffic), and (c) limited duration (nonpermanent activities, e.g., construction). The 2003 standard does not include acceptable levels of vibration. The consensus of opinion is that sufficient information was not available at the time for establishing appropriate vibration levels given the complexity of human response to building vibration. The standard does indicate that adverse comments about residential building vibration may occur when the magnitudes or levels are only slightly higher than the perception levels (ISO 2631-1:1997, Annex C).[33] Other complaints may be due to secondary effects such as reradiated noise (ISO 2631-2:2003, Annex B).[34] There should be no reason to consult the Health Guidance Caution Zones in ISO 2631-1:1997, Annex B, except in an extremely rare building vibration environment.

The standard ISO 2631-5:2001,[36] entitled "Part 5: Method for Evaluation of Vibration Containing Multiple Shocks," directs attention to the health of the lumbar spine. Exposures to multiple shocks may occur in the operation of equipment and vehicles over rough terrain or rough seas. A biomechanical model is used to predict the response of the human spine to a given input and to generate an acceleration dose. The standard provides guidelines on using the acceleration dose to assess the health effects of multiple shocks based on the probability of an adverse health effect that depends on the relationship between the ultimate strength of the lumbar spine, the age of the person, and the number of years of exposure.

Airborne Whole-Body Vibration Criteria

Current guidelines for airborne vibration are given in terms of the noise exposure. The Air Force Occupational, Safety, and Health Standard AFOSHSTD 48-19[14] recommends that, for minimizing whole-body vibration effects, no octave- or one-third-octave-band noise level exceed 145 dB for frequencies in the range of 1–40,000 Hz and that the overall A-weighted sound pressure level be below 150 dBA with no time limits. The ACGIH[38] recommends that one-third-octave-band levels between 1 and 80 Hz should not exceed 145 dB, and the overall unweighted SPL should not exceed 150 dB. The assessment of airborne vibration exposure may differ depending on which guideline is used. Minimal research has been conducted on the physiological and pathological effects that may be associated with airborne vibration.

Hand-Transmitted Vibration Criteria

The ISO provides basic guidelines for assessing hand-transmitted vibration in ISO 5349, "Mechanical Vibration—Measurement and Evaluation of Human Exposure to Hand-Transmitted Vibration." The standard consists of two parts: Part 1: General Requirements (ISO 5349-1:2001)[30] and Part 2: Practical Guidance for Measurement at the Workplace (ISO 5349-2:2001).[39] For hand-transmitted vibration, the center of the coordinate system is the head of the third metacarpal with the z axis defined as the longitudinal axis of the third metacarpal, the y axis in the general direction of the tool handle (basicentric coordinate system), and the x axis passing from the top to the bottom of the hand. Figure 19.10 illustrates the frequency weightings or factors associated with the center frequencies of one-third-octave bands for assessing the effects of hand-transmitted vibration.

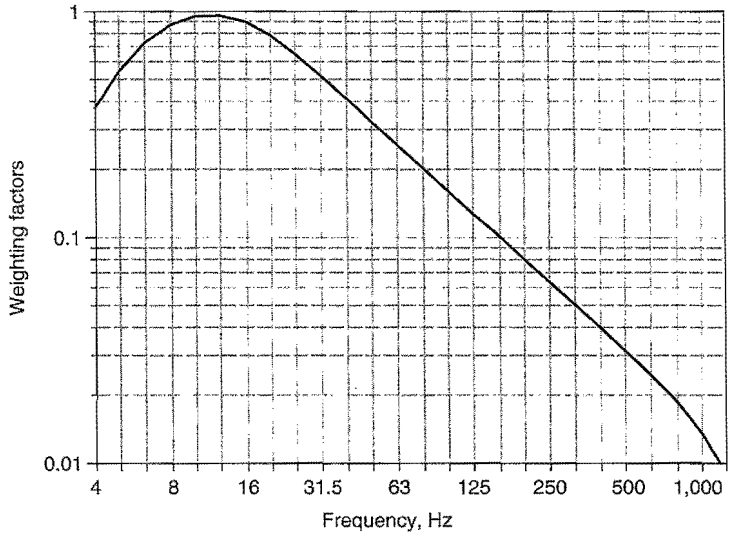


FIGURE 19.10 ISO 5349-1:2001 Frequency-weighting curve W_h for hand-transmitted vibration.[33] (Redrawn with permission. Copyright by the International Organization for Standardization. Standard can be obtained from any member body or directly from the ISO Central Secretariat, ISO, Casepostal 56, 1211 Geneva 20, Switzerland.)

The quantity used to assess health effects is the 8-hr energy-equivalent vibration total value [$A(8)$], or daily vibration exposure. It is assumed that the health risk for hand-transmitted vibration applies to all three orthogonal directions. Therefore, the same weighting curve (Fig. 19.10) is applied to vibration in each of the three orthogonal axes. The vector sum of the overall weighted accelerations estimated for each axis defines the vibration total value (a_{hv}). Figure 19.11 depicts the daily exposure values [$A(8)$] expected to produce vibration-induced white finger in 10% of persons exposed for a given number of years, D_y. The standard ISO 5349-2:2001[39] provides additional guidelines for measuring hand-transmitted vibration in the workplace, determining the daily vibration exposure, and selecting appropriate operations. The measurement of vibration entering the hand may not always be practical. Part 2 includes practical measurement locations for selected power tool types and summarizes the location of accelerometers used in vibration-type test standards for a variety of power tools. These locations are usually close to the hand.

Additional Exposure Standards and Guidelines

Other organizations and countries have generated standards and guidelines that compliment, supplement, or even differ from the human vibration standards described above, particularly the ISO 2631-1:1997. The ACGIH[38] provides guidelines for whole-body as well as hand-transmitted vibration. The European Union

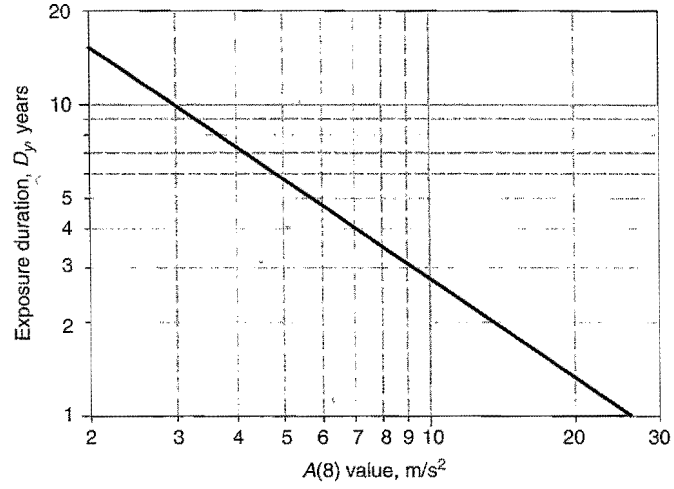


FIGURE 19.11 Vibration exposure for predicted 10% prevalence of vibration-induced white finger in a group of exposed persons. (Redrawn from ISO 5349-1:2001[30] with permission. Copyright by the International Organization for Standardization. Standard can be obtained from any member body or directly from the ISO Central Secretariat, ISO, Casepostal 56, 1211 Geneva 20, Switzerland.)

has recently published a directive on health and safety requirements for exposure to both whole-body and hand-transmitted vibration. It is important that designers and assessors understand the similarities and differences among the various standards and the appropriateness of their applicability. It is also critical to use current editions of these standards since new information could have significant influences on defining health risk.

REFERENCES

1. U.S. Environmental Protection Agency (EPA), "Information on Levels of Environmental Noise Requisite to Protect Public Health and Welfare with an Adequate Margin of Safety," Report No. 550/9-74004, EPA, Washington, DC, March 1974.
2. H. E. Von Gierke, D. Robinson, and S. J. Karmy, "Results of the Workshop on Impulse Noise and Auditory Hazard," ISVR Memorandum 618, Institute of Sound and Vibration Research, Southampton, United Kingdom, October 1981. Also *J. Sound Vib.*, **83**, 579–584 (1982).
3. J. Tonndorf, H. E. Von Gierke, and W. D. Ward, "Criteria for Noise and Vibration Exposure," in C. M. Harris (Ed.), *Handbook of Noise Control*, 2nd ed., McGraw-Hill, New York, 1979.
4. C. W. Nixon, "Excessive Noise Exposure," in S. Singh (Ed.), *Measurement Procedures in Speech, Hearing, and Language*, University Park Press, Baltimore, MD, 1975.

5. International Organization for Standardization (ISO), "Acoustics—Determination of Occupational Noise Exposure and Estimation of Noise-Induced Hearing Impairment," ISO 1999.2, ISO, Geneva, Switzerland, 1990.
6. K. D. Kryter et al., "Hazardous Exposure to Intermittent and Steady-State Noise," paper presented before the NAS-NRC Committee on Hearing, Bioacoustics, and Biomechanics, WG 46, Washington, DC, 1965.
7. Occupational Safety and Health Administration, "Occupational Noise Exposure; Hearing Conservation Amendment," *Fed. Reg.*, **48**(46), 9738–9785 (1983).
8. National Center for Health Statistics, "Hearing Levels of Adults by Age and Sex," Vital Statistics, Public Health Service Publication No. 1000, Series-11-No. 11, U.S. Government Printing Office, Washington, DC, 1965.
9. M. R. Stephenson, C. W. Nixon, and D. L. Johnson, "Long Duration (24–48 Hours) Exposure to Continuous and Intermittent Noise," Joint EPA/USAF Report, AFAMRL Technical Report No. 82–92, Wright Patterson AFB, OH, 1982.
10. W. D. Ward et al., "Proposed Damage Risk Criteria for Impulsive Noise (Gunfire)," paper presented before the NAS-NRC Committee on Hearing, Bioacoustics, and Biomechanics, WG 46, Washington, DC, 1968.
11. R. R. A. Coles, G. R. Garinther, D. C. Hodge, and C. G. Rice, "Hazardous Exposure to Impulse Noise," *J. Acoust. Soc. Am.*, **43**, 336–343 (1968).
12. C. W. Nixon, H. H. Hille, H. C. Sommer, and E. Guild, "Sonic Booms Resulting from Extremely Low Altitude Supersonic Flight: Measurements and Observations on Houses, Livestock, and People," AAMRL Technical Report No. 68-52, Wright Patterson AFB, OH, 1968.
13. C. W. Nixon, "Human Auditory Response to an Air Bag Inflation Noise," PB-184-837, Clearinghouse for Federal Scientific and Technical Information, Arlington, VA, 1969.
14. Office of the Air Force Surgeon General, Air Force Occupational Safety and Health (AFOSH) Program, "Hazardous Noise Program," AFOSHSTD 48-19, March 31, 1994, Washington, DC.
15. G. C. Mohr, J. N. Cole, E. Guild, and H. E. Von Gierke, "Effects of Low Frequency and Infrasonic Noise on Man," *Aerospace Med.*, **36**, 817–824 (1965).
16. C. W. Nixon and D. L. Johnson, "Infrasound and Hearing," in W. D. Ward (Ed.), *International Congress on Noise as a Public Health Problem*, 550/9-73-008, U. S. Environmental Protection Agency, Washington, DC, May 1973.
17. H. E. Von Gierke and D. E. Goldman, "Effects of Shock and Vibration on Man," in C. M. Harris (Ed.), *Shock and Vibration Handbook*, 3rd ed., McGraw-Hill, New York, 1988.
18. H. E. Von Gierke, "To Predict the Body's Strength," *Aviat. Space Environ. Med.*, **59**, A107–A115 (1988).
19. E. B. Magid, R. R. Coermann, and G. H. Ziegenruecker, "Human Tolerance to Whole Body Sinusoidal Vibration," *Aerospace Med.*, **31**, 915–924 (1960).
20. W. B. Hood, R. H. Murray, C. W. Urschel, et al., "Cardiopulmonary Effects of Whole-Body Vibration in Man," *J. Appl. Physiol.*, **21**(6), 1725–1731 (1966).
21. H. Dupuis and G. Zerlett, *The Effects of Whole-Body Vibration*, Springer-Verlag, Berlin, Heidelberg, New York, Tokyo, 1986.

22. H. Seidel and R. Heide, "Long-Term Effects of Whole-Body Vibration: A Critical Survey of the Literature," *Int. Arch. Occup. Environ. Health*, **58**, 1–26 (1986).
23. R. R. Coermann, "The Mechanical Impedance of the Human Body in Sitting and Standing Position at Low Frequencies," ASD Technical Report 61–492, Aeronautical Systems Division, Air Force Systems Command, U. S. Air Force, Wright Patterson AFB, OH, 1961.
24. M. J. Moseley and M. J. Griffin, "Effects of Display Vibration and Whole-Body Vibration on Visual Performance," *Ergonomics*, **29**(8), 977–983 (1986).
25. M. J., Griffin, *Handbook of Human Vibration*, Academic, London, 1990, pp. 128–134.
26. M. J. Wells and M. J. Griffin, "Benefits of Helmet-Mounted Display Image Stabilisation under Whole-Body Vibration," *Aviat. Space Environ. Med.*, **55**(1), 13–18 (1984).
27. H. E. Von Gierke and C. W. Nixon, "Effects of Intense Infrasound on Man," in W. Tempest (Ed.), *Infrasound and Low Frequency Vibration*, Academic, New York, 1976, pp. 115–150.
28. J. C. Guignard and P. F. King, "Aeromedical Aspects of Vibration and Noise," AGARDograph No. 151, NATO Advisory Group for Aerospace Research and Development (AGARD), 1972.
29. S. D. Smith, "Characterizing the Effects of Airborne Vibration on Human Body Vibration Response," *Aviat. Space Environ. Med.*, **73**(1), 36–45 (2001).
30. International Organization for Standardization (ISO), "Mechanical Vibration and Shock—Measurement and Evaluation of Human Exposure to Hand-Transmitted Vibration—Part 1: General Requirements," ISO 5349-1: 2001, ISO, Geneva, Switzerland.
31. W. Taylor and P. L. Pelmear (Eds.), *Vibration White Fingers in Industry*, Academic, London, 1975.
32. U.S. Department of Health and Human Service, National Institute for Occupational Safety and Health (NIOSH), "Occupational Exposure to Hand-Arm Vibration," DHHS Publication No. 89–106, NIOSH, Washington, DC, 1989.
33. International Organization for Standardization (ISO), "Mechanical Vibration and Shock—Evaluation of Human Exposure to Whole-Body Vibration—Part 1: General Requirements," ISO 2631-1:1997, ISO, Geneva, Switzerland.
34. International Organization for Standardization (ISO), "Mechanical Vibration and Shock—Evaluation of Human Exposure to Whole-Body Vibration—Part 2: Vibration in Buildings (1–80 Hz)," ISO 2631-2:2003, ISO, Geneva, Switzerland.
35. International Organization for Standardization (ISO), "Mechanical Vibration and Shock—Evaluation of Human Exposure to Whole-Body Vibration—Part 4: Guidelines for the Evaluation of the Effects of Vibration and Rotational Motion on Passenger and Crew Comfort in Fixed-Guideway Transport Systems," ISO 2631-4:2001, ISO, Geneva, Switzerland.
36. International Organization for Standardization (ISO), "Mechanical Vibration and Shock—Evaluation of Human Exposure to Whole-Body Vibration—Part 5: Method for Evaluation of Vibration Containing Multiple Shocks," ISO 2631-5:2004, ISO, Geneva, Switzerland.
37. American National Standards Institute, "Guide for the Evaluation of Human Exposure to Whole-Body Vibration," ANSI S3.18–2002, Acoustical Society of America, Melville, NY, 2002.

38. American Conference of Governmental Industrial Hygienists (ACGIH), "2003 TLVs® and BEIs®, Based on the Documentation of the Threshold Limit Values for Chemical Substances and Physical Agents & Biological Exposure Indices," ACGIH, Cincinnati, OH, 2003.

39. International Organization for Standardization (ISO), "Mechanical Vibration and Shock—Measurement and Evaluation of Human Exposure to Hand-Transmitted Vibration—Part 2: Practical Guidance for Measurement at the Workplace," ISO 5349-2:2001, ISO, Geneva, Switzerland.

CHAPTER 20

Criteria for Noise in Buildings and Communities

LEO L. BERANEK

Consultant
Cambridge, Massachusetts

One of the early steps in the architectural design of a building is the specification of acceptable noise levels in the spaces for occupancy by human beings. Noise sources in rooms include the air-handling and conditioning system (HVAC), the occupants themselves, machinery in the room, and vibration of the surfaces of the room by machinery outside. In this chapter, the sources of the noise in a space are, in general, not discussed. However, in many cases, such as in offices, dwellings, schools, auditoriums, and studios, it is generally true that the most likely annoying noise is created by the HVAC system. In those cases the criteria presented here apply to the HVAC noise alone as measured without the presence of people. In shops, manufacturing plants, and restaurants, the principal noise sources are machinery or large numbers of people. In such spaces the designer only has to make sure that the HVAC levels do not exceed the liberal limits suggested in this chapter.

20.1 SOUND LEVELS: DEFINITIONS

The sound (noise) levels, all in decibels, that are used in this chapter are taken from Chapter 1, which, in turn, were taken from U.S. and international standards:

- Sound pressure level (SPL) L_p [see Eq. (1.21)].
- A-weighted sound pressure level L_A [see Eq. (1.22)].
- The equivalent sound level L_{eq}, which is broadly defined by

$$L_{eq} = L_{av,T} = 10 \log(1/T) \frac{\int_0^T p_A^2(t)\, dt}{p_{ref}^2} \quad \text{dB} \tag{20.1}$$

where T is the time over which the averaging takes place and must be specified [see Eq. (1.23)].

38. American Conference of Governmental Industrial Hygienists (ACGIH), "2003 TLVs® and BEIs®, Based on the Documentation of the Threshold Limit Values for Chemical Substances and Physical Agents & Biological Exposure Indices," ACGIH, Cincinnati, OH, 2003.

39. International Organization for Standardization (ISO), "Mechanical Vibration and Shock—Measurement and Evaluation of Human Exposure to Hand-Transmitted Vibration—Part 2: Practical Guidance for Measurement at the Workplace," ISO 5349-2:2001, ISO, Geneva, Switzerland.

CHAPTER 20

Criteria for Noise in Buildings and Communities

LEO L. BERANEK

Consultant
Cambridge, Massachusetts

One of the early steps in the architectural design of a building is the specification of acceptable noise levels in the spaces for occupancy by human beings. Noise sources in rooms include the air-handling and conditioning system (HVAC), the occupants themselves, machinery in the room, and vibration of the surfaces of the room by machinery outside. In this chapter, the sources of the noise in a space are, in general, not discussed. However, in many cases, such as in offices, dwellings, schools, auditoriums, and studios, it is generally true that the most likely annoying noise is created by the HVAC system. In those cases the criteria presented here apply to the HVAC noise alone as measured without the presence of people. In shops, manufacturing plants, and restaurants, the principal noise sources are machinery or large numbers of people. In such spaces the designer only has to make sure that the HVAC levels do not exceed the liberal limits suggested in this chapter.

20.1 SOUND LEVELS: DEFINITIONS

The sound (noise) levels, all in decibels, that are used in this chapter are taken from Chapter 1, which, in turn, were taken from U.S. and international standards:

- Sound pressure level (SPL) L_p [see Eq. (1.21)].
- A-weighted sound pressure level L_A [see Eq. (1.22)].
- The equivalent sound level L_{eq}, which is broadly defined by

$$L_{eq} = L_{av,T} = 10 \log(1/T) \frac{\int_0^T p_A^2(t)\, dt}{p_{ref}^2} \quad \text{dB} \tag{20.1}$$

where T is the time over which the averaging takes place and must be specified [see Eq. (1.23)].

- A-weighted equivalent sound level $L_{eq,A}$ is that given by Eq. (20.1), but with the A-weighted frequency response in place in the measuring instrument. Often this quantity is simply labeled L_{eq} and the A weighting is known through its expression in dBA [see Eq. (1.24)].
- The band average sound level is that given in Eq. (19.1), but with the band width specified.
- The averaging time T can be a matter of fractional seconds, minutes, hours, days, or even a year. Always, it must be specified.
- Day–night sound level L_{dn} [see Eq. (1.25)]. Note, in some nations, the 24-h period is divided into three intervals, day, evening, and night, for which Eq. (1.25) must have three integrals with the interval times specified.
- A-weighted sound (noise) exposure $E_{A,T}$ (proportional to energy flow, intensity times time, in a sound wave in the time period T) [see Eq. (1.26)].
- A-weighted sound (noise) exposure level L_{EAT} [see Eq. (1.27)].
- Speech interference level SIL is the average of the sound pressure levels in the four octave bands, whose midfrequencies are 500, 1000, 2000, and 4000 Hz.

20.2 EVALUATION OF ROOM NOISE: SURVEY METHOD, ENGINEERING METHOD, AND PRECISION METHOD[1]

Current-Day Sound-Level Meters

Current-day sound-level meters are used to determine the sound levels in some or all of the ten octave bands with midfrequencies from 16 to 8000 Hz. The meter "speed" can be set to slow, fast, or impulse. When the meter speed is set to "fast," a running integration time of about 125 ms is achieved. The output of the meter can be set to read or store the following levels: L_{eq}, the equivalent noise level over the measurement time period; the peak level L_{max}, and the statistical levels L_{10}, L_{50}, L_{90}, and L_{95}, where the subscript means that level is exceeded 10, 50, 90, or 95% of the time. The 50% level is the median level. When measuring A-weighted sound levels, the meter speed is set at "slow." For monitoring, the meters usually have storage capacity from 1 s up to 24 h. The stored data can be sampled as often as every 100 ms. Acoustical consultants say that their measuring time of HVAC noise at a particular location in a room is usually under a minute.

Survey Method — L_A

An A-weighted sound level L_A is often used for surveying whether a measured noise level satisfies a specified noise criterion. It is readily measured with the simplest sound-level meters. The measurement of L_A is the average of the maximum meter readings, with the meter response set at slow, and obtained by moving the microphone about the room, avoiding positions near the surfaces or the geometric center. It is assumed that the measured noise is free of pure tones and HVAC surging. The presence of HVAC surging can usually be detected by listening or by observing the meter swings using the "flat" (or "C") frequency weighting and the fast meter response.

Because L_A lacks specific spectral information, it can be misleading in evaluating noise other than that arising from reasonably well-designed HVAC systems. The values given in Table 20.1 are recommended for estimating whether measured A-weighted levels may be suitable for the purposes indicated. The numbers presented in that table are largely influenced by the results of a request to a number of consulting firms for examples of excessive noise situations.[2] Fourteen firms responded. The acceptable and unacceptable octave-band levels in school rooms, auditoria, offices, and hotel rooms resulted. Those data indicated that the best method to use in writing specifications, where HVAC surging and large sound fluctuations are not expected, is to use noise criterion (NC) curves, described in the next section. (*Note*: The acceptable NC curves for various occupancies of the spaces are given in Table 20.2. Table 20.1 was determined from Table 20.2 and the NC curves of Fig. 20.1 as follows: For each of the NC curves the speech interference level (SIL) and the A-weighted effective level (L_A) were calculated and $L_A - \text{SIL}$ found. These differences were added to the levels in Table 20.2 to obtain the levels of Table 20.1. For example, $L_A - \text{SIL}$ for the NC-40 criterion curve is 8 dB, which means that where 40 dB appears in Table 20.2, 48 dB appears in Table 20.1. Also in reference 2, the octave-band levels for 14 cases of excessive noise at low frequencies revealed that $L_A - \text{SIL} = 14$ dB is clearly unacceptable, while in offices with acceptable noise levels $L_A - \text{SIL}$ did not exceed approximately 7.5 dB.)

Engineering Method: NC Curves

The most widely used method today for evaluating the suitability of the noise in a space for human occupancy and for writing noise specifications employs the NC curves shown in Fig. 20.1.[3,4] The numerical values from which Fig. 20.1 was plotted are given in Table 20.2 (rounded to the nearest decibel). In measuring a noise the sound-level meter (with octave-band filtering) is set to yield L_{eq} with a slow meter, flat response. The integration time T can be of any desired length—seconds, hours, or months. If each octave-band meter reading slowly fluctuates over a small range, the average value is used.

For writing specifications, the suggested NC ratings for various occupancies are shown in Table 20.2. For example, for small offices, NC-35 to NC-40 is listed.

When evaluating a measured noise spectrum, the octave-band levels are plotted on the set of curves in Fig. 20.1. The rating given to the noise is set by the band level that "touches" the highest NC curve (interpolated to the nearest decibel). For example, assume that the levels in the eight bands from 31.5 to 4000 Hz were 68, 65, 61, 58, 50, 42, 37, and 30 dB, respectively. The highest NC rating

TABLE 20.1 Recommended A-Weighted Sound-Level Criteria for HVAC Systems for Rooms (Unoccupied) of Various Uses

Occupancy	A-Weighted Sound Level L_A in dBA
Small auditoriums	35–39
Large auditoriums, large drama theaters, and large churches (for very good speech articulation)	30–35
TV and broadcast studios (close microphone pickup only)	16–35
Legitimate theaters	30–35
Private residences	
Bedrooms	35–39
Apartments	39–48
Family rooms and living rooms	39–48
Schools	
Lecture and classrooms	
With areas less than 70 m^2	44–48
With areas greater than 70 m^2	39–44
Open-plan classrooms	44–48
Hotels/motels	
Individual rooms or suites	39–44
Meeting/banquet rooms	35–44
Service support areas	48–57
Office buildings	
Offices	
Executive	35–44
Small, private	44–48
Large, with conference tables	39–44
Conference rooms	
Large	35–39
Small	39–44
Open-plan areas	44–48
Business machines, computers	48–53
Public circulation	48–57
Hospitals and clinics	
Private rooms	35–39
Wards	39–44
Operating rooms	35–44
Laboratories	44–53
Corridors	44–53
Public areas	48–52
Movie theaters	39–48
Churches, small	39–44
Courtrooms	39–44
Libraries	44–48
Restaurants	48–52
Light maintenance shops, industrial plant control rooms, kitchens and laundries	52–62
Shops and garages	57–67

Note: Data based on L_A − SIL for NC curves of Table 20.2.

TABLE 20.2 Recommended NC and RNC Noise Criteria for HVAC Systems for Rooms (Unoccupied) of Various Uses

Occupancy	NC and RNC Recommended Criterion Curve
Recording studios	Lowest curve of Fig. 20.1
Broadcast studios (distant microphone pickup used)	10
Concert halls, opera houses, and recital halls (listening to faint musical sounds)	15–18
Small auditoriums	25–30
Large auditoriums, large drama theaters, and large churches (for very good speech articulation)	20–25
TV and broadcast studios (close microphone pickup only)	15–25
Legitimate theaters	20–25
Private residences	
Bedrooms	25–30
Apartments	30–40
Family rooms and living rooms	30–40
Schools	
Lecture and classrooms	
With areas less than 70 m^2	35–40
With areas greater than 70 m^2	30–35
Open-plan classrooms	35–40
Hotels/motels	
Individual rooms or suites	30–35
Meeting/banquet rooms	25–35
Service support areas	40–50
Office buildings	
Offices	
Executive	25–35
Small, private	35–40
Large, with conference tables	30–35
Conference rooms	
Large	25–30
Small	30–35
Open-plan areas	35–40
Business machines, computers	40–45
Public circulation	40–50
Hospitals and clinics	
Private rooms	25–30
Wards	30–35
Operating rooms	25–35
Laboratories	35–45
Corridors	35–45
Public areas	40–45
Movie theaters	30–40
Churches, small	30–35
Courtrooms	30–35
Libraries	35–40
Restaurants	40–45
Light maintenance shops, industrial plant control rooms, kitchens and laundries	45–55
Shops and garages	50–60

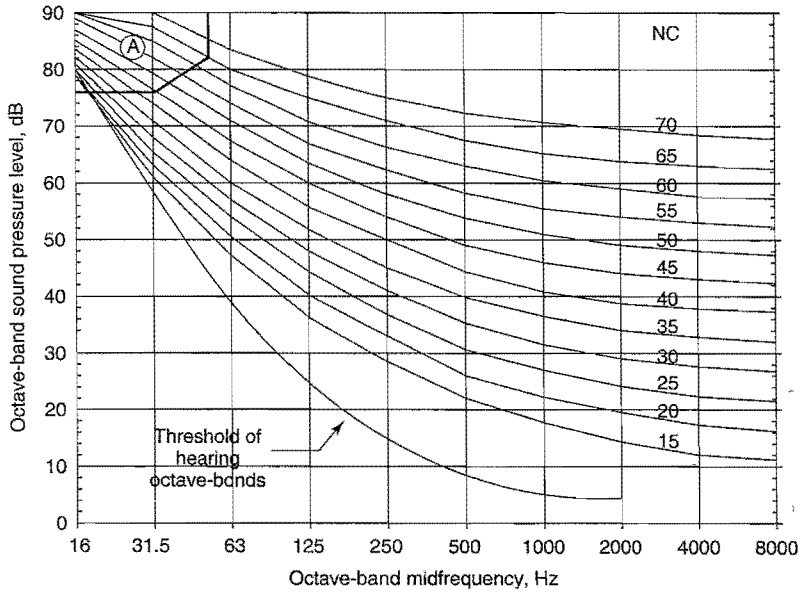


FIGURE 20.1 Noise criteria curves derived from interviews and simultaneous noise measurements extended to low frequencies by comparison with balanced NC (NCB) curves. These NC curves are used to rate noises by the "tangency method."[2,3,5,10] Region *A* indicates low-frequency levels that may produce feelable vibrations and rattles from lighting fixtures in lightweight constructions if fluctuations or surging is present. The threshold of hearing is taken from ANSI S12.2–1995.

curve "touched" by this spectrum is determined by the 58-dB level in the 250-Hz band and equals NC-50. This is the so-called tangency method of rating.

The NC curves were originally derived from a survey of noise in a large number of offices and spaces in a military Air Force base[5] and in several office buildings.[6] The surveys were conducted by asking occupants of rooms how they rated the noise both generally and at that instant (on a scale with six divisions from "very quiet" to "intolerably noisy") and then measuring the noise at that instant. It was determined that the activity most affected by the noise was speech communication both person to person and by telephone. However, it was also found that even though speech communication might be satisfactory in a space, the low-frequency noise levels could be so high as to be annoying. How much higher can the low-frequency noise be compared to the midfrequency noise? It was found that the overall loudness of the noise had to be taken into consideration. To answer this question, two quantities were measured, the SIL and the loudness level of the noise.

The SIL is a measure of the degree of interference of a noise with speech communication. It is standardized as the average sound pressure level, in decibels, in the four octave bands 500, 1000, 2000, and 4000 Hz.[7]

TABLE 20.3 Noise Criteria Curves from Fig. 20.1 to Nearest Decibel

	By Octave-Band Center Frequencies, Hz									
NC CURVE	16	31.5	63	125	250	500	1000	2000	4000	8000
NC-70	90	90	84	79	75	72	71	70	68	68
NC-65	90	88	80	75	71	68	65	64	63	62
NC-60	90	85	77	71	66	63	60	59	58	57
NC-55	89	82	74	67	62	58	56	54	53	52
NC-50	87	79	71	64	58	54	51	49	48	47
NC-45	85	76	67	60	54	49	46	44	43	42
NC-40	84	74	64	56	50	44	41	39	38	37
NC-35	82	71	60	52	45	40	36	34	33	32
NC-30	81	68	57	48	41	35	32	29	28	27
NC-25	80	65	54	44	37	31	27	24	22	22
NC-20	79	63	50	40	33	26	22	20	17	16
NC-15	78	61	47	36	28	22	18	14	12	11

The loudness level is determined by a standardized computational procedure which yields results in units called phons.[8] Needed are measured octave- or one-third-octave-band levels in all the frequency bands.

The studies revealed that the loudness level (in phons) should not exceed the SIL (in decibels) by more than about 24 units if the space is not to be annoying to the occupants. Because low-frequency sounds are less loud than high-frequency sounds, their levels can be higher. Thus with increasing frequency the NC curves slope downward monotonically and their shape is determined to resemble that of well-known "equal-loudness" curves.[9] The amount of slope and the shape of the spectrum are determined by the 24-unit difference just mentioned. (*Note*: The average of the levels in the four speech interference bands for each NC curve in Fig. 20.1 is between 0.25 and 1 dB higher than the designating number shown for the curve. The reason is that a shift in the frequency limits for the octave bands was standardized some years after these curves were developed. However, the decibel values for the points and the designating numbers on these curves are exactly the same as originally presented.)

It must be emphasized that the NC curves so derived give the upper permissible limit of the low-frequency noise once the SIL is known. Thus, the shape of a NC curve is not the shape of an ideal noise spectrum, but rather is the shape of a "not-to-be-exceeded" spectrum.

Two basic assumptions concerning the curves of Fig. 20.1 are that the noise contains no pure tones and there is no surging of the noise from fans that drive the HVAC system.

Concerning the measurement of sound levels at each point on a NC curve, the meter response is set to suit the desired result. If the equivalent noise level over a period of hours or days is decided, the slow meter response is selected. For short samples of the measured noise, the fast response is used. For example, a series of 100–1000 samples each 100 ms long requires fast response. The meter

can show the equivalent level L_{eq} in decibels for the sequence, or the maximum level L_{max}, or the level above which 10% of the interval levels are found, called L_{10}, or the L_{50} level, which is the mean level, or the L_{90} level. Some consultants believe the L_{50} level correlates well with people's judgment of the acceptability of their noise environment, provided that the speech intelligibility requirement is met.

Comments about NC Curves. The NC curves as originally derived did not extend down to the 31.5- and 63-Hz octave bands. These two bands have been added by the author to the original curves, based on the studies that led to the balanced noise criterion (NCB) curves that are briefly discussed below. The revised curves of Fig. 20.1 have been shown in two studies to predict successfully all known cases of sizable complaints by occupants of existing building spaces.[10,11*] In none of these cases was surging detected.

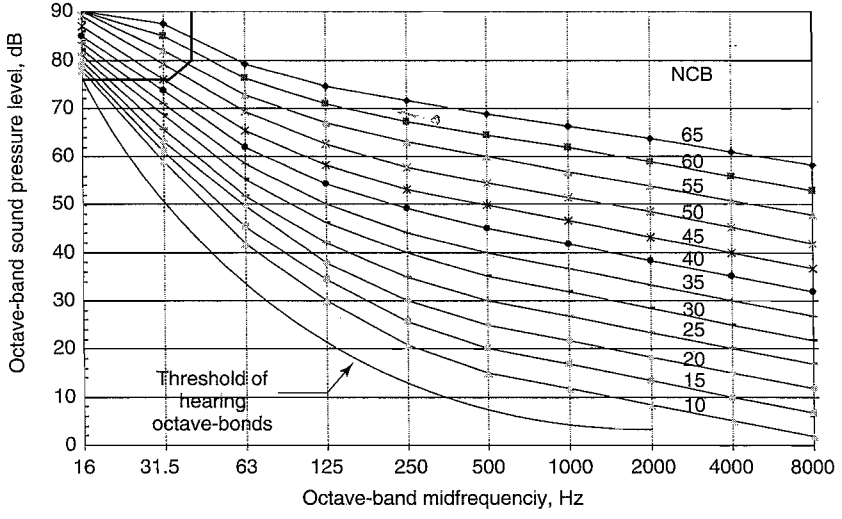


FIGURE 20.2 Balanced noise criteria curves, taken from ANSI S12.2–1995. These curves are used to rate noises with a procedure described in the standard and ref. 10.

*In ref. 11, 238 measured sound-pressure-level spectra were obtained from the consulting files of Cavanaugh Tocci Associates. Plots were made of the relation between NC (tangency method) and NCB (tangency method). The two were closely related with an $R^2 = 0.97$. Similarly, the NCB rating was plotted in relation to the RC or RC II rating, with a correlation of $R^2 = 0.98$, except that the RC values are about 2 dB greater than the NC values because the NC curves are based on the average of the levels in the 500-, 1000-, 2000-, and 4000-Hz bands, while the RC curves are labeled based on the average of the levels in the 500-, 1000-, and 2000-Hz bands.

NCB Curves

The NCB curves shown in Fig. 20.2[7] were derived from the following premises: (1) the rating number for each curve should equal its four-band SIL; (2) the calculated octave-band loudness for those bands from 125 to 8000 Hz should contain the same number of critical (hearing) bands, and for the two lower bands, the loudnesses should be weighted downward in proportion to the fraction of critical bands contained; and (3) the difference between the SIL (in decibels) and the loudness level (in phons) for a criterion curve should not exceed 24 units. The detailed method of applying NCB curves to the evaluation of HVAC noise is not discussed here, because they have not found widespread use, in spite of their being contained in ANSI S12.2–1995. As mentioned above, the NC curves have been extended to the 16- and 31.5-Hz bands by comparison with the rationale that led to the NCB curves. Except for the method of applying them to the rating of a noise, the NCB curves differ little from the NC curves of Fig. 20.1.

The levels taken from the NCB curves (rounded to the nearest decibel) are listed in Table 20.4.

RC (Originally Called "Revised Criteria") Curves

The RC criteria curves for evaluating noise in a room or for specifications were built around the point of view that sound levels lower than those shown by the NC curves of Fig. 20.1 should always be specified for the bottom three-octave frequency bands (31.5, 63, and 125 Hz). The primary reason given is that if there are strong fluctuations or surging in the HVAC noise, the specified low-frequency octave-band levels for the RC curves ought to be low enough so that the noise is not disturbing.

The basis for the RC curves was a set of measurements made in the early 1970s of the noise in 68 offices where the HVAC noise levels were judged satisfactory.

TABLE 20.4 Balanced Noise Criteria Curves from Fig. 20.2 to Nearest Decibel

	By Octave-Band Center Frequencies, Hz									
NCB CURVE	16	31.5	63	125	250	500	1000	2000	4000	8000
NCB-65	97	88	79	75	72	69	66	64	61	58
NCB-60	94	85	76	71	67	64	62	59	56	53
NCB-55	92	82	72	67	63	60	57	54	51	48
NCB-50	89	79	69	62	58	55	52	49	45	42
NCB-45	87	76	65	58	53	50	47	43	40	37
NCB-40	85	73	62	54	49	45	42	38	35	32
NCB-35	84	71	58	50	44	40	37	33	30	27
NCB-30	82	68	55	46	40	35	32	28	25	22
NCB-25	81	66	52	42	35	30	27	23	20	17
NCB-20	80	63	49	38	30	25	22	18	15	12
NCB-15	79	61	45	34	26	20	17	13	10	7
NCB-10	78	59	43	30	21	15	12	8	5	2

When plotted, those noise-level spectra, on average, sloped off linearly with frequency at the rate of 5 dB/octave in the bands from 63 to 4000 Hz. It was concluded that if the measured spectra in satisfactory office environments had that characteristic, the −5 dB/octave line is "optimum," but no comparisons with other spectra were made.

The RC curves are shown in Fig. 20.3 and the values are listed in Table 20.5.[12]

In this chapter, only the Mark II version of the RC method is employed, which differs from the original version in that the levels in the 16- and 31.5-Hz bands are equal instead of the 16-Hz band being 5 dB higher than the 31.5-Hz band. Also the procedure for evaluating measured data is different.

An RC curve suitable for a particular type of room may be determined from Table 20.6. The values there were chosen to permit satisfactory speech intelligibility, where that is important, or to provide noise levels that are not above normal activity sounds.

When evaluating a noise spectrum using the RC method, the first step is to determine the average of the measured sound levels in the 500-, 1000-, and 2000-Hz octave bands, the *midfrequency average*, which Reference 11 calls *level at midfrequencies* (LMF). This number identifies the level of the measured spectrum in the frequency region most important to speech communication, and it selects the reference RC curve used as a starting point for the analysis that follows. For example, if the LMF is 36 dB, the RC-36 becomes the reference curve. If that LMF is suited to the activities that take place in the space in which

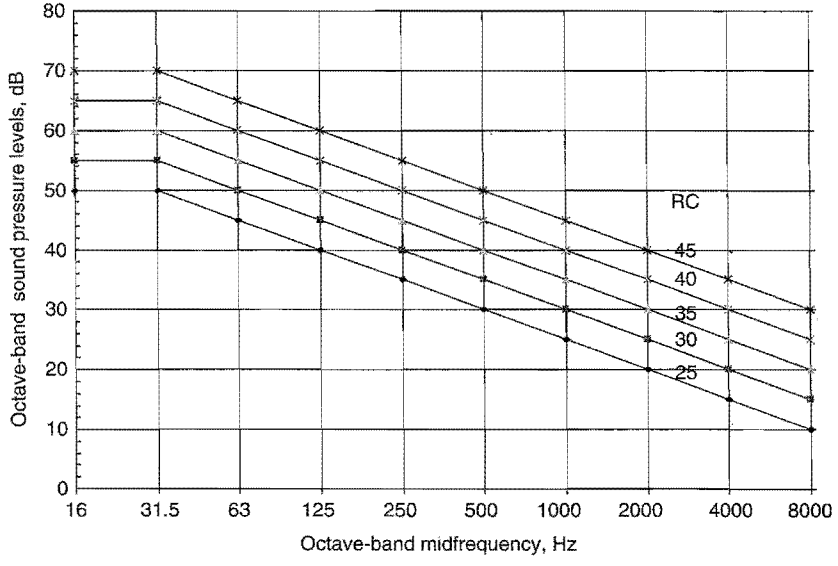


FIGURE 20.3 Noise criteria RC Mark II curves, derived from measurements of HVAC noise in offices. These RC curves are used to rate noises by a procedure detailed in ref. 12.

TABLE 20.5 Noise Criteria RC Curves from Fig. 20.3 to Nearest Decibel

	By Octave-Band Center Frequencies, Hz									
RC CURVE	16	31.5	63	125	250	500	1000	2000	4000	8000
RC-25	50	50	45	40	35	30	25	20	15	10
RC-26	51	51	46	41	36	31	26	21	16	11
RC-27	52	52	47	42	37	32	27	22	17	12
RC-28	53	53	48	43	38	33	28	23	18	13
RC-29	54	54	49	44	39	34	29	24	19	14
RC-30	55	55	50	45	40	35	30	25	20	15
RC-31	56	56	51	46	41	36	31	26	21	16
RC-32	57	57	52	47	42	37	32	27	22	17
RC-33	58	58	53	48	43	38	33	28	23	18
RC-34	59	59	54	49	44	39	34	29	24	19
RC-35	60	60	55	50	45	40	35	30	25	20
RC-36	61	61	56	51	46	41	36	31	26	21
RC-37	62	62	57	52	47	42	37	32	27	22
RC-38	63	63	58	53	48	43	38	33	28	23
RC-39	64	64	59	54	49	44	39	34	29	24
RC-40	65	65	60	55	50	45	40	35	30	25
RC-41	66	66	61	56	51	46	41	36	31	26
RC-42	67	67	62	57	52	47	42	37	32	27
RC-43	68	68	63	58	53	48	43	38	33	28
RC-44	69	69	64	59	54	49	44	39	34	29
RC-45	70	70	65	60	55	50	45	40	35	30

the measurements were made (from Table 20.6), and if the spectrum closely approximates the reference curve, the noise is given a rating of "N," neutral.

If the measured spectrum is not "neutral," the RC (latest version, Mark II) rating procedure begins with the reference curve derived from it. Next, determination of three quantities is calculated from the measured spectrum, each called, *energy-average spectral deviation factor*. Three frequency regions are chosen for this analysis—low (16–63 Hz), middle (125–500 Hz), and high (1000–4000 Hz)—dubbed the LF, or "rumble," the MF, or "roar," and the HF, or "hiss," regions.

The procedure is as follows: First, for each octave-frequency band in the measured spectrum, the difference in decibels between that spectrum and the reference RC curve is found. The sign may be either positive or negative. For each of the three frequency regions, LF, MF and HF, the three octave-band differences therein are summed on an *energy basis*, which yields an energy-average spectral deviation factor for that region. For example, assume the three-octave-band differences in the LF region are 4, 5, and 9 dB, giving an averaged energy level of 4.54, and 10 log 4.54 = 6.57 dB. This factor is also determined for the MF and HF regions, which, as an example here, we shall assume are equal to 4.82 and −0.92 dB. Next, the *quality assessment index* QAI is defined

TABLE 20.6 Recommended RC Criteria for HVAC Systems for Rooms (Unoccupied) of Various Uses

Occupancy	RC Criterion Curve[a]
Private residences	
Bedrooms	25–30 (N)
Apartments	30–35 (N)
Family rooms and living rooms	30–40 (N)
Schools	
Lecture and classrooms	30–35 (N)
Open-plan classrooms	35–40 (N)
Hotels/motels	
Individual rooms or suites	30–35 (N)
Meeting/banquet rooms	30–35 (N)
Halls, corridors, lobbies	35–40 (N)
Service support areas	40–50 (N)
Office buildings	
Executive offices	25–35 (N)
Private offices	30–35 (N)
Private offices with conference tables	25–30 (N)
Conference rooms	25–30 (N)
Open-plan areas	35–40 (N)
Business machines/computers	40–45 (N)
Public circulation	40–50 (N)
Hospitals and clinics	
Private rooms	25–30 (N)
Wards	30–35 (N)
Operating rooms	25–35 (N)
Laboratories	35–45 (N)
Corridors	35–45 (N)
Public areas	40–45 (N)
Churches	30–35 (N)
Libraries	35–40 (N)
Courtrooms	30–40 (N)
Restaurants	40–45 (N)

[a]N = neutral spectrum.

as the difference (in decibels) between the maximum and minimum values of the three spectral deviation factors just determined. In our example QAI = 6.57 − (−0.92) = 7.5 dB.

By the RC Mark II procedure, a *neutral* spectrum is one for which QAI is less than 5 dB and L_{16} and $L_{31.5}$ are at most 65 dB. If the highest *positive* spectral deviation factor occurs in the LF region, the spectrum is evaluated as having (i) a "marginal rumble" if 5 dB < QAI ≤ 10 dB or (ii) an "objectionable rumble" if QAI > 10 dB. If the highest positive factor falls in the MF or the HF regions, the same decibel ranges for QAI are listed for evaluating a spectrum as having "marginal or objectionable roar or hiss." For example, a measured spectrum might be designated as RC-45 (i.e., reference curve), roar (i.e., MF region), and probably objectionable (i.e., QAI exceeds 10 dB).[12]

The RC procedure would seem to mean that in writing a specification, a particular RC curve would be specified, but with the understanding that the measured levels in *any one* of the three frequency regions can be exceeded by about 5 dB without penalty.

It must be noted that in the 68 offices originally studied, the A-weighted slow meter sound level only covered a range of 40 to 50 dB, and thus none of the sound levels were considered that are found in spaces like concert halls at one extreme or factory spaces at the other. Second, the RC spectra are typical of HVAC practice in quality offices of the 1970 period and may not be typical at any future time.

The difficulty with the undisciplined use of the RC curves is that they penalize those HVAC installations that are free of surging or of large low-frequency fluctuations. In concert halls or other sites where very low background noise is required, the HVAC systems must be of highest quality, free of surging or significant low-frequency fluctuations. The measured NC noise spectra for concert halls usually are specified to be in the range of NC-15 to NC-18 (See Fig. 20.1 and Table 20.2). The levels in the completed halls usually follow a NC curve down to the 63-Hz band or lower. If RC curves equal to RC-15 to RC-20 were to be specified at such a site, 15 or more decibels of noise reduction would be required in the lowest bands. The cost of such an unnecessary reduction at low frequencies would be prohibitive. Of course, the perceived danger, from the specification point of view, is that a supplier might be told to meet, say, the NC-20 criterion curve, but that he or she might, in fact, install a low-cost HVAC system whose air supply source exhibited surging and then insist that the system meets the specification based on measurements in the octave bands with the usual sound-level meter set to slow response. Advanced techniques for evaluating spectra to determine whether the HVAC noise exhibits surging or large random fluctuations are presented in the next section.

Precision Method — RNC Curves[13,14]

There is a need to evaluate HVAC systems in which surging from the driving fan(s) takes place and to write specifications for the design of HVAC systems to avoid the chance of surging. To listeners, surging is very apparent and disturbing, and it must be addressed both in the writing of specifications and when diagnosing the seriousness of the noise afterward. Surging cannot be determined by a conventional sound-level meter with the slow meter speed and "A" frequency-weighted response in place, partly because surging primarily affects the levels in the low-frequency bands and partly because surging may be averaged out if the slow speed is used.

HVAC: Well Behaved or Surging? Surging usually can be heard aurally or it can be seen visually on a standard sound-level meter by observing the levels in the 16-, 31-, and 63-Hz octave bands. The sound-level meter must be set for fast response and flat frequency characteristic (or C weighting). If surging is found from listening or observing the levels in the octave bands above, then the RNC method of evaluation should be used to determine the seriousness of the noise condition.

First, Some Psychoacoustics. In devising a more precise method of evaluating whether the HVAC noise in a room is intrusive for its primary use, one must turn to the field of psychoacoustics for help. First, the ear only integrates (lumps together) significant variations in the level of a sound provided they occur within a short time period, that is, if the variations occur within a time period that is less than about 125 ms. That is, any fluctuations in HVAC noise that occur within a time interval of about 100 ms are perceived as though the noise were continuous (with the same energy) in that period without fluctuations.

A second reality is that the ear integrates the sound energy that falls within frequency bands called *critical bands*. Critical bands increase in width at about the same rate as the widths of the octave frequency bands increase except at low frequencies. In the frequency region below 125 Hz, the critical bands are about 100 Hz wide. Hence, the 16-, 31.5-, and 63-Hz octave-band levels must be combined in some manner into one band centered, say, at 31.5 Hz, in order that it can be treated in the same way as the higher frequency bands.

A third fact arising from the properties of hearing involves the loudness of sounds at low frequencies, that is, at frequencies below about 200 Hz. For the three octave bands 16, 31.5, and 63 Hz, a change of approximately 5 dB in level creates a doubling in the subjective loudness of a sound. For the 125-Hz band, a change of about 8 dB causes a doubling of loudness. For octave bands with midfrequencies of 250 Hz and above, a change of 10 dB is necessary to create a doubling in loudness. Thus, variations in level of the successive 100-ms intervals for the four lowest frequency bands must be treated differently from variations in level of the 100-ms intervals for the higher frequency bands. The RNC procedures, about to be described, are designed to take into account these three characteristics of the hearing system when evaluating the noise of a space.

Large Random Fluctuations. Even though surging is not observed orally or visually, the presence of large random fluctuations at low frequencies is still a possibility. The simplest test for this requires the observation of the differences between the L_{max} and L_{eq} levels or the L_{10} and the L_{eq} levels in the 16-, 31-, 63-, and 125-Hz bands with the meter set on fast. If the difference between L_{max} and L_{eq} for any one of the three lowest bands (16-, 31-, and 63-Hz octave bands) is greater than 7 dB, or $L_{10} - L_{eq} > 4$ dB, or if the difference between L_{max} and L_{eq} for the 125-Hz band is greater than 6 dB, or $L_{10} - L_{eq} > 3$ dB, large random fluctuations are indicated and the full RNC method should be used.

Well-Behaved HVAC Noise—Use NC Curves. When no surging or large-scale fluctuations are observed, L_{eq} measurements (slow scale) can be made in all the octave bands for any length of time T (fractions of minutes or longer) and the results compared with the NC curves of Fig. 20.1. The microphone used for the decibel measurements can be at one place in the room if the noise field is uniform throughout, or by measuring at a number of points and averaging the results, or simply by rotating the microphone at arm's length (2-m-diameter circle) and taking the average of the results.

Again, it must be borne in mind that all of the methods described in this chapter assume that there are no pure tones audible in the noise. If a pure tone(s) is suspected, narrow-band measurements (one-third octave or less) should be made to determine its frequency and intensity. Then, the pure-tone source should be located and steps taken to reduce its level before evaluating the remaining HVAC noise.

Found or Suspected Surging or Large Low-Frequency Fluctuations in HVAC Noise—Use RNC Curves. When surging or large low-frequency fluctuations are found or suspected, the RNC procedure is recommended to determine the penalty. It requires the use of a contemporary sound-level meter and a computer. The method incorporates the psychoacoustic facts discussed above. The RNC curves are shown in Fig. 20.4. Each RNC-X curve (e.g., RNC-40, RNC-50)

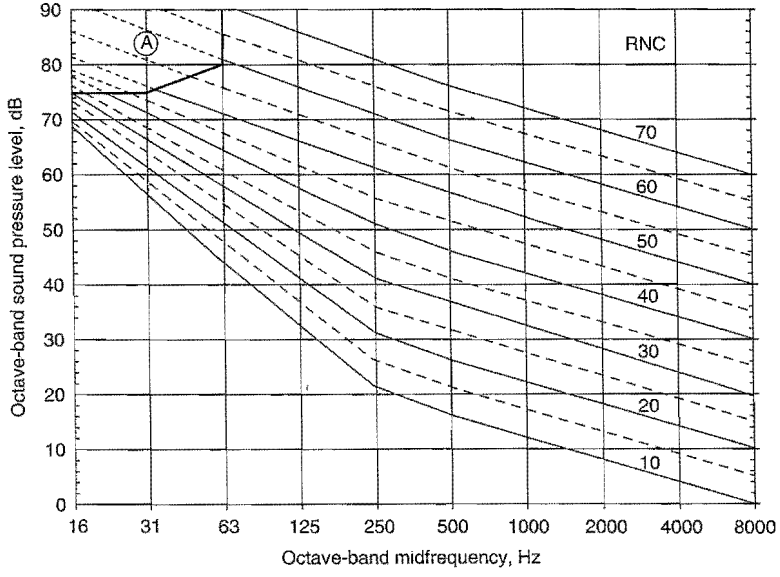


FIGURE 20.4 Balanced Noise criteria curves, devised in refs. 1,13, and 14 to rate noises that exhibit HVAC surging or large random fluctuations. In well-behaved HVAC systems the curves yield the same ratings as NC curves. When there are clearly audible HVAC surging or random vibrations, the curves yield ratings more like those of the RC curves—a penalty is imposed for surging that requires lower levels as measured with a "slow," sound-level meter setting.

TABLE 20.7 Coefficients Used in Eqs. (20.2) and (20.3) to Calculate RNC-X Curves of Fig. 20.4

Octave Band, Hz	Sound-Level Range, dB	K_{1ob}[a]	K_{2ob}
16	≤81	64.3333	3
	>81	31	1
31	≤76	51	2
	>76	26	1
63	≤71	37.6667	1.5
	>71	21	1
125	≤66	24.3333	1.2
	>66	16	1
250	All	11	1
500	All	6	1
1000	All	2	1
2000	All	−2	1
4000	All	−6	1
8000	All	−10	1

[a]The four-decimal figures are only to give calculated RNC-X even-decibel values.

can be derived from

$$L_{ob} = \frac{\text{RNC-}X}{K_{2ob}} + K_{1ob} \tag{20.2}$$

where RNC-X is the number on the curve, L_{ob} is the x-axis level for the particular octave band, and the constants K_{2ob} and K_{1ob} are taken from Table 20.7 for the particular octave bands.

Example 20.1. Calculate the SPL of the 63-Hz band for the RNC-20 curve of Fig. 20.4:

$$L_{ob} = (20/1.5) + 37.6667 = 13.3333 + 37.6667 = 51 \text{ dB}.$$

Conversely, the nearest RNC evaluation curve for a measured octave-band level can be obtained from

$$\text{RNC-}X = (L_{ob} - K_{1ob}) \times K_{2ob} \tag{20.3}$$

Example 20.2. Assume the measured level in the 125-Hz octave band L_{ob} is 55 dB. Determine which RNC curve (to nearest decibel) that measurement touches:

$$\text{RNC-X} = (55 - 24.3333) \times 1.2 = \text{RNC-37}$$

Recommended RNC Curves. The recommended RNC curves for spaces are the same as those for the NC curves and are given in Table 20.2.

If there is no surging or large scale-fluctuations, so that L_{eq} levels can be measured with the slow meter and flat frequency response, evaluation by the new RNC curves will yield results that are approximately equal to those from the NC curves. Therefore, the permissible L_{eq} levels at low frequencies compared to the SIL at midfrequencies will be as large as those shown in Fig. 20.1.

If surging and fluctuations exist, the RNC method "penalizes" the L_{eq} levels in the octave frequency bands below 300 Hz, so that if the disturbance in those frequency bands is large, the permissible L_{eq} levels may approach the low-frequency levels of the RC curves, as in Fig. 20.3.

Corrections to Measured Levels in Octave Bands at 16, 31.5, and 63 Hz When Surging or Large Fluctuations Exist. If surging and fluctuations exist, the RNC method penalizes the L_{eq} levels in the octave frequency bands below 300 Hz, so that if the disturbance in those frequency bands is large, the permissible L_{eq} levels may approach the low-frequency levels of the RC curves, as in Fig. 20.3. Contemporary sound-level meters can store up to 24 h of data for later downloading to a computer. The data should be recorded with a fast meter setting and a flat frequency response. The stored data (of whatever total time length) in bands or overall is sampled every 100 ms, forming the required octave-band time series for the RNC method. For the total time period, L_{peak}, L_{10}, and L_{50} are also available.

Each of the successive 100-ms samples is labeled i, where the ultimate i should be between 150 and 1000 depending on the suspected magnitude of the surging.

Because the loudness of a sound, at a given level, is considerably less at 16 Hz than at 31.5 Hz and, in turn, the loudness is considerably less at 31.5 Hz than that at 63 Hz, in the RNC method the three octave bands with midfrequencies at 16, 31.5, and 63 Hz are combined and replaced by a "three-band-sum" at 31.5 Hz. To do this, all of the measured 100-ms samples for the 16-Hz octave band are reduced by 14 dB and the samples for the 63-Hz octave band are increased by 14 dB. These adjusted levels for the 16- and 63-Hz bands are combined with the measured levels in the 31.5-Hz band on *an energy basis* and the new level (in decibels) is called a three-band-sum.

The ith 100-ms sample of this three-band-sum is called L_{LFi}. Calculate $L_{LF,eq}$ for the three-band-sum by summing the energies of the samples and dividing by the number of samples and taking 10 log of the result. Also, calculate L_{LFm}, the mean level of the set of three-band-sum samples.

The object now is to determine a correction K_{LFC} to be added to the *measured* L_{eq} at 31.5 Hz (not the three-band-sum) that takes into consideration both the L_{LFi} values and the fact that a change of only 5 dB is needed for a doubling of loudness at 31.5 Hz—and at 125 Hz, 8 dB is needed. Let δ stand for this change.

First calculate the correction at 31.5 Hz, K_{LFC}:

$$K_{LFC} = K_{LF\delta} - (L_{LF,eq} - L_{LFm}) \tag{20.4}$$

where

$$K_{LF\delta} = 10 \log \left(\frac{1}{N} \sum_{i=1}^{N} 10^{L\alpha/10} \right) \tag{20.5}$$

and where, at 31.5 Hz ($\delta = 5$ dB),

$$L\alpha = \frac{10}{\delta}(L_{LFi} - L_{LFm}) = 2(L_{LFi} - L_{LFm}) \tag{20.6}$$

The quantity K_{LFC} is added to the *measured* equivalent level L_{eq} (long time energy average) in the 31.5-Hz octave band and is plotted on Fig. 20.4 (no numbers are plotted in the 16- and 63-Hz bands). If data are not available for the 16-Hz band, the three-band-sum is determined for the 31.5- and 63-Hz bands.

Correction to Measured Level in Octave Band at 125 Hz If Surging Is Observed or Suspected. The level of each element of the 100-ms series at 125 Hz is called L_{125i}. Calculate L_{125eq} at 125 Hz by combining the energies of the samples and dividing by the number of samples and taking 10 log of the result. Also, calculate L_{125m}, the mean level of the set of samples at 31.5 Hz. The correction to be added to the *measured* 125-Hz octave-band L_{eq} is called K_{125C} and is given by

$$K_{125C} = K_{125\delta} - (L_{125eq} - L_{125m}) \tag{20.7}$$

where

$$K_{125\delta} = 10 \log\left(\frac{1}{N}\sum_{i=1}^{N} 10^{L\beta/10}\right) \tag{20.8}$$

and where, at 125 Hz ($\delta = 8$ dB),

$$L\beta = \frac{10}{\delta}(L_{125i} - L_{125m}) = 1.25(L_{125i} - L_{125m}) \tag{20.9}$$

Example for Surging. Used is a set of random data having a Gaussian distribution with a standard deviation of about 3 dB for the combined 16–31.5–63-Hz band. Superimposed is a sinusoidal variation with a peak-to-peak amplitude of 15 dB. Shown in Table 20.8 are 10 of the 1000 measured octave-band levels each 100 ms in length. The three-band-sum defined above is given in the last column.

The summary data for 1000 samples are listed in Table 20.9. The correction K_{LFC} to be added to the L_{eq} at 31.5 Hz comes from Eq. (20.4) and equals 11.5 dB, yielding the adjusted 31.5-dB band level equal to 73.1 dB. From Eq. (20.7), the correction K_{125C} is found to be 1.6 dB, yielding 44.7 dB. The corrected spectrum is shown in the last line of Table 20.9. When the corrected spectrum is plotted in Fig. 20.4 or is determined from Eq. (20.3), it is found that the highest RNC curve touched is RNC-44 (at 31.5 Hz). If there had been no correction, the highest curve touched would have been RNC-22. The strong surging and turbulence has changed the rating from RNC-22 to RNC-44.

TABLE 20.8 Ten 100-ms Samples from a Total of 1000 Samples[a]

ith Band Numbers	By Octave-Band Mid frequencies, Hz										L_{LFi} Three-Band-Sum, (dB)
	16	31.5	63	125	250	500	1000	2000	4000	8000	
1	41.3	52.0	32.4	33.8	26.7	21.7	14.2	10.7	7.4	3.4	53.1
2	63.8	53.8	35.3	35.8	28.5	24.7	17.7	14.1	8.3	4.0	56.3
3	48.8	46.9	41.9	32.5	24.8	22.2	16.1	10.0	5.7	2.5	56.4
4	69.6	54.8	39.6	42.3	31.8	28.2	21.1	19.4	12.9	9.3	59.5
5	67.3	55.7	45.8	46.4	41.0	36.7	29.2	25.2	22.3	17.4	61.9
6	75.5	52.3	44.6	39.0	32.3	26.8	22.7	19.2	12.7	8.7	63.6
7	59.7	52.8	50.0	50.3	37.8	33.8	28.5	25.5	19.5	16.8	64.4
8	61.8	63.0	46.8	47.8	41.4	35.9	27.6	25.2	18.7	16.1	65.1
9	65.2	65.2	46.6	44.3	39.5	34.1	26.7	23.9	19.1	14.3	66.6
10	64.8	66.5	44.2	42.7	34.2	30.0	24.0	19.2	15.3	12.4	67.2
Mean level L_{LFm} of these 10 samples.											61.4
Standard deviation σ of these 10 samples.											4.8
Equivalent sound level L_{eq} of these 10 samples.											63.4

[a]Data Represent a Gaussian noise with a superimposed surge implemented by a sine wave with a 2-s period and a 15-dB peak-to-peak amplitude.

Simplified Method: Corrections to Measured Levels in 16–125-Hz Octave Bands When There Are Large Random Reflections and Not Strong Surging. By this method, the same equations are used to determine the corrections to the adjusted 31- and 125-Hz bands, that is, Eqs. (20.4) and (20.7), but the quantities $K_{LF\delta}$ and $K_{125\delta}$ are calculated from

$$K_{LF\delta} = 0.115\left(\frac{10}{\delta}\right)^2 \sigma_{LF}^2 = 0.115(2)^2\sigma_{LF}^2 = 0.46\sigma_{LF}^2 \tag{20.10}$$

where σ_{LF} is the standard deviation of the L_{LFi} (three-band-sum) series, and

$$K_{125\delta} = 0.115\left(\frac{10}{\delta}\right)^2 \sigma_{125}^2 = 0.115(1.2)^2\sigma_{125}^2 = 0.166\sigma_{125}^2 \tag{20.11}$$

where σ_{125} is the standard deviation of the L_{125i} series.

20.3 ACOUSTICALLY INDUCED VIBRATIONS AND RATTLES

From experience, primarily on the West Coast of the United States, an assessment has been made of the probability of acoustically induced vibration and rattles in lightweight wall and ceiling constructions (including light fixtures, windows, and some furnishings). Obviously, significant fluctuations or surging must be present in the HVAC noise. The region of likely probability where such vibrations in lightweight construction can be clearly felt is shown as A in Figs 20.1–20.4.[11] In

TABLE 20.9 Summary Data for RNC Example[a]

		Octave-Band Mid frequencies, Hz								
	Three-Band-Sum	16	31.5	63	125	250	500	1000	2000	4000	8000
L_{eq}	64.5	68.6	61.8	46.0	43.2	35.9	30.9	24.9	20.9	17.0	12.9
L_m (mean)	60.3	60.2	62.0	54.9	42.1	39.9	32.9	28.0	22.0	18.0	14.0
$L_{eq} - L_m$	4.2	6.6	6.8	3.9	3.2	2.9	2.9	2.9	2.9	2.9	2.9
Eqs. (20.5) and (20.8)	15.5	—	—	—	4.8						
Eqs. (20.4) and (20.7)											
Band corrections	—	—	11.3	—	1.6						
Corrected spectrum	—	—	73.1	—	44.7	35.9	30.9	24.9	20.9	17.0	12.9
Highest RNC curve "touched"	—	—	44	—	25	25	25	23	23	23	22

[a]The L_{eq} is the energy average level in each octave band for all 1000 of the 100-ms samples. The three-band-sum correction of 11.3 dB is added to the L_{eq} of the 31.5-Hz octave band to give an adjusted (for surging) level of 73.1 dB. At 125 Hz the adjusted level is 44.8 dB, 1.6 dB above the L_{eq} level.

very well built structures, such as are expected in concert halls and opera houses, the sound levels can extend into region A without expectation of feelable surface vibrations or audible rattles. In office and school buildings attention should be paid to L_{eq} levels that reach 70 dB or more in the 16- and 31.5-Hz octave bands because of current trends in HVAC design and installation.

20.4 CRITERIA FOR NOISE ANNOYANCE IN COMMUNITIES

The major sources of noise in communities are road, rail and air traffic, industries, construction, and public works. The most common metric used in the United States for estimating the annoyance or disturbance of community noise is the A-weighted day–night sound level (L_{dn}) [see Eq. (1.25)] with slow meter response. The A weighting discriminates against low-frequency sound energy, similar to the way that the hearing apparatus judges loudness. The sound energy of each noise-producing event is summed separately into the total. All of the energy of a noise that rises and falls as a source approaches and departs is summed into the total. The sound energy of each event at night is multiplied by 10 before it is added into the total. This treatment means that a few aircraft fly-bys at night may be as annoying to residents as a large number in the daytime. The European Union countries, for the most part, use a day–evening–night level.

The day–night sound level (L_{dn}) that is agreed on by nearly all agencies, boards, and standards-setting bodies to be the threshold for noise impact in urban residential areas is $L_{dn} = 55$ dBA.[15] In other words, people will begin to complain seriously about the noise if the level is higher. Some agencies speak of this energy-average level as being determined over a period of 12 months. Only the U.S. Federal Aviation Administration (FAA) and the Department of Defense (DOD) speak of a L_{dn} equal to 65 dBA as being the level at which noise begins to impact unfavorably on people in residential areas. Some studies indicate that in urban communities just under half of the U.S. population is exposed to L_{dn} levels of 55 dBA or greater. The World Health Organization (WHO, 1999) has stated that serious annoyance may occur for a L_{dn} of approximately 55 dBA, while moderate annoyance will have a threshold of about 50 dBA. It further recommends that the maximum level L_{max} at night should not exceed 40 dBA.

A possible reason for the 65-dBA level used by the FAA and DOD is that people near airports, on average, have learned to accept higher noise levels or, if not, they have moved away. This also assumes that the airport's relations with the communities surrounding it are good. Quiet rural communities seem to demand lower (5–10 dBA) noise levels.

20.5 TYPICAL URBAN NOISE

A summary of A-weighted noise levels measured in U.S. city areas, daytime and nighttime, is given in Fig. 20.5. Trucks and buses are principal sources of

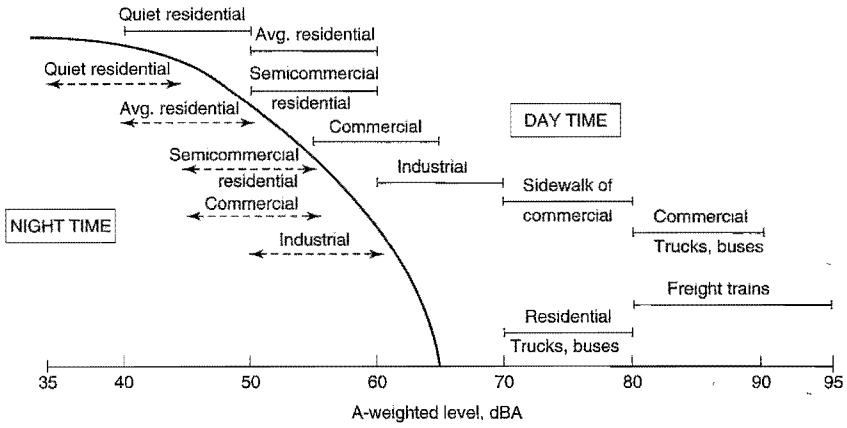


FIGURE 20.5 Schematic display of typical A-weighted noise levels by day and by night in different U.S. urban areas.[4] Noise around industrial areas is frequently caused by trucks.

noise. Parenthetically, the levels in this figure are not L_{dn}, but rather A-weighted levels in a residential area that vehicles produce when they travel on the streets surrounding that neighborhood. In urban residential areas, the noise is frequently the roar of traffic on thoroughfares that may be up to a kilometer away. Traffic noise is likely to be relatively steady and go on all night at a reduced level. If thoroughfares exist on two or more sides of an area, the noise is often nearly uniform over the area.

REFERENCES

1. American National (Draft) Standard ANSI S12.2-200x, "Criteria for Evaluating Room Noise" (not yet subject to extended comment or vote, 2004).
2. L. L. Beranek, "Applications of NCB and RC noise criterion curves for specification and evaluation of noise in buildings," *Noise Control Eng. J.*, **45**, 209–216 (1997).
3. L. L. Beranek, "Revised Criteria for Noise Control in Buildings," *Noise Control*, **3**, 19–27 (1957).
4. L. L. Beranek, *Noise and Vibration Control*, rev. ed., Institute of Noise Control Engineering, Marstun Itall, Iowa State University, Ames, IA, 1988.
5. L. L. Beranek, "Criteria for Office Quieting Based on Questionnaire rating Studies," *J. Acoust. Soc. Am.*, **28**, 833–852 (1956).
6. L. L. Beranek, *Transactions Bulletin No. 18*, Industrial Hygiene Foundation, Pittsburgh, PA, 1950.
7. ANSI S3.14–1977 (R-1986), "*Rating Noise with Respect to Speech Interference*," Acoustical Society of America, Melville, NY, 1986.
8. ANSI S3.3–1960 (R 1992), "*Procedure for the Computation of the Loudness of Noise*," Acoustical Society of America, Melville, NY, 1992.

9. D. W. Robinson, and L. S. Whittle, "The Loudness of Octave Bands of Noise," *Acustica*, **14**, 24–35 (1964).
10. L. L. Beranek, "Balanced Noise Criterion (NCB) Curves," *J. Acoust. Soc. Am.*, **86**, 650–664 (1989); "Application of NCB Noise Criterion Curves," *Noise Control Eng. J.*, **33**, 45–56 (1989).
11. G. C. Tocci, "Room Noise Criteria—The State of the Art in the Year 2000," *NOISE/NEWS International*, **8**, 106–119 (2000).
12. W. E. Blazier, "RC Mark II: A Refined Procedure for Rating the Noise of Heating, Ventilating and Air-Conditioning (HVAC) Systems in Buildings," *Noise Control Eng. J.*, **45**, 243–250 (1997).
13. P. D. Schomer, "Proposed Revisions to Room Noise Criteria," *Noise Control Eng. J.*, **48**, 85–96 (2000).
14. P. D. Schomer, and J. S. Bradley, "A Test of Proposed Revisions to Room Noise Criteria Curves," *Noise Control Eng. J.*, **48**, 124–129 (2000).
15. P. D. Schomer, *A White Paper: ASSESSMENT OF NOISE ANNOYANCE*, Schomer and Associates, Champaign, IL, April 22, 2001.

CHAPTER 21

Acoustical Standards for Noise and Vibration Control

ANGELO CAMPANELLA

Consultant
Columbus, Ohio

PAUL SCHOMER

Consultant
Champaign, Illinois

LAURA ANN WILBER

Consultant
Wilmette, Illinois

21.1 WHERE TO FIND AND HOW TO SELECT U.S. NATIONAL AND ISO STANDARDS

This chapter is arranged to provide the titles of North American and international (ISO) standards of interest to noise control engineers, according to specific noise control technology categories such as absorption and insulation (isolation). Acoustical terminology may be found in ANSI S1.1-1994 (R1999), *Acoustical Terminology* and ASTM C634, *Standard Terminology Relating to Environmental Acoustics*. The titles of some standards listed here are truncated to save space. Verbal descriptions, if offered, are brief. As with any technology, state-of-the-art advances bring updated versions of many of these documents. These standards are periodically reviewed and possibly revised by the responsible committees, often on a five-year cycle. A few ANSI standards have become an adoptation of the corresponding ISO document, indicated as "Adoption" or "NAIS" (Nationally Adopted International Standard). The reader is encouraged to search anew for recent revisions of these documents. Be advised that some engineering applications may specify past versions, especially as part of a long procurement program or arbitrated contract. It is up to the reader to determine, in participation with interested parties as necessary, which version to use. For the latest standards version, often listed according to the standard's numeral title (e.g., ANSI S12.19 can be found by searching www.ansi.org for S12.19), see the

public Internet web page listing by the providing agencies. Some of these agency pages are:

www.ANSI.org (ANSI)
www.ari.org (ARI—free downloads)
www.asastore.aip.org (ANSI + ISO standards available)
www.ashrae.com (ASHRAE)
www.asme.org (ASME)
www.astm.org (ASTM)
www.iec.ch (IEC)
www. iso.ch (ISO)
www.nssn.org (National Standards Systems Network, all standards available)
www.sae.org (SAE)

21.2 SOUND LEVEL MEASUREMENTS

Instrumentation

Standards for noise-measuring instruments, generally measuring sound pressure level (SPL) or "sound level," are listed separate from hearing-measuring instruments (audiometry). Common sound-measuring instruments include sound-level meters, calibrators, filters, and microphones. The most common sound measurement instruments for noise control are specified in ANSI S1.4. Such an instrument comprises a pressure sensor such as a condenser microphone, an amplifier with special wide-band and narrow-band filters, time-averaging circuits, a display, and some memory functions. The precision varies as type 0 (most accurate) to type 2 (least accurate). This entire system can be calibrated at any time with an appropriate calibrator. The acoustical velocity is rarely measured in practice, except for the use of dynamic (velocity) microphones for some audio purposes. The "intensity" method combines SPL and acoustical velocity measurements at a point to compute the intensity value at that point. Applicable standards are as follows:

ANSI S1.4-1983 (R2001), *Specification for Sound Level Meters.* Conforms closely to the IEC standard for sound-level meters, Publication 651, first edition, issued in 1979, but improved for measurement of transient sound signals and it permits the use of digital displays, rigorous definition of the fast and slow exponential time averaging, increase in the crest factor requirement to 10 for type 1 instruments, specification of a type 0 laboratory instrument with generally smaller tolerance limits than specified for type 1, and deletion of the type 3 survey instrument. The corresponding IEC standard (IEC 61672-1:2002 and IEC 61672-2:2003) contains more stringent environmental requirements. In 2003, ANSI S1.4 was under revision to better correspond.

ANSI S1.6-1984 (R2001), *Preferred Frequencies, Frequency Levels, and Band Numbers for Acoustical Measurements.*

ANSI S1.8-1989 (R2001), *Reference Quantities for Acoustical Levels.*

ANSI S1.9-1996 (R2001), *Instruments for the Measurement of Sound Intensity.* Requirements for instruments to measure sound intensity employing the two-microphone technique. Similar to IEC 1043.

ANSI S1.10-1966 (R2001), *Method for the Calibration of Microphones.*

ANSI S1.11-1986 (R1998), *Specification for Octave-Band and Fractional-Octave-Band Analog and Digital Filters.* Performance requirements for fractional-octave-band bandpass filters, in particular octave-band and one-third-octave-band filters, applicable to passive or active analog filters that operate on continuous-time signals to analog and digital filters that operate on discrete-time signals and to fractional-octave-band analyses synthesized from narrow-band spectral components. Four accuracy grades are allowed: the most accurate for precise analog and digital filters. The two least accurate grades meet the requirements of S1.11-1966. Also see IEC 61260:1995.

ANSI S1.14-1998, *Recommendations for Specifying and Testing the Susceptibility of Acoustical Instruments to Radiated Radio-Frequency Electromagnetic Fields, 25 MHz to 1 gHz.*

ANSI S1.15-1997/Part 1 (R2001), *Measurement Microphones.* Part 1: *Specifications for Laboratory Standard Microphones.* This is comparable to the international standard IEC 1094-1:1992, "Measurement Microphones—Part 1: Specifications for Laboratory Standard Microphones."

ANSI S1.16-2000, *Method for Measuring the Performance of Noise Discriminating and Noise Canceling Microphones.*

ANSI S1.17-2004/Part 1, *Measurement and Specifications of Insertion Loss of Wind Screens in Still or Slightly Moving Air.* Determines the insertion loss of wind screens when installed on measuring microphones over a defined frequency range.

ANSI S1.40-1984 (R2001), *Specification for Acoustical Calibrators.* Requirements for coupler-type acoustical calibrators, including the SPL in the coupler, the frequency of the sound, and the determination of the influence of atmospheric pressure, temperature, humidity, and magnetic fields on the pressure level and frequency of the sound produced by the calibrator. (Also see IEC 60942:2003.)

ANSI S1.42-2001, *Design Response of Weighting Networks for Acoustical Measurements.*

ANSI S1.43-1997 (R2002), *Specifications for Integrating Averaging Sound Level Meters.* Consistent with the relevant requirements of ANSI S1.4-1983 (R1997) but specifies additional characteristics needed to measure the time-average SPL of steady, intermittent, fluctuating, and impulsive sounds. (See also IEC 61672-1:2002 and IEC 61672-2:2003.)

ANSI S12.3-1985 (R2001), *Statistical Methods for Determining and Verifying Stated Noise Emission Values of Machinery and Equipment.* Preferred methods for determining and verifying noise emission values for machinery and equipment which are stated in product literature or labeled by other means.

SPL Measurement Techniques

ANSI S1.13-1995 (R1999), *Measurement of Sound Pressure Levels in Air.* Procedures for the measurement of sound levels in air at a single point indoors but

may be utilized in outdoor measurements under specified conditions. Includes identification of prominent discrete tones.

ASTM E1014-2000. *Measurement of Outdoor A-Weighted Sound Levels.* A guide for measuring outdoor sound levels over various time periods, intended to be used by practitioners in the field as well as by members of the general public who have little or no special technical training in areas relating to acoustics.

ANSI S1.25-1991 (R2002), *Specification for Personal Noise Dosimeters.* Makes provision for three exchange rates: 3, 4, and 5 dB per doubling of exposure time. Provides tolerances for the entire instruments, parameters, including frequency response, exponential averaging employing slow and fast transient time response, threshold, and dynamic range, for SPL measurement in a random-incidence sound field without the presence of a person wearing the instrument.

ANSI S12.19-1996 (R2001), *Measurement of Occupational Noise Exposure.* Methods that can be used to measure a person's noise exposure received in a workplace. Provides uniform procedures and repeatable results for the measurement of occupational noise exposure.

ISO 11204:1995, *Noise Emitted by Machinery and Equipment—Measurement of Emission Sound Pressure Levels at a Work Station and at Other Specified Positions—Method Requiring Environmental Corrections.*

Intensity Instruments and Measurement Techniques

ANSI S1.9-1996 (R2001), *Instruments for the Measurement of Sound Intensity.* Requirements for instruments to measure sound intensity employing the two-microphone technique. Similar to IEC 1043.

ANSI S12.12-1992 (R2002), *Standard Engineering Method for the Determination of Sound Power Levels of Noise Sources Using Sound Intensity.* Measures the sound power level of noise sources in indoor or outdoor environments using sound intensity instrumentation.

ISO 9614-1:1993, *Determination of Sound Power Levels of Noise Sources Using Sound Intensity.* Part 1: *Measurement at Discrete Points.* Part 2: *Measurement by Scanning.*

21.3 SOUND POWER MEASUREMENT TECHNIQUES

ANSI S12.5-1990 (R1997), *Requirements for the Performance and Calibration of Reference Sound Sources.* Requirements, including free-field laboratory calibration above a reflecting plane, for reference sound sources used in the substitution measurement of sound power.

ANSI S12.11-1987 (R1997), *Method for the Measurement of Noise Emitted by Small Air-Moving Devices.* Measures sound power emitted by small air-moving devices, reported as the noise power emission level in bels. Includes device-mounting methods, test environmental conditions, and device operation method during the tests.

ISO 10302:1996, *Method for the Measurement of Airborne Noise Emitted by Small Air-Moving Devices.*

ANSI S12.15-1992 (R2002), *Measurement of Sound Emitted by Portable Electric Power Tools, Stationary and Fixed Electric Power Tools, and Gardening Appliances.* Methods for SPL measurement and the subsequent calculation of sound power levels.

ANSI S12.23-1989 (R2001), *Method for the Designation of Sound Power Emitted by Machinery and Equipment.* Expressing the noise emission of machinery and equipment as overall A-weighted sound power on labels or other noise emission documentation.

ANSI S12.30-1990 (R2002), *Guidelines for the Use of Sound Power Standards and for the Preparation of Noise Test Codes.* Six standards for determining the sound power levels of equipment for sound test codes for machines and equipment.

ANSI S12.35-1990 (R2001), *Precision Methods for the Determination of Sound Power Levels of Noise Sources in Anechoic and Hemi-Anechoic Rooms.* Determination of the sound power levels of noise sources in laboratory anechoic or hemi-anechoic room, the instrumentation, installation, source operation, SPL measurement surface; calculation of sound power level, directivity index, and directivity factor.

ANSI S12.44-1997 (R2002), *Methods for Calculation of Sound Emitted by Machinery and Equipment at Workstations and Other Specified Positions from Sound Power Level.* Determining emission SPLs from the sound power level values of machinery and equipment at workstations and other locations.

ANSI S12.50-2002 National Adopted International Standard (NAIS), *Determination of Sound Power Levels of Noise Sources—Guidelines for the Use of Basic Standards.* Adoption of ISO 3740:2000. Summaries of ISO 3741–3747 and selection of one or more standards appropriate to any particular type (Clause 6 and Annex D). Used in the preparation of noise test codes (see ISO 12001) and noise testing where no specific noise test code exists.

ANSI S12.51-2002 (including Corrigendum 1 : 2001) NAIS standard, *Acoustics—Determination of Sound Power Levels of Noise Sources Using Sound Pressure—Precision Method for Reverberation Rooms.* Adoption of ISO 3741:1999, a direct method and a comparison method for determining the sound power level produced by a source in a standard environment.

ANSI S12.53/1-1999 ISO 3743-1:1994, *Determination of Sound Power Levels of Noise Sources—Engineering Methods for Small, Movable Sources in Reverberant Fields.* Part 1: *Comparison Method for Hard-Walled Test rooms. (Adoption of ISO 3743-1.)* Part 2: *Methods of Special Reverberation Test Rooms. (Adoption of ISO 3743-2.)*

ANSI S12.54-1999 ISO 3744:1994, *Determination of Sound Power Levels of Noise Sources Using Sound Pressure—Engineering Method in an Essentially Free Field over a Reflecting Plane.* Adoption of ISO 3744, sound power engineering accuracy, measurement by the comparison method in an anechoic environment.

ANSI S12.56-1999 ISO 3746:1995, *Determination of Sound Power Levels of Noise Sources Using Sound Pressure—Survey Method Using an Enveloping Measurement Surface over a Reflecting Plane.* Adoption of ISO 3746, determining the sound power level of sound sources In Situ, especially if nonmovable, in

octave bands from which the A-weighted sound power level is calculated. The accuracy will be that of either an engineering method or a survey method.

ARI 250-2001, *Performance and Calibration of Reference Sound Sources.*

ARI 280-95, *Requirements for the Qualification of Reverberant Rooms in the 63 Hz Octave Band.*

ASTM E1124-97, *Standard Test Method for Field Measurement of Sound Power Level by the Two-Surface Method.* An In Situ survey measurement of sound power level with sound pressure measurements at two concentric surfaces.

ISO 3740:2000, *Determination of Sound Power Levels of Noise Sources—Guidelines for the Use of Basic Standards.*

ISO 3741:1999, *Determination of Sound Power Levels of Noise Sources Using Sound Pressure—Precision Methods for Reverberation Rooms.*

ISO 3743-1:1994, *Determination of Sound Power Levels of Noise Sources—Engineering Methods for Small, Movable Sources in Reverberant Fields.* Part 1: *Comparison Method for Hard-Walled Test Rooms.* Part 2: *Methods for Special Reverberation Test Rooms.*

ISO 3744:1994, *Determination of Sound Power Levels of Noise Sources Using Sound Pressure—Engineering Method in an Essentially Free Field over a Reflecting Plane.*

ISO 3745:1977, *Determination of Sound Power Levels of Noise Sources—Precision Methods for Anechoic and Semi-Anechoic Rooms.*

ISO 3746:1995, *Determination of Sound Power Levels of Noise Sources Using Sound Pressure—Survey Method Using an Enveloping Measurement Surface over a Reflecting Plane.*

ISO 3747:2000, *Determination of Sound Power Levels of Noise Sources Using Sound Pressure—Comparison Method In Situ.*

ISO 5135:1997, *Determination of Sound Power Levels of Noise from Air-Terminal Devices, Air-Terminal Units, Dampers and Valves by Measurement in a Reverberation Room.*

ISO 5136:1990, *Determination of Sound Power Radiated into a Duct by Fans—In-Duct Method.*

ISO 6926:1999, *Requirements for the Performance and Calibration of Reference Sound Sources Used for the Determination of Sound Power Levels.*

21.4 MACHINERY NOISE EMISSION MEASUREMENT TECHNIQUES

ANSI S12.1-1983 (R2001), *Guidelines for the Preparation of Standard Procedures to Determine the Noise Emission from Sources.* Included are the general questions to be asked during development of a measurement procedure. Included are prefatory material, measurement conditions, measurement operations, data reduction, preparation of a test report, and guidelines for the selection of a descriptor for noise emission.

ANSI S12.10-2002 ISO 7779:1999 NAIS standard, *Measurement of Airborne Noise Emitted by Information Technology and Telecommunications Equipment.* Adoption of ISO 7779:1999 and its amendment ISO 7779: 1999/FDAM 1.

ANSI S12.16-1992 (R2002), *Guidelines for the Specification of Noise of New Machinery.* Methods to calculate workplace noise SPL from test data produced by manufacturers of stationary equipment. This references existing ANSI, trade, and professional association measurement standards and techniques to be used by manufacturers to produce individual raw machine sound power or SPL test data.

ANSI S12.43-1997 (R2002), *Methods for the Measurement of Sound Emitted by Machinery and Equipment at Workstations and Other Specified Positions.* Three methods to measure SPLs: (1) in a free field over a reflecting plane, (2) in normal operating environments, and (3) when operating in their normal environments when less accurate measurements are acceptable.

ARI 530-95, *Method of Measuring Sound and Vibration of Refrigerant Compressors.*

ARI 575-94, *Method of Measuring Machinery Sound within an Equipment Space.*

ISO 4412-1:1991, *Hydraulic Fluid Power—Test Code for Determination of Airborne Noise Levels.* Part 1: *Pumps.* Part 2: *Motors.* Part 3: *Pumps—Method Using a Parallelepiped Microphone Array.*

ISO 4871:1996, *Declaration and Verification of Noise Emission Values of Machinery and Equipment.*

ISO 7574-1:1985, *Statistical Methods for Determining and Verifying Stated Noise Emission Values of Machinery and Equipment.* Part 1: *General Considerations and Definitions.* Part 2: *Methods for Stated Values for Individual Machines.* Part 3: *Simple (Transition) Method for Stated Values for Batches of Machines.* Part 4: *Methods for Stated Values for Batches of Machines.*

ISO 7779:1999, *Measurement of Airborne Noise Emitted by Information Technology and Telecommunications Equipment.*

ISO 9295:1988, *Measurement of High-Frequency Noise Emitted by Computer and Business Equipment.*

ISO 9296:1988, *Declared Noise Emission Values of Computer and Business Equipment.*

ISO 9611:1996, *Characterization of Sources of Structure-Borne Sound with Respect to Sound Radiation from Connected Structures—Measurement of Velocity at the Contact Points of Machinery When Resiliently Mounted.*

ISO 11200:1995, *Noise Emitted by Machinery and Equipment—Guidelines for the Use of Basic Standards for the Determination of Emission Sound Pressure Levels at a Work Station and at Other Specified Positions.*

ISO 11201:1995, *Noise Emitted by Machinery and Equipment—Measurement of Emission Sound Pressure Levels at a Work Station and at Other Specified Positions—Engineering Method in an Essentially Free Field over a Reflecting Plane.*

ISO 11202:1995, *Noise Emitted by Machinery and Equipment—Measurement of Emission Sound Pressure Levels at a Work Station and at Other Specified Positions—Survey Method* In Situ.

ISO 11203:1995, *Noise Emitted by Machinery and Equipment—Determination of Emission Sound Pressure Levels at a Work Station and at Other Specified Positions from the Sound Power Level.*

ISO 10846, *Acoustics and Vibration—Laboratory Measurement of Vibro-Acoustic Transfer Properties of Resilient Elements.* Part 1—1997: *Principles and Guidelines.* Part 2—1997: *Dynamic Stiffness of Elastic Supports for Translatory Motion—Direct Method.* Part 3—2002: *Indirect Method for Determination of the Dynamic Stiffness of Resilient Supports for Translatory Motion.*

ISO 11690-1, *Recommended Practice for the Design of Low-Noise Workplaces Containing Machinery.* Part 1: *Noise Control Strategies.* Part 2: *Noise Control Measures.* Part 3: *Sound Propagation and Noise Prediction in Workrooms.*

21.5 IMPACT OF NOISE IN WORKPLACE

Two qualities of workplace noise are of concern as they affect damage to hearing and speech communication. Environmental noise includes vibration and infrasound. Hearing conservation measurements are of two forms: measurement of hearing acuity and measurement of noise levels in work and recreational environments.

Hearing Testing (Audiometry) Equipment and Procedures

ANSI S3.1-1999, *Maximum Permissible Ambient Noise Levels for Audiometric Test Rooms.* Specifies maximum permissible ambient noise levels (MPANLs) allowed in an audiometric test room.

ANSI S3.6-1996, *Specification for Audiometers.* The audiometers covered in this specification are devices designed for use in determining the hearing threshold of an individual in comparison with a chosen standard reference threshold level.

ANSI S3.21-1978 (R1997), *Methods for Manual Pure-Tone Threshold Audiometry.* Outlines the procedure for pure-tone threshold audiometry used in the assessment of an individual's threshold of hearing for pure tones.

ISO 226:1987, *Normal Equal-Loudness Level Contours.* Data in this standard formed the basis for the dBA and dBC curves used in noise measurement.

ISO 389, 1964 Acoustics, *Standard Reference Zero for the Calibration of Pure-Tone Audiometers.* Part 1: *Reference Equivalent Sound Pressure Levels for Pure Tones and Supra-Aural Earphones.* Part 2: *Reference Equivalent Threshold Sound Pressure Levels for Pure Tones and Insert Earphones.* These data are also shown in ANSI S3.6-1996.

ISO 6189:1983, *Pure Tone Air Conduction Threshold Audiometry for Hearing Conservation Purposes.* Outlines the procedure for testing hearing thresholds as well as describes the conditions of the testing. Part of this standard is similar to information found in ANSI S3.21-1978 (R1997).

ISO 7029:2000, *Statistical Distribution of Hearing Thresholds as a Function of Age.* Gives expected threshold values for men and women without a history of noise exposure. Data are utilized in ISO 1999 and ANSI S3.44-1996.

ISO 8253-1:1989, *Audiometric Test Methods*—Part 1: *Basic Pure Tone Air and Bone Conduction Threshold Audiometry.* Part 2: *Sound Field Audiometry with Pure Tone and Narrow-Band Test Signals.* Part 3: *Speech Audiometry.*

ISO 11904-1:2002, *Determination of Sound Immission from Sound Sources Placed Close to the Ear.* Part 1: *Technique Using a Microphone in a Real Ear (MIRE Technique).* Some of the data in this standard are similar to that in ANSI S12. 42-1995 (R1999).

IEC 60645-1 Ed 2.0 b: 2001, *Electroacoustics—Audiological Equipment.* Part I: *Pure-Tone Audiometers.* Has material also found in ANSI S3.6-1996.

Hearing Conservation Programs

ANSI S3.44-1996 (R2001), *Determination of Occupational Noise Exposure and Estimation of Noise-Induced Hearing Impairment.* Adoption of ISO 1999:1990(E) of the same name; however, S3.44 allows assessment of noise exposure using a time–intensity trading relation other than a 3-dB increase per halving of exposure time.

ANSI S12.6-1997 (R2002), *Methods for Measuring the Real-Ear Attenuation of Hearing Protectors.* Specifies laboratory-based procedures for measuring, analyzing, and reporting the noise-reducing capabilities of conventional passive hearing protection devices.

ANSI Technical Report S12.13 TR-2002, *Evaluating the Effectiveness of Hearing Conservation Programs through Audiometric Data Base Analysis.* Describes methods for evaluating the effectiveness of hearing conservation programs in preventing occupational noise-induced hearing loss by using techniques for audiometric database analysis.

ANSI S12.42-1995 (R1999), *Microphone-in-Real-Ear and Acoustic Test Fixture Methods for the Measurement of Insertion Loss of Circumaural Hearing Protection Devices.* Describes the microphone-in-real-ear and the acoustical test fixture methods for the measurement of the insertion loss of circumaural earmuffs, helmets, and communications headsets.

ISO 1999:1999, *Acoustics—Determination of Occupational Noise Exposure and Estimation of Noise-Induced Hearing Impairment.* Similar to ANSI S3.44-1996 except that ISO 1999 is more restrictive.

ISO 4869-1:1990, *Hearing Protectors*—Part 1: *Subjective Method for the Measurement of Sound Attenuation.* Part 2: *Estimation of Effective A-Weighted Sound Pressure Levels When Hearing Protectors Are Worn.* Part 3: *Simplified Method for the Measurement of Insertion Loss of Ear-Muff Type Protectors for Quality Inspection Purposes.* Part 4: *Measurement of Effective Sound Pressure Levels for Level-Dependent Sound-Restoration Ear-Muffs.*

ISO 7029:2000, *Statistical Distribution of Hearing Thresholds as a Function of Age.*

ISO 9612:1997, *Guidelines for the Measurement and Assessment of Exposure to Noise in a Working Environment.*

Speech Communication Metrics

ANSI S3.2-1989 (R1999), *Method for Measuring the Intelligibility of Speech over Communication Systems.* A revision of ANSI S3.2-1960 (R1982). Provides three alternative sets of lists of English words to be spoken by trained talkers over the speech communication system to be evaluated.

ANSI S3.4-1980 (R1997), *Procedure for the Computation of Loudness of Noise.* Specifies a procedure for calculating the loudness of certain classes of noise.

ANSI S3.5-1997 (R2002), *Methods of the Calculation of the Speech Intelligibility Index (SII).* Computation of the SII based on the intelligibility of speech as evaluated by speech perception tests given a group of talkers and listeners.

ASTM 1130-2002, *Objective Measurement of Speech Privacy in Open Offices Using Articulation Index (AI).* Computation of the Articulation Index (AI) from standard speech levels, ambient noise, and articulation weighting factors.

ANSI S3.14-1977 (R1997), *Rating Noise with Respect to Speech Interference.* Defines a simple numerical method for rating the expected speech-interfering aspect (Speech Interference Level, SIL) of noise using acoustical measurements of the noise.

ISO/TR 3352, 1974, *Acoustics—Assessment of Noise with Respect to Its Effect on the Intelligibility of Speech.* This technical report has never been approved as a standard in part because of the concern over whether the impact of noise is similar for each language.

ISO/TR 4870:1991, *The Construction and Calibration of Speech Intelligibility Tests.*

Environmental Noise SPL Measurement Methods

Environmental noise SPL measurements are typically made outdoors to mirror most regulations. Sound measurement locations are often near houses or in empty fields and near transportation and industrial noise sources. In addition to meeting all the requirements of ANSI S1.4, this acoustical equipment and its application must be tolerant of wind, rain, birds, insects, and mechanical abuse. Primary noise sources include transportation (aircraft, road traffic, trains, etc.), industrial facilities, neighborhood noise (pets, heating, ventilation, and air conditioning), recreational noise (shooting ranges, races, and music venues).

ANSI S12.18-1994 (R1999), *Procedures for Outdoor Measurement of Sound Pressure Level.* Procedures for the measurement of SPLs outdoors, considering ground effects and refraction due to wind and temperature gradients and to turbulence. Measurement of SPLs produced by specific sources outdoors. Method 1: general method, outlines conditions for routine measurements. Method 2: precision method, describes strict conditions for more accurate measurements, providing short-term A-weighted SPL or time-averaged SPL, A-weighted or in octave- or in one-third-octave or narrow-band SPL, but does not preclude determination of other sound descriptors.

ASTM E1014-84(2000), *Standard Guide for Measurement of Outdoor A-Weighted Sound Levels.* Basic technique for performing a reliable A-weighted sound-level measurement outdoors.

ASTM E1503-97, *Standard Test Method for Conducting Outdoor Sound Measurements Using a Digital Statistical Analysis System.* Covers the measurement of outdoor sound levels at specific locations using a digital statistical analyzer and a formal measurement plan.

ISO 7196: 1995, *Frequency-Weighting Characteristic for Infrasound Measurements.*

ISO 10843:1997, *Methods for the Description and Physical Measurement of Single Impulses or Series of Impulses.*

Environmental Noise Measurement Applications

ANSI S12.7-1986 (R1998), *Methods for Measurement of Impulse Noise.* Measures impulse noise from discrete events, such as quarry and mining explosions or sonic booms, or from multiple-event sources such as pile drivers, riveting, or machine-gun firing. Data may be reported as time variation of the sound pressure, with or without frequency weighting, and sound exposure level.

ANSI S12.8-1998 (R2003), *Methods for Determining the Insertion Loss of Outdoor Noise Barriers.* Determine the insertion loss of outdoor noise barriers, including direct before and after measurements, indirect before measurements at an "equivalent" site, and indirect predictions of "before" sound levels. Indirect before measurements and indirect before prediction methods require direct measurements of "after" sound levels. May use sound sources naturally present at a site, controlled natural sound sources, or controlled artificial sound sources. Receiver location and atmospheric, ground, and terrain conditions may be chosen. Worksheets are provided

ANSI S12.9-1988 (R2003), *Quantities and Procedures for Description and Measurement of Environmental Sound.* Part 1: *Basic Quantities for Description of Sound in Community Environments and General Procedures for Measurement of These Quantities.* Part 2: *Measurement of Long-Term, Wide Area Sound.* Part 3: *Short-Term Measurements with an Observer Present.* Part 4: *Noise Assessment and Prediction of Long-Term Community Response.* Part 5: *Sound Descriptors for Determination of Compatible Land Use.* Part 6: *Methods for Estimation of Awakenings Associated with Aircraft Noise Events Heard in Homes.*

ANSI/ASME PTC 36-1985 (R1998), *Measurement of Industrial Sound.* Procedures for measuring and reporting airborne sound emissions from mechanical equipment.

ARI 260-2001, *Sound Rating of Ducted Air Moving and Conditioning Equipment.*

ARI 270-95, *Sound Rating of Outdoor Unitary Equipment.*

ARI 275-97, *Application of Sound Rating Levels of Outdoor Unitary Equipment.*

ARI 300-2000, *Sound Rating and Sound Transmission Loss of Packaged Terminal Equipment.*

ARI 350-2000, *Sound Rating of Non-Ducted Indoor Air-Conditioning Equipment.*

ARI 370-2001, *Sound Rating of Large Outdoor Refrigerating and Air-Conditioning Equipment.*

ISO 1996, *Description and Measurement of Environmental Noise.* Part 1-2003: *Basic Quantities and Assessment Procedures.* Part 2-1987: *Acquisition of Data Pertinent to Land Use.* Part 3-1987: *Application to Noise Limits.*

ISO 3891:1978, *Procedure for Describing Aircraft Noise Heard on the Ground.*

ISO 8297:1994, *Determination of Sound Power Levels of Multisource Industrial Plants for Evaluation of Sound Pressure Levels in the Environment—Engineering Method.*

ISO 10847:1997, *In-Situ Determination of Insertion Loss of Outdoor Noise Barriers of All Types.* See also ANSI S12.8.

ISO/TS 13474:2003, *Impulse Sound Propagation for Environmental Noise Assessment.*

SAE J1075 (revised June 2000), *Surface Vehicle Standard (R) Sound Measurement—Construction Site.* Procedures and instrumentation to be used for determining a representative sound level during a representative time period at selected measurement locations on a construction site boundary.

Environmental Sound Propagation Outdoors

ANSI S1.18-1999, *Template Method for Ground Impedance.* Procedures for obtaining the real and imaginary parts of the specific acoustical impedance of natural ground surface outdoors.

ANSI S1.26-1995 (R1999), *Method for Calculation of the Absorption of Sound by the Atmosphere.* Still-atmosphere absorption losses of sound for a wide range of meteorological conditions.

ANSI S12.17-1996 (R2001), *Impulse Sound Propagation for Environmental Noise Assessment Response.* Engineering methods to calculate the propagation and attenuation of high-energy impulsive sounds through the atmosphere. It estimates the mean C-weighted sound exposure level of impulsive sound at distances ranging from 1 to 30 km, applicable for explosive masses between 50 and 1000 kg.

ISO 9613, *Attenuation of Sound during Propagation Outdoors.* Part 1-1993: *Calculation of the Absorption of Sound by the Atmosphere. Attenuation of Sound During Propagation Outdoors.* Part 2-1996: *General Method of Calculation.* Propagation attenuation, including barrier attenuation calculations, excess attenuation by hard and soft ground surfaces, and attenuation of sound by rows of buildings and by trees and shrubs.

ISO/TS 13474:2003, *Impulse Sound Propagation for Environmental Noise Assessment.*

Environmental Vibrations

ANSI S3.18-2002, *NAIS Standard Mechanical Vibration and Shock—Evaluation of Human Exposure to Whole-Body Vibration.* Part 1: *General Requirements.* Part of ISO 2631 defining methods for the measurement of periodic, random, and transient whole-body vibration. It indicates the principal factors that combine to determine the degree to which a vibration exposure will be acceptable.

ANSI S3.29-1983 (R2001), *Guide to the Evaluation of Human Exposure to Vibration in Buildings.* Reactions of humans to vibrations of 1–80 Hz inside buildings are assessed as degrees of perception and associated vibration levels and duration.

ANSI S3.34-1986 (R1997), *Guide for the Measurement and Evaluation of Human Exposure to Vibration Transmitted to the Hand.* The recommended method for the measurement, data analysis, and reporting of human exposure to hand-transmitted vibration.

ANSI S3.40-2002, *NAIS Standard Mechanical Vibration and Shock—Hand-Arm Vibration—Method for the Measurement and Evaluation of the Vibration Transmissibility of Gloves at the Palm of the Hand.* Adoption of ISO 10819:1996. A method for the laboratory measurement, data analysis, and reporting of the vibration transmissibility of gloves of vibrations from a handle to the palm of the hand in the frequency range 31.5–1250 Hz.

ISO 2631, *Mechanical Vibration and Shock—Evaluation of Human Exposure to Whole-Body Vibration.* Part 1-1997: *General Requirements.* Part 2-1989: *Continuous and Shock-Induced Vibrations in Buildings (1 to 80 Hz).* Part 4-2001: *Guidelines for The evaluation of the Effects of Vibration and Rotational Motion on Passenger and Crew Comfort in Transport Systems.*

ISO 2671:1982, *Environmental Tests for Aircraft Equipment—Part 3.4: Acoustic Vibration.*

ISO 4866:1990, *Mechanical Vibration and Shock—Vibration of Buildings—Guidelines for the Measurement of Vibrations and Evaluation of Their Effects on Building.*

ISO 4867:1984, *Code for the Measurement and Reporting of Shipboard Vibration Data.*

ISO 5007:2003, *Agricultural Wheeled Tractors—Operator's Seat—Laboratory Measurement of Transmitted Vibration.*

ISO 5008:2002, *Agricultural Wheeled Tractors and Field Machinery—Measurement of Whole-Body Vibration of the Operator.*

ISO 5347-3:1993, *Calibration of Vibration and Shock Pick-ups.* Part 3: *Secondary Vibration Calibration.* Part 4: *Secondary Shock Calibration.* Part 5: *Calibration by Earth's Gravitation.* Part 6: *Primary Vibration Calibration at low Frequencies.* Part 7: *Primary Calibration by Centrifuge.* Part 8: *Primary Calibration by Dual Centrifuge.* Part 10: *Primary Calibration by High Impact Shocks.* Part 11: *Testing of Transverse Vibration Sensitivity.* Part 12: *Testing of Transverse Shock Sensitivity.* Part 13: *Testing of Base Strain Sensitivity.* Part 14: *Resonance Frequency Testing of Undamped Accelerometers on a Steel Block.* Part 15: *Testing of Acoustic Sensitivity.* Part 16: *Testing of Mounting Torque Sensitivity.* Part 17: *Testing of Fixed Temperature Sensitivity.* Part 18: *Testing of Transient Temperature Sensitivity.* Part 19: *Testing of Magnetic Field Sensitivity.* Part 22: *Accelerometer Resonance Testing—General Methods.*

ISO 5348:1998, *Mechanical Mounting of Accelerometers.*

ISO 5349-1:2001, *Mechanical Vibration—Guidelines for the Measurement and the Assessment of Human Exposure to Hand-Transmitted Vibration.* Parts of this standard are similar to ANSI S3.34-1986 (R1997). Part 2: *Practical Guidance for Measurement at the Workplace.*

ISO 5805:1997, *Mechanical Vibration and Shock—Human Exposure—Vocabulary.*

ISO 8041:1990, *Human Response to Vibration—Measuring Instrumentation.*

ISO 13091-1:2001, *Mechanical Vibration—Vibrotactile Perception Thresholds for the Assessment of Nerve Dysfunction.* Part 1: *Methods of Measurements at the Fingertips.*

ISO 8042:1988, *Characteristics to be Specified for Seismic Pick-Ups.*

ISO 9022-10:1998, *Optics and Optical Instruments—Environmental Test Methods.* Part 10: *Combined Sinusoidal Vibration and Dry Heat or Cold.* Part 15: *Combined Digitally Controlled Broad-Band Random Vibration and Dry Heat or Cold.*

21.6 VEHICLE EXTERIOR AND INTERIOR NOISE

There are many SAE and ISO standards dealing with the source of noise emissions of various motor vehicles, including road vehicle (automobiles, trucks, buses, and motorcycles), trains, boats, aircraft, construction equipment (e.g., dozer), agricultural equipment (e.g., tractor), and small-engine equipment (e.g., lawn edger). Full listings of these standards are maintained at the SAE and ISO websites. The following is a sampling of these standards. Quite a few are identically SAE and ISO standards.

Vehicle Noise — Interior Noise Measurement Techniques

ISO 2923:1996, *Measurement of Noise on Board Vessels.*

ISO 3095:1975, *Measurement of Noise Emitted by Railbound Vehicles.*

ISO 3381:1976, *Measurement of Noise Inside Railbound Vehicles.*

ISO 5128:1980, *Measurement of Noise Inside Motor Vehicles.*

ISO 5129:2001, *Measurement of Sound Pressure Levels in the Interior of Aircraft During Flight.*

ISO 5130:1982, *Measurement of Noise Emitted by Stationary Road Vehicles—Survey Method.*

ISO 5131:1996, *Tractors and Machinery for Agriculture and Forestry—Measurement of Noise at the Operator's Position—Survey method.*

ISO 7188:1994, *Measurement of Noise Emitted by Passenger Cars under Conditions Representative of Urban Driving.*

ISO 11819-1:1997, *Measurement of the Influence of Road Surfaces on Traffic Noise.* Part 1: *Statistical Pass-By Method.*

Road Surface Sound Absorption

See ISO 13472 below under Sound Absorption.

Vehicle Noise — Exterior Noise Measurement (Noise Emission) Techniques

SAE J366, *Exterior Sound Level for Heavy Trucks and Buses (APR 2001).* Test procedure, environment, and instrumentation for determining the maximum exterior sound level for highway motor trucks, truck tractors, and buses.

ISO 3095:1975, *Measurement of Noise Emitted by Railbound Vehicles.* Obtaining reproducible and comparable measurement results of levels and spectra of noise emitted by all kinds of vehicles operating on rails or other types of fixed track except for track maintenance vehicles in operation.

SAE J34 (June 2001), *Exterior Sound Level Measurement Procedure for Pleasure Motorboats.* Procedure for measuring the maximum exterior sound level of pleasure motorboats while being operated under wide open-throttle conditions.

ISO 362:1998, *Measurement of Noise Emitted by Accelerating Road Vehicles—Engineering Method.* (Available in English only.)

SAE J16395 (ISO 6395) (February 2003), *Measurement of Exterior Noise Emitted by Earth-Moving Machinery—Dynamic Test Conditions.* Determining the noise emitted to the environment by earth-moving machinery in terms of the A-weighted sound power level while the machine is working under dynamic test conditions.

SAE J17216 (ISO 7216) (February 2003), *Agricultural and Forestry Wheeled Tractors and Self-Propelled Machines—Measurement of Noise Emitted When in Motion.* Measuring the A-weighted SPL in an extensive open space of the noise emitted by agricultural and forestry wheeled tractors and self-propelled machines fitted with elastic tires while the vehicle is in motion. It is not applicable to special forestry machinery, for example, forwarders, skidders, etc., as defined in ISO 6814.

ISO 4872:1978, *Measurement of Airborne Noise Emitted by Construction Equipment Intended for Outdoor Use.* Method for determining compliance with noise limits

ISO 6393:1998, *Measurement of Exterior Noise Emitted by Earth-Moving Machinery—Stationary Test Conditions.* (Available in English only.)

ISO 6394:1998, *Measurement at the Operator's Position of Noise Emitted by Earth-Moving Machinery—Stationary Test Conditions.* (Available in English only.)

ISO 6395:1988, *Measurement of Exterior Noise Emitted by Earth-Moving Machinery—Dynamic Test Conditions.*

ISO 6396:1992, *Measurement at the Operator's Position of Noise Emitted by Earth-Moving Machinery—Dynamic Test Conditions.*

ISO 6798:1995, *Reciprocating Internal Combustion Engines—Measurement of Emitted Airborne Noise—Engineering Method and Survey Method.*

ISO 7216:1992, *Agricultural and Forestry Wheeled Tractors and Self-Propelled Machines—Measurement of Noise Emitted When in Motion.*

ISO 7182:1984, *Measurement at the Operator's Position of Airborne Noise Emitted by Chain Saws.*

ISO 9645:1990, *Measurement of Noise Emitted by Two-Wheeled Mopeds in Motion—Engineering Method.*

ISO 11094:1991, *Test Code for the Measurement of Airborne Noise Emitted by Power Lawn Mowers, Lawn Tractors, Lawn and Garden Tractors, Professional Mowers, and Lawn and Garden Tractors with Mowing Attachments.*

21.7 ARCHITECTURAL NOISE CONTROL IN BUILDINGS

There are three categories of sound control standards for buildings. The first is for testing materials that limit sound transmission from one room to another. The second is to test the sound absorption capability of materials. The third tests the general capabilities of rooms to cope with sounds within it for favorable (offices, classrooms, and auditoria) and unfavorable or noisy situations.

Sound Transmission

ASTM E90-02, *Standard Test Method for Laboratory Measurement of Airborne Sound Transmission Loss of Building Partitions and Elements.* Laboratory measurement of airborne sound transmission loss of building partitions such as walls of all kinds, operable partitions, floor–ceiling assemblies, doors, windows, roofs, panels, and other space-dividing elements.

ASTM E336-97, *Standard Test Method for Measurement of Airborne Sound Insulation in Buildings.* Determining the sound insulation in the field between two rooms in a building. The evaluation may be made including all paths by which sound is transmitted or attention may be focused only on the dividing partition. The word "partition" in this test method includes all types of walls, floors, or any other boundaries separating two spaces. The boundaries may be permanent, operable, or movable.

ASTM E413-87 (1999), *Classification for Rating Sound Insulation.* The method of calculating, from laboratory or field sound insulation measurements at frequencies from 125 to 4000 Hz the single-number acoustical rating called sound transmission class (STC) or field sound transmission class (FSTC) and the single-number rating between two spaces called the noise isolation class (NIC).

ASTM E497, *Practice for Installing Sound-Isolating Lightweight Partitions.* Preferred design methods for constructing high-noise-insulation walls and floor/ceilings.

ASTM E557, *Practice for Architectural Application and Installation of Operable Partitions.* Preferred design and installation methods for constructing high-noise-insulation operable partitions in the field.

ASTM E596-96 (2002), *Standard Test Method for Laboratory Measurement of Noise Reduction of Sound-Isolating Enclosures.* The reverberation room measurement of the noise reduction of sound-isolating enclosures.

ASTM E597, *Practice for Determining a Single-Number Rating of Airborne Sound Isolation for Use in Multi-Unit Building Specifications.* A short test method for field use where a sound source of a standard spectrum is used to test the noise insulation between two existing rooms in a building. Broadband A-weighted sound levels are measured. Computation provides a single number sound insulation value analogous to FSTC.

ASTM E966-02, *Standard Guide for Field Measurements of Airborne Sound Insulation of Building Facades and Facade Elements.* Procedures for measuring the sound insulation of an installed building facade or facade element (window, door). These values may be used separately to predict interior levels or combined into a single number such as by classification E 413 (STC with precautions) or classification E 1332 (outside–inside transmission class, OITC) for sound insulation against transportation noises.

ASTM E492-90 (1996), *Standard Test Method for Laboratory Measurement of Impact Sound Transmission through Floor-Ceiling Assemblies Using the Tapping Machine.* Measurement of impact sound levels (e.g., footfalls) produced by the ISO tapping machine. Results are used to determine the impact isolation class (IIC) by E989.

ASTM E989-89 (1999), *Standard Classification for Determination of Impact Insulation Class (IIC).* A single-number rating of data from ASTM E492 and E1007 for comparing floor–ceiling assemblies for general building design purposes. The rating is called an impact insulation class (IIC).

ASTM E1007-97, *Standard Test Method for Field Measurement of Tapping Machine Impact Sound Transmission through Floor-Ceiling Assemblies and Associated Support Structures.* A field measurement analogous to E492.

ASTM E1123-86 (1998), *Standard Practices for Mounting Test Specimens for Sound Transmission Loss Testing of Naval and Marine Ship Bulkhead Treatment Materials.* Describes test specimen mountings for test method E90, to be used for naval and marine ship bulkhead noise insulation measurement.

ASTM E1222-90 (2002), *Standard Test Method for Laboratory Measurement of the Insertion Loss of Pipe Lagging Systems.* Covers the measurement of the insertion loss of pipe lagging systems under laboratory conditions.

ASTM E1289-97, *Standard Specification for Reference Specimen for Sound Transmission Loss.* Construction and installation of a standard reference specimen for interlaboratory sound transmission loss measurement evaluation using test method E90.

ASTM E1332-90 (1998), *Standard Classification for Determination of Outdoor-Indoor Transmission Class.* A single-number rating for exterior doors, windows, and walls for their noise insulation against ground and air transportation noise, including aircraft roadway vehicles and trains.

ASTM E1408-91 (2000), *Standard Test Method for Laboratory Measurement of the Sound Transmission Loss of Door Panels and Door Systems.* Laboratory measurement of the sound transmission loss for door panels and door systems. It includes specimen-mounting instructions and the force required to close, latch, unlatch, and open a door.

ASTM E1414-00, *Standard Test Method for Airborne Sound Attenuation between Rooms Sharing a Common Ceiling Plenum.* Uses a special laboratory space

to simulate a pair of adjacent offices or rooms separated by a partition and sharing a common plenum space (a common economical construction method used for walls between offices and classrooms). The only significant laboratory sound transmission path is by way of the ceiling structure and the plenum space.

ISO 140-1:1997, *Measurement of Sound Insulation in Buildings and of Building Elements*. Part 1: *Requirements for Laboratory Test Facilities with Suppressed Flanking Transmission*. Part 2: *Determination, Verification and Application of Precision Data*. Part 3: *Laboratory Measurements of Airborne Sound Insulation of Building Elements*. Part 4: *Field Measurements of Airborne Sound Insulation between Rooms*. Part 5: *Field Measurements of Airborne Sound Insulation of Façade Elements and Façades*. Part 6: *Laboratory Measurements of Impact Sound Insulation of Floors*. Part 7: *Field Measurements of Impact Sound Insulation of Floors*. Part 8: *Laboratory Measurements of the Reduction of Transmitted Impact Noise by Floor Coverings on a Heavyweight Standard Floor*. Part 9: *Laboratory Measurement of Room-to-Room Airborne Sound Insulation of a Suspended Ceiling with a Plenum Above It*. Part 10: *Laboratory Measurement of Airborne Sound Insulation of Small Building Elements*. Part 12: *Laboratory Measurement of Room-to-Room Airborne and Impact Sound Insulation of an Access Floor*. Part 13: *Guidelines*. (Available in English only.)

ISO 717-1:1996, *Rating of Sound Insulation in Buildings and of Building Elements*. Part 1: *Airborne Sound Insulation*. Part 2: *Impact Sound Insulation*.

ISO 9052-1:1989, *Determination of Dynamic Stiffness*. Part 1: *Materials Used under Floating Floors in dwellings*.

ISO 3822, *Laboratory Tests on Noise Emission from Appliances and Equipment Used in Water Supply Installations*. Part 1-1999: *Method of Measurement*. Part 2-1995: *Mounting and Operating Conditions for Draw-Off Taps and Mixing Valves*. Part 3-1997: *Mounting and Operating Conditions for In-Line Valves and Appliances*. Part 4-1997: *Mounting and Operating Conditions for Special Appliances*.

ISO 11546-1:1995, *Determination of Sound Insulation Performances of Enclosures*. Part 1: *Measurements under Laboratory Conditions (for Declaration Purposes)*. Part 2: *Measurements In Situ (for Acceptance and Verification Purposes)*.

ISO 11957:1996, *Determination of Sound Insulation Performance of Cabins—Laboratory and In Situ Measurements*.

ISO 15186-1:2000, *Measurement of Sound Insulation in Buildings and of Building Elements Using Sound Intensity*. Part 1: *Laboratory Measurements*.

Sound Absorption

ASTM C384-98, *Standard Test Method for Impedance and Absorption of Acoustical Materials by the Impedance Tube Method*. The use of an impedance tube (standing-wave apparatus) for the measurement of impedance ratios and the normal-incidence sound absorption coefficients of acoustical materials.

ASTM C423-02, *Standard Test Method for Sound Absorption and Sound Absorption Coefficients by the Reverberation Room Method*. Measures the random-incidence sound absorption coefficients of material test specimens, mounted according to ASTM E795, in a reverberation room by measuring sound decay rate.

ASTM E477, *Test Method for Measuring Acoustical and Airflow Performance of Duct Liner Materials and Prefabricated Silencers*. Laboratory measurement method for the sound insertion loss provided by duct sound attenuators.

ISO 7235:1991, *Measurement Procedures for Ducted Silencers—Insertion Loss, Flow Noise and Total Pressure Loss*.

ISO 11691:1995, *Measurement of Insertion Loss of Ducted Silencers without Flow—Laboratory Survey Method*.

ISO 11820:1996, *Measurements on Silencers In Situ*.

ISO 11821:1997, *Measurement of the In Situ Sound Attenuation of a Removable Screen*.

ASTM C522-87(1997), *Standard Test Method for Airflow Resistance of Acoustical Materials*. The measurement of airflow resistance, specific airflow resistance, and airflow resistivity of porous materials. Materials may be thick boards or blankets to thin mats, fabrics, papers, and screens.

ISO 9053:1991, *Materials for Acoustical Applications—Determination of Airflow Resistance*.

ASTM E756-98, *Standard Test Method for Measuring Vibration-Damping Properties of Materials*. Measures the vibration-damping properties—loss factor η, Young's modulus E, and shear modulus G—of materials over a frequency range of 50 Hz to 5 kHz and over the useful temperature range of the material. This method tests materials that have application in structural vibration, building acoustics, and the control of audible noise. Test materials include metal, enamel, ceramics, rubber, plastic, reinforced epoxy matrix, and wood that can be formed to the test specimen bar configuration.

ASTM E795-00, *Standard Practices for Mounting Test Specimens during Sound Absorption Tests*. Standard specimen mountings for tests performed in accordance with C423.

ASTM E1042, *Classification for Acoustically Absorptive Materials Applied by Trowel or Spray*.

ASTM E1050-98, *Standard Test Method for Impedance and Absorption of Acoustical Materials Using a Tube, Two Microphones, and a Digital Frequency Analysis System*. The two-microphone impedance tube method, including a digital frequency analysis system, to measure the normal-incidence sound absorption coefficients and normal specific acoustical impedance ratios of materials.

ISO 354. 2003, *Acoustics—Measurement of Sound Absorption in a Reverberation Room*. Similar to ASTM C423.

ISO 10534-1:1996, *Determination of Sound Absorption Coefficient and Impedance in Impedance Tubes*. Part 1: *Method Using Standing Wave Ratio*. Similar to ASTM C384.

ISO 11654:1997, *Sound Absorbers for Use in Buildings—Rating of Sound Absorption*.

ISO 10844:1994, *Specification of Test Tracks for the Purpose of Measuring Noise Emitted by Road Vehicles.*

ISO 13472-1:2002, *Measurement of Sound Absorption Properties of Road Surfaces In Situ.* Part 1: *Extended Surface Method.* A vertical impedance tube test method for measuring In Situ the sound absorption coefficient of road surfaces as a function of frequency in the range from 250 Hz to 4 kHz.

Architectural Acoustics, Reverberation, and Noise Control Design

ANSI S12.2-1995 (R1999), *Criteria for Evaluating Room Noise.* Defines NC, NCB, RC, and perceptible acoustically induced low-frequency vibration criterion curves for the octave-band SPL spectrum of noise and gives rules for using them to evaluate room background noise.

ANSI S12.60-2002, *Acoustical Performance Criteria, Design Requirements, and Guidelines for Schools.* Acoustical performance criteria, design requirements, and design guidelines for new school classrooms and other learning spaces to achieve a high degree of speech intelligibility in learning spaces. Conformance test procedures are provided.

ASTM E1041, *Guide for Measurement of Masking Sound in Open Offices.*

ASTM E1110-01, *Standard Classification for Determination of Articulation Class.* Provides a single figure rating that can be used for comparing building systems and subsystems for speech privacy purposes. The rating is designed to correlate with transmitted speech intelligence between office spaces.

ASTM E1111-02, *Standard Test Method for Measuring the Interzone Attenuation of Ceiling Systems.* Measures the sound reflective characteristics of ceiling systems with partial-height space dividers, used in offices and sometimes in schools to achieve speech privacy between work zones in the absence of full-height partitions. Restricted to a fixed space divider height of 5 ft, a ceiling height of nominally 9 ft, a source height of 4 ft, and microphone positions at 4 ft height.

ASTM E1130-02, *Standard Test Method for Objective Measurement of Speech Privacy in Open Offices Using Articulation Index (AI).* Measuring speech privacy objectively between existing locations in open offices. Uses acoustical measurements, published information on speech levels, and speech intelligibility to compute the Articulation Index (AI).

ASTM E1179-87 (1998), *Standard Specification for Sound Sources Used for Testing Open Office Components and Systems.* Specifies the sound source used for measuring the speech privacy between open offices or for measuring the laboratory performance of acoustical components (see E1111 and E1130).

ASTM E1375-90 (2002), *Standard Test Method for Measuring the Interzone Attenuation of Furniture Panels Used as Acoustical Barriers.* Measurement of the interzone attenuation of furniture panels used as acoustical barriers in open-plan spaces to provide speech privacy or sound isolation between working positions.

ASTM E1376-90 (2002), *Standard Test Method for Measuring the Interzone Attenuation of Sound Reflected by Wall Finishes and Furniture Panels.* Measures the degree to which reflected sound is attenuated by vertical surfaces in open-plan spaces.

ASTM E1573-02, *Standard Test Method for Evaluating Masking Sound in Open Offices Using A-Weighted and One-Third Octave Band Sound Pressure Levels.* Procedures to evaluate the spatial and temporal uniformity of masking sound in open offices using A-weighted or one-third-octave-band SPLs.

ASTM E1574-98, *Standard Test Method for Measurement of Sound in Residential Spaces.* Practical measurement of residual building interior noise SPLs.

ASTM E2235, *Standard Test Method for the Measurement of Decay Rates for Use in Sound Insulation Test Methods.* Measurement of sound decay rate ($60/T$) in any room, where T is the reverberation time, seconds.

ISO 3382:1997, *Measurement of the Reverberation Time of Rooms with Reference to Other Acoustical Parameters.* Measurement of reverberation time T in performance spaces. Specifies additional measures of auditorium gain (G), early decay (EDT), clarity (C80), Deutlichkeit (D50), central time (CT) lateral energy fraction (LF) and interaural cross correlation (IACC) and of T in any room.

ISO 10053-1991, *Measurement of Office Screen Sound Attenuation under Specific Laboratory Conditions.* Similar to ASTM E1375.

APPENDIX A

General References

M. Belanger, *Digital Processing of Signals: Theory and Practice*, Wiley, New York (1985).

J. S. Bendat and A. G. Piersol, *Random Data, Analysis and Measurement Procedures*, 2nd ed., Wiley, New York (1986).

L. L. Beranek, *Acoustics*, reprinted with changes by the Acoustical Society of America, New York (1986).

L. L. Beranek, *Acoustical Measurements*, rev. ed., Acoustical Society of America, New York (1988).

D. A. Bies and C. H. Hansen, *Engineering Noise Control*, Unwin Hyman, London (1988).

M. P. Blake and W. S. Mitchell, *Vibration and Acoustic Measurement Handbook*, Spartan Books, New York (1972).

R. N. Bracewell, *The Fast Fourier Transform and Its Applications*, 2nd ed., McGraw-Hill, New York (1986).

L. Cremer and H. A. Mueller, *Principals and Applications of Room Acoustics*, Vols. 1 and 2, translated by T. J. Schultz, Applied Science, London and New York (1982).

M. J. Crocker, *Noise Control*, Van Nostrand Reinhold, New York (1984).

J. D. Erwin and E. R. Graf, *Industrial Noise and Vibration Control*, Prentice-Hall, Englewood Cliffs, NJ (1979).

F. Fahy, *Sound and Structural Vibration—Radiation, Transmission and Response*, Academic, New York (1985).

C. M. Harris, Ed., *Shock and Vibration Handbook*, 3rd ed., McGraw-Hill, New York (1988).

M. C. Junger and D. Feit, *Sound, Structures, and Their Interaction*, 2nd ed., MIT Press, Cambridge, MA (1986).

L. E. Kinsler, A. R. Frey, A. B. Coppens, and J. V. Sanders, *Fundamentals of Acoustics*, 3rd ed., Wiley, New York (1982).

H. Kuttruff, *Room Acoustics*, Applied Science Publishers, London (1973).

R. L. Lyon, *Statistical Energy Analysis of Dynamical Systems*, MIT Press, Cambridge, MA (1975).

A. V. Oppenheim and R. W. Schafer, *Digital Signal Processing*, Prentice-Hall, Englewood Cliffs, NJ (1975).

R. B. Randall, *Frequency Analysis*, 3rd ed., Bruel & Kjaer, Naerum, Denmark (1987).

APPENDIX B

American System of Units

The American system of units [which used to be referred to as the English system of units until England converted to the meter-kilogram-second (mks) system] is inherently confusing. In everyday American life, the *pound* (abbreviated lb) is used either as a force or as a weight, both having the units of force. To further complicate matters, some technical writers seek to provide a system parallel to the metric system by using either of two quantities for force and either of two corresponding quantities for mass. Thus, some adopt the pound as the unit of force and define a *slug* as the unit of mass. Others define a *poundal* as the unit of force and adopt the pound as the unit of mass. Neither the slug nor the poundal has found general acceptance in the literature, although we use the former in this text.

As one well-traveled acoustician said, "I have determined that 1 kg of butter bought in Zurich is exactly the same amount as 2.2 lb bought in New York. Whenever I wish to solve a technical problem in America without confusion, I immediately divide the number of pounds by 2.2 to obtain the equivalent number of kilograms. Then I work in the mks system, where force and mass are clearly distinguished." Let us take a moment to distinguish further between mass and force.

The mass of a body is defined as $m = F/\ddot{x}$, where F is the vector sum of all forces acting on the center of gravity of the unrestrained body and $\ddot{x}$ is the acceleration produced in the direction of the force F.

The weight of a body is defined as $w = mg$, where g is the acceleration of gravity (9.81 m/s^2 on earth) and w is the force that must act on the otherwise unrestrained body to keep it stationary when exposed to the gravitational field. Consequently, a body has the same mass but different weight on the moon than on earth. On earth the weight of a 1-kg mass, which is designated as one kilopond (1 kp), is 1 kp weight = 1 kg mass $\times$ 9.81 m/s^2 = 9.81 newtons.

CONSISTENT SYSTEMS OF UNITS USED IN THIS TEXT

Two consistent systems of units are used in this text, the *mks* and the *fss* systems. To describe them, let us start with Newton's second law:

$$\text{Force} = \text{mass} \times \text{acceleration} \tag{B.1}$$

In the *meter-kilogram-second* system

$$\text{No. of newtons} = \text{no. of kg} \times \text{no. of m/s}^2 \tag{B.2}$$

In the *foot-slug-second* system

$$\text{No. of pounds force (lb)} = \text{no. of slugs} \times \text{no. of ft/s}^2 \tag{B.3}$$

The relations among the magnitudes of the units are

$$1\text{kp} = 2.205\text{lb weight}$$
$$1\text{ kg} = 0.0685\text{slug}$$
$$1\text{slug} = 14.59\text{ kg}$$
$$1\text{ newton} = 0.225\text{lb force}$$
$$1\text{lb force} = 4.448\text{ newtons}$$
$$1\text{slug} = 32.17\text{lb weight}$$
$$1\text{lb weight} = 0.03108\text{slug} = 0.454\text{ kg}$$

Example. If 1 kg mass is to be accelerated 1 m/s^2, we see, by Eq. (B.2), that a force of 1 newton is required. How many pounds (force) is required for the same result?

Solution 1 kg equals (2.205/32.17) slug and 1 m/s^2 = 3.28 ft/s^2. Thus, by Eq. (B.3), 0.225 lb (force) is required.

INCONSISTENT SYSTEMS OF AMERICAN UNITS USED IN THE LITERATURE

Two inconsistent systems of American units are commonly encountered, the *fps* and the *ips* systems.

In the *foot-pound-second* system (inconsistent system)

$$\text{No. of pounds force (lb)} = \frac{\text{no. of pounds weight (lb)}}{g} \times \text{no. of ft/s}^2 \tag{B.4}$$

where g is the acceleration due to gravity in units of ft/s^2, that is, 32.17 ft/s^2.

In the *inch-pound-second system* (inconsistent system)

$$\text{No. of pounds force (lb)} = \frac{\text{no. of pounds weight (lb)}}{g} \times \text{no. of in./s}^2 \tag{B.5}$$

where g is the acceleration due to gravity in units of in./s^2, that is, 3.86 in./s^2. Mechanical engineers often use the *in.-lb-s* system in the field of shock and vibration.

Example. A 1-kg mass is accelerated 5 m/s^2. Find the force necessary to do this in newtons and pounds (force).

Solution

$$1\text{ kg} = 2.2\text{ lb weight} = 0.0685\text{ slug}$$
$$5\text{ m/s}^2 = 16.4\text{ ft/s}^2$$
$$F\text{ (newtons)} = 1 \times 5 = 5\text{ newtons}$$
$$F\text{ (lb)} = 0.0685 \times 16.4 = 1.124\text{ lb (force)}$$

APPENDIX C

Conversion Factors

The following values for the fundamental constants were used in the preparation of the factors:

$$1 \text{ m} = 39.37 \text{ in.} = 3.281 \text{ ft}$$

$$1 \text{ lb (weight)} = 0.4536 \text{ kp} = 0.03108 \text{ slug}$$

$$1 \text{ slug} = 14.594 \text{ kg}$$

$$1 \text{ lb (force)} = 4.448 \text{ newtons}$$

$$\text{Acceleration due to gravity} = 9.807 \text{ m/s}^2$$

$$= 32.174 \text{ ft/s}^2$$

$$\text{Density of } H_2O \text{ at } 4^\circ\text{C} = 10^3 \text{ kg/m}^3$$

$$\text{Density of Hg at } 0^\circ\text{C} = 1.3595 \times 10^4 \text{ kg/m}^3$$

$$1 \text{ U.S. lb} = 1 \text{ British lb}$$

$$1 \text{ U.S. gallon} = 0.83267 \text{ British gallon}$$

$$^\circ\text{F} = (\tfrac{9}{5})^\circ\text{C} + 32$$

$$^\circ\text{C} = (\tfrac{5}{9})(^\circ\text{F} - 32)$$

TABLE C.1 Conversion Factors

To convert	Into	Multiply by	Conversely, multiply by
acres	ft^2	4.356×10^4	2.296×10^{-5}
	$miles^2$ (statute)	1.562×10^{-3}	640
	m^2	4,047	2.471×10^{-4}
	hectare (10^4 m^2)	0.4047	2.471
atm	in. H_2O at 4°C	406.80	2.458×10^{-3}
	in. Hg at 0°C	29.92	3.342×10^{-2}
	ft H_2 O at 4°C	33.90	2.950×10^{-2}
	mm Hg at 0°C	760	1.316×10^{-3}
	$lb/in.^2$	14.70	6.805×10^{-2}

(*continued overleaf*)

TABLE C.1 (*continued*)

To convert	Into	Multiply by	Conversely, multiply by
	newtons/m^2	1.0132×10^5	9.872×10^{-6}
	kp/m^2	1.033×10^4	9.681×10^{-5}
°C	°F	$(°C \times \frac{9}{5}) + 32$	$(°F - 32) \times \frac{5}{9}$
cm	in.	0.3937	2.540
	ft	3.281×10^{-2}	30.48
	m	10^{-2}	10^2
circular mils	$in.^2$	7.85×10^{-7}	1.274×10^6
	cm^2	5.067×10^{-6}	1.974×10^5
cm^2	$in.^2$	0.1550	6.452
	ft^2	1.0764×10^{-3}	929
	m^2	10^{-4}	10^4
cm^3	$in.^3$	0.06102	16.387
	ft^3	3.531×10^{-5}	2.832×10^4
	m^3	10^{-6}	10^6
deg (angle)	radians	1.745×10^{-2}	57.30
dynes	lb (force)	2.248×10^{-6}	4.448×10^5
	newtons	10^{-5}	10^5
dynes/cm^2	lb/ft^2 (force)	2.090×10^{-3}	478.5
	newtons/m^2	10^{-1}	10
1 in. H_2O	N/m^2	249.18	4.013×10^{-3}
ergs	ft-lb (force)	7.376×10^{-8}	1.356×10^7
	joules	10^{-7}	10^7
ergs/cm^3	ft-lb/ft^3	2.089×10^{-3}	478.7
ergs/s	watts	10^{-7}	10^7
	ft-lb/s	7.376×10^{-8}	1.356×10^7
ergs/s-cm^2	ft-lb/s-ft^2	6.847×10^{-5}	1.4605×10^4
fathoms	ft	6	0.16667
ft	in.	12	0.08333
	cm	30.48	3.281×10^{-2}
	m	0.3048	3.281
ft^2	$in.^2$	144	6.945×10^{-3}
	cm^2	9.290×10^2	0.010764
	m^2	9.290×10^{-2}	10.764
ft^3	$in.^3$	1728	5.787×10^{-4}
	cm^3	2.832×10^4	3.531×10^{-5}
	m^3	2.832×10^{-2}	35.31
	liters	28.32	3.531×10^{-2}
ft H_2O at 4°C	in. Hg at 0°C	0.8826	1.133
	lb/$in.^2$	0.4335	2.307
	lb/ft^2	62.43	1.602×10^{-2}
	newtons/m^2	2989	3.345×10^{-4}
gal (liquid U.S.)	gal (liquid Brit. Imp.)	0.8327	1.2010
	liters	3.785	0.2642
	m^3	3.785×10^{-3}	264.2
gm	oz (weight)	3.527×10^{-2}	28.35

TABLE C.1 (*continued*)

To convert	Into	Multiply by	Conversely, multiply by
	lb (weight)	2.205×10^{-3}	453.6
hp (550 ft-lb/s)	ft-lb/min	3.3×10^4	3.030×10^{-5}
	watts	745.7	1.341×10^{-3}
	kW	0.7457	1.341
in.	ft	0.0833	12
	cm	2.540	0.3937
	m	0.0254	39.37
$in.^2$	ft^2	0.006945	144
	cm^2	6.452	0.1550
	m^2	6.452×10^{-4}	1550
$in.^3$	ft^3	5.787×10^{-4}	1.728×10^3
	cm^3	16.387	6.102×10^{-2}
	m^3	1.639×10^{-5}	6.102×10^4
kg	lb (weight)	2.2046	0.4536
	slug	0.06852	14.594
	g	10^3	10^{-3}
kg/m^2	lb/$in.^2$ (weight)	0.001422	703.0
	lb/ft^2 (weight)	0.2048	4.882
	g/cm^2	10^{-1}	10
kg/m^3	lb/$in.^3$ (weight)	3.613×10^{-5}	2.768×10^4
	lb/ft^3 (weight)	6.243×10^{-2}	16.02
liters	$in.^3$	61.03	1.639×10^{-2}
	ft^3	0.03532	28.32
	pints (liquid U.S.)	2.1134	0.47318
	quarts (liquid U.S.)	1.0567	0.94636
	gal (liquid U.S.)	0.2642	3.785
	cm^3	1000	0.001
	m^3	0.001	1000
$\log_e n$, or $\ln n$	$\log_{10} n$	0.4343	2.303
m	in.	39.371	0.02540
	ft	3.2808	0.30481
	yd	1.0936	0.9144
	cm	10^2	10^{-2}
m^2	$in.^2$	1550	6.452×10^{-4}
	ft^2	10.764	9.290×10^{-2}
	yd^2	1.196	0.8362
	cm^2	10^4	10^{-4}
m^3	$in.^3$	6.102×10^4	1.639×10^{-5}
	ft^3	35.31	2.832×10^{-2}
	yd^3	1.3080	0.7646
	cm^3	10^6	10^{-6}
microbars (dynes/cm^2)	lb/$in.^2$	1.4513×10^{-5}	6.890×10^4
lb/ft^2	2.090×10^{-3}	478.5	

(*continued overleaf*)

TABLE C.1 (*continued*)

To convert	Into	Multiply by	Conversely, multiply by
	newtons/m^2	10^{-1}	10
miles (nautical)	ft	6080	1.645×10^{-4}
	km	1.852	0.5400
miles (statute)	ft	5280	1.894×01^{-4}
	km	1.6093	0.6214
$miles^2$ (statute)	ft^2	2.788×10^7	3.587×10^{-8}
	km^2	2.590	0.3861
	acres	640	1.5625×10^{-3}
mph	ft/min	88	1.136×10^{-2}
	km/min	2.682×10^{-2}	37.28
	km/h	1.6093	0.6214
nepers	db	8.686	0.1151
newtons	lb (force)	0.2248	4.448
	dynes	10^5	10^{-5}
newtons/m^2	$lb/in.^2$ (force)	1.4513×10^{-4}	6.890×10^3
	lb/ft^2 (force)	2.090×10^{-2}	47.85
	dynes/cm^2	10	10^{-1}
lb (force)	newtons	4.448	0.2248
lb (weight)	slugs	0.03108	32.17
	kg	0.4536	2.2046
lb H_2O (distilled)	ft^3	1.602×10^{-2}	62.43
	gal (liquid U.S.)	0.1198	8.346
$lb/in.^2$ (weight)	lb/ft^2 (weight)	144	6.945×10^{-3}
	kg/m^2	703	1.422×10^{-3}
$lb/in.^2$ (force)	lb/ft^2 (force)	144	6.945×10^{-3}
	N/m^2	6894	1.4506×10^{-4}
lb/ft^2 (weight)	$lb/in.^2$ (weight)	6.945×10^{-3}	144
	gm/cm^2	0.4882	2.0482
	kg/m^2	4.882	0.2048
lb/ft^2 (force)	$lb/in.^2$ (force)	6.945×10^{-3}	144
	N/m^2	47.85	2.090×10^{-2}
lb/ft^3 (weight)	$lb/in.^3$ (weight)	5.787×10^{-4}	1728
	kg/m^3	16.02	6.243×10^{-2}
poundals	lb (force)	3.108×10^{-2}	32.17
	dynes	1.383×10^4	7.233×10^{-5}
	newtons	0.1382	7.232
slugs	lb (weight)	32.17	3.108×10^{-2}
	kg	14.594	0.06852
slugs/ft^2	kg/m^2	157.2	6.361×10^{-3}
tons, short (2,000 lb)	tonnes (1000 kg)	0.9075	1.102
watts	ergs/s	10^7	10^{-7}
	hp (550 ft-lb/s)	1.341×10^{-3}	745.7

INDEX

A

Absorption of sound, *see* Sound absorption
Acceleration level, 20
ACGIH, *see* American Conference of Governmental Industrial Hygienists
Acoustical efficiency (throttling valves), 647–649
Acoustical enclosures, 521–552. *See also* Small enclosures, sound in
  close-fitting, sealed enclosures, 531–537
  for cooling towers, 667
  for feed pumps, 672
  for industrial gas turbines, 673
  intermediate-size enclosures, 537–538
  large, with interior sound-absorbing treatment, 540–551
    effect of sound-absorbing treatment, 547, 548
    flanking transmission through floor, 549, 550
    inside-outside vs. outside-inside transmission, 549–550
    key parameters influencing insertion loss, 544–545
    leaks, 547, 548
    machine position, 549
    machine vibration pattern, 549
    model for insertion loss at high frequencies, 541–544
    wall panel parameters, 545–547
  large, without internal sound-absorbing treatment, 538–540
  partial, 551–552
  performance of:
    insertion loss as measure for, 522–523
    measures for, 518–519
    qualitative description, 523–525
  size of, 521
  small, sealed enclosures, 525–531
  for transformers, 679
Acoustical impedance, 39–41
  characteristic 40
  complex 39–40
  specific 40
Acoustically induced vibrations and rattles, 905, 907
Acoustical levels, 12–24
Acoustical modal response, 149–151
Acoustical privacy, 203–204. *See also* Speech privacy
Acoustical standards, *see* Standards
Acoustical terminology, 1–41, 911
Acoustical wave equation, 25–34, 149
Active machinery isolation, 840–845
Active noise and vibration control (ANVC), 721–849
  actuators:
    locations of, 806–808
    number of, 804–806
    placement and selection of, 722–730
    sizing of, 808–809
  controller architecture and performance simulations, 814–817
  control sensors/architectures, 730–732
  design considerations, 800–801
  digital filters, 740–751
    adaptive design for, 749–751
    description of, 741–747
    optimal design for, 747–749
  feedback control systems, 779–800
    alternate suboptimum control filter estimation, 784–800
    basic architecture, 779–781
    optimal control filter estimation, 781–784
  feedforward control systems, 751–779
    adaptive control, 760–765
    basic architecture, 751–754
    control of aliasing effects, 765–769
    extension to MIMO systems, 777–779
    optimal control filter estimation, 754–760
    system identification, 769–777
  identifying performance goals for, 801–804
  implementation and testing of, 827–829
  performance expectations, 732–733
  placement and selection of control sources/actuators, 722–730
  prototype ANVC systems, 733–740
    active machinery isolation, 840–845
    airborne noise in high-speed patrol craft, 845–849
    MIMO feedforward active locomotive exhaust with passive component, 829–840

TABLE C.1 (*continued*)

To convert	Into	Multiply by	Conversely, multiply by
	newtons/m^2	10^{-1}	10
miles (nautical)	ft	6080	1.645×10^{-4}
	km	1.852	0.5400
miles (statute)	ft	5280	1.894×01^{-4}
	km	1.6093	0.6214
miles^2 (statute)	ft^2	2.788×10^7	3.587×10^{-8}
	km^2	2.590	0.3861
	acres	640	1.5625×10^{-3}
mph	ft/min	88	1.136×10^{-2}
	km/min	2.682×10^{-2}	37.28
	km/h	1.6093	0.6214
nepers	db	8.686	0.1151
newtons	lb (force)	0.2248	4.448
	dynes	10^5	10^{-5}
newtons/m^2	lb/in.^{2} (force)	1.4513×10^{-4}	6.890×10^3
	lb/ft^2 (force)	2.090×10^{-2}	47.85
	dynes/cm^2	10	10^{-1}
lb (force)	newtons	4.448	0.2248
lb (weight)	slugs	0.03108	32.17
	kg	0.4536	2.2046
lb H_2O (distilled)	ft^3	1.602×10^{-2}	62.43
	gal (liquid U.S.)	0.1198	8.346
lb/in.^{2} (weight)	lb/ft^2 (weight)	144	6.945×10^{-3}
	kg/m^2	703	1.422×10^{-3}
lb/in.^{2} (force)	lb/ft^2 (force)	144	6.945×10^{-3}
	N/m^2	6894	1.4506×10^{-4}
lb/ft^2 (weight)	lb/in.^{2} (weight)	6.945×10^{-3}	144
	gm/cm^2	0.4882	2.0482
	kg/m^2	4.882	0.2048
lb/ft^2 (force)	lb/in.^{2} (force)	6.945×10^{-3}	144
	N/m^2	47.85	2.090×10^{-2}
lb/ft^3 (weight)	lb/in.^{3} (weight)	5.787×10^{-4}	1728
	kg/m^3	16.02	6.243×10^{-2}
poundals	lb (force)	3.108×10^{-2}	32.17
	dynes	1.383×10^4	7.233×10^{-5}
	newtons	0.1382	7.232
slugs	lb (weight)	32.17	3.108×10^{-2}
	kg	14.594	0.06852
slugs/ft^2	kg/m^2	157.2	6.361×10^{-3}
tons, short (2,000 lb)	tonnes (1000 kg)	0.9075	1.102
watts	ergs/s	10^7	10^{-7}
	hp (550 ft-lb/s)	1.341×10^{-3}	745.7

INDEX

A

Absorption of sound, *see* Sound absorption
Acceleration level, 20
ACGIH, *see* American Conference of Governmental Industrial Hygienists
Acoustical efficiency (throttling valves), 647–649
Acoustical enclosures, 521–552. *See also* Small enclosures, sound in
  close-fitting, sealed enclosures, 531–537
  for cooling towers, 667
  for feed pumps, 672
  for industrial gas turbines, 673
  intermediate-size enclosures, 537–538
  large, with interior sound-absorbing treatment, 540–551
    effect of sound-absorbing treatment, 547, 548
    flanking transmission through floor, 549, 550
    inside-outside vs. outside-inside transmission, 549–550
    key parameters influencing insertion loss, 544–545
    leaks, 547, 548
    machine position, 549
    machine vibration pattern, 549
    model for insertion loss at high frequencies, 541–544
    wall panel parameters, 545–547
  large, without internal sound-absorbing treatment, 538–540
  partial, 551–552
  performance of:
    insertion loss as measure for, 522–523
    measures for, 518–519
    qualitative description, 523–525
  size of, 521
  small, sealed enclosures, 525–531
  for transformers, 679
Acoustical impedance, 39–41
  characteristic 40
  complex 39–40
  specific 40
Acoustically induced vibrations and rattles, 905, 907
Acoustical levels, 12–24
Acoustical modal response, 149–151
Acoustical privacy, 203–204. *See also* Speech privacy
Acoustical standards, *see* Standards
Acoustical terminology, 1–41, 911
Acoustical wave equation, 25–34, 149
Active machinery isolation, 840–845
Active noise and vibration control (ANVC), 721–849
  actuators:
    locations of, 806–808
    number of, 804–806
    placement and selection of, 722–730
    sizing of, 808–809
  controller architecture and performance simulations, 814–817
  control sensors/architectures, 730–732
  design considerations, 800–801
  digital filters, 740–751
    adaptive design for, 749–751
    description of, 741–747
    optimal design for, 747–749
  feedback control systems, 779–800
    alternate suboptimum control filter estimation, 784–800
    basic architecture, 779–781
    optimal control filter estimation, 781–784
  feedforward control systems, 751–779
    adaptive control, 760–765
    basic architecture, 751–754
    control of aliasing effects, 765–769
    extension to MIMO systems, 777–779
    optimal control filter estimation, 754–760
    system identification, 769–777
  identifying performance goals for, 801–804
  implementation and testing of, 827–829
  performance expectations, 732–733
  placement and selection of control sources/actuators, 722–730
  prototype ANVC systems, 733–740
    active machinery isolation, 840–845
    airborne noise in high-speed patrol craft, 845–849
    MIMO feedforward active locomotive exhaust with passive component, 829–840

Active noise and vibration control (ANVC) (*continued*)
sensors:
control sensors/architectures, 730–732
number/location of, 809–814
performance of, 813–814
reference, 809, 812–813
residual, 809–812
Actuators (ANVC):
locations of, 806–808
number of, 804–806
placement and selection of, 722–730
sizing of, 808–809
Actuator channels, 806
Adaptive control algorithm, 760–765
A/D converters, *see* Analog-to-digital converters
Added mass, 348, 355, 383–384
Added mass coefficient, 348
Added mass/fluid density, 348
Added volume, 348, 355
Admittance, 41
Aeroacoustical sources, 611–616
aerodynamic dipoles, 612–613
aerodynamic monopoles, 611–612
aerodynamic quadrupoles, 613–614
of fractional orders, 614
influence of source motion, 615–616
Aerodynamic dipoles, 614
Aerodynamic monopoles, 614
Aerodynamic sound, 611, 643–656. *See also* Gas flow noise
AFOSHSTD (Air Force Occupational, Safety, and Health Standard), 881
AI, *see* Articulation index
Air bag deployment noise, 869
Airborne excitation, simultaneous dynamic excitation and, 462–465
Airborne sound (noise):
outdoors, 121
Airborne whole-body vibration criteria, 881
Air compressors, predicting noise from, 660–662
Air-Conditioning and Refrigeration Institute (ARI), 911
Air-cooled condensers, predicting noise from, 667–668
Aircraft interior noise control, 736
Airflow velocity (HVAC systems), 701–703
fans, 707
near grilles, 701–702
terminal boxes/valves, 708–709
Airfoils:
"singing" of, 640
sound generation by, 639–640
Air Force Occupational, Safety, and Health Standard (AFOSHSTD), 881
Air mounts, 739
Air Movement and Control Association (AMCA), 670
Air pressure ratios, 648
Air spring isolators, 577
Aliasing, 817
active control of, 765–769
in spectral analysis, 54
All zero filters, 743
AMCA (Air Movement and Control Association), 670
American Conference of Governmental Industrial Hygienists (ACGIH), 871, 881, 882
American National Standards Institute (ANSI), 878, 911
American Society of Heating, Refrigerating, and Air-Conditioning Engineers (ASHRAE), 706, 711, 911
American Society of Mechanical Engineers (ASME), 911
American Society of Testing and Materials (ASTM), 911
American system of units, 935–937
Amplification at resonance, 583
Analog-to-digital (A/D) converters, 741–742, 766, 767
for ANVC systems, 819–825
sampling process of, 817
Anechoic spaces/rooms, 82, 97–98, 211
ANSI, *see* American National Standards Institute
Antialiasing filters, 54, 57, 765–769
and ANVC performance, 815
selection of, 817–819
ANVC, *see* Active noise and vibration control
Applications Handbook (ASHRAE), 711
Architectural acoustics ,standards for, 930–931
Architectural noise control in buildings, standards for, 926–931
Area sources, 122
ARI (Air-Conditioning and Refrigeration Institute), 911
ARMA filters, 744
Armed forces sound exposure criteria, 863, 867–868, 874
Articulation index (AI), 203–204
ASHRAE, *see* American Society of Heating, Refrigerating, and Air-Conditioning Engineers
ASHRAE handbooks, 706, 711
ASME (American Society of Mechanical Engineers), 911
ASTM (American Society of Testing and Materials), 911
Asymptotic threshold shift (ATS), 865, 866
Atmospheric absorption, 136
Atmospheric pressure, 1
Attenuation:
active noise control, 721–849
ducts, lined, 311–313

of sound:
by atmosphere, 136
by barriers, 132–135, 137–139
by ground cover and trees, 137
total, 137
Audio frequency region, 859–867, 873
Auralization, 190
Autocorrelation function, 60
Automotive interior noise control system, 735–736
Autoregressive moving average filters, 744
Autospectral density functions, 55–59
Averages, 8, 19:
linear, 48
running, 49–50
synchronous averaging, 51–52
unweighted (linear), 48, 49
weighted, 48–49
Average A-weighted sound level, 17
Average diffuse-field surface absorption coefficient, 184–185
Average sound level, 16
A-weighted sound level, 17, 887–891
A-weighted sound (noise) exposure level, 18, 858, 859
coal car shakers, 664
diesel-engine-powered equipment, 668
transformers, 677–678
A-weighted sound power level, 73–75
air compressors, 661
in diffuse field, 81
estimates of, 659
feed pumps, 673
steam turbines, 676
wind turbines, 680
A-weighted sound pressure level, 15–16
long-term, 139
for noise exposure, 858, 859
for outdoor sound, 121
overall, 142–143

B

Background noise:
in classrooms, 196–197
for speech intelligibility, 192–193
Baffled pistons, sound power output of, 35, 36
Balanced noise criterion (NCB) curves, 894, 895
Bandwidths:
of continuous-spectrum sound, 7–9
conversion of, 10–11
half-power, 165
with tapering, 57
Barriers, 132
cooling towers, 667
effectiveness of, 345
for open-plan offices, 202–203
for outdoor sound, 120, 132–135
close to trees, with gaps and slots, 138–139
interaction of ground and, 137–138
and uncertainty of attenuation, 141–142
with transformers, 679
Beams:
damping due to reinforcements, 591–592
infinite:
effective length connecting force and moment impedance, 502
transmission through, 395–397
power transmission to plate from, 410–413
viscoelastic damping of:
three-component beams, 602–606
two-component beams, 599–600
Beam-tracing techniques, 189–190
BEM (boundary element model), 121
Bending waves:
complete power transmission for, 412–413
reflection loss of, 407–410
in beams, 411–412
and change in cross-sectional area, 407
free bending waves at *L*-junctions, 408
in plates with vibration break, 415–416
through cross junctions and T-junctions, 409–410
through infinite plates, 417–418
Bias error, 59
in coherent output power calculations, 65
in gain factor estimates, 62
in intensity measurement, 105, 106
Blocked pressure, 626, 629
Block's formula for shallow cavities, 641–642
Boilers, predicting noise from, 662–663
Boundaries, damping due to, 591
Boundary conditions, 150, 151
forced sound pressure response, 159
Boundary element method, 156
Boundary element model (BEM), 121
Breakin noise, HVAC, 703–705
Breakin sound transmission loss, 450–451
Breakout noise, HVAC, 703–705
Breakout sound transmission loss, 448–450
Broadband disturbance control, 756–760
Broadband regulation filter, 790–795, 797
Bucket ladder unloaders, 664
Butterworth filters, 817–818

C

Cabins:
acoustical performance measures of, 520
defined, 517
Cauer filters, 817–818
Cavities, flows past, 640–643
Ceilings, for mechanical rooms, 710
Central-processing units (CPUs), 825, 827
CHABA, *see* National Academy of Sciences–National Research Council, Committee on Hearing, Bioacoustics and Biomechanics
Characteristic resistance, 40

Choked jets, 621
Circular effects (with FFT), 50
Clamshell bucket unloaders, 664
Classrooms, 191–197
  controlling sound in, 196–197
  predicting acoustical quality of, 193–196
  speech intelligibility in, 192–193
Closed-loop system identification, 771, 772, 774–776, 827, 828
Closed offices, sound pressure levels in, 190–191
Close-fitting enclosures:
  defined, 522
  sealed, 531–537
    free standing, 531–534
    machine-mounted, 535–537
  wrappings vs., 552
Coincidence frequency, 432–434, 436. *See also* Critical frequency for orthotropic plates, 437
Coal car shakers, 663–664
Coal crushers, 665
Coal-handling equipment:
  diesel-powered, 668
  predicting noise from, 663–665
Coal mills and pulverizers, 665
Coal transfer towers, 665
Coefficient of variation, 50
Coherence functions (coherency squared), 58–59
Coherent output power relationship, 64–65
Coil spring isolators, 576
Combination mufflers, 335–338
Combustion noise (gas turbine engines), 624–626
Community noise, 907
Comparison method (sound power output), 81, 88–89
Compensation filter (feedback control), 792–800
Compensator-regulator architecture (feedback control), 784–785
Complex admittance, 41
Complex impedance, 38–40, 588
Complex sound spectra, 12
Composite partitions, sound transmission through, 451
Composite structures (statistical energy analysis), 456
Composite transmission factor, 461, 462
Comprehensive models (noise prediction), 198
Compression waves, 6, 390–391
  and change in cross-sectional area, 407
  in plates with vibration break, 414–415
Compressive force, 347–348
Concentric-tube resonator (CTR), 304–311
Concurrent system identification, 771
Conference rooms, 191, 890, 891, 898
Construction equipment, diesel-powered, 668
Continuous spectra, 2–3, 7–11
Control authority (ANVC), 730
Conversion factors, 939–942
Cooley-Tukey algorithm, 53–54
Cooling towers, predicting noise from, 666–667
Core noise, 624–625, 679
Correlation functions, 60–61
Cosine-squared taper, 55, 57
Coulomb damping, 588
Coupling loss factor, 456
CPUs, *see* Central-processing units
Criteria for noise limits in buildings, 886–907
  survey method, L_A, 888–889
  engineering method, NC, 889, 892–894
  precision method, RNC, 899–905
Critical bands, 900
Critical frequency, 432–433, 436. *See also* Coincidence frequency
Critical damping coefficient, 559, 581
Critical damping ratio, 162
Cross-correlation function, 67–69
Cross junctions, reflection loss of bending waves through, 409–410
Cross-sectional area:
  of HVAC ducts, 687, 691
  power transmission owing to change in, 406–407
Cross-spectral density (CSD) matrix, 804–808, 810–814
Cross-spectral density functions, 57–59
CSD matrix, *see* Cross-spectral density matrix
CTR, *see* Concentric-tube resonator
Cylindrical array (microphones), 93, 94, 96
Cylindrical sound sources, 4

D

D/A converters, *see* Digital-to-analog converters
Damage risk criteria:
  for hearing, 858–874
    impulse noise, 867–869
    infrasound exposure, 869, 870
    noise exposure criteria for audio frequency region, 861–867
    protection of, 871–874
    ultrasound exposure, 869–871
  human vibration response, 874–883
    exposure guidelines, 877–883
    hand-transmitted vibration effects, 877
    whole-body vibration effects, 875–877
Damping, 174–176
  critical damping ratio, 162
  effect of, 561
  in HVAC ducts, 701, 703
  structural, 561, 579–607
    analytical models of, 588
    due to boundaries and reinforcements, 591–592
    due to energy transport, 592–594
    effects of, 579–580
    energy dissipation and conversion, 589–590
    measurement of, 586–588
    measures of, 580–586
    models of, 588–589
    viscoelastic, 594–607
  in two-stage isolation systems, 573, 574
  viscous, 561
Damping capacity, 584
Damping ratio, 559, 561, 581
Dashpots, 395
  in mass-spring-dashpot system, 557–560
  point force impedance for, 394
Data analysis, 43–69
  analog, 52
  correlation functions, 60–61
  deterministic data, 44–45
  mean-square values, 3, 47–48
  mean values, 47
  for periodic excitation source identification, 63–64
  for propagation path identification, 66–69
  random data, 45–47
  for random excitation source identification, 64–66
  running averages, 49–50
  spectral functions, 52–59
    auto (power) spectral density functions, 55–58
    coherence functions, 58–59
    FFT algorithm, 52–54
    line and Fourier spectral functions, 54–55
  statistical sampling errors, 50–51, 59
  synchronous averaging, 51–52
  for system response properties identification, 62–63
  types of data signals, 43
  weighted averages, 48–49
Data signals, 43
  deterministic, 44–45
  random, 45–47
Day-night sound (noise) level, 17, 888, 907
dB, *see* Decibels
Decay, *see* Sound decay
Decay distance, 603
Decay rates, 582, 587. *See also* Reverberation time
Decibels (dB):
  fractions of, 24
  and reference quantities, 12
  sound power expression, 75
  sound pressure level expression, 15, 17
Deflection, 599
Deformation of solids, 492
Department of Defense (DOD), 907

Deterministic data signals, 44–45
  spectral computations for, 55
  statistical sampling errors with, 59
DI, *see* Directivity index
Diesel-engine-powered equipment, predicting noise from, 668–669
Diffuse-field theory, 184–187
Diffuse (reverberant) field, 76–77
  control of, 200–201
  driving freely hung panel, 457–459
  measurement in, 82
  sound power determination in, 81
  sound power in, 81, 85–91
Diffusers:
  HVAC, 701–703
  in reverberations rooms, 209–210
Digital data:
  mean-square value of, 47–48
  mean values of, 47
Digital filters (ANVC), 740–751
  adaptive design for, 749–751
  advantages of, 740–741
  description of, 741–747
  optimal design for, 747–749
Digital signal processor (DSP) chips, 740–741, 825–827
Digital signal processors, 825–827
Digital-to-analog (D/A) converters, 767, 770, 815–816
  for ANVC systems, 819–825
  sampling process of, 817
Dilatation resonance, 439
Dipoles:
  aerodynamic, 614, 633
  sound power output of, 34, 35
Direct-estimation algorithm, MIMO, 778
Direct field, control of, 200
Directional sources, 72, 73, 78–79
Directivity:
  defined, 72
  determination of, 113–117
Directivity factor, 113–116
Directivity index (DI), 115–117, 123
Directivity pattern, 113, 114
Direct method (sound power output), 81, 89–91
Displacement level, 582
Displacement ventilation systems, 703
Dissipation, 165–166
Dissipative silencers, 311–335
  economic considerations, 335
  effect of flow on silencer attenuation, 329–331
  factors in acoustical performance of, 282–283
  flow-generated noise, 331–333
  key performance parameters, 313–316
  lined ducts, 281–313
  parallel-baffle silencers, 316–325
  pod silencers, 328–329

Dissipative silencers (*continued*)
prediction of silencer pressure drop, 333–335
round silencers, 325–328
Distributed sound-masking systems, 206
Doppler factor, 615
Dose-response curve (DRC), 868
Double-layer partitions, sound transmission through, 443–449
Double-tuned expansion chamber (DTEC), 297–300
Drag, 633
DRC (dose-response curve), 868
Driving point force impedance, 496–500
Dry cooling systems, *see* Air-cooled condensers
Dry friction damping, 588
DSP chips, *see* Digital signal processor chips
DTEC, *see* Double-tuned expansion chamber
Ducts:
flow noise in, 635–638
HVAC, noise transmission attentuation for, 685–699
by cross-sectional area changes, 687, 691
by divisions, 687
by elbows, 691–693
end-reflection loss, 697–698
by plenums, 696–697
prefabricated sound attenuators, 693–696
room effect, 698–699
in straight ducts, 686–691
lined, 280–313
for rooftop air conditioning units, 715–716
sound power determination in, 112–113
transmission loss of, 448–451
Dynamic absorbers, 593
Dynamic capability (of instruments), 105–107
Dynamic excitation:
by point force, 393–394
simultaneous airborne excitation and, 462–465

E

Early decay time (EDT), 183
ECMA International, 112
EDT (early decay time), 183
Effective value, 2, 31. *See also* Root-mean-square sound pressure
Eigenfrequency, 400
Elastic surface layer, improvement of impact noise isolation with, 479–483
Elastomeric isolators, 576–577
Elbows, HVAC ducts, 691–693
Elementary radiators, sound power output of, 35–36
Emission, 71
HVAC outdoor noise, 717–718
immission vs., 73
machinery noise measurement standards, 916–918
noise power emission level, 75n.
strength descriptors for, 71
Empirical models of sound in rooms, 190
Enclosures, *see* Acoustical enclosures
End-reflection loss, HVAC, 697–698
Energy, dissipated, *see* Damping
Energy-average spectral deviation factor, 897
Energy speed, 391, 393
English system of units, 835
Entrance loss (dissipative mufflers), 313–314
Environmental corrections, 80, 98–101
Environmental Protection Agency (EPA), 863
Environmental sound (noise):
measurement application standards, 921–922
measurement method standards, 920–921
outdoor propagation of, 922. *See also* Outdoor sound propagation
Environmental vibrations standards, 922–924
EPA (Environmental Protection Agency), 863
Equipment (machine) mounted enclosures, 522, 535–537
Equivalent continuous A-weighted noise level, 17
Equivalent sound absorption area, 99
Equivalent sound power level, estimating, 659–660
Equivalent viscous damping, 589n.
Excitation:
of freely hung panel, 457–459
by incident waves vs. other means, 427
by point force, 393–394
of solid structures:
extension of reciprocity to, 473–476
with sound field vs. point force, 462–465
sources of:
and gain factors, 62–63
periodic, 63–64
random, 64–66
Exit loss (dissipative mufflers), 314
Expansion chamber mufflers, 293–300
double-tuned, 297–299
extended-outlet, 294–297
general design guidelines for, 299–300
simple, 293–294
Extended-outlet muffler, 294–297
Eyring approach (diffuse-field theory), 185

F

FAA (Federal Aviation Administration), 907
Fans:
air-cooled condensers, 667
cooling towers, 667
HVAC, 705–707
industrial, 669–672
industrial gas turbines, 674
for mechanical equipment, 718
transformers, 677–679

Far field, 5, 6, 76–77
cooling towers, 667
transformers, 678–679
Fast-field program (FFP), 121
Fast Fourier transform (FFT) algorithms, 50, 52–55
Federal Aviation Administration (FAA), 907
Federal Highway Administration (FHWA), 132
Feedback control systems, 779–800
alternate suboptimum control filter estimation, 784–800
architecture for, 731–732, 779–781
optimal control filter estimation, 781–784
residual sensor channels for, 809
system identification in, 771–777
Feedback neutralization, 775
Feedforward control systems, 751–779
adaptive control, 760–765
architecture for, 731–732
basic architecture, 751–754
control of aliasing effects, 765–769
extension to MIMO systems, 777–779
MIMO active locomotive exhaust with passive component, 829–840
optimal control filter estimation, 754–760
reference sensor channels for, 809
residual sensor channels for, 809
system identification, 769–777
Feed pumps, predicting noise from, 672–673
FFP (fast-field program), 121
FFT algorithms, *see* Fast Fourier transform algorithms
FFT analyzer, 104
FHWA (Federal Highway Administration), 132
Field-incidence mass law, 435
Field-incidence sound transmission, 435–437
Field-incidence transmission loss, 546
Filtered-U algorithm, 775
Filtered-x LMS algorithm, 761–765, 771, 775, 778, 779
Finite-element method, 156–159
Finite impulse response (FIR) filters, 743, 744, 746–749
Finite panels, sound transmission through, 439–443
FIR filters, *see* Finite impulse response filters
5-dB rule, 859
Fixed diffusers, 209
Fixed -point DSPs, 827
Flanking sound transmission, 451–453, 549, 550
Flexible-wall effect on sound pressure, 166–171
coupled structural–acoustical response, 169–170
wall as noise source, 166–168
wall as reactive impedance, 167, 169
Floating floors:
checking performance of, 486
impact noise isolation with, 482
locally reacting, 482–382
for mechanical rooms, 710
resonantly reacting, 483
Floating-point DSPs, 825, 827
Flow(s):
past cavities, 640–643
in pipes, 630–631
separated, 627
and silencer attenuation, 329–331
Flow-generated noise:
gas flow noise, 611–656
aeroacoustical sources, 611–616
aerodynamic noise of throttling valves, 643–656
airfoils and struts sound generation, 638–640
in flows past cavities, 640–643
from fluid flow in pipes, 630–631
gas jet noise, 616–624
gas turbine engine combustion noise, 624–626
grid or grille noise, 635–638
spoiler noise, 631–635
turbulent boundary layer noise, 626–630
HVAC:
in duct systems, 699–700
flow-generated sound power, 694
of silencers, 331–333
Flow resistance, flow resistivity, 235–237
Fluctuating drag (flow spoilers), 633
Fluctuating lift forces (flow spoilers), 633
Fluids, propagation speed of sound in, 351–352
Foot-pound-second system of units, 936
Foot-slug-second system of units, 936
Forced sound pressure response, 159–161
Formstiff small enclosures, 527–530
4-dB rule, 859
Fourier spectral functions, 54–55
Fraction of critical damping, 581. *See also* Damping ratio
Free field, 4, 32, 76
measurement in, 82
outdoor sound propagation in, 126–128
sound power determination in, 91–98
Free-field approximation, for sound intensity, 79–81
Free-field radiation, from jet in ideal acoustical medium, 616
Free standing enclosures, 522, 531–534
Frequency response function, 62, 161
Frequency spectral density, 638–639
Fresnel number, 132
Fresnel zones, 134
Friction force, 347
Furnishings, sound in rooms and, 184

G

Gain factor estimates, 62–63
Gas flow noise, 611–656
  aeroacoustical sources, 611–616
  aerodynamic noise of throttling valves, 643–656
    acoustical efficiency, 647–649
    aerodynamic noise, 643–647
    due to high velocities in valve outlet, 652
    methods of valve noise reduction, 652–656
    pipe transmission loss coefficient, 649–651
  airfoils and struts sound generation, 638–640
  in flows past cavities, 640–643
  from fluid flow in pipes, 630–631
  gas jet noise, 616–624
  gas turbine engine combustion noise, 624–626
  grid or grille noise, 635–638
  spoiler noise, 631–635
  turbulent boundary layer noise, 626–630
Gas jet noise, 616–624
  flight effects, 624
  from imperfectly expanded jets, 621–623
  jet mixing noise, 616–621
Gas turbines:
  engine combustion noise, 624–626
  industrial, predicting noise from, 673–675
Gauges of metal plates, 513–514
Generalized-terrain PE, 121
Gradient, 25, 26, 103
Gradient descent algorithms, 749–750
Graphical user interface (GUI), 829
Grid noise, 635–638
Grilles:
  HVAC, 701–703
  noise from, 635–638
Ground cover, outdoor sound propagation and, 137
Group speed (energy speed), 391, 393
GUI (graphical user interface), 829

H

Half-power bandwidth, 165
Half-power points, 583n.
Hand-arm vibration syndrome (HAVS), 857, 877
Hand-transmitted vibration criteria, 881–882
Hand-transmitted vibration effects, 877
Hanning window, 55, 57
HAVS, *see* Hand-arm vibration syndrome
Head-related transfer functions (HRTFs), 190
Hearing, 858–874
  damage risk criteria, 858–861
  impulse noise, 867–869
  infrasound exposure, 869, 870
  noise exposure criteria for audio frequency region, 861–867
  protection of, 871–874
  psychoacoustics, 900
  and sound pressure, 1
  standards for testing equipment/procedures, 918–919
  ultrasound exposure, 869–871
Hearing conservation program standards, 919
Hearing impairment (hearing loss), 18
Hearing threshold, 18, 19, 894
Hearing threshold levels, 18
Heating, ventilating, and airconditioning (HVAC) systems, 685–718
  airflow velocity, 701–703
  A-weighted sound-level criteria for, 890–891
  diffuser selection, 703
  duct-borne noise transmission attentuation, 685–699
    by cross-sectional area changes, 687, 691
    by divisions, 687
    by elbows, 691–693
    end-reflection loss, 697–698
    by plenums, 696–697
    prefabricated sound attenuators, 693–696
    room effect, 698–699
    in straight ducts, 686–691
  duct sizes, 700
  for especially quiet spaces, 700–703
  fans, 705–707
  flow noise in ducted systems, 699–700
  grille selection, 703
  mechanical plant room sound isolation and noise control, 709–710
  NCB criteria curves for, 901
  NC criteria curves for, 901
  noise breakout/break-in, 703–705
  outdoor noise emissions, 717–718
  RC criteria curves for, 898
  RNC criteria curves for, 900–902
  rooftop air conditioning units, 715–717
  terminal boxes/valves, 707–709
  vibration isolation considerations, 711–715
Heat recovery steam generators (HRSGs), 674
Helmholtz equation, 126
Helmholtz resonators, 149, 384, 640, 642–643
Hemi-anechoic spaces/rooms, 82, 92–97, 211
Hemispherical array (microphones), 92–94, 100–101
Hemispherical spaces, directivity index in, 116
Horizontal translational motions, stiffness of isolators and, 564–565
HRSGs (heat recovery steam generators), 674
HRTFs (head-related transfer functions), 190
Human-occupancy areas, noise criteria for, 887–908
  acoustically induced vibrations and rattles, 905, 907
  evaluation methods for, 888–906

    A-weighted sound level, 888–891
    current-day sound-level meters, 888
    NCB curves, 895
    NC curves, 889, 892–894
    RC curves, 895–899
    RNC curves, 899–906
  noise annoyance in communities, 907
  sound level definitions, 887–888
  typical urban noise, 907–908
Human systems, effect of noise/vibration on, 857–858. *See also* Hearing
Human vibration response, 874–883
  exposure guidelines, 877–883
  hand-transmitted vibration effects, 877
  whole-body vibration effects, 875–877
Huygens' model for wave fields, 133–134
HVAC systems, *see* Heating, ventilating, and airconditioning systems

I

IEC, *see* International Electrotechnical Commission
IIR filters, *see* Infinite impulse response filters
IL, *see* Insertion loss
Image sources, method of, 188–189
Immission, 71
  emission vs., 73
  preferred descriptor of, 71
Impact dampers, 590
Impact noise, 477–487
  coal-handling equipment:
    car shakers, 664
    rotary car dumpers, 664
  with elastic surface layer, 479–483
  noise isolation vs. sound transmission loss, 483–486
  standard tapping machine, 477–479
Impedance, 38–41
  complex, 39, 588
  equivalent lumped, 397–398, 496
  of infinite plates and beams, 393–397
  mechanical, 40; 394–395
  moment, 501
  plane-wave, 39, 352–354
  point force, 394–396, 496–500
  separation, 430–434
Impulse noise. *See also* Impact noise
  exposure to, 860
  and hearing, 867–869
  protection against, 874
Impulse response (digital systems), 742–746
Inch-pound-second system of units, 936
Incident sound waves:
  excitation of structures by, 427
  sound absorption:
    normal incidence on porous layer in front of rigid wall, 248–251
    oblique incidence, 251–254
  sound transmission through infinite plate:
    normal-incidence waves, 427–430
    oblique-incidence waves, 430–433
    random-incidence (diffuse) sound, 433–439
Industrial fans, predicting noise from, 669–672
Industrial gas turbines, predicting noise from, 673–675
Industrial workshops, 197–201
  noise control for, 200–201
  noise prediction for, 198–200
Inertia bases, 561–562, 712
Inertia force, 347
Infinite impulse response (IIR) filters, 744, 746, 750
Infinite rigid pistons, 417
Infrasound exposure, 859, 860
  and hearing, 869, 870
  protection against, 872–873
Inhomogeneous atmosphere, refraction of sound in, 129–132
Inner model transform, 781. *See also* Youla transform
Insertion loss (IL), 170, 284–286
  as acoustical performance measure, 522–523
  air compressors, 662
  close-fitting enclosures:
    free standing, 532–534
    machine-mounted, 535–537
  HVAC ducts, 690–693
  large enclosures:
    and flanking, 549, 550
    at high frequencies, 541–544
    inside-outside vs. outside-inside transmission, 549–550
    key parameters influencing, 544–545
    and leaks, 547, 548
    and machine position, 549
    and machine vibration pattern, 549
    and sound-absorbing treatment, 547, 548
    and wall panel thickness, 545–547
    without internal sound-absorbing treatment, 538–540
  small enclosures:
    leaky, 530–531
    sealed, 525–530
Instrumentation standards:
  intensity instruments, 914
  noise-measuring instruments, 912–913
Insulation, thermal-acoustical blanket, 672
Intensity, *see* Sound intensity
Intermediate office speech level (IOSL), 205
Intermediate-size enclosures, 537–538
Internal friction, 589
International Electrotechnical Commission (IEC), 104, 911
International Organization for Standardization (ISO), 82, 878, 911
Inverse square law, 4–5

IOSL (intermediate office speech level), 205
ISO, *see* International Organization for Standardization
Isolation effectiveness, 568–569
  and isolator mass effects, 570–571
  with two-stage isolation, 573–575
Isolation efficiency, 560
Isolation range, 559

J

Jet mixing noise, 616
Joint input-output method, 776–777

K

Kronecker delta function, 742
Kuttruff model, 198–199

L

Large enclosures:
  with interior sound-absorbing treatment, 540–551
    analytical model for insertion loss at high frequencies, 541–544
    effect of sound-absorbing treatment, 547, 548
    flanking transmission through floor, 549, 550
    inside-outside vs. outside-inside transmission, 549–550
    key parameters influencing insertion loss, 544–545
    leaks, 547, 548
    machine position, 549
    machine vibration pattern, 549
    wall panel parameters, 545–547
  without interior sound-absorbing treatment, 538–540
Large partitions, sound transmission of, 425–427
Lateral quadrupole, 349–350
Leakage, in filtered-x algorithm, 762
Leakage errors, 54
Leaky enclosures, 522
  large, 547, 548
  small, 530–531
Lecture rooms, 191. *See also* Classrooms
Levels, 12–18
  average A-weighted sound level, 17
  average sound level, 16
  A-weighted sound (noise) exposure level, 18
  A-weighted sound pressure level, 15–16
  day–night, 17
  equivalent continuous A-weighted, 17
  hearing impairment (hearing loss), 18
  hearing threshold levels:
    associated with age, 18
    associated with age and noise, 18
    for setting "zero" at each frequency on a pure-tone audiometer, 18
  noise-induced permanent threshold shift, 18
  overall levels, determining, 22–24
  sound intensity level, 14–15
  sound power level, 13–14
  sound pressure level, 15, 17
Level at mid-frequencies (LMF), 896, 897
Linear average, 48
Linear isolators, massless, 569–570
Lined ducts, 280–313
Line sources, 122
Line spectral function, 54–55
Line spectrum, 2
L-junctions, reflection loss of free bending waves at, 408
LMF, *see* Level at mid-frequencies
LMS algorithm, 750–751
  adaptive control based on, 760
  filtered-x, 761–762, 771, 775
Logarithmic decrement, 581, 587
Longitudinal quadrupole, 350
Longitudinal waves, 6
  in beams, reflection loss for, 410–411
  resonance of, 640–641
Long-term A-weighted sound pressure level, 139
Loss factor:
  damping, 584
  for panels/uniform plates, 591
  in piping, 630–632
  structural damping, 561
  of three-component beam, 604–606
  of viscoelastic material, 595–596
Loudness, perceived, 900
Loudspeakers, 729
Low-noise compressors, 660

M

Machine-mounted enclosures, *see* Equipment mounted enclosures
Machinery noise:
  active machinery isolation, 840–845
  emission measurement standards, 916–918
  inertia bases, 561–562
  prediction of, *see* Prediction of machinery noise
Machinery vibration, active control of, 739–740
Mach number, 304
Masking of sound, 205, 206
Mass, 394, 579
Mass-controlled boundaries, 169
Mass law, 443
Massless linear isolators, 569–570
Massless springs, 395
  in mass-spring-dashpot system, 557–560
  point force impedance for, 394
Mass-spring-dashpot system, 557–560, 580
  energy dissipation in, 585

  steady-state response of, 584
  time variation of, 581
Material damping, 589
Mean-square error (FIR filters), 748–749
Mean-square (ms) value (variance), 47–48
  in data analysis, 47–48
  normalized random error of, 50, 51
Mean-square sound pressure:
  and bandwidth conversion, 10–11
  for complex spectra, 12
  for contiguous frequency bands, 8, 9
  of continuous-spectrum sound, 7, 11
Measurement environments, 82
Measurement surfaces, 92
Mechanical hysteresis, 589
Mechanical impedance, 40, 394–395
Mechanical induced-draft cooling towers, 666–667
Mechanical plant rooms, sound isolation/noise control in, 709–710
Mercury RACE++, 825, 827
Metallic isolators, 576
Meteo-BEM, 121
Meteorology, outdoor sound propagation and, 139–140
Meter-kilogram-second (mks) system of units, 936
Method of image sources, 188–189
Micrometeorology, 130
Microphones (for measurements), 102
  for hemi-anechoic spaces, 92–97
  for reverberation rooms, 87–88
Midfrequency average, 896
MIMO systems, *see* Multiple-input, multiple-output systems
mks system of units, 936
Mobility, (admittance, 43), 396
  measurement of, 588
  receiver, 569
  in two-stage isolation systems, 575–576
Modal analysis technique, 159
Modal damping, 163, 164
Modal damping constant (decrement), 159
Modal density, 400–402, 454, 507–508
Modal energy, 453–455
Modal parameter extraction instrumentation, 588
Modal testing, 588
Modern optimal control theory, 781
Mode shapes, 150, 152–155, 400, 507–508
Modes of vibration:
  equal energy of, 455
  modal energy, 453–455
  system of modal groups, 453–454
Momn-Obukhov boundary layer theory, 121
Monopoles:
  aerodynamic, 611–612, 614
  sound power output of, 34, 35
Motion sickness guidelines, 880
Moving-average filters, 743
Moving sound sources:
  outdoor, 124–126
  reciprocity in moving, 476–477
ms, *see* Mean-square value
Mufflers. *See also* Silencers
  combination, 335–338
  expansion chamber, 293–300
  feed pumps, 674
  for industrial fans, 670
  perforated-element, 300–311
  steam vents, 677
  transformers, 679
Multilayer partitions, sound transmission through, 443–448
Multiple-input, multiple-output (MIMO) systems, 740
  feedforward, 754
  feedforward active locomotive exhaust with passive component, 829–840
    actuator number/location, 832–834
    control actuator design, 834–836
    control architecture, 835–836
    hardware selection, 837–838
    performance goals, 831–832
    problem description, 829–830
    sensor number/location, 832, 834, 835
    system performance, 838–840
  LMS algorithms for, 751
  optimal design of, 777–779
  Youla feedback architecture in, 783
Music, exposure criteria for, *867*
Music waves, superposition principle and, 36

N

National Academy of Sciences–National Research Council, Committee on Hearing, Bioacoustics and Biomechanics (CHABA), 861–862, 867
Natural-draft cooling towers, 666
Natural frequencies, 150, 152–155
  of finite structures, 400
  and horizontal stiffness of isolators, 565
  of mechanical equipment isolators, 711
  for pure vertical vibration, 563
  of rigid and nonrigid masses, 563
  for rocking, 564
  in two-stage isolation systems, 572–573
NCB curves, *see* Balanced noise criterion curves
NC curves, *see* Noise criterion curves
Near field, 76
NEMA values (transformer noise level), 678, 679
Net oscillatory force, 349
Neutralizers, 593
Newton's second law of motion, 25, 26
Nichols plot, 787–788, 794

NIPTS, *see* Noise-induced permanent threshold shift
NITTS, *see* Noise-induced temporary threshold shift
Noise annoyance (in communities), 907
Noise-cancellation headsets, 736–738
Noise control, 345
  active, *see* Active noise and vibration control
  in buildings, acoustical standards for, 926–931
  in classrooms, 196–197
  design standards for, 930–931
  for industrial workshops, 200–201
  in mechanical plant rooms, 709–710
  in solid structures, *see* Solid structures, interaction of sound waves with
  as system problem, 81
  transformers, 679
  in very small enclosures, 145–146
Noise criterion (NC) curves, 889, 892–894, 901
Noise exposure:
  A-weighted, 858
  criteria for audio frequency region, 861–867, 886–906
  duration of, 865–866
Noise exposure level, A-weighted, 18
Noise-induced hearing loss, 857, 859
Noise-induced permanent threshold shift (NIPTS), 861–862, 864, 865
Noise-induced temporary threshold shift (NITTS), 866, 867
Noise level, perceived, 4
Noise mapping, computer software for, 139
Noise power emission level (NPEL), 75n.
Noise reduction (NR), 284, 286, 345, 382–387
  active, 345
  actuators, 807
  air compressors, 662
  coal-handling equipment:
    car shakers, 664
    crushers, 665
    rotary car dumpers, 664
    transfer towers, 665
    unloaders, 664
  cooling towers, 666, 667
  feed pumps, 673
  HVAC systems:
    criteria for noise control in, 886–906
    by duct cross-sectional area changes, 687, 691
    by duct divisions, 687
    by elbows, 691–693
    for especially quiet spaces, 700–703
    by plenums, 696–697
    for straight ducts, 686–691
  industrial fans, 669–670
  by minimizing added mass, 383–384
  passive, 345–346
  at specific frequencies, 384–387
  steam turbines, 676
  throttling valves, 652–656
  wind turbines, 680
Noise reduction coefficient (NRC), 207
Noise sources, *see* Sound (noise) sources
Nondirectional sources, 72, 78
Nondispersive waves, 391–392
Nonperiodic steady-state signals, 44
Nonrecursive filters, 743
Nonrigid masses:
  natural frequencies of, 563
  transmissibility of, 565–567
Nonstationary random data, 46–47, 49–50
Non-volume-displacing sound sources, radiation by, 361–377
  effect of surrounding point force by rigid pipe, 375–377
  force acting on fluid, 371–375
  response of bounded fluid to point force excitation, 375
  response of unbounded fluid to excitation by oscillating small rigid body, 363
  in response to excitation of fluid by oscillating small rigid sphere, 363–371
Normal-incidence sound transmission, 427–430
Normalized LMS algorithm, 751
Normalized random error, 50, 65
Normal modes, 150
Normal-mode expansion, 159
Normal mode of vibration, *see* Resonance
Normal specific acoustical impedance, 41
Nosoacusis, 860
NPEL (noise power emission level), 75n.
NR, *see* Noise reduction
NRC (noise reduction coefficient), 207
Nyquist frequency, 53, 54, 57
Nyquist plots, 583, 585, 786–788, 794, 798, 799
Nyquist's sampling theorem, 815
Nyquist stability criterion, 785

O

OAPWL, *see* Overall sound power level
OASPL, *see* Overall sound pressure level
Oblique-incidence sound transmission, 430–433
Occupational Safety and Health Administration (OSHA), 862
Octave-band sound power level:
  air compressors, 661
  estimates of, 659
  feed pumps, 673
  steam turbines, 676
  with surging or large fluctuations, 903–905
Octave-band sound pressure level, 15, 678
Octave-band source spectra, 122–123

Offices:
  closed, sound pressure levels in, 190–191
  criteria for noise control in, 890, 891
  open-plan, 201–208
One-dimensional wave equation:
  backward-traveling plane wave, 32
  general solution to, 27–28
  intensity, 31–32
  outwardly traveling plane wave, 28–31
  particle velocity, 31
  root-mean-square sound pressure, 31
  solutions to, 27–34
  spherical wave, 32–34
Open area ratio, 306, 307
Open-loop system identification, 770–772, 774, 775, 827, 828
Open-plan offices, 201–208
  barriers for, 202–203
  design parameters for, 206–208
  rating acoustical privacy of, 203–204
  speech and noise levels in, 205–206
  workstation acoustical design, 204–205
Optimal control theory, 781
Oscillating rigid bodies, radiation efficiencies of, 418–419
Oscillating small rigid bodies:
  fluid excitation, 363–371
    force acting on fluid, 371–375
    harmonic excitation, 363–365
    predicting body length, 366–370
    predicting radiated sound power, 366, 371
    random excitation, 371
    sound radiation of nonspherical bodies, 365
    unbounded fluid, 363
  point force excitation, 375–377
  radiation by, 348–349
Oscillating spheres, sound power output of, 34, 35
Oscillating three-dimensional bodies, radiation efficiencies of, 418–419
OSHA noise exposure criteria, 862
OSHA (Occupational Safety and Health Administration), 862
Outdoor noise emissions, from HVAC systems, 717–718
Outdoor sound propagation, 119–143
  accounting for meteorology, 139–140
  airborne, 121
  atmospheric absorption, 136. *See also* Air absorption
  barriers, 132–135
  computer software for noise mapping, 139
  effects of ground cover and trees, 137
  in homogeneous free space over ground, 120–121, 126–128
  inhomogeneity of atmosphere, 129–132
  interaction of barriers and ground, 137–138
  moving sources, 124–126
  point sources at rest, 120–124
  reflectors and reverberation, 135–136
  refraction of sound, 129–132
  relevance of criteria for, 119–120
  standard regulations for interactions, 137
  standards for, 922
  uncertainties of, 140–143
Outwardly traveling plane wave, 28–31
Overall A-weighted sound pressure level, 17, 142–143
Overall level (OA), 22–24
Overall sound power level (OAPWL):
  air compressors, 661
  air-cooled condensers, 667
  boilers, 662
  coal-handling equipment:
    car shakers, 663
    crushers, 665
    mills and pulverizers, 665
    rotary car dumpers, 664
    transfer towers, 665
    unloaders, 664
  diesel-engine-powered equipment, 668–669
  feed pumps, 672
  for gas turbine engines, 625
  industrial fans, 670–672
  industrial gas turbines, 675
  steam turbines, 676
  steam vents, 676–677
Overall sound power output (cooling towers), 666
Overall sound pressure level (OASPL), 618–621, 624
Overlapped processing, 57

P

Parabolic equation (PE), 121
Parallel-baffle silencers, 311, 312, 316–325
  baffle thickness, 324–325
  cross-sectional area, 322
  effect of temperature on, 322–324
  predicting acoustical performance of, 316–322
  quantitative considerations with, 317
Parallelepiped array (microphones), 93, 95, 100
Particle velocity, 5–6
  measurement of, 102–103
  for outwardly traveling plane wave, 31
  for spherical waves, 33–34
Partitions, sound transmission by:
  composite partitions, 451
  double-layer partitions, 443–449
  large partitions, 425–427
  multilayer partitions, 443–447
  small partitions, 421–425
Passive silencers, 279–338
  combination mufflers, 335–338
  dissipative, 311–335
    economic considerations, 335

Passive silencers (*continued*)
effect of flow on silencer attenuation, 329–331
flow-generated noise, 331–333
key performance parameters, 313–316
lined ducts, 281–313
parallel-baffle silencers, 316–325
pod silencers, 328–329
prediction of silencer pressure drop, 333–335
round silencers, 325–328
expansion chamber mufflers, 293–300
double-tuned expansion chamber, 297–299
extended-outlet muffler, 294–297
general design guidelines for, 299–300
simple expansion chamber muffler, 293–294
perforated-element mufflers, 300–311
acoustical performance, 303–310
back pressure, 310–311
range of variables for, 300–303
performance metrics for, 281–286
reactive, 286–293
representation by basic silencer elements, 287–288
transfer matrices for, 288–293
Pendulum isolators, 577–578
Perceived noise level, 49
Perforated-element mufflers, 300–311
acoustical performance, 303–310
back pressure, 310–311
range of variables for, 300–303
Perforated plates, open area of, 515
Performance:
ANVC systems:
and controller architecture, 814–817
goals for, 801–804
and doors/windows/ventilation openings, 660
insertion loss as measure of, 522–523
measures of, 518–519
qualitative description of, 523–525
Periodic excitation sources, identification of, 63–64
Periodic signals, 44
mean-square value for, 48
spectral computations for, 54
statistical sampling errors with, 59
Permanent threshold shifts (PTSs), 862
Permissible exposure level (PEL), 862
Phase speed, 391–393
Pipes:
fluid flow in, 630–631
to isolated mechanical equipment, 714
with open side branch, sound radiation in, 355
transmission loss of, 448–451
Pipe transmission loss coefficient (throttling valves), 649–651
Pipe wrappings, 554–555
Piston-in-cylinder isolators, 577
Plane boundaries, sound radiation and, 377–382
oscillating moment in infinite liquid, 381–382
pressure-release boundaries, 379–381
rigid boundaries, 378–379
Plane waves, 6
backward-traveling, 32
outwardly traveling, 28–31
reflection and transmission at interfaces of, 403–406
sound pressure and particle velocity relationship, 38
Plane-wave impedance, 352–354
Plane-wave transfer matrix method, 280–281
Plant transfer functions, 770–771
Plateau method (sound transmission), 442–443
Plates:
finite, point-excited, 420–421
infinite, 395–397, 417–418
effective length connecting force and moment impedance, 502
normal-incidence plane waves, 427–430
oblique-incidence plane waves, 430–433
point-excited, 420–421
random-incidence sound, 433–439
inhomogeneous, 438–439
orthotropic, 437–438
perforated, open area of, 515
power transmission from beam to, 410–413
steel, gauges and weights of, 513–514
thin isotropic, field-incidence transmission for, 435–437
transmission through, 395–397
normal-incidence plane waves, 427–430
oblique-incidence plane waves, 430–433
random-incidence sound, 433–439
with vibration break, power transmission between, 413–416
with viscoelastic coatings, 601–602
with viscoelastic interlayers, 606–607
Plenums:
HVAC ducts, 696–697
for rooftop air conditioning units, 715
Plug muffler, 304–311
Pneumatic isolators, 577
Pod silencers, 328–329
Point force:
active control of disturbance, 725–727
dynamic excitation by, 393–394
excitation by sound field vs., 462–465
Point force impedance, 394–396, 496–500
Point input admittance (mobility), 396
Point moment, dynamic excitation by, 393–394
Point moment impedance, 394–395, 501
Point sound sources, 122–124, 361

Poisson's ratio, 391, 493
Pole-zero filters, 744
Position-keeping system, 739, 796
Positive definite (quadratic function), 748
Power, *see* Sound power
Power balance:
and response of finite structures, 399–403
in two-structure system, 456–457
Power balance equation, 406
Power law damping, 588
PowerPC (PPC) chips, 825–827
Power spectral density (PSD) functions, 55–58, 172–174
Power spectral density spectrum, 9
Power transmission between structural elements, 406–416
from beam to plate, 410–413
and change in cross-sectional area, 406–407
plates separated by thin resilient layer, 413–416
reflection loss:
of bending waves through cross junctions/T-junctions, 409–410
of free bending waves at *L*-junctions, 408
PPC chips, *see* PowerPC chips
Prediction of machinery noise, 659–681
air compressors, 660–662
air-cooled condensers, 667–668
boilers, 662–663
coal-handling equipment, 663–665
cooling towers, 666–667
diesel-engine-powered equipment, 668–669
feed pumps, 672–673
industrial fans, 669–672
industrial gas turbines, 673–675
steam turbines, 675–676
steam vents, 676–677
transformers, 677–679
wind turbines, 679–681
Prefabricated sound attenuators, HVAC, 693–696
Presbyacusis, 860
Pressure, *see* Sound pressure
Pressure-residual intensity index, 106
Privacy, in open-plan offices, 201–204
Processor-to-processor communications, 825
Propagation of sound:
in fluids, 351–352
identifying propagation paths, 66–69
outdoor, *see* Outdoor sound propagation
in rooms, 182
Propagation speed:
in solids, 492
velocity vs., 391
PSD functions, *see* Power spectral density functions
PTSs (permanent threshold shifts), 862
Pulsating small rigid bodies, radiation by, 348
Pulsating sphere:
maximum achievable volume velocity of, 359–361
sound radiation of, 355
Pumps:
feed, predicting noise from, 672–673
at transformers, 677
Pure tones, 2
in continuous spectrum, 7, 8
and hearing thresholds, 18
setting pure-tone audiometers, 18
and spectral density, 9

Q

Quadrupoles, aerodynamic, 613–614
Quality assessment index (QAI), 897–899
Quantization noise, 822–823
Quarter-spherical spaces, directivity index in, 116–117

R

Radiation efficiency, 418–420, 509–511
Radiation fields of sources, 75–77
Radiation impedance of sphere, 364
Radiation of sound:
by thin plates, 417, 420
effect of plane boundaries on, 377–382
oscillating moment in infinite liquid, 381–382
pressure-release boundaries, 379–381
rigid boundaries, 378–379
global cancellation, 722
by non-volume-displacing sound sources, 361–377
effect of surrounding point force by rigid pipe, 375–377
force acting on fluid, 371–375
response of bounded fluid to point force excitation, 375
response of unbounded fluid to excitation by oscillating small rigid body, 363
in response to excitation of fluid by oscillating small rigid sphere, 363–371
by small rigid bodies, 346–355
acoustical parameters, 351–354
lateral quadrupole, 349–350
longitudinal quadrupole, 350
oscillating small rigid bodies, 348–349
by pipe with open side branch representing pulsating sphere, 355
by piston in rigid tube with open side branch, 354–355
pulsating small rigid bodies, 348
radiated sound power, 351
in solid structures, 416–421
tonal components in, 635
by vibrating structures, 593–594
by volume-displacing sound sources, 356–361

Radiators, elementary, 35–36
Random-analysis theory, 172–174
Random data signals, 45–47
  cross-spectral density function, 57–58
  mean values for, 47
  statistical sampling errors with, 59
  tapering windows with, 57
Random error, 62
Random excitation sources, identification of, 64–66
Random-incidence (diffuse) sound transmission, 433–439
Random-incidence mass law, 435
Random sound pressure response, 170, 172–175
Rattles, acoustically induced, 905, 907
Rayleigh, Lord, 119, 129
Raynaud's phenomenon, 877
Ray theory, 121
Ray-tracing techniques, 189–190, 198
RC curves, 895–899
RC filter, 48
Reactive silencers, 286–293
  factors in acoustical performance of, 282–283
  representation by basic silencer elements, 287–288
  transfer matrices for, 288–293
Receiver mobility, 569
Reciprocity, 162, 465–477
  extension to sound excitation of structures, 473–476
  for higher order excitation sources/responses, 512
  in moving media, 476–477
  prediction of noise from multiple correlated forces, 470–471
  source strength identification by, 471–473
  theorem, 162
Reconstruction filters, 817–819
Recursive filters, 744
Reference quantities, 12, 19–22
"Reference Quantities for Acoustical Levels" (ANSI S1.9–1989, Reaffirmed2001), 19, 20
Reference sensors (ANVC), 809, 812–813
Reflection loss:
  for bending waves:
    in beams, 411–412
    and change in cross-sectional area, 407
    at interfaces, 404–405
    free bending waves at *L*-junctions, 408
    in plates with vibration break, 415–416
    through cross junctions and T-junctions, 409–410
  for compression waves:
    and change in cross-sectional area, 407
    in plates with vibration break, 414–415
  for longitudinal waves in beams, 410–411
Reflection of sound:
  at plane interfaces, 37, 403–406
  by room surfaces, 183
Reflectors, outdoor, 135–136
Refraction of sound, 129–132
Regularization (ANVC sensors), 814
Regulation filter design (feedback control), 785–792
Reinforcements, damping due to, 591–592
Relative bandwidth, 583
Residual sensors (ANVC), 809–812
Resonance, 38, 150, 640–643
Resonance frequencies, 165
  of boilers, 663
  of finite structures, 400, 401, 507–508
  standing-wave, 570
Resonance transmission loss, 460
Reverberant field, *see* Diffuse (reverberant) field
Reverberation:
  in classrooms, 197
  in industrial workshops, 197–198
  outdoor sound propagation, 135–136
  for speech intelligibility, 193
  standards for, 930–931
  with steam turbines, 676
Reverberation rooms, 82, 209–210
  characteristics of, 85–86
  experimental setup for, 87–88
  qualification requirements for, 86–87
Reverberation time, 175–176, 582
Reynolds stresses, 119, 613
Rigid masses, 395, 563. *See also* Three-dimensional masses
Rigid tube with open side branch, sound generation in, 354–355
Ring frequency, 500
Rms sound pressure, *see* Root-mean-square sound pressure
RNC curves, 899–906
Road surface sound absorption standards, 924
Rocking motions, vertical motions coupled with, 563–564
Rooftop air conditioning units, 715–717
Rooms, sound in, 181–211
  air absorption, 183
  alternative prediction approaches, 187–188
  anechoic and hemi-anechoic chambers, 211
  auralization, 190
  classrooms, 191–197
  criteria for noise control in, 886–907
  diffuse-field theory, 184–187
  domestic rooms and closed offices, 190–191
  empirical models, 190
  and furnishings, 184
  from HVAC ducts, 698–699
  industrial workshops, 197–201
  method of image sources, 188–189
  open-plan offices, 201–208

  propagation of sound, 182
  ray and beam tracing, 189–190
  reverberation rooms, 209–210
  sound decay, 182–183
  surface absorption and reflection, 183
Room noise evaluation:
  engineering method, 889, 892–894
  precision method, 899–905
  survey method, 888–889
Root-mean-square (rms) sound pressure, 2
  for contiguous frequency bands, 8, 9
  of continuous-spectrum sound, 7, 11
  normalized random error of, 50, 51
  for outwardly traveling plane wave, 31
Rotary coal car dumpers, 664
Rotating diffusers, 209–210
Round silencers, 312, 325–328
Running averages, 49–50

S

SA A/D converters, *see* Successive-approximation A/D converters
Sabine approach (diffuse-field theory), 185–186
Sampling errors, *see* Statistical sampling errors
Schroeder frequency, 209
Screech tones, 621, 622
SEA, *see* Statistical energy analysis
Seals, for mechanical rooms, 710
Sealed enclosures:
  close-fitting, 531–537
  defined, 522
  small, 525–531
SECM, *see* Simple expansion chamber muffler
Seismic restraint of equipment, 713
SEL, *see* Sound exposure level
Self-noise, 639
Sensors (ANVC), 730–732
  performance of, 813–814
  reference, 809, 812–813
  residual, 809–812
Separation impedance, 430–434
Shakers (ANVC), 730
Shear modulus (viscoelastic material), 391, 595–596
Shear parameter (3-component beam), 603
Sheet Metal and Air Conditioning National Association (SMACNA), 686
Shock-associated noise, 616, 621–623
Shock response spectrum, 55
Side-lobe leakage, 54
Sigma-delta A/D converters, 820–822
Signal-to-noise ratio (SNR):
  ANVC converters, 823–825
  for classrooms, 196
  for open-plan offices, 203–204
  for synchronous averaged signal, 52
SII, *see* Speech intelligibility index
SIL, *see* Speech interference level
Silencers. *See also* Mufflers
  active noise control, 280
  defined, 280
  dissipative mufflers, 314, 315
  downstream of valves, 654, 655
  effect of flow on attenuation, 329–331
  flow-generated noise of, 331–333
  for HVAC ducts, 693–696, 705
  modeling, 283–286
  passive, *see* Passive silencers
  for rooftop air conditioning units, 716
  selection factors for, 281–282
Simple expansion chamber muffler (SECM), 293–294, 299–300
Simplified models (noise prediction), 198–199
Single-input, single-output (SISO) systems, 733
  feedback, 779–781
  feedforward, 754
  filtered-x algorithm for, 762
  LMD algorithm for, 751
Singular-valued decomposition (SVD), 804–807, 810, 813
SISO systems, *see* Single-input, single-output systems
SMACNA (Sheet Metal and Air Conditioning National Association), 686
Small enclosures, sound in, 145–178. *See also* Rooms, sound in
  acoustical modal response, 149–151
  enclosure driven at resonance, 164–166
  flexible-wall effect on sound pressure, 166–171
  forced sound pressure response, 159–161
  natural frequencies and mode shapes, 150, 152–155
  numerical methods for acoustical analysis, 156–159
  random sound pressure response, 170, 172–175
  sealed enclosures, 525–531
  steady-state sound pressure response, 161–164
  transient sound pressure response, 174–178
  very small enclosures, 145–149
Small partitions, sound transmission of, 421–425
Small rigid bodies:
  oscillating, *see* Oscillating small rigid bodies
  radiation by, 346–355
    acoustical parameters of, 351–354
    lateral quadrupole, 349–350
    longitudinal quadrupole, 350
    pipe with open side branch representing pulsating sphere, 355
    piston in rigid tube with open side branch, 354–355

Small rigid bodies: (*continued*)
pulsating bodies, 348
radiated sound power, 351
Smoothing filters (ANVC) 815
Snell's law, 405
Sociacusis, 860
Soft parameters, 827, 828
Solids:
key acoustical parameters of, 493–495
wave motion in, 390–393
Solid structures, interaction of sound waves with, 389–515
impact noise, 477–487
impact noise isolation vs. sound transmission loss, 483–486
improvement of impact noise isolation by elastic surface layer, 479–483
standard tapping machine, 477–479
mechanical impedance, 394–395
power balance and response of finite structures, 399–403
power input, 395–399
power transmission between structural elements, 406–416
from beam to plate, 410–413
and change in cross-sectional area, 406–407
plates separated by thin resilient layer, 413–416
reflection loss of bending waves through cross junctions/T-junctions, 409–410
reflection loss of free bending waves at *L*-junctions, 408
reciprocity, 465–477
in moving media, 476–477
prediction of noise from multiple correlated forces, 470–471
and sound excitation of structures, 473–476
source strength identification by, 471–473
reflection and transmission at plane interfaces, 403–406
and simultaneous airborne/dynamic excitation, 462–465
sound radiation, 416–421
sound transmission:
flanking, 451–453
of large partitions, 425–427
loss in ducts and pipes, 448–451
of normal-incidence waves through infinite plate, 427–430
of oblique-incidence waves through infinite plate, 430–433
of random-incidence (diffuse) sound through infinite plate, 433–439
of small partitions, 421–425
through composite partitions, 451
through double- and multilayer partitions, 443–449
through finite-size panel, 439–443
statistical energy analyses, 453–462
composite structures, 456
diffuse sound field driving freely hung panel, 457–459
equal energy of modes of vibration, 455
modal energy, 454–455
noncorrelation between waves in two systems, 455
power balance in two-structure system, 456–457
realization of equal coupling loss factor, 456
SEA method, 459–462
system of modal groups, 453–454
transmission loss through simple homogeneous structure, 459–462
superposition, 465–467
wave motion in solids, 390–393
Sound absorption, 215–274
by air in rooms, 183
atmospheric, 136
design charts for fibrous sound-absorbing layers, 254–264
monolayer absorbers, 255–259
multilayer absorbers, 261
thin porous surface layers, 261–264
two-layer absorbers, 259–261
for enclosures, 521
equivalent sound absorption area, 99
large flat absorbers, 246–265
normal incidence on porous layer in front of rigid wall, 248–251
oblique sound incidence, 251–254
plane sound waves at normal incidence, 247–248
limp porous layer, 225–229
multiple limp porous layers, 229
by non-sound absorbers, 218–221
in open-plan offices, 206–207
by plate and foil absorbers, 271–274
by porous bulk materials and absorbers, 229–246
acoustical properties of porous materials, 238–239
analytical characterization of porous granular/fibrous materials, 238
empirical prediction of flow resistivity, 237
empirical predictions from regression analyses of measured data, 239–243
flow resistance and flow resistivity, 235–237
plastic foams, 244–245
polyester fiber materials, 241, 243–244
porosity, 231–233
process of, 231
and temperature, 245–246
theoretical prediction of flow resistivity, 237–238
tortuosity, 232, 234
process of, 216
by resonance absorbers, 264–271
absorption cross section of individual resonators, 266–268
acoustical impedance of resonators, 265–266
internal resistance of resonators, 268–271
nonlinearity and grazing flow, 268
resonance frequency, 266
spatial average impedance of resonator arrays, 271
by rigid porous layer, 221–225
by room surfaces, 183
sound absorption coefficients, 216–218
standards for, 928–930
by thin-flow resistive layer in front of rigid wall, 221
waveguide absorbers, 593
for wrappings, 521
Sound absorption average (SAA), 206–208
Sound attenuation, *see* Noise reduction; Silencers
Sound barriers, *see* Barriers
Sound decay, 182–183, 186
Sound energy density, 7
Sound exposure, A-weighted, 18
Sound exposure level (SEL), 125–126
Sound generation, 345–387
effect of nearby plane boundaries on, 377–382
non-volume-displacing sound sources, 361–377
effect of surrounding point force by rigid pipe, 375–377
force acting on fluid, 371–375
response of bounded fluid to point force excitation, 375
response of unbounded fluid to excitation by oscillating small rigid body, 363
in response to excitation of fluid by oscillating small rigid sphere, 363–371
reducing sound radiation, 382–387
small rigid bodies, 346–355
acoustical parameters of, 351–354
lateral quadrupole, 349–350
longitudinal quadrupole, 350
oscillating small rigid bodies, 348–349
by pipe with open side branch representing pulsating sphere, 355
by piston in rigid tube with open side branch, 354–355
pulsating small rigid bodies, 348
radiated sound power, 351
volume-displacing sound sources, 356–361

Sound intensity, 3–4
for cylindrical sound source, 4
defined, 3
in determining sound power, 101–112
free-field approximation for, 79–81
instrumentation for measuring, 104–105
for outwardly traveling plane wave, 31–32
and sound power, 22
sound power vs., 14–15
and sound pressure, 4
for spherical sound source, 4
for spherical waves, 34
standards for measurement instruments/techniques, 914
Sound intensity analyzer, 103–104
Sound intensity level, 14–15
reference quantities for, 19–22
and sound power level, 22
Sound isolation, in mechanical plant rooms, 709–710
Sound levels, *see* Levels
Sound level measurement standards, 912–914
Sound (noise) sources, 71–117, 887
aeroacoustical, 611–616
in classrooms, 192, 196
cylindrical, 4
dipole-type, 638
directional, 72, 73
directivity of, 113–117
excitation sources:
and gain factors, 62–63
periodic, 63–64
random, 64–66
measurement environments for, 82
nondirectional (monopole), 34, 72
outdoor:
moving sources, 124–126
point sources at rest, 122–124
point (monopole), 34, 361
radiation by, 35, 361–377
radiation field of, 75–77
sound intensity:
free-field approximation for, 14, 35, 79–81
and sound power, 14, 77–79
sound power levels, 14, 73–74
determination of, 82–85
in diffuse field, 81, 85–91
in ducts, 112–113
environmental corrections in determining, 98–101
in free field, 14, 91–98
and sound intensity, 14, 77–79
sound intensity in determining, 14, 101–112
spherical, 4, 5, 35
volume-displacing:
radiation by, 35, 356–361
in workshops, 199

Sound power, 4, 5
  of baffled pistons, 36
  defined, 4, 14
  in diffuse field, 81, 85–91
  of dipoles, 34, 35
  in ducts, 112–113
  in free field, measurement of, 91–98
    anechoic spaces, 97–98
    hemi-anechoic spaces, 92–97
    measurement surfaces, 92
  of monopoles, 34
  of oscillating spheres, 34, 35
  radiated, 351
  and sound intensity, 4, 22, 77–79
Sound power input:
  in solid structures, 395–399
  to structures, 503–506
Sound power level, 13–14, 73–74
  defined, 72
  and environmental corrections, 98–101
  environmental noise:
    measurement application standards, 921–922
    measurement method standards, 920–921
  expression of, 75
  HVAC duct-borne noise, 685–686
  with impact noise, 479
  ISO standards for determining, 82–85
  reference quantities for, 19–22
  and sound intensity level, 22
Sound power measurement standards, 914–916
Sound power output:
  air-cooled condensers, 667
  cooling towers, 666
  small boilers, 662
Sound pressure, 1
  in determination of sound power, 4, 91–98
  flexible-wall effect on, 166–171
  forced sound pressure response, 159–161
  and particle velocity, 5–6
  in plane waves, 32, 38
  random sound pressure response, 170, 172–175
  and sound intensity, 4
  sound power vs., 4, 14–15
  space-averaged squared, 7
  for spherical waves, 32–33
  steady-state sound pressure response, 161–164
  transient sound pressure response, 174–178
Sound pressure level, 15, 17
  A-weighted, 15–16
  calculation of, 18, 72, 73
  defined, 18, 71
  expression of, 75
  long-term A-weighted, 16, 139
  overall A-weighted, 142–143
  reference pressure for, 19
  reference quantities for, 19–22
Sound propagation:
  in industrial workshops, 197, 198
  between office workstations, 202, 204–205
  underwater, 121
Sound radiation, *see* Radiation of sound
Sound spectra, 7–12
  complex, 12
  continuous, 7–11
Sound transmission, *see* Transmission
Sound waves, 1–7
  compressional, 6
  interference of, 36–37
  inverse square law for, 4–5
  longitudinal, 6
  and noise, 1
  and particle velocity, 5–6
  period of, 2
  plane, 6, 28–31
  reflection, 36–38, 404–405
  resonant, 38
  root-mean-square amplitude of, 2
  sound energy density, 7
  and sound spectra, 2–3. *See also* Sound spectra
  speed of, 6
  spherical, 32–34
  standing, 37–38
  transverse, 6
  traveling, 37
  wave equation, 25–34
  wavelength, 7
Source dimensionality, 805
Space-averaged sound energy density, 7
Space-averaged squared sound pressure, 7
Spacers, 600n.
Spatial decay rate, 582
Specific acoustical impedance, 40
Spectral density function, 50
Spectral functions:
  data analysis, 52–59
    auto (power) spectral density functions, 55–58
    coherence functions, 58–59
    FFT algorithm, 52–54
    line and Fourier spectral functions, 54–55
    statistical sampling errors, 59
  time domain procedures for, 60
Spectral method (underwater sound), 121
Spectral (spectrum) density, 9
Speech communication metrics standards, 920
Speech intelligibility, in classrooms, 192–193
Speech intelligibility index (SII), 204, 206–208
Speech interference level (SIL), 888, 889, 892, 893

Speech privacy, 203–204
  and ambient noise levels, 206
  and voice levels, 205
Speech waves, superposition principle and, 36
Speed of sound, 6
  group (energy) speed, 391, 393
  phase speed, 391–393
  propagation speed vs. velocity, 391
  in solids, 492
Spherical sound sources, 4, 5, 116
Spherical waves, 32–34
Spinal injury, vibration-related, 857
Spoiler noise, 631–635
Spring isolators, 712–713
Squared correlation coefficient function, 61
Square law damping, 588
Standards, 911–931
  for architectural noise control in buildings, 926–931
    acoustics, reverberation, and noise control design, 930–931
    sound absorption, 928–930
    sound transmission, 926–928
  for criteria for noise in rooms, 886–906
  for environmental correction, 98–101
  finding/selecting, 911–912
  hand-transmitted vibration criteria, 881–882
  for HVAC silencers, 694
  for impact noise isolation, 486
  for impact of noise in workplace, 918–924
    environmental noise measurement applications, 921–922
    environmental noise SPL measurement methods, 920–921
    environmental sound propagation outdoors, 922
    environmental vibrations, 922–924
    hearing conservation programs, 919
    hearing test equipment/procedures, 918–919
    speech communication metrics, 920
  for industrial workshop noise, 201
  for intensity measurement, 108, 109–112
  for intensity measurement instrumentation, 104, 108
  for machinery noise emission measurements, 916–918
  for noise control by enclosures and cabins, 517–521
  noise-induced hearing impairment, 864–865
  occupational noise exposure, 864–865
  for outdoor sound, 131, 132, 134–135, 140
  for qualification of reverberation rooms, 86–90
  for sound level measurements, 912–914
    intensity instruments and measuring techniques, 914
    noise-measuring instrumentation, 912–914
    SPL measurement techniques, 913–914
  for sound power, 82–85
    in anechoic space, 97–98
    in ducts, 112–113
    in hemi-anechoic space, 92–96
    in reverberation rooms, 209–210
  for sound power measurements, 914–916
  for speech intelligibility, 193
  structure-borne whole-body vibration, 878–881
  for vehicle exterior/interior noise, 924–926
    exterior noise measurement techniques, 925–926
    interior noise measurement techniques, 924
    road surface sound absorption, 924
  for wind turbines, 681
Standard tapping machine, 477–479
Standard threshold shift (STS), 862
Standing-wave resonance frequencies, 570
Standing waves, 37–38
Stationary random data, 45–46
Stationary signals, ms value of, 47–48
Statistical energy analysis (SEA), 453–462
  composite structures, 456
  diffuse sound field driving freely hung panel, 457–459
  equal energy of modes of vibration, 455
  modal energy, 454–455
  noncorrelation between waves in two systems, 455
  power balance in two-structure system, 456–457
  principle of, 455
  realization of equal coupling loss factor, 456
  system of modal groups, 453–454
  transmission loss through simple homogeneous structure, 459–462
Statistical sampling errors:
  with correlation functions, 61
  with mean and ms value calculation, 50–51
  with spectra calculation, 59
Steady state, diffuse-field theory prediction of, 186
Steady-state drag, 633
Steady-state particle velocity, 38
Steady-state response:
  damping, 587
  forced vibrations, 582–584
Steady-state signals:
  ms value of, 47–48
  nonperiodic, 44
Steady-state sound pressure, 38
Steady-state sound pressure level, 15, 187
Steady-state sound pressure response, 161–164, 167
Steam turbines, predicting noise from, 675–676
Steam vents, predicting noise from, 676–677

Steel plates, gauges and weights of, 513–514
Stiffness-controlled boundaries, 169
Stochastic transients, 46–47
Strouhal number, 619, 620, 640, 641
Structural–acoustical analogy, 156, 158
Structural–acoustical coupling, 169–170
Structural acoustics, 389
Structural damping, 561, 579–607
  analytical models of, 588
  due to boundaries and reinforcements, 591–592
  due to energy transport, 592–594
  effects of, 579–580
  energy dissipation and conversion, 589–590
  measurement of, 586–588
  measures of, 580–586
    complex stiffness, 584–586
    decay of unforced vibrations with viscous damping, 580–582
    interrelation of, 586
    steady forced vibrations, 582–584
  models of, 588–589
  retarding force in, 588
  viscoelastic, 594–607
    materials and material combinations, 594–595
    mechanical properties of viscoelastic materials, 595–599
    plates with viscoelastic coatings, 601–602
    plates with viscoelastic interlayers, 606–607
    structures with viscoelastic layers, 599
    three-component beams with viscoelastic interlayers, 602–606
    two-component beams, 599–600
Structural dynamics, 389
Structure-borne sound, 611
Structure-borne whole-body vibration criteria, 878–881
Struts, sound generation by, 638–639
Successive-approximation (SA) A/D converters, 820–822, 825
Superposition, 465–467
  with multiple correlated force input, 470
  in source strength identification, 471–473
Supersonic jets, 621
Surging in HVAC noise, 903–905
SVD, *see* Singular-valued decomposition
Synchronous averaging, 51–52
Systems of units, 20, 935
System identification, 769–777, 827
  closed-loop, 771, 772, 774–776, 827, 828
  in feedback control systems, 771–777
  open-loop, 771, 772, 774, 775, 827, 828
System response properties, identification of, 62–63

T

Tapering functions and windows, 54–57
Tapped delay line filters, 743
Tapping machine, *see* Standard tapping machine
Temperature, refraction of outdoor sound and, 129–130
Temperature-frequency equivalence (viscoelastic materials), 597
Temporary threshold shifts (TTSs), 862, 869, 870
Terminal boxes/valves, HVAC, 707–709
Thermal-acoustical blanket insulation, 672
3-dB rule, 859
Three-dimensional masses, vibration isolation for, 563–567
Three-dimensional silencer analysis, 280
Three-duct muffler, 304–311
Throttling valves, aerodynamic noise of, 643–656
  acoustical efficiency, 647–649
  aerodynamic noise, 643–647
  due to high velocities in valve outlet, 652
  methods of valve noise reduction, 652–656
  pipe transmission loss coefficient, 649–651
Time constant, 48
Time history signals, 43–44
Time-varying signals, 44–45
Time-varying transfer functions (ANVC systems), 771
Time-weighted average (TWA), 862
T-junctions, reflection loss of bending waves through, 409–410
TL, *see* Transmission loss
TNM (Traffic Noise Model), 132
Tonal disturbance control, 754–760
Tonal noise:
  boilers, 663
  industrial fans, 669–671
  steam turbines, 676
  transformers, 677, 679
  from turbofan engines, 737–738
Tonal oscillations, 635
Tones:
  in continuous spectrum, 7, 8
  pure, 2
  in sound spectra, 2–3
Traffic noise, 124–126, 132
Traffic Noise Model (TNM), 132
Trailing-edge noise, 640
Transfer function, 62
Transfer matrices (silencers), 280–281, 288–293
  cross-sectional discontinuities, 289–291
  pipe with uniform cross section, 289
  resonators, 291–293
Transformers:
  active noise control for, 723, 725
  predicting noise from, 677–679
Transient signals, 45, 55

Transient sound pressure response, 174–178
Transmissibility, 557–560
  and damping, 561
  and inertia base, 561–562
  and isolation effectiveness, 569
  and isolator mass effects, 570
  and machine speed, 562
  of nonrigid masses, 565–567
  with two-stage isolation, 572–574
Transmission, sound transmission, 71
  flanking, 451–453
  of large partitions, 425–427
  of small partitions, 421–424
  loss of ducts and pipes, 448–451
  at plane interfaces, 403–406
  of small partitions, 421–425
  standards for, 926–928
  structural, 592–593
  through composite partitions, 451
  through double- and multilayer partitions, 443–449
  through finite-size panel, 439–443
  through infinite plate:
    normal-incidence plane sound waves, 427–430
    oblique-incidence plane sound waves, 430–433
    random-incidence (diffuse) sound, 433–439
Transmission coefficient, 425
Transmission loss (TL), 284, 286
  breakin, 450–451
  breakout, 448–450
  classical definition of, 439
  for double partitions, 447–449
  for ducts, 448–451
  field-incidence, 435–436
  of finite panels, 439–443
  flanking, 439–443
  impact noise isolation vs., 483–486
  for inhomogeneous plates, 438–439
  and mass law barrier, 443
  for multilayered partitions, 443–447
  normal-incidence, 427–430
  oblique-incidence, 430–433
  for orthotropic plates, 437
  for pipes, 448–451
  pipe transmission loss coefficient, 649–651
  random-incidence, 434–435
  resonance, 460
  for single partitions, 442–443
  through partitions, 425–427
  through simple homogeneous structure, 459–462
Transversal filters, 743
Transverse waves, 6
Traveling waves, 37
Travel-limited isolators, 713
Trees, outdoor sound propagation and, 137–139
Trigger signal (synchronous averaging), 52
TTS, *see* Temporary threshold shifts
Tuned dampers, 593
Turbines:
  industrial gas turbines, 673–675
  steam turbines, 675–676
  wind turbines, 679–681
Turbofan engine noise control, 737–738
Turbulent boundary layer noise, 626–630
Two-stage vibration isolation, 572–576
Two-structure system:
  noncorrelation between waves in, 455
  power balance in, 456–457

U

Ultrasonic waves, 1
Ultrasound exposure, 859, 860, 869–871, 873–874
Uncertainty, in outdoor sound propagation, 140–143
Underexpanded jets, 621
Underwater sound propagation, 121
Uniform pressure mode, 154, 162
Unit-area acoustical impedance, 41
U.S. armed forces hearing conservation criterion, 863, 867, 868, 874
Unit-sample sequence, 742
Unweighted (linear) averages, 48, 49
Urban noise, 907–908

V

Vacuum bubbles, 385–387
Vacuum pumps, 660
Variation, coefficient of, 50
VDV (vibration dose value), 879
Vehicle exterior/interior noise standards, 924–926
Velocity, propagation speed vs., 391
Vents, steam, predicting noise from, 676–677
Vertical motions, rocking motions coupled with, 563–564
Vibration break, 413
Vibration data, 43
Vibration dose value (VDV), 879
Vibration-induced white finger (VWF), 877
Vibration isolation, 557–578
  active, *see* Active noise and vibration control
  active machinery isolation, 840–845
  for building mechanical systems, 711–715
  classical model, 557–563
    damping effect, 561
    inertia base effects, 561–562
    isolation efficiency, 560
    limitations of, 562–563
    machine speed effect, 562
    mass-spring-dashpot system, 557–560
    transmissibility, 557–560
  high-frequency considerations in, 567–572

Vibration isolation (*continued*)
practical isolators, 576–578
for rooftop air conditioning units, 716
for three-dimensional masses, 563–567
two-stage, 572–576
uses of, 557
Vibration sources:
acoustic, 905, 907
loading of, 567–568
Vibration total value (VTV), 879
Viscoelastic damping, 594–607
beams:
three-component, with viscoelastic interlayers, 602–606
two-component, 599–600
materials and material combinations, 594–595
mechanical properties of viscoelastic materials, 595–599
plates:
with viscoelastic coatings, 601–602
with viscoelastic interlayers, 606–607
structures with viscoelastic layers, 599
Viscous damping, 561, 589n.
Viscous damping coefficient, 580
Viscous damping ratio, 583
Volume-displacing sound sources, radiation by, 356–361
Volume velocity, 146–147, 359–361
Voyager lightweight aircraft, 866
VTV (vibration total value), 879
VWF (vibration-induced white finger), 877

W

Walls:
flexible-wall effect on sound pressure, 166–171
for mechanical rooms, 710
Wall pressure wavenumber-frequency spectrum, 627, 629–630
Wave equation, 25–34, 149
continuity equation in, 27
equation of motion in, 25–26
gas law in, 26–27
one-dimensional:
backward-traveling plane wave, 32
general solution to, 27–28
intensity, 31–32
outwardly traveling plane wave, 28–31
particle velocity, 31
root-mean-square sound pressure, 31
solutions to, 27–34
spherical wave, 32–34
in rectangular coordinates, 27
Waveguide absorber, 593
Wavelength, 7
Wave motion (in solids), 390–393
Wavenumber, 29
Weighted averages, 48–49
WHO, *see* World Health Organization
Whole-body vibration effects, 875–877
Wiener filter, 749
Wiener–Khinchine relationship, 50
Wind turbines, predicting noise from, 679–681
Workplace noise standards, 918–924
Workshops, *see* Industrial workshops
Workstations, sound propagation between, 202, 204–205
World Health Organization (WHO), 871, 907
Wrappings, 552–555
acoustical enclosures vs., 521
close-fitting enclosures vs., 552
defined, 517

Y

Youla transform, 781–784
Young's modulus, 391, 493, 595

Z

"Zone of silence," 345, 846, 847
Zoom transforms, 57